TECHNICAL DIGEST

1995

ORGANIC THIN FILMS FOR PHOTONICS APPLICATIONS

SEPTEMBER 11–14, 1995

PORTLAND, OREGON

1995 TECHNICAL DIGEST SERIES
VOLUME 21

COSPONSORED BY
OPTICAL SOCIETY OF AMERICA
THE AMERICAN CHEMICAL SOCIETY
DIVISION OF POLYMER CHEMISTRY, INC.
DIVISION OF POLYMERIC MATERIALS
AND ENGINEERING, INC.

DISCLAIMER NOTICE

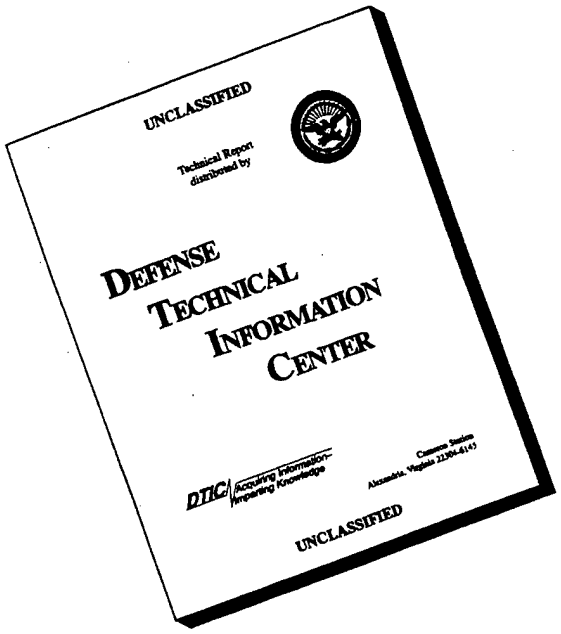

THIS DOCUMENT IS BEST QUALITY AVAILABLE. THE COPY FURNISHED TO DTIC CONTAINED A SIGNIFICANT NUMBER OF PAGES WHICH DO NOT REPRODUCE LEGIBLY.

CONFERENCE EDITION

1995

Summaries of the papers presented at the topical meeting

ORGANIC THIN FILMS FOR PHOTONICS APPLICATIONS

September 11–14, 1995
Portland, Oregon

1995 Technical Digest Series
Volume 21

Cosponsored by
Optical Society of America

The American Chemical Society
Division of Polymer Chemistry, Inc.
Division of Polymeric Materials Science and Engineering, Inc.

Optical Society of America
2010 Massachusetts Avenue NW
Washington DC 20036-1023

Articles in this publication may be cited in other publications. To facilitate access to the original publication source, the following form for the citation is suggested:

Name of Author(s), "Title of Paper," in *Organic Thin Films for Photonics Applications*, Vol. 21, 1995 OSA Technical Digest Series (Optical Society of America, Washington DC, 1995), pp. xx-xx.

Optical Society of America

ISBN

Conference Edition	1-55752-411-4
Postconference Edition (Note: Postconference Edition includes postdeadline papers.)	1-55752-412-2
1995 Technical Digest Series	1-55752-368-1

Library of Congress Catalog Card Number

Conference Edition	95-68688
Postconference Edition	95-68689

Printed in the U.S.A.

Contents

ORGANIC THIN FILMS FOR PHOTONICS APPLICATIONS
TECHNICAL PROGRAM COMMITTEE

Kenneth Singer, *Case Western Reserve University, Chair*
Charles Y.-C. Lee, *Air Force Office of Scientific Research, Chair*
Hilary S. Lackritz, *Purdue University, Program Chair*
George I. Stegeman, *University of Central Florida/CREOL, Program Chair*
***Gary C. Bjorklund,** *Optivision Inc.*
Julian Bristow, *Honeywell Technology Center*
Susan Ermer, *Lockheed Research and Development Division*
Anthony F. Garito, *University of Pennsylvania*
Alan Heeger, *University of California, Santa Barbara*
Yasuhiro Koike, *Keio University, Japan*
Mark G. Kuzyk, *Washington State University*
Geoffrey A. Lindsay, *U.S. Navy*
Rick Lytel, *Akzo Nobel Electronic Products, Inc.*
Seth Marder, *California Institute of Technology*
Tobin Marks, *Northwestern University*
W. E. Moerner, *IBM Almaden Research Center*
Peter Palffy-Muhoray, *Kent State University*
Paras N. Prasad, *State University of New York at Buffalo*
William H. Steier, *University of Southern California*
James T. Yardley, *AlliedSignal Inc.*

INTERNATIONAL ADVISORY COMMITTEE

Donal D. C. Bradley, *University of Sheffield, UK*
Peter Gunter, *Swiss Federation Institute of Technology, Switzerland*
Winfried Horsthuis, *Akzo Nobel Electronic Products, The Netherlands*
François Kajzar, *CEA Saclay, France*
Toshikuni Kaino, *NTT Opto Electronics Laboratory, Japan*
Wolfgang Knoll, *Max-Planck-Institut fur Polymerforschung, Germany*
Seizo Miyata, *Tokyo University of Agriculture and Technology, Japan*
Hachi Nakanishi, *Tohoku University, Japan*
Almira Natansohn, *Queen's University, Canada*
Andre P. Persoons, *University of Leuven, Belgium*
Hiroyuki Sasabe, *Institute of Physical and Chemical Research (RIKEN), Japan*
Guiseppe Zerbi, *Politecnico di Milano, Italy*
Joseph Zyss, *Centre National d'Etudes des Telecommunications, France*

*OSA Technical Council Representative

HOLLADAY ROOM

8:00am–8:15am
Opening Remarks

8:15am–10:00am
MA • Passive Devices
Andre Pierre Persoons, *University of Leuven, Belgium, Presider*

8:15am (Invited)
MA1 • High-speed polymer optical fiber and amplifier, Yasuhiro Koike, *Keio Univ., Japan.* A 2.5-Gbit/s graded-index (GI) polymer optical fiber was achieved with red laser diode and basic performance of high power GI polymer optical fiber amplifier is proposed. **(p. 2)**

8:45am (Invited)
MA2 • Toward the practical application of polymeric optical interconnection technology, James T. Yardley, L. Eldada, K. M. T. Stengel, L. W. Shacklette, Chengjiu Wu, C. Xu, *AlliedSignal Corporate Research and Technology.* We have developed a number of new polymeric materials that make possible the fabrication of complex point-to-point optical interconnections with controlled numerical aperture and geometry. Practical applications for these technologies include optical backplanes, on-chip or on-module interconnection, and sensor circuitry. **(p. 6)**

9:15am
MA3 • Polyimide optical waveguides fabricated by direct electron beam writing, T. Maruno, T. Sakata, Y. Y. Maruo, S. Sasaki, *NTT Interdisciplinary Research Laboratories, Japan;* T. Ishii, T. Tamamura, *NTT Opto-electronics Laboratories, Japan.* Polyimide optical waveguides are fabricated by direct electron beam writing.They operate in a single mode, and have an optical loss of 0.4 dB/cm at a 1.3-μm wavelength. **(p. 10)**

9:30am
MA4 • Polymer waveguide applications in multichip modules and board level optical interconnects, Yue Liu, Julian Bristow, Terry Marta, Sommy Bounnak, Klein Johnson, *Honeywell Technology Center;* Yung Liu, Herb Cole, *GE Corporate Research and Development.* We describe polymer waveguide applications for multichip modules and board level optical interconnects that use established materials, processes, and equipment in electronic industry. **(p. 14)**

9:45am
MA5 • Nonlinear spectroscopy of DANS side-chain polymers, Myoungsik Cha, *Punsan Univ., South Korea;* Akira Otomo, William E. Torruellas, George I. Stegeman, *Univ. Central Florida;* David Beljonne, Jean Luc Bredas, *Univ. Mons-Hainaut, Belgium;* Winfried H. G. Horsthuis, Guus R. Möhlmann, *Akzo-Nobel Electronic Products, The Netherlands.* A complete nonlinear spectroscopic study compared to a molecular orbital calculation of the second and third order nonlinear response of DANS polymers are presented. **(p. 18)**

LLOYD CENTER BALLROOM

10:00am–10:30am
Coffee Break

HOLLADAY ROOM

10:30am–12:00m
MB • Fibers
Yasuhiro Koike, *Keio University, Japan, Presider*

10:30am (Invited)
MB1 • Studies of polymer optical fibers, W. D. Chen, R. F. Shi, A. F. Garito, *Univ. Pennsylvania.* Polymer optical fibers (POFs) offer many significant advantages over inorganic glass optical fibers in short-distance data communications systems, especially in those cases where ease of handling and installation are very important. The current status of step-index and graded-index POFs is reviewed. **(p. 22)**

11:00am
MB2 • All-optical switching in a single-mode polymer optical fiber, D. W. Garvey, M. G. Kuzyk, R. Kruhlak, *Washington State Univ.;* C. W. Dirk, S. Martinez, H. Selnau, Jr., P. Craig, L. Green, *Univ. Texas–El Paso.* We report on the all-optical switching characteristics of a single-mode polymer optical fiber with a squaraine dye-doped poly(methyl)methacrylate core using a Sagnac interferometer. **(p. 26)**

11:15am
MB3 • Transparent birefringence-free copolymer and its application, Shuichi Iwata, Hisashi Tsukahara, Eisuke Nihei, Yasuhiro Koike, *Keio Univ., Japan.* Birefringence-free copolymer for any degree of orientation was successfully synthesized. The polarization preserving fiber made of this copolymer was proposed. **(p. 30)**

11:30am
MB4 • Development of plastic optical fiber devices and multiple-core plastic optical fibers, Aruna R. Nagarur, Sathya Gopalan, Carl W. Dirk, *Univ. Texas–El Paso.* We describe the process of fabricating multiple-core plastic optical fibers. Plastic optical fibers for nonlinear optical device structures and sensors will be presented. **(p. 34)**

11:45am
MB5 • Polarization-insensitive crystalline organic waveguides, R. B. Taylor, Z. Shen, S. R. Forrest, *Princeton Univ.* We describe new polarization-insensitive rib waveguides with a guiding layer composed of a vacuum deposited crystalline organic semiconductor, 3,4,9,10 perylenetetracarboxylic dianhydride (PTCDA). **(p. 38)**

12:00m–1:30pm
Lunch (on your own)

HOLLADAY ROOM

1:30pm–3:45pm
MC • $\chi^{(3)}$
Carl Dirk, *University of Texas at El Paso, Presider*

1:30pm (Invited)
MC1 • Linear and nonlinear spectroscopy of β-carotene and other oligo-polyenes: experimental and theoretical studies, F. Rohlfing, D. D. C. Bradley, *Univ. Sheffield, UK;* J. Cornil, D. Beljonne, J. L. Brédas. *Univ. Mons Hainaut, Belgium;* A. Eberhardt, K. Müllen, *Max-Planck-Institute für Polymerforschung, Germany.* We report studies of linear- and electro-absorption spectra which allow new insights into the electronic structure of polyenes and their nonlinear response. **(p. 44)**

2:00pm
MC2 • Large enhancement in the third order response of asymmetric β-carotenoids, Vincent Ricci, William E. Torruellas, George I. Stegeman, *Univ. Central Florida;* Sandra Gilmour, Seth Marder, *Jet Propulsion Laboratory;* Mireille Blanchard-Desce, *College de France, France.* An enhancement of a factor of up to 43 in the third order susceptibility of trans-β-carotene is achieved by mono-substituting a series of electron acceptors. **(p. 46)**

2:15pm (Invited)
MC3 • Electronic and nonlinear optical properties of organic molecules: assessment of the influence of the molecular structure, Fabienne Meyers, *Univ. Mons-Hainaut, Belgium,* and *Calif. Institute of Technology;* David Beljonne, Jean-Luc Brédas, *Univ. Mons-Hainaut, Belgium;* Chin-Ti Chen, Seth R. Marder, *Calif. Institute of Technology.* We present a theoretical study relating the molecular structure of symmetrical and unsymmetrical squaraine dyes, as well as of various push-push, push-pull, and pull-pull polyenes, to their nonlinear optical properties. **(p. 49)**

2:45pm (Invited)
MC4 • Organic thin-films for spatial light modulation, J. M. Nunzi, S. Delysse, N. Pfeffer, F. Charra, *LETI, France.* Optically addressed spatial light modulators are key components for optical beam handling. A figure of merit for the comparison of materials is derived. Resonant processes in organic thin-films are evaluated in terms of switching efficiency. Real-time holography and *Q*-switching applications are demonstrated. **(p. 53)**

3:15pm
MC5 • Nonlinear absorption in the liquid crystal 5CB, T. Kosa, P. Palffy-Muhoray, *Kent State Univ;* A. Dogariu, E. W. Van Stryland, *Univ. Central Florida.* Nonlinear absorption in the liquid crystal 5CB is shown to be 5th order using picosecond Z-scan and time resolved absorption measurements. A 5-level model is proposed. **(p. 57)**

3:30pm
MC6 • Two-photon resonant contributions to the third-order susceptibility of C_{60} in the solid state, F. J. Bartoli, S. R. Flom, J. R. Lindle, *U.S. Naval Research Laboratory.* The spectral dispersion of the third-order susceptibility is calculated for C_{60} films using three- and four-level models and compared with experimental data at infrared wavelengths. **(p. 60)**

LLOYD CENTER BALLROOM

3:45pm–5:15pm
MD • Poster Session/Coffee Break
Mark G. Kuzyk, *Washington State University, Presider*

MD1 • Interference phenomena in nonlinear dielectrics, P. Kaatz, P. Nosbaum, Ch. Bosshard, P. Günter, *Swiss Federal Institute of Technology, Switzerland.* Generalizations are presented of the Maker fringe technique for determining the magnitude and sign of multilayer and multicomponent second and third order nonlinear optical susceptibilities. **(p. 66)**

MD2 • Collision-induced hyper-Rayleigh light scattering in CCl_4, Philip Kaatz, David Shelton, *Univ. Nevada–Las Vegas.* Hyper-Rayleigh scattering from carbon tetrachloride due to molecular collisions is shown to influence measured depolarization ratios and consequently, ratios of hyperpolarizability components. **(p. 70)**

MD3 • Donor/acceptor systems derived from tetraethynylethene, Rik R. Tykwinski, Martin Schreiber, François Diederich, *ETH-Zentrum, Switzerland;* Rolf Spreiter, Christian Bosshard, Peter Günter, *ETH-Hönggerberg, Switzerland;* Corinne Boudon, Jean-Pierre Gisselbrecht, Maurice Gross, *Univ. Louis Pasteur, France.* Trends in the electrical (redox potentials) and optical (UV, fluorescence, $\chi^{(3)}$) properties for a series of donor/acceptor functionalized tetraethynylethene monomers and oligomers as a function of substitution degree and pattern are presented. **(p. 74)**

MD4 • Passive polymer directional couplers: theory and experiment, Lou Bintz, Wei Feng, Jiong Ma, Sihan Lin, Darja Tomic, Alan Mickelson, *Univ. Colorado–Boulder.* We present a Computer Aided Design model of a polymer directional coupler and show some preliminary comparision of the predicted characteristics with characteristics of directional couplers fabricated in a side-chained PMMA/DR1. **(p. 77)**

MD5 • Novel nonlinear optical polymers for second harmonic generation, Naoto Tsustumi, Osamu Matsumoto, Wataru Sakai, Tsyuoshi Kiyotsukuri, *Kyoto Institute of Technology, Japan.* This paper presents a novel nonlinear optical polymer whose dipole moment is aligned transverse to main chain. Poled polymer has large second order nonlinearity of 1.6×10^{-7} esu (67 pm/V) with its long-term thermal stability. **(p. 81)**

MD6 • Growth and characterization of vacuum deposited organic thin film, Kang I. Seo, Isaac Jones, Calvin W. Lowe, *Alabama A & M Univ.* Organic thin films preparation and characterization techniques for optimal growth conditions are demonstrated. Structure of deposited samples is observed with respect to various evaporation temperatures. **(p. 85)**

MD7 • Fabrication of organic thin films by laser ablation deposition for electro-optics devices, Takeo Fujii, Hiroki Shima, Naotaka Matsumoto, Fumihiko Kannari, *Keio Univ., Japan.* Non-polymer organic thin films such as copper-phthalocyanine and 4-dialkylamino-4'-nitrostilbene were fabricated by KrF laser ablation. Crystalline thin films with accurate composition transfer from the target material were deposited when reducing the laser ablation fluence close to the ablation threshold fluence. **(p. 89)**

MD8 • Dependency of side-chain chromophore orientations on Langmuir–Blodgett polymer structures, D. West, D. L. Williams, T. A. King, Z. Ali-Adib, P. Hodge, D. Dunne, *Univ. Manchester, UK.* Some combinations of polymeric materials yield thick Langmuir–Blodgett films of consistent structure. Side-chain composition variations can optimize the chromophore orientation in such films. **(p. 93)**

MD9 • Electro-optic measurement of the electric-field distributions in coplanar-electrode poled polymers, J. W. Wu, *Ewha Womans Univ., Korea.* Electric field distributions inside the coplanar-electrode polymer film are determined by the linear electro-optic measurement. Electrostatic factors obtained by theoretical analysis is compared with the experimental values. **(p. 97)**

MD10 • Electro-refraction and electro-absorption in poled-polymer films, Ned O'Brien, Vince Dominic, *Univ. Dayton;* Steve Caracci, *USAF Wright Laboratories.* We simultaneously measure electro-refraction and electro-absorption in poled-polymer Fabry–Perot cavities by rotating the etalon and observing an asymmetric signal. **(p. 101)**

MD11 • Guest-host crosslinked polyimides for integrated optics, T. C. Kowalczyk, T. Z. Kosc, K. D. Singer, *Case Western Reserve Univ.;* A. J. Beuhler, D. A. Wargowski, *Amoco Chemical Co.;* P. A. Cahill, C. H. Seager, M. B. Meinhardt, *Sandia National Laboratories.* We report on the optical and electrical characterization of aromatic, organic soluble, thermally and photochemically crosslinkable, guest-host polyimides for electro- and integrated optics. **(p. 105)**

MD12 • Photocarrier generation efficiency of pyrromethene-doped polymers, Kwang-Sun Kang, Wade N. Sisk, Faramarz Farahi, M. Yasin Akhtar Raja, *Univ. North Carolina.* The photocarrier generation efficiency of pyromethene-doped-polymers is studied for the first time as a function of composition, temperature, and laser power by transient photocurrent measurements. **(p. 109)**

MD13 • Surface-functionalized nanostructured gold/polymer composites, K. E. Gonsalves, G. Carlson, X. Chen, *Univ. Connecticut;* J. Kumar, *Univ. Massachusetts;* R. Perez, M. Jose-Yacaman, *Univ. Nacional Autonoma de Mexico.* Stable nanometric gold particles were synthesized using a phase-transfer reaction which stabilized the particle surfaces with thiol groups. Composites of these particles in PMMA exhibited third-order nonlinear optical susceptibility. **(p. 113)**

MD14 • Studies of photopolymerization at metal surfaces, Suchitra Subrahmanyan, Fang Chen, Hilary S. Lackritz, *Purdue Univ.* Surface second harmonic generation and other spectroscopies are used to investigate reactions and deposition during and following photopolymerization of vinyl monomers onto metal surfaces for coating applications. **(p. 117)**

MD15 • Detection of molecular chirality using different optical second-harmonic generation techniques, R. Stolle, F. Lohr, G. Marowsky, *Laser-Laboratorium Göttingen e.V., Germany.* We have investigated several samples regarding their molecular chirality using two different nonlinear optical techniques: (a) second-harmonic rotation pattern analysis using linear polarized light and (b) the novel method of second-harmonic circular dichroism. **(p. 121)**

MD16 • Polymer waveguide taps for optical signal distribution, Claire L. Callender, Lucie Robitaille, Julian P. Noad, *Communications Research Centre, Canada.* Coupling of light from polymer ridge waveguides into underlying semiconductor substrates has been investigated. The potential for integration of polymer waveguides with photodetectors in GaAs optoelectronic integrated circuits is discussed. **(p. 125)**

MD17 • Pyroelectric, dielectric and electro-optical investigation of cross-linking in red acid magly, S. Bauer, S. Bauer-Gogonea, S. Yilmaz, C. Dinger, W. Wirges, R. Gerhard-Multhaupt, *Heinrich Hertz Institut für Nachrichtentechnik, Germany;* F. Michelotti, E. Toussaere, R. Levenson, J. Liang, J. Zyss, *France Telecom CNET.* The electrical and optical responses from the chromophores in cross-linking NLO polymers are sensitive to mobility restrictions and thus permit monitoring of the cross-linking process. **(p. 129)**

MD18 • Physical aging after photo-induced or thermally assisted poling for enhancing the stability of polymeric dipole glasses, S. Bauer-Gogonea, S. Bauer, W. Wirges, R. Gerhard-Multhaupt, *Heinrich Hertz Institut für Nachrichtentechnik, Germany;* H. J. Wintle, *Queen's Univ., Canada.* Aging at elevated temperatures under an electric field is shown to improve the thermal stability of poled NLO-polymer electrets as determined with pyroelectric techniques. **(p. 133)**

MD19 • In situ RHEED observation of MBE growth of organic thin films, Tadashi Ishibashi, Shin'ichiro Tamura, Jun'etsu Seto, *Sony Corp., Japan;* Masahiko Hara, Hiroyuki Sasabe, Wolfgang Knoll, *Institute of Physical and Chemical Research (RIKEN), Japan.* Abstract not available. **(p. 137)**

MD20 • Structure and properties of fluoro-aluminum tetraphenylporphyrin (FAITPP) thin films, Yuji Yakura, *Sony Corp., Japan* and *Univ. Washington;* Rebecca Shia, Tomikazu Sasaki, Fumio Ohuchi, *Univ. Washington.* In an attempt to design molecular array with adjustable periodicity in two dimensions, FAITPP was synthesized. The results are discussed about fabricated thin films. **(p. 141)**

MD21 • Optical nonlinearity of co-polymers caused by charge injection, Barak Lavi, Garry Berkovic, *Weizmann Institute of Science, Israel.* Asymmetric charge injection can create second-order optical nonlinearity in polymer-dye systems. Unlike corona poling, nonlinearity caused charge injection effect saturates at low (ca 10%) dye concentration. **(p. 145)**

MD22 • Fabrication of out-of-plane branching mirrors on polymer channel waveguide, Manabu Kagami, *Toyota Central R&D Labs., Inc., Japan.* A method of simultaneously fabricating out-of-plane branching mirrors and optical channel waveguides from a polymer film has been developed by improved dry etching process. **(p. 148)**

MD23 • Third-order nonlinear optical effects in organic nickel complexes and triarylmethyl cations, Daniel R. Greve, Thomas Bjornholm, *Univ. Copenhagen, Denmark;* Tommy Geisler, *Aalborg Univ., Denmark;* Jan C. Petersen, *Danish Institute of Fundamental Metrology, Denmark.* Third-harmonic generation and semi-empirical calculations show that charge transfer transitions in triarylmethyl cations are important for obtaining high values of the 2nd order hyperpolarizability. **(p. 152)**

MD24 • Design and characterization of phthalocyanine thin film materials, Steven R. Flom, James S. Shirk, Richard G. S. Pong, F. J. Bartoli, Arthur W. Snow, *U.S. Naval Research Laboratory;* Young H. Chang, Warren T. Ford, *Oklahoma State Univ.* The design and nonlinear optical characterization of phthalocyanines that form neat thin films of good optical quality and simultaneously maintain desirable NLO properties is reported. **(p. 156)**

MD25 • Optically aligned liquid crystal cells as diffractive optical elements, T. Kosa, P. Palffy-Muhoray, *Kent State Univ.* Diffractive liquid crystal elements, based on the principle that orthogonal polarizations do not interfere, are proposed and studied. Nematic orientation is controlled via optical buffing. **(p. 160)**

MD26 • Nonlinear optical anisotropy of highly oriented poly (p-phenylene benzobisthiazole) Langmuir–Blodgett films, Liming Wang, Hiroyuki Sasabe, Wada Tatsuo, *The Institute of Physical and Chemical Research (RIKEN), Japan;* Tomoyuki Yuba, Masaaki Kakimoto, Yoshio Imai, *Tokyo Institute of Technology, Japan.* The in-plane third-order nonlinear optical anisotropy properties of the PBT LB films fabricated through precursor route were studies by optical third-harmonic generation measurement. **(p. 162)**

MD27 • Investigation of the stability of electro-optical dyes, Lixia Zhang, Priya Calamegham, Carl Dirk, *Univ. Texas–El Paso;* Susan Ermer, *Lockheed Research and Development Division;* R. J. Twieg, *IBM Almaden Research Center.* We are reporting the thermal stability of some organo-optic materials and the quantitative analysis of the structure-property relationship. **(p. 166)**

MD28 • Nonlinear optical properties of self-assembled main-chain polymer films, W. N. Herman, J. A. Cline, J. M. Hoover, A. Chafin, G. A. Lindsay, *U.S. Navy, NAWCWD;* K. J. Wynne, *U.S. Office of Naval Research.* We report on the structure and nonlinear optical properties of a 24-layer ABAB type Langmuir–Blodgett film fabricated from two main-chain polymers, both of which are optically nonlinear. **(p. 170)**

MD29 • Defeating the nonlinearity/transparency tradeoff, Christopher R. Moylan, I.-Heng McComb, Robert J. Twieg, *IBM Almaden Research Center;* Susan Ermer, Steven M. Lovejoy, Doris S. Leung, *Lockheed Research and Development.* An apparently fundamental tradeoff between chromophore nonlinearity and transparency exists. Two different classes of compounds are shown to evade this tradeoff; the results are explained. **(p. 174)**

MD30 • Efficiency and time-dependence of luminescence in a high electron affinity conjugated polymer, I. D. W. Samuel, R. H. Friend, *Cavendish Laboratory, UK;* G. Rumbles, C. J. Collison, B. Crystall, *Imperial College, UK;* S. C. Moratti, A. B. Holmes, *University Chemical Laboratory, UK.* Luminescence efficiency and time-dependence measurements of a high electron affinity derivative of poly(*p*-phenylene vinylene) show important differences from those of the unsubstituted material. **(p. 178)**

MD31 • Anisotropic self-alignment of supramolecular amylose inclusion of chromophores for second-order nonlinear optical materials, Oh-Kil Kim, Ling-Siu Choi, *U.S. Naval Research Laboratory;* He-Yi Zang, Xue-Hua He, Yan-Hua Shih, *Univ. Maryland Baltimore County.* A novel supramolecular inclusion complex of nonlinear chromophores with rigid-rod helical amylose was developed. Its thin films demonstrated a long-range anisotropic self-alignment and exceptional nonlinear stability. **(p. 180)**

MD32 • Structural and solvatochromic studies of a series of chromophoric TCNQ derivatives with large second order nonlinearities. Marek Szablewski, Philip Thomas, Graham Cross, Jacqueline Cole, *Univ. Durham, UK.* Solvatochromism and structural studies are used to demonstrate the features in common of a range of highly nonlinear amino-TCNQ chromophores. **(p. 184)**

MD33 • Photobleaching in side-chain NLO polymers, Manfred Eich, Hanno Beisinghoff, Hubertus Feix, W. Görtz, Jan Vydra, *German Telekom Research Center, Germany.* Abstract not available. **(p. 188)**

MD34 • Enhanced photo-oxidative stability and nonlinear optical response of a dialkoxy-substituted poly-phenylenevinylene through C_{60} addition, H. W. Sarkas, S. R. Flom, F. J. Bartoli, Z. H. Kafafi, *U.S. Naval Research Laboratory.* The addition of C_{60} to the nonlinear optical polymer, poly-[2-methoxy, 5-(2'-ethylhexyloxy-p-phenylenevinylene] was found to greatly enhance its stability against photo-oxidation. Composites of this polymer and C_{60} were prepared by spin-coating and were spectroscopically characterized. The nonlinear optical properties of these composite materials were studied at 590.5 nm, near the absorption tail of the π–π^* transition of the polymer. **(p. 189)**

MD35 • Preparation, optical spectroscopy, and fluorescence of molecular organic composites for light-emitting diodes, Harry W. Sarkas, Charles D. Merritt, Zakya H. Kafafi, *U.S. Naval Research Laboratory.* Nanostructures of highly fluorescent organic molecules dispersed in a dual function electroluminescent metal chelate host were prepared by vacuum deposition and were spectroscopically characterized. Quantum yields based on the photoluminescence spectra of the composite films are significantly enhanced relative to those of the guest and host in the solid state. Preliminary results on the function of an organic light-emitting diode based on these nanostructures are reported. **(p. 193)**

MD36 • Two-beam coupling in a photorefractive polymer waveguide, Dan Kokron, Stephen M. Evanko, L. Michael Hayden, *Univ. Maryland Baltimore County.* We report the launching and amplification of guided waves in a polymeric photorefractive slab waveguide by optically pumping the surface of the waveguide. The output power and rise time versus pump incidence angle and power are determined. **(p. 197)**

MD37 • Growth of thin single crystalline films of m-nitroaniline and their nonlinear optical characterization, A. Leyderman, M. Espinosa, *Univ. Puerto Rico–Mayaguez.* We report crystallization features of thin single crystalline films of *m*-nitroaniline grown between two plates with thickness ranging from 0.5 to 20 μ. The intensity of the second harmonic generated by organic film versus incident angle of the Nd:YAG 1.064 μm beam has been measured. **(p. 201)**

MD38 • Recent progress in polymer electroluminescence: electron transport polymers and microcavity devices, D. O'Brien, M. S. Weaver, M. Pavier, A. Bleyer, D. G. Lidzey, S. J. Martin, A. Tajbakhah, M. A. Pate, T. A. Fisher, T. Richardson, T. M. Searle, M. S. Skolnick, D. D. C. Bradley, *Univ. Sheffield, UK;* Sun Meng, *Fudan Univ., China.* We present results concerning the design, synthesis and characterization of new electron transport polymers and the fabrication and operation of polymer microcavity LEDs. **(p. 204)**

MD39 • Chi-electric relaxation: frequency domain chromophore dynamics in nonlinear optical polymers, J. A. Cline, W. N. Herman, *U.S. Navy.* Using second harmonic generation as a probe, we report measurements of chromophore mobility as a function of the frequency of an applied electric field at various temperatures. Characteristic curves are similar to dielectric relaxation data. **(p. 206)**

MD40 • Preparation of high-quality thin films: SHG properties of Y-type LB films prepared by using moving-wall type LB deposition system, M. Talukder, G. Lindsay, *U.S. Naval Air Warfare Center;* S. Fujita, T. Watanabe, S. Miyata, *Tokyo Univ., Japan.* Y-type LB films were prepared from a syndioregic polymer by using a moving-wall type trough. Strong SHG was observed for y-type films. It is normally unusual for y-type films to give SHG. These results suggest that even y-type LB films possess the noncentrosymmetric structures without poling. **(p. 210)**

LLOYD CENTER BALLROOM

6:30pm–8:30pm
Conference Reception

HOLLADAY ROOM

8:00am–9:30am
TuA • Symposium on Displays Base on Organic Thin Films I (Joint with OSA Annual Meeting)
Peter Palffy-Muhoray, *Kent State University, Presider*

8:00am (Invited)
TuA1 • Electroluminescence from conjugated polymers, Richard Friend, *Cavendish Laboratory, UK.* Conjugated polymers can be processed as thin films, and can be used as the emissive or charge-transport layers in thin-film electroluminescent diodes. I will discuss the present understanding of the operation these devices, including the improvement to the efficiency that can be produced by the use of heterojunction devices. **(p. 216)**

8:30am (Invited)
TuA2 • Current conduction and electroluminescence mechanisms in molecular organic light emitting devices, S. R. Forrest, P. E. Burrows, Z. Shen, V. Bulovic, D. M. McCarty, M. E. Thompson, *Princeton Univ.* We determine the mechanisms of current conduction and electroluminescent color and intensity in molecular organic light emitting devices. **(p. 217)**

9:00am
TuA3 • Double heterostructure and MQW organic light-emitting diodes for flat panel displays, Dirk Ammermann, Achim Böhler, Christoph Rompf, Wolfgang Kowalsky, *Technische Univ. Braunschweig, Germany.* Optimized double heterostructure organic light-emitting diodes show a maximum optical output power of 0.3 mW and an internal quantum efficiency of 5.5%. The emission wavelength can be detuned up to 140 meV by multiple quantum well structures. **(p. 221)**

9:15am
TuA4 • Highly scattered optical-transmission polymer for the liquid crystal display backlight, Akihiro Horibe, Megumi Izuhara, Eisuke Nihei, Yasuhiro Koike, *Keio Univ., Japan.* The new optical-transmission polymer was applied to the backlight for the liquid crystal display that was simpler and brighter than in a conventional system. **(p. 225)**

LLOYD CENTER BALLROOM

9:30am–9:45am
Coffee Break

HOLLADAY ROOM

9:45am–11:15am
TuC • Symposium on Displays Based on Organic Thin Films II (Joint with OSA Annual Meeting)
Stephen R. Forrest, *Princeton University, Presider*

9:45am (Invited)
TuC1 • Optical alignment of liquid crystal displays and devices via polarized light, Wayne M. Gibbons, Paul J. Shannon, Shao-Tang Sun, *Alliant Techsystems.* In this presentation, we discuss the use of optical alignment as a non-contact method to align liquid crystal displays. Issues such as the pre-tilt angle and the dielectric properties of the optically controlled alignment polymer will be addressed. **(p. 230)**

10:15am (Invited)
TuC2 • TN and GH-LCDs fabricated by non-rubbing techniques and an overview of LCDs in Japan, S. Kobayashi, Y. Iimura, T. Saitoh, H. Suzuki, *Tokyo Univ. A&T, Japan;* T. Hashimoto, T. Sugiyama, K. Katoh, *Stanley Electric Co., Japan.* Amorphous TN(twisted by 90°) and amorphous highly twisted chiral nematic (N*)(twisted by 300°) are utilized for fabricating TN and GH-LCDs, respectively, and furthermore, photopolymer films are utilized for fabricating TN-LCD and hybrid aligned N-LCD. These NLC alignment techniques are non-rubbing techniques, and they make it possible to overcome the disadvantages of current rubbing technique. An overview of LCDs in Japan is also given. **(p. 233)**

10:45am
TuC3 • Electroluminescence from organometallic thin films, R. A. Campos, I. Kovalev, Y. Guo, T. Skotheim, *Moltech Corp.* We report current-voltage and luminance-voltage characteristics for electroluminescent cells containing emitter materials based on lanthanide complexes and short-chain polymers. **(p. 236)**

11:00am
TuC4 • Accelerated degradation studies of MEH-PPV, H. B. Radousky, A. D. Madden, K. Pakbaz, T. W. Hagler, H. W. H. Lee, *Lawrence Livermore National Laboratory.* The degradation rate in MEH-PPV films was studied using photoluminescence, and is strongly influenced by thickness, oxygen exposure during preparation, and the measuring environment. **(p. 240)**

OREGON CONVENTION CENTER BALLROOM 203/204

11:30am (OSA Annual Meeting Plenary)
TuB3 • The creation of new information paradigms through flat panel displays, Malcolm Thompson, *Xerox PARC, and U.S. Display Consortium.* Abstract not available.

12:30pm–1:30pm
Lunch (on your own)

HOLLADAY ROOM

1:30pm–3:30pm
TuD • Chromophores I
Charles Y.-C. Lee, *U.S. Air Force Office of Scientific Research, Presider*

1:30pm (Invited)
TuD1 • Experimental and theoretical studies of nonlinear optical chromophores, M. Ahlheim, M. Staehelin, B. Zysset, *Sandoz Huningue S. A., France;* J.-L. Brédas, C. Dehu, A. Fort, F. Meyers, *Univ. Mons-Hainaut, Belgium;* M. Barzoukas, C. Runser, *IPCMS, France;* P. V. Bedworth, Z. Hu, S. R. Marder, J. W. Perry, *California Institute of Technology;* Y. Cai, A. K.-Y. Jen, *ROI Technologies;* M. Blanchard-Desce, *Ecole Normale Supérieure, France.* We will describe how the nonlinear optical properties of dyes vary as a function of ground state polarization and how dyes with reasonable thermal stability and large second-order optical nonlinearities can be synthesized and characterized. **(p. 244)**

2:00pm (Invited)
TuD2 • New polymers for second-order nonlinear optics, G. Lindsay, J. Stenger-Smith, A. Chafin, R. Hollins, L. Merwin, R. Yee, R. Nissan, M. Nadler, R. Henry, W. Herman, *U.S. Navy;* K. Wynne, *U.S. Office of Naval Research;* P. Ashley, *U.S. Army Missile Command;* L. Hayden, *Univ. Maryland Baltimore County.* Progress on mainchain syndioregic polymers for $\chi^{(2)}$ applications is reported. An electro-optic coefficient, r_{33} of 8.5 pm/V @ 1.3 microns and loss of <1 dB/cm was measured in a Mach-Zehnder interferometer waveguide fabricated by parallel plate electrode poling and photobleaching. This EO film has been stable at ambient room temperature for many months, and the long term thermal stability is estimated to be ≥125°C if protected from UV radiation and air. Preliminary results on the preparation of a series of related polymers designed for low temperature fabrication of $\chi^{(2)}$ thin films will be reported. **(p. 247)**

2:30pm (Invited)
TuD3 • High performance chromophores and polymers for E–O applications, Alex K.-Y. Jen, Varanasi Pushkara Rao, Tian-An Chen, Yongming Cai, Kevin J. Drost, Yue-Jin Liu, J. T. Kenney, Robert M. Mininni, *ROI Technologies;* Peter V. Bedworth, Seth R. Marder, *California Institute of Technology;* Larry Dalton, *Univ. Southern California.* We will describe the structure/property relationship of several classes of thermally and chemically stable chromophores. The incorporation of these chromophores in polyimides and polyquinolines produces very efficient E–O materials. **(p. 251)**

3:00pm
TuD4 • Polyurethane-based polymers with improved stability of electrooptic properties, J. Zieba, C.-K. Park, B. Swedek, P. N. Prasad, *SUNY–Buffalo;* Kwang-Sup Lee, *Han Nam Univ., Korea;* Ki-Jeong Moon, Hong-Ku Shim, *Korea Advanced Institute of Science and Technology, Korea.* Two types of polyurethane based second order NLO polymers are presented from the point of view of their nonlinear parameters and their temporal and thermal stabilities. **(p. 255)**

3:15pm
TuD5 • Design and synthesis of soluble thermally stable nonlinear optical chromophores based on the dicyanomethylenepyran moiety, Steven M. Lovejoy, Susan Ermer, Doris S. Leung, *Lockheed Missiles and Space Company, Inc.;* Carl W. Dirk, Priya Kalamegham, Lixia Zhang, *Univ. Texas–El Paso;* Christopher R. Moylan, *IBM Almaden Research Center.* A series of soluble thermally stable nonlinear optical chromophores based on the dicyanomethylenepyran moiety have been developed. Their synthesis, physical properties, and EFISH measurement values are discussed. **(p. 259)**

LLOYD CENTER BALLROOM

3:30pm–4:00pm
Coffee Break

HOLLADAY ROOM

4:00pm–6:00pm
TuE • Chromophores II
Susan P. Ermer, *Lockheed Research and Development Division, Presider*

4:00pm (Invited)
TuE1 • Permanent all optical poling of an octupolar dye, Joseph Zyss, Ifor Samuel, *France Télécom-CNET, France;* Céline Fiorini, Fabrice Charra, Jean-Michel Nunzi, *Centre d'Etudes de Saclay, France.* Permanent optical poling of an octupolar dye has been achieved by interference between one and two-photon absorption in a guest-host system leading to a $\chi^{(2)}$ of 1.2 pm/V. **(p. 264)**

4:30pm (Invited)
TuE2 • Potentials of ionic organic chromophores for second-order nonlinear optical thin film materials, H. Nakanishi, X.-M. Duan, S. Okada, H. Oikawa, M. Matsuda, *Tohoku Univ., Japan.* Ionic compounds like stilbazolium cation, *p*-toluenesulfonate anion and their related ions are potential chromophores having shorter cut-off wavelength and larger β than so-far-known neutral ones. **(p. 268)**

5:00pm (Invited)
TuE3 • Ferroelectric liquid crystals for second-order nonlinear optics, David M. Walba, Peter L. Cobben, Daniel J. Dyer, Uwe Müller, Renfan Shao, Noel A. Clark, *Univ. Colorado–Boulder.* Ferroelectric liquid crystals (FLCs) have a polar supermolecular structure that suggests they should be useful in second-order nonlinear optics applications. Useful NLO FLCs however, have not yet been realized. Here we report on a new FLC structural class wherein the disperse red 1 chromophore is oriented along the polar axis. These new FLCs should show useful NLO properties. **(p. 272)**

5:30pm
TuE4 • Self-assembly approaches to organic second-order nonlinear optical thin film materials, George K. Wong, Weiping Lin, Haitian Zhou, David Hahn, Paul M. Lundquist, Wenbin Lin, Stephen B. Roscoe, Shlomo Yitzchaik, Tobin J. Marks, *Northwestern Univ.* We have used new topotactic approaches to prepare self-assembled stilbazolium superlattices which show very high structural regularity and very large second-order nonlinearity. **(p. 275)**

5:45pm
TuE5 • Photochemical stability and performance of second-order nonlinear optical chromophores and polymers, R. J. Twieg, V. Y. Lee, R. D. Miller, C. R. Moylan, W. Volksen, *IBM Almaden Research Center;* A. Knoesen, R. A. Hill, D. R. Yankelevich, *UC–Davis.* Studies indicate a remarkable and unanticipated influence of the identity of the polymer on the extent of optical damage of poled polymer films. **(p. 279)**

HOLLADAY ROOM

8:00am–10:00am
WA • Active Devices I
Tony Ticknor, *Akzo Nobel Electronic Products, Presider*

8:00am (Invited)
WA1 • Electro-optic polymer waveguide devices–materials, fabrication, and applications, William H. Steier, *Univ. Southern California.* Some of the important applications for electro-optic polymer waveguide devices will be discussed along with examples of progress and fabrication techniques in each area. **(p. 284)**

8:30am (Invited)
WA2 • Progress toward practical polymer electro-optic devices, Susan Ermer, William W. Anderson, Timothy E. Van Eck, Dexter G. Girton, James A. Marley, Alex Harwit, Steven M. Lovejoy, Doris S. Leung, *Lockheed Research and Development Division.* High speed analog and digital switching has been demonstrated in a polymer Mach–Zehnder modulator with a voltage-length product of 13 V-cm. Materials and process optimization and anisotropic V-groove etching for fiber attachment will also be discussed. **(p. 285)**

9:00am (Invited)
WA3 • Incorporation of thermally stable nonlinear optical polymers into electro-optic devices, D. M. Burland, R. G. Devoe, M. C. Jurich, V. Y. Lee, R. D. Miller, C. R. Moylan, J. I. Thackara, R. J. Twieg, T. Verbiest, W. Volksen, *IBM Almaden Research Center.* High thermal stability and substantial optical nonlinearity have been achieved in a class of electro-optic polyimides. Mach-Zehnder 2 × 2 switches have been fabricated from these materials. **(p. 289)**

9:30am (Invited)
WA4 • 60-GHz electro-optic modulation from polymer waveguide phase modulators, Harold R. Fetterman, Wenshen Wang, Datong Chen, *UC–Los Angeles;* Yongqiang Shi, James H. Bechtel, *TACAN Corp.;* Srinath Kalluri, William H. Steier, Larry R. Dalton, *Univ. Southern California.* 60-GHz electro-optic modulation from polymer phase modulators was demonstrated using an optical heterodyne technique. The devices exhibited good temporal stability and optical power handling capability. **(p. 293)**

LLOYD CENTER BALLROOM

10:00am–10:30am
Coffee Break

HOLLADAY ROOM

10:30am–12:30pm
WB • Active Devices II
William H. Steier, *University of Southern California, Presider*

10:30am
WB1 • Integration of NLO polymer waveguides with indium gallium arsenide p-i-n photodiodes, Jeffrey S. Cites, *Aegis Research Corp.;* Paul R. Ashley, *U.S. Army Missile Command;* Richard P. Leavitt, *U.S. Army Research Laboratory.* Nonlinear optical (NLO) polymer waveguides have been integrated with InGaAs p-i-n detectors at 1.3 μm, exhibiting coupling efficiencies over 98% and system responsivities greater than 0.2 A/W. **(p. 298)**

10:45am
WB2 • Arrays of flip-chip mounted, surface-illuminated, crystalline-organic optoelectronic modulators on glass substrates, D. Yap, *Hughes Research Laboratories;* P. E. Burrows, S. R. Forrest, *Princeton Univ.* Conventional III–V device processing techniques have been used for the first time to fabricate, with micron-level tolerances, arrays of crystalline 3,4,9,10-perylenetetracarboxylic dianhydride optoelectronic modulators. **(p. 302)**

11:00am
WB3 • Light-induced spatial modulation of second-order optical nonlinearity via a photoconducting layer, Rami Cohen, Garry Berkovic, *Weizmann Institute of Science, Israel.* Second-order optical nonlinearity in polymer-dye systems can be spatially modulated by light using a bilayer structure comprising the nonlinear optical polymer and an organic photoconductor. **(p. 306)**

11:15am
WB4 • Miniature integrated optical wavelength analyzer chip, R. E. Kunz, J. Dübendorfer, *Paul Scherrer Institute, Switzerland.* A novel integrated optical chip suitable for realizing compact miniature wavelength analyzers is presented. Monitoring the mode spectrum of a laser diode is experimentally demonstrated. **(p. 309)**

11:30am
WB5 • Photomechanical multistability and logic in a polymer optical fiber, D. J. Welker, M. G. Kuzyk, *Washington State Univ.* We have demonstrated both optical and mechanical multistability in a mesoscale polymer optical fiber waveguide Fabry–Perot interferometer of ≈1-cm length and 100-μm diameter. **(p. 313)**

11:45am
WB6 • Vertical integration of polymer electro-optic devices on electronic circuits, Srinath Kalluri, Antao Chen, Mehrdad Ziari, William H. Steier, Zhiyong Liang, Larry R. Dalton, *Univ. Southern California;* Datong Chen, Bahram Jalali, Harold R. Fetterman, *UC–Los Angeles.* Polymer electro-optic phase modulators were fabricated on non-planar Si circuitry. Results on the protection of MESFET devices during the poling and fabrication cycles of a modulator are also presented. **(p. 317)**

12:00m
WB7 • C_{60}:electron donor nanocomposites and multilayer structures for nonlinear optics, Harry W. Sarkas, Zakya H. Kafafi, *U.S. Naval Research Laboratory.* Organic nanocomposites and multilayer structures of C_{60} with various electron donors have been prepared by vacuum deposition and spectroscopically characterized. The appearance of new absorption bands in the optical spectra of the nanocomposite films reveals the formation of neutral charge transfer complexes where C_{60} acts as the electron acceptor. The optical spectra of the organic multilayer structures reveal analogous effects at the layer interfaces. Significant enhancements in the nonlinear optical response have been observed for the composites and proposed for the multilayer structures. **(p. 321)**

12:15pm
WB8 • Photo excitation stability and bias voltage stability of electro-optic polymer modulators for broadband analog transmission systems, Yongqiang Shi, David J. Olson, James H. Bechtel, *TACAN Corp.;* Srinath Kalluri, William H. Steier, *Univ. Southern California;* Wenshen Wang, Datong Chen, Harold R. Fetterman, *UC–Los Angeles.* Optical power and quadrature bias voltage stability of electro-optic polymer modulators were tested for broadband analog signal transmission system. Experimental results are presented. **(p. 325)**

12:30pm–1:30pm
Lunch (on your own)

HOLLADAY ROOM

1:30pm–3:30pm
WGG • Symposium on Data Storage I (Joint with OSA Annual Meeting)
George I. Stegeman, *University of Central Florida, Presider*

1:30pm (Invited)
WGG1 • Photorefractive polymers for holographic optical storage, W. E. Moerner, C. Poga, Y. Jia, R. J. Twieg, *IBM Almaden Research Center.* Holographic optical storage in photorefractive polymers requires many performance characteristics to be simultaneously present in the same material; recent proofs-of-principle and current problems are described. **(p. 330)**

2:00pm (Invited)
WGG2 • High-efficiency photorefractive polymers, B. Kippelen, K. Meerholz, B. L. Volodin, Sandalphon, N. Peyghambarian, *Univ. Arizona.* The performance of recently developed highly efficient photorefractive polymers based on a plasticized poly(N-vinylcarbazole) host is investigated and the origin of the high refractive index changes is identified. **(p. 334)**

2:30pm (Invited)
WGG3 • Photo-induced birefringence, holographic surface gratings and photorefractive properties of azo polymers, Mei Sing Ho, Almeria Natansohn, *Queen's Univ., Canada;* Chris Barrett, Paul Rochon, *Royal Military College, Canada.* This is a review of the most recent discoveries in azo polymer research. Photo-induced birefringence, holographic surface gratings inscription and also photorefractive properties are included. The possible implications for all-azo optical devices are discussed. **(p. 338)**

3:00pm
WGG4 • High-efficiency photorefractive polymer with immunity to crystallization, C. Poga, R. J. Twieg, W. E. Moerner, *IBM Almaden Research Center.* We have fabricated a new high-performance photorefractive polymer, PVK:FDEAMNST:C_{60}, which is immune to crystallization because the chromophore is liquid at room temperature. Measurements of the photorefractive performance are presented. **(p. 342)**

3:15pm
WGG5 • Two-photon absorption based optical recording in organic planar waveguide, Ram Piyaket, Ilkan Cokgor, Frederick B. McCormick, Sadik Esener, *UC–San Diego;* Alexander S. Dvornikov, Peter M. Rentzepis, *UC–Irvine.* We discuss the possibility of storing information in a planar waveguide made from spirobenzopyran doped PMMA. The limitations of the approach are studied using relevant experimental data. **(p. 346)**

LLOYD CENTER BALLROOM

3:30pm–4:00pm
Coffee Break

HOLLADAY ROOM

4:00pm–5:45pm
WTT • Symposium on Data Storage II (Joint with OSA Annual Meeting)
W. E. Moerner, *IBM Almaden Research Center, Presider*

4:00pm (Invited)
WTT1 • Liquid crystalline polymer based optical data storage, Nico Maaskant, *Akzo Nobel Electronic Products BV, The Netherlands.* After a short overview of the optical data storage market and its trends, some examples of liquid crystalline polymer based optical data storage systems will be discussed. **(p. 352)**

4:30pm (Invited)
WTT2 • Photochromic diarylethenes for erasable optical memory, Masahiro Irie, *Kyushu Univ., Japan.* Recent advances in photochromic memory media for photo-mode erasable optical recording are reported. Photochromic media having fatigue resistant character and readout stability have been developed. **(p. 354)**

5:00pm
WTT3 • Photochromic azo-polymer structures for photonic applications, Z. Sekkat, J. Wood, M. Büchel, E. F. Aust, *Max-Planck-Institut für Polymerforschung, Germany;* Y. Geerts, *Massachusetts Institute of Technology;* R. D. Miller, *IBM Almaden Research Center;* W. Knoll, *Max-Planck-Institut, Germany,* and *The Institute of Physical and Chemical Research (RIKEN), Japan.* We report on photoisomerization induced linear and nonlinear-optical properties in photochromic films consisting of ultrathin silane layers, Langmuir–Blodgett–Khun structures, and bulk polymers. **(p. 357)**

5:15pm
WTT4 • Azobenzene side-chain polymer films for optically induced holographic surface relief gratings, D. Y. Kim, Lian Li, J. Kumar, S. K. Tripathy, *Univ. Massachusetts.* Polarized laser-induced erasable holographic surface relief gratings with large amplitude were directly created on azobenzene side-chain polymer films without any subsequent processing steps. **(p. 361)**

5:30pm
WTT5 • Photo-induced refractive index changes in PMMA films including a photochromic Fulgide, Shin'ya Morino, Takeo Yamazaki, Shinjiro Machida, Takashi Yamashita, Kazuyuki Horie, *Univ. Tokyo, Japan.* Photo-induced refractive index changes were measured for PMMA films including a Fulgide. The minimum switching energy of optical switching devices using photochromic reactions was estimated. **(p. 365)**

HOLLADAY ROOM

8:00am–10:00am

ThA • Characterization

George I. Stegeman, *University of Central Florida, Presider*

8:00am (Invited)

ThA1 • Spatial and temporal orientational correlations between nonlinear optical chromophores probed by femtosecond hyper-Rayleigh scattering, Koen Clays, Marvin Wu, André Persoons, *Univ. Leuven, Belgium.* Spatial and temporal orientational correlation in a thin film or a solution of nonlinear optical chromophores has been probed by hyper-Rayleigh scattering using femtosecond pulses. **(p. 370)**

8:30am (Invited)

ThA2 • Measurements of first hyperpolarizabilities β: anomalous hyper-Rayleigh scattering results, Marinus C. Flipse, Roel de Jonge, *Akzo Nobel Central Research, The Netherlands;* Albert W. Marsman, Cornelis A. van Walree, Leonardus W. Jenneskens, *Utrecht Univ., The Netherlands.* First hyperpolarizabilities of well-known chromophores were determined with HRS. Anomalous results were obtained due to fluorescence at the second-harmonic induced by two-photon absorption. **(p. 374)**

9:00am

ThA3 • Evanescent wave surface enhanced Raman scattering from organic molecules bonded to "optical chemical benches," Wenbo Xu, Mark P. Andrews, *McGill Univ., Canada.* Guided evanescent wave surface enhanced Raman spectroscopy is used to probe the vibrational structure of submonolayer coverages of organosiloxanes grafted to planar waveguide surfaces. **(p. 378)**

9:15am

ThA4 • Two-slit electro-optic coefficient measurement technique and efficient in-plane poling of polymer thin films, Sean Garner, Srinath Kalluri, Mehrdad Ziari, William H. Steier, Zhiyong Liang, Larry R. Dalton, *Univ. Southern California;* Yongqiang Shi, *TACAN Corp.* A novel and simple electro-optic coefficient measurement technique for in-plane poled polymer thin films is presented. Efficient in-plane poling is demonstrated. **(p. 382)**

9:30am

ThA5 • Optical response of a chiral molecule and circular dichroism in second-harmonic generation, Jeffery J. Maki, Martti Kauranen, Thierry Verbiest, André Persoons, *Univ. Leuven, Belgium.* We calculate the circular dichroism in second-harmonic generation from a chiral surface using a simple classical model of an electron bound to a helix. **(p. 386)**

9:45am

ThA6 • Linearly and circularly polarized probes of second-order optical activity of chiral surfaces, Thierry Verbiest, Martti Kauranen, Jeffery J. Maki, André Persoons, *Univ. Leuven, Belgium;* M. N. Teerenstra, A. J. Schouten, *Univ. Groningen, The Netherlands;* R. J. M. Nolte, *Univ. Nijmegen, The Netherlands.* Surface chirality can be studied by second-harmonic generation using fundamental light with circular and appropriately chosen linear polarizations. **(p. 390)**

LLOYD CENTER BALLROOM

10:00am–10:30am

Coffee Break

HOLLADAY ROOM

10:30am–12:15pm

ThB • SHG Devices

Gerd Marowsky, *Laser-Laboratorium Göttingen, Germany, Presider*

10:30am

ThB1 • Effect of poling-induced polymer film deformation on second-harmonic generation in periodically poled polymer channel waveguides, M Jäger, G. I. Stegeman, *Univ. Central Florida;* W. Brinker, S. Yilmaz, S. Bauer, *Heinrich-Hertz-Institut für Nachrichtentechnik Berlin, Germany;* W. H. G. Horsthuis, G. R. Möhlmann, *Akzo Nobel Electronic Products, The Netherlands.* Second harmonic generation has been demonstrated in periodically poled DANS channel waveguides with phase-matching over 2 mm. Electrode penetration on poling has also been observed. **(p. 396)**

10:45am

ThB2 • Enhanced Cerenkov-radiative SHG with uv-induced nonlinear optical susceptibility-corrugation, Heihachi Sato, Hiroaki Matsuno, *National Defense Academy, Japan;* Iwao Seo, *Mitsubishi Chemistry Co. Ltd., Japan.* Irradiating ArF 193-nm laser beam onto uniformly poled VDCN/VAc copolymer with covering by fine-structure masks to induce nonlinear optical corrugation, the Cerenkov-radiative SHG power has been extremely enhanced. **(p. 400)**

11:00am

ThB3 • Frequency doubling in a poled polymer waveguide using anomalous dispersion phase-matching, T. C. Kowalczyk, K. D. Singer, *Case Western Reserve Univ.;* P. A. Cahill, *Sandia National Laboratories.* We demonstrate anomalous dispersion phase-matched second harmonic generation in a poled polymer waveguide. Phase-matching is achieved between the lowest order TM modes at a fundamental wavelength of 815 nm. **(p. 404)**

11:15am

ThB4 • Quasi-phase-matched sum frequency generation in active-passive hybrid waveguides, S. Lehmann, G. Marowsky, *Laser-Laboratorium Göttingen e.V., Germany.* Sum frequency generation in passive channel waveguides covered with a nonlinearly active poled polymer film has been demonstrated. The nonlinearity of the polymer has been modulated by the photobleaching technique to achieve quasi-phasematching. **(p. 408)**

11:30am

ThB5 • Quasi-phase-matched second-harmonic generation in an electro-optic polymer waveguide, Satoru Tomaru, Toshio Watanabe, Makoto Hikita, Itaru Yokohama, Michiyuki Amano, Yoshito Shuto, Hiroki Itoh, Masaki Asobe, *NTT Opto-electronics Laboratories, Japan.* Quasi-phase-matched second-harmonic generation from an electro-optic polymer waveguide has been realized with an efficiency of about 10^{-3}/W around a 1.55-μm fundamental wavelength. **(p. 412)**

11:45am

ThB6 • Bulk-type phase-matched SHG devices of poled polymer, X. T. Tao, T. Watanabe, H. Ukuda, S. Miyata, *Tokyo Univ. Agriculture and Technology, Japan.* Bulk phase-matched second-harmonic generation has been realized from a drawn and poled polymer by prism and end-fire coupling at 1.064 μm. **(p. 416)**

12:00m
ThB7 • Thin films of organic salts with large optical nonlinearities by organic vapor phase deposition, P. E. Burrows, S. R. Forrest, T. Buma, L. S. Sapochak, J. Schwartz, *Princeton Univ.;* V. S. Ban, J. L. Forrest, *PD-LD Inc.* We describe a novel technique, organic vapor phase deposition, for the growth of thin films of optically nonlinear organic salts with >95% purity on various substrates. **(p. 420)**

12:15pm–1:30pm
Lunch (on your own)

HOLLADAY ROOM

1:30pm–2:15pm
ThC • Electroluminescent Polymers
Kenneth D. Singer, *Case Western Reserve University, Presider*

1:30pm (Invited)
ThC1 • High efficiency white and colored organic electroluminescence, R. H. Jordan, A. Dodagbalapur, M. Strukelj, L. J. Rothberg, R. E. Slusher, T. M. Miller, *AT&T Bell Laboratories.* White light organic electroluminescence is described, which employs a blue-emitting species as a layer sandwiched between the hole transporter bis(triphenyl)diamine and the electron transporter tris(8-hydroxyquinoline)aluminum. Improved electroluminescent efficiency is obtained by using microcavity enhanced surface-emission in a structure which uses the hole transporter and the (organic dye doped) electron transporter. **(p. 426)**

2:00pm
ThC2 • Polymer light-emitting electrochemical cells, Qibing Pei, Gang Yu, Chi Zhang, Yang Yang, Alan J. Heeger, *UNIAX Corp.* Light-emitting electrochemical cells are reported based on a *p-n* junction diode created *in-situ* through simultaneous *p*-type and *n*-type doping on opposite sides of a thin conjugated polymer film. **(p. 429)**

HOLLADAY ROOM

2:15pm–3:45pm
ThD • Organics Towards Devices
Kenneth D. Singer, *Case Western Reserve University, Presider*

2:15pm (Invited)
ThD1 • Effects of drawing on second-order nonlinear optical coefficients of poled polymers, T. Watanabe, X. T. Tao, M. Nakayama, J. Kim, T. Deguchi, S. Miyata, *Tokyo Univ., Japan.* The effects of drawing on second order nonlinear optical coefficients of poled polymers were examined using Λ type main chain polymers and a side chain polymer. **(p. 434)**

2:45pm
ThD2 • Neodymium-chelate-doped polymer waveguides, Sihan Lin, Robert J. Feuerstein, Alan R. Mickelson, *Univ. Colorado–Boulder.* Neodymium ions have been incorporated into polymers using chelates. The photoluminescence has been observed at 1.06-μm wavelength in the chelate-doped fluorinated polyimide waveguides. **(p. 438)**

3:00pm
ThD3 • Optical second harmonic generations of the thermotropic liquid crystalline main-chain polymer (aromatic polyesters), Tadahiro Asada, *Kyoto Univ., Japan.* The second harmonic generation of liquid crystalline aromatic copolyesters of 2-hydroxy-6-naphtoic acid and 4-hydroxybenzoic acid with various compositions have been investigated both experimentally and by molecular simulation. **(p. 442)**

3:15pm
ThD4 • Diagnostics of femtosecond laser pulses using films of poly(p-phenylenevinylene), B. Luther-Davies, M. Samoc, A. Samoc, M. Woodruff, *Australian National Univ.;* J. Swiatkiewicz, *SUNY–Buffalo;* R. Trebino, K. Delong, *Sandia National Laboratories.* Poly(p-phenylenevinylene) films can be used for diagnostics of femtosecond Ti-sapphire laser pulses by single shot-autocorrelation and frequency resolved optical gating (FROG). **(p. 446)**

3:30pm
ThD5 • Polarized electroluminescence in liquid crystalline main-chain polymers containing arylene vinylene units, R. Festag, A. Greiner, G. Lüssem, C. Schmidt, V. Stümpflen, J. H. Wendorff, *Philipps Univ., Germany.* New liquid crystalline polymers carrying arylene vinylene units with a high thermal stability are presented. The orientation behavior in the liquid crystalline phase was investigated. **(p. 448)**

LLOYD CENTER BALLROOM

3:45pm–4:15pm
Coffee Break

HOLLADAY ROOM

4:15pm–5:45pm
ThE • Processing
Hilary Lackritz, *Purdue University, Presider*

4:15pm
ThE1 • Optically initiated orientation of nonlinear photoisomers, R. A. Hill, P. Prêtre, A. Knoesen, *UC–Davis;* D. R. Yankelevich, *Centro de Investigación Científica y de Educación Superior de Ensenada, Mexico;* R. Twieg, *IBM Almaden Research Center.* We are investigating the dynamics of the trans-cis isomerization and orientation of nonlinear stilbene molecules in the presence of an electric field by monitoring the changes in the second order nonlinearity. **(p. 454)**

4:30pm
ThE2 • Electro-optic and second harmonic generation studies of dye-doped polymers, Fassil Ghebremichael, Hilary S. Lackritz, *Purdue Univ.* Second harmonic generation and electro-optic techniques were used to study dye-doped polymer dynamics for better understanding of the polymer's temporal and thermal stability. **(p. 458)**

4:45pm
ThE3 • Relaxation processes in nonlinear optical side-chain polyimide polymers, P. G. Kaatz, Ph. Prêtre, U. Meier, U. Stalder, P. Günter, *ETH Hönggerberg, Switzerland;* B. Zysset, M. Stähelin, M. Ahlheim, F. Lehr, *Sandoz Optoelectronics Research, France.* Relaxation times of polyimide side-chain polymers above and below T_g have been modeled using the Adam–Gibbs expression for structural relaxations with the aid of a scaling relation. **(p. 462)**

5:00pm
ThE4 • Toward a physical interpretation of the activation volumes for chromophore reorientation in corona poled polymers, Shane C. Brower, L. Michael Hayden, *Univ. Maryland, Baltimore County.* Activation volumes for several rod-like molecules doped into poly(n-alkyl methacrylates) are measured using second harmonic generation. The results are compared to activation volumes from pressure dielectric relaxation measurements on the pure polymers, obtained from the literature. **(p. 466)**

5:15pm
ThE5 • Current flow in doped and undoped electro-optic polymer films during poling, D. G. Girton, W. W. Anderson, J. A. Marley, T. E. Van Eck, S. Ermer, *Lockheed Research and Development Division.* A procedure for measuring current in polymer films during poling is presented, with data on selected films as a function of time and applied field. **(p. 470)**

5:30pm
ThE6 • Electric field effects in poled polymer thin films, Mark H. Ostrowski, Hilary S. Lackritz, *Purdue Univ.* Electric field and polymer relaxation characterization was performed on doped poly(methyl methacrylate) films to understand and optimize the poling process for second order nonlinear optical applications. **(p. 474)**

5:45pm–6:00pm
Closing Remarks

Monday, September 11, 1995

Passive Devices

MA 8:15 am-10:00 am
Holladay Room

Andre Pierre Persoons, *Presider*
University of Leuven, Belgium

High speed polymer optical fiber and amplifier

Yasuhiro Koike
Faculty of Science and Technology
Keio University
3-14-1, Hiyoshi, Kohoku-ku, Yokohama 223, JAPAN
Phone: +81-45-563-1141 ext. 3454
Fax: +81-45-562-7625

I. Introduction

Growing needs for processing and transmission of information have led to the increasing use of optical fibers for high speed communication. Although most long-haul communication has utilized single-mode glass fibers, inorganic glasses are not a universally ideal material especially for fiber connection and handling problem. The large core polymer optical fibers (POFs) will solve such problems because of great flexibility.

As all commercially available POFs have been of the step-index (SI) type whose bandwidth is about 50 MHz for 100 m transmission due to the modal dispersion, it can not cover the required bandwidth for the high speed multimedia network. However, high-bandwidth graded-index POF [1-3] enables gigabit signal transmission over 100 m. In this paper, basic performances of high bandwidth GI POF and high power GI polymer optical fiber amplifier were described.

II. GI Polymer Optical Fiber

The GI POF was prepared by the interfacial-gel polymerization technique we previously reported[1-3]. In this process, the GI preform rod with a 20~30-mm diameter was heat-drawn into the GI POF with a 0.5-mm diameter.

All deuterated PMMA-based GI POF and partially fluorinated polymer(synthesized at Hoechst AG, Germany) based GI POF were also prepared in order to eliminate the attenuation at the near infrared region. The attenuation spectra of the all deuterated MMA base and partially fluorinated polymer based GI POFs are

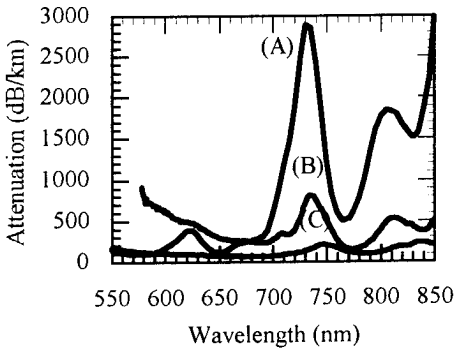

Fig. 1 Total attenuation spectra of the GI POFs.
(A): PMMA-base (B): partially fluorinated polymer-base
(C): all deuterated PMMA-base

shown in Fig. 1 compared with that of MMA based GI POF. In the fluorinated polymer GI POF, the attenuation at 780-nm wavelength of the MMA-based fiber (about 800 dB/km) could dramatically decrease to 150 dB/km[4] which is almost the same as that of PMMA-d8 based GI POF.

III. 2.5 Gbps transmission in 100 m GI POF link

Data transmission experiment was carried out[5] by using the edge emitting red LD with 647 nm wavelength which was newly developed by NEC Co. Ltd. for high speed data transmission.

Power penalty dependencies on the bit rates both for SI POF and GI POF in the 100 m link are shown in Fig. 2. If the power penalty is allowed up to 1 dB, available bit rates with SI POF and GI POF were 90 Mb/s and 3 Gb/s, respectively.

When considering the dispersion of POF, only modal dispersion has been

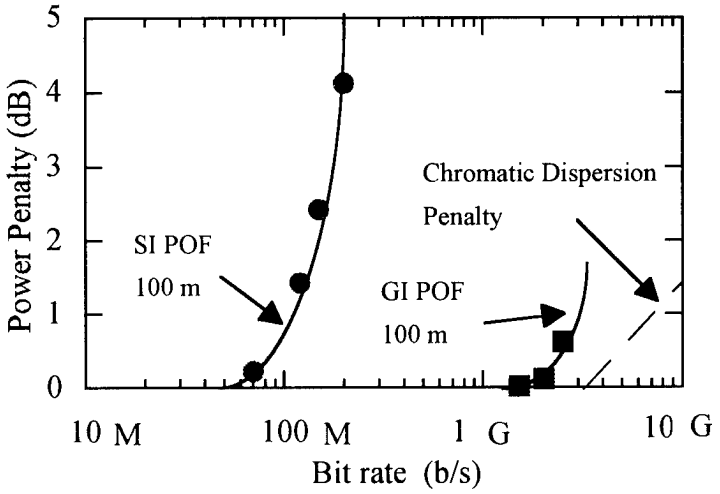

Fig. 2 Power penalty dependencies on bit rates.

discussed because material dispersion and waveguide dispersion are so small compared with the modal dispersion in the case of the SI POF. However, since the modal dispersion can be minimized when the optimum refractive-index distribution is formed in the GI POF, we must investigate the material dispersion. Figure 3 shows the calculated material dispersion of the PMMA and partially fluorinated polymer. It should be noted that even at 650-nm wavelength, the material dispersion of partially fluorinated polymer was -0.136 (ns/ nm·km) which was approximately half of that of PMMA (-0.248 (ns /nm· km). Furthermore, at 780-nm wavelength, which is one of the optical window of the partially fluorinated polymer based GI POF, the calculated material dispersion(-0.078 (ns /nm·km)) is smaller than that at 650 nm. Therefore, the use of fluorinated polymer as the core matrix polymer of the GI POF will offer several advantages: low absorption loss, low water absorption, and small material dispersion.

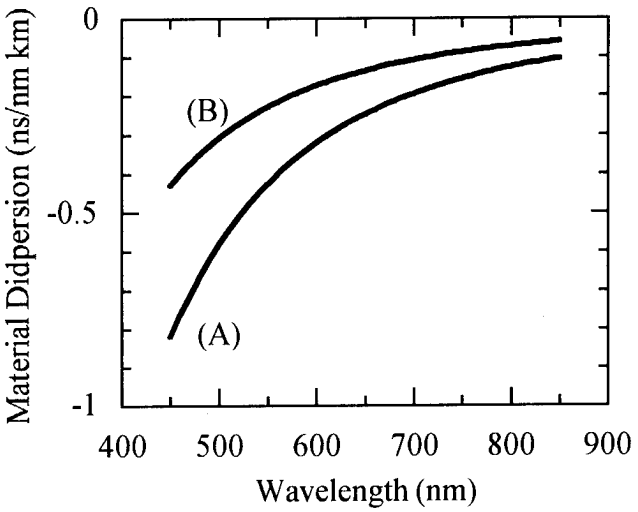

Fig. 3 Material Dispersion of the matrix polymer of the GI POF
(A): PMMA (B): partially fluorinated polymer

IV. GI polymer optical fiber amplifier

Graded-index (GI) type organic dye-doped polymer optical fiber amplifiers (POFA) were successfully prepared for the first time at Keio university[6,7]. High-power and high-gain optical amplification in a short length of the GI POFA is possible due to the extremely large absorption and emission cross sections of the doped dye (approximately 10,000 times larger than those of rare-earth elements), and a large core diameter (more than 500 μm). In addition, a lot of choice of organic dye dopants is possible, resulting in amplification covering wide range in the visible region. These advantages offer attractive applications such as an amplifier in polymer optical fiber LAN, a booster for a laser diode or other light sources, and so on.

The signal gain of the GI POFA against the launched pump power is shown in Figure 4. The pump source was a doubled Q-switched Nd:YAG laser at 532 nm wavelength and the signal source was a dye laser at 591 nm wavelength. The pump and signal lights were combined by means of a beamsplitter and were coaxially launched into a rhodamine B (RB)-doped GI POFA. After through a spectroscope, the output from the GI POFA at a launched signal power of 1 W was detected by a photomultiplier tube connected to a oscilloscope.

The maximum power of 620 W (the signal gain of 28 dB) was obtained with the launched pump power of 11 kW. As far as we know, such a high-power amplification with the signal and pump pulses of several nanosecond duration in the visible region was realized for the first time.

In order to quantitatively analyze the amplification, we assume the fast three-level system where the decay of the vibrational energy in the first excited singlet state S_1 is extremely fast. Figure 4 shows the calculated signal gain with respect to the signal wavelength for a RB-doped type, a rhodamine 6G-doped type, and a DCM-doped type GI POFA assuming the launched pump power of 10kW. This means that high gain of more than 26dB (about 400 times) can be obtained through the region of

approximately 50 nm wavelength (540~590 nm). Especially, high gain of 33 dB (about 2000 times) can be achieved around 579n m.

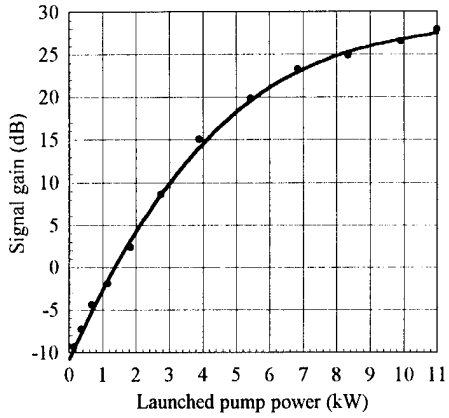

Figure 4 Signal gain against launched pump power for a rhodamine B-doped GI POFA prepared from the methyl methacrylate solution of 1ppm-rhodamine B. Core diameter = 500μm. Launched signal power (at 591nm, FWHM = 3.5ns) = 1W. Pump wavelength (FWHM = 6ns) = 532nm. Fiber length = 1m.

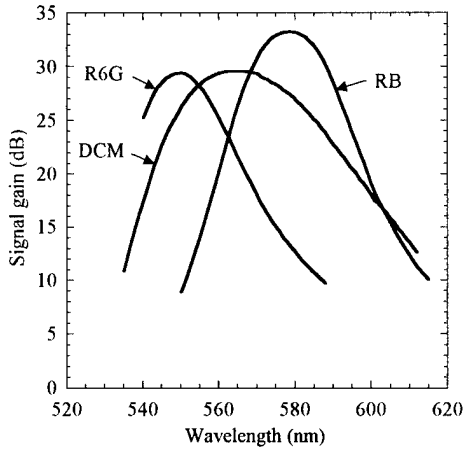

Figure 5 Signal gain against signal wavelength for a rhodamine B-type, a rhodamine 6G-type and a DCM-doped type GI POFA. Launched signal power (FWHM = 3.5ns) = 1W. Launched pump power (at 532nm, FWHM = 6ns) = 10kW. Rhodamine B density = 0.18ppm, Rhodamine 6G density = 1.00ppm, DCM density = 0.20ppm.

V. References

1. Y. Koike, ECOC'92, Proc. Vol.2, 679(1992)
2. T. Ishigure, E. Nihei, and Y. Koike, Appl. Opt. **33** (19), 4261 (1994).
3. T. Ishigure, A. Horibe, E. Nihei, and Y. Koike, Electron. Lett. **30** (14) 1169 (1994)
4. T. Ishigure, E. Nihei, Y. Koike, C. E. Forbes, L. LaNieve, R. Straff, and H. A. Deckers, IEEE Photon. Technol. Lett. **7** (1995), in press.
5. T. Ishigure, E. Nihei, S. Yamazaki, K. Kobayashi, and Y. Koike, Electron Lett. **31** (6), 487 (1995)
6. A. Tagaya, Y. Koike, T. Kinoshita, E. Nihei, T. Yamamoto, and K. Sasaki, Appl. Phys. Lett. **63**(7), 1(1993).
7. A. Tagaya, Y. Koike, E. Nihei, S. Teramoto, K. Fujii, T. Yamamoto, and K. Sasaki, Appl. Opt. **34**(6), 998 (1995)

Toward the Practical Application of Polymeric Optical Interconnection Technology

James T. Yardley, L. Eldada, K. M. T. Stengel, L. W. Shacklette,
Chengjiu Wu, and C. Xu
AlliedSignal Corporate Research and Technology
PO Box 1021
Morristown, NJ 07962-1021

INTRODUCTION

Intrinsic resistance and capacitance limit the rate at which information can be moved through conventional electronic circuitry. In principle, optics provides means for much higher data transfer rates. In addition, optical information pathways are insensitive to electromagnetic interference. Today glass optical fibers are routinely used for high speed data transfer in many applications. Although these fibers provide a very convenient means for carrying optical information over long distances, they are very inconvenient for complex high density optical circuitry. Furthermore, interconnection devices fabricated from glass optical fibers are difficult to fabricate and are very fragile. Polymeric materials, on the other hand, offer the potential to create highly complex optical interconnection circuitry on a planar substrate. In addition, they provide the possibility for a much higher degree of ruggedness. What has been needed is development and characterization of suitable polymeric materials, development of fabrication techniques for polymeric optical devices, development of technology for interconnection of polymer waveguides with glass optical fibers and full characterization of the resulting optical circuitry. We have developed a technology for polymeric optical interconnection which addresses these needs. The key features of this technology and some example applications will be described here.

MATERIALS

We have developed a wide variety of optically transparent polymers which are based on combinations of acrylate monomers. These monomer systems form highly cross-linked polymers which have very low intrinsic absorption in the wavelength range from about 400 nm to about 900 nm for non-fluorinated monomers, and from about 400 nm to about 1300 nm for moderately to heavily fluorinated monomers. This synthetic scheme allows the precise adjustment of index of refraction within a range from about 1.3 to 1.6. Since many of these monomers are fully miscible, any desired index can be obtained by varying the proportions of the monomers used. Thus the numerical aperture of waveguides fabricated from these polymers can be precisely controlled by using the same or different monomers in appropriate proportions as cladding (or underlying buffer) and core. At the same time, other physical properties of the polymer can be controlled such as surface energy and adhesive characteristics, as well as flexibility and toughness.

A characteristic of key importance for application is the thermal stability of the polymers. All organic materials are susceptible to yellowing upon exposure to elevated temperatures. This yellowing typically results from the formation of partially conjugated molecular groups characterized by a broad ultraviolet absorption band that tails off in intensity at longer wavelengths. Such an absorption pattern gives rise to a yellowing and eventually a browning of the polymer. The yellowing rate can, of course, be influenced by the chemical structure of the original polymer. Although the monomers used here all contain acrylate substituents, the chemical characteristics can vary widely, for example, from simple aliphatic, to aromatic, to ether, to urethanes. The choice of these linkages in the monomers employed ultimately determines, to a significant degree, the characteristics of the resulting polymer including flexibility, toughness, and stability against yellowing. The other major influence on polymer properties is

the number and distribution of crosslinking sites (acrylate groups), which control crosslink density and affect a wide variety of physical properties such as shrinkage upon polymerization, thermal expansion coefficient, toughness, and flexibility.

We have developed a large number of polymer compositions with varying properties. Typically compositions with index greater than about 1.54 are useful as core materials and those with index less than about 1.52 are useful as buffer (or cladding) materials. One prototypical waveguide system consists of a core material of index 1.545 which we designate, C2, and a buffer and cladding consisting of a mixture of C2 with another monomer of lower index. The ratio of the latter monomers was adjusted to obtain an appropriate index to give our targeted numerical aperture of 0.29. We have measured the thermal stability of this system as a function of both temperature and wavelength of the transmitted light. Figure 1 shows a plot of the observed yellowing rate expressed in engineering units of dB/cm per hour for degradation of C2 in air obtained from thin film samples. We have made measurements predominantly at short wavelengths and at high temperature in order to collect useful information in a reasonable amount of time. Figure 1 also shows rate constants for yellowing extrapolated from a simple Ahrrenius law. These extrapolations are consistent with the observed data and allow us to estimate losses induces over very long periods of time at lower temperatures.

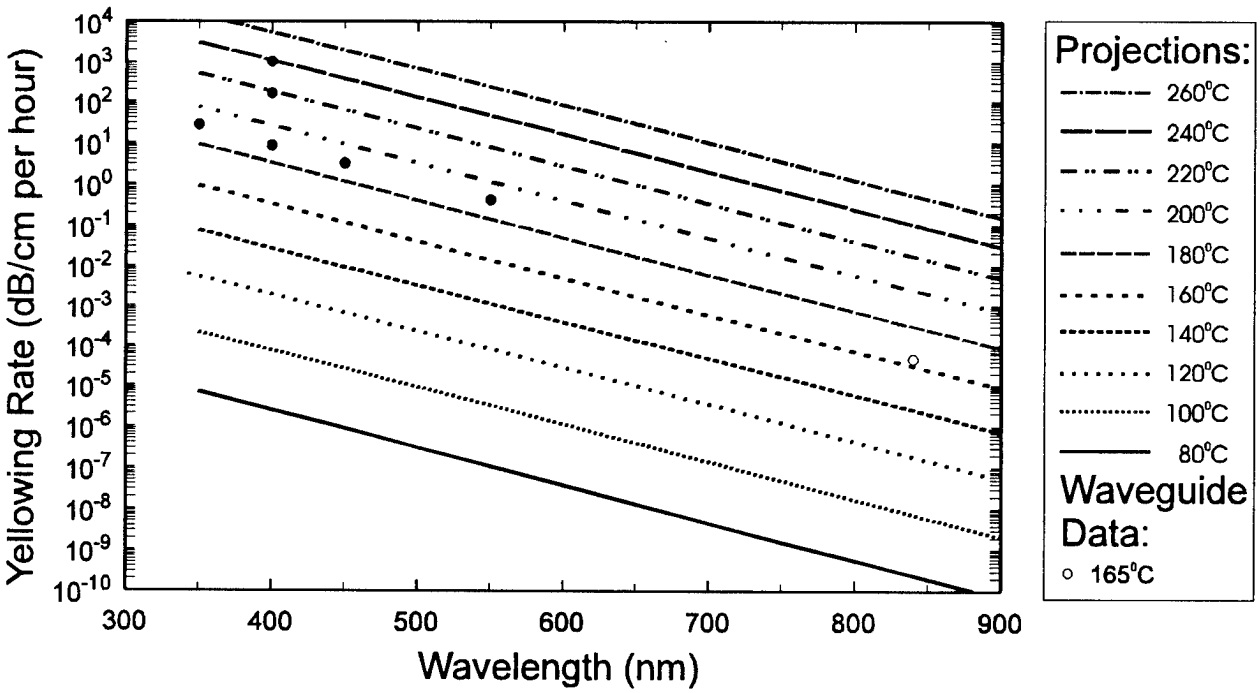

Figure 1. Thermal stability of the polymer waveguide core material, C2, is plotted as a function of temperature and wavelength. Line plots are predicted values for yellowing rate at increments of 20 °C beginning with 80 °C for the bottom most line. The closed circles represent data taken on thin film samples exposed to air at temperatures of 190, 218, and 240 °C. The open circle is the rate of yellowing observed for an encapsulated waveguide at 165 °C over a period of 20 days.

We have also made measurements on an actual waveguide device consisting of a 5-cm long straight guide fabricated between glass sheets and sealed at the edges with epoxy. In this case the polymeric structure is protected from oxygen exposure and thus is not perfectly analogous to the data shown above. The device was pigtailed with glass fiber, which was in turn fitted with SMA connectors, and illuminated with 840-nm light from a diode source. The source was fed through a 1 x 2 splitter to provide a reference signal as well as a sample signal. The power loss as a function of time and temperature was monitored through the ratio of these signals. The value obtained through this

measurement was close to that projected by the model inferred from the behavior of the thin film samples. The point representing this waveguide data is also depicted in Figure 1. Projections using the thermal aging model developed here indicate that the lifetime with respect to yellowing could be up to 75 years at 120 °C for an 840-nm wavelength.

DEVICE FABRICATION

Polymeric optical waveguide devices may be fabricated in many ways. For the materials described above, a photolithographic fabrication scheme is most appropriate. Within our approach, photosensitive polymerization initiators are added to the monomer mixtures to provide a means for photochemically initiating the polymerizations. We thus place a thin or thick film of photosensitive monomer mixture on an appropriate substrate (which can be glass, quartz, glass filled polyimide printed circuit board substrate, or flexible polyimide film for example). We expose to an appropriate dose of ultraviolet radiation (typical sensitivity is about 100mJ/cm^2) with a laser in direct write mode or with a conventional arc lamp light source through an appropriate photomask. We then remove unpolymerized material by conventional wet development with organic solvent such as methanol. This lithographic process offers very high contrast response allowing us to define sharply polymeric features with dimensions ranging from a few microns to millimeters with a high degree of accuracy and process latitude. As an example, Figure 2 shows an electron micrograph of part of an 8X8 star coupler device created with a conventional photomask before overcoating with cladding material where waveguide dimensions of about 100μ are employed to match commercial glass optical fiber. It is clear from this micrograph that very sharply defined features can be readily fabricated.

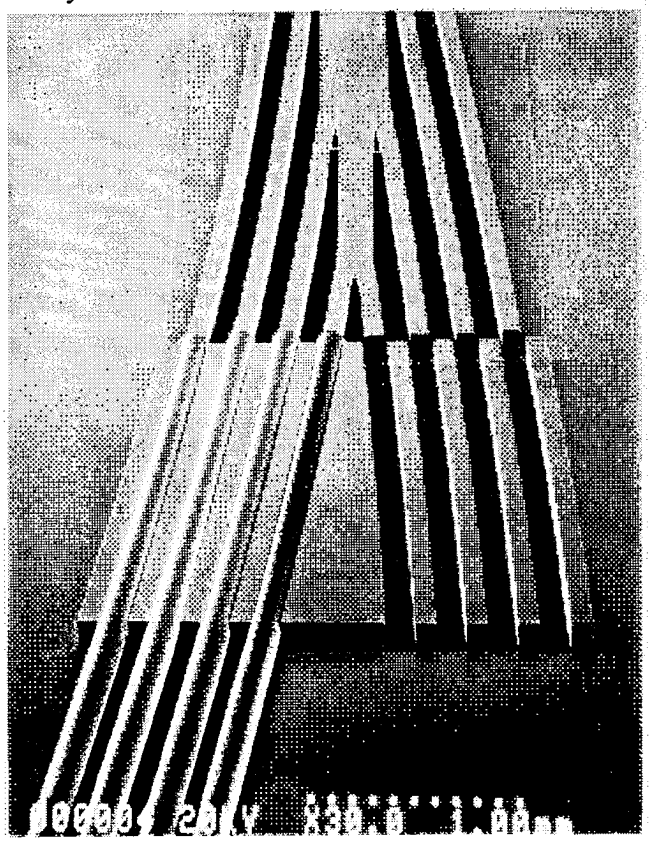

Figure 2. Electron micrograph of partially fabricated 8X8 star coupler device built on 100μ waveguide structures. Also shown are fiber optic to waveguide interconnection technology.

APPLICATIONS

Within AlliedSignal, we employ polymeric interconnect technology as discrete devices for interconnecting numerous optical devices uses in aerospace avionic sensor applications. Specific advantages of optical interconnection for avionic sensor applications include immunity from electromagnetic interference, light weight, overall circuit simplicity, thermal stability and mechanical ruggedness. For example we have developed a simple 1X2 coupler which allows a light source to interrogate a remote engine speed detector and return signal to be analyzed with both output and return signals carried over a single optical fiber. Devices such as these satisfy exacting aerospace specifications and are currently being qualified for commercial and military aircraft use. AlliedSignal is also participating in a demonstration fly-by-light system funded by ARPA and managed by McDonnell Douglas in which we will use polymeric waveguides to fabricate an optical backplane suitable for avionics use.

The POINT program, funded by ARPA and carried out by a consortium including GE, Honeywell, AMP, AlliedSignal, Columbia University, and University of Southern California is developing low cost high speed data processing modules employing polymeric interconnections. In particular, the program will demonstrate a high speed optical parallel data link within multichip modules and between modules. One aspect of this program will be direct in-situ writing of optical waveguides on electronic modules using AlliedSignal materials.

These and other programs are demonstrating the practical efficacy of polymeric optical waveguide interconnect circuitry. At this point in time, we may consider the technology to be technically viable. As optical interconnection businesses mature, we may be assured that polymeric materials will allow these technologies to become commercially viable as well.

Polyimide Optical Waveguides Fabricated by Direct Electron Beam Writing

NTT Interdisciplinary Research Laboratories, *NTT Opto-electronics Laboratories
T. Maruno, T. Sakata, *T. Ishii, Y. Y. Maruo, S. Sasaki, and *T. Tamamura
9-11, Midori-cho 3-chome Musashino-shi, Tokyo 180 Japan
Telephone: +81 422 59 4241
Facsimile: +81 422 59 2918

Polymer optical waveguides are attractive for fabricating economical and practical optoelectronic devices and interconnections in optical communication systems [1,2]. Channel waveguides, therefore, have been produced using several polymers such as poly(methyl methacrylate), polystylene, poly(organosiloxane), and polyimide [3-6]. One of the first priorities for polymer waveguides is high thermal stability so that soldering can be used in conventional device fabrication. Fluorinated polyimides are promising candidates for waveguide materials because they show high thermal stability and low optical loss near the IR wavelength region. We have previously developed novel fluorinated polyimides [7] and manufactured a single-mode optical waveguide for them by using conventional reactive ion etching (RIE) [8]. Moreover, we recently clarified that the refractive index of fluorinated polyimides can be controlled by electron beam irradiation [9], and that optical waveguides can thus be fabricated by direct electron beam writing (DEBW) [10,11]. This method is very useful because the fabrication process becomes simpler than when using RIE. In this paper, we propose a new optical waveguide fabricated by DEBW, which consists of a single material and a simple two-layer structure.

The chemical structure of the fluorinated polyimide (**I**) used in this study is shown in Figure 1. Poly (amic acid) precursor solutions of **I** were prepared by the reaction of 2,2-bis(3,4-dicaboxyphenyl) hexafluoropropane dianhydride (6FDA) and 2,2'-bis(trifluoromethyl)-4,4'-diaminobiphenyl (TFDB) in *N,N*-dimethylacetamide. A non-fluorinated polyimide (**II**) derived from the reaction of pyromellitic dianhydride and 2,2'-dimethyl-4,4'-diaminobiphenyl was also used as a comparison.

Figure 2 shows the relationship between the percentage of refractive-index change and the electron-beam dose. The refractive index was measured with a prism coupler (Metricon) for a large irradiated (4mm x 4mm) 8-μm-thick film. The Δn of **I** increases as the dose increases, and exceeds 0.3% at a dose of 1500 μC/cm^2. On the other hand, Δn of **II** scarcely changes as the dose is increased. As is well known, Δn of 0.25-0.7% is suitable for fabricating single mode optical waveguides [12]. Figure 2 clearly demonstrates

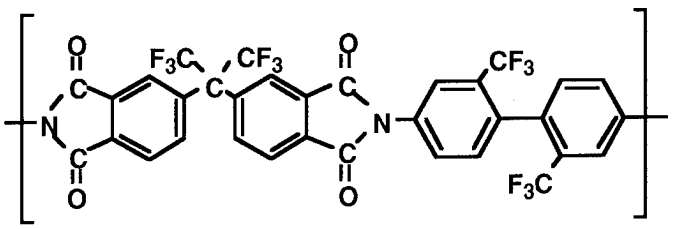

Figure 1 Chemical structure of fluorinated polyimide (**I**).

that sufficient Δn for single-mode operation can be obtained by electron-beam irradiation on the fluorinated polyimide.

Figure 3 shows a schematic diagram of the fabrication process for polyimide waveguides. First, a 30-μm-thick film of **I** is formed on an substrate by spin-coating and curing. Then, the film is exposed to an electron beam of 25 keV with a diameter of 0.2 μm in an electron beam lithography system (JEOL JBX-5FE), and line patterns are drawn for the core of the waveguides. Finally, a 20-μm-thick film of **I** is formed as an over-cladding on the irradiated polyimide film by spin-coating and curing. This method reduces the number of fabrication processes to less than half compared with the conventional RIE method.

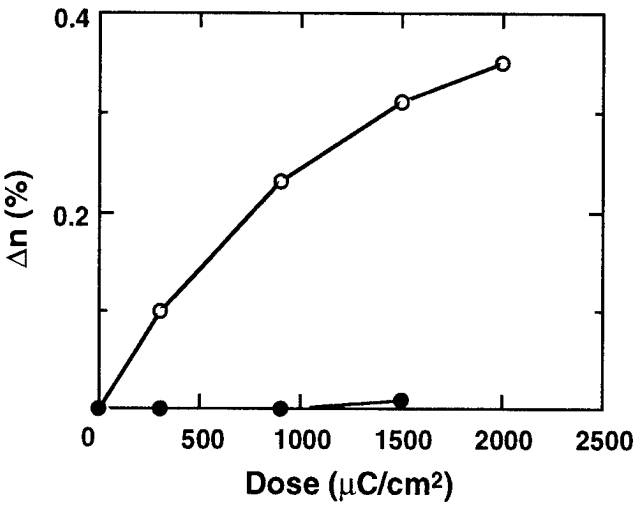

Figure 2 Relationship between percentage of refractive-index change and electron-beam dose of fluorinated polyimide (I, ○) and non-fluorinated polyimide (II, ●)

The fabricated waveguides had core widths ranging from 7 to 12 μm, and lengths of 66 mm. Figure 4(a) is a cross-section micrograph of a waveguide fabricated with a dose of 1500 μC/cm^2 and a core width of 8 μm. Contrast change was clearly observed at the electron beam irradiated area. The interference pattern in the cross-section of this waveguide was observed with a transmitted dual-beam interference microscope (Mizojiri Kogaku Co. Ltd.), and then the refractive index profile was calculated from the pattern by using

$$n(x,y) = 10^{-6} \bullet \lambda d(x,y)/Dt \quad (1)$$

Here n(x,y) is the refractive index difference, d(x,y) is the interference deviation, D is the intervel between

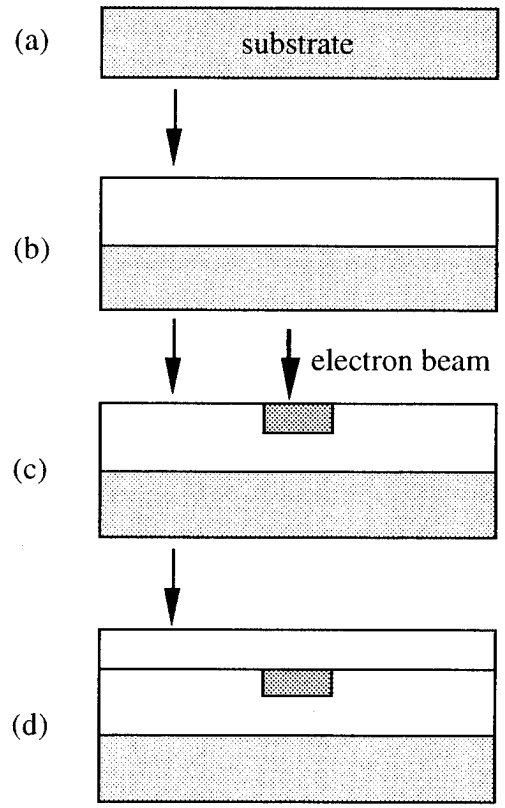

Figure 3 Fabrication sequence for embedded channel waveguides: formation of (a) the substrate, (b) the 6FDA/TFDB under-cladding layer by spin-coating; the layer is followed by (c) electron-beam irradiation and (d) spin-coating of the 6FDA/TFDB over-cladding layer.

interference patterns, λ is the wavelength of the light source (546nm), and t is the sample thickness. Figure 4(b) shows the interference pattern and the refractive index profile of a 50-μm-thick sliced waveguide. The waveguide refractive index varies with the depth below the surface. The maximum refractive index is more than 0.8%, which is about three times larger than that of the large area irradiated film in Figure 2. The core depth was estimated to be about 9μm because the refractive index did not change at a deeper level. Monte Carlo simulation of electron trajectories shows that the energy density profile is similar to the refractive index profile in the waveguide. The result indicates that the refractive index change was induced by the interaction between the electrons and polyimide.

Figure 5 shows typical near-field patterns for fabricated wavuguides.

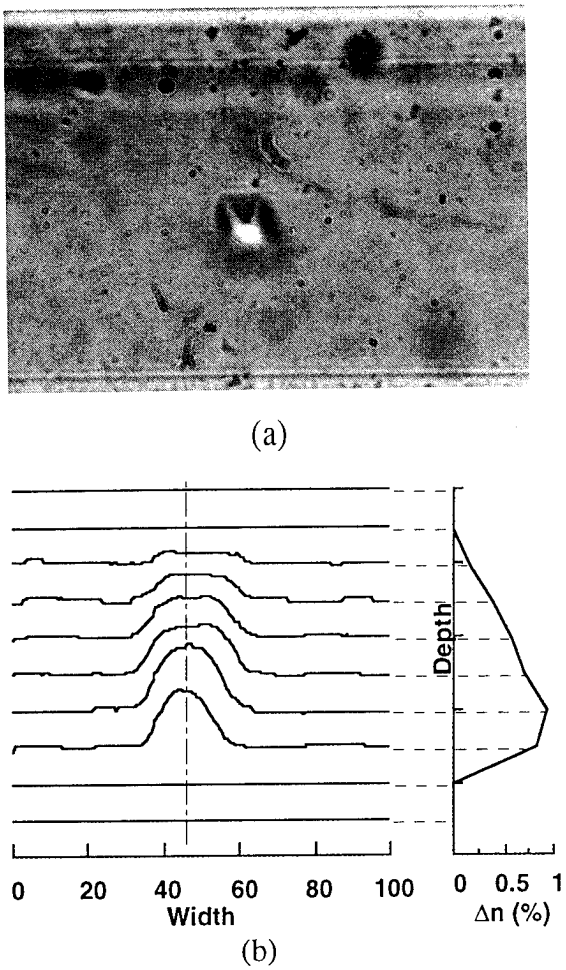

Figure 4 Cross-section micrograph of the embedded waveguide (a), and interference pattern and refractive-index profile (b).

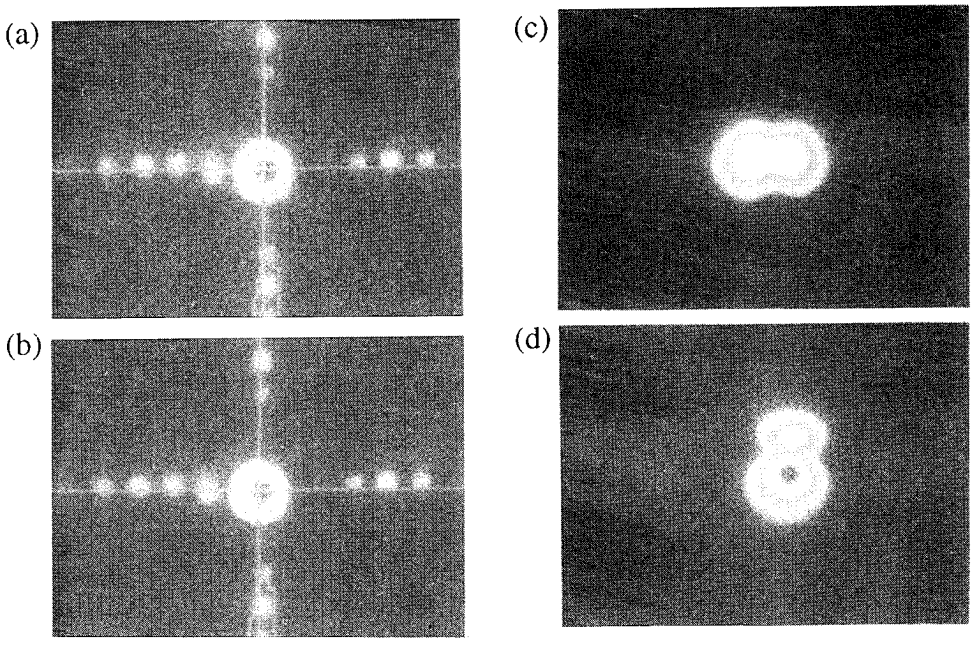

Figure 5 Near-field pattern at a 1.3 μm wavelength: mode profiles for (a) core width of 8 μm and TE-polarized incident light, (b) 8 μm and TM, (c) 11 μm and TE, and (d) 11 μm and TM.

Figures 5(a) and (b) indicate that the waveguide with an 8μm core width operates in a single mode for both TE and TM polarized incident light. These near-field pattern measurements demonstrate that wave-guides with a core width of less than or equal to 8 μm operate in a single mode at a wavelength of 1.3 μm, but the wave-guides with a core width of more than 8 μm operate in multiple modes.

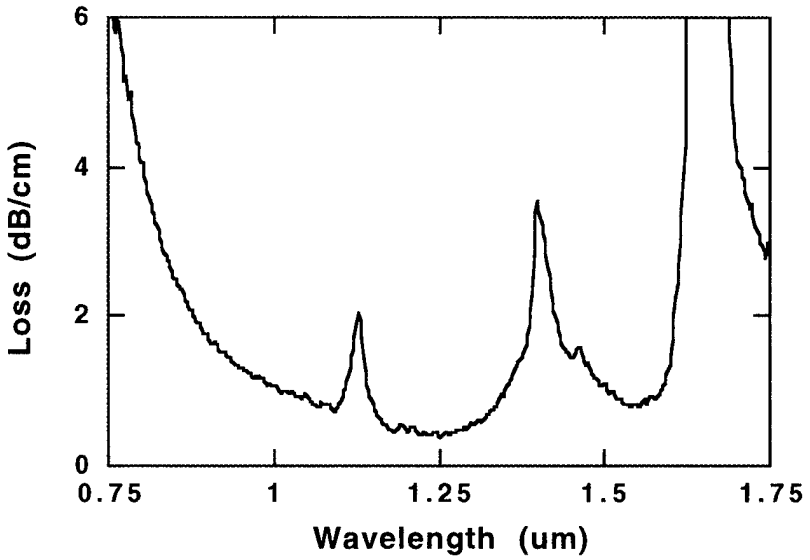

Figure 6 Loss spectrum of waveguide with a core width of 8 μm.

Figure 6 shows the loss spectrum of wave-guides with a core width of 8μm. There are low loss windows at optical communication wavelengths of 1.3 and 1.55 μm. The lowest optical loss at 1.3 μm among the waveguides, which operated in a single mode when the core width was 8 μm,was 0.4 dB/cm for TE and 0.7 dB/cm for TM polarized incident light.

In conclusion, we showed that the magnitude of refractive index change caused by direct electron beam writing is sufficient for single-mode waveguide fabrication. By optimizing the irradiation conditions, embedded channel waveguides with single mode transmission and low optical loss can be manufactured using a single fluorinated polyimide.

References

1. T. Izawa et al., ECOC-IOOC 91, Paper Web6-1, pp. 97-100 (1991).
2. B. L. Booth, J. Lightwave Technol., LT-7, 1445-1453 (1989).
3. S. Imamura, R. Yoshimura, and T. Izawa, Electron Lett., 27, 1342-1343 (1991).
4. D. A. Christensen, Proc. Soc. Photo-opt. Instrum. Eng., 836, 359-363(1987).
5. M. Usui, et al., Electron Lett., 30, 958-959 (1994).
6. R. Reuter, H. Franke, and C. Feger, Appl. Opt., 27, 4565-4571 (1988).
7. T. Matsuura, et al., Macromolecules, 26, 419-423 (1993).
8. T. Matsuura, et al., Electron Lett., 29, 2107-2108 (1993).
9. Y. Y. Maruo, et al., J. Vac. Sci. Technol., to be published.
10. Y. Y. Maruo, et al., Appl. Optics, 34, 1047-1052 (1995).
11. Y. Y. Maruo, et al., J. Lightwave Technol., to be published.
12. S. Suzuki, et al., Trans. IEICE, J77-C-I, 184-193 (1994).

Polymer Waveguide Applications in Multichip Modules (MCMs) and Board Level Optical Interconnects

Yue Liu, Julian Bristow, Terry Marta, Sommy Bounnak, and Klein Johnson
Honeywell Technology Center, 3660 Technology Drive, Minneapolis, MN 55418
(612)951-7843

Yung Liu, and Herb Cole
GE Corporate Research and Development, 1 River Road, Schenectady, NY 12301

I. Introduction

Optical backplanes are of increasing interest for commercial and military avionics processors. For such systems that competes on the basis of throughput per unit volume (and/or weight), increased component counts dictates a move from conventional packaging and board assembly technology to chip-on-board or multichip module (MCM) technologies as clock speeds and number of I/Os increase, and greater functionality are being demanded in a given system. Optical interconnects is likely to find its first introduction in such systems where practical density limits are being reached. Such situations include the maximum pin numbers in a manufacturable board-to-backplane connectors, or the maximum number of I/Os can be provided in an MCM.

While fiber optics technology has successfully implemented between cabinets as replacement for twisted wire and coax cable point-to-point link, its application inside a cabinet on the board level is severely limited due the bulk of fibers and connectors, and significant labor/cost involved in assembling that scale directly with degree of parallelism in the interconnect. Polymer optical waveguide interconnect technology, on the other hand, is particularly suitable for board level applications for its high density and potential low cost. It can be viewed as an "optical" equivalent of electrical printed circuit board (PCB) technology in which the fabrication cost is independent of the interconnect functionality and complexity. In order to take advantage of the high density of polymer waveguide to address the pinout limitation in systems employing multichip module, one must locate optoelectronic devices (such as lasers and photodetectors) with electronic die in the same MCM package. If optical waveguide can be fabricated, integrated and packaged into the MCM and board level with existing MCM and board fabrication equipment and technologies, further economies can be introduced by implementing optical interconnect within established electronic capital infrastructure.

Desirable features of a waveguide system for MCM and board level interconnects are:
- Compatibility with PCB board fabrication techniques;
- Compatibility with established MCM fabrication techniques;
- Acceptable lifetime (20 years) in typical operation environment;
- Optical properties compatible with typical system insertion requirements (loss budget)
- Low manufacturing cost

Our approach to meeting these requirements has been to develop a passive, multimode polymer waveguide system which can be directly applied to both MCMs and PCBs, and to develop connector interface technologies which allow these components to be integrated into systems using materials, processes, practices, and equipment that are compatible with established electrical industry. In this paper, we will describe each of the components, and present recent results on the performance of both individual components and a number of subsystem demonstrations.

II. Board integrated polymer waveguides

Our passive multimode polymer waveguide [1] fabricated on a thin (5 mil, Kapton substrate with standard electronic process equipment Multimode operation offers sufficient bandwidth (100-200

MHz.cm), and high density (four to five times that of electrical interconnects) while ensuring non-critical manufacturing techniques are used.

The typical process procedure are as follows. First a bottom buffer layer of benzocyclobutene (BCB) is deposited on too of the Kapton substrate, followed by a layer of polyetherimide (GE Ultem) as waveguide core. The BCB material is commercially available from Dow Chemical under trade name "Cyclotene" while the Ultem is a purified version of commercial thermal plastic material from GE. A SiO_2 layer is then deposited on the Ultem, and is subsequently patterned with waveguide features using typical contact lithography. The waveguide features is then transferred into Ultem using oxygen reactive iron etch. After removing the SiO_2 mask, the Ultem waveguide core is overcoated with another layer of BCB to yield a rectangular core completely encapsulated in BCB cladding. The competed waveguide layer is a rugged flexible sheet and maybe handled without special care.

The waveguide system is developed such that it then can be incorporated as an "optical layer" into standard electrical multi-layer printed circuited board using standard board lamination procedure. We have measured no additional loss after the waveguide layer is laminated onto circuit board at 20 psi and 375F. Losses of the multimode waveguide system were measured to be 0.24 dB/cm at 830 nm wavelength. While these figures are not as low as that of some acrylic waveguide system, the polyetherimide and BCB materials does not appear to suffer the degradation of loss at elevated temperatures which can occur in acrylic systems.

III. Optoelectronic packaging in MCM.

In optoelectronic component level, recent developments offer very encouraging candidates that are suitable for MCM applications which demand, compared to other commercial applications, higher performance in speed, temperature, and large element array devices. Vertical cavity surface emitting lasers (VCSELs) can offer very low threshold current (1mA or less) with much less temperature sensitive, moderate optical power (a few mW), high bandwidth (a few GHz), and larger operating temperature range. Planar configuration of VCSEL allows manufacturable fabrication and low cost wafer level testing and salability to 1D and 2D arrays [2]. In the short wavelength range (0.7 to 0.85 μm) integrated GaAs receivers (photodetector and amplifiers), and receiver array are also available through various foundries and laboratories[3].

As greater functionality is conferred on the optical interconnect, a large number of optoelectronic device must be incorporated into the module. Therefore a scaleable packaging scheme is essential to allow for progressively large number of optoelectronic devices to be added without increasing the time and cost associated with assembling the package.

Our approach to optoelectronic packaging for MCM is to insert optical interconnects using existing MCM fabrication equipment, techniques, and materials. The packaging scheme we adopted is in GE's HDI (High Density interconnect, MCM technology. Fig. 2 shows the general approach of this package. This is a "chip-first" MCM packaging approach in which electronic and optoelectronic die are pick-and-placed into a MCM substrate with prefabricated slots. Thus yields a planar top surface for subsequent lamination of dielectric layers (Kaptons), and fabrication of via, metal electrical interconnect lines, as well as polymer optical waveguides. To accommodate inevitable misplacement of each die, The HDI process uses a pattern recognition system to locate precise position of each die, and detects any displacement of each interconnect pads from its ideal position, and then adaptively on-line generates modified via positions, and interconnect paths that fits current module layout. The via holes are produced using excimer laser ablation, and the metal interconnects are produced by laser "writing" of photoresist followed by metal etching. After all necessary layers of electrical interconnects to both electronic and optoelectronic die are completed, an optical waveguide layer is fabricated, as an additional interconnect layer, using the same Ultem /BCB combination. The Ultem waveguide interconnect patterns are generated using the same HDI rule which allow waveguide to be written adaptively to exact active regions of the optoelectronic device.

The HDI process can locate target and generate patterns on 1.5 um step size grid. This is well within the typical alignment tolerance at the interfaces between the multimode waveguides and optoelectronics devices. Excess losses are expected due to bend in waveguide path to accommodate the die misplacement (max. of ±25 um for a typical pick-and-place machine) and limited step size. A 90 degree directional change is required at the both interfaces for the waveguide (horizontal), to collect light emitted from VCSEL (vertical) and to inject light into the detector. This achieved by terminate the waveguide with a 45 degree facet using a controlled laser ablation process similar to what is used to produce electrical via hole. Figure 3 shows a cross section of a waveguide with 45-degree reflector end facet fabricated with HDI process. We have measured excess loss of 1 dB per reflector facet (air bounded by total internal reflection) at 830 nm wavelength.

We have successfully package a 32 element VCSEL array using HDI process with complete electrical interconnects, optical waveguide array, and 45-degree interfaced with the VCSELs. A complete gigabit per second parallel optical link module is being fabricated using HDI which includes optoelectronic devices such as VCSEL and detector arrays, electronic devices such as laser drivers, pre-amplifiers, and post amplifier, and optical waveguides

IV. MCM-to-board connector interface

Figure 4 shows the schematic of our board-to-MCM connector. This connector approach used a flexible waveguide ribbon with special alignment "bars" built with the waveguide core. The ribbon is fabricated using the same technique described for the board-level waveguides, followed by a process that opens up the alignment bars. This process is simple, non-critical alignment step based on selective reactive ion etch technique. Yet it yields physical alignment slots that are precisely registered with respect to the waveguide array on each end of the connector ribbon. Same technique applies both to MCM- and on board-level waveguide interfaces. A rigid "key" piece completed with polymer ribs that matches to the dimension and spacing of alignment slots. The "key" is used to assemble components, providing passive self-alignment of the ribbon to the board- and MCM-level waveguides.

This interface shown good self-align properties. Couple losses were measured at each channels of a 1x32 array interfaces. The coupling losses among the 32 channels are 1.28 ± 0.6 dB, which includes a systematic variation across the array due to curling of the flexible waveguide. All results shown were obtained without recourse to additional alignment.

V. Summary

We describe our approach and recent works of polymer waveguide applications for MCM- and board-level optical interconnects. Our focus has been on developing practical low-cost optical solutions that are compatible with established materials, processes, and equipment in electronic industry.

References:

1. J. Bristow, et al., "Polyetherimide Based Waveguides for Passive Multimode Board and MCM Optical interconnects", Polymer Preprints, Americal Chemical Society, August 1994.

2. M.K.Hibbs-Brenner, et al.,"Record performance of planar, implanted GaAs/AlGaAs top-emitting veritical-vacity surface-emitting lasers (VCSELs) grown by MOCVD", IEEE LEOS '94 PD1.5, Picsataway, NJ, 1994.

3. Y.M. Wong, et al., "Technology development of a high-desity 32-channel 16-Gbps optical data link for optocal interconntion applocation for the Optoelectronic Technology Consortium (OETC)", to be published in the IEEE Journal of Lightwave Technology.

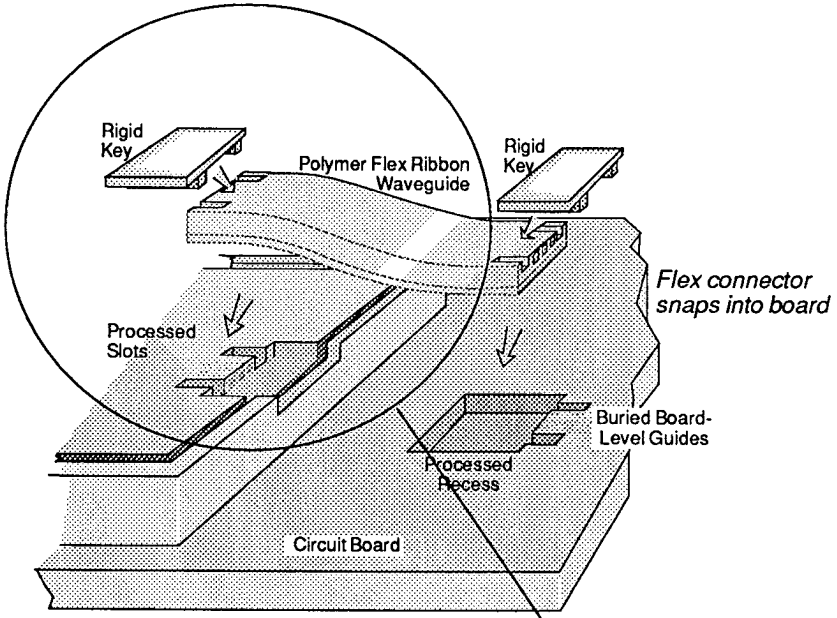

Figure 1(c): MCM-to-Board connector assembly

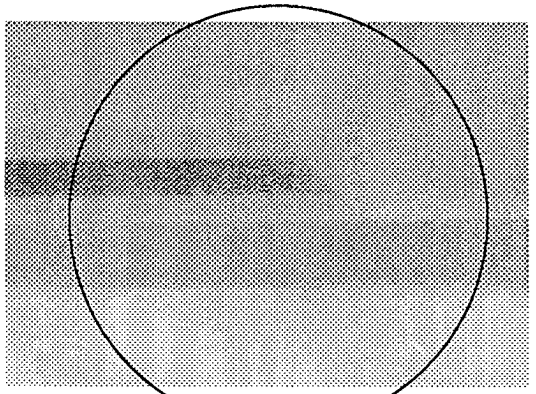

Figure 1(b): Cross section of waveguide with 45-degree facet processed using HDI

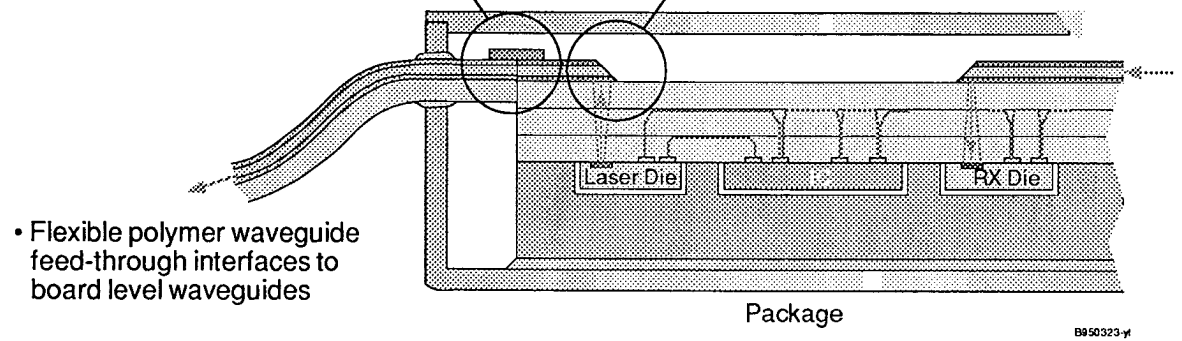

Figure 1(a): MCM package using HDI process

NONLINEAR SPECTROSCOPY OF DANS SIDE CHAIN POLYMERS

Myoungsik Cha
Laboratory for Dielectric Studies
Punsan University
South Korea

Akira Otomo, William E. Torruellas, George I. Stegeman
C.R.E.O.L., University of Central Florida
12424 Research Parkway, Orlando, FL 32826
tel.: 407 - 658 3918

David Beljonne, Jean Luc Brédas
Centre de Recherche en Electronique et Photonique Moléculaire
Université de Mons-Hainaut
Place du Parc 20, B7000 Mons (Belgium)

Winfried H.G. Horsthuis, Guus R. Möhlmann
AKZO-NOBEL Electronic Products
Arnhem, Netherlands

Molecular systems, in particular polymers, with π-electron donor-acceptor groups are becoming potential candidates in applications where large bandwidth and low costs are desired for electro-optical modulation of optical information. Di-Phenyl molecules including Disperse-Red-1 and Di-Amino-Nitro-Stilbene (DANS) embody most of the requirements in stability, high loading, processability and very large electro-optical figures of merit[1]. However little is known about their electronic structure represented by their excited state spectrum and responsible for their nonlinear optical response, for both second and third order. We present a complete spectroscopic study of the DANS molecular system and compare our theoretical predictions to the second order nonlinear spectrum and four third order nonlinear optical spectra of amorphous DANS side-chain polymers. In particular we can successfully explain shifts of the nonlinear spectrum compared to the linear absorption one by properly accounting for Frank-Condon type displacements[2].

In the field of nonlinear spectroscopy an interesting question has been whether a gas phase molecular theory can predict the universal response of π-electron conjugated molecules. In the case of relatively small molecules like DANS a complex approach such as the INDO/MRD-CI calculation is performed based on an optimized geometry. When appropriate Raman modes are included in these calculations a very good

agreement with the position, strength and line-width of the linear absorption spectrum can be obtained, Fig.1. When such results are included in the expression of the second and third order susceptibility, shifts of the experimental results, for instance the two-photon absorption spectrum, are observed, Fig.2. We have attributed these shifts to a distribution of Frank-Condon factors, different from that obtained from the linear absorption spectrum. For the latter effect to occur the well established empirical two-level model is expanded to a three level model which includes the ground state, the so-called charge transfer (CT) band and a weakly one photon allowed state located above CT, the latter resulting from our calculations. A large inter-state coupling between CT and the highest energy state results on the IR shifts observed experimentally, Fig.2-3. In this calculation local field factors have properly been taken into account under the Lorentz-Lorentz approximation. Three additional nonlinear optical spectra confirm the validity of our theoretical approach.

REFERENCES

1) G. Stegeman, W. Torruellas, *MRS proceedings*, vol. 328, 397, Boston, Fall 1993.

2) S. Aramaki, W.E. Torruellas, R. Zanoni, G.I. Stegeman, *Opt. Comm.*, **85**, 527 (1991).

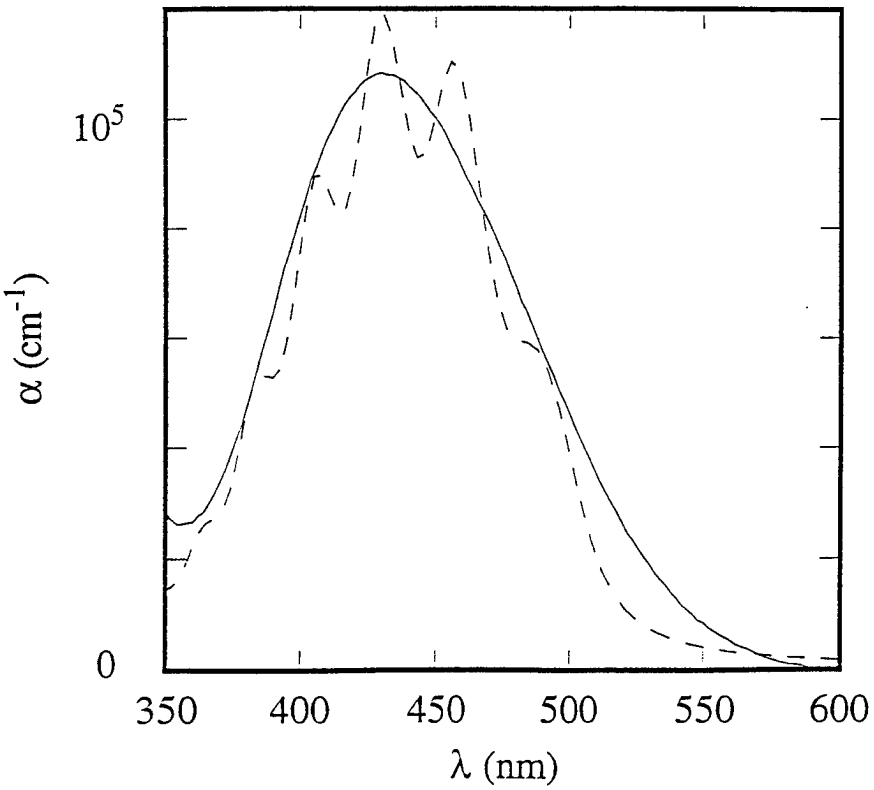

Figure 1:

DANS linear absorption spectrum. The solid line is the experimentally measured spectrum, the dashed line shows the results of the INDO/MRD-CI calculation.

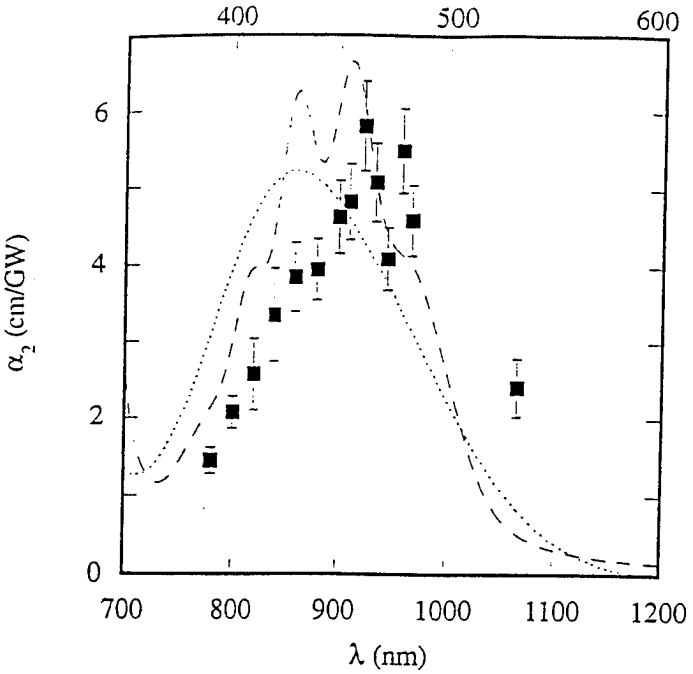

Figure 2:

Two-Photon absorption spectrum for DANS side chain polymers. The squares are the experimentally determined values, the dotted line is the linear absorption spectrum at twice its wavelength range, while the dashed line shows the results of our calculation.

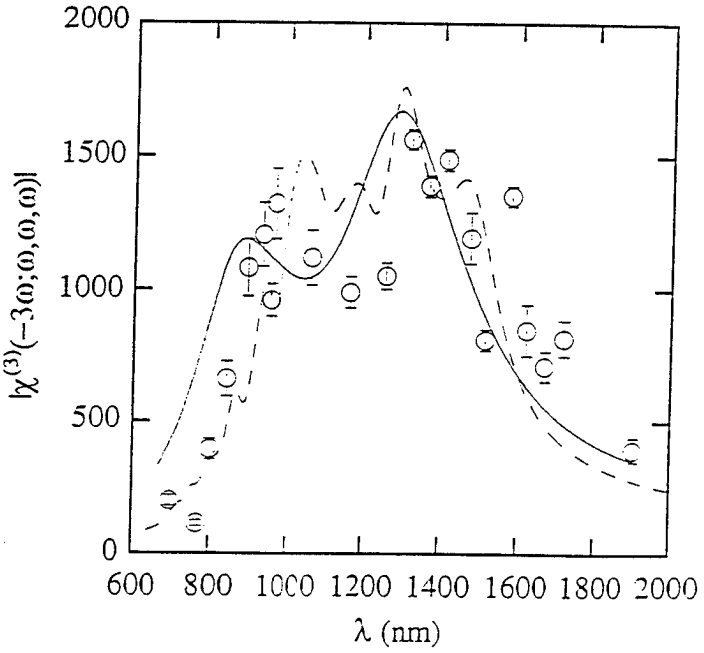

Figure 3:

Third harmonic generation spectrum of disordered DANS side chain polymer. The solid line is the fit twoan empirical two-level model while the dashed line shows the results of our calculation.

Monday, September 11, 1995

Fibers

MB 10:30 am-12:00 m
Holladay Room

Yasuhiro Koike, *Presider*
Keio University, Japan

Studies of Polymer Optical Fibers

W. D. Chen, R. F. Shi, and A.F. Garito,
Department of Physics,
University of Pennsylvania, Philadelphia, PA 19104
Tel: (215) 898-5810 Fax: (215) 898-2010

1. Introduction

The growing demands in local area networks (LANs) for low cost broad band data communications are providing a major opportunity for further technology developments important to polymer optical materials and devices. Polymer optical fibers (POF) can satisfy requirements for high-bandwidth, quick-connect, fiber optics for short distance (100 m) data transmission in data links, multimedia, and multi-noded bus networks[1-4]. Figure 1 illustrates the variety of application areas together with their required transmission bandwidths.

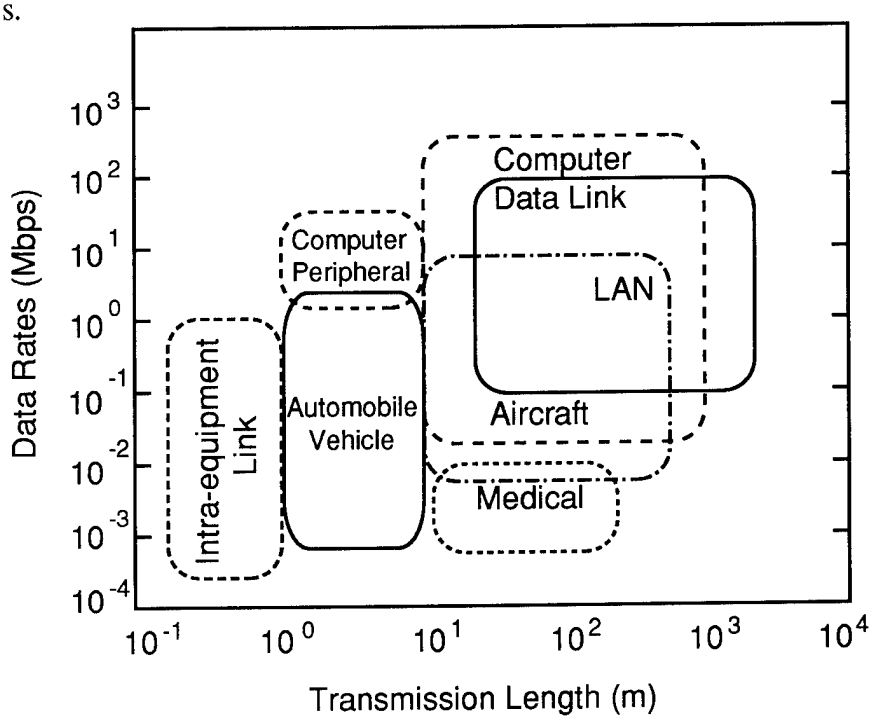

Figure 1. Potential applications for polymer optical fibers and their required bandwidths.

2. Optical Attenuation and Bandwidth Limits

POFs come in two forms, namely multimode step index (SI) and graded index (GI) fibers which provide, respectively, bandwidths in the range from 10 MHz-km to 1 GHz-km [3]. As shown in the accompanying optical attenuation spectrum of Figure 2, POFs

made of PMMA have three loss windows at 570, 650, and 780 nm between the various CH overtone modes. Current interest is centered on the 650 nm wavelength where the loss can be as low as 160 dB/km and where both LED and laser diode sources have been developed for ready availability [4].

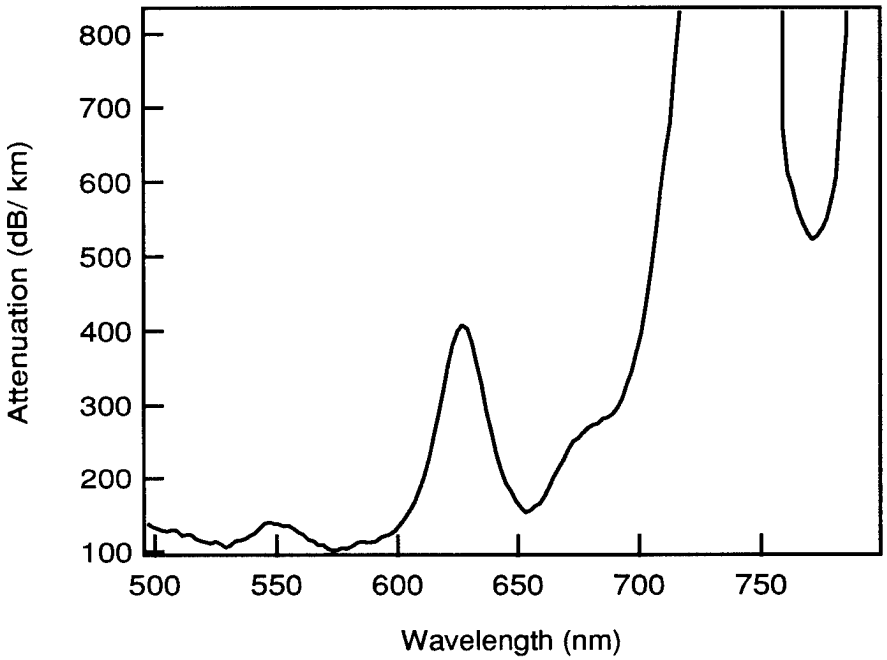

Figure 2. Optical loss spectrum of PMMA based step-index polymer optical fiber.

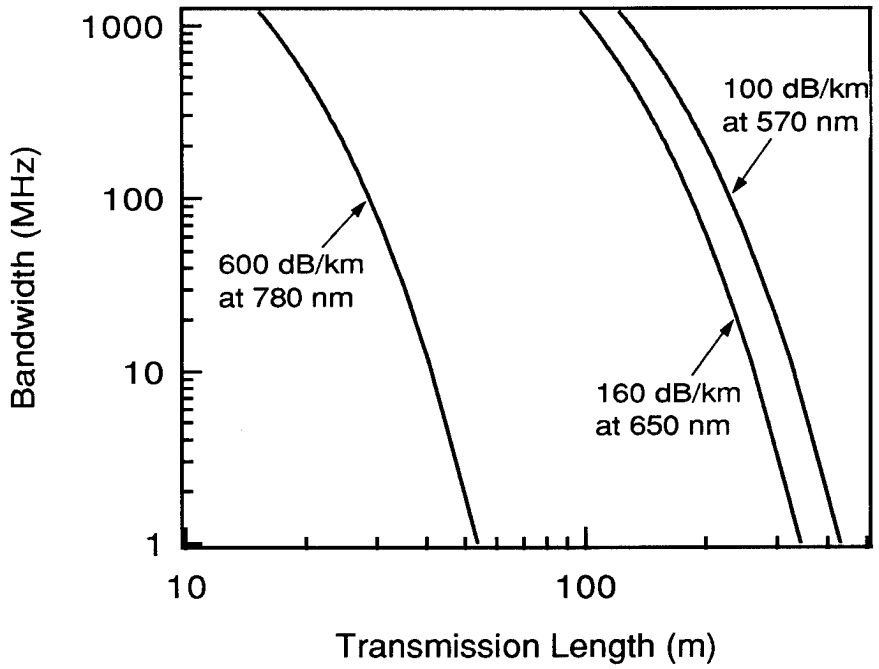

Figure 3. Attenuation limited bandwidth in PMMA at 570, 650, and 780 nm.

The background loss in each of these windows limits the bandwidth, or equivalently, the data rate at which data can be transmitted. Figure 3 shows the bandwidth-length limits for PMMA at 570, 650, and 780 nm wavelengths. In general, signal transmission will not be attenuation-limited for values of bandwidth-length that fall to the lower left of each curve. Thus, at 650 nm with a loss of 160 dB/km, the fiber attenuation will allow approximately 50 MHz transmission band width over fiber lengths of about 200m.

3. Mode Dispersion and Bandwidth Limits

In the absence of attenuation, the bandwidth of a POF is determined primarily by inter modal dispersion in group velocity and is measured through the broadening of picosecond optical pulses inserted into the fiber under well specified launch conditions. Typical results for similar length SI and GI POFs are compared in Figure 4. The 46 ps input pulse is broadened considerably in the 44 m length SI POF to 696 ps. In contrast, the broadening in the 68 m length GI POF is only 98 ps. From the data, the bandwidth of the SI POF is 280 MHz-100 m, while the bandwidth of the GI POF is about 3.46 GHz-100 m.

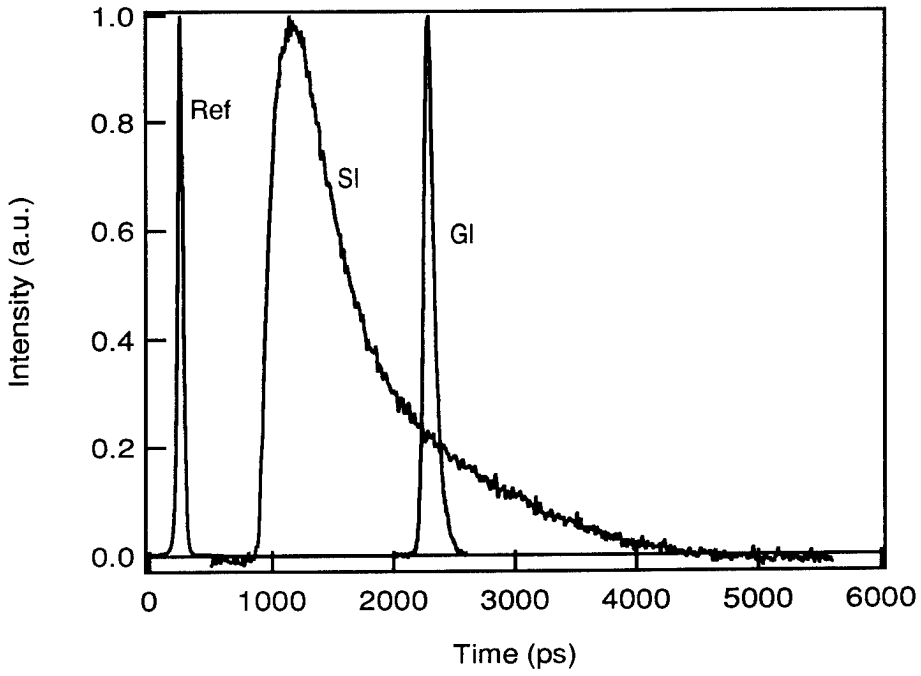

Figure 4. Broadening of 46 ps input pulse in 44 m step-indexed (SI) and 68 m graded-indexed (GI) polymer optical fibers.

4. Numerical Aperture: Fiber Coupling and Beam Insertion

Short distance communications require many junctions and connections of optical fibers. In the case of a single mode optical fiber, the core diameter is about 5 micrometers, so that in the connection of two fibers, a slight misalignment, as small as a few micrometers, causes a significant coupling loss. A POF with a relatively large diameter of order 1 millimeter helps in solving this problem [1].

High efficiencies in beam insertion are also achievable in POFs because of their high numerical apertures (NA). The NA represents the light-gathering ability of the fiber and is related to the difference in refractive index between the core and the cladding. The high NAs in POFs derive from the tunability of polymer refractive indices over a wide range. These indices vary from 1.3 for highly fluorinated materials to around 1.6 for oxygen containing resins. A typical POF has an NA of around 0.5, equivalent to an acceptance angle of 60 degrees, compared to 0.14 and 16 degrees for a comparable glass fiber. The large acceptance angle greatly eases the alignment tolerances for POF connectors, significantly reducing their complexity.

Thus, POFs offer many significant advantages over inorganic glass optical fibers in short-distance data communications systems, especially in those cases where ease of handling and installation are very important.

Acknowledgment: Research generously supported by AFOSR, ARPA, and NSF.

References:

1. T. Kaino, "Polymer Optical Fibers", in *Polymers for Lightwave and Integrated Optics: Technology and Applications*, L.A. Hornak, ed. (Marcel Dekker, New York 1992) p. 1.

2. M. G. Kuzyk, U. C. Paek, C. W. Dirk, "Guest-host Polymer Fibers for Nonlinear Optics", *Appl. Phys. Lett.* **59** (8), 902 (1992).

3. Y. Koike, "High Bandwidth Low Loss Polymer Fibers", Proc. ECOC'92, 1992, p. 679.

4. S. Yamazaki, et. al., "A 2.5 Gb/s 100m GRIN Plastic Optical Fiber Data Link at 650nm Wavelength", Proc. ECOC'94 Post deadline Paper, p. 1, 1994.

All-Optical Switching in a Single-mode Polymer Optical Fiber

D.W. Garvey, M.G. Kuzyk, and R. Kruhlak
Department of Physics, Washington State University, Pullman, WA 99164-2814

C.W. Dirk, S. Martinez, H. Selnau, Jr., P. Craig, L. Green
Department of Chemistry, University of Texas, El Paso, Texas 79968-0513

Motivated by the demonstration of all optical switching in a silica glass fiber, we are investigating the use of dye-doped polymer optical fiber as the switching medium. Because of the dye's larger nonlinear response, devices in the 1 meter length range are possible. Measurements of the intensity dependent phase shift in these fibers are already within an order of magnitude of providing a π phase shift. In this contribution we report on the switching characteristics of a first generation Sagnac switch.

In order for a material to function as a suitable nonlinear medium for the construction of an all optical switch, there are several parameters which need to be maximized. The intensity of light used in the device is limited by onset of optical damage to a peak power of about 150W in a 15 micron diameter core. At present we are attempting to increase this limit by purifying the monomer that is used in fabricating the fibers. Given that there is an upper bound on the intensity, the material must also have as large of a third order susceptibility as possible. The class of squaraine dyes was reported to have a large $\chi^{(3)}$ and is the material under study in the present work. The most convenient material class that allows for ease of fabrication is the guest/host system in which a highly nonlinear molecule is placed in a transparent host. Silica glass is a well known high quality optical material that has been used in optical devices made from silica glass fibers. The squaraine dyes, however, break down at temperatures required to process glass into a fiber, so polymers have been used as a more suitable host material owing to their lower processing temperatures. In particular we have chosen poly(methyl)methacrylate (PMMA) as our host material. At present the maximum concentration of ISQ squaraine dye that we have been able to get into monomer solution is 0.1% by weight of dye to polymer. The nonlinearity of the material can be incremented by increasing solubility. Another consideration is the value of the two photon absorption coefficient (the imaginary part of $\chi^{(3)}$) which must be small compared to the size of the real part of the third order nonlinearity. While initial results for the squaraine ISQ suggest that it may not be suitable in this regard, several additional squaraine dyes are under investigation.

We have been able to fabricate step index single-mode polymer (PMMA) optical fibers. Single-mode polymer fibers with squaraine doped cores have the ideal geometry for construction of an all optical device since they provide high intensities over long interaction lengths.

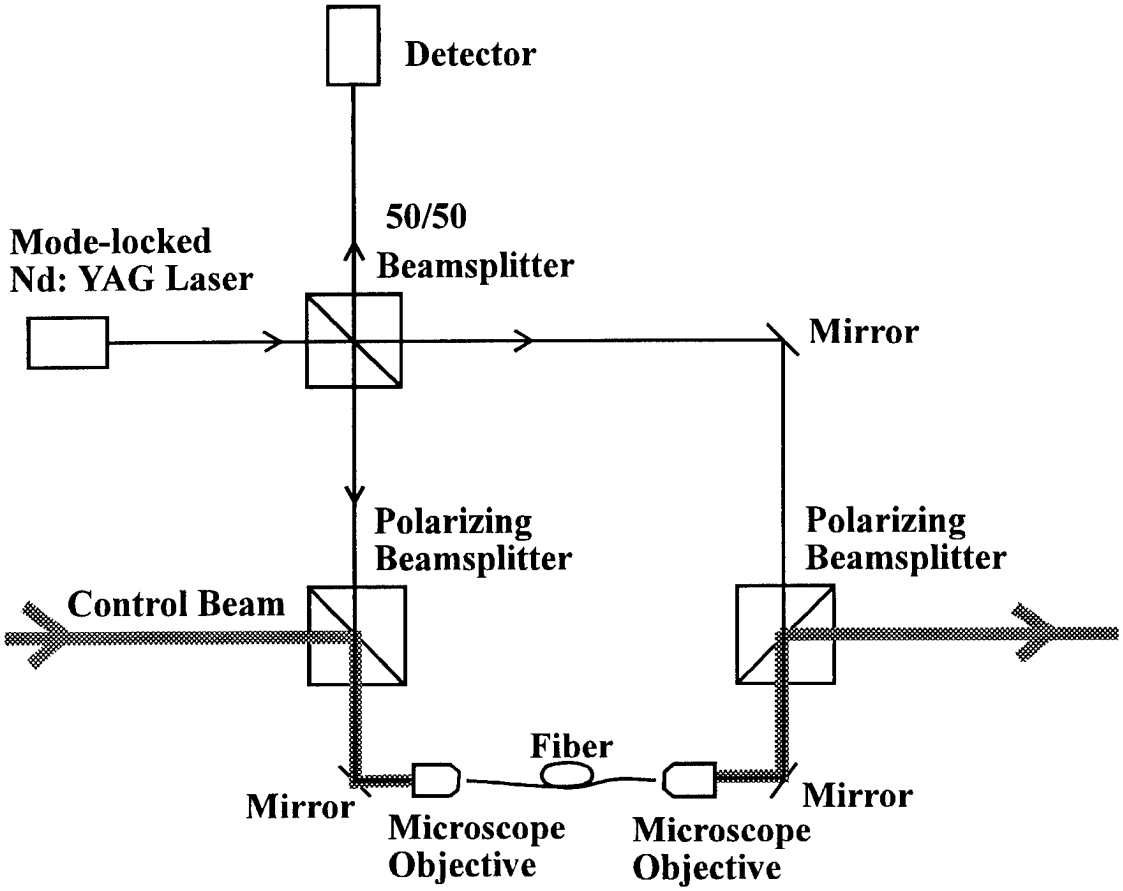

Figure 1. Sagnac Switch

The main thrust of our polymer optical fiber research is to create an all optical switch in which light output can be switched from one state to another by purely optical means. Two versions of such a switch are under development. Figure 1 shows the basic configuration of a Sagnac interferometer switch. A low intensity pulse of light enters the interferometer and is split into two equal parts by a 50/50 beamsplitter which then counterpropagate around the ring. Part of the path of both beams includes traveling through a 20cm length of squaraine-doped fiber. The intensities of both of these beams is low enough that the nonlinear effects are negligible. These pulses will interfere constructively when they are recombined at the detector since they have followed identical paths around the ring. This would be the "on state" of our device. The device can be switched to its "off state" by means of a control pulse that is introduced into the interferometer by the polarizing beamsplitter in the left leg of the interferometer. The polarization of the two counterpropagating pulses is orthogonal to that of the control pulse so that they will pass through the polarizing beamsplitter unaffected. The control pulse is launched into the interferometer so that it travels with one of the counterpropagating pulses. Furthermore the intensity of control pulse is high enough to induce an intensity dependent phase shift on itself and on the lower intensity pulse upon which it is superimposed. The control pulse is then removed from the interferometer by the polarizing beamsplitter in the right leg of the interferometer. The low intensity

counterpropagating pulses will then be recombined at the detector and interfere. The output intensity depends on the phase shift. A full π phase shift would lead to complete destructive interference and would correspond to the "off state" of the device. At present we have observed 1/40th of the full half wavelength phaseshift in a 20 μm diameter with 0.1% ISQ doping and a laser source at a peak power of 150W. The phase shift can be substantially increased with either higher power input or smaller core diameter.

The other optical switch design under investigation is the dual core polymer optical fiber. For low intensities, where nonlinear effects do not contribute, a beam that is introduced into one of the two cores will gradually bleed over into the other core. After propagating over a length called the coupling length, the light is found to be completely in the other

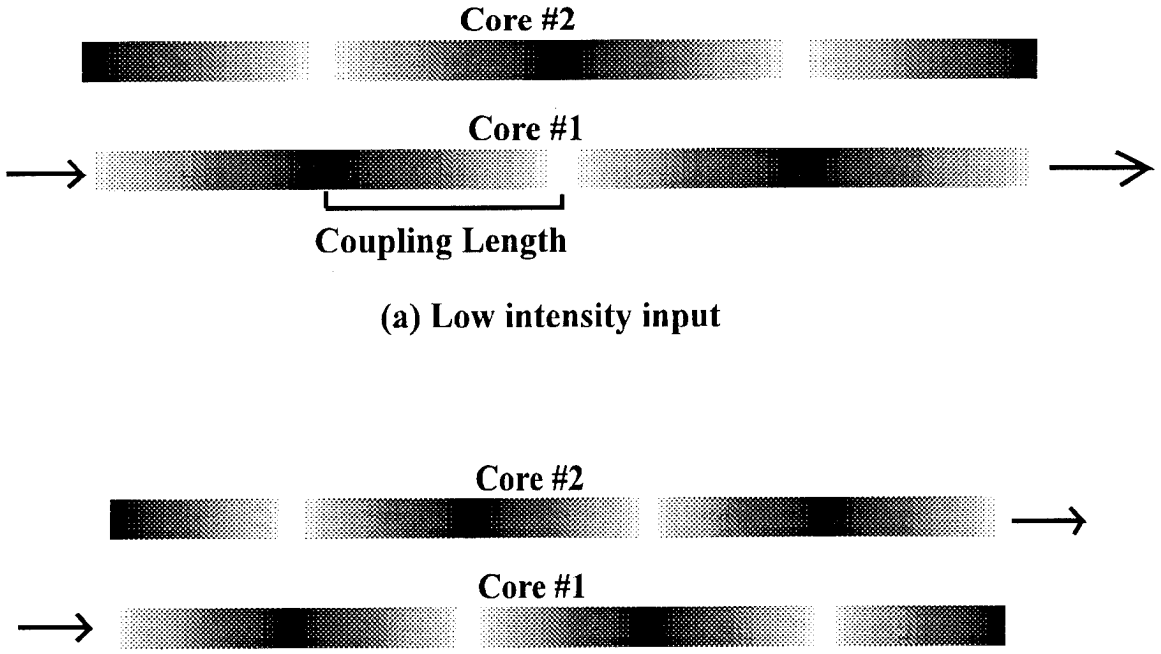

Figure 2. Dual Core All-optical Switch

core. The coupling length is a function of the distance between the cores and the difference in the index of refraction between the core and cladding material. If the core material has an intensity dependent refractive index, the coupling length will also be a function of the intensity of the light. To make this function as a switch we must choose a length of dual core fiber that is an integral multiple of the coupling length. An example of this is shown in Figure 2. The length of fiber is chosen so that the light makes four complete hops to emerge from the same core into which it was originally introduced. If the intensity of the light is increased so that the hopping distance decreases by 25%, the light is then able to complete five hops and will emerge from the other core. The function of this switch is to convert intensity information into a binary output.

One of the problems we have encountered is an unwanted nonlinear effect of stimulated Brillouin scattering. The pulses traveling through the fiber affect the material in such a way as to set up a traveling acoustical wave. The changes in the index of refraction induced by these compressions and rarefactions act as a moving grating and causes some of the light to be reflected back down the fiber. The magnitude of the effect is proportional to the intensity of the light. The strength of Brillouin scattering seems also to depend on material. We will discuss the role of Brillouin scattering on all optical switching. Because stimulated Brillouin scattering acts as a source of light, it must be minimized. We believe that better purification of the polymeric materials will lead to less stimulated Brillouin scattering.

In conclusion, we report on the first generation all optical switch made from a single-mode polymer optical fiber and discuss its operational characteristics.

We acknowledge the support of the following agencies:

Air Force Office of Scientific Research
National Science Foundation MRCE
Texas Higher Education Coordinating Board
The University of Texas at El Paso

Transparent Birefringence-free Copolymer and its Application

Shuichi Iwata, Hisashi Tsukahara, Eisuke Nihei, and Yasuhiro Koike

Faculty of Science and Technology, Keio University,

3-14-1, Hiyoshi, Kohoku-ku, Yokohama 223, Japan

TEL : +81-45-563-1141 ext.3454

FAX : +81-45-562-7625

SUMMARY

The birefringence-free copolymer was prepared by randomly copolymerizing positive and negative birefringent monomers. The birefringence-free copolymer showed excellent transparency and no microscopic heterogeneous structures were observed. As a novel application of the birefringence-free copolymer, we propose the polarization preserving polymer optical fiber (POF).

INTRODUCTION

Birefringence caused by orientation of polymer chains in extrusion or injection molding takes disadvantage of optical applications. As the method of compensation for birefringence, the blend of positive and negative birefringent polymers has been studied and some pairs of polymer blends have been proposed[1),2)]. But polymer blends can not be practically used because of the problems in the transparency and the difficulty in mixing polymers homogeneously. In order to solve the problems of the blend method, we propose a new method which compensates birefringence by the copolymerization of positive and negative birefringent monomers.

BIREFRINGENCE-FREE COPOLYMER

We selected MMA as the negative birefringent monomer, and benzyl methacrylate (BzMA) as the positive one. The monomer reactivity ratios, r_1 and r_2, between the two monomers calculated by using Q and e values are about unity. Therefore the two monomers can be quite randomly copolymerized. These two monomers were copolymerized with various compositions at 70℃ for one day. The copolymer film having uniform thickness of about 100 μm was prepared by casting the polymer solution on a glass plate. The film was uniaxially stretched to various draw ratio at 90℃. Birefringence was determined by measuring the optical path difference between parallel and perpendicular rays to the drawing direction.

Figure 1 shows the birefringence Δn ($= n_{//} - n_{\perp}$) of the poly(MMA-co-BzMA) film as a function of the draw ratio. Here $n_{//}$ and $n_{\perp}$ denote refractive indices parallel and perpendicular to the drawing direction, respectively. The drawn PMMA has a negative birefringence ($\Delta n < 0$), while PBzMA has a positive birefringence ($\Delta n > 0$). The value and the sign of birefringence were changed with varying the composition of copolymers. When the copolymer was synthesized at the composition of MMA/BzMA=82/18(wt./wt.), the birefringence became always zero in spite of any degree of draw ratio.

Since the birefringence is compensated in the scale of only several monomer units on polymer chain, this copolymer causes no birefringence for any orientation of polymer chain in injection molding. Figure 2 shows photographs of PMMA and poly(MMA-co-BzMA) plates (3.2 mm thickness and 12.5 mm width) prepared by the injection molding, which were placed between crossed polarizers. The birefringence Δn of the PMMA (a) is -2.16×10^{-5}, while the Δn of the poly(MMA-co-BzMA) is almost zero.

The light scattering measurement was done to quantitatively investigate the isotropic and anisotropic scattering loss of the birefringence-free copolymer. Details of the light scattering measurement have been shown in Refs. 3) and 4).

Table 1 shows the scattering parameters for the copolymer samples. The α_1^{iso} means the scattering loss of the isotropic scattering, while the α^{aniso} means that of anisotropic one. The total scattering loss α_{total} is the sum of α_1^{iso} and α^{aniso}. It is noteworthy that the α_{totai} of the birefringence-free poly(MMA-co-BzMA) is 30.4 dB/km and is competitive with those of the homopolymers.

POLARIZATION PRESERVING PROPERTIES of POF

The novel polarization preserving graded-index (GI) POF is proposed. The GI preform was prepared by the interfacial-gel copolymerization[5] of MMA and BzMA (MMA/BzMA=82/18 (wt./wt.)). The refractive-index distribution of the preform is shown in Figure 3. The GI preform was heat-drawn into the GI POF having a diameter of 0.5 mm at 210℃.

The polarization preserving properties of different types of POFs are shown in Figure 4 in which the linearly polarized He-Ne laser beam was injected into the POF. The abscissa indicates the angle between the directions of two polarizer located at input and output sides of the POF, respectively, and the ordinate shows the output intensity through the fiber. In the case of the step-index (SI) POF commercially available, the output intensity is almost independent of angle through

0° to 180°, which means that the linearly polarized incident beam became random polarization at output. The main factors of the depolarization through the SI POF were due to both the birefringence inside core and the reflection at core-cladding boundary. The MMA-BzMA SI POF and the PMMA GI POF could not also preserve the polarization phase due to reflection or birefringence. On the other hand, the MMA-BzMA GI POF almost could preserve the incident polarization with the same length. Namely, the output intensity at 90° angle in Figure 4 is almost zero. The MMA-BzMA GI POF has a small birefringence distribution because of the refractive-index distribution inside a core region. However, since rays passing through the GI POF has sinusoidal trajectories, the phase retardation is almost compensated by transmitting in both positive and negative birefringent regions. The extinction ratio of the MMA-BzMA POF was 18.2 dB, while the SI POF had the extinction ratio of 0.7 dB.

CONCLUSIONS

The birefringence-free copolymer could be prepared by randomly copolymerizing positive and negative birefringent monomers. The total scattering loss of the birefringence-free poly(MMA-co-BzMA) was 30.4 dB/km and superior to polymer blends in transparency. As one application of the birefringence-free copolymer, we proposed the multi-mode polarization preserving GI POF by utilizing the interfacial-gel copolymerization. It was noteworthy that the MMA-BzMA GI POF almost could preserve the incident polarization phase through the 50-cm fiber, although the polarization phase became almost random in the case of the PMMA SI POF with the same length.

REFERENCES

1) B. R. Hahn, and J. H. Wendorff, *Polymer*, 26, 1619(1985)

2) H. Saito, and T. Inoue, *J. Polym. Sci. Part B*, 25, 1629(1987)

3) N. Tanio, Y. Koike, and Y. Ohtsuka, *Polymer Journal*, 21, 3, 259(1989)

4) Y. Koike, S. Matsuoka, and H. E. Bair, *Macromolecules*, 25, 4807(1992)

5) Y. Koike, *Polymer*, 32, 1737(1990)

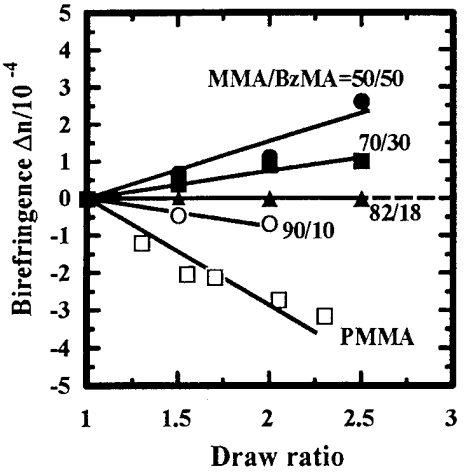

Figure 1 Birefringence of poly(MMA-co-BzMA).

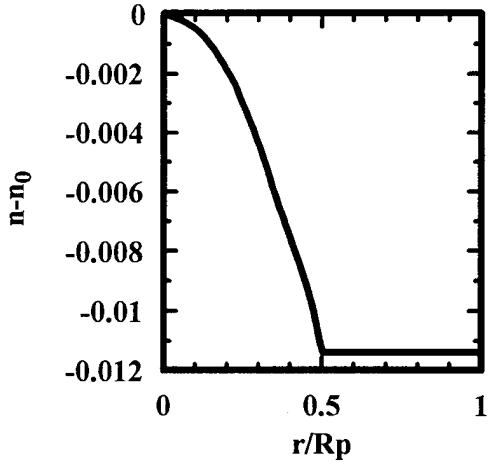

Figure 3 The refractive-index distribution of the (MMA-BzMA) GI POF.

Table 1 Scattering losses of polymers.

MMA/BzMA (wt./wt.)	α_1^{iso} (dB/km)	α^{aniso} (dB/km)	α_{total} (dB/km)
100/0	7.5	4.7	12.2
80/20	20.0	10.4	30.4
0/100	7.8	45.1	52.9

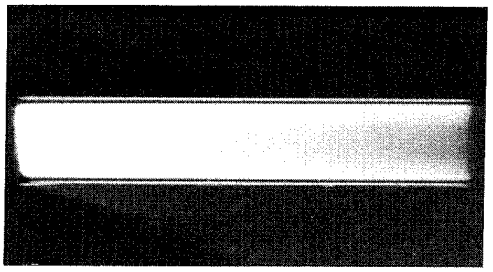

(a) PMMA

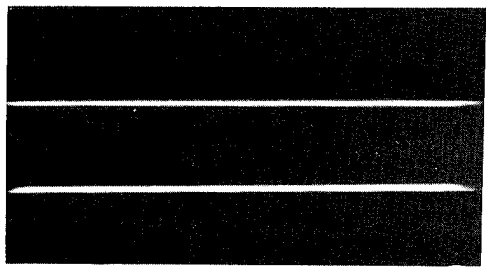

(b) Poly(MMA-co-BzMA)

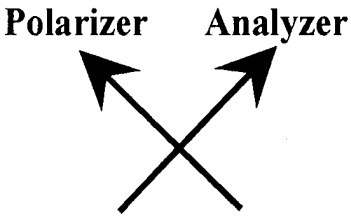

Figure 2 Photographs of injection molded polymers placed between crossed polarizers.

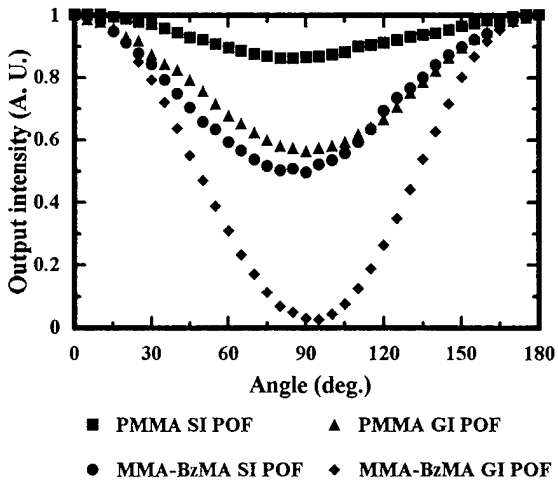

Figure 4 Polarization preserving properties of POFs. (Fiber length : 0.5 m)

Development Of Plastic Optical Fiber Devices and Multiple-Core Plastic Optical Fibers

Aruna R. Nagarur, S. Gopalan and Carl W. Dirk
Department of Chemistry
The University of Texas at El Paso
El Paso, TX 79968
Tel: (915) 747-5964
Fax: (915) 747-5748

A vast amount of research has been done on optical fibers. Most of the work has been done on Glass optical fibers (GOFs). Much less has been done on Plastic optical fibers (POFs), and very little with regards to applications of nonlinear optics.[1] Plastic optical fibers are currently under intense investigation and are used for Local Area Networks (LAN), vehicular systems[2] and optical sensor applications. Though they have much greater losses than Glass optical fibers they display advantages with regard to easy fabrication, flexibility, porosity and permeability (sensors), optical modification by organic dyes and cost.

The preparation procedure for clad and unclad POF are reported, as well as their application to nonlinear optics and optical chemical sensing.

We also report here, possibly for the first time, a general and simple procedure for the preparation of multiple-core plastic optical fibers. By 'multiple-core', we mean a fiber which contains more than one waveguiding core in the same cladding matrix. Such a fiber is drawn as a single component, after first preparing a multiple-core preform. Multiple-core fibers offer the advantage of using a single macroscopic fiber structure to support several cores, each of which could serve a different function.

Preparation of Multiple-core Plastic Optical Fibers:

The making of plastic optical fibers involved the synthesis of the core and the cladding. The core was a copolymer made by bulk polymerizing 60 mole percent of methylmethacrylate (MMA) and 40 mole percent of styrene in test-tubes using ter-butyl peroxide (0.4 mole %) as the initiator and n-butanethiol (1 mole %) as the chain transfer agent, at a temperature of 85°C.

Nonlinear Optical cores:

Doping of squarylium dyes into the fibers has been done. Fibers of this type are currently under investigation at Washington State University for use as all-optical signal processing devices.

Cladding

The cladding was synthesized by bulk polymerizing MMA along with the initiator, ter butyl peroxide (0.4 mole %) and the chain transfer agent, n-butanethiol (1 mole %) in an apparatus that was custom designed in our lab. The apparatus is shown in figure 1 below. It consisted of a thick-walled, four feet long pyrex glass tube. Two neckings were performed on the

tube with a distance of 30" between them. Two plugs held the teflon wire(s) firmly under tension. The tube was sealed at one end. The procedure for polymerizing the monomer involved systematically polymerizing short depths of the monomer, then adding more monomer, and simultaneously lowering the reaction tube into an oil bath maintained at 85°C to polymerize and densify that section of monomer. By short depths, we mean that as long as the diameter of the tube was atleast 1/3 the depth of the unpolymerized monomer, densification occurred smoothly with no void formation. If the length of the unpolymerized monomer was increased even by twice the length, void formation was observed. So, therefore polymerization of long lengths (30") of the monomer could not be carried out as it resulted in a preform that had a lot of voids. The problem was that the polymer was ca. 30% denser than the monomer, so that over the course of the neat polymerizations, polymer viscosity eventually prevented polymer flow to allow voids to collapse and close. The new procedure for synthesizing the cladding preform took about 20-30 days. The preform was obtained by breaking open the glass tube.

Synthesis of the core and POF preforms:

The core was baked in a squeezer-clamp designed in our lab, for a week at 120°C to remove moisture and bubbles trapped during the course of the polymerization. The preform was then drawn in the fiber drawing tower to the required diameter, to fit into the channel(s) in the cladding. The preform, consisting of the core fiber surrounded by the cladding was then baked in a 15/32" squeezer clamp at 120°C to fuse the core to the cladding..

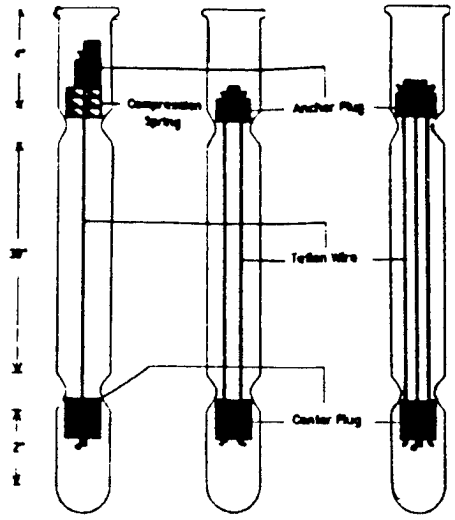

A schematic view of the single-core, dual-core and triple-core polymerization reaction vessels.

FIG-1

Fiber drawing:

The preform, approximately 0.5" in diameter, is then fed into the tube oven of the fiber drawing tower. The required diameter of the fiber was drawn by setting the speed of the take-up spool and the speed at which the preform is lowered into the oven appropriately.

Analysis of the polymers:

The glass transition temperature of the polymer preforms and fibers were analyzed. The refractive index of the cladding was found to be 1.492 and that of the core was found to be 1.547.

The measurements of the refractive index were taken on an ellipsometer for the thin films of the polymers spun on silicon wafer. The POFs were examined under an optical microscope.

Plastic optical fiber chemical sensors:

The field of optical fiber sensors is broad and well developed with respect to Glass optical fiber sensors. Plastic optical fiber sensor work is much less well developed, and still in its infancy relative to silica glass optical fiber sensors. The main research area of plastic optical fiber sensors appears to be confined to chemical sensors[3,4,5]. Given our expanding capability at the manufacture of specialty POF structures, we undertook an investigation to evaluate our fibers for chemical sensing. This is to some extent a preliminary step in the eventual development of multiple-core fiber sensors or smart materials capable of sensing and signal processing. We report ammonia and carbon monoxide POF sensors that are based on measuring optical loss.

Ammonia Fiber sensor:

The sensing agent used in the detection of ammonia is Bromocresol Purple (BCP), an acid-type indicator. Ammonia fiber sensors using a copolymer (PMMA/PS-60/40) and a homopolymer (PMMA) have been made. In both cases, BCP was dissolved in the monomer mixture, and polymerized with 0.4 mole % of the initiator (ter butyl peroxide) and 1 mole % of the chain transfer agent (n-butanethiol). The rest of the procedure is as described for the synthesis of the cores. The concentration of BCP in the copolymer monomer mixture was 0.02 mole % and 0.01% in the homopolymer monomer mixture. Fibers having the copolymer core with BCP and PMMA cladding have been made. Clad and unclad fibers were tested for sensor capability. The sensor measurement setup is as shown in figure 2. The graph shows the detection of ammonia at 0.8M concentration (figure 3). The detection is indicated by a decrease in signal after the addition of ammonium hydroxide. Ammonia at 0.8M could be detected in less than 5 seconds. The reaction is considerably more fascile for aqueous solution than for gas phase measurements implying that water is involved. Response is slow, suggesting that more porous structures need to be made.

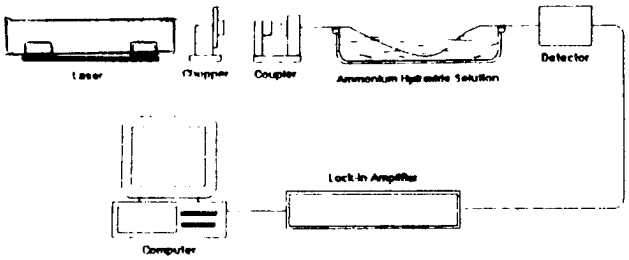

Experimental Setup
for Aqueous Ammonia Detection

FIG 2

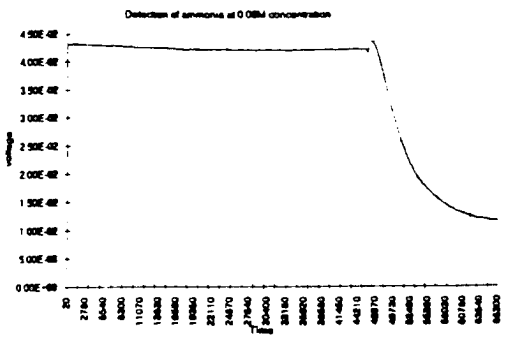

FIG. 3

Carbon monoxide fiber sensor.

The sensing agent used here is palladium chloride. Sensors using a copolymer(PMMA/PS-60/40) and a homopolymer (PMMA) were made. In both cases, Palladium

chloride was dissolved in the monomer mixture, and polymerized with 0.4 mole % of the initiator (ter butyl peroxide) and 1 mole % of the chain transfer agent (n-butanethiol). The rest of the procedure is as described for the synthesis of the cores. The concentration of Palladium chloride in the copolymer monomer mixture was 0.002 mole % and 0.01% in the homopolymer monomer mixture. Fibers having a copolymer core with palladium chloride and a PMMA cladding have also been made. The graph (Figure 4) shows the detection of carbon monoxide at 100% concentration. The chemical reaction involved the reduction of palladium chloride to metallic palladium and the oxidation of carbon monoxide to carbon dioxide. It is clear that the reaction is slow, necessitating structural modifications to future fibers.

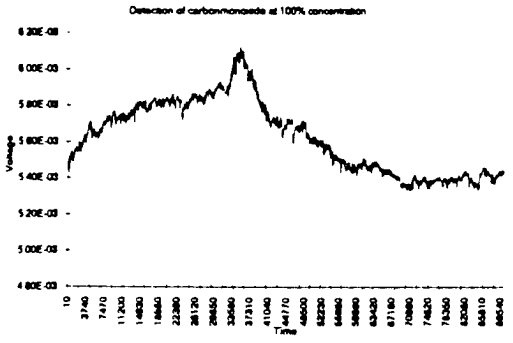

FIG. 4

Thermal studies and refractive index measurements of the sensor fiber materials have been done. Dual-core sensors having an ammonia sensing core and a carbon monoxide sensing core have also been made. These fibers are also currently under investigation.

Conclusions:

We have worked out a procedure to manufacture multiple-core POFs. This technology is new and the fiber structures are both new and an entirely unique development in POF research. Sensor development using multiple core fibers is underway. Nonlinear optical work using POF structures seems to offer some promise for all-optical devices. The use of multiple core fibers able to perform sensing, nonlinear optical processes, and signal processing offers a new avenue for the development of smart materials.

References:

1. M. G. Kuzyk U. C. Paek, C. W. Dirk *Applied Physics Letters*, ***59***, 902-904 (1991).
2. ***Plastic Optical Fibers and Applications***, **Vol. 25,** Information Gatekeepers Inc., Boston, Massachusetts (1994).
3. Zhou, Q and Sigel, G.H., *International Journal of Optoelectronics*, **4**, 415-423 (1989).
4. Zhou, Q *et al*, *Applied Optics*, **28**, 2022-2025 (1989).
5. Peterson, J.I. *et al*, *Analytical Chemistry*, **52**, 864-869 (1980).

Polarization Insensitive Crystalline Organic Waveguides

R.B. Taylor, Z. Shen and S.R. Forrest
Advanced Technology Center for Photonics and Optoelectronic Materials (ATC/POEM)
Department of Electrical Engineering
Princeton University
Princeton, NJ. 08544
Phone: 609-258-2856 Fax 609-258-1954

Interest in crystalline organic semiconductors has increased recently due to their diverse optical and electronic properties which have numerous device applications. Considerable effort has been focused on utilizing the large optical nonlinearities found in many of these materials.[1] One crystalline organic semiconductor: 3,4,9,10 perylenetetracarboxylic dianhydride (PTCDA), has been of particular interest due to its excellent electronic properties, giant dielectric anisotropies[2] and potential uses in optoelectronic devices. Recent research with PTCDA has yielded considerable success with waveguide structures.[3,4]. Special properties of PTCDA such as low optical absorption loss at near-infrared wavelengths, environmental stability, and capability of patterning make waveguide integrated devices and organic - semiconductor hybrid devices very attractive.

A few attempts to make organic crystalline waveguides have been reported using zone melting growth[5], filling the core of an optical fiber with an organic crystal[6], and by vapor deposition[7], but these types of organic crystalline waveguides have suffered from high scattering losses due to crystalline defects. Very low loss rib PTCDA waveguides (~ 2 dB/cm) were grown using organic molecular beam deposition (OMBD)[3], but these guides were not capable of guiding the TM polarization. TM polarizations are difficult to guide in PTCDA because of the very low index of refraction perpendicular to the film[2] ($n_\perp = 1.36$). A very low index ($n < 1.36$), patternable, and durable buffer layer is required to guide TM modes. TE polarizations are relatively easy to guide in PTCDA because the parallel index of refraction is high[2] ($n_\parallel = 2.017$) and many dielectrics have an index lower than this. TM polarizations, however are important for devices such as polarization splitters, modulators, and waveguide coupled detectors. In this work we report the first realization of low loss organic crystalline (PTCDA) rib waveguides which support both TE and TM polarizations.

The PTCDA waveguides were grown by OMBD in a method similar to [3]. Rib waveguides were fabricated on polished (100) InP substrates. The cladding layer consists of

approximately 2 μm of Teflon AF-1601S amorphous polymer (n = 1.31) spun directly on the InP substrate. A mask layer of SiO was evaporated onto the Teflon. A series of stripes with widths ranging from 2 μm to 50 μm and approximately 1 cm in length were photolithographically patterned onto the SiO layer. The Teflon film was dry-etched in an O_2 plasma at a pressure of 100 mTorr and an input power of 50 W. After etching, the SiO mask layer was stripped off. Vacuum deposition of PTCDA directly onto the Teflon surface does not produce continuous films, but the addition of the SiO layer results in high quality PTCDA crystalline films. Thus, a thin ~ 100 Å layer of SiO was evaporated onto the Teflon film to provide surface "wetting" for the PTCDA core layer. The thickness of the PTCDA guiding layer is approximately 0.7 μm. The InP wafers along with the guides were then cleaved along the (110) direction perpendicular to the guide axis orientation to facilitate end-fire coupling. An electron micrograph of a rib waveguide showing the top surface and the cleaved edge is shown in Fig. 1. The guide side walls are smooth and the cleaved edge of the PTCDA film is sharp.

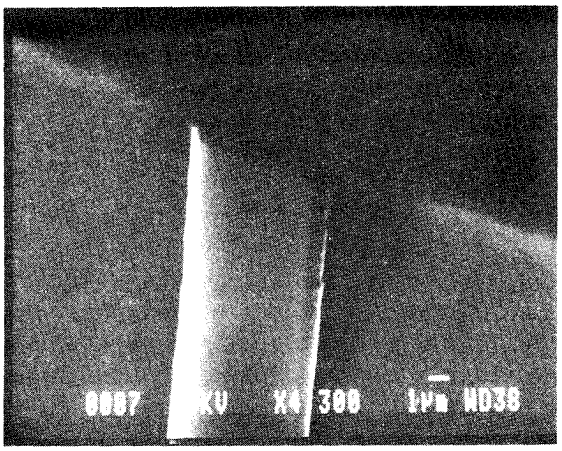

Figure 1 Electron micrograph of a PTCDA rib waveguide cross section

The output mode patterns from 5 mm long waveguides of various widths are shown in Fig. 2. Both TE and TM polarizations are supported by these guides. Here, nearly perfect TE_{00}, TE_{02} and TE_{03} -like modes as well as TM_{01}, TM_{03} and TM_{05} -like modes are clearly observed at the output of the guides. These modes exhibit very strong TE or TM-like characteristics. The relative contributions of the electric field components can be experimentally obtained by measuring the intensity of the output modes for x and y polarizations. The ratio, R, of these intensities describes the effective behavior of the mode, and is given by:

$$R = \sqrt{\frac{|I_y|}{|I_x|}}$$

Here I_x and I_y are the integrated intensities of the modes in the x and y directions, respectively. For R >> 1 the mode is effectively TE-like, and when R << 1 the mode is effectively TM-like. For R~1 the mode can be described as a mixed mode. Modal intensity experiments show the modes are either TE or TM-like for TE or TM incident polarized light. Average values for guide widths larger than 2 μm were R = 10, with the smallest ratio measured being R = 2.21 for TE incident

light on a 4 μm wide guide. R values generally decrease as the waveguide width is reduced, culminating in complete polarization rotation from TE into TM and from TM into TE in 2 μm waveguides. This is expected as the decreasing width changes the waveguides from guides with slab-like properties to guides with channel-like properties.

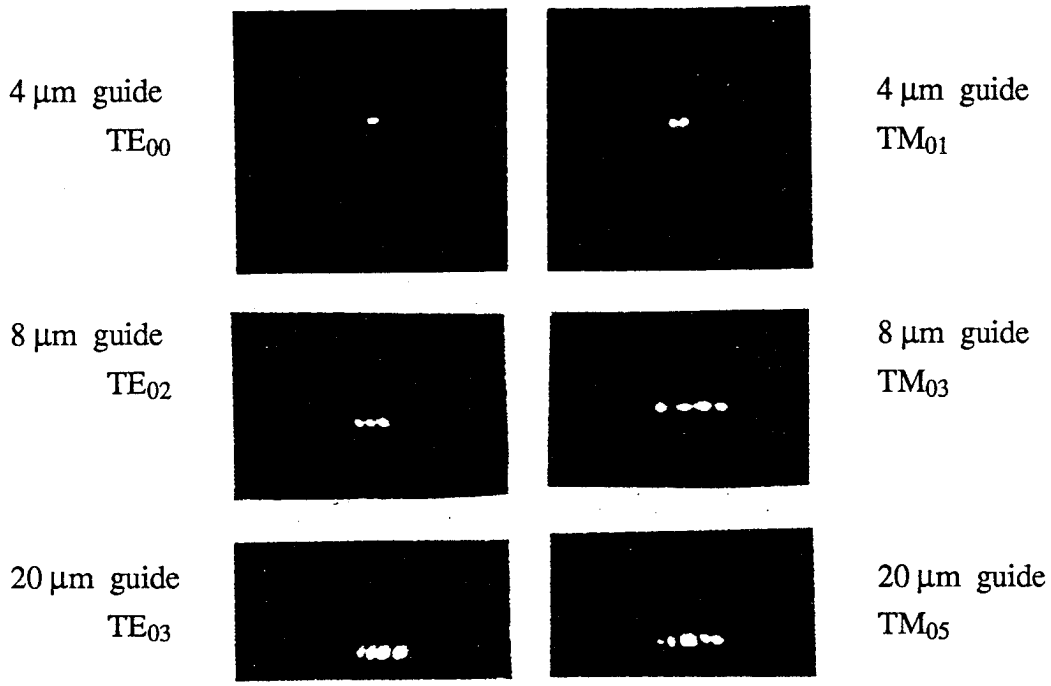

Figure 2 TE and TM modal patterns for various waveguides

Modal solutions for anisotropic waveguides have shown that pure TE or TM modes can only exist if the optical (c) axis of the crystal is aligned with the y axis of the waveguide or is in the x-z plane of the waveguide[8] (see Figure 3). For PTCDA films deposited in vacuum, the molecules form stacks so that the optical axis lies 11° from the waveguide x axis, but one would expect, a priori, that the orientation of the optical axis with respect to the z-axis of the waveguide is arbitrary. In such a case, mixed modes would dominate. However, the TE-like or TM-like nature of the modes in slab-like waveguides indicates that the c-axis is generally aligning with the x-z plane. This surprising preferential orientation of the c-axis with respect to the waveguide indicates that the structure of the film is being influenced by the patterned stripes during vacuum deposition.

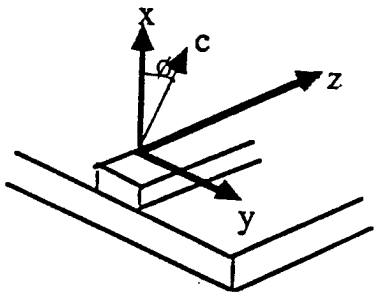

Figure 3 Waveguide and crystal axis

Waveguide losses were approximated by measuring the intensity of scattered light radiating from the top surface of the guide with a CCD camera and a profile analyzer. The intensity of scattered light from the top surface is assumed to be proportional to the intensity of light in the guide. By measuring the decay in intensity from the top scattered light, propagation losses of < 5 dB/cm were obtained for an incident wavelength of $\lambda = 1.064$ μm. Light that is scattered from both the front facet of the waveguide and the substrate will cause this measurement to overestimate the actual waveguide loss.

In conclusion, we have demonstrated polarization insensitive waveguiding in PTCDA channel waveguides on InP substrates. Propagation losses of < 5 dB/cm at $\lambda = 1.064$ μm were observed. Hybrid modes with strong TE-like or TM-like characteristics were observed indicating that the crystalline c-axis is generally aligned along the waveguides stripe during vacuum deposition. Such observations reveal a high degree of structural ordering in the PTCDA film.

The realization of these polarization-independent PTCDA waveguides is an important step toward achieving a variety of optical organic devices such as polarization splitters, modulators and waveguide coupled detectors. Such devices can be integrated monolithically with semiconductor optoelectronic devices (e.g., lasers and photodetectors) for uses in many applications including optical communications, optical computing, and optical information processing.

The authors thank AFOSR and ARPA for support of this work. We also thank P.E. Burrows for his helpful discussions.

References

1. D.S. Chemla and J.Zyss (eds.), "Nonlinear Properties of Organic Molecules and Crystals", *Academic*, NY, 1989.

2. D.Y. Zang, F.F. So, and S.R. Forrest, Appl. Phys. Lett., **59**, 823 (1991).

3. D.Y. Zang, Y.Q. Shi, F.F. So, S.R. Forrest and W.H. Steier, Appl. Phys. Lett. **58**, 562 (1991).

4. D.Y. Zang and S.R. Forrest, Appl. Phys. Lett., **60**, 189 (1992).

5. S. Tomaru, M. Kawachi, and M. Kobayashi, Opt. Commun., **50**, 154 (1984).

6. B.K. Neyer, 6th Topical Meeting opn Integrated and Guided Wave Optics, Tech. Dig., paper ThA2, January 6-8, 1982.

7. G.H. Hewig and K. Jain, Opt. Commun., **47**, 347 (1983).

8. W.K. Burns and J. Warner, J. Opt.Soc. Am., **64**, 441 (1974).

$\chi^{(3)}$

MC 1:30 pm-3:45 pm
Holladay Room

Carl Dirk, *Presider*
University of Texas at El Paso

Linear and Nonlinear Spectroscopy of β-Carotene and Other Oligo-polyenes: Experimental and Theoretical Studies

F. Rohlfing, D.D.C. Bradley*

Department of Physics and Sheffield Centre for Molecular Materials,

University of Sheffield, Hicks Building, Hounsfield Road, Sheffield S3 7RH, UK.

* tel: +44-114-276 8555 ext 4575, fax: +44-114-272 8079,

e-mail: D.Bradley@Sheffield.ac.uk

J. Cornil, D. Beljonne, J.L. Brédas,

Service de Chemie Des Materiaux Nouveaux, Université de Mons Hainaut,

Place du Parc 20, B-7000 Mons, Belgium.

A. Eberhardt and K. Müllen,

Max-Planck-Institute für Polymerforschung, Ackermann Weg 10,

Postfach 3148, 55021 Mainz, Germany.

We report studies of linear- and electro-absorption spectra which allow new insights into the electronic structure of polyenes and their nonlinear response.

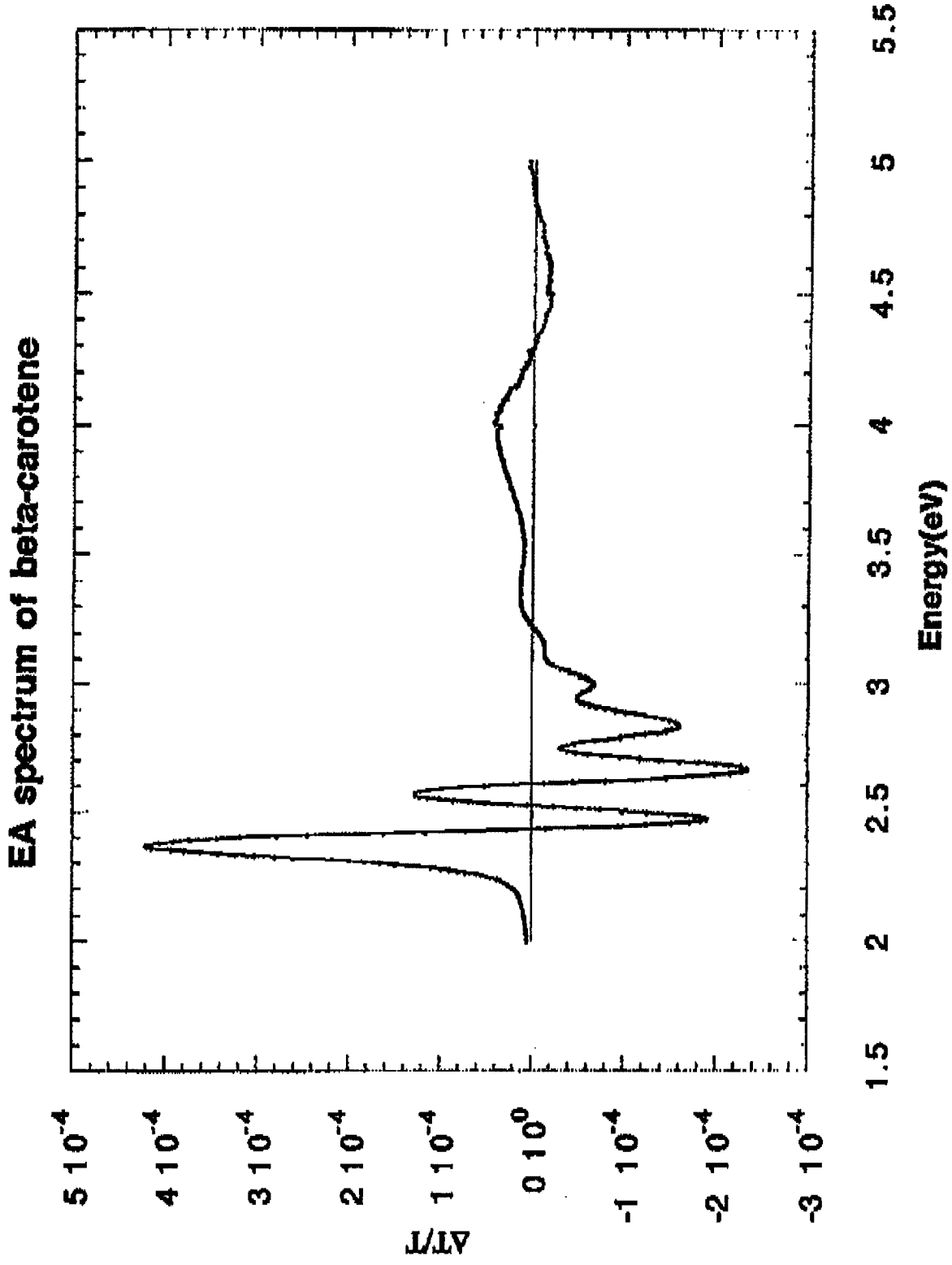
EA spectrum of beta-carotene
ΔT/T
5 10^-4
4 10^-4
3 10^-4
2 10^-4
1 10^-4
0 10^0
-1 10^-4
-2 10^-4
-3 10^-4
1.5
2
2.5
3
3.5
4
4.5
5
5.5
Energy(eV)

LARGE ENHANCEMENT IN THE THIRD ORDER RESPONSE OF ASYMMETRIC β-CAROTENOÏDS

Vincent Ricci, William E. Torruellas, George I. Stegeman
C.R.E.O.L., University of Central Florida
12424 Research Parkway, Orlando, FL 32826
tel.: 407 - 658 3918

Sandra Gilmour, Seth Marder
California Institute of Technology
Jet Propulsion Laboratory
4800 Oak Grove Drive
Pasadena, CA 91109

Mireille Blanchard-Desce
Collège de France
11, Place Marcelin Berthelot
75005 Paris, France

Trans-β-Carotene shows one of the largest instantaneous off-resonant nonlinearities reported to date.[1] Increasing the electron conjugation with longer back bones, polymers, has been the most common approach to enhance such a nonlinear optical response[2]. However it has been recognized that molecular asymmetrization represents another viable route for increasing the third order susceptibility without having to pay a price for smaller molecular densities, an increased molecular instability and poor solubility[3]. Here we report an enhancement of approximately a factor of 50.

In addition to trans-β-carotene, we have investigated a family of six carotenoïds with a single acceptor being attached to one end of trans-β-carotene. As an example we show our spectroscopic third harmonic generation results for one of the carotenoïds, Fig.1. The transition dipole moment and the mesomeric moment increase with the amount of assymetrisation represented by the shift of the peak wavelength of the so-called charge transfer band and account with the latter for the observed enhancement shown in Fig.2. Note the seventh power dependence on the peak wavelength of the CT band predicted by Perry and his coworkers.

The magnitude of the third order susceptibility was taken at the peak of the measured nonlinear dispersion curve of 4% molar loading in PMMA thin films. In the case of the molecule with the largest susceptibility, increasing its present loading fraction to the commonly 40% found in side chain polymers, would result in a disordered polymer with one of the largest third order nonlinear responses known to us.

to the commonly 40% found in side chain polymers, would result in a disordered polymer with one of the largest third order nonlinear responses known to us.

References

1) J.P. Hermann, J. Ducuing, *J. Appl. Physics.*, **45**, 5100 (1974).
2) K.H. Haas, A. Ticktin, A. Esser, H. Fisch, J. Paust, W. Schrof, *J. Phys. Chem.*,**97**, 8675 (1993).
3) A.F. Garito, J.R. Heflin, K.Y. Wong, O. Zamani-Khamiri, *In Organic Materials for Nonlinear Optics: Royal Society of Chemistry Special Publication*, **69**, 16 (1989), Ed. R.A.Hann and D. Bloor.

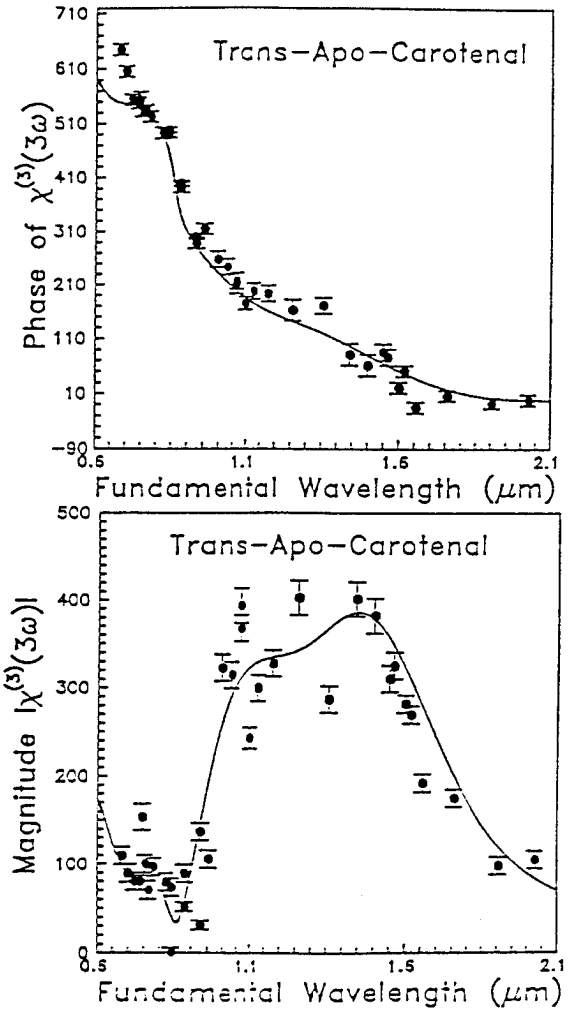

Figure 1:

Third harmonic generation spectrum, magnitude and phase, of trans-β-apocarotenal. The filled circles are the measured third order susceptibilities of 4% doped PMMA thin films. The solid line is a best fit to a two excited-state model.

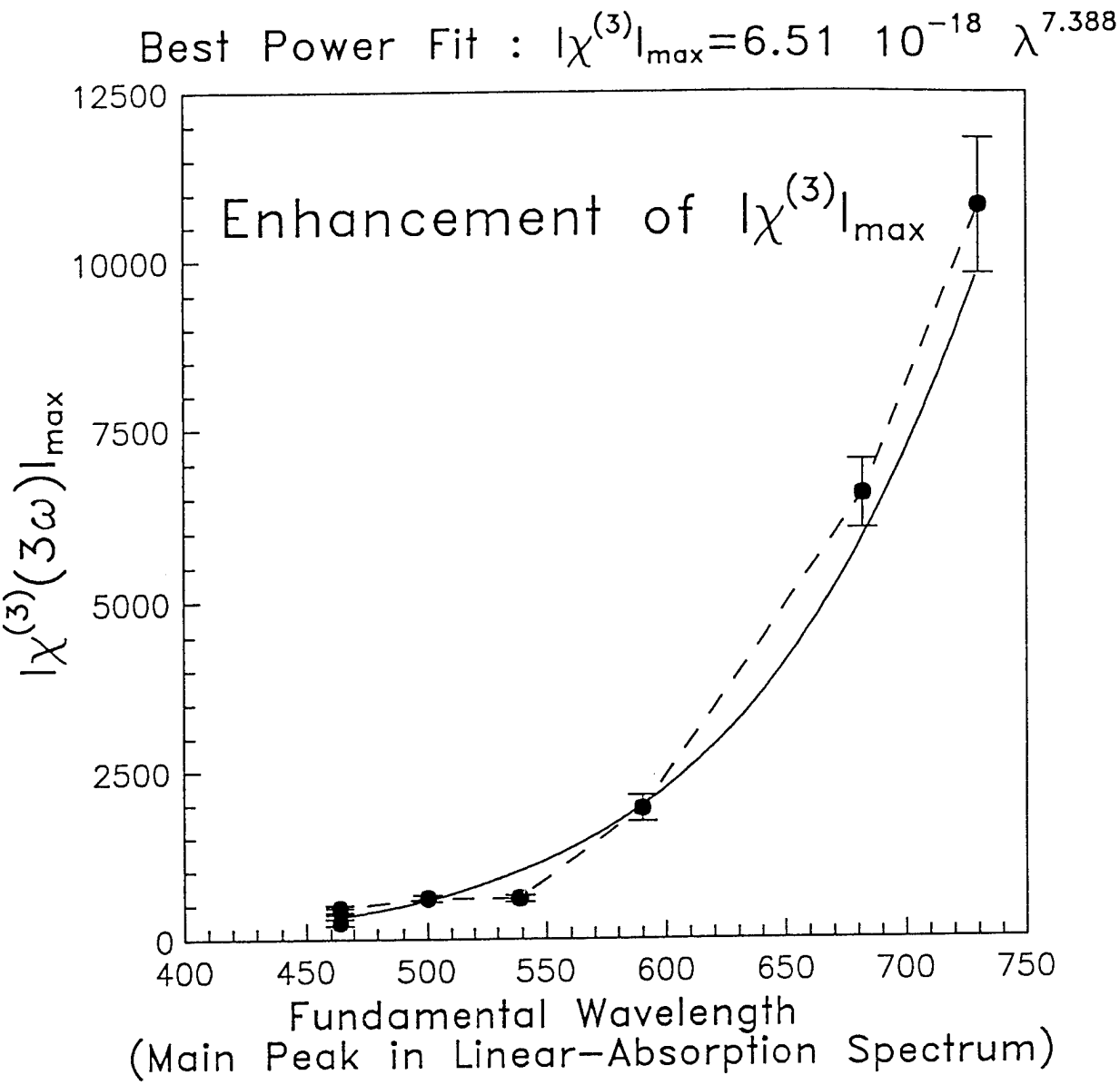

Figure 2:

Enhancement of the third order susceptibility versus the position of the peak of the CT band. The amplitude of the third order response was taken at the peak value of THG spectra.

ELECTRONIC AND NONLINEAR OPTICAL PROPERTIES OF ORGANIC MOLECULES: ASSESSMENT OF THE INFLUENCE OF THE MOLECULAR STRUCTURE

Fabienne Meyers,[a,b] Chin-Ti Chen,[b] David Beljonne,[a] Jean-Luc Brédas,[a] and Seth R. Marder,[b,c]

a: Université de Mons-Hainaut, Place du Parc 20, B-7000 Mons, Belgium.

b: The Beckman Institute, California Institute of Technology, Pasadena, CA 91125.

c: The Jet Propulsion Laboratory, California Institute of Technology, Pasadena, CA 91109.

In a previous work, using computational approaches, we analyzed how the polarizability, α, second-order polarizability, β, and third-order polarizability, γ, are controled by the ground state polarization [1-4]. To do so, we investigated the influence of an external, static electric field upon the nonlinear optical (NLO) properties, for a set of push-pull polyenes [1]. The calculated effect of the external electric field on the molecular structure and electronic properties of the chromophores is similar to that resulting from donor-acceptor substituents on a segment of the chromophore, or from changing the dielectric properties of the environment around the molecule, *e.g.*, increasing the polarity of the solvent. The structure/properties relationships derived from that study are summarized in Figure 1, and have allowed us to propose chemical design prescriptions for the optimization of second- and third-order optical nonlinearities in organic molecules [3].

In the present work, we aim at extending the range of validity of our analysis regarding these structure/NLO properties relationships, by focusing on molecules that display a two-directional $D^+ \rightarrow A^- \leftarrow D^+$ (D for donor and A for acceptor) configuration, the squaraine dyes; the molecular structure of such dyes is, for example:

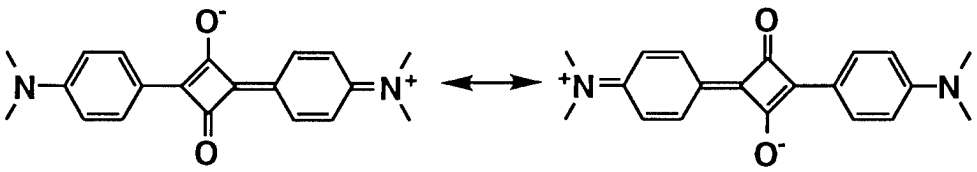

These canonical resonance structures may be, in fact, compared to those describing the underlying straight-chain polymethine cyanine:

With respect to Figure 1, the squaraine and cyanine molecules may be related to a push-pull polyene in its so-called cyanine limit, *i.e.*, where the bond-length alternation is zero; in this case, there occurs an equal mixture of two the degenerate resonance forms that results into a non alternating polyene structure for the cyanine and an equivalent form for the squaraine. Such molecules are known to show negative third-order nonlinearities [5-7], which is consistent with the structure/NLO properties relationships presented earlier, and that can be rationalized within the simple three-term model [2,5,8,9] derived from static perturbation theory.

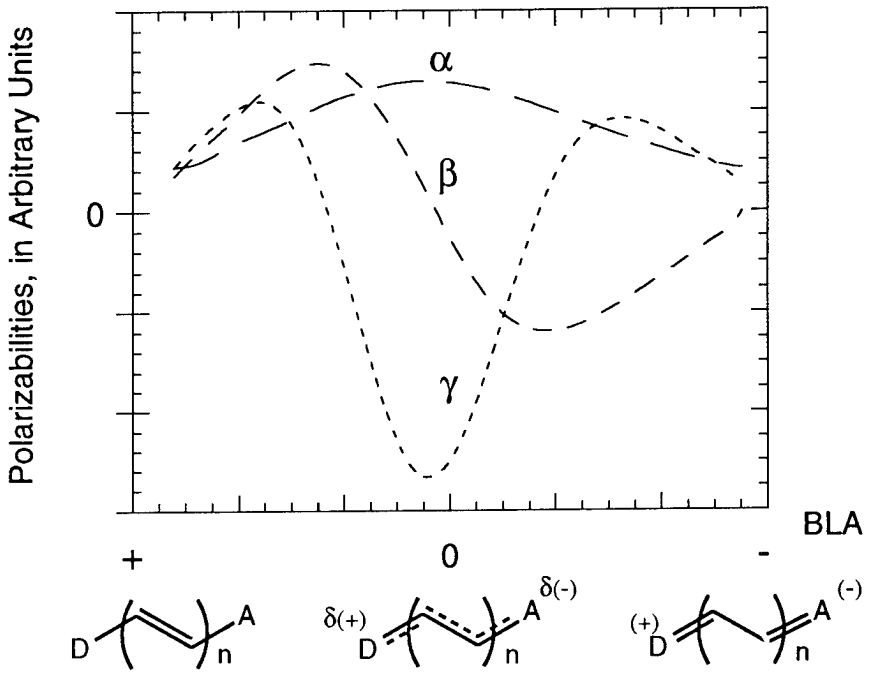

Figure 1: Qualitative evolutions of the polarizabilities α, β, and γ (in arbitrary units), as a function of the ground-state polarization, translated in terms of bond-length alternation, BLA, for a generic push (donor, D) / pull (acceptor, A) polyene.

The questions that we will address are: (i) How realistic is a three-term model expression to describe the third-order NLO properties of such bidirectional dyes? (ii) What are the relative

contributions of the first and/or higher excited states to the NLO response? (iii) What is the relevant structural parameter, that could be used in a way comparable to the bond-length alternation, BLA, in polymethines?

Moreover, we will present an analysis of the geometric and electronic structure of unsymmetric squaraines, implying substitution by two different donor groups instead of two dimethyl-amino groups, as depicted above. Indeed, unsymmetric squaraine dyes have been lately considered as a new class of compounds for second-order NLO properties [10,11]. Again, if one refers to the evolution of β as function of BLA (Figure 1), it can be seen that β is maximum for an intermediate structure, between the polyene- (where BLA is positive) and cyanine- (where BLA is zero) limits. For push-pull polyenes, the usual approach to optimize β, *i.e.*, by increasing the strength of the donor and acceptor substituents, corresponds to following the left part of the β-curve starting at the polyene-limit and continuously increasing β. Our approach is opposite here since rather than starting near the polyene limit and decreasing the magnitude of BLA by searching for stronger donors or/and acceptors, we consider optimizing β by introducing asymmetry into highly polarizable cyanine-like structures. From an experimental point of view, this alternative strategy has already been successfully applied [10,11]. A theoretical study may provide a generalized picture of the structure/properties relationships, and therefore allow for a fine tuning of the hyperpolarizabilities by controling the molecular structure of organic compounds other than substituted polyenes.

Finally, we will present a theoretical analysis of the influence of substitutions on the geometric and electronic structure of polyenes [12]. The calculations performed in this study include an extended configuration interaction technique coupled to an Intermediate Neglect of Differential Overlap (INDO) Hamitonian to describe the lowest excited states [13]. Based on these excited states, the sum-over-states formalism provides an estimate of the linear and nonlinear molecular polarizabilities [14] of various substituted polyenes, such as those sketched below:

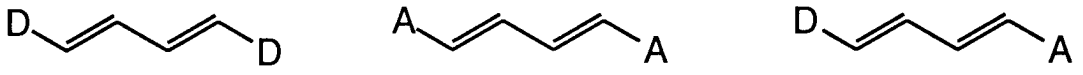

where the donor group D is either NH_2, OH, or NMe_2, and the acceptor group A is either CHO, CN, or NO_2.

We will compare the effect induced by the end groups attached to the conjugated segment on the NLO properties. Focusing mainly on the description of the third-order polarizability, it

appears that compared to a bisdonor-substituted butadiene, a bisacceptor compound leads to a stronger enhancement [12,15]. On the other hand, when looking at the chain-length dependence, evolving from a substituted butadiene to decapentaene, the bisdonor polyenes appear to be more promising candidates in order to achieve large nonlinearities in longer chains [12,16]. These results are in agreement with those from the experimental study of Pucetti *et al.* [17]. We will also provide an overall description of the evolution upon substitution, of these excited states of the D/D, A/A, and D/A polyenes, that are important in the NLO processes.

References:

[1] F. Meyers, S. R. Marder, B. M. Pierce and J. L. Brédas, *J. Am. Chem. Soc.*, 1994, **116**, 10703.
[2] F. Meyers, S. R. Marder, B. M. Pierce and J. L. Brédas, *Chem. Phys. Lett.*, 1994, **228**, 171.
[3] S. R. Marder, C. B. Gorman, F. Meyers, J. W. Perry, G. Bourhill, J. L. Brédas and B. M. Pierce, *Science,* 1994, **265**, 632.
[4] C. B. Gorman and S. R. Marder, *Proc. Natl. Acad. Sci. U.S.A.*, 1993, **90**, 11297.
[5] C. W. Dirk, L. T. Cheng and M. G. Kuzyk, *Int. J. Quantum Chem.*, 1992, **43**, 27.
[6] C.W. Dirk, W.C. Herndon, F. Cervantes-Lee, H. Selnau, S. Martinez, P. Kalamegham, A. Tan, G. Campos, M. Velez, J. Zyss, and L.-T. Cheng, *J. Am. Chem. Soc.*, 1995, **117**, 2214.
[7] Y.Z. Yu, R.F. Shi, A.F. Garito, and C.H. Grossman, *Optics Lett.*, 1994, **19**, 786.
[8] B. M. Pierce, *Proc. SPIE-Int. Soc. Opt. Eng.*, 1991, **1560**, 148.
[9] A. F. Garito, J. R. Heflin, K. Y. Wong and O. Zamani-Khamiri, *Proc. SPIE-Int. Soc. Opt. Eng.*, 1988, **971**, 2.
[10] C. T. Chen, S. R. Marder and L. T. Cheng, *J. Am. Chem. Soc.*, 1994, **116**, 3117.
[11] C. T. Chen, S. R. Marder and L. T. Cheng, *J. Chem. Soc. - Chem. Commun.* , 1994, 259.
[12] D. Beljonne, F. Meyers, and J.L. Brédas, submitted for publication.
[13] J. Ridley and M. Zerner, *Theoret. Chim. Acta (Berlin)*, 1973, **32**, 111 ; R.J. Buenker and S.D. Peyerimhoff, *Theoret. Chim. Acta* , 1974, **35**, 33.
[14] B.J. Orr and J.F. Ward, *Mol. Phys.*, 1971, **20**, 513.
[15] F. Meyers and J.L. Brédas, *Synth. Met.*, 1992, **49**, 181.
[16] F. Meyers and J.L. Brédas, in "Organic Materials for Non-linear Optics III", G.J. Ashwell and D. Bloor, eds., (Royal Society of Chemistry, London, 1993), pp. 1-6.
[17] G. Puccetti, M. Blanchard-Desce-M, I. Ledoux, J.M. Lehn, and J. Zyss, *J. Phys. Chem.*, 1993, **97**, 9385.

Organic Thin-Films For Spatial Light Modulation

Jean-Michel Nunzi, Stephane Delysse, Nicola Pfeffer and Fabrice Charra
Groupe Composants Organiques,
LETI (CEA - Technologies Avancées)
CE Saclay, F91191 Gif sur Yvette, France
phone: 33 1 69086812
fax: 33 1 69087679
internet: nunzi@serin.cea.fr

In the field of image and beam processing, there is great need for devices in which a spatial light-intensity profile such as an image can be recorded and transformed into a transmission or a phase retardation profile. A solution in order to process a still increasing volume of information issued from sensors and data banks is indeed to treat it in parallel. And as information is often available as optical images, a simple idea is to pre-process or to compress it prior to acquisition. This is performed using correlation or novelty filtering techniques [1]. A key device in this respect is the optically addressed spatial light modulator (SLM) [2]. It permits the achievement of input functions in optical image processors based on holographic and Fourier optics. The principle of the SLM process is the same as with the more classical silver-halide photography, except that SLM must perform real-time operations. The drawback of silver-halide photography is indeed the delay, larger than a minute, between exposure and processing. Different techniques, with commercially available devices, already permit the achievement of real-time spatial light modulation. They use a juxtaposition of photoconductor and liquid-crystal films in an artificial photorefractive-like sandwich [3]. However, operation with typical pixel densities of $1\mu m^2$, beam surfaces of $1cm^2$ and processing speeds larger than 100MHz is far from being realised with commercial SLMs. It is the reason for considering the performances offered by organic thin films in this respect [4].

SLM performances may be characterized by the minimum pixel surface, the exposure sensitivity per pixel (in pJ/px), and the switching time. For several applications, a target performance for an optimized SLM would be sub-μm^2 pixels with sub-pJ/px sensitivity and sub-μs response time. For the comparison, the xerographic process could be used for SLM with typically $10\mu m^2$-pixel size, 0.5pJ/px exposure sensitivity and a minimum 0.1s-*switching* time [5]. With liquid-crystal light valves, pixel size is typically $10\mu m^2$, exposure sensitivity 5pJ/px, and switching time 1ms. However, the major drawback with *classical* SLMs is not with switching time, but with spatial resolution which permits poor holographic processing capability. Indeed, in order to fully exploit the parallel addressing capabilities of light, an optimized SLM should have a spatial resolution limited by diffraction. This limits the maximum thickness t of the device to an optical wavelength; that is $t \approx 1\mu m$. That is the main reason for using organic thin films in order to optimize SLM performances and to fully exploit the parallel processing capabilities of light beams.

For an SLM to give a high contrast ratio in transmission, or a high efficiency in diffraction, the complex phase retardation $\delta\varphi = 2\pi\delta nt/\lambda$ induced inside the sample must exceed 1. With a thickness $t=\lambda$, this corresponds to a complex index change as large as $\delta n=0.2$. No such index change can be achieved in materials without use of resonant nonlinearities. For instance, the large nonlinear *cascading* phase-retardation reported in organic single-crystals corresponds to $\delta n \approx 2\times10^{-3}$ [6], and the 210cm^{-1}-net gain obtained in *photorefractive* polymers corresponds to $\delta n \approx 5\times10^{-3}$ [7]. Additionally, optimization of the exposure sensitivity imposes severe restrictions on useful materials. For instance, for third-order $\chi^{(3)}$-materials to switch with less than 1pJ/μm^2 energy, their figure of merit $\chi^{(3)}/\tau$ must exceed 10^{-3} m^{2}V^{-2}s^{-1} $\approx 10^5$ *esu*. Obviously, such magnitude corresponds to resonance with optical transitions [4]. It can be achieved with *photochromic* materials in which resonant excitation brings molecules with high quantum efficiency into a metastable state from which an excited state transition with large oscillator strength permits efficient beam modulation. Molecular engineering rules of such photochromic have been defined in order to optimize molecules for sub-nanosecond switching times [8]. The key feature of optimized molecules was identified as a spectral narrowing of excited state transitions, leading to excited state absorption cross sections σ larger than 10^{-15}cm^2. The phenomenon was initially identified in thiophene oligomers [9]. It was named *spectral concentration*. It can be reproduced in several polyene-like poly-aryl oligomers whose photoinduced absorption energies are displayed in Figure 1 [10]. Spectral norrowing of excited state transitions with respect to ground state transitions in those oligomers ranges within a factor 4 to 5. It induces amplification of the absorption cross section in the same proportions.

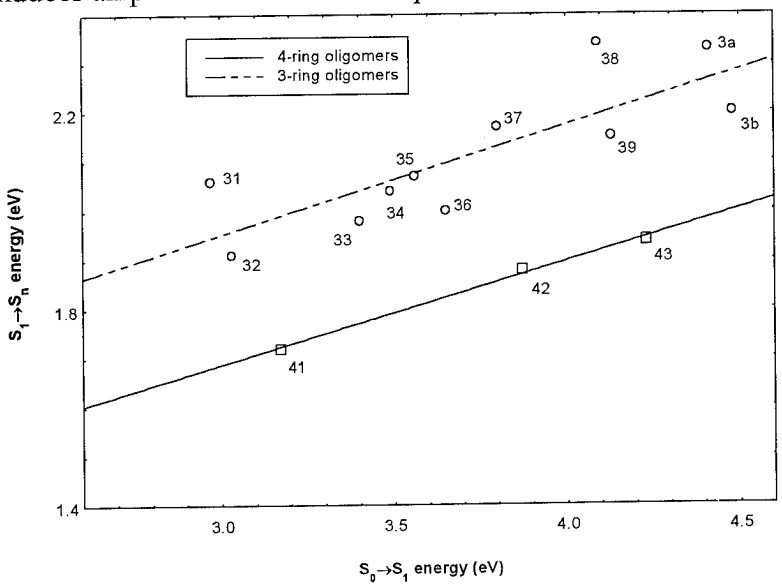

Figure 1: Photoinduced singlet state transition energies of 3-ring (circles) and 4-ring oligomers (squares), as a function of ground state transition energies. Slope of fitted lines is 1/4.5. Oligomers are: dibutylaminonitrostilbene in paraffin oil (31), αα'-dibromo,ω-nitroterthiophene in cyclohexane (32), αω-dibromoterthiophene (33), terthiophene (34), bithienylbenzene (35), dithienylethylene (36), biphenylthiophene (37), diphenyloxazole (38), stilbene (39), diphenyloxadiazole (3a), terphenyl (3b) and quaterthiophene (41), biphenylbutadiene (42), quaterphenyl (43).

High modulation efficiency can also be achieved with saturable absorbers. They indeed have a large SLM figure of merit. We have studied saturable absorbing dyes in the 1064nm-wavelength domain using the picosecond *Kerr ellipsometry* technique. In the case of the Kodak-IR5 dye, SLM figure of merit is $\chi^{(3)} / \tau = 2 \times 10^{-2}$ $m^2V^{-2}s^{-1}$. The spectral dispersion of the real and imaginary parts of the nonlinear index of refraction measured in the 0.9-1.3µm wavelength domain for the Bis(4-diethylaminodithiobenzil)nickel (BDN) dye dissolved into a PMMA matrix is reported in Figure 2. We can observe transient hole-burning features above 1064nm-wavelength. Relaxation (switching) time is 6ns. Quenching of the nonlinearity takes place at higher concentrations.

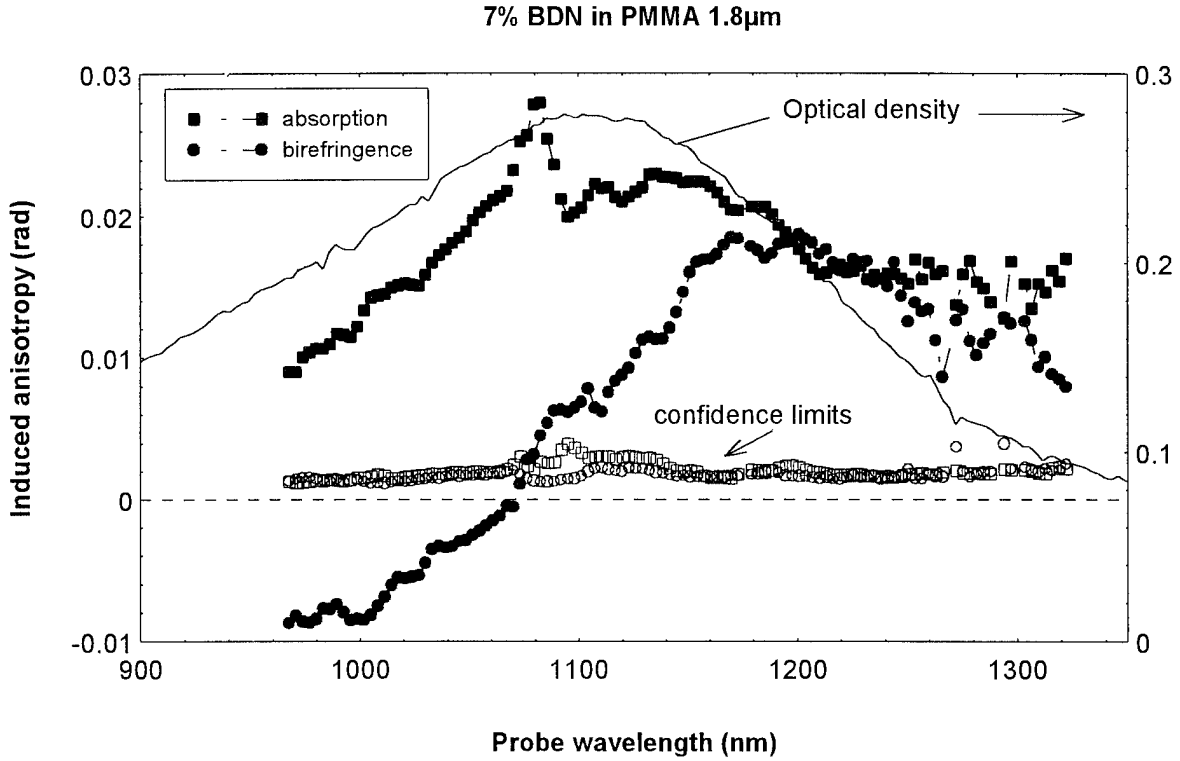

Figure 2: Dispersion of the nonlinear absorption (full squares) and refraction (full circles) phase retardations measured under saturable absorption conditions with picosecond excitation at 1064nm in a PMMA film doped with BDN-dye. Open squares and circles represent 70% confidence limits.

As an application, using micrometer thickness spin-coated polymer films, Q-switching of a compact diode-pumped Nd-YAG microlaser was demonstrated. The laser provides stable and reproducible 2.5µJ pulses with less than 700ps duration at 15KHz repetition rate under continuous pumping conditions [11]. Power fluence inside the laser cavity is 0.4GWcm^{-2}.

In order to demonstrate the possibility of handling information with diffraction limited pixel density in organic thin-films, we performed a real-time holography experiment under large F/1 aperture angle conditions. The holographic exposure source was a continuous argon ion laser delivering 500mW power at the green 514nm-wavelength. It was splitted into two equal parts

using a roof prism. The first part crossed a transmission object and the interference pattern between the two parts was recorded by the SLM. The useful hologram size was $4cm^2$. The SLM was made with 10%-(w) DR1-dye doped into a PMMA matrix. A 4μm thickness film was spin-coated from a chlorobenzene solution onto a 5cm diameter BK7-glass plate. Its optical density at 514nm was 1.6. Holographic readout using the 633nm red output of a He-Ne laser permitted real-time holography monitoring with $\approx 0.1s$ switching time. The diffraction limited pixel density performance is demonstrated by the large $\approx 45°$ viewing angle with which the hologram is recorded. It corresponds to a $\approx 1\mu m$-pixel size (fringe pitch). The photochromic process with DR1 is a succession of *trans-cis* isomerization cycles which induce a net molecule reorientation [12]. Such SLM can be used continuously during days without apparent damage. The SLM is not optimized as concerns exposure sensitivity but it approximately 50 times better than classical photochromic molecules such as the nitro-BIPS spiropyran-dye [4].

The realization of organic SLMs using thin-films in which optical modulation is achieved on a molecular scale opens the door to devices for the processing of large quantities of parallel information or complex images. As organic materials have an ultrafast response time and typical room temperature triplet relaxation times in the μs range, their resonant third order optical nonlinearity opens the door to optical image processing above MHz frequency rates. With their processing ease and chemical tailoring capability, organic films may play a significant role in the field of image and optical beam handling. A molecular engineering strategy is being currently developed for the optimization of photchromic nonlinear optical materials for spatial light modulation.

[1] A. Vanderlugt, *Optical signal processing*, Wiley (New York, 1992).
[2] C. Warde and A.D. Fisher, in *Optical signal processing*, J.L. Horner (ed.), Academic, p.477 (New York, 1987).
[3] J. Grinberg, A. Jacobson, W. Bleha, L. Miller, L. Fraas, D. Boswell, G. Myer, *Opt. Eng.* **14**, 217 (1975).
[4] J.M.Nunzi and F.Charra, *Nonlinear Optics* **10**, 447 (1994).
[5] W. Gerhartz, *Imaging and information technology*, VCH (Weinheim, 1992).
[6] D.Y. Kim, W.E. Torruellas, J. Kang, C. Bosshard, G.I. Stegeman, P.Vidakovic, J. Zyss, W.E. Moerner, R. Twieg and G. Bjorklund, *Opt. Lett.* **19**, 868 (1994).
[7] K. Meerholz, B.L. Volodin, Sandalphon, B. Kippelen and N. Peyghambarian, *Nature* **371**, 497 (1994).
[8] J.M. Nunzi, F. Charra and N Pfeffer, *Journal de Physique III* **3**, 1401 (1993).
[9] D. Fichou, J.M. Nunzi, F. Charra and N. Pfeffer, *Adv. Mater.* **6**, 64 (1994).
[10] N. Pfeffer, *PhD dissertation*, Université Paris-Nord (October 1994).
[11] E. Molva, J.J. Aubert, J. Marty and J.M. Nunzi, *French patent* #9313564 (1993), extended to Europe (1994).
[12] C. Jones and S. Day, *Nature* **351**, 15 (1991).

Nonlinear Absorption in the Liquid Crystal 5CB

T. Kosa*, A. Dogariu†, P. Palffy-Muhoray*, and E.W. Van Stryland†
*Liquid Crystal Institute, Kent State University, Kent, OH 44242
†Center for Research in Electro-Optics and Lasers, University of Central Florida, Orlando, FL 32816

T. Kosa, Liquid Crystal Institute, Kent State University, Kent, OH 44242.
tel.: (216) 672-4056, fax.: (216) 672-2796.

Nematic liquid crystals exhibit large optical nonlinearities in response to laser fields. Since these materials are highly transparent in the visible, they are attractive candidate materials for device applications. A variety of mechanisms are responsible for the observed nonlinearities, operating on different time scales. In earlier studies, the response on the nanosecond timescale was investigated in a geometry where director reorientation is not expected to occur. In the present work, nonlinear absorption on the picosecond timescale is studied in detail.

The samples consist of a $40\mu m$ thick nematic 5CB slab between two glass plates, which were spin-coated with polyimide and unidirectionally buffed. The nematic director aligns parallel to the buffing direction. The samples were irradiated with a frequency doubled, passively modelocked Nd:YAG laser. Pulses with $28ps$ (FWHM) duration and energy up to $3\mu J$ were focussed to a $33\mu m$ (FWHM) waist.

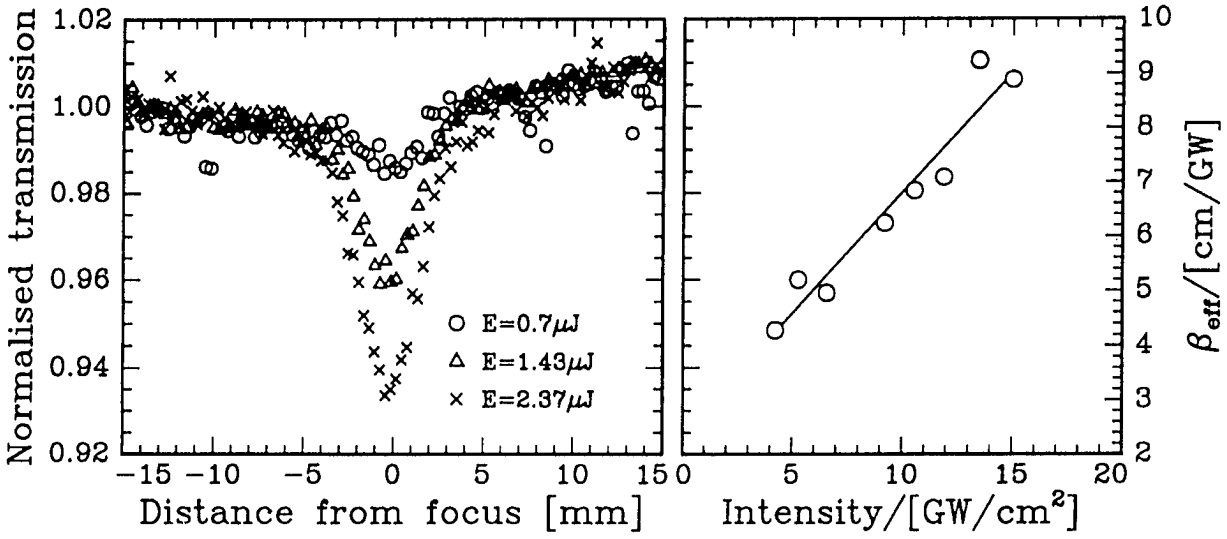

Fig.1.: Open aperture Z-scan curves for 5CB for different intensities.

Fig.2.: β_{eff} as function of intensity.

In the Z-scan technique, the sample is translated along the optic axis (z-direction) through the focal plane of the focussing lens, while the far field transmitted intensity is monitored either with (closed aperture) or without (open aperture) a diaphragm in front of the detector. In pump-probe measurements, the sample is fixed in the focal plane where the pump and probe beams overlap each other with a ratio of 6:1. Using a delay stage, the probe pulses can be delayed by up to $3.3ns$ relative to the pump. Fig.1 shows open aperture Z-scan curves with pump polarization parallel to the director. Near the focal plane, the transmitted intensity decreases, indicating nonlinear absorption. The nonlinear absorption coeffient β_{eff} can be calculated from the modulation amplitude [1]. As shown in Fig. 2, β_{eff} is nearly proportional to intensity, indicating that the mechanism is not pure two-photon absorption (TPA), which would give an intensity independent β. The zero intensity extrapolated value of β_{eff} ,which indicates the third order contribution, is small and can only be determined from our measurements with relatively large uncertainty. A linear fit of $\beta_{eff} = \beta_0 + \gamma I$ gives $\beta_0 = 0.3 \pm 0.2cm/GW$ and $\gamma = 0.5 \pm 0.05cm^3/GW_2$.

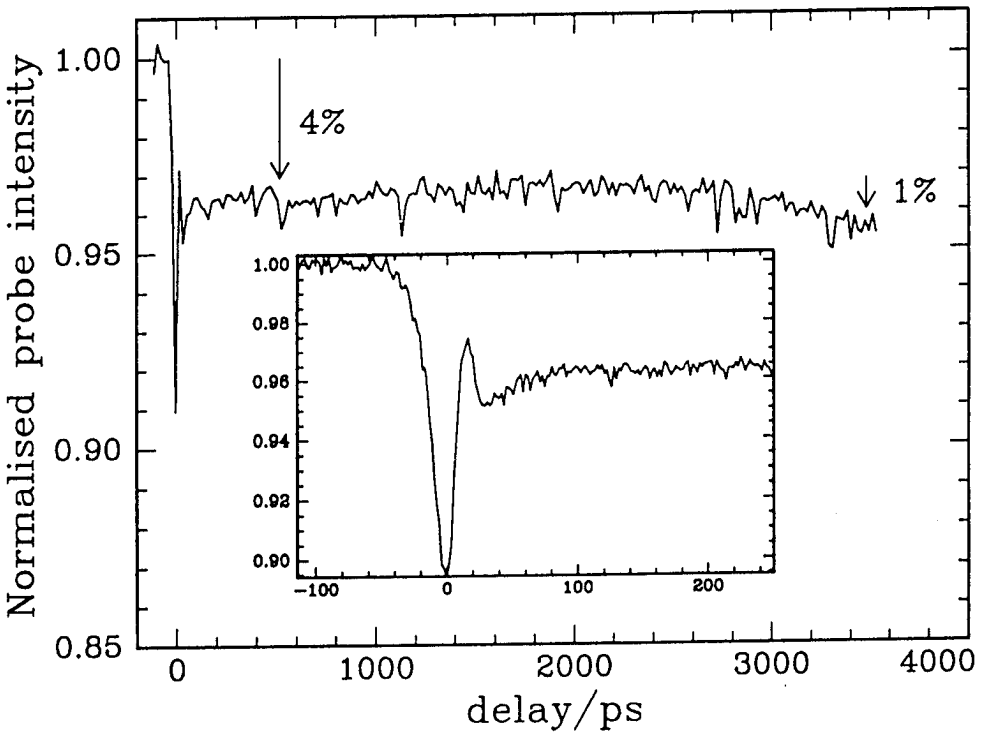

Fig.3.: Probe intensity as function of time delay.

We interpret the linear increase of β_{eff} with intensity as the result of a 5^{th} order process such as excited state absorption (ESA) accessed via TPA.[3][5] Fig.3. shows results of the pump-probe measurements up to a $3.2ns$ probe delay, while the inset show the results for

the first $300ps$. The important features are as follows. At zero delay, TPA dominates, but immediately after the pump pulse TPA generated ESA can bee seen. The ESA decays with the lifetime of the excited state, this, however, is not seen on the time scale of our measurements. Instead, at around $3ns$ the onset of a new absorption channel is observed. This is consistent with the measurement of a large β_{eff} in the ns regime [2][5] and also with time resolved absorption measurements[3][4][6].

To account for these observations we propose a simple 5-level model, shown in Fig. 4. Electrons excited through TPA either give rise to one photon excited state absorption ESA1, or first make a nonradiative transition with characteristic time τ and then give rise to excited state absorption ESA2. Our pump-probe measurements indicate that $\tau > 3ns$. Further time resolved measurements are needed with delay times $> 3ns$ to fully characterise these processes.

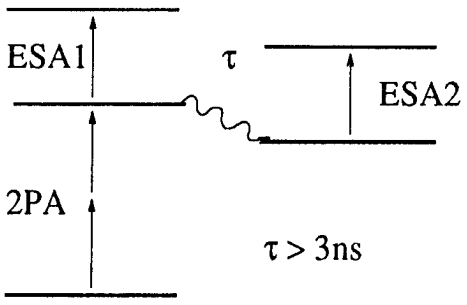

Fig.4.: Schematic of 5-level model.

References

[1] A.A. Said, M.Sheik-Bahae, D.J. Hagan, T.H. Wei, J. Wang, J. Young, and E.W. Van Stryland, *J. Opt. Soc.Am.* **B 9**, 405, 1992.

[2] W. Zhao, J.H. Kim and P. Palffy-Muhoray, *SPIE Proc.* **2229**,131, 1994.

[3] P. Palffy-Muhoray, T. Wei and W. Zhao, *Mol. Cryst. Liq. Cryst.*, **251**,19, 1994.

[4] L. Li, H.J. Yuan, G. Hu and P. Palffy-Muhoray, *Liquid Crystals*, **16**, 703, 1994.

[5] A. Hochbaum, Y.-Y.Hsu and J.L. Fergason, *SPIE Proc.* **2229**,131, 1994.

[6] K.J. McEwan and R.C. Hollins, *SPIE Proc.* **2229**,131, 1994.

Two-Photon Resonant Contributions to the Third-Order Susceptibility of C_{60} in the Solid State

F. J. Bartoli, S. R. Flom and J. R. Lindle
Optical Sciences Division, Naval Research Laboratory
Washington, DC 20375
Phone: (202) 767-3612
Fax: (202) 404-8613

The role two-photon states play in the third-order optical response of organic systems has received much recent attention.[1] Third harmonic generation (THG) measurements are especially useful since they directly probe coherent electronic processes involving two- and three-photon resonances.[2,3] Degenerate four-wave mixing (DWFM) and nonlinear transmission (NLT) are complementary techniques which are also sensitive to two-photon states, but may also contain contributions from incoherent excited-state processes. The advantage of the latter experiments is that they yield information on the third-order coefficient $\chi^{(3)}(-\omega;\omega,\omega,-\omega)$ which is directly related to the nonlinear refractive index of interest for device applications. A direct comparison of DFWM and NLT results, when coherent electronic processes dominate, to $\chi^{(3)}(-3\omega;\omega,\omega,\omega)$ determined by THG should yield useful information concerning the origin of the nonlinear optical response.

The highly delocalized spherical fullerene C_{60}, which has generated widespread interest as a nonlinear optical material, appears to be an ideal choice for such a comparison at near-infrared wavelengths. Extensive third-harmonic generation (THG) experiments by Kajzar and coworkers[5] have measured the electronic $\chi^{(3)}(-3\omega;\omega,\omega,\omega)$ for C_{60} films in the 800-1900 nm spectral region. In this region the measurement wavelength is far below any one-photon resonance and should access only the lowest two-photon and three-photon states. Although DFWM and NLT investigations[5] in the visible region have shown a significant excited-state contribution, picosecond measurements on fullerene films at 1064 nm have been attributed to two-photon resonantly enhanced electronic processes.[6] Other optical evidence for such a two-photon state in this region has been reported[7]. Recent DWFM experiments of Strohkendl *et al.*,[8] performed between 750 nm and 875 nm using femtosecond pulse excitation, also show the pulse-limited response expected for an electronic process.

In the present work, lowest-order sum-over-states calculations of the dispersion of $\chi^{(3)}(-\omega;\omega,\omega,-\omega)$ and $\chi^{(3)}(-3\omega;\omega,\omega,\omega)$ are performed for C_{60} in the solid state. DWFM data in the near-infrared region are compared with THG results, and with the calculated results based on three-level and four-level models. Evidence for a second low-lying two-photon state is discussed.

A schematic energy level diagram is illustrated in Fig. 1, showing the lowest strongly allowed dipole transition at ω_{01}, and two two-photon states at ω_{02} and ω_{0n}, well below the one-

photon state. Assuming a centrosymmetric system, with only one one-photon state and one or more two-photon states, the sum-over-states expression for the third-order susceptibility can be written,[1,9]

$$\chi^{(3)}_{ijkl}(-\omega_\sigma;\omega_1,\omega_2,\omega_3) = \frac{NF}{4\hbar^3}\left[\sum_m \mu_{01}^2\mu_{1m}^2 D_{1m1} - \mu_{01}^4 D_{11}\right] . \qquad (1)$$

N is the number density, F is the local field factor, μ_{1m} is the transition dipole moment, and D_{1m1} and D_{11} are frequency dependent factors.[10] D_{1m1} contains the two-photon resonance terms expected to be important here. The local field factor is given by $F \equiv f_\omega^4$ for degenerate four-wave mixing and $f_\omega^3 f_{3\omega}$ for third harmonic generation, where $f_\omega = (n_\omega^2+2)/3$ and n_ω is the refractive index at ω for C_{60}. The refractive index data of Ren *et al.*[11] were used.

Figure 2 compares the value of $|\chi^{(3)}_{xxxx}(-\omega;\omega,\omega,-\omega)|$ for C_{60} films (square), measured[6] at 1064 nm by DFWM, with the measured dispersion in $\chi^{(3)}_{xxxx}(-3\omega;\omega,\omega,\omega)$ reported by Kajzar *et al.*[4] in the 850 nm to 1500 nm spectral region (circles). Note that the value of $\chi^{(3)}_{xxxx}(-3\omega;\omega,\omega,\omega)$ at 1064 nm is an order of magnitude larger than that determined by degenerate four-wave mixing. The upper curve represents a fit of the dispersion in $\chi^{(3)}_{xxxx}(-3\omega;\omega,\omega,\omega)$ to the THG data. The calculation employed a three-level model (Eq. 1) with parameters[12] ($\hbar\omega_{01}$=3.54 eV, $\hbar\omega_{02}$= 1.88 eV, $\hbar\Gamma_1$=0.14 eV, $\hbar\Gamma_2$= 0.1 eV, μ_{01}=9.1D and μ_{01}=9.1D) similar to those reported by Kajzar

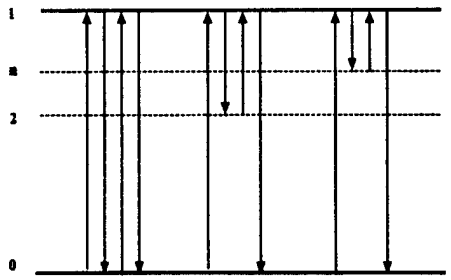

Figure 1. Schematic energy level diagram for C_{60}, illustrating the three- and four-level models employed. State 1 has a symmetry opposite to that of the ground state (0) and 0-1 dipole transitions are strongly allowed. States 2 and n, lower in energy than state 1, are one-photon forbidden and two-photon allowed.

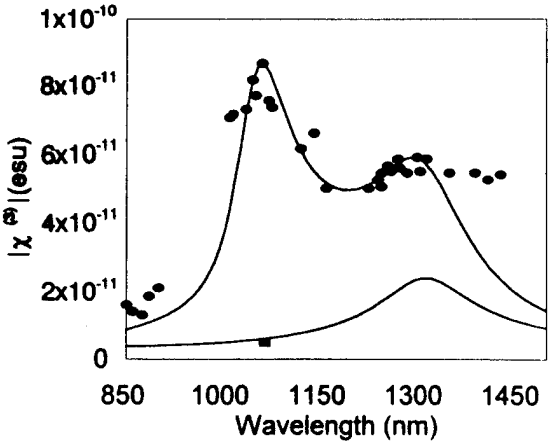

Figure 2. Calculated dispersion of $\chi^{(3)}_{xxxx}(-\omega;\omega,\omega,-\omega)$ (lower curve) and $\chi^{(3)}_{xxxx}(3\omega;\omega,\omega,\omega)$ (upper curve) obtained using the three-level model. The DFWM results of Ref. 6 (square) and the THG results of Ref. 4 (circles) are shown for comparison.

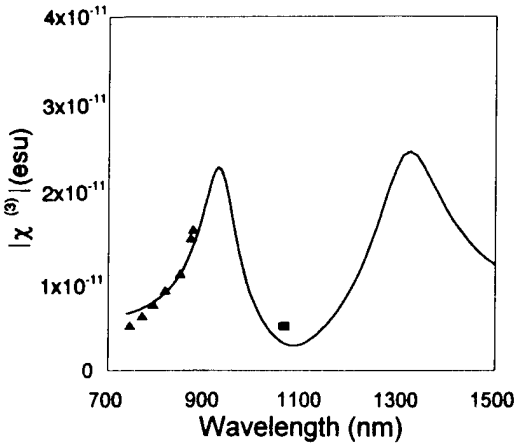

Figure 3. Calculated dispersion of $\chi^{(3)}_{xxxx}(-\omega;\omega,\omega,-\omega)$ (solid curve) obtained using the four-level model. The DFWM results of Ref. 6 (square) and Ref. 8 (triangles) are shown for comparison.

et al.[4] They assigned the peak at 1300 nm as a two-photon resonance with a two-photon state at $\hbar\omega_{02}$ = 1.88 eV and that between 1000 nm and 1100 nm as a three-photon resonance. The calculated results are in reasonable agreement with the THG data, consistent with the findings of reference 4.

The same parameters used above were employed here without further adjustment to calculate the dispersion in $\chi^{(3)}_{xxxx}(-\omega;\omega,\omega,-\omega)$ using Eq. 1, and the results compared with the DFWM data at 1064 nm. This three-level model (lower curve in Fig. 2) correctly predicts the experimental $|\chi^{(3)}_{xxxx}(-\omega;\omega,\omega,-\omega)|$ measured by DFWM. The calculations also predict a two-photon peak near 1300 nm, approximately 0.4 times that of the THG result. The additional enhancement of THG result near 1300 nm is due to the proximity of the three-photon resonance.

While the three-level model, fit to the THG results, predicts the magnitude of $\chi^{(3)}_{xxxx}$ for DFWM, it also predicts $\mathrm{Re}\chi^{(3)}_{xxxx}(-\omega;\omega,\omega,-\omega) \gg \mathrm{Im}\chi^{(3)}_{xxxx}(-\omega;\omega,\omega,-\omega)$. This is contrary to experimental observations[6] at 1064 nm. When $\mathrm{Im}\chi^{(3)}_{xxxx}(-\omega;\omega,\omega,-\omega)$, determined by nonlinear transmission measurements, is compared to $|\chi^{(3)}_{xxxx}(-\omega;\omega,\omega,-\omega)|$, obtained from degenerate four-wave mixing, it appears that $\chi^{(3)}_{xxxx}(-\omega;\omega,\omega,-\omega)$ possesses an imaginary component that is comparable to or larger than the real part. Shortcomings of the three-level model in describing the wavelength dispersion of the third-order susceptibility in the near infrared region is made more obvious when one considers the femtosecond DFWM data of Strohkendl *et al.*[8] at wavelengths between 740 nm and 880nm. Shown as the triangles in figure 3, this data clearly is not accounted for by the above three-level calculation for $\chi^{(3)}_{xxxx}(-\omega;\omega,\omega,-\omega)$ which was derived from THG data. Figure 3 shows the results of a four-level model which includes a second two-photon state at $\hbar\omega_{0n}$ = 2.65 eV. The calculated results agree reasonably well with the measured $|\chi^{(3)}_{xxxx}(-\omega;\omega,\omega,-\omega)|$ as shown in the figure, and correctly predicts the signs of the real and imaginary parts of $\chi^{(3)}_{xxxx}(-\omega;\omega,\omega,-\omega)$ reported in Ref. 8. Because of cancellation in the real contributions from the two-photon states, the four-level model also predicts a smaller $\mathrm{Re}(\chi^{(3)}_{xxxx})$ at 1064 nm, in better agreement with the experimental results.

In conclusion, direct comparison of THG and DFWM, when it can be established that the latter is dominated by coherent electronic processes, provides a powerful tool for understanding

the origin of the third-order response. While further measurement of the dispersion of $\chi^{(3)}_{xxxx}(-\omega;\omega,\omega,-\omega)$ is needed to more thoroughly test model calculations, the calculated results clearly suggest the importance of the higher-lying two-photon state, and supports the conclusion that the DFWM result for C_{60} in the near-infrared is a two-photon resonantly enhanced electronic process.

REFERENCES

1. J. R. Heflin, Y. M. Cai, and A. F. Garito, J. Opt. Soc. Am. B **8**, 2132 (1991).
2. J. H. Andrews, J. D. V. Khaydarov, and K. D. Singer, Opt. Lett. **19**, 984 (1994).
3. Y. Z. Yu, R. F. Shi, A. F. Garito, and C. H. Grossman, Opt. Lett. **19**, 786 (1994).
4. F. Kajzar, C. Taliani, M. Muccini, R. Zamboni, S. Rossini, and R. Danieli, Proc. SPIE, **2284**, 58 (1994); F. Kajzar, C. Taliani, R. Danieli, S. Rossini, and R. Zamboni, Chem. Phys. Lett. **217**, 418 (1994).
5. S. R. Flom, R. G. S. Pong, F. J. Bartoli, and Z. H. Kafafi, Phys. Rev. B **46**,15598 (1992); M. J. Rosker, H. O. Marcy, Tallis Y. Chang, J. T. Khoury, K. Hansen, and RT. L. Whetten, Chem. Phys. Lett. **196**, 427 (1992).
6. Z. H. Kafafi, J. R. Lindle, R. G. S. Pong, F. J. Bartoli, L. J. Lingg and J. Milliken, Chem. Phys. Lett. **188**, 492 (1992); J. R. Lindle, R. G. S. Pong, F. J. Bartoli, and Z. H. Kafafi, Phys. Rev. B 48, 9447 (1993).
7. R.Zamboni, M. Muccini, R. Danieli, C. Taliani, H. Mohn, W. Müller, and H. U. Ter Meer, Proc. SPIE, **2284**, 120 (1994).
8. F. P. Strohkendl, R. J. Larsen, L. R. Dalton, R. W. Helwarth, H. W. Sarkas, and Z.H.Kafafi, Proc. SPIE, **2284**, 78 (1994).
9. B. J. Orr and J. F. Ward, Mol. Phys. **20**, 513 (1971).
10. M. G. Kuzyk and C. W. Dirk, Phys. Rev. A **41**, 5098 (1990).
11. S. L. Ren, Y. Wang, A. M. Raon, E. McRae, J. M. Holden, T. Hager, KaiAn Wang, Wan-Tse Lee, H. F. Ni, J. Selegue, and P. C. Eklund, Appl. Phys. Lett. **59**,2678 (1991).
12. The parameters employed are similar but not identical to those of reference 4. The main difference is in the lower values used here for the dipole moment matrix elements which are more consistent with that found for other organic systems (e.g., see Refs. 1 and 2).

Monday, September 11, 1995

Poster Session

MD 3:45 pm-5:15 pm
Lloyd Center Ballroom

Mark G. Kuzyk, *Presider*
Washington State University

Interference Phenomena in Nonlinear Dielectrics

P. Kaatz, P. Nosbaum, Ch. Bosshard, and P. Günter
Nonlinear Optics Laboratory, Institute of Quantum Electronics
Swiss Federal Institute of Technology
ETH Hönggerberg, CH-8093 Zürich, Switzerland
(Phone: + 41-1-633 22 90; FAX: + 41-1-633 10 56)

I. Introduction.

The Maker fringe technique remains the most common and reliable method for evaluating relative magnitudes of nonlinear optical (NLO) susceptibilties. In this work we discuss generalizations of this technique to multilayer and multi-component determination of NLO susceptibilties for second (SHG) and/or third (THG) harmonic generation. Many authors have discussed SHG and/or THG from a single crystal or slab of NLO material for the case of neglible depletion of the fundamental wave, (see e.g. [1]). If the reflected harmonic wave from the far boundary surface is neglected, the intensity of SHG (n=2) or THG (n=3) from a fundamental beam at λ_ω can be written as (refractive indices $n^a_{n\omega}$, n^a_ω and angles $\vartheta^a_{n\omega}$, ϑ^a_ω are in the crystal):

$$I_{n\omega} = \left[(t^a_\omega)^2 \, I_\omega \right]^n \left[(A_1 - A_2)^2 + 4 A_1 A_2 \sin^2\left(\frac{\delta_a}{2}\right) \right] \quad \text{with} \quad \delta_a = 2n\pi \frac{d_a}{\lambda_\omega} \left(n^a_{n\omega} \cos \vartheta^a_{n\omega} - n^a_\omega \cos \vartheta^a_\omega \right) \quad (1)$$

where $A \propto \chi^{(n)} / \Delta\varepsilon_{n\omega}$, $\Delta\varepsilon_{n\omega} = (n^2_{n\omega} - n^2_\omega)$, and not including transmission factors in A_1 and A_2. The crystal thickness is given by d_a. Weak absorption at ω or $n\omega$ can be incorporated in A_1 and A_2. In general, the refractive indices and transmission factors are angle dependent.

II. Bilayer System.

Using the same boundary conditions and approximations, the NLO interference pattern for two successive nonlinear media, denoted by a, b (where just one component in each medium contributes a signal) can be written as:

$$I_{n\omega} = \left[(t^a_\omega)^2 \, I_\omega \right]^n \left[(A_1 - A_2)^2 + 4 A_2 (A_1 - B_2) \sin^2\left(\frac{\delta_a}{2}\right) + (B_1 - B_2)^2 + 4 B_1 (B_2 - A_1) \sin^2\left(\frac{\delta_b}{2}\right) \right.$$
$$\left. + 2(A_1 - A_2)(B_1 - B_2) + 4 A_2 B_1 \sin^2\left(\frac{\delta_a + \delta_b}{2}\right) \right] \quad (2)$$

where the nonlinear phase shifts δ_a, δ_b, and the NLO susceptibility components A and B are described similarly to the case of a single NLO medium.

a). SHG from Two Successive Crystals.

Equation (2) shows that harmonic generation from two successive media allows the detemination of both the relative magnitude and the sign of the two NLO components in question. Although often used in THG, it seems to have been neglected for SHG measurements. Figure 1 illustrates SHG from two successive NLO crystals, $KNbO_3$ and $LiNbO_3$.

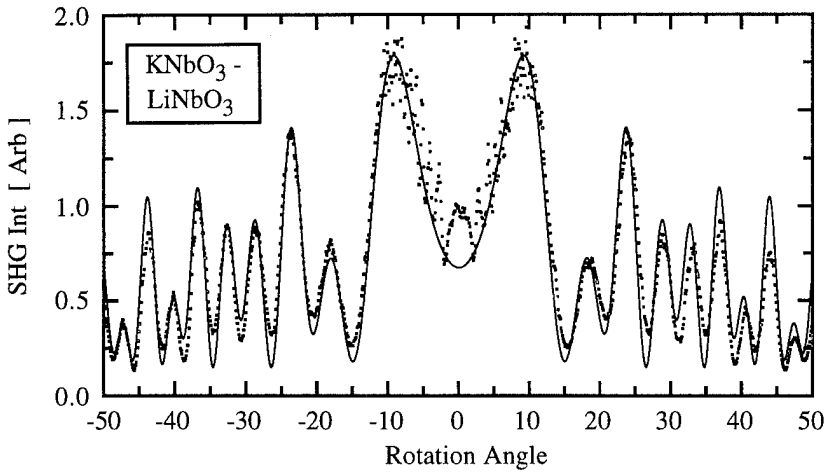

Figure 1. SHG signal from two successive NLO crystals, $KNbO_3$ and $LiNbO_3$ optically contacted together. The input and output polarization as well as the rotation axis are along the c axis of the crystals. The analysis of the SHG measurement gives d_{33} ($KNbO_3$) = 0.82 ± 0.05 d_{33} ($LiNbO_3$) at 1338 nm. The measurement indicates that the sign of d_{33} ($KNbO_3$) and d_{33} ($LiNbO_3$) are the same (negative by an absolute measurement of $LiNbO_3$, see [2]).

b). THG from Two Isotropic Dielectrics.

The THG variant of this measurement is quite common for the determination of the relative nonlinear susceptiblity of polymer films, as illustrated in Figure 2. Eqn. (2) was used for the fit.

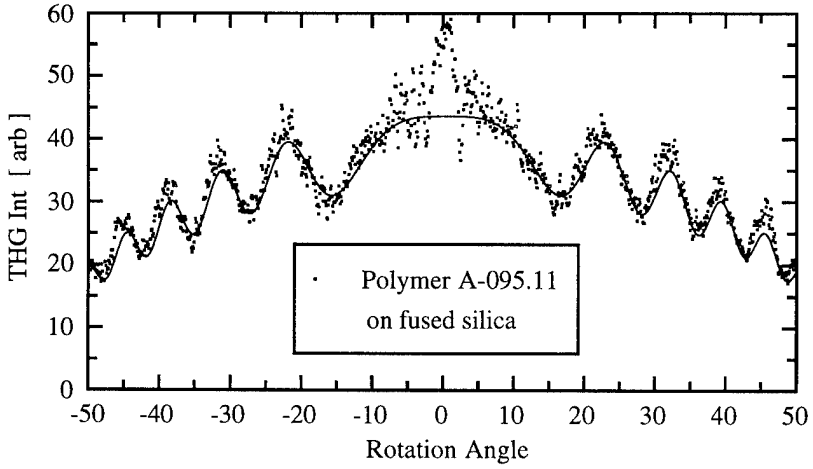

Figure 2. THG signal from a 400 nm thick polymer film (A-095.11) [3] on fused silica. Input and output polarization are parallel with the rotation axis. Analysis of the interference pattern gives $\chi^{(3)}$ (polymer) ≈ (200 ± 10) $\chi^{(3)}$ (fused silica) at 1907 nm. The polymer refractive indices are 1.65 @ 1907 nm and 1.84 @ 636 nm.[3] Correction was made for a slight absorbance at 636 nm.

III. Intracrystal Harmonic Generation.

Intracrystal harmonic generation also allows the determination both the relative magnitude and the sign of the two NLO susceptibility components. In this case the intensity is described by:

$$I_{n\omega} = \left[(A_1 - A_2)^2 + 4A_1(A_1 + B_2)\sin^2\left(\frac{\delta_a}{2}\right) + (B_1 - B_2)^2 + 4B_1(A_1 + B_2)\sin^2\left(\frac{\delta_b}{2}\right) + 2(A_1 - A_2)(B_1 - B_2) - 4A_1B_1\sin^2\left(\frac{\delta_a - \delta_b}{2}\right)\right] \quad (3)$$

(compare eqn. (2)), where the nonlinear phase shifts δ_a, δ_b, and NLO susceptibility components A and B are defined as in **I** and **II** with the appropriate NLO coefficients and phase shifts as described below.

a). SHG in a single crystal.

The use of a polarizer and an analyzer in front and behind a SHG active crystal allows the determination of the relative **d** coefficients. For a crystal of mm2 symmetry, A and B are given by:

$$A_1 = \left(t_\omega^s\right)^2 t_b^{2s}\, \chi_s^{(2)}/\Delta\varepsilon_s \cos^2\alpha \qquad A_2 = \left(t_\omega^s\right)^2 t_f^{2s}\, t_b^s\, \chi_s^{(2)}/\Delta\varepsilon_s \cos^2\alpha$$

$$B_1 = \left(t_\omega^p\right)^2 t_b^{2p}\, \chi_p^{(2)}/\Delta\varepsilon_p \sin^2\alpha \qquad B_2 = \left(t_\omega^p\right)^2 t_f^{2p}\, t_b^p\, \chi_p^{(2)}/\Delta\varepsilon_p \sin^2\alpha$$

with s,p polarization. α is the polarization angle of the fundamental wave relative to the rotation axis. The phase shifts δ_a and δ_b are similar to those in **II**, with the use of the appropriate refractive indices. This measurement has been used previously for the case when the analyzer is adjusted to an angle where $A = -B$, for which the interference pattern reduces to the expression given in **I**.[4] However, equation (3) can be used at any arbitrary angle of the polarizer as illustrated in Figure 3.

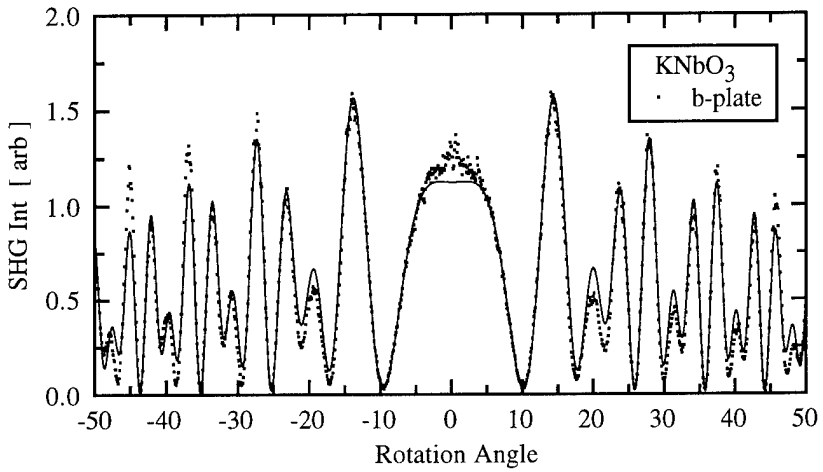

Figure 3. SHG signal from a single $KNbO_3$ b-plate. The input polarization was at 60° from the c axis. The SHG polarization and the rotation axis was about the c axis. The SHG interference comes from mixing of d_{33} and d_{31}. Analysis of the SHG signal gives $d_{31} = 0.59 \pm 0.05\ d_{33}$ at 1338 nm. The measurement indicates that d_{31} and d_{33} have the same sign (negative from the results of Figure 1).

b). Cascading of SHG and THG.

The interference pattern describing intracrystal cascading of a second harmonic wave with the fundamental wave determined by $\chi_a^{(2)}(3\omega;2\omega,\omega)$ to give THG is also given by eqn. (3) with

$$A_1 = (t_\omega)^3\, t_{3\omega}^f\, t_{3\omega}^b \left[\frac{\chi_a^{(3)}}{\Delta\varepsilon_{3\omega}} - \frac{2\,\hat{\chi}_a^{(2)}\,\chi_a^{(2)}}{\Delta\varepsilon_{3\omega}\,\Delta\varepsilon_{2\omega}}\right] \qquad B_1 = (t_\omega)^3\, t_{3\omega}^f\, t_{3e}^b\, \frac{2\,\hat{\chi}_a^{(2)}\,\chi_a^{(2)}}{\Delta\varepsilon_{s\omega}\,\Delta\varepsilon_{2\omega}}$$

$$A_2 = (t_\omega)^3\, t_{3\omega}^{f3} \left[\frac{\chi_a^{(3)}}{\Delta\varepsilon_{3\omega}} - \frac{2\,\hat{\chi}_a^{(2)}\,\chi_a^{(2)}}{\Delta\varepsilon_{3\omega}\,\Delta\varepsilon_{2\omega}}\right] \qquad B_2 = (t_\omega)^3\, t_{3\omega}^{fe}\, \frac{2\,\hat{\chi}_a^{(2)}\,\chi_a^{(2)}}{\Delta\varepsilon_{s\omega}\,\Delta\varepsilon_{2\omega}}$$

where

$$\chi_a^{(3)} = \chi_a^{(3)}(3\omega;\omega,\omega,\omega) \qquad \hat{\chi}_a^{(2)} = \chi_a^{(2)}(3\omega;2\omega,\omega) \qquad \chi_a^{(2)} = \chi_a^{(2)}(2\omega;\omega,\omega)\ ,$$

and

$$\delta_a = \delta_{3\omega}\ ;\ \ \delta_b = \delta_{3\omega} - \delta_{2\omega}\ ;\ \ \delta_a - \delta_b = \delta_{2\omega}\ ,$$

where $\Delta\varepsilon_{s\omega} = n_e^2 - n_\omega^2$ and $n_e = (2n_{2\omega} + n_\omega)/3$ see also [5], (the transmission coefficents also are given in [5]). The THG measurement gives a determination of the ratio $R = \chi_a^{(3)}/(\hat{\chi}_a^{(2)}\,\chi_a^{(2)})$. Figure 4 shows a measurement of cascading in an a-plate of $KNbO_3$.

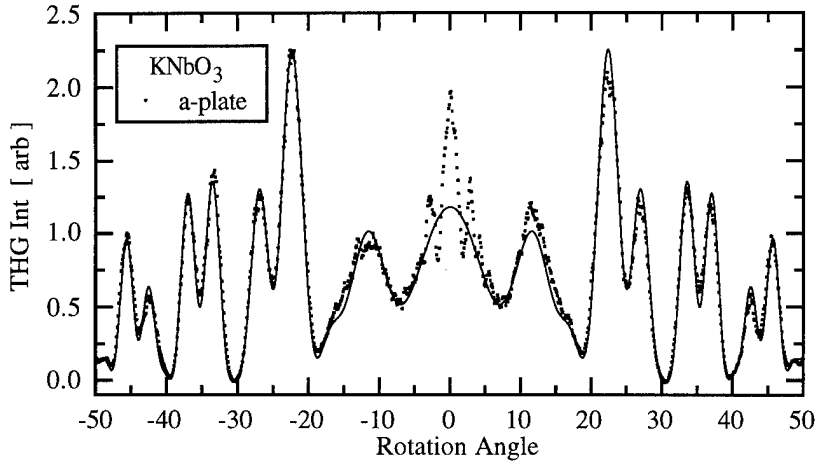

Figure 4. Cascaded THG signal from a 1310 μ $KNbO_3$ a-plate. The input and output polarization as well as the rotation axis are along the c axis of the crystal. The THG measurement gives a ratio $R = 2.4 \pm 0.1$ at 1907 nm.

IV. THG from Three Successive Isotropic Media.

The THG intensity from liquids in cuvettes (vacuum) can be similarly written as:

$$I_{3\omega} = \left[(t_\omega^a)^2 \, I_\omega \right]^3 \left[(A_1 - A_2)^2 + 4A_2(A_1 - B_2)\sin^2\left(\frac{\delta_a}{2}\right) + (B_1 - B_2)^2 + 4(B_1 - C_2)(B_2 - A_1)\sin^2\left(\frac{\delta_b}{2}\right) \right.$$
$$+ (C_1 - C_2)^2 + 4C_1(C_2 - B_1)\sin^2\left(\frac{\delta_c}{2}\right) + 2(A_1 - A_2)(B_1 - B_2) + 4A_2(B_1 - C_2)\sin^2\left(\frac{\delta_a + \delta_b}{2}\right)$$
$$\left. + 2(B_1 - B_2)(C_1 - C_2) + 4C_1(B_2 - A_1)\sin^2\left(\frac{\delta_b + \delta_c}{2}\right) + 2(A_1 - A_2)(C_1 - C_2) + 4A_2 C_1 \sin^2\left(\frac{\delta_a + \delta_b + \delta_c}{2}\right) \right]$$

with A ,C the NLO coefficients of the two cuvette windows and B of the liquid. The phase shifts are written similarly to that in **I**. This eqn. gives results equivalent to those previously obtained.[6]

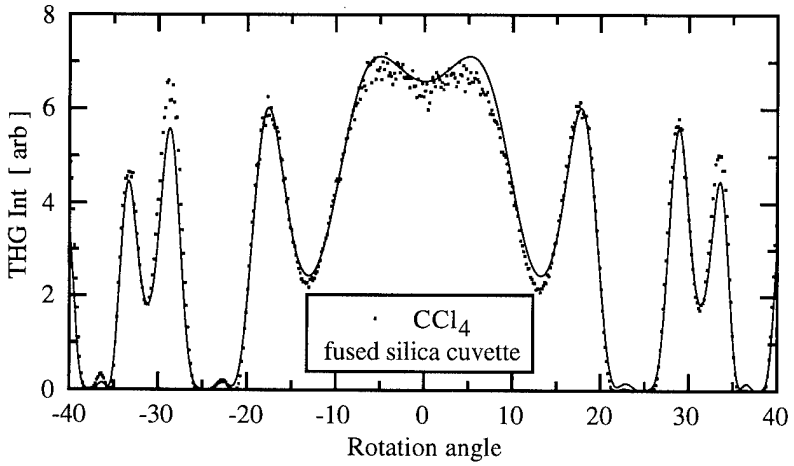

Figure 5. THG signal from CCl_4 in a fused silica cuvette (Hellma). Input and output polarization are parallel with the rotation axis. The liquid cavity is ≈ 1000 μm thick with cell walls ≈ 1250 μm. The THG measurement gives $\chi^{(3)}$ (CCl_4) = 2.7 ± 0.1 $\chi^{(3)}$ (fused silica) at 1907 nm and a coherence length of 29.39 μm. The measurement is done in vacuum.

V. References

[1] Kurtz, S. K. in *Laser Handbook*; F. T. Arecchi and E. O. Schulz-Dubois, Eds.; North-Holland: Amsterdam, 1972; Vol. 1; pp 923-974.

[2] Miller, R. C.; Nordland, W. A. *Phys. Rev. B* **1970**, *2*, 4896-4902.

[3] Prêtre, P.; Kaatz, P.; Bohren, A.; Günter, P.; Zysset, B.; Ahlheim, M.; Stähelin, M.; Lehr, F. *Macromolecules* **1994**, pp. 5476-5486.

[4] Miller, R. C.; Nordland, W. A. *Appl. Phys. Lett.* **1970**, *16*, 174-176.

[5] Meredith, G. R. *Phys. Rev. B* **1981**, *24*, 5522-5532.

[6] Kajzar, F.; Messier, J. *Phys. Rev. A* **1985**, *32*, 2352-2363.

Collision Induced Hyper-Rayleigh Light Scattering in CCl_4

Philip Kaatz and David Shelton
Department of Physics
University of Nevada - Las Vegas
Las Vegas, NV USA 89154 - 4002
Phone: (702) 895 - 17 27; FAX: (702) 895 - 08 04

Introduction

Hyper-Rayleigh and hyper-Raman light scattering (HRS) were among the first nonlinear optical (NLO) phenomena to be investigated both theoretically and experimentally.[1,2] A revival of interest in this technique has occured as it is a more general method of investigating the second order NLO properties of molecules.[3] The HRS experiment allows the characterization of molecules having dipolar or octupolar symmetry, in contrast to electric-field induced second harmonic generation (EFISH), in which only species having dipolar symmetry may be probed.[4] Moreover, if a polarization analysis is made of the scattered light, relative ratios of the components of the second order NLO polarizability tensor may be determined.[5,6] In this work we report evidence for the collision-induced modulation of HRS. We find that is necessary to consider the intermolecular collision contribution to HRS in order to obtain accurate ratios of the first (β) hyperpolarizability components. Vapor phase HRS measurements are also reported, where the vapor phase intensities are directly compared with the liquid phase intensities. Local field factors are able to correct for the differences between vapor and liquid phases for the intramolecular contribution to HRS.

Experimental

Carbon tetrachloride (spectroscopic grade) was filtered through a 0.2 μ micropore filter directly into a spectroscopic fused silica cell. Temperature control was accomplished by a thermostatted aluminum block. The source radiation at 1064 nm was obtained from a acousto-optically *Q*-switched Nd:YAG laser (Quantronix 116) and focused into the sample cell with a 4X objective lens. The laser produced trains of $\approx$ 150 ns pulses at a repetition rate of 3 kHz. Input power levels and polarization properties were selected by a set of crossed Glan-Taylor polarizers and a Soleil-Babinet compensator. Scattered light was collected at 90° with f/2 optics and focused onto a spectrometer (Jobin-Yvon Ramonor U 1000). The liquid measurements were done with a spectral slit width of 2.4 cm^{-1}. For vapor phase measurements the slits were opened to 13 cm^{-1}. The polarization of the scattered light was analyzed with a sheet polariod. The dispersed light was detected by a PMT (Hamatsu R943) and stored in a multichannel analyzer (Nucleus PCA).

Results and Discussion

Depolarized Rayleigh Scattering in Liquids

Einstein first calculated the intensity of light scattered by thermal fluctuations from simple fluids. His conclusions suggested that the elastically scattered light would preserve the polarization of the incident beam. Later experiments, however, have shown that the light scattered by such fluids includes a nonnegligible depolarized component. Intermolecular interactions are generally attributed to be the source of this unexpectedly large depolarized component. Discussions of

mechanisms for collision-induced scattering from liquids generally conclude that the frequency shifted, $\Delta\omega$, profile can be described as:[7]

$$I(\Delta\omega) = f(\Delta\omega)\exp(-|\Delta\omega|/\omega_0) \ , \qquad (1)$$

where $f(\Delta\omega)$ typically has a power law dependence. The depolarized Rayleigh scattering from liquid CCl_4 at 22° C is shown in Figure 1. The asymmetry in the Stokes-antiStokes wings is accounted for by multiplying by $\exp(\Delta\omega/2kT)$, where $2kT$ = 410 cm^{-1} at 22° C. [8]

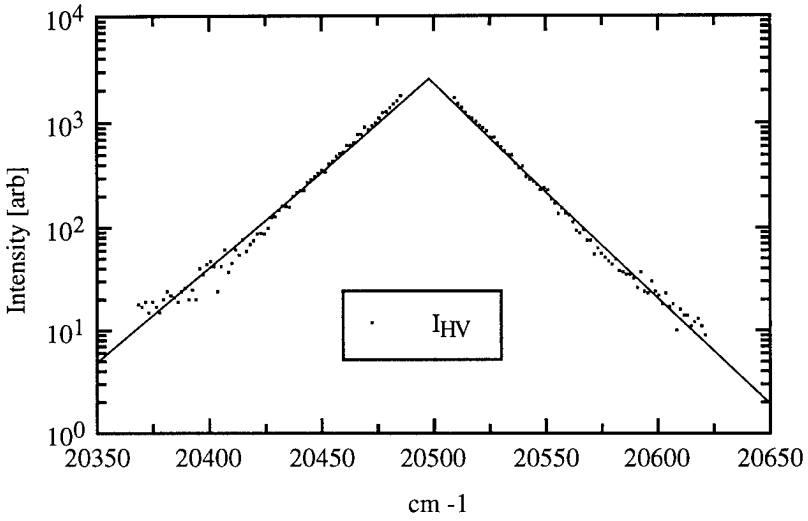

Figure 1. Depolarized I_{HV} Rayleigh wing scattering from liquid CCl_4 @ 22° C. An Ar^+ laser @ 488 nm was used as the radiation source. A fit of the broad Rayleigh wing scattering to eqn. (1) gives ω_0 = 22 cm^{-1}, with $f(\Delta\omega)$ = 1.

Hyper-Rayleigh Scattering in Liquids

Assuming the second harmonic scattered light is broadened by rotational diffusion having a Debye-type relaxation time τ_l, the spectral distribution of the second harmonic scattered light is a sum of Lorentzian lineshapes from the dipolar, $\overline{\beta}^{[1]}$, and octupolar, $\overline{\beta}^{[3]}$, components;[9]

$$I_{VV}^{2\omega}(\Delta\omega) \propto \frac{1}{5} g_1(\Delta\omega)\left|\overline{\beta}^{[1]}\right|^2 + \frac{2}{35} g_3(\Delta\omega)\left|\overline{\beta}^{[3]}\right|^2 \ , \qquad (2)$$

and

$$I_{HV}^{2\omega}(\Delta\omega) \propto \frac{1}{45} g_1(\Delta\omega)\left|\overline{\beta}^{[1]}\right|^2 + \frac{4}{105} g_3(\Delta\omega)\left|\overline{\beta}^{[3]}\right|^2 \ , \qquad (3)$$

where

$$g_l(\Delta\omega) = \frac{2\tau_l}{1+(\Delta\omega\,\tau_l)^2} \ . \qquad (4)$$

For tetrahedral molecules, the description of HRS simplifies considerably as there is only one nonzero component $\overline{\beta}_{xyz}$ of the first hyperpolarizability tensor. For intramolecular HRS, then

$$\overline{\beta}^{[1]} = 0 \qquad \text{and} \qquad \overline{\beta}^{[3]} = \overline{\beta}_{xyz} \ , \qquad (5)$$

where the overbar indicates molecule fixed coordinates. Equations (2-5) predict a depolarization ratio $I_{VV}^{2\omega}/I_{HV}^{2\omega} = 1.5$ for contributions to HRS from single molecules of T_d symmetry.

Typical HRS I_{VV} and I_{HV} spectra for CCl4 at 22 °C are shown in Figure 2. To explain the experimental results, the spectra were assumed to be composed of two components - a Lorentzian component describing the intrinsic molecular nonlinear optical properties, and a broad exponential component due to collision-induced modulation of the first hyperpolarizability tensor, $\overline{\beta}_{xyz}$.

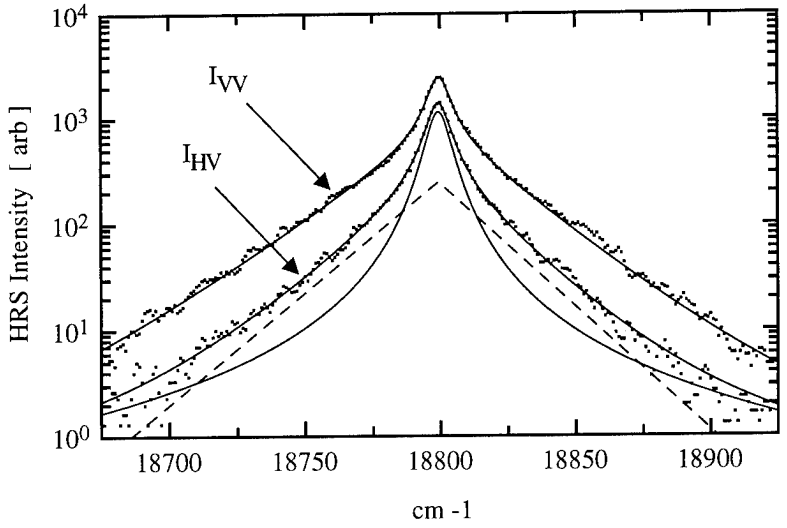

Figure 2. HRS from CCl_4 at 22° C. The Lorentzian contributes 46% of the total scattering for I_{VV} and 68% for I_{HV}. The FWHM for both I_{VV} and I_{HV} of the Lorentzian is 9.6 ± 0.1 cm^{-1}. The exponential decay constant is ω_0 = 22 cm^{-1} (I_{VV}) , 20 cm^{-1} (I_{HV}). An integration of the total scattering gives a depolarization ratio I_{VV}/I_{HV} = 2.40±0.05 whereas integration of the Lorentzian term gives a depolarization ratio I_{VV}/I_{HV} = 1.50±0.05 as predicted for T_d symmetry.

Decomposing the HRS spectra into an octupolar and a dipolar term $\left|\overline{\beta}^{[1]}\right|^2 \propto I_{VV} - 3/2\, I_{HV}$ confirms the above collision-induced hypothesis. As CCl_4 has no intrinsic dipole moment, the strong dipolar HRS scattering shows the influence of intermolecular contributions. Figure 3 shows that the dipolar contribution can be entirely represented by the exponential term.

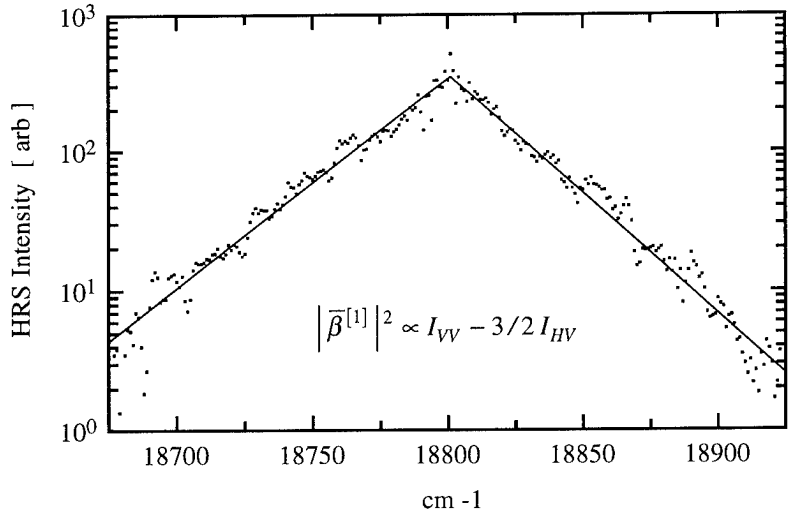

Figure 3. Decomposition of the HRS spectra into the dipolar term given by I_{VV} - 3/2 I_{HV} shows only a contribution from collision-induced scattering. The fit to an exponential decay gives ω_0 = 27 cm^{-1}.

Hyper-Rayleigh Scattering in Gases

Vapor phase HRS measurements were also done in the same spectroscopic cell above the liquid, at several temperatures ranging from 25 - 70 °C. Accounting for rotational transitions, the HRS intensity for molecules of T_d symmety is given by:[10]

$$I_{VV}^{2\omega} \propto (E^{\omega})^4 \,(2J+1)(2J'+1)\left(\overline{\beta}_{xyz}\right)^2 exp(-BJ(J+1)/kT)\ , \qquad (6)$$

with the selection rules,

$$\Delta J = 0, \pm 1, \pm 2, \pm 3 \quad , \quad J + J' \geq 3 \quad \text{and} \quad \Delta k = \pm 2\ .$$

A comparison of the theoretical HRS spectrum and the composite experimental results is shown in Figure 4.

As the vapor and liquid measurements were made in the same cell with the same focusing and collection optics, a direct comparison can be made of any potential local field enhancement of the nonlinear polarizabilty $\overline{\beta}_{xyz}$ due to environmental effects. After correction for density, source length, collection geometry, and reflection loss differences in the liquid and vapor, we find that the total scattering in the liquid in enhanced by 1.5 ± 0.1 times the total scattering of the vapor, with the Lorentz local field given by $(n^2+2)/3$. With the above measurements in the liquid indicating that only 46% of the scattering in the liquid is due from intramolecular contributions, we find the enhancement of the liquid HRS signal compared to vapor is 1.0 ± 0.1. The excess enhancement is interpreted as being due to the collision-induced HRS scattering present in the liquid.

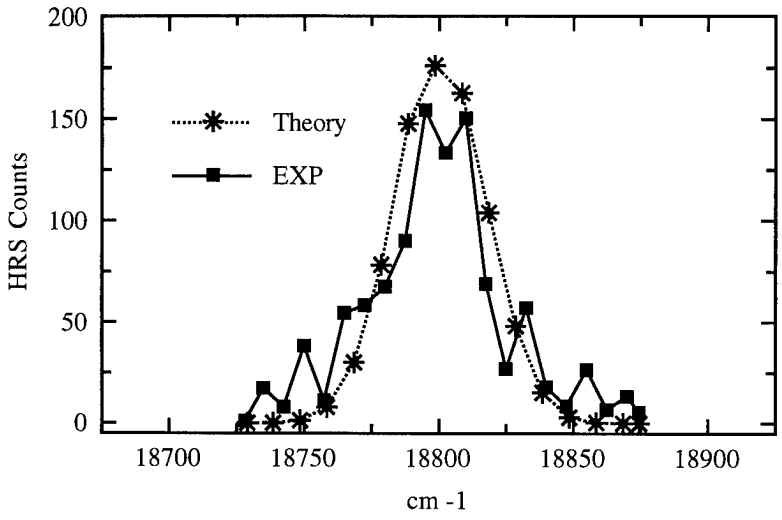

Figure 4. HRS intensity from CCl_4 vapor done in the I_{VV} geometry. The experimental curve is a composite from several scans of the vapor at temperatures ranging from 25-70 °C with a total integration time of ≈ 24 hrs. The theoretical curve was calculated with B = 0.057 cm^{-1}, T = 25 °C and convolved with a 13 cm^{-1} box slit function.

References

(1) Kielich, S. *Acta Phys. Polon.* **1964**, *26*, 135-154.

(2) Terhune, R. W.; Maker, P. D.; Savage, C. M. *Phys. Rev. Lett.* **1965**, *14*, 681-684.

(3) Clays, K.; Persoons, A.; De Maeyer, L. In *Adv. Chem. Phys.*; M. Evans and S. Kielich, Eds.; J. Wiley & Sons: **1994**; Vol. *LXXXV*; pp 455-498.

(4) Zyss, J.; Ledoux, I. *Chem. Rev.* **1994**, *94*, 77-105.

(5) Bersohn, R.; Pao, Y. H.; Frisch, H. L. *J. Chem. Phys.* **1966**, *45*, 3184-3198.

(6) Heesink, G. J. T.; Ruiter, A. G. T.; van Hulst, N. F.; Bölger, B. *Phys. Rev. Lett.* **1993**, *71*, 999-1002.

(7) Gelbart, W. M. in *Adv. Chem. Phys.*; I. Prigogine and S. A. Rice, Eds.; J. Wiley & Sons: 1974; Vol. 26; pp 1-106.

(8) Shelton, D. P.; Tabisz, G. C. *Mol. Phys.* **1980**, *40*, 299-308.

(9) Maker, P. D. *Phys. Rev. A* **1970**, *1*, 923-951.

(10) Altmann, K.; Strey, G. *J. Raman Spec.* **1982**, *12*, 1-15.

Donor-Acceptor Systems Derived from Tetraethynylethene

Rik R. Tykwinski,[a] Martin Schreiber,[a] Rolf Spreiter,[b] Christian Bosshard,[b] Corinne Boudon,[c] Jean-Paul Gisselbrecht,[c] François Diederich,[a] Peter Günter[b] and Maurice Gross[c]

[a]Laboratorium für Organische Chemie, ETH-Zentrum, Universitätstr. 16, CH-8092 Zürich (Switzerland), tel. +41-1-632 26 36, Fax +41-1-632 11 09, [b]Institut für Quantenelektronik, ETH-Hönggerberg, CH-8093 Zürich (Switzerland), and [c]Laboratoire d'Electrochemie, Université Louis Pasteur, F-67008 Strasbourg Cedex (France).

An increasing number of conjugated, organic molecules and polymers are finding application as materials for electronics and photonics due to their inherent synthetic flexibility, potential ease of processing and the possibility of tailoring material characteristics to suit a desired property.[1] To more efficiently design organic materials to specific tasks, it is necessary to understand how and to what degree alteration of molecular electronic structure affects materials properties. Investigation of a comprehensive series of synthetically related molecules and the relationship between their electronic and physical properties is perhaps the best approach to the rational design of useful organic materials. Hence, we have synthesized a complete series of conjugated, electronically varied molecules based on a tetraethynylethene (TEE, **1**) framework. Study of the optical and electrical properties of these electronically diverse building blocks will aid in tuning specific properties for the ultimate formation of functionalized polytriacetylenes (PTAs, **2**).

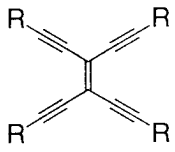

1

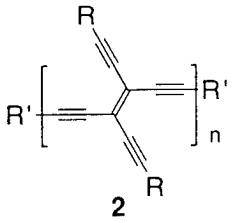

2

Utilizing the large variety of known TEE precursors as building blocks,[2] the series of functionalized TEEs was assembled via palladium catalyzed couplings, and includes representatives of all regiochemistries about the TEE core as well as several dimers (**3**-**8**). Of particular interest was the formation of *trans*-substituted TEEs, **3**, which would be subsequently used as monomers toward the formation of laterally functionalized PTAs.[3] Trends in the electrical (redox potentials) and optical (UV-Vis, fluorescence, NLO) properties as a function of substitution degree and pattern for monomers **3**-**7** and several representative dimers **8** have been

investigated. These analyses reveal that the extent and mode of conjugation (*gem*, *cis*, or *trans*) and the extent of functionalization (mono-, di-, tri-, or tetra-substituted) have profound effects on the overall optical properties of the molecules, whereas the substituent effects on the redox potential are relatively minor.

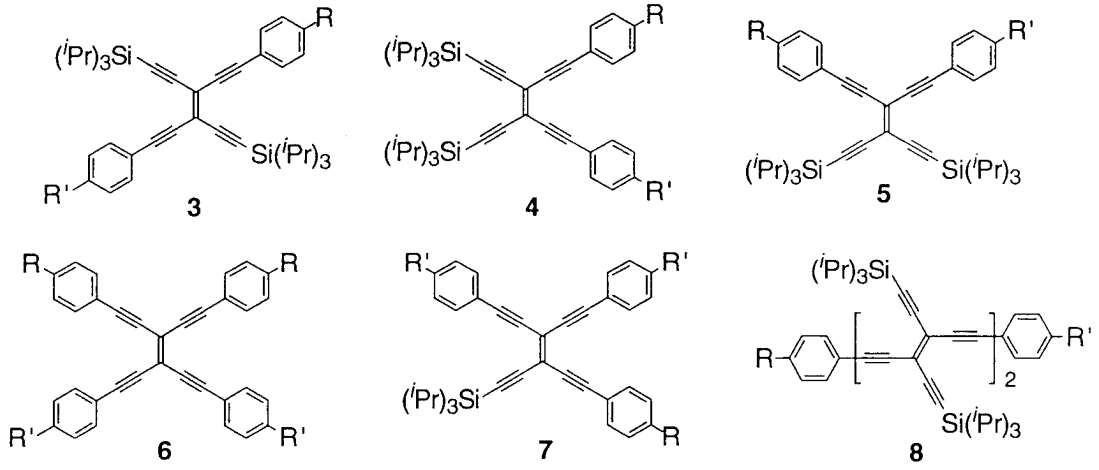

Recent work has shown that single strand, conjugated PTAs, **2**, possess intriguing optical and electrical properties, high environmental stability, high solubility and the ability to form high quality films. The versatility of functionalized TEEs as precursors to polymers is now demonstrated by the synthesis of laterally donor/acceptor functionalized PTAs via oxidative coupling of selected monomers **3**. For example, as outlined below, the oxidative coupling of *trans*-bisdeproteced TEE, **9,** in the presence of 0.01 eq. 3,5-bis(*t*butyl)phenylacetylene as an endcapping reagent affords the stable, electron rich PTA **10**. Materials properties trends in the series of monomers as well as recent advances in the synthesis of functionalized PTAs will be presented.

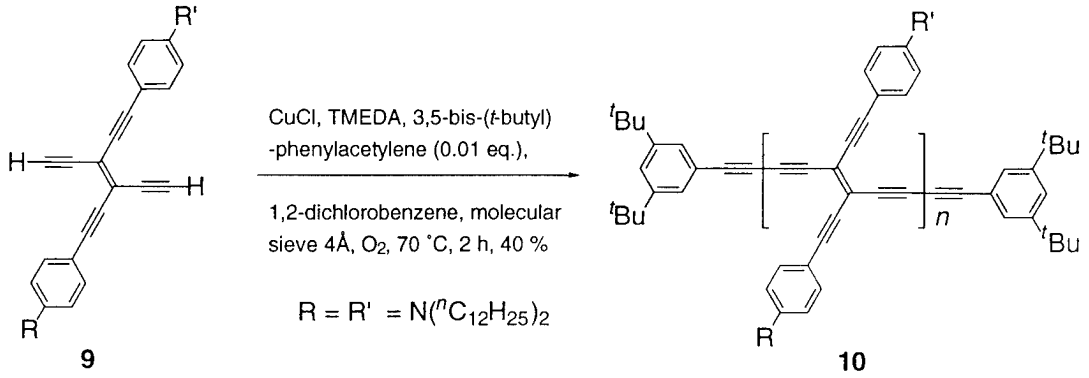

References

1. *Conjugated Polymers and Related Materials*; Salaneck, W.R., Lundström, I., Rånby, B., Eds.; Oxford University Press: Oxford, 1993. *Organic Materials for Non-linear Optics III*; Ashwell, G. J., Bloor, D., Eds.; Bookcraft: Bath, 1993. *Organic Molecules for Non-Linear Optics and Photonics*; Messier, J., Kajzar, F., Prasad, P., Eds.; Kluwer Academic Publishers: Dordrecht, 1991. Miller, J. S. *Adv. Mater.* **1993**, *5*, 671-676. Bäuerle, P. *Adv. Mater.* **1993**, *5*, 879-886.

2. Anthony, J.; Boldi, A. M.; Rubin, Y.; Hobi, M.; Gramlich, V.; Knobler, C. B.; Seiler, P.; Diederich, F. *Helv. Chim. Acta* **1995**, *78*, 13-45.

3. Schreiber, M.; Anthony, J.; Diederich, F.; Spahr, M. E.; Nespar, R.; Hubrich, M.; Bommeli, F.; Degiorgi, L.; Wachter, P.; Kaatz, P.; Bosshard, C.; Günter, P.; Colussi, M.; Suter, U. W.; Boudon, C.; Gisselbrecht, J.-P.; Gross, M. *Adv. Mater.* **1994**, *6*, 786-790.

Passive Polymer Directional Couplers: Theory and Experiment

By
Lou Bintz, Wei Feng, Jiong Ma, Sihan Lin, Darja Tomic, and Alan Mickelson

Guided Wave Optics Laboratory
University of Colorado, Boulder, CO, 80309-0425

Abstract:
We present a Computer Aided Design model of a polymer directional coupler and show some preliminary comparision of the predicted characteristics with characteristics of directional couplers fabricated in a side-chained PMMA/DR1. This model encompasses many of the physical processes and effects encountered in the manufacture of passive polymer directional couplers, including actual transverse index profile induced by bleaching, longitudinal variations in the effective index of the polymer due random variations in the material, and the coupling between wave guides in the s-bend transition region of the directional coupler.

Introduction

Polymer directional couplers are potentially high quality, inexpensive, and easily manufactured optical modulators[1,2]. However, in order to realize this potential and fabricate economically feasible devices requires a design tool which models in detail a physically realizable directional coupler. In this paper we present a design tool, based on finite element forward beam propagation, which includes modeling of the non-ideal processes which occur during manufacture of the device, inherent random characteristics present in the composition of the polymer films and coupling between wave guides in the s-bend region of the coupler. This model can then predict the performance characteristics of the manufactured device, including the effective coupling length and the predicted crosstalk of the directional coupler. In Figure 1 is a flow chart representation of the design tool, which shows the major elements of the model including the central computational element, the discrete beam propagation algorithm.

By using a finite element forward beam propagation model, we can include local perturbations of the wave guide. Though coupled-mode theory allows us to calculate the coupling length of an ideal passive directional coupler, it can not take into account the coupling in the s-bend region. And since the ideal wave guide coupled-mode calculation predicts zero crosstalk between the channels, without analytically decomposing the wave guide into sections whose length is on the order of the local coherence length of

small random variations in the index of the polymer material, no information about the crosstalk of a real device can be gleaned from the coupled mode theory model. Parameters characterizing the longitudinal variation in the material, and the transverse index profile of the wave guide, which are calculated in separate modules of the design tool, can also be incorporated in the finite element beam propagation model.

The transverse index profile of the wave guide is manufactured by selectively bleaching the polymer film. The bleaching process of the polymer is represented by a calibrated model in the bleaching module. The bleaching module returns a calculated transverse index profile which is used to calculate the local mode profile. An analytical model of the random variations in the polymer wave guide calculates an effective local coherence length and local crosstalk of the wave guide. More detailed analysis of these modules will be discussed in the following sections.

The Bleaching Model

One of the most efficient ways to prepare non-linear optical polymer channel waveguides is by photobleaching. We have developed a bleaching model that is able to predict the transverse optical index profiles for photobleached polymer films[2]. The fabrication parameters of the directional coupler are input into the module (intensity of the u.v. light, thickness and temperature of polymer layer being bleached, and duration of the bleaching process) and the optical characteristics of the polymer channel waveguides are calculated from the calibrated model. The model has been successfully applied and calibrated for photobleached PMMA/DR1 and Ultem/DEDR1 wave guides.

The Crosstalk Model

The crosstalk in passive directional couplers is limited to roughly -30 to (-35) dB. A theoretical analysis based on small random index flucuations shows that even very small, difficult to measure, random spatial variations in refractive index can result in the crosstalk levels that have been experimentally measured. The crosstalk module returns the analytical solution for the relation between crosstalk, index variation and correlation length.

Experimental Results

The passive polymer directional couplers that were fabricated had the following physical characteristics . The s-bend region had a radius of the curvature of 1 cm with a 2 cm transition length and a 100 μm lateral offset. With this bending radius the optical loss of the bend was negligible. The width of the channel wave guide was 3.6 μm, the height 2.17 μm, and the interaction gap 2.9 μm. The coupling length varied from 0 μm to 1330 μm in 70 μm steps. The PMMA/DR1 thin film was spun onto glass

substrates. After baking, we bleached the sample through a mask for 54 hours. The end face of the device was prepared using a cleaving technique.

Fig. 2 shows the comparison between the preliminary simulation results and the measurements on fabricated devices. There was good agreement between simulation results and experimental measurement. We have achieved -26 dB crosstalk.

References

[1] D.G.Girton,S.L.Kwiatkowski,G.F. Lipscomb, and R.S. Lytel," 20 Ghz electro-optic polymer Mach- Zender modulator,"*Appl. Phys. Lett.*, vol 58, no 16 , pp. 1730-1732, Apr 1991

[2] C.C. Teng "Traveling-wave polymetric optical intensity modulator with more than 40 Ghz of 3-db electrical bandwidth," *Appl. Phys. lett.* vol. 60, no. 13, pp. 1538-1540, Mar 1992

[3]Jiong Ma, Sihan Lin, Wei Feng, Robert J. Feuerstein, Brian Hooker and Alan R. Mickelson, "Modeling photobleached optical polymer waveguides", Guided wave optics laboratory report, NO. 58, April 1994, submitted to Applied Optics.

Flow Chart of Passive Directional Coupler Cad Tool

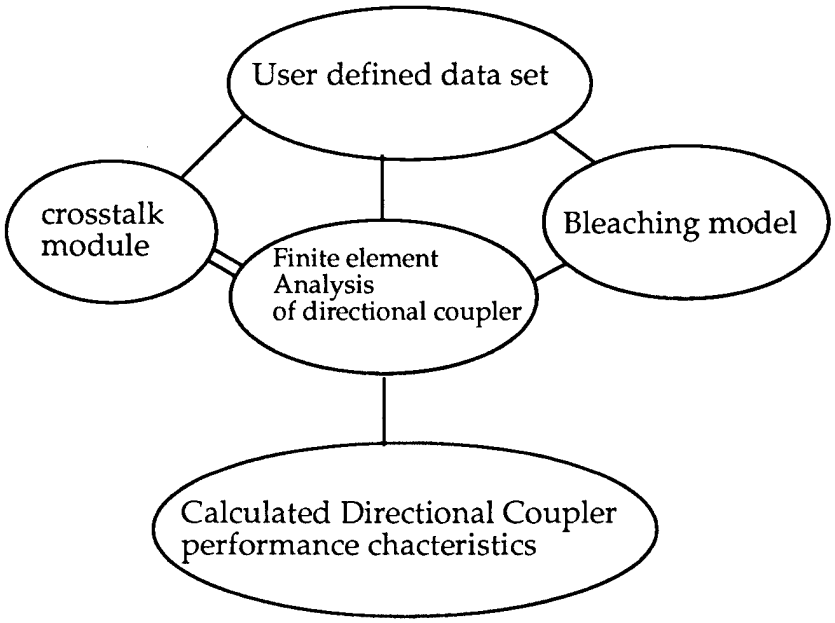

Fig.1

The comparison of measured output (points)
vs
simulated results (solid line)

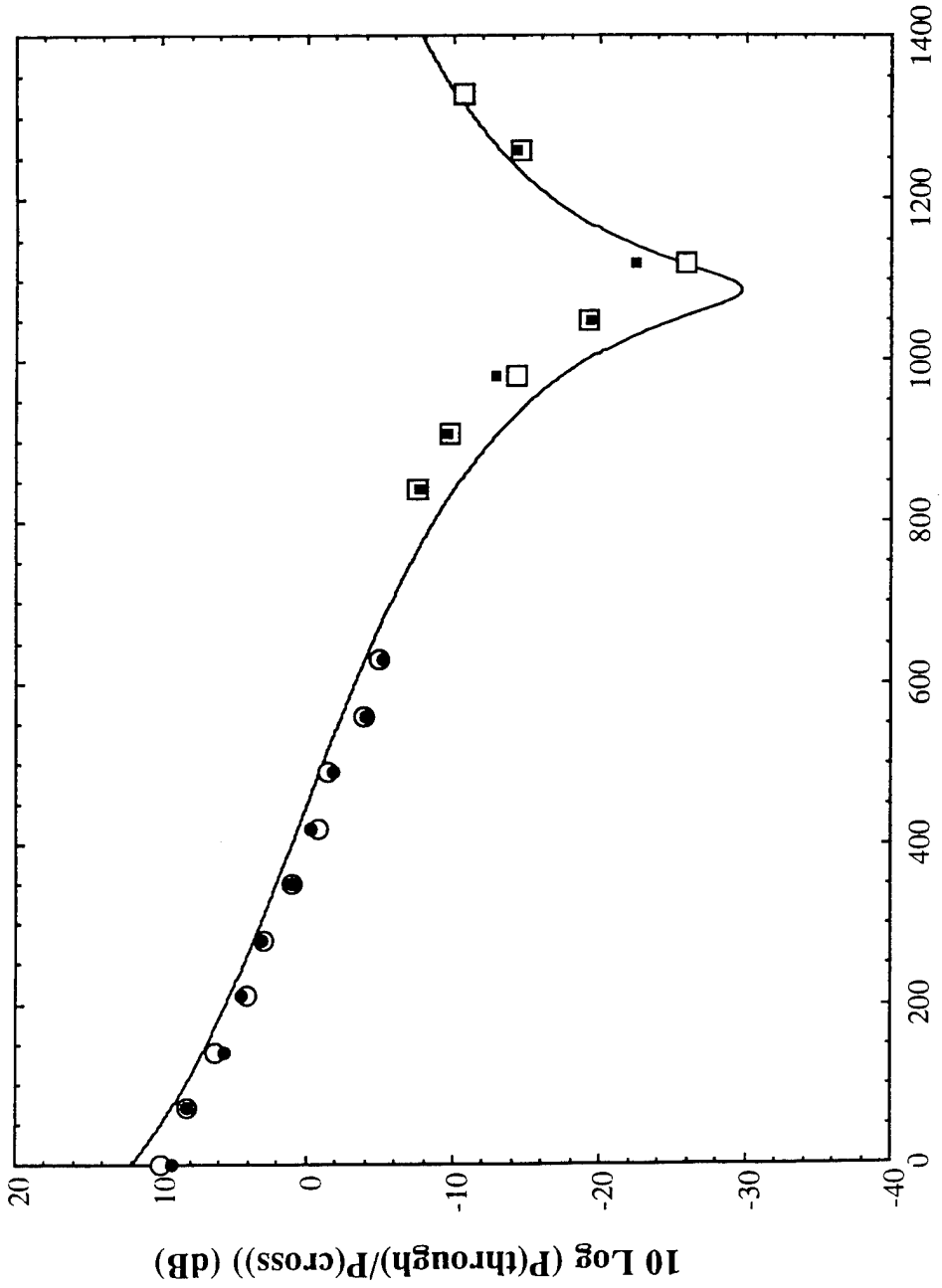

fig 2

Novel Nonlinear Optical Polymers for Second Harmonic Generation

Naoto Tsustumi*, Osamu Matsumoto, Wataru Sakai and Tsuyoshi Kiyotsukuri
Departement of Polymer Science & Engineering, Kyoto Institute of Technology, Matsugasaki, Sakyoku, Kyoto 606, Japan
Tel : 81-75-724-7810, Fax : 81-75-724-7710

Introduction

Recently, we have synthesized a new type of NLO phore whose dipole moment is aligned transverse to the main chain backbone, and resultant poled polymer film shows large second harmonic efficiency with its good thermal stability. In this paper, we present the second harmonic generation (SHG) properties of this novel type of NLO polymer material whose dipole moment is aligned transverse to the main chain backbone and compare these properties to those for the polymer with NLO phore in the main chain backbone.

Experimental

3-(2-Hydroxyethylamino)-5-(hydroxymethyl)-4'-nitroazobenzene (T-AZODIOL) was used as the NLO phore whose dipole moment is aligned transverse to the main chain backbone. T-AZODIOL was synthesized via 2 step reactions; First, 3-(2-hydroxylamino)-benzylalcohol (DIOL) was prepared from *m*-aminobenzyl alcohol with 2-chloroethanol. Then the coupling reaction of DIOL with diazotized *p*-nitroaniline gave rise to T-AZODIOL. 4-[N-(2-Hydroxyethyl)-N-methylamino]-3'-(hydroxymethyl)azobenzene (AZODIOL) dye was the NLO phore monomer for preparing the polymer with NLO phore in the main chain backbone. AZODIOL was synthesized through the coupling reaction of *m*-aminobenzyl alcohol with diazotized N-(2-hydroxylethyl)-N-methylaniline. Chemical structures of these NLO phore monomers are shown in Figure 1.

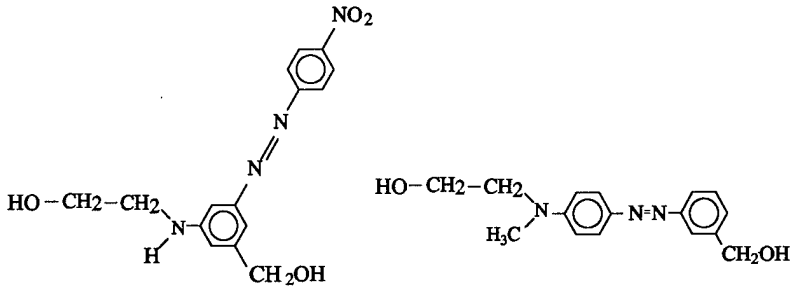

T-AZODIOL AZODIOL

Figure 1. Chemical structures and codes for NLO phore monomers.

T-polymer was prepared from T-AZODIOL with tolylene 2,4-diisocyanate in DMAc at the temperature of 85°C for 20 min in nitrogen atmosphere. L-polymer was prepared from AZODIOL with tolylene 2,4-diisocyanate in the same condition as T-polymer prepared.

The corona poling technique was employed to orient NLO phore to the poling direction. The distance between 0.1 ϕ tungsten wire for corona poling and the sample was

kept 1.4 cm. Maker fringe method was employed to measure SHG.

Results and Discussion

Poling caused the decrease of absorption intensity and shorter wavelength shift of absorption peak. Thermal annealing at the condition of the same temperature and time dose not cause the change of intensity and spectral shift. Thus, intensity change is ascribed to the orientation of azobenzene dye to the direction of the film thickness induced by poling. The spectral blue shift has been reported for other cross-linked main chain polymers, which is contrast to the red shift observed in the most side-chain polymers.

The refractive indices (RI) for transverse electric field (TE) mode are measured using m-line method at wavelength of 632.8 and 830 nm. RI values at wavelength of 632.8 and 830 nm were listed for unpoled polymer films in Table I. Wavelength dispersion of RI can be fitted to a one-oscillator Sellmeier-dispersion formula,

$$n_f^2(\lambda) - 1 = \frac{q}{1/\lambda_0^2 - 1/\lambda^2} + A \qquad (1)$$

where λ_0 is the absorption wavelength of the dominant oscillator, q is a measure for the oscillator strength, and A is a constant containing the sum of all the other oscillators. RI values of at 532 and 1064 nm for the use of SHG calculation are obtained from the predicted plot and also listed in Table I for both T-polymer and L-polymer.

Table I. RI values at wavelength of 632.8 and 830 nm measured and those at 532 and 1064 nm predicted using Eq. (1).

	Wavelength (nm)			
Polymer	632.8	830	532	1064
T-polymer	1.6957	1.6686	1.779	1.661
L-polymer	1.6828	1.6499	1.745	1.638

The SHG coefficients of the polymers are made relative to a Y-cut quartz plate (d_{11}=1.2 × 10^{-9} esu). The typical Maker fringe pattern could be observed for both the case of p-polarized and s-polarized fundamental beam.

It is important to optimize the poling condition (poling voltage, temperature and time) to obtain better SHG activities.

For T-polymer, SHG coefficient increased with increasing applied voltage and leveled out at the voltage above 8.0 kV. Increase of poling temperature causes the increase of SHG coefficient with large increment of coefficient at the temperature around 95°C. Poling time increased SHG coefficient with leveled out SHG coefficient at the time above 1h. When the sample film was poled at the optimum condition of poling voltage of 8 kV, temperature of 95°C and time of 60 min, d_{33} value of 1.6 × 10^{-7} esu (67 pm/V) were

obtained. This value is larger than SHG coefficient of lithium niobate ($LiNbO_3$).

For L-polymer, poling at the temperature above 70°C caused the film surface opaque. SHG coefficient increased with increasing applied voltage up to 7 kV with its decrease above 8 kV.

In the theoretical expression of SHG coefficient d_{33} can be written as

$$d_{33} = \frac{N f_\omega^2 f_{2\omega} \beta \mu_g E_p}{10kT} \tag{2}$$

where N is the number density of noncentrosymmetric NLO guest molecules, β is the hyperpolarizability of the NLO guest, f_ω and $f_{2\omega}$ are Lorentz-Lorenz local field factors of the form $(\varepsilon + 2)/3$, and T is the poling temperature. The value of ε has been taken as the square of the refractive index of the sample at either the fundamental or second harmonic frequency. The number of density N is calculated using the film density. To evaluate d_{33} values from eq. (2), β, μ_g and E_p values must be estimated from the absorption spectra data.

E_p was determined from the intensity change in absorbance caused by the orientation of NLO phore, using the electrochromic theory. The orientation-induced intensity change in absorbance can be related to the electric field, using the electrochromic theory.

$$\frac{A(p)}{A(0)} = 1 - \frac{3\coth(u)}{u} + \frac{3}{u^2} \tag{3}$$

where $A(p)$ and $A(0)$ are the absorbance with and without electric field, respectively and $u=(\mu_g E_p)/(kT)$.

β can be calculated using the two level model,

$$\beta = \frac{9e^2}{4m}\left(\frac{h}{2\pi}\right)^2 \frac{W}{[W^2-(2h\nu)^2][W^2-(h\nu)^2]} f \Delta\mu \tag{4}$$

where e is an elementary electric charge in esu, m is a rest mass of electron, h is Planck's constant, W is the energy at the absorption wavelength of the dominant oscillator, and $h\nu$ and $2h\nu$ are the energies of the fundamental and second harmonic light. f is the oscillator strength of the dominant oscillator and can be evaluated from the absorption spectrum of the dominant oscillator.

Assuming the dipole moment at the ground state μ_g and the dipole moment difference between ground and excited states $\Delta\mu$ ($=\mu_e - \mu_g$) from those for well known azobenzene dyes, β and d_{33} could be calculated. For T-polymer, d_{33} can be calculated as 1.0×10^{-7} esu using E_p of 2.7 MV/cm, μ_g of 8 D and β of 119×10^{-30} esu, whereas experimentally obtained d_{33} was 0.91×10^{-7} esu. Experimentally obtained d_{33} value is in good agreement with theoretically calculated one.

Figure 2 shows the long-term thermal stability of d_{33} for both T-polymer and L-polymer when the sample films were stored at room temperature for the time which are

shown in the horizontal axis in the figure. Plot in the figure is in the form of SHG coefficients d_{33} normalized by that measured at time of zero. It is noted that T- polymer has good long-term thermal stability. Both polymers have the glass transition temperature (T_g) around 35°C.

Figures 3 and 4 shows the SHG activity profile for T-polymer and L-polymer, respectively, which is first carried out at 30°C and then at higher fixed temperature shown in the horizontal axis in the figure. T-polymer does not show significant loss at the temperature around 65°C and the large activity loss occurs at the temperature above 80°C. These temperatures are far from the T_g of T-polymer. Further and detailed investigation for thermal stability of SHG activity when T-polymer film is stored at the temperature of 50 and/or 60°C is in progress. Whereas, for L-polymer, initial SHG loss starts at the temperature around 40°C (initial SHG loss temperature) which is close to T_g for the sample. Significant large activity loss occurs at the temperature around 50 - 55°C.

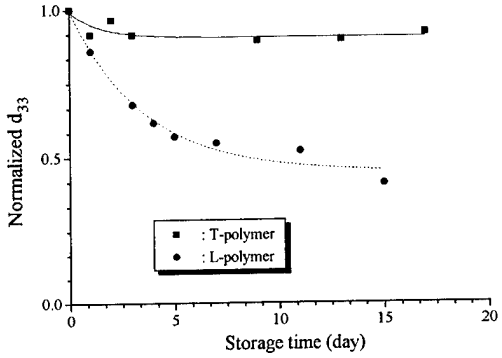

Figure 2. Long-term thermal stability of d_{33} values when the sample films are stored at room temperature.

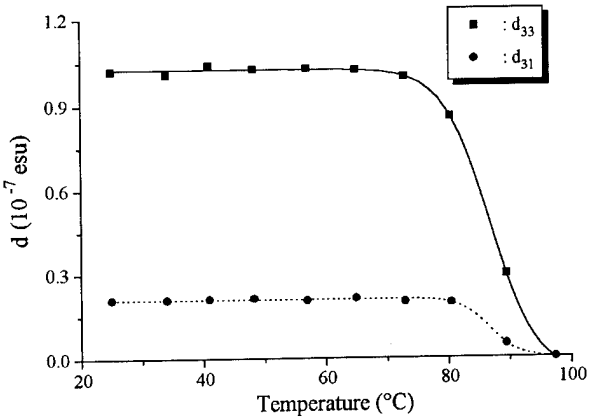

Figure 3. Temperature profile of d_{33} and d_{31} for T-polymer

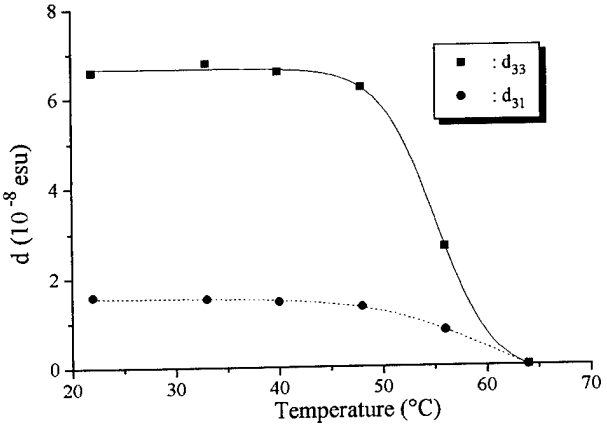

Figure 4. Temperature profile of d_{33} and d_{31} for L-polymer.

Growth and Characterization of Vacuum Deposited Organic Thin Films

Kang I. Seo, Isaac Jones and Calvin W. Lowe
Department of Physics, Alabama A & M University, Normal AL 35762

1. INTRODUCTION

The properties of vacuum evaporated thin films are of current interest both from applied and fundamental standpoints, as they may lead to useful and unusual devices. While such thin films have traditionally been composed of inorganic materials, it has recently been known that organic thin films can also have potentially useful electrical and optical behavior related to their large nonlinear optical susceptibilities. Thin films of large stable organic molecules such as perylenetetracarboxylic dianhydride (PTCDA) on semiconductor surfaces were extensively studied by Forrest *et al.* [1-4].

Vacuum evaporation, one of the oldest and the most widely used techniques in depositing solid films, is the basis of our organic molecular beam deposition (OMBD) stations. The vacuum system is made up of a stainless-steel custom vacuum chamber baked to 200 °C to reach a normal base pressure of 2×10^{-9} Torr after 8 hours.

Ellipsometry and prism coupled waveguiding are use to measure refractive index and thickness at various positions across the substrate. Infrared spectra of the deposited films are compared to the organic powders to study any change that might occur during deposition at elevated temperatures. Morphology of the films is checked with a scanning electron microscopy. The degree of orientation of the crystallites in the films is studied by X-ray diffraction.

The aim of the experiment is to find the optimal conditions for thin film growth of various organic materials. The film structure is influenced by the relationship between the pressure inside the chamber and the temperature of the effusion cell.

2. EXPERIMENTAL DETAILS

All commercial organic materials were purified by repeated vacuum sublimation and were finally obtained as small needle-like crystals. Two aromatic dianhydrides, 3,4,9,10-perylenetetracarboxylic dianhydride (PTCDA) and 3,4,7,8-naphthalenetetracarboxylic dianhydride (NTCDA), were separately deposited on (100) Si wafers with various growth conditions [5]. Typical sublimation temperatures under atmospheric pressure were approximately 465°C and 300°C for PTCDA and NTCDA, respectively. One of the organic materials that has received great attention is mixed methyl-(2,4-dinitrophenyl)-aminopropanoate : 2-methyl-4-nitroaniline (MAP:MNA); a new nonlinear optical material [6].

The molecular beams are generated under UHV conditions from custom designed quartz effusion cells, whose temperatures are accurately regulated by PID controllers with K-type thermocouplers. The intensity of the beam incident on the substrate surface is controlled by varying the temperature of the effusion cell.

3. RESULTS AND DISCUSSIONS

Deposited films of PTCDA on Si wafers are red and transparent, while films of NTCDA and of mixed MNA: MAP are light yellow.

Ellipsometry at 6328 Å (He-Ne laser line) was performed using a Gaertner Scientific Ellipsometer Model L116. We varied the ellipsometric angles for the incident beam to profile the refractive index of the thin film. We found that the refractive index of NTCDA is 1.542 and that of PTCDA is 1.696. The refractive index, n=1.622, of mixed MNA:MAP was measured by prism coupler with 6328 Å wavelength. Once the refractive index was determined for the deposited film, the index was fixed to obtain the film thickness of samples.

An ellipsometric thickness survey was taken over the 1cm x 2cm surface of PTCDA and NTCDA films. Though the substrates were not rotated during deposition, we found no more than 4.5 % thickness variations. The design of our crucible and the operating conditions of our vacuum station are the most likely cause. A computer model of film uniformity for inorganic films agree reasonably well with our results [7,8].

The IR spectra were measured by a Perkin-Elmer FT-IR 1725X spectrometer. An IR spectrum of a 941 Å PTCDA film (400 °C crucible temperature ; film#2) on a Si wafer is shown in Fig. 1. IR spectra of a purified PTCDA solid on a KBr plate and with various crucible temperatures included.

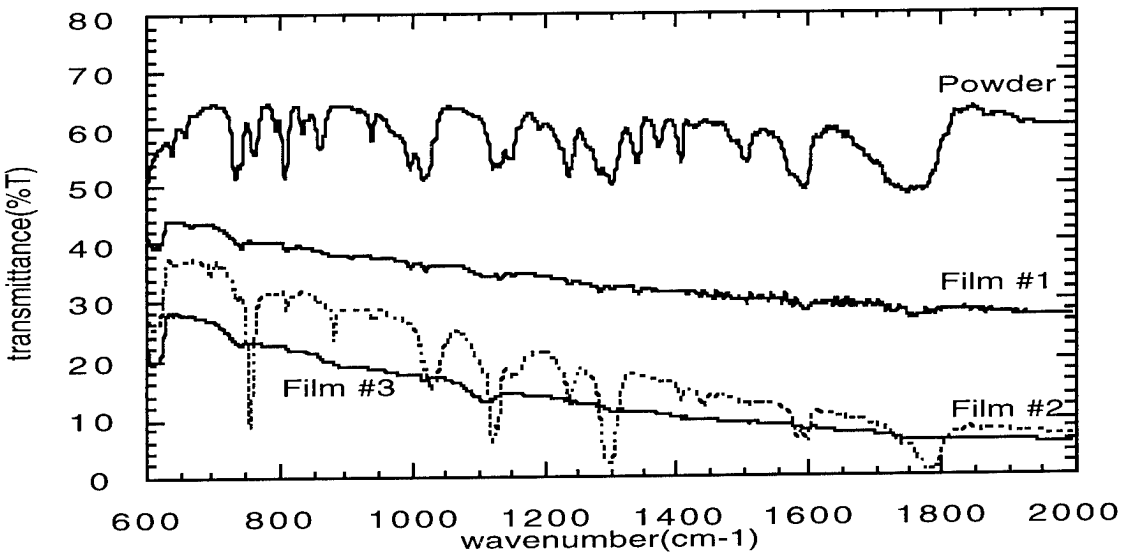

Fig. 1 Infrared spectra of PTCDA samples with various effusion cell temperatures (#1=500 °C ; #2=400 °C ; #3=375 °C) and powder pellet

Taking the 1299 cm^{-1} band in Fig. 1, one can notice that the ring stretching vibration in a film has a sharper peak than in a KBr pellet because of molecular orientation. Similarly, in the NTCDA spectrum, bands are seen at 1581 and 1455 cm^{-1} in the film

that are assigned to benzene ring stretch vibrations. The 1768 cm^{-1} band is observed for C=O stretch vibration. Several bands occurring in the KBr pellet, often with a large intensity, disappear in the single crystal spectrum (300 °C of crucible temperature) due to thermal decomposition.

The scanning electron microscopy (SEM) image of the NTCDA film is continuous and made of densely packed crystallites. The planar NTCDA molecules tend to deposit smoothly on the substrate. The SEM images of PTCDA films of various thickness on Si substrate are shown in Fig. 2. The films were also continuous and consisted of densely packed crystallites. The effect of substrate temperature during deposition was studied in the case of PTCDA. On the lower-temperature substrate, the continuity is high with smaller crystallites. It is evident that a low-temperature substrate is better for film growth from the viewpoint of continuity.

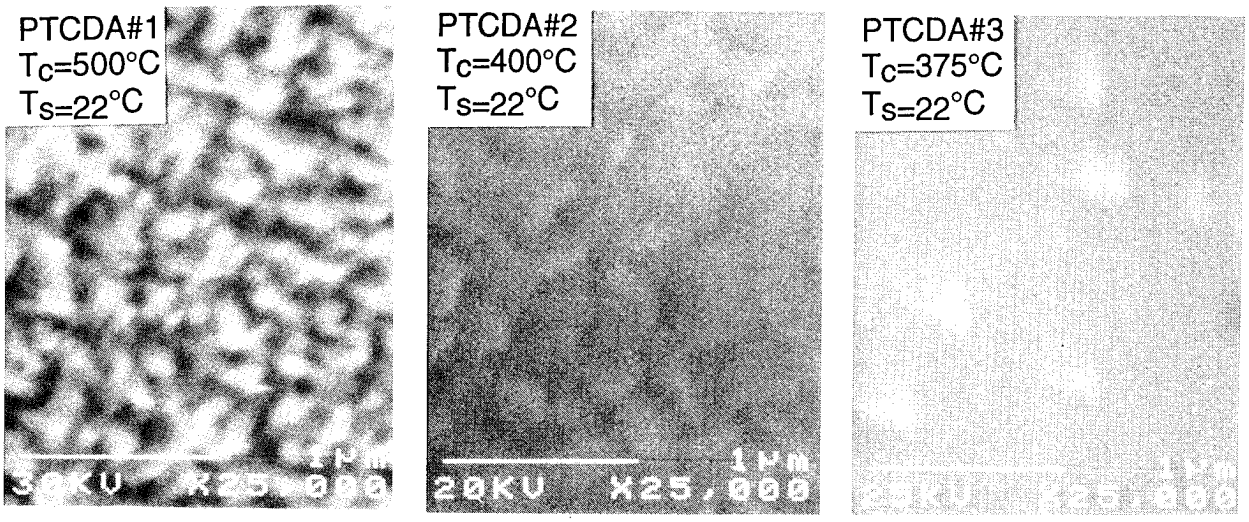

Fig.2 scanning electron micrographs of PTCDA with various growth conditions

X-ray diffraction measurements were carried out at room temperature using an X-ray diffractometer (PW 1840, Philips) operated with Cu Kα(λ = 1.5405 Å) radiation. The peak value for NTCDA samples is indicated at 2θ =33.37° for 300°C of crucible temperature. Clear diffraction peaks are seen for PTCDA films prepared with crucible temperatures of 500°C,400°C and 375°C. The sharpness of those peaks indicates a single orientation of the molecule with respect to the substrate surface. The broad background peak in Fig. 3 is due to X-ray reflections from the substrate.

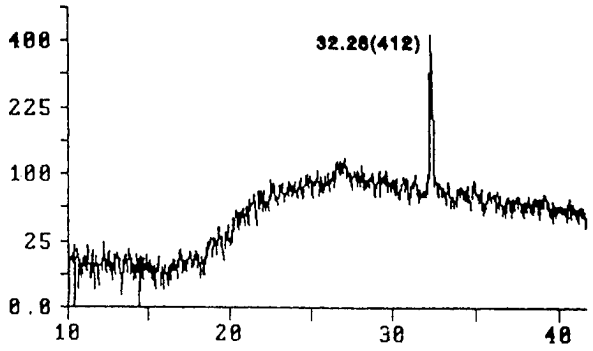

Fig. 3 X-ray diffraction pattern of PTCDA

The samples of mixed MNA:MAP are made with an effusion cell temperature of 105°C with various substrate temperatures. Fig. 4 shows a SEM image of mixed MNA:MAP at a substrate temperature of 22 °C . The SEM images show the increase in cluster size with lower substrate temperature.

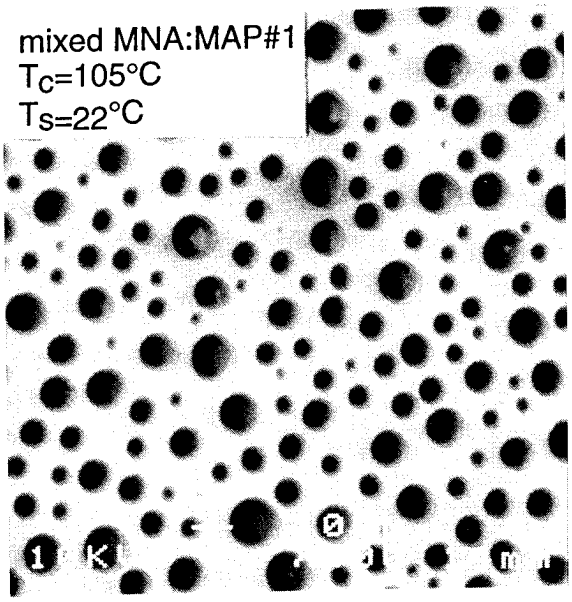

Fig. 4 SEM image of mixed MNA:MAP

4. CONCLUSION

PTCDA, NTCDA and mixed MNA:MAP have been used as model materials for other thin film materials. Vacuum-deposited organic materials have been shown to exhibit optimized properties including uniformity, optical absorption, orientation of molecules, and electrophotographic performance when the condensation (substrate) temperatures are held at room temperature or lower- temperature.

The OMBD technique was successfully applied to obtain organic thin films on (100) Si wafer with appropriate cell and substrate temperatures, the deposited films were continuous and made of densely packed crystallites. The film surface is made smooth and uniform without sample rotation by specially designed effusion cell.

References

[1] S. R. Forrest, M. L. Kaplan and P. H. Schmidt, J. Appl. Phys. **56**, 543 (1984)
[2] S. R. Forrest, M. L. Kaplan P. H. Schmidt and J. M. Parsey, Jr., J. Appl. Phys. **58**, 867 (1985)
[3] F. F. So, S. R. Forrest, Y. Q. Shi and W. H. Steier, Appl. Phys. Lett. **56,** 674 (1990)
[4] F. F. So and S. R. Forrest, Phys. Rev. Lett. **66**, 2649 (1991)
[5] Obtained from Aldrich Chemical Co.Inc., Milwaukee, Wisc. 53233
[6] S. M. Rao, A. K. Betra, R. B. Lal, R. A. Evans, B. H. Loo, R. M. Metzger and W. J. Lee, J. Appl. Phys. **70**, 6674 (1991)
[6] R. M. Metzger, J. L. Atwood, W. J. Lee, S. M. Rao, R. B. Lal and B. H. Loo, Acta Cryst. **C49**, 738 (1993)
[7] J. A. Curless, J. Vac. Sci. Technol. **B3**, 531 (1985)
[8] K. I. Seo and C. W. Lowe, to be published

Fabrication of Organic Thin Films by Laser Ablation Deposition for Electro-Optics Devices

Takeo FUJII, Hiroki SHIMA, Naotaka MATSUMOTO, and Fumihiko KANNARI

Department of Electrical Engineering, Faculty of Science and Technology,
Keio University,
3-14-1, Hiyoshi, Kohoku-ku, Yokohama 223, JAPAN

Tel. +81-45-563-1141
Fax. +81-45-563-2773

1. Introduction

Various functions of organic materials in opto-electronics have been received much attention. Development of process technologies of various organic films, which are especially aimed for controlling their architectures in nanometer size, is also growing interest. Although inorganic films such as high-temperature ceramic superconducting materials or ferroelectric ceramics have been successfully fabricated in laser ablation deposition schemes, there is less experimental results available on organic thin film deposition with laser ablation.

Recently, we succeeded in fabrication of crystalline thin films of polytetrafluoroethylene (PTFE) by F_2 laser (157 nm) ablation [1]. X-ray photoemission spectra indicated that the composition of deposited films was similar to the source material. The significance of the laser ablation deposition technique is its controllability from shot-to-shot. Therefore, laser ablation processes are suitable for fabricating new material structures consisting of different types of materials, such as organic and inorganic, with nanometer-size resolution.

In this work, we experimentally studied the fabrication of non-polymer organic thin films with UV laser ablation method. Since most of organic molecules studied for opto-electronics applications have complex structures with relatively long chemical chains, reconstruction of such chemical structures on a substrate from decomposed target fragments, which was succeeded for simple molecular structures of PTFE polymers even with 10 times as high as the laser fluence at an ablation threshold (~90 mJ/cm^2) [1], seems to be more difficult [2]. When decreasing the laser beam energy to minimum, the process is effectively equivalent to a moderate molecular beam generation with keeping the original molecular structures, which is more like a laser desorption from solid surface, followed by layer formation on a substrate. Therefore, it is important to find a laser energy range allowed for organic thin film fabrications with accurate structure transfer from the target.

2. Experimental Methods

The thin film deposition was carried out in Ar atmosphere of ~200 mTorr or in vacuum of

~10^{-5} Torr. The KrF laser beam with the pulse length of ~25 ns [a full width at half maximum (FWHM)] was incident through a focusing lens (f=200 mm) on CuPc or DANS targets, which were fabricated by casting the powder under high mechanical stress. The films were grown on a monocrystal silicon (100) substrate or a glass substrate located at 3-cm apart from the target under the substrate temperature of ~300 K. Film surface analyses were performed by X-ray photoemission spectroscopy (XPS), scanning electron microscopy (SEM), X-ray diffraction (XRD), and Fourier transform infrared (FTIR). Electrical property of CuPc thin films was examined by fabricating a Schottky diode.

3. Results and Discussion

Once molecules are decomposed in laser ablation, reconstruction of thin films with the same molecular structures as those of the target material seems to be difficult. Therefore, a first step of our experiments was aimed to clarify whether a process, in which only inter-molecular bonds are dissociated by the laser ablation with minimizing the decomposition of molecules, is possible when reducing the laser fluence to the laser ablation threshold as close as possible. We measured the laser ablation threshold of CuPc with the KrF laser to ~20 mJ/cm^2.

When a large laser fluence of 1.5 J/cm^2 was used, although there is no clear energy shift in the XPS spectra compared with those of CuPc target, the relative concentration of nitrogen to carbon (N/C) extremely decreased. It is speculated that nitrogen atoms are easily removed during the laser ablation and never recontained again in the reconstructed film. In the FTIR spectrum obtained at 1.5 J/cm^2, the peaks that can be observed below 1400 cm^{-1} in a vacuum evaporated CuPc film completely disappeared. Therefore, at higher laser fluences, CuPc molecules are significantly decomposed to small fragments. On the other hand, the XPS spectra obtained for the CuPc film with a low laser fluence of 30 mJ/cm^2 show almost the same N/C ratio as that of the target. FTIR obtained at 30 mJ/cm^2 also shows the similar spectra to that of the vacuum evaporated film. Therefore, it seems that the main architecture of CuPc can be kept in the thin films at near the ablation threshold fluences.

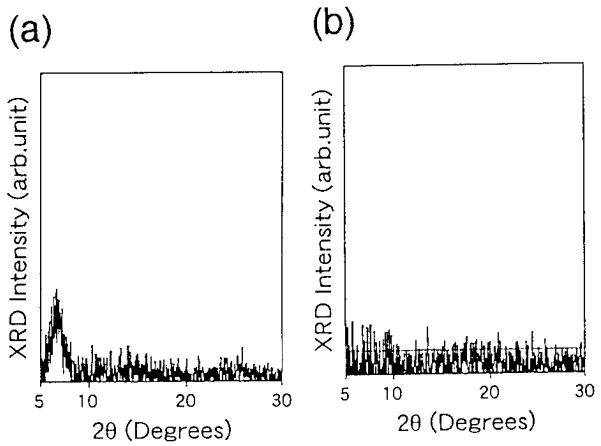

Fig. 1 2θ XRD scans of CuPc thin films deposited by KrF laser ablation at (a) 30 mJ/cm^2; (b) at 1500 mJ/cm^2

Crystallinity of CuPc films was evaluated with XRD. Although the CuPc target exhibits many

peaks with a highest peak at 7°, the film deposited with the vacuum evaporation shows only a single peak at 7°, which characterize an α-type molecular orientation. Figure 1 shows the 2θ XRD scans of films deposited by the laser ablation in 10^{-5} Torr at room temperature. Although the film deposited at 1.5 J/cm^2 does not show any crystalline peak, the film deposited at 30 mJ/cm^2 exhibits a single peak at 7° indicating that an α-type molecular orientation is dominant in the film.

The SEM of CuPc films deposited at room temperature by the laser ablation shows many particles and porous structures on the film. The films fabricated by the vacuum evaporation is more smooth surface. However, as demonstrated in PTFE thin film deposition with a F_2 laser ablation, slight increases in substrate temperature will drastically improve the surface morphology [1].

V-I curves of Schottky diode constructed between an Al electrode and the thin films deposited by laser ablation shows a clear unidirectional V-I characteristics. Therefore, CuPc thin films deposited by laser ablation still keep the electrical characteristics of CuPc.

Similar thin film depositions were repeated for DANS with the KrF laser ablation. DANS film fabricated at a laser fluence of 30 mJ/cm^2 shows similar XPS spectra to that fabricated by the vacuum evaporation, although N1s peak corresponding to the NO_2 bond indicates that N-O bonds were slightly depleted relative to N-C bonds in the ablation deposited film. Figure 2 shows FTIR spectra of DANS. Since the DANS target was fabricated by casting DANS powder under high pressure, FTIR spectrum shows many broadened structures, indicating a random molecule orientations. The DANS thin film deposited by the laser ablation shows narrower spectra that

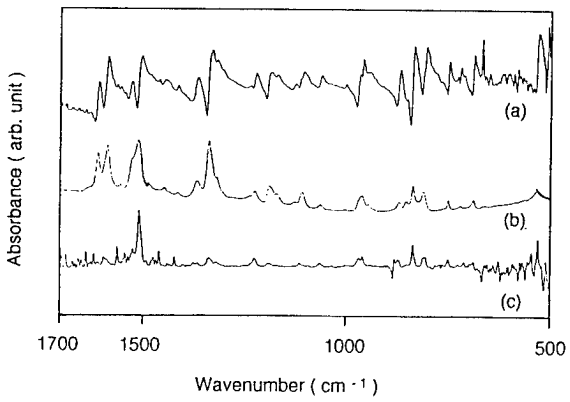

Fig. 2 FTIR spectra of DANS thin films: (a) target; (b) KrF laser ablation at 30 mJ/cm^2; (c) vacuun evapolation

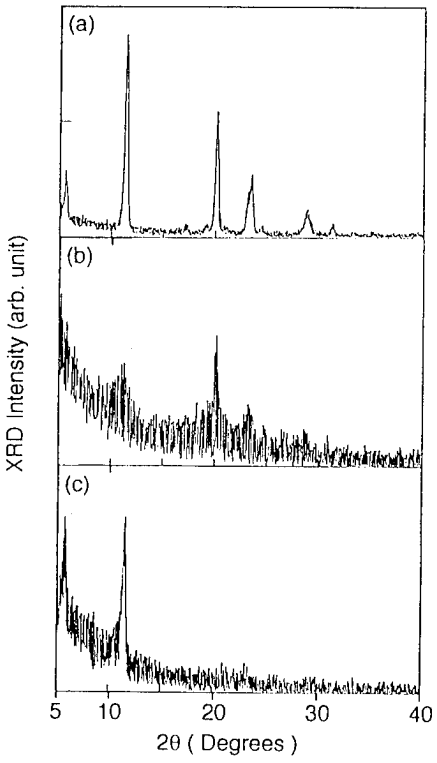

Fig. 3 2θ XRD scans of DANS thin films: (a) target; (b) KrF laser ablation at 30 mJ/cm^2; (c) vacuum evapolation

basically correspond to the spectra of target. FTIR spectrum obtained for DANS film fabricated by the vacuum evaporation shows only selected peaks. Therefore, the vacuum evaporation process holds the selectivity in DANS molecular orientation. Figure 3 shows 2θ XRD scans of DANS. The target shows peaks at 6, 12 23 and 25°. The vacuum evaporated DANS shows large peaks at 6 and 12°. However, DANS fabricated by the laser ablation shows a strong peak at 20° with weak and broader peaks at 12, 23 and 25°. Therefore, XRD measurements also indicated the absence of selectivity of crystal orientation in the laser ablation process at room temperarure.

4. Conclusion

Non-polymer organic thin films of CuPc and DANS were deposited by the KrF laser ablation. Crystalline thin films with accurate composition transfer from the target material were fabricated when reducing the laser ablation fluence close to the ablation threshold fluence. Higher laser fluences cause the decomposition of molecules to smaller size fragments, which can not be reconstructed on the substrate to the original molecular architectures. Electrical contact between the Al and CuPc films fabricated at a laser fluence of 30 mJ/cm^2 under 10^{-5} Torr shows V-I characteristics of Schottky diode, indicating that the film still maintains electrical property of semiconductor. Similarly, DANS films with no significant modification in the molecular structure were fabricated with the laser ablation. However, both FTIR and XRD spectra indicated that the thin films deposited at a substrate temperature at 300 K have no molecular orientation selectivity for DANS.

In order to use the organic thin film fabrication with the laser ablation scheme for novel functional materials, the controls of molecular orientations and achievement of uniformity at the surface and boundaries between different layers have to be developed. Epitaxial film growth of organic materials with laser ablations, which is already an established technique in inorganic materials, is growing interest.

References

1. Y. Ueno, T. Fujii, and F. Kannari, Appl. Phys. Lett. **65**(1994) 1370.

2. K. Higaki, C. Nagai, O. Murata and H. Itoh, J. Photopolymer Sci. Technol. **6**(1993) 429.

Dependency of Sidechain Chromophore Orientations on Langmuir-Blodgett Polymer Structures

D. West, D.L. Williams, T.A. King
Department of Physics & Astronomy, Brunswick St., University of Manchester,
M13 9PL, UK. Tel +44 161 275 4292 Fax +44 161 275 4293
dave.west@man.ac.uk

Z. Ali-Adib, P. Hodge, D. Dunne
Department of Chemistry, Brunswick St., University of Manchester, M13 9PL, UK

The LB technique allows optical chromophores to be placed within a predetermined series of organic molecular layers. Moreover, the orientations of the chromophores can be controlled when they are positioned in the apolar tail sections of the amphiphiles that are used. The fragility, the tendency to reorganise and even the diffusion mobility of dyes included in an LB film may be greatly reduced if polymeric materials are used. In addition to thermal and mechanical stability, polymers offer an amorphous structure in the plane of the film layers with a reduction in optical scatter relative to monomer films of materials such as fatty acids[1].

Individual molecular layers are extremely thin, and a thicker film (of the order of a micron thick) is advantageous for many optical techniques. In optical configurations where light is transmitted through the film plane, a thicker film gives increased optical path lengths in the film. Waveguided configurations require a film thick enough to support guided modes. However, when several hundred molecular layers are deposited in sequence to build up a thicker film, the layers deposited later are often considerably more disordered than the initial layers. This problem has been particularly common in alternating layer "AB" films with non-centrosymmetry in the direction perpendicular to the layer planes, such as have been developed for SHG studies. We have shown that it is possible using polymeric materials to deposit such alternating layer LB films of consistently high sidechain structural order with up to 600 layers[2].

For correct interpretation of optical studies on these thicker films it is important to check carefully that structure is preserved throughout the transverse structure of the film[3]. Accordingly a range of checks are used, including the trough deposition ratio, optical density measurements as a function of number of layers deposited, the number of small angle X-ray diffraction peaks observed from the film, ellipsometry for the complex refractive index, birefringence and thickness of the films, and waveguide m-line spectroscopy.

Some aspects of the sidechain packing may be deduced from the X-ray diffraction Bragg spacing and FT-IR spectroscopy. For nonlinear alternating layer LB films, the study of SHG as a function of angle of incidence is the most sensitive test of the ordering, revealing the angle of tilt of the nonlinear chromophores and the consistency of the structure as thicker films are built up. By observing the rate of change of the square root of second harmonic intensity as the number of layers is increased, a profile of the effective nonlinearity can be deduced as a function of the

distance from the substrate. This effective nonlinearity is partially dependent on the tilt angle and packing of the chromophores in the apolar sidechains. For applications such as SHG and electro-optic devices, it is advantageous in these films to lift the chromophores up from the plane of the molecular layers towards the perpendicular to the film.

Experimental

The requirements to produce uniformly structured thicker nonlinear LB films restrict the choice of materials that can be used successfully. However, we show that there is scope within these restrictions to vary the sidechain structure of the polymers in the film considerably increasing the elevation of the dipolar chromophores. In principle any dipolar chromophore could be used[4], and we have continued to use hemicyanine-based polymers alternated with a long chain polyvinyl pyridinium salt as a convenient example, studied by SHG from an Nd:YAG laser at 1064 nm wavelength.

A series of comparative studies of novel materials is presented. The effect on the chromophore tilt of varying the length of the alkyl group at the end of the active sidechain in a copolymer can be dramatic, varying from an essentially flat 78° to a range of tilts around 57° from the upright. Using an alkyl chain length matched to that of the pyridinium salt layer is in this case counterproductive (figure 1). Where there is a poor match between active sidechain and passive sidechain in the copolymer, the more upright orientation of chromophores is not stable and different sample films show widely varying structures.

A closer resemblence between active and passive sidechain units in the copolymer has been used in a series of films designed to examine the effects of increasing the distance of the delocalised electron systems of the sidechains from the main chain of the polymer. Saturated hydrocarbon chains of three differing lengths have been used to link the chromophore to the polymer backbone (figure 2). This does not affect chromophore tilt but does appear to affect the nonlinear response of the films.

Using a series based on an analogous homopolymeric nonlinear polymer, the effect of the size of the alkyl group at the end of the sidechains is the reverse of the copolymer case: here, a match between the alkyl end groups of the nonlinear polymer and the pyridinium polymer provides the optimal structure and film chromophore response (figure 3). For a 45° angle of propagation through the film, the effective nonlinear susceptibility of 30 pmV^{-1} in thick films of this structure is the best result possible based on the chromophore response for hemicyanine and the LB tilted chromophore structure, which yields maximal SHG efficiency for this experimental configuration when chromophores are elevated approximately 45° from the plane of the film.

In conclusion, using the "AB" alternating layer Langmuir-Blodgett film structure it is possible to produce films hundreds of layers thick with uniform structure for each successive polymeric bilayer. In this structure, the angle from the vertical at which the nonlinear chromophores rest in the sidechains is to some extent controllable. We note that the nonlinear response of the films do not vary linearly with chromophore loading. The origin of tilt-angle independent variations in

film nonlinear response may be found in local field effects and interactions between delocalised electron systems.

References

[1] P. Hodge and N.B. McKeown, in "Principles and Applications of Nonlinear Optical Materials" eds R.W. Munn and C.N. Ironside, Chapman & Hall, London 1993.
[2] "Efficient second harmonic generation from all-polymeric Langmuir-Blodgett "AB" films containing up to 600 layers" P. Hodge, Z. Ali-Adib, D. West and T.A. King, Thin Solid Films **244**(1994) 1007-1011.
[3] "Order in thin organic films" R.H. Tredgold, Cambridge University Press 1994.
[4] "Second harmonic generation from thick all-polymeric Langmuir-Blodgett films prepared using polyurethanes" M. Conroy, Z. Ali-Adib, P. Hodge, D. West and T. King, J Mater Chem **4(1)** (1994) 1-4.

Acknowledgement
One author (DW) gratefully acknowledges financial support from the Royal Commission for the Exhibition of 1851.

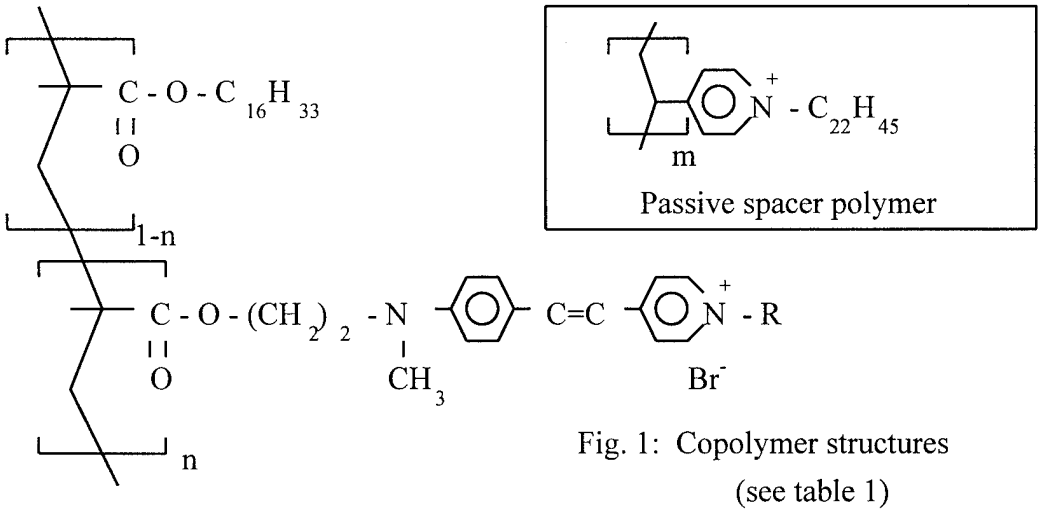

Fig. 1: Copolymer structures (see table 1)

table 1: Properties of first series of copolymers

End group R	loading, n	Nonlinearity χ_2 (pmV^{-1})	Chromophore tilt angle
$C_{22}H_{45}$	37%	1.5	78°
C_5H_{11}	45%	*approx.* 10	57°

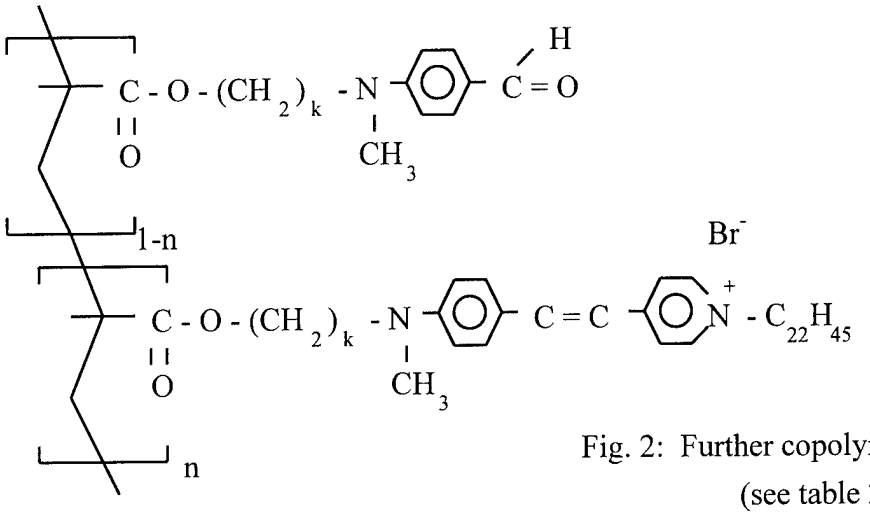

Fig. 2: Further copolymer structures
(see table 2)

table 2: Properties of second series of copolymers			
Alkyl bridge length, k	Loading, n	Nonlinearity χ_2 (pmV^{-1})	Chromophore tilt angle
2	60%	3	53°
3	68%	18	53°
4	30%	5	52°

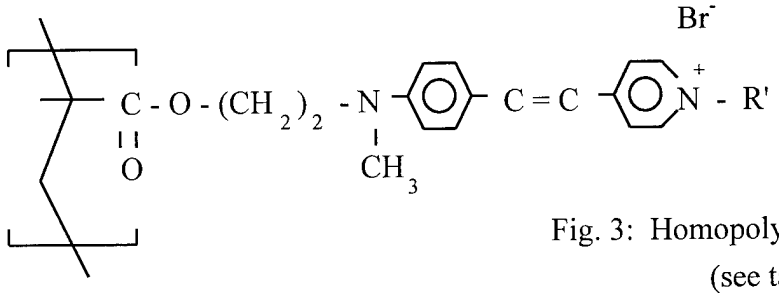

Fig. 3: Homopolymer structures
(see table 3)

table 3: Properties of homopolymeric series		
End group, R'	Nonlinearity χ_2 (pmV^{-1})	Chromophore tilt angle
$C_{12}H_{25}$	15	54°
$C_{16}H_{33}$	11	52°
$C_{18}H_{37}$	12	56°
$C_{22}H_{45}$	30	53°

Electro-optic measurement of the electric-field distributions in coplanar-electrode poled polymers

J.W. Wu

Department of Physics, Ewha Womans University, Seoul 120-750, South Korea

(TEL) +82-2-360-2369, (FAX) +82-2-312-2367, e-mail jwwu@ewhahp3.ewha.ac.kr

In electro-optic thin film samples, two configurations of electrodes are commonly adopted for the electric field poling, parallel and coplanar. In the parallel-plate configuration, electro-optic (EO) polymer is sandwiched between two thin electrode plates on top of a substrate. Because the size of electrodes is larger than the polymer thin film thickness, the electric field distribution is almost uniform inside the polymer film between the top and bottom electrodes. In the coplanar electrode structure, two thin separate electrodes with a narrow gap in between them are deposited on top of substrate, and EO polymer film is spin coated. Here the film covers both electrodes and the dc poling and EO effect measuring fields pass through and above the film making the electric field distribution complicated. Furthermore the electric field lines have different shapes for different thickness of thin films, since the dielectric constant of polymer films is different from that of the air.

The electric field distribution is obtained theoretically from the electrostatic potential satisfying the Laplace equation. We note that the presence of the polymer film itself distorts the field lines due to the introduction of a new boundary condition. Dielectric constants of polymer films being different from that of the air, the presence of a film on top of the electrodes provides another boundary condition for the Laplace equation. By introducing the image charge (the position and size of the image charges depend on the thickness), the electric field distribution of a thick polymer film is obtained as shown in Figure(1).

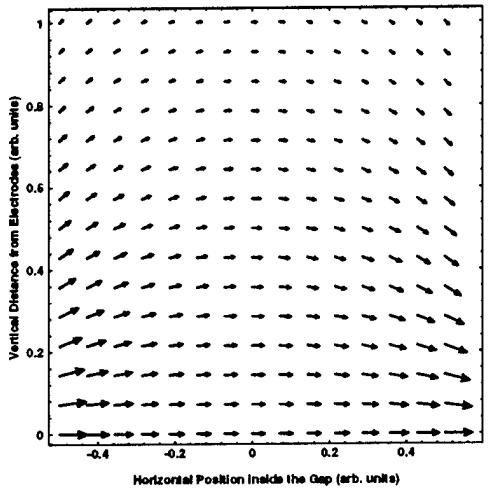

Figure 1

Field strength gradually decreases as the vertical distance from the substrate increases. Field components along the substrate, responsible for the EO effect in the coplanar electrode configuration, also are not uniform across the gap. These variations will lead to a change of EO effects for films with different thicknesses.

To determine the electric field distribution from electro-optic measurement, we selected 4-(dicyanomethylene)-2-methyl-6-(p-dimetylaminostyryl-4H-pyran) (DCM)/LQ2200 compound (*Hitachi Chemical Co.*) guest/host system. DCM/LQ2200 system is known to be isotropic dielectrically as well as optically. Charge injection occurs in the coplanar electrode configuration when the dc poling field is applied at temperatures above the glass transition temperature T_g of polymer. In order to take care of this charge injection problem, the poling temperature is kept at least 50°C below T_g. In preparing samples, 10μm gap coplanar chromium electrodes were patterned on top of fused quartz. An 8% weight concentration of DCM in LQ2200 polyimide was prepared by overnight-stirring of DCM in LQ2200 polyamic acids. In order to study the electric field distribution vertical to the electrode plane, six samples were prepared. Sample 1 has the EO polymer (DCM/LQ2200) of 2μm thickness right on top of the coplanar electrodes. After curing

at 250°C for half an hour, it was poled at the poling field strength of 50V/μm at 200°C (about 50°C below T_g) for 1 minute to minimize the charge injection. In sample 2, the base polymer with thickness of 2μm was spin coated on top of coplanar electrodes and fully cured at 300°C. After that, the same EO polymer was spin-coated on top of the fully cured bare polymer, and cured again at 250°C for half an hour. The poling was performed at the identical condition as sample 1. The same step was repeated for samples 3-6. EO effect coming from the active EO polymer on the top layer was measured by the cross-polarizer lock-in technique. Figure(2) shows the measured EO signal as a function of the film thickness. Nonlinear optical molecules residing inside the EO polymer give rise to the measured EO signal, the magnitude providing informations on the field distributions in the top layer. The electric field distribution determines both the orientational distribution function of guest molecules and the amount of detected EO response. Different thickness samples will sample the field distribution at different vertical positions above the coplanar electrodes. As expected, the EO signal decreases rapidly as the film gets thicker.

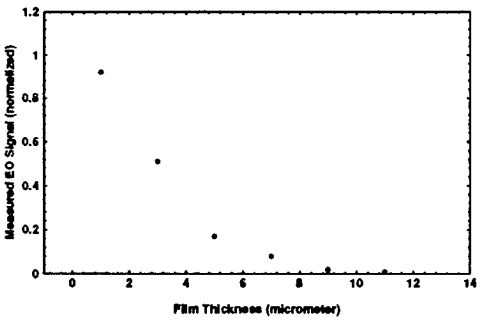

Figure 2

From the simple variation of the field distribution, two effects accumulate to result in a large difference in the EO effect for films with different thicknesses. First, the orientational

distribution of nonlinear optical molecules is different. Ratio of the dipolar interaction energy to the thermal energy, $x = \frac{\mu E_p}{kT}$, varies inside the polymer film since the electric field distribution is not uniform. In other words, the order parameter related to the achieved alignment of the nonlinear optical molecules varies as a function of the vertical distance from the substrate as well as the lateral position inside the gap. The second effect comes in when the linear EO effect is measured. Change of the refractive index experienced by an optical light on the application of a dc field E_k^0, which is the very EO effect, is described by an effective linear polarizability α_{ij}^{eff}.

$$\alpha_{ij}^{eff}(-\omega;\omega,0) = \chi_{ijk}^{(2)}(-\omega;\omega,0)E_k^0$$

For a given field distribution of the modulating electric field E_k^0, the amount of refractive index change is not homogeneous across the gap between two electrodes. Distortion of the electric field results in the distortion of the index change accordingly. These two effects combine to give an overall variation on the EO effect for coplanar electrode poled polymer thin films with different thicknesses. Since both the preparation (poling) of samples and the measurement of EO effect involve dc electric fields, the distortion effect is doubled, giving an enhanced effect in the end. The phase-shift difference $\Delta\phi = \phi_{\|} - \phi_{\perp}$ between the parallel and perpendicular components of a linearly polarized light along 45° relative to the poling field direction can be expressed in terms of the EO molecular hyperpolarizability $\beta_{ijk}(-\omega;\omega,0)$. For a linearly shaped molecule like DCM, $\beta_{333}(-\omega;\omega,0)$ is dominant. In the lowest order, $\Delta\phi$ is

$$\Delta\phi \propto \beta_{333}(-\omega;\omega,0)\frac{\mu E_p}{kT}E^0$$

Here both the poling field E_p and the measuring field E^0 have distorted field distribution as shown in Figure (2), while the optical field E^ω passing through the film is not affected by field distortions. Rapid descease of the measured EO response as the film thickness increases agrees well with the calculated electric field distributions when proper boundary conditions are taken into account.

Electro-refraction and electro-absorption in poled-polymer films

Ned O'Brien and Vince Dominic
Center for Electro-Optics
University of Dayton
Dayton, Ohio 45469-0245
Phone: (513) 229 - 2797
FAX: (513) 229 - 2471

and

Steve Caracci
WL/MLPO Bldg. 650
3005 P St. STE6
WPAFB, Ohio 45433-7707
Phone: (513) 255 - 4474 Ext. 3216
FAX: (513) 255 - 4913

Poled-polymer investigations largely concentrate on the electro-optic effect since most proposed devices are phase controlled. Relatively few papers discuss the concurrent electro-absorption effect.[1-5] The well-known resonant enhancement of electro-refraction near the chromophore absorption band also leads to increased electro-absorption. One might significantly over- or under-estimate the electro-optic coefficient if electro-absorption is ignored.

We describe a wonderfully simple experimental technique that measures the field-induced change in both the refractive index and the absorption. References 4 and 5 describe techniques that make the same measurement but not with the simplicity of our method. The poled-polymer samples consist of a glass substrate coated with a transparent ITO electrode, a thin polymer/chromophore layer, and an evaporated gold contact. The gold and ITO serve as electrodes across the poled region of the polymer whereas the gold and air/glass interface serve as the mirrors in our Fabry-Perot cavity. As shown in Fig. 1, we pass a HeNe laser beam through the poled region of the sample and loosely focus the transmitted light onto a photodiode. A sinusoidal voltage (±16 V, 5kHz) applied across the ≈2 μm thick polymer layer induces refractive index and absorption changes in the sample. A lockin amplifier measures both the average and time-varying components of the transmitted light signal while a controlled actuator slowly rotates (±3°) the sample. The electro-refractive and electro-absorptive effects are measured at each of the five HeNe wavelengths (λ = 543.5 nm, 594.1 nm, 604.8 nm, 611.9 nm, and 632.8 nm).

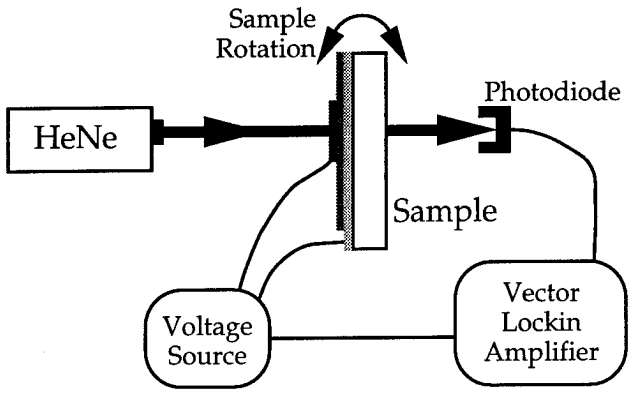

Figure 1) Schematic drawing of the experimental setup. A photodiode monitors the laser transmission through our poled-polymer Fabry-Perot structure. The rotation axis is centered on the incidence spot within the poled region. The sample consists of the following layers: gold electrode, polymer layer, ITO contact, and the glass substrate.

Figure 2 displays the angular variation of the average photodiode signal along with the magnitude of the lockin signal. The appearance of an electro-absorptive effect is immediately apparent in Fig. 2 by observing the asymmetry of the lockin signal. The average signal, by contrast, shows the expected low-finesse Airy function behavior. The asymmetry in the lockin signal arises from the interference between the electro-optic and electro-absorptive effects. Consider an incidence angle θ_1 where the average signal has a positive slope. At θ_1, increasing the optical path length within the cavity increases the transmission so that if a positive applied field ($E_{applied}$) gives a positive index change ($\Delta n > 0$) then the transmittance is increased. If a positive $E_{applied}$ decreases the absorption ($\Delta\alpha < 0$) then the electro-absorption and electro-refraction signals add constructively. On the other hand, destructive interference occurs at incidence angles with negative slope, such as θ_2. At these angles a positive $E_{applied}$ still increases the optical path length but this now reduces the transmittance. The electro-absorption signal does **not** switch sign at θ_2 and so still increases the transmittance for a positive $E_{applied}$. Therefore, at θ_2 the electro-absorptive and electro-optic signals add out phase whereas θ_1 at they add in phase. Our method thus gives a simple way to identify the influence of electro-absorption.

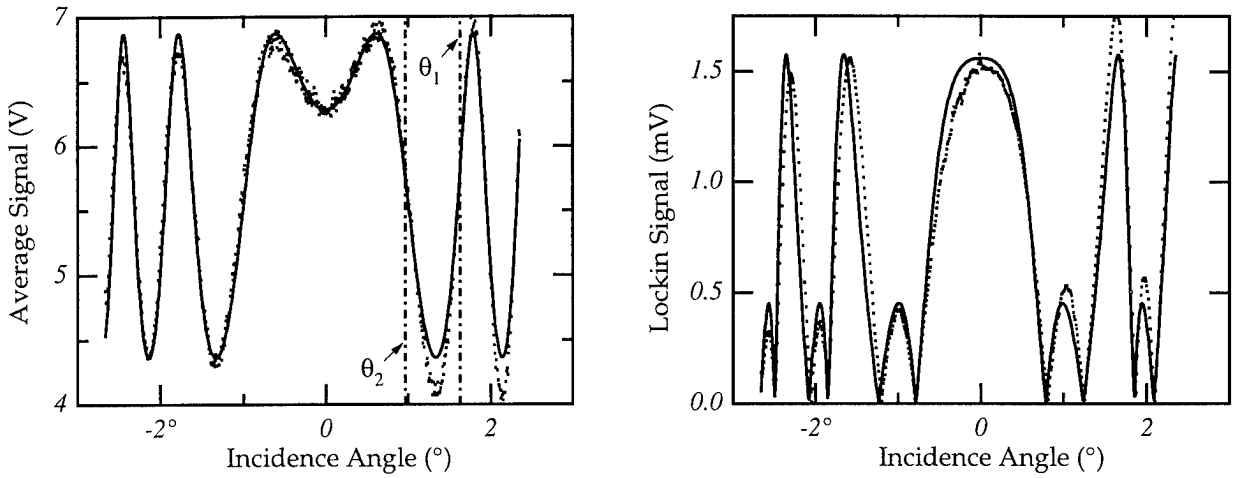

Figure 2) a) Average photodiode signal and theoretical fit (dots=data, line=fit) at λ = 632.8 nm as the Fabry-Perot is rotated. b) Lockin signal dependence on the incidence angle with the raw data (dots) and the theoretical fit (solid line).

With our method we made a quick initial study of the electro-optic and electro-absorption dispersion in a Dow Chemical Company sample. The sample is golden yellow and has an absorption edge at approximately λ = 520 nm. Figure 3 indicates that the measured signal is dominated by electro-absorption at λ = 543.5 nm because the signal never decreases to zero (compare with Fig. 2b). Figure 4 shows the wavelength dependence of both the electro-refractive and electro-absorptive effects. Note the strong increase near the absorption edge. We are currently planning more detailed dispersion measurements and pursuing theoretical models. We expect that the electro-absorption will scale as the derivative of the absorption spectrum.

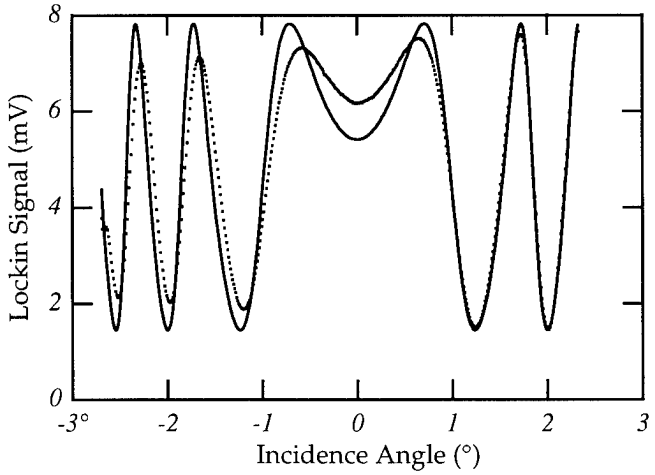

Figure 3) Lockin signal dependence on the incidence angle at λ = 543.5 nm. The dots are raw data and the solid curve is the theoretical fit. The signal magnitude does not reach zero because the electro-absorptive effect dominates.

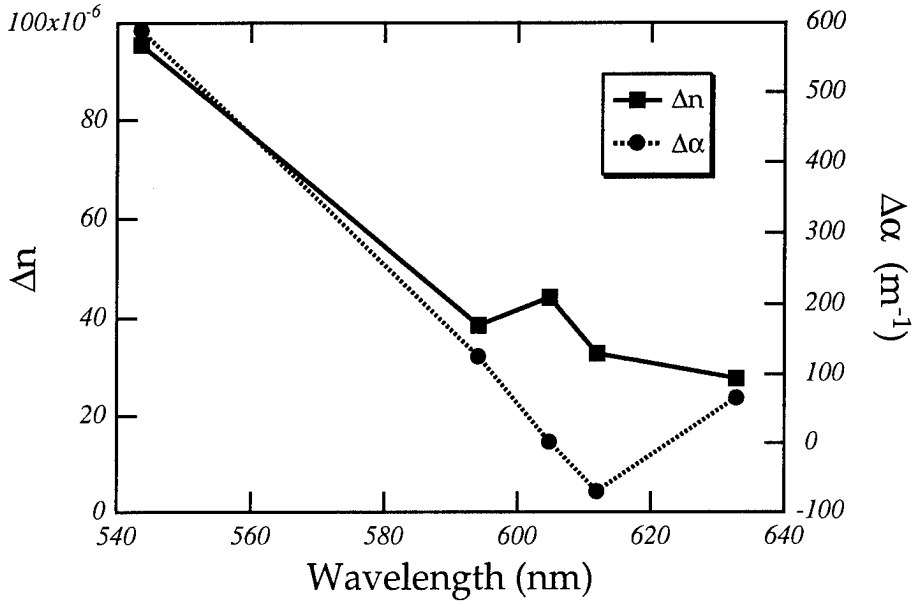

Figure 4) Dispersion of the electro-optic and electro-absorptive effects for the five HeNe wavelengths. Notice that the electro-absorption changes sign near 615 nm. The sample (labeled TP86) was supplied by the Dow Chemical Company.

References

1. J. L. Stevenson, S. Ayers, and M. M. Faktor, "The linear electrochromic effect in meta-nitroaniline," J. Phys. Chem. Solids **34**, 235-239 (1973).

2. R. H. Page, M. C. Jurich, B. Reck, A. Sen, R. J. Twieg, J. D. Swalen, G. C. Bjorklund, and C. G. Willson, "Electrochromic and optical waveguide studies of corona-poled electro-optic polymer films," J. Opt. Soc. Am. B **7** (7), 1239-1250 (1990).

3. A. Horvath, H. Bassler, and G. Weiser, "Electroabsorption in conjugated polymers," Phys. Stat. Sol. B **173**, 755-764 (1992).

4. K. Clays and J. S. Schildkraut, "Dispersion of the complex electro-optic coeficient and electrochromic effects in poled polymer films," J. Opt. Soc. Am. B **9** (12), 2274-2282 (1992).

5. F. Qiu, K. Misawa, X. Cheng, A. Ueki, and T. Kobayashi, "Determination of complex tensor components of electro-optic constants of dye-doped polymer films with a Mach-Zehnder interferometer," Appl. Phys. Lett. **65** (13), 1605-1607 (1994).

Guest-Host Crosslinked Polyimides for Integrated Optics

T.C. Kowalczyk, T.Z. Kosc, and K.D. Singer
Case Western Reserve University, Department of Physics, Cleveland, OH 44106-7079
Phone: (216) 368-4017 Fax: (216) 368-4671

A.J. Beuhler and D.A. Wargowski
Amoco Chemical Co., P.O. Box 3011, Naperville, IL 60566
Phone: (708) 961-7717 Fax: (708) 420-3534

P.A. Cahill, C.H. Seager, and M.B. Meinhardt
Sandia National Laboratories, Division 1811, Albuquerque, NM 87185-0368
Phone: (505) 844-5754 Fax: (505) 844-9624

We report on our approach to the development of device-quality electro-optic materials. We have sought to optimize the optical losses and processing properties first, and later to functionalize the materials having learned how to synthesize and process them for devices.[1,2] We started with perfluorinated, preimidized fully aromatic polyimides. Preimidization makes processing doped polymer systems more flexible, by making functionalizing easier (no harsh imidization process) while allowing spin coating of soluble fully-imidized polymers. Fluorination increases solubility while decreasing optical loss and refractive index. Fully aromatic polymers allow for the best high temperature properties. We found that by introducing alkylated crosslinking groups which can be photo- or thermally activated, optical losses were further reduced, so that high quality waveguides could be fabricated.[1] Another advantage of the crosslinking groups is that they open up new processing capabilities.[2] For example, cross-linking allows for simple multilayer formation, permits a liquid etch process to define waveguides, and provides a chemical hook to which chromophores may be covalently attached. We have uncovered a number of issues relating to functionalization, such as increased optical loss due to long absorption tails in the chromophore and enhanced mobility of small chromophores. We have also studied poling issues related to multilayer films. We believe that this approach, focused on the processing and operation of devices, has led to a flexible material system which shows exceptional promise for the development of electro-optic polymer devices.

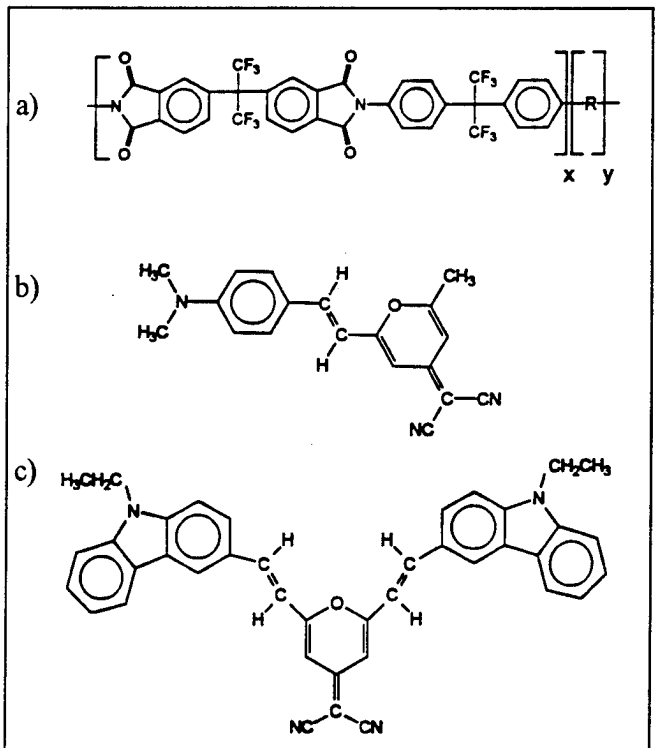

Figure 1. Chemical structure of a) Ultradel 9020D, b) DCM, and c) DADC.

We studied optical loss mechanisms in neat polyimide waveguides fabricated from a series of perfluorinated soluble and fully imidized polyimide polymers.[1] We found that the dominant loss mechanism is absorption tails, probably from electronic charge transfer states of these aromatic polyimides. These losses could be minimized by the incorporation of alkylated cross linking groups leading to generic structures as depicted in Figure 1. Optical losses as low as 0.3 dB/cm at 1300 nm wavelength were observed in the Ultradel 9020D series of Figure 1.

We report here on our progress in developing poled electro-optic materials based on this high optical quality material. First, we studied the excess loss introduced by the incorporation of the nonlinear optical chromophores, DCM[3] and DADC[4] into these polymers (see Fig. 1 for structures). Figure 2 presents photothermal deflection spectrographs (PDS) of the doped and undoped polymers.[5] It is apparent that the introduction of these chromophores into the polymer lead to significant excess loss well into the infrared. These long absorption tails are difficult to discern except by sensitive techniques such as PDS, and have a significant impact on the applicability of these chromophores in devices. It is likely that these absorption tails are an important property to study in any chromophore/polymer system one contemplates for device application.

We have also studied the poling process and resultant nonlinear optical and electro-optic properties in these doped systems. Samples were prepared by doping the fully imidized Ultradel 9020D with 17% weight fraction of both chromophores. Films were dissolved in a solvent mixture and spin-coated onto substrates. The films were soft-baked below 200 C to remove solvent. It has been found that cross-linking occurs just above 200 C; this reaction was used to lock-in the poled order. It was found that the poling and stability of contact poled films was insensitive to the poling temperature and time as long as the temperature was above 200 C and the time longer than 15 minutes. The electro-optic coefficient was measured using a Mach-Zehnder interferometer as a function of the poling field strength. The measured coefficients were found to be in excellent agreement with the standard thermodynamic model.[6] We found an electro-optic coefficient (r_{33}) for DADC doped films to be about 5 pm/V with a poling field of 1.2 MV/cm which was the maximum attainable in single-layer films. The large molecular weight of DADC makes it difficult to load to a high number density and thus limits the electro-optic coefficient. Higher nonlinearity chromophores may be incorporated at high density into the polymer by linking them into the polymer on the alkylated sites during the crosslinking process leading to more useful optical nonlinearities. The DCM doped samples exhibited higher nonlinearities due to higher number density, but sublimed from the polymer during poling.[7]

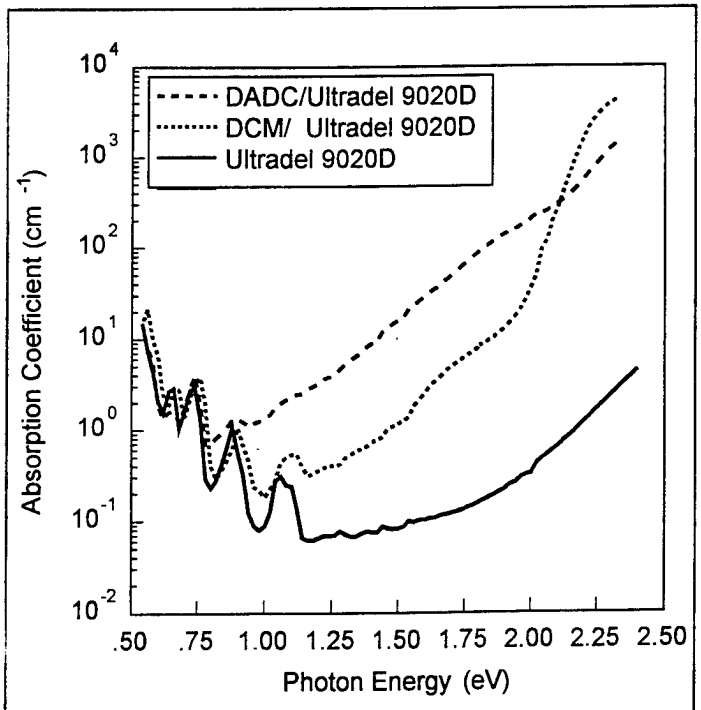

Figure 2. Photothermal deflection spectra of doped and undoped polymer films.

The poled electro-optic polymers exhibited no orientational decay at room temperature. The stability of the electro-optic coefficient for both chromophores at 125 C is depicted in Figure 3. Though the stability is good, we expect better stability if the chromophores are reacted into the polymer as described above. Both materials systems exhibited similar behavior.

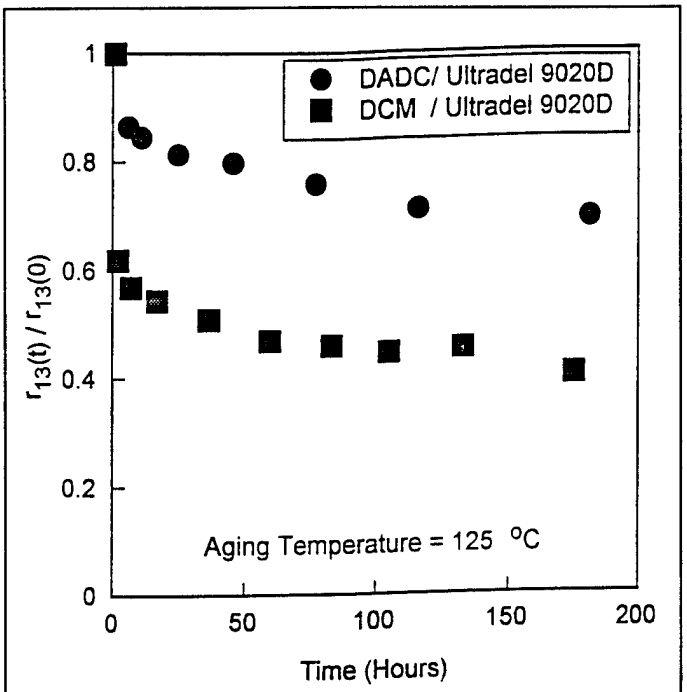

Figure3. Decay of the electro-optic coefficient of poled polymer.

Finally, we explored three layer waveguide structures. We have described earlier, a wet etching technique to form high quality channel structures.[2] Since these polymers are photocrosslinkable leading to a strong differential solubility, channel structures are easily defined without the need for additional photoresist processing steps. Further, multilayer structures are easily formed by thermally crosslinking the cladding layers prior to deposition of the waveguiding layer. Multilayer rib waveguides fabricated from Ultradel 9020D exhibited no excess losses over multilayer slab waveguides indicating that the etched rib introduced little scattering. The flexible chemistry of these materials allows for precise tuning of the refractive index for optimum waveguide design. We fabricated three layer systems consisting of DADC doped Ultradel 9020D as the center layer with undoped Ultradel 9020D as the cladding. Two sets of data points are shown in Fig. 4. The open data points depict the susceptibility as a function of the poling field assuming the resistance of all three layers is the same. Shaded data points use a scaling factor to fit the experimental data to the poling field values predicted by the poling model. The best fit scaling factor is 0.11. We independently measured the resistivities of each layer at the poling temperature. Along with the layer thickness data, we calculated the correction factor U using a resistance divider model where the effective poling field is related to the applied poling field by,[8]

$$V_{eff} = UV_{applied} = \frac{R_{core}}{R_{core} + 2R_{cladding}} V_{applied}$$

where R_{core} and $R_{cladding}$ are the resistances of the core and cladding layers respectively. From direct measurements, the value of U was determined to be 0.1 in excellent agreement with that determined by the data fit indicating the validity of the resistive division model. We have been able to adjust the conductivity of the cladding by reducing the degree of fluorination of the cladding polymer. We believe that the poling of multilayers can be optimized in this manner.

To conclude, we have examined the electro-optic properties of a crosslinkable polyimide polymer system which has been shown to form exceptional waveguide structures. We have found that the polymers can be effectively poled in accordance with existing poling models to form thermally stable materials and device structures. Further work is necessary to

improve the material properties. Reacting an efficient nonlinear optical material by attachment to the existing alkylated crosslinking sites seems like the obvious path to increasing nonlinearity and stability. The most troublesome result from these studies, which probably applies to many chromophore functionalized systems, is the presence of long absorption tails due to the introduction of the chromophores which may lead to unacceptable waveguide losses. This issue is an important one to study further.

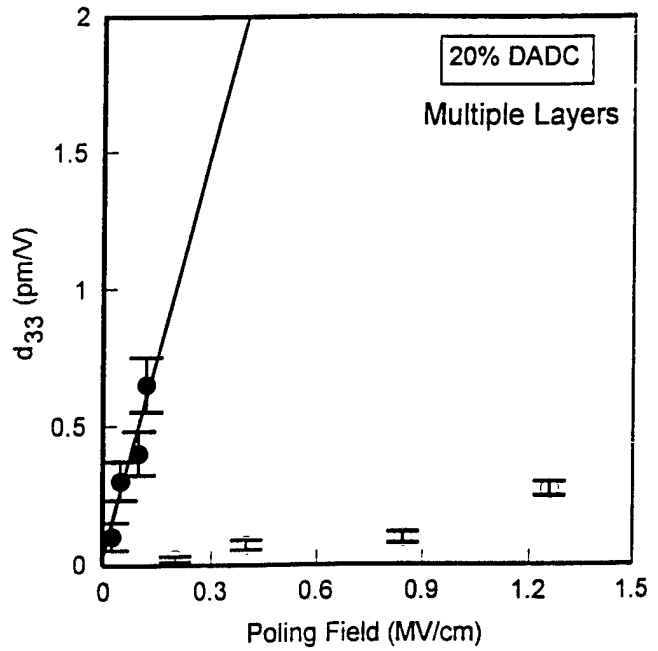

Figure 4. Poling field dependence of triple layer films. Open circles are the raw data, solid circles corrected for voltage division by a theoretical fit to the thermodynamic model.

Acknowledgements

The authors are grateful to Dr. Susan Ermer for synthesis of DADC, and Cynthia Allen for experimental assistance. This work was partially supported by AFOSR under grant no 49620-93-1-0202 and the U.S. Department of Energy under contract DE-AC04-94AL85000.

References

1. T.C. Kowalczyk, T.Z. Kosc, K.D. Singer, P.A. Cahill, C.H. Seager, M.B. Meinhardt, A. Beuhler, and D.A. Wargowski, *J. Appl. Phys.* **76**, 1111 (1994).
2. A. Beuhler, D.A. Wargowski, T.C. Kowalczyk, and K.D. Singer, *Proc. SPIE* **1849**, 92 (1993).
3. S. Ermer, J.F. Valley, R. Lytel, G.F. Lipscomb, T.E. Van Eck, and D.G. Girton, *Appl. Phys. Lett.* **61**, 2272 (1992).
4. S. Ermer, D. Leung, S. Lovejoy, J. Valley and M. Stiller, *in Organic Thin Films for Photonic Applications Technical Digest* **17**, 50 (Optical Society of America, 1993).
5. T.C. Kowalczyk, T.Z. Kosc, K.D. Singer, A.J. Beuhler, D.A. Wagowski, P.A. Cahill, C.H. Seager, and M.B. Meinhardt, submitted *J. Appl. Phys.*
6. K.D. Singer, M.G. Kuzyk, and J.E. Sohn, *J. Opt. Soc. Am. B* **4**, 968 (1987).
7. H.H. Fujimoto, S. Das, J.F. Valley, M. Stiller, L. Dries, D. Girton, T. Van Eck, S. Ermer, E.S. Binkley, J.C. Nurse, and J.T. Kenney, *Proc. MRS* **328**, 553 (1994).
8. H.C. Ling, W.R. Holland, and H.M. Gordon, *J. Appl. Phys.* **70**, 6669 (1991).

Photocarrier Generation Efficiency of Pyrromethene-Doped Polymers

Kwang-Sun Kang and Wade N. Sisk
Chemistry Department, University of North Carolina, Charlotte, NC 28223
Tel: (704) 547-4433, Fax: (704)547-3151

Faramarz Farahi and M. Yasin Akhtar Raja
Physics Department, University of North Carolina, Charlotte, NC 28223
Tel: (704) 547-2818, 547-2826, Fax: (704) 547-3160

I.Introduction

Solid-state dye lasers based on polymethylmethacrylate (PMMA) polymers and pyrromethene laser dyes are currently being evaluated for lasing yield, damage threshold, and device lifetime.[1] The fluorescence pathway in these solid-state dyes competes with the carrier production path. Popovic[2] has demonstrated the connection between fluorescence yield and carrier generation for the phthalocyanines, namely higher fluorescence yield correlates with lower carrier yield. An improved understanding of the mechanism of organic photoconductors may enable selective optimization of conditions for lasing (fluorescence) or photocarrier production. Since pyrromethene dyes are known to exhibit strong fluorescence under zero field conditions[3], low photocarrier yield and thus a high activation barrier for carrier production is predicted. The objective of this study is to determine the activation energy of photocarrier production in laser excited pyrromethene/PMMA samples by measuring the temperature dependence of the photoresponse. The dependence of charge generation on electron donor dopants, dye concentration, and laser intensity are also investigated; consequently information on charge traps and thermal decomposition rates is obtained.

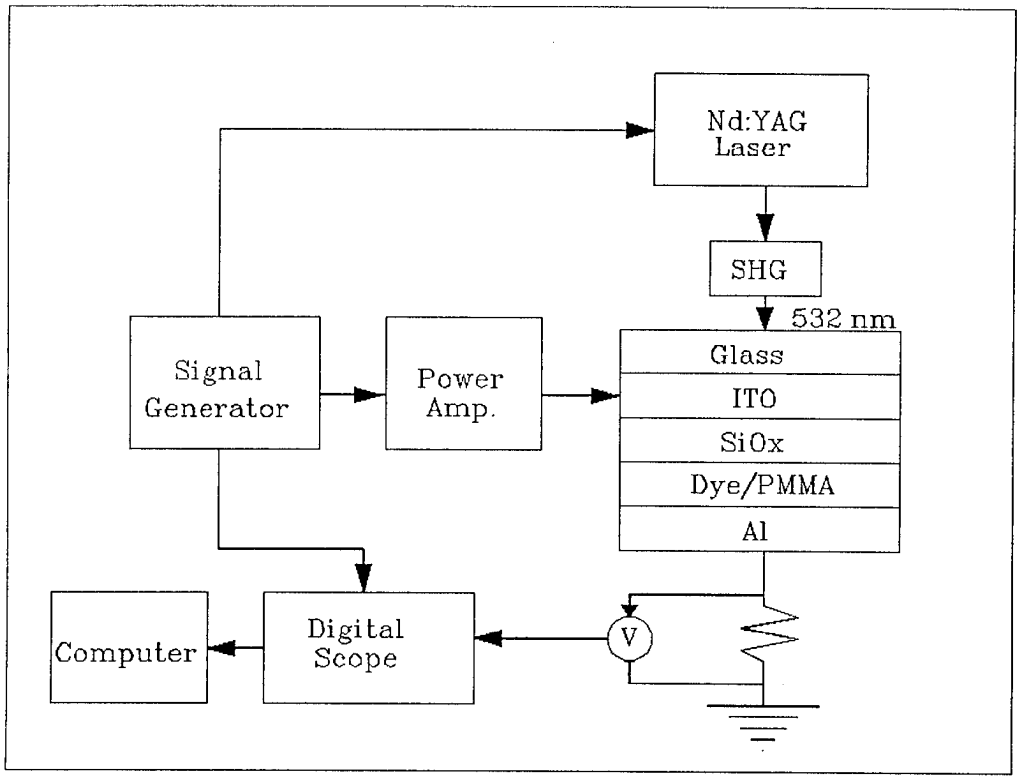

Figure 1: Schematic view of transient photocurrent apparatus

II. Experimental

Pyrromethene 567 (PM567 from Exciton) dispersed in PMMA and dissolved in tetrachloroethane was used to prepare thin film samples. For several samples various amounts of triphenylamine (TPA) was added to the solution in order to study the effects of donor dopants, in a fashion similar to previous studies.[4,5] This solution was spin-coated onto a silicon oxide/indium-tin-oxide/glass substrate, after which aluminum electrodes were vacuum deposited at 10^{-6} Torr. Figure 1 shows a schematic of the apparatus for measuring the relative photoresponse. The 0.7 μm thick sample is subjected to an applied voltage (0-140 V) generating electric fields from 0 to 2×10^6 V cm^{-1}. This sample is simultaneously excited by the second harmonic of a Nd:YAG laser (532 nm @ 0.5 mJ/pulse). The photocurrent traverses a 50 Ω resistor resulting in a voltage profile. This voltage profile is integrated over time to obtain the photoresponse, R. In order to compare different samples, the relative photocarrier generation efficiency, R′, was determined by normalizing R to the absorbance. In addition to the above, absorbance measurements were also performed using a ultraviolet-visible spectrometer.

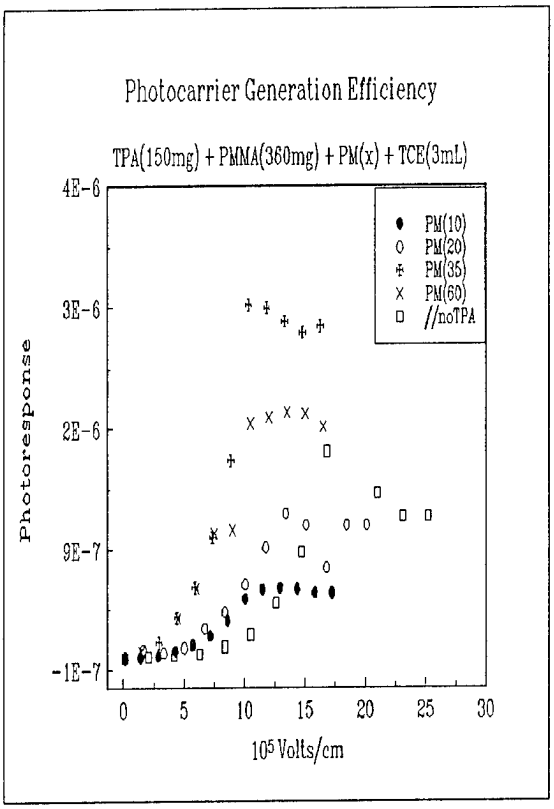

Figure 2a: Photoresponse of Pyrromethene 567

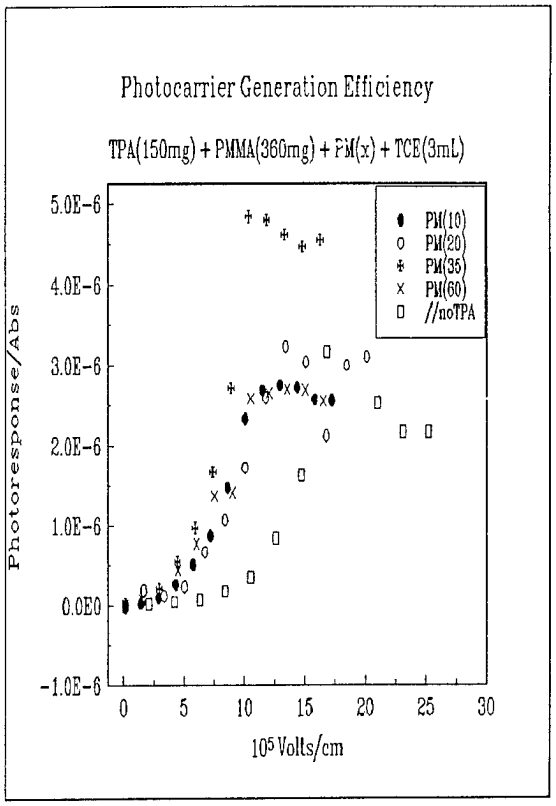

Figure 2b: Normalized Photoresponse of Pyrromethene 567

III. Results and Discussion

A. Field Dependence of Photocarrier Yield

Figure 2 shows the dependence of photocarrier response on electric field strength. Similar to previous studies conducted with rhodamine dyes[5], the photoresponse and relative photocarrier efficiency curves exhibit a dye concentration maximum. That is, at a given field strength the 35 mg PM567 sample has a larger photoresponse than the 60 mg PM567 sample. Two mechanisms might be responsible for this observation: (1) aggregate and dimer formation and (2) trap center behavior by pyrromethene.[5]

The half-saturation field, $E_{1/2}$, is approximately $7x10^5$ V cm^{-1} for the present compositions (Fig. 2). This field, $E_{1/2}$, for the 60 mg PM567/PMMA sample which contains no TPA ($\sim 1.4x10^6$ V cm^{-1}) exceeds the 60 mg sample containing 150 mg TPA ($\sim 7.5x10^5$ V cm^{-1}), consistent with TPA facilitating the formation of a charge transfer state with the electronically excited dye.

B. Photocarrier Yield Temperature Dependence

The absorbance measured at a wavelength of 532 nm as a function of time at 100°C (10 minute lead time) is shown in Fig. 3 for various compositions of dye/dopant (PM567/TPA/PMMA) thin films. The decomposition rate increases with both dopant (TPA) and dye (PM567) content. Comparison of initial rates shows a first order dependence on PM567. No decomposition was observed in the absence of TPA.

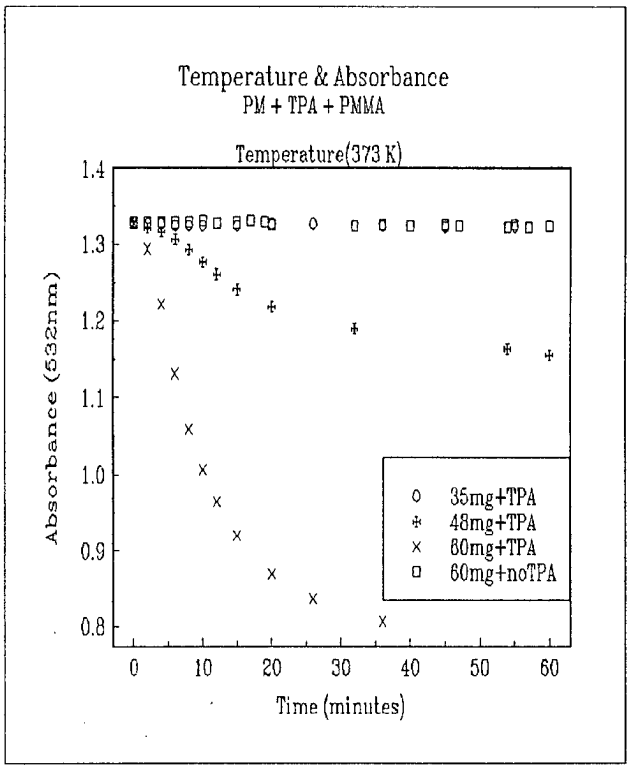

Figure 3: Thermal Decomposition of Pyrromethene

The natural logarithm of the normalized photoresponse R′ as a function of temperature exhibits a linear dependence in the 40 - 80°C range. The activation energies versus field strengths were fitted to a quadratic expression as shown in Fig. 4. A zero field activation energy of 0.11 eV was extrapolated. This value is significantly larger than low activation energies measured for pthalocyanines (0.02-0.06 eV).[2,6] This is consistent with phthalocyanines serving as good zero-field charge generators and pyrromethene dyes as good fluorescent media.

C. Photocarrier Efficiency vs. Laser Power

The photoresponse, R, may be represented as a function of light intensity, I, according to the equation:

$$R = KI^{\alpha} \quad (1)$$

Where K is a proportionality constant and α is related to the trap energy distribution. As shown in Fig. 5 the value of α dramatically increases with increasing dye concentration. This dependence may be attributed to different trapping mechanisms for low and high dye concentrations. Previously α values from 0.5 to 1 have been reported for organic thin films.[7] Observed changes in α may be interpreted as changes in the population and trap energy distribution. Values near 1 and 0.5 reflect uniform and exponential trap energy level distributions, respectively.

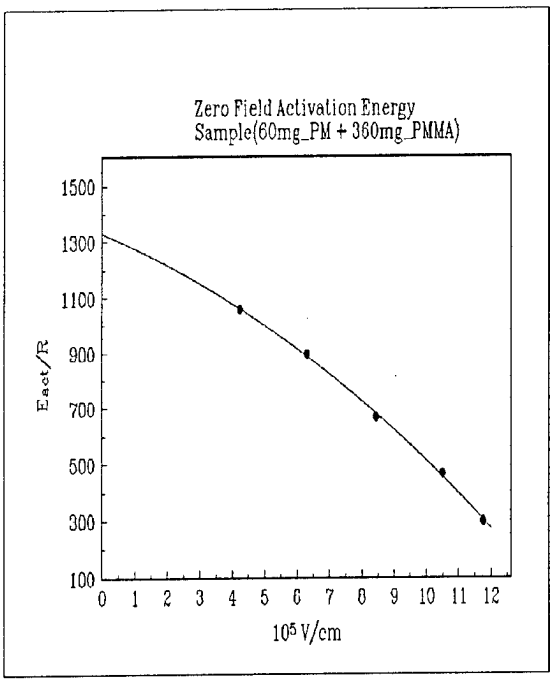

Figure 4: Activation Energy Field Dependence

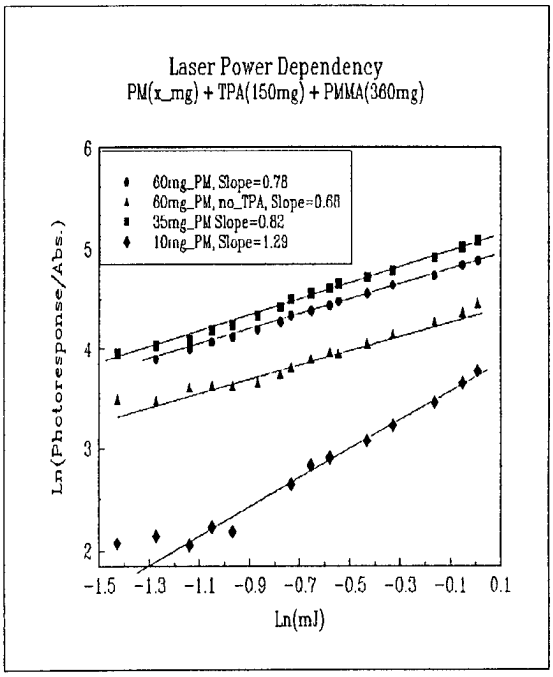

Figure 5: Excitation Intensity Dependence

IV. Summary and Conclusion

For the first time photocurrents have been observed in pyrromethene dyes subjected to an electric field. This investigation measured the relative photocarrier generation efficiency of polymethylmethacrylate/pyrromethene guest-host polymers as a function of applied field, temperature and laser intensity. The photocarrier yield versus dye concentration peaks for a particular dye concentration in accordance with previous observations for rhodamine dyes.[4] The half-saturation field strengths depend strongly on the presence of the donor dopants, TPA. Samples doped with TPA exhibited photodecomposition at elevated temperatures. The temperature dependence studies of samples not containing TPA led to the determination of the activation energy, resulting in a value of ~ 0.11 eV. The trap energy distribution has been obtained from the photoresponse variation with laser intensity: the low dye concentrations bore a more sensitive dependence, which is attributed to a difference in trap energy distributions.

In the future the fluorescence/charge generation mechanism will be investigated for various donor/acceptor dopants and direct observation of fluorescence.

V. Bibliography

[1]T.H. Allik, Proceedings of The Solid-State Dye Laser Technology Workshop, August 1994.
[2]Z.D. Popovic, J. Chem. Phys. **76**, 2714 (1982).
[3]T. Allik, S. Chandra, R. Hermes, J. Hutchinson, M. Soong, and J. H. Boyer, Proceedings of Advanced Solid-State Lasers **15**, 271 (1993).
[4]S. Grammatica and J. Mort, J. Chem. Phys. **67**, 5628 (1977).
[5]N. G. Kuvshinskij, V. M. Komko, and S. E. Kostjuk, Molec. Phys. **73**, 805 (1991).
[6]T. Saito, W. Sisk, T. Kobayashi, S. Suzuki, and Takao Iwayanagi, J. Phys. Chem. **97**, 8026 (1993).
[7]J.W. Pankow, C. Arbour, J.P. Dodelet, G.E. Collins, and N.R. Armstrong, J. Phys. Chem. **97**, 8485 (1993).

SURFACE FUNCTIONALIZED NANOSTRUCTURED GOLD/POLYMER COMPOSITES

by K. E. Gonsalves[1,2], G. Carlson[1], X. Chen[2],J. Kumar[3], R. Perez[4], M. Jose-Yacaman[5]

[1]Polymer Science Program, Institute of Materials Science and [2]Department of Chemistry,University of Connecticut, Storrs, CT 06269.

[3]Center for Advanced Materials, Department of Physics,University of Massachusetts, Lowell, Lowell, MA 01854.

[4]Instituto de Fisica-Laboratorio Cuernavaca, Universidad Nacional Autonoma De Mexico, Apartado Postal 139-B, C. P. 52191 Cuernavaca, Morelos, Mexico.

[5]Instituto de Fisica, Universidad Nacional Autonoma de Mexico, Apartado Postal 20-364, C. P. 01000 Mexico, D. F., Mexico.

Abstract—*Nanometric gold particles were synthesized by a liquid/liquid phase-transfer reaction. Composites of these particles were prepared by free-radical polymerization of solutions of the particles in methyl methacrylate monomer. Concentrations of 1.0, 0.7, and0.3 mg/mlwere prepared, with no noticeable agglomeration of particles during processing. PMMA/gold films showed a linear absorption peak at 530 nm, which is characteristic of nanosized gold. High-resolution electron microscopy measurement showed that the particle diameters varied from 5 to 11 nm. Degenerate four-wave mixing experiments on 10-micron films yielded a maximum value of 1.4 x 10^{-11} e.s.u. for the third-order nonlinear optical susceptibility at 532 nm.*

1. INTRODUCTION

Nano-scale metal particles exhibit an enhancement of many properties, such as magnetic and optical polarizability[1], Raman scattering[2], and chemical reactivity[3]. Nanosized gold is especially useful because of its optical nonlinearity[4], which arises from the quantum confinement of the metal's electron cloud. By incorporating these particles into a clear polymer matrix, "quantum dots" are obtained in a readily processable form. This optical nonlinearity can be exploited to make materials for photonics and electro-optics.

The work described herein consists of a) the chemical synthesis of gold nanoparticles which are surface-functionalized to prevent their agglomeration, b) the dispersion of these particles into a polymer matrix, and c) the characterization of the resulting materials. We have also initiated a measurement of the third-order optical nonlinearity ($\chi^{(3)}$) of gold nanoparticles suspended in polymer matrices using the degenerate four-wave mixing (DFWM) technique.

2. RESULTS

2.1 Synthesis

Stable gold particles were made by a phase-transfer reaction of gold ions with dodecanethiol[5]. Tetraoctylammonium bromide, gold chloride [$HAuCl_4$], dodecanethiol, sodium borohydride (Sigma Chemical) were used as received. Water and HPLC grade toluene (Aldrich) were refluxed overnight under nitrogen and filtered through a 0.45 micron syringe cartridge before use. Reagent grade ethanol was used as received from Aldrich.

A waxy, brown solid was obtained. The material is stable for months in air at room temperature and may be handled like a simple compound. The product consists of gold nanoparticles with the surface atoms bound to thiol groups. The twelve-carbon surface functionality introduces steric repulsion, which inhibits particle agglomeration.

2.2 Film Preparation

Methyl methacrylate monomer (Aldrich) was vacuum distilled to remove the hydroquinone initiator. Polymerization of 23 ml MMA (in a scintillation vial) was

initiated with ~5 mg AIBN. The mixture also contained 25 mg of the thiol-derivatized gold particles. After 125 min at 65 °C, the reaction was quenched by cooling. The nanoparticles did not agglomerate, although their presence did slow the reaction. Concentration was varied by diluting this mixture with pure, prepolymerized MMA. Loadings of 1.0, 0.7, and 0.3 mg/ml were prepared. Then, 3mg of benzoin, a photoinitiator, was stirred into each of the resulting viscous liquids. Films of this prepolymer were spin-coated onto a clean quartz substrates (3000 rpm, ~8 sec) and cured by exposing to light overnight. The films were transparent, with the same purple color as the nanoparticles.

2.3 Characterization

The surface-functionalized structure of the nanoparticles (see Fig. 1) was verified by elemental analysis, nuclear magnetic resonance spectroscopy (NMR,) and high-resolution transmission electron microscopy (HRTEM).

The elemental analysis (Galbraith Laboratories) showed weight percentages of 19.82 C, 3.69 H, 74.87 Au, and 1.62 S (by difference); which is consistent with the proposed structure. The sulfur/gold ratio of 13.2% is in close agreement with the theoretical ratio of 12.2%, calculated for a 10-nm particle. The carbon/hydrogen ratio is also as expected (45%).

The UV/vis spectrum of a thin (~ 10 micron) PMMA/gold composite film was measured on a Perkin-Elmer Lambda 9 spectrophotometer from 200 to 1200 nm. A film of with plain PMMA used as a blank. The spectrum showed a broad absorption peak centered at 530 nm, which agrees with previous studies[6] of nano-scale gold.

NMR spectra of the particles and dodecanethiol were obtained on a Bruker AC-270 instrument (300 MHz). The similarity of these two spectra, particularly the strong S-H singlet at 7.6 ppm, shows that intact dodecanethiol is part of the structure of the stable material.

Direct evidence of the particle size, size distribution, and morphology was obtained using HRTEM. The instrument was a JEOL-4000EX with a point-to-point resolution of approximately 1.7 angstroms. Samples were prepared from methanol dispersions of the particles. These were deposited on copper grids with a carbon film. The HRTEM observations show very few particles with a diameter of less than 5 nm. Most of the nanometric gold particles are in the range of 7 to 10 nm. This is illustrated in Fig. 2, the size distribution. Fig. 3 shows a HRTEM image of the gold particles. All particles display the characteristic lattice fringes of the common HRTEM images. Some of the gold particles clearly have faceting as indicated by the arrows[7].

3. MEASUREMENT OF NONLINEAR OPTICAL PROPERTIES

Third-order nonlinear optical properties of gold nanoparticles in PMMA were studied using degenerate four-wave mixing (DFWM). In this technique[8], a diffraction grating is formed in the region of interaction between the sample and two interfering light waves. A third light wave diffracts off this grating and causes the fourth wave, the signal. The two interfering beams are referrred to as the 'pump' (or 'write') beams, and the third as the 'probe' (or 'read') beam. The characteristics of the grating, such as diffraction efficiency and decay time, together with the dependence of FWM signal on parameters such as beam intensities, crossing angles, and polarization, provide information about the nonlinear optical properties of the material.

Fig. 1 Thiol-derivatized nanometric gold.

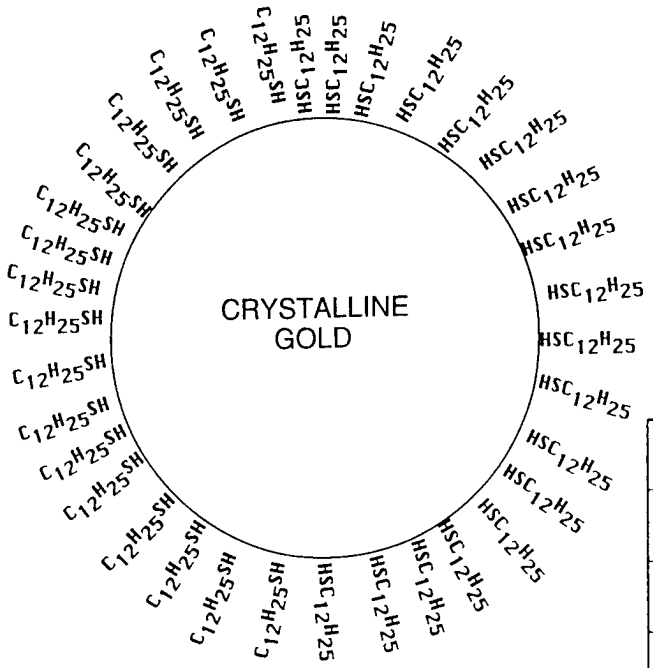

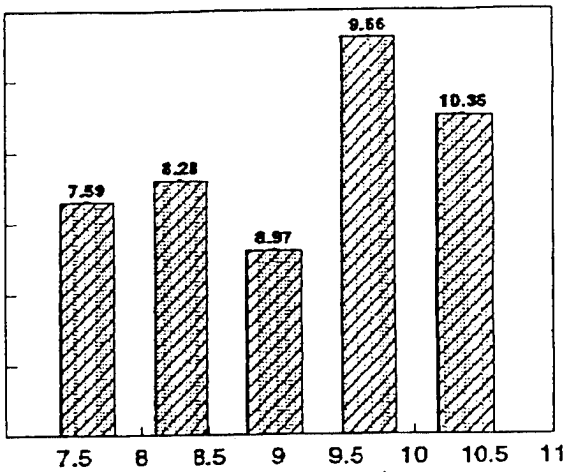

Fig.2 Gold particle size distribution (nm)

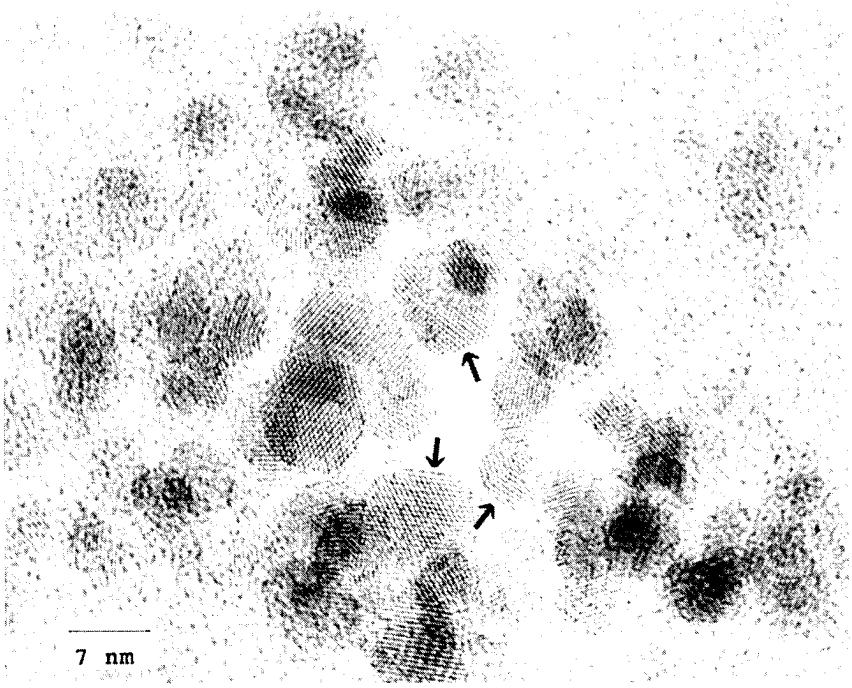

Fig.3 HRTEM image of gold nanoparticles

The 532-nm, 25-ps pulses from a Q-switched neodynium-doped yttrium-aluminum-garnet (Nd:YAG) laser (Quantel) were used. The laser operated at a 10-Hz repetition rate. A neutral density filter was placed in the probe beam to to reduce its intensity to about 1% that of the pump beams. The crossing angle was 6°. Fast silicon photodiodes calibrated against a laser-energy meter were used to monitor the signal, the probe and the pump pulse energies.

The magnitude of the third-order nonlinear susceptibility, $\chi^{(3)}$, of the gold suspension in PMMA was estimated from a measurement of the FWM signal of the sample relative to that of a reference sample of CS_2 placed in a quartz cell of 2-mm path length. The value of $\chi^{(3)}$ was obtained from[9]:

$$\chi^{(3)} / \chi_R^{(3)} = (\eta / \eta_R)^{1/2} \; (n / n_R)^2 \; L/L_R \; (I_{1R} \, I_{2R} / I_1 I_2)^{1/2}, \qquad (1)$$

where the subscript R refers to parameters pertaining to the reference, L is the effective interaction length, n is the refractive index, I_1 and I_2 are the intensities of the pump beams, and

$$\eta = I_s / I_p, \qquad (2)$$

is the diffraction efficiency. I_s and I_p are the intensities of the signal and transmitted probe beams, respectively.

The measured $\chi^{(3)}$ values of the samples were, as expected, proportional to particle concentration. For the 1.0, 0.7, and 0.3 mg/ml concentrations, the susceptibilities were 1.4×10^{-11}, 9.8×10^{-12}, and 6.7×10^{-12} e.s.u., respectively.

4. CONCLUSION

In summary, surface-functionalized gold nanoparticles have been synthesized, characterized by elemental analysis, optical absorption, NMR, and HRTEM. Polymer/gold composites have been prepared by free-radical polymerization of methyl methacrylate monomers containing the particles. Nonlinear optical properties of the gold in poly(methyl methacrylate) were measured using degenerative four-wave mixing.

Future work will include further studies of the nonlinear optical properties of composite films and investigation of the effect of the gold nanoparticles on polymerization rate and ultimate polymer properties.

5. ACKNOWLEDGEMENT

The authors gratefully acknowledge the support of this work, which was provided by ONR N0014-94-1-0833. Also, thanks to Francisco Aranda, P. Sanchez and L. Rendon for technical assistance.

6. REFERENCES

1. M. J. Bloemer, J. W. Haus, P. R. Ashley, *J. Opt. Soc. Am. B*, 7, no. 5, May, 1990, 790.
2. A. Otto, T. Bornemann, U. Erturk, I. Mrozek, C. Pettenkofer, *Surf. Sci.*, 210, 1989, 363-386.
3. R. W. Siegel, *Mater. Sci. Eng.*, B19, 1993, 37-43.
4. T. Dutton, B. VanWonterghem, S. Saltiel, N. V. Chestnoy, P. M. Rentzepis, T. P. Shen, D. Rogovin, *J. Phys. Chem.*, 94, 1990, 1100-1105.
5. M. Brust, M. Walker, D. Bethell, D. J. Schiffrin, R. Whyman, *J. Chem. Soc., Chem. Commun.*, 1994, 801.
6. D. G. Duff, A. Baiker and P. P. Edwards, *J. Chem. Soc., Chem. Commun.*, 1993, 96.
7. M. J. Yacaman, K. Heinemann, and H. Poppa, *CRC Chemistry and Physics of Solid Surfaces,* 1982, 3, 109.
8. P. N. Prasad, D. J. Williams, Introduction to Non-linear Optical Effects in Molecules and Polymers, Wiley & Sons, New York, 1992.
9. A. R. Bogdan, Y. Prior, and N. Bloembergen, *Opt. Lett.*, 6, 1981, 82.

Studies of Photopolymerization at Metal Surfaces

Suchitra Subrahmanyan, Fang Chen and Hilary S. Lackritz
School of Chemical Engineering
Purdue University
West Lafayette, IN 47907-1283
Tel: (317) 494-4065
Fax: (317) 494-0805

Introduction

Surface second harmonic generation is used to study surface reactions during photopolymerization of vinyl monomers on metal surfaces. Photopolymerization shows promise in making defect-free insulating and abrasion resistant coatings, and in the fabrication of microelectronic devices[1]. Although researchers have studied the gas phase reaction in some detail, little is known about the surface reactions[2]. Also, the effects of various physical parameters such as monomer pressure, light intensity, and the nature of metal and the monomer on the physical properties of polymer films are not known.

Photopolymerization of vinyl monomer on metal surfaces is a free radical reaction and often involves three steps: photoinitiation, propagation, and termination[3]. In the presence of a metallic substrate, photoinitiation can occur on the metallic substrate, in the gas phase or a combination of both. The conventional method for studying gas phase reaction kinetics is to determine the time dependence of pressure as a function of light intensity, which gives the apparent rate of polymerization. However, the kinetics of surface reaction during the photopolymerization are currently unknown. Because there are few appropriate surface specific techniques with high sensitivity and good time resolution there have been limited number of studies of the kinetics and mechanism of photopolymerization. Recently, surface second harmonic generation (SSHG) has proven to be a surface specific technique with submonolayer sensitivity and high time resolution.

The surface photopolymerization kinetics will be determined by monitoring the second harmonic intensity from the surface as the reaction proceeds, i.e. the second harmonic intensity, I, is measured simultaneously along with the pressure change during the photopolymerization. The surface second harmonic intensity is given by the following[4]:

$$I^{1/2} \propto \chi^{(2)} = \chi_s^{(2)} + \theta\chi_m^{(2)} + (1-\theta)\chi_p^{(2)}$$

where θ is the fraction of unreacted monomer and $\chi_s^{(2)}, \chi_m^{(2)}, \chi_p^{(2)}$ are the equilibrium second order nonlinear susceptibilities of metal surface, monomer/metal, and polymer/metal, respectively. By following the decrease in signal from the metal during photopolymerization, the surface reaction dynamics can be determined. The goal of this project is therefore to develop SSHG as a surface analytical tool to study photopolymerization reaction *in-situ* and in real time and also to determine final film characteristics as a function of processing conditions.

By simultaneously studying the gas phase kinetics and surface kinetics during photopolymerization , the mechanism and important procsessing variables were determined. The chemical structure of the polymer film formed was characterised by Fourier transform infrared-attenuated total internal reflection (FTIR-ATR) spectroscopy. The metal substrate was characterized by X-ray photoelectron spectroscopy (XPS).

Experimental

Light from a nanosecond Nd: YAG laser was polarized by passing it through a half wave plate and polarizer. The polarized light was focused and was incident on the sample at 70° with respect to the surface normal. The reflected second harmonic light at 532 nm is detected by a

photomultiplier tube, averaged by a boxcar and analysed by computer. A more detailed description of the experimental setup is published elsewhere[5].

Acrolein (97%, Aldrich) was passed through an inhibitor removal column prior to use, then vacuum distilled to remove water and other impurities. Gold samples were prepared by vapor deposition onto a silicon substrate. Aluminum foil from Johnson Matthey was polished using 0.05 μm alumina gel to remove the oxide layer.

Purified monomer was degassed via freeze-pump-thaw cycles. It was then introduced into the reaction cell by equilibration with Schlenk tube containing the purified monomer. The photopolymerization was carried out by irradiation with Hg(Xe) lamp. A filter was used to transmit light only between 300 - 340 nm to avoid thermal polymerization. Monomer pressure was measured using a pressure transducer that has linear response over a range of 0-15 psia.

Results and Discussion

The surface reaction rate can be obtained by monitoring the decay of second harmonic generation as the reaction proceeds. Metals have a large nonlinear optical response because of the polarizability arising from free electrons. When the surface is covered by adsorbates, some of the metal electrons are localized, giving rise to smaller nonlinear susceptibility values. Two metal substrates (gold and aluminum) and acrolein have been investigated in this work. The bare gold substrate gave rise to a large second harmonic signal. Polyacrolein was then deposited on gold surface by photopolymerization using UV light. No appreciable second harmonic signal was obtained from the polyacrolein/gold interface. Similar results were also obtained in the case of aluminum. Therefore, we have established that second harmonic generation can clearly distinguish between pure metal and metal/polymer interface. Work is in progress to obtain surface polymerization kinetics .

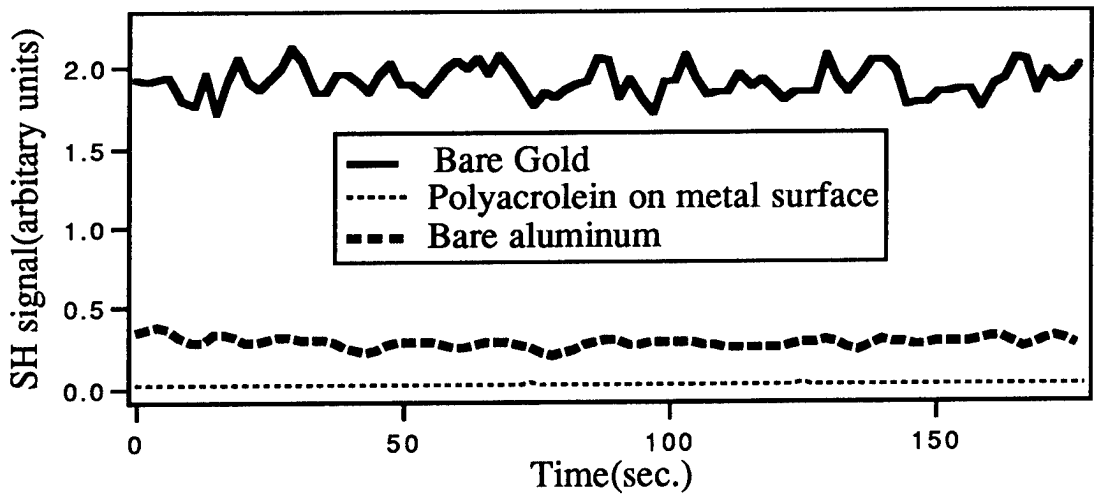

Figure 1. Steady state surface second harmonic signal from bare gold, aluminum, and polymer/metal surface

The monomer pressure of acrolein as a function of time has been measured during photopolymerization on aluminum and nickel. Preliminary results indicate that the monomer/metal system reaches equilibrium in about 24 hours after the introduction of the monomer vapor over the metal surface. On irradiation both systems show an induction time of about 30 minutes. Also, the reaction rate in the initial stages is found to be first order with respect to monomer vapor pressure and then becomes zero order after 110 min. It was found that there was no dark reaction in the case of aluminum or nickel. More detailed studies of the gas phase kinetics are in progress.

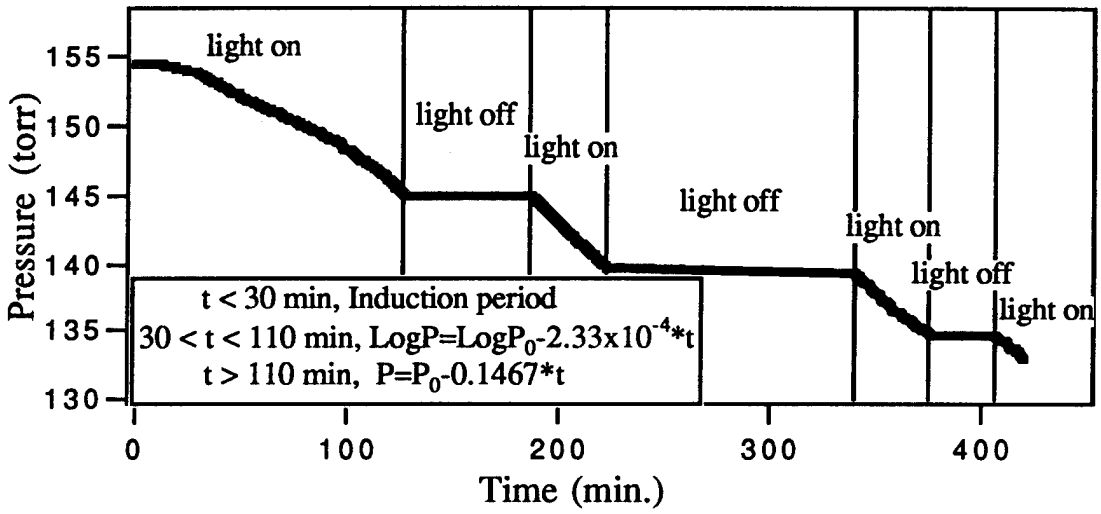

Figure 2. Time dependence of acrolein vapor pressure during photopolymerization on aluminum

Earlier studies have shown that the elemental composition and the concentration of oxide sites on the metal surface may play an important role in the photopolymerization reaction[2]. Therefore reproducible sample preparation and characterization of the metal surface is of paramount importance. XPS has been used successfully for surface characterization of gold and aluminum.

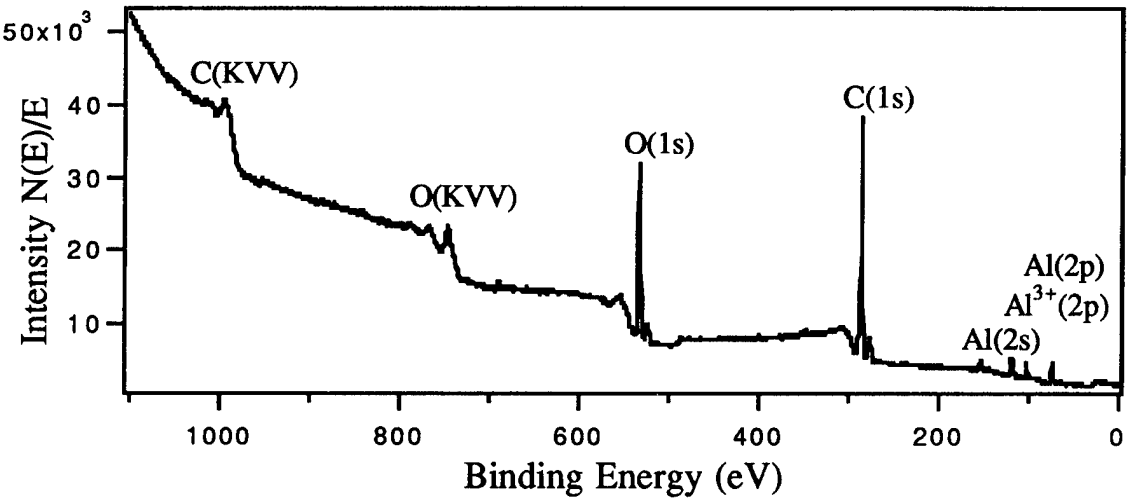

Figure 3. X-Ray photoelectron spectrum of aluminum

The polymer obtained as a result of photopolymerization was characterized by FTIR/ATR. The IR spectra of polyacrolein formed on gold is shown in Figure 4. The spectra shows bands corresponding to the ether, acetal, carbonyl, and unsaturated hydrocarbonyl functional groups. The spectra is in agreement with the structure of polyacrolein reported in the literature[6]. Polyacrolein is a complex crosslinked polymer with cyclic acetal and hemiacetal (tetrahydropyran) structural units as well as free aldehyde and hydroxyl groups. The unsaturated hydrocarbonyl bands are probably due to the trapped unreacted monomer.

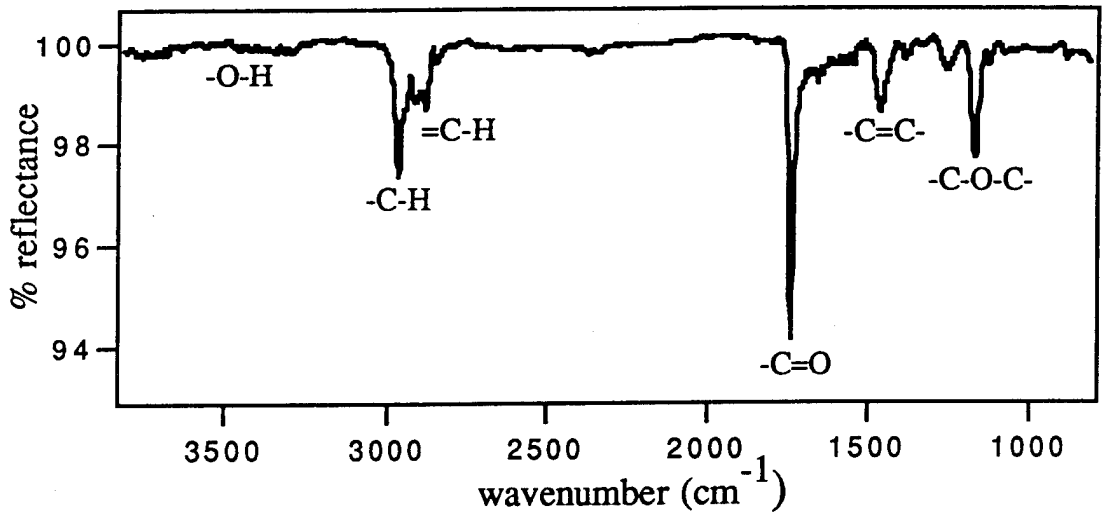

Figure 4. Fourier transform infrared-attenuated total internal reflection of polyacrolein on aluminum surface

Scanning electron microscopy was used to characterise the morphology the polyacrolein formed by photopolymerization on the metal and is shown in Figure 5. The polyacrolein particles are aymmetric in shape with their size ranging from 5-15 μm. It is interesting to note that the particles are not aggregated, but are distributed uniformly on the metal surface.

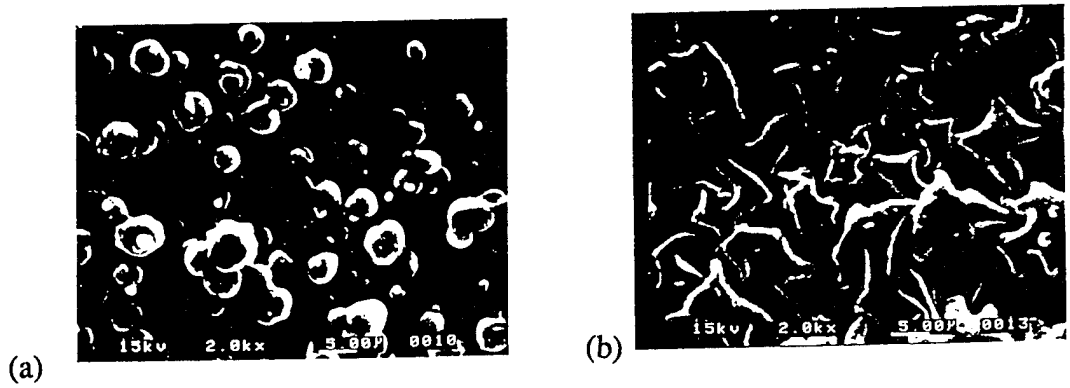

Figure 5. Scanning electron micrographs (x 2000) of polyacrolein on (a) aluminum and (b) gold

Efforts are in progress to measure the final film thickness and homogeneity of the polymer by using spectroellipsometry and profilometry. Furthermore, the effects of various parameters such as nature of metal, nature of monomer, monomer pressure and light intensity on the physical properties of polymer films will be investigated.

References

1. Wright, A.N., in "Polymer Surfaces" Clark, D.T. and Feast, W.J. Eds., John Wiley and Sons, NY, 1978, Ch. 8
2. Lewis, F.D., Marshall, N.J., Hampsch, H.L., Tetrahedron, 43(7), 1987, 1635
3. Odian, G., "Principles of Polymerization", John Wiley and Sons, NY, 1981, p.179
4. Berkovic, G., Rasing, Th., Shen, Y.R., J. Chem. Phys., 85(12), 1986, 7374
5. Manuscript in preparation to be submitted to Macromolecules.
6. Fischer, R.F. in "Acrolein," Smith, C.W., Ed., John Wiley and Sons, NY, 1962, p.211

Detection of Molecular Chirality using different Optical Second-Harmonic Generation Techniques

R. Stolle, F. Lohr and G. Marowsky

Laser–Laboratorium Göttingen e.V.,

Hans-Adolf-Krebs-Weg 1, 37077 Göttingen, Germany

Tel. (49) 551 50350

In the past, second-harmonic (SH) studies of monolayers have often been applied to systems with $C_{\infty,v}$-symmetry, in most cases to systems consisting of rodlike molecules [1]. These samples are axialsymmetric with respect to the surface and possess a mirror plane of symmetry normal to the surface. If the molecules are replaced by chiral molecules of one enantiomer, this mirror symmetry is broken and the system exhibits C_{∞}-symmetry. In the following, this is called *surface chirality.* Because these monomolecular films are very thin, this symmetry break can hardly be detected using linear optical techniques such as optical activity measurements. However, if the molecular chirality influences the part of the nonlinear structure responsible for SH generation, surface chirality can be detected by using nonlinear optical techniques.

For a sample with C_∞-symmetry, the underlying second-order susceptibility tensor $\chi^{(2)}$ is given by

$$\chi_S^{(2)} = \begin{pmatrix} 0 & 0 & 0 & \chi_{xyz} & \chi_{xzx} & 0 \\ 0 & 0 & 0 & \chi_{yzy} & \chi_{yxz} & 0 \\ \chi_{zxx} & \chi_{zyy} & \chi_{zzz} & 0 & 0 & 0 \end{pmatrix}, \tag{1}$$

with χ_{zzz} ; $\chi_{zxx} = \chi_{zyy}$; $\chi_{xzx} = \chi_{yzy}$ (as in the case of $C_{\infty,v}$-symmetry without microscopic chirality), and the additional components $\chi_{xyz} = -\chi_{yxz}$. Two different techniques can be used to distinguish between C_∞-symmetry (surface chirality) and C_∞, v-symmetry (no surface chirality). First, one can record a rotation pattern ti detect the s-component of the SH signal [2]. Whereas in the case of $C_{\infty,v}$-symmetry the pattern shows an eightfold symmetry, this symmetry is reduced to a fourfold pattern for a sample with C_∞-symmetry. Alternatively, one can use the novel technique of second-harmonic circular dichroism (SH-CD) [3, 4, 5]: The SH intensities $I_{left}^{(2\omega)}$ and $I_{right}^{(2\omega)}$, generated by the left- and right-circular polarized fundamental, are detected separately. The existence of SH-CD is equivalent to $I_{SH-CD}^{(2\omega)} \neq 0$ when the definition

$$I_{SH-CD}^{(2\omega)} := I_{left}^{(2\omega)} - I_{right}^{(2\omega)}$$

is used. In the dipole approximation, a complex-valued susceptibility tensor $\chi^{(2)}$ is necessary for the possibility of SH-CD. This condition is fulfilled if the frequency of the fundamental or

the harmonic radiation hits a resonant absorption of the molecular layer. Alternatively, the experiment can be performed in total internal reflection with the underlying nonlinear Fresnel coefficients being complex valued [2]. If the experimental arrangement is mirror symmetric, the observation of SH-CD is equivalent to surface chirality [5].

We present experimental results using both of the experimental techniques mentioned above. The kind of molecular chirality detectable by these methods is discussed. These results may be of interest for the molecular engineering of chiral molecules or for the investigation of biological systems.

References

[1] Y. R. Shen. Surface properties probed by second-harmonic generation and sum-frequency generation. *Nature*, **337**:519–525, 1989.

[2] B. U. Felderhof, A. Bratz, G. Marowsky, O. Roders, and F. Sieverdes. Optical second-harmonic generation from adsorbate layers in total-reflection geometry. *J. Opt. Soc. Am. B*, **10**(10):1, 1993.

[3] T. Petralli, T. M. Wong, J. D. Byers, H. I. Yee, and J. M. Hicks. Circular dichroism spectroscopy at interfaces: A surface second harmonic generation study. *J. Phys. Chem.*, **97**:1383–1388, 1993.

[4] J. D. Byers, H. I. Yee, and J. M. Hicks. A second-harmonic generation analogon of optical rotatory dispersion for the study of chiral monolayers. *J. Chem. Phys.*, **101**(7):6233–6241, 1994.

[5] R. Stolle, M. Loddoch, and G. Marowsky. Theory of second-harmonic circular dichroism at surfaces. *Nonlinear Optics*, 8:79–85, 1994.

Polymer Waveguide Taps for Optical Signal Distribution

Claire L. Callender, Lucie Robitaille and Julian P. Noad

Communications Research Centre, P.O. Box 11490, Station H,
Ottawa, Ontario, Canada K2H 8S2
Tel: (613)-998-2726 Fax: (613)-990-8382

Introduction

GaAs optoelectronic integrated circuit (OEIC) technology is having an increasing impact in the areas of communications and signal processing, with applications such as high speed broad-band switching, high-speed interconnects for multiprocessor local area networks (LANs) and optically controlled phased-array antennas. A major component of the production of OEICs is the low cost, robust and reliable integration of optoelectronic devices for generating, amplifying and detecting optical signals. Recently, there has been considerable interest in the integration of photodetectors with optical waveguide circuits. Monolithic integration of metal-semiconductor-metal (MSM) detectors with semiconductor optical waveguides has been achieved by evanescent coupling from a waveguide layer into an absorbing detector layer grown epitaxially on top of the waveguide[1,2]. In this paper we examine the potential of polyimide waveguides as integrated light distribution systems in monolithic OEICs. Polymer guides can be formed on top of complex semiconductor circuitry by spin coating and photolithography. Polymer waveguides offer the advantages of ease of processing, low cost, and low optical losses. As well, vertical coupling facilitates alignment of light sources and detectors without additional components such as gratings or 45° facets.

Waveguide Fabrication

Waveguides were patterned in films of Ultradel 9020D polymer, a photosensitive fluorinated polyimide material from Amoco Chemical Company. Substrates were polished GaAs or Si wafers coated with a 1-2 μm layer of evaporated SiO_2 to act as a cladding layer. Polymer films ranging from 3-6 μm thickness were deposited by spin coating. Ultimately, the application of polymer waveguides to OEIC fabrication will require GaAs or InP substrates, but Si can be utilized in the development stages due to its low cost and similar refractive index. Ridge waveguides of widths 5 - 75 μm were photolithographically defined and hard baked to 300°C. Propagation losses, estimated by measuring the intensity of the scattered light from the guides using a video camera and framegrabber or a scanning fiber bundle, were typically 0.8-1.3 dB/cm at 633 nm and 830 nm.

To assess the efficiency of vertically integrating polymer guides with planar MSM photodetectors, regions of varying length were etched in the SiO_2 buffer layer to expose the bare semiconductor substrate. These "bufferless regions" ranged in size from 50 μm to 500 μm long. Etching was achieved by first evaporating and patterning a 4000 Å layer of Al on top of the SiO_2 layer, followed by a wet etch using buffered HF. Polymer films were then

spun on top of the patterned buffer layer and ridge waveguides patterned orthogonally to the bufferless regions as shown in Figure 1.

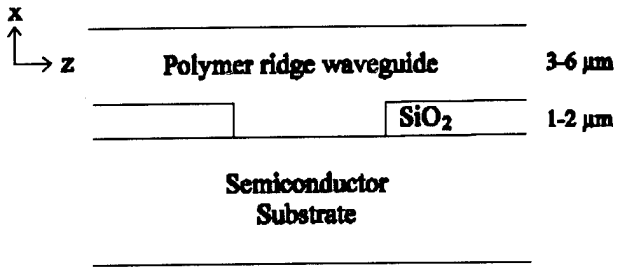

Figure 1. Geometry of polymer ridge waveguides patterned over gaps in SiO_2 buffer layer

Loss Measurements

The samples were cleaved perpendicular to the ridge waveguides and light was coupled into the waveguides via butt coupling from an optical fiber. Figure 2 shows the decrease in the scattered light signal at 830 nm from a 25 μm wide guide passing over two consecutive 250 μm long bufferless absorbing regions on a Si substrate (5.1 ± 0.4 dB for each) . Similar data were collected for 15, 25, 50 and 75 μm ridge guides over 50, 100, 250 and 500 μm bufferless regions. No dependence of the losses on the width of the waveguide was observed.

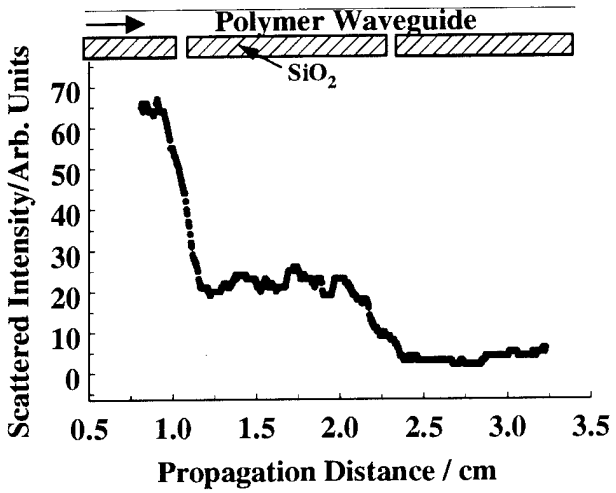

Figure 2. Optical loss at 830 nm from a 25 μm polyimide ridge waveguide on passing over two 250 μm bufferless regions. Each region results in 5.1 ± 0.4 dB of light coupled out of the guide.

The loss is attributed to coupling of light out of the guide into the substrate, where it

is absorbed, and not scattering out of the guide. We observed some scattering at each edge, where the guide crosses over the etched regions; the dependence of this effect on the thickness of the guides, thickness of the buffer layer and nature of the substrate will be discussed. The logarithmic dependence of the depletion of the guided light as a function of the length of a bufferless region on Si for wavelengths of 633 nm and 830 nm is presented in Figure 3. Each data point is derived from an average of 5-20 measurements.

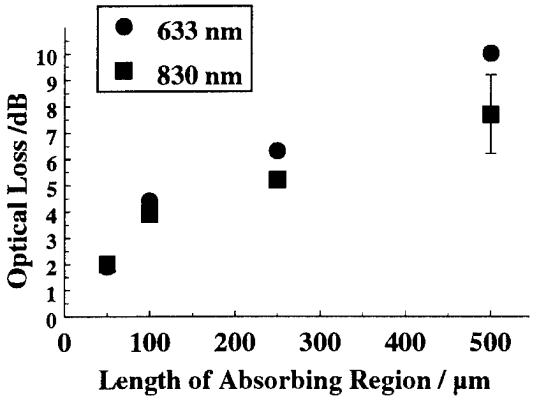

Figure 3. Optical loss from polyimide ridge waveguides at 633 nm and 830 nm as a function of the gap in the SiO_2 buffer layer

Studies of evanescent coupling from semiconductor waveguides have predicted and observed a simple exponential loss of power along the length of the guide for thick absorbing layers[1]. We observe a simple exponential loss (linear loss in dB vs. absorber length) for absorber lengths greater than 100 μm with deviation at low lengths. Significant deviations from exponential behaviour have been observed previously[1], and it has been noted that a finite distance is required before power can be coupled from the waveguide to the absorbing layer[3]. Coupling efficiency is determined by a number of factors and requires careful modelling to predict accurately. The coupling efficiency in our system should be dominated by the large refractive index difference between guide and semiconductor and not the material absorption coefficient. We expect that the absorption from polymer guides, n=1.55, into Si or GaAs substrates (n=3.7+0.005i and 3.7+0.08i at 830 nm respectively)[4] to be of similar magnitude. The efficiency of the optical coupling between guide and absorber can be increased by lowering the refractive index discontinuity; we will discuss the possibility of introducing a further "matching" layer, with an intermediate refractive index, between guide and absorber.

Empirically we have established that with a Si substrate, we can absorb between 20 and 90 % of the light with absorber lengths varying from 25 and 500 μm. Similar results are expected for GaAs and this system is currently under study. Using these data, we have designed a series of taps for a 1 x 4 array of MSM photodetectors, which can be used in a high speed optoelectronic switch, currently under investigation in our laboratory[5]. Typically an MSM detector for operation at 830 nm consists of an epitaxial layer of undoped GaAs grown on a semi-insulating GaAs substrate. Absorption of light in the epitaxial layer results

in generation of carriers which are collected by application of an electric field via an interdigitated metal-contact pattern with spacing of 1-3 μm between the electrode fingers. This arrangement maximizes speed and gain of the device. The use of optically opaque metal electrodes means that the length of exposed GaAs available for absorption is appreciably reduced. For integration with polymer waveguides we propose the use of indium tin oxide (ITO) electrodes, which are transparent at 830 nm. This allows our calculated absorber lengths to be translated directly in detector lengths. MSM detectors employing ITO electrodes have previously been characterized in our laboratory[6] and demonstrate an increase in responsivity of a factor of 2. The proposed structure is shown in Figure 4. To minimize device capacitance, the width of the detectors is 25-50 μm with a polymer guide of the same size patterned on top. The lengths of the detectors are approximately 25, 40, 90 and 250 μm which, allowing for a nominal scattering loss at each input and output of 2%, divides the input signal equally among the 4 detectors.

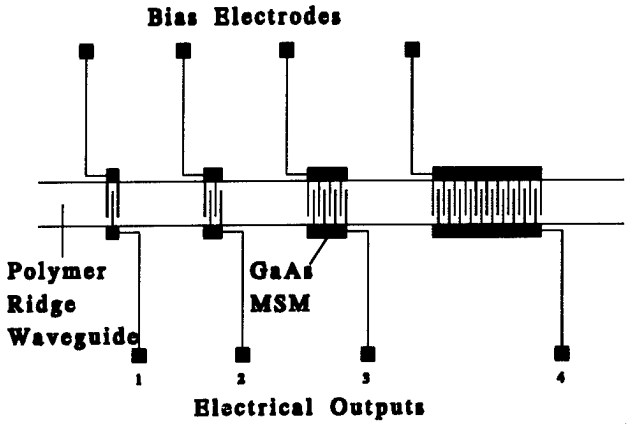

Figure 4. Schematic representation of light distribution to a 1 x 4 array of MSM photodetectors using vertically integrated polymer waveguides

References

1. R.J. Deri, IEEE J. Lightwave Technol., 11 , (1993) 1296-1313.
2. M. Erman, Ph. Riglet, Ph. Jarry, B.G. Martin, M. Renaud, J.F. Vinchant and J.A. Cavailles, IEE Proc.-J, 138 (1991) 101-108.
3. W. Ng, A. Narayanan, R.R. Hayes, D. Persechini and D. Yap, IEEE Photonics Technol. Lett. 5, (1993) 514-517.
4. E.D. Palik (Ed.), "Handbook of Optical Constants of Solids", Academic Press, NY (1985).
5. F. Gouin, C. Beaulieu and J. Noad, submitted to Photonics East, Philadelphia, 22nd-26th October, 1995.
6. C. Beaulieu, F. Gouin, J. Noad, W. Hartman, E. Lisicka-Skrzek, K. Vineberg and E. Berolo, Proc. Photonics West, San Jose, February 4-10th, 1995.

Pyroelectric, dielectric and electro-optical investigation of cross-linking in Red Acid Magly

S. Bauer, S. Bauer-Gogonea, S. Yilmaz, C. Dinger,
W. Wirges and R. Gerhard-Multhaupt
Heinrich Hertz Institut für Nachrichtentechnik
Einsteinufer 37, D-10587 Berlin, Germany
and
F. Michelotti, E. Toussaere, R. Levenson, J. Liang and J. Zyss
France Telecom CNET, Lab. de Bagneux
196, A. Henri Ravera, F-92220 Bagneux, France

Introduction

Cross-linking of nonlinear optical polymers during the poling process is an interesting way to increase the thermal stability of the dipole orientation [1]. For the optimization of the poling process in cross-linking polymers, experimental techniques for the in-situ characterization of the polar order are highly desirable. Recently, Aramaki et al.[2] introduced in-situ electro-optical measurements by the ellipsometric method in order to follow the cross-linking process by optical means. They also established a direct connection between dielectric and in-situ electro-optical measurements [3]. Here we report a comprehensive study of the cross-linking process of Red Acid Magly by means of dielectric, in-situ electro-optical and pyroelectrical measurements. In addition we extend the model in [3] for the interpretation of in-situ electro-optical measurements and their connection to the dielectric properties.

Sample Preparation

The following experiments were performed on the cross-linkable Red Acid Magly polymer, details of the synthesis were already reported in [4]. Samples with a thickness of approximately 1μm were prepared from a suitable solution by means of spin-coating onto ITO-coated glass substrates. The sample preparation was completed after evaporation of a top aluminum or gold electrode.

Dielectric Measurements

The dielectric function is measured by use of a Hewlett-Packard HP4284 LCR setup in the frequency range of 20Hz to 1MHz. The dielectric function can be expressed as [5]

$$\epsilon = \epsilon_\infty + N\mu < \cos\theta > = \epsilon_\infty + \frac{N\mu^2}{3kT}\frac{1}{[1+(i\omega\tau)^\alpha]^\beta} \qquad (1)$$

where ϵ_∞ is the unrelaxed dielectric constant, N is the dipole density, μ the dipole moment, α and β parameters describing the asymmetry and the width of the dielectric loss function and $< \cos\theta >$ is the average over the cosine of the angle θ between

the electric field and the chromophore axis.

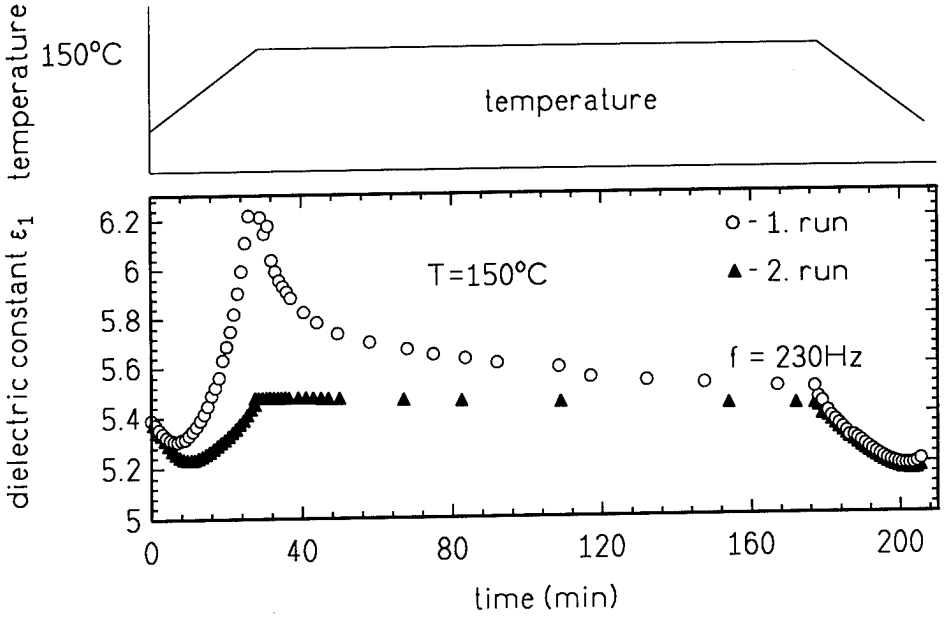

Fig1: Dielectric constant during heating, cross-linking and cooling, measured at 230Hz.

In order to investigate the cross-linking process following scheme is adopted. In the first step the polymer sample is heated with a constant rate to the temperature at which the cross-linking is performed and finally the sample is cooled to room temperature with the same rate. Fig. 1 shows the dielectric constant ϵ_1 measured at 230Hz as a function of time when cross-linking is performed at 150°C. First the dielectric constant is decreasing with increasing temperature due to the thermal expansion of the polymer sample. Then the dipole mobility increases so that they can follow the applied electric field and thus the dielectric constant increases. The effect is more pronounced at the low measurement frequency. During the isothermal step, the dielectric constant decreases with increasing time. This decrease is due to the cross-linking process which reduces the mobility of the dipoles. Finally, by cooling the polymer sample to room temperature, the dielectric function decreases (because the dipole mobility is frozen) and increases again due to the effect of thermal expansion. Also shown in Fig. 1 is a second run after cross-linking was completed. In this case we see, as expected, no decrease of the dielectric constant during the isothermal process step. Thus, dielectric measurements are very helpful in order to investigate the cross-linking of NLO polymers.

In-situ Electro-optic Measurements During Poling

Electro-optic (EO) measurements were performed with the ellipsometric technique described in [6]. For the in-situ EO measurements, the applied electric field is a superposition of the poling field E_{dc} and an ac-field E_{ac} with an angular frequency Ω. According to [2], [3] the measured signal has contributions arising from birefringence and from the EO-effect. In extension of [3], the measured signal is proportional to:

$$\Delta n(\Omega) \sim \frac{N}{n}[\frac{12\pi}{45}\Delta\alpha(\frac{\mu}{kT})^2\frac{1}{[1+(i\omega\tau)^\alpha]^\beta} + \frac{2}{15}\frac{\mu\beta}{kT}(1+\frac{1}{[1+(i\omega\tau)^\alpha]^\beta})]E_{dc}E_{ac}e^{i\omega t} \quad (2)$$

Eq. (2) takes into account the broad distribution of relaxation times which is typical for polymers and also introduces a frequency dependency of the EO effect. A detailed derivation of Eq. (2) will be reported in a forthcoming publication.

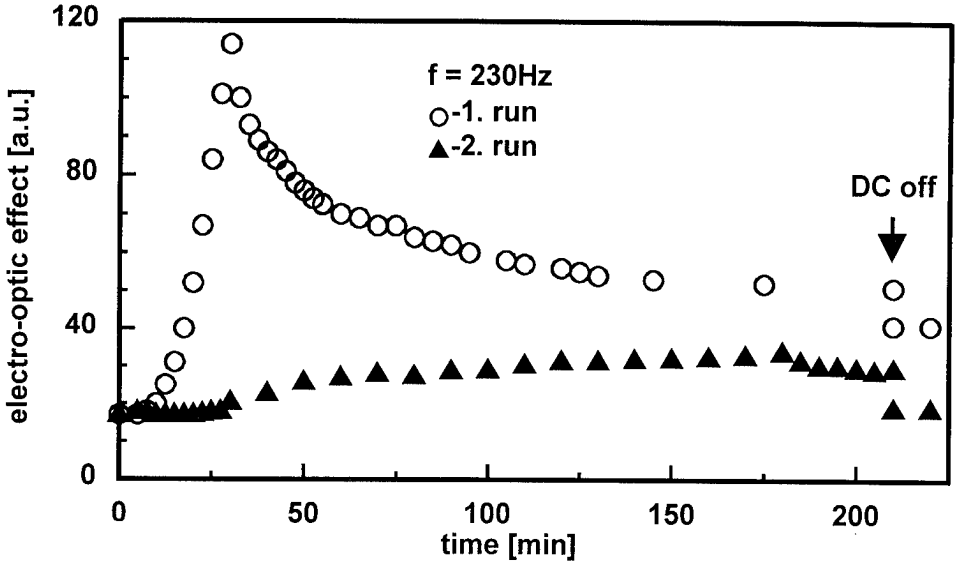

Fig.2 In-situ EO response during heating, cross-linking and cooling measured at 230Hz.

For the in-situ EO measurements the same procedure was applied as for the dielectric measurements. The results in Fig. 2 show the measurement performed at 230Hz. The signal at room temperature is due to the dc-induced EO-effect. During heating, first an increase of the EO signal due to the enhanced mobility of the dipoles occurs. During the isothermal cross-linking at 150°C, the EO signal decreases in the same way as the dielectric function. Upon cooling the complete freezing of the cross-linked dipoles can be followed. After removing the dc-field, an EO signal drop is observed as the dc-induced contribution vanishes. The remaining signal is the real EO-effect. In a second run, in-situ EO measurements were performed on an already cross-linked polymer sample. Again, no changes in the signal during the isothermal process can be observed. However, as cross-linking is completed, the resulting EO-signal is smaller than the signal after in-situ poling during cross-linking. Thus in-situ EO measurements are very attractive for optical investigation of cross-linking processes.

Pyroelectric Thermal Analysis (PTA)

The stability of the dipole orientation after the poling and cross-linking processes were investigated with the recently introduced PTA technique [7]. Fig 3 shows the experimental results obtained with 8% and 30% Red Acid Magly samples. The enhanced thermal stability of the 30% polymer sample is obvious from the measurement

and shows the larger increase in the glass-transition temperature due to the larger amount of cross-linking sites. Also included is the PTA result after photo-induced poling (PIP) of an already cross-linked sample. PIP was performed at T=110°C with unpolarized light with an intensity of 25mW/cm^2 (wavelength range 360-800 nm) for 120min. As observed in other polymers, the thermal stability of the PIP sample is less good than compared to the samples poled during cross-linking. However, improvements of the thermal stability by aging will be the topic of further investigations.

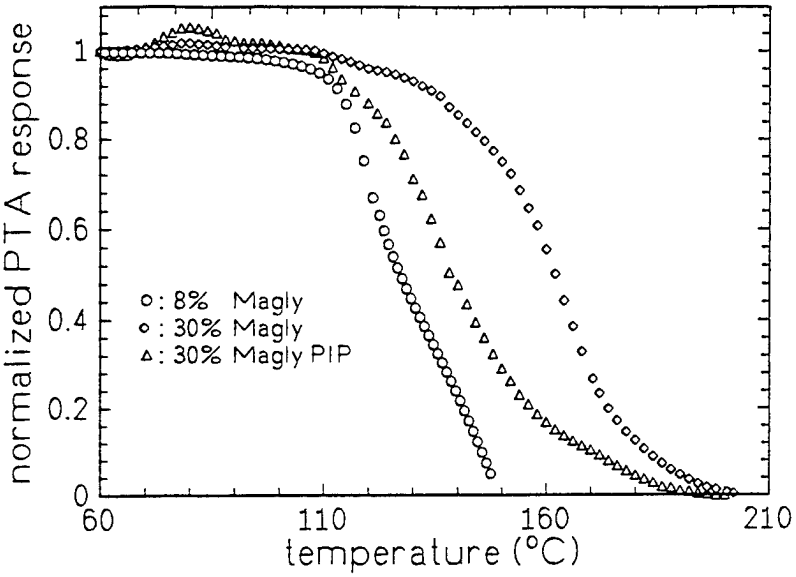

Fig.3 PTA results for the different Red Acid Magly samples.

Conclusion

It has been shown that pyroelectrical, dielectric and electro-optical investigations are powerfu l techniques for the optimization of cross-linking processes in NLO polymers.

F. Foll, A. Rousseau, and B. Boutevin from the Laboratoire de Chimie Appliquée of ENSCM in Montpellier are greatefully acknoledged for the supply of Red-Acid Magly synthesized under a CNET contract.

References

[1] M. Eich, B. Reck, D. Y. Yoon, C. G. Wilson, and G. C. Bjorklund, J. Appl. Phys., **66**, 3241 (1989).

[2] S. Aramaki, Y. Okamoto, and T. Murayama, Jpn. J. Appl. Phys. **33**, 5759 (1994).

[3] S. Aramaki, Jpn. J. Appl. Phys. **34**, L47 (1995).

[4] J. Liang, R. Levenson, C. Rossier, E. Toussaere, J. Zyss, A. Rousseau, B. Boutevin, E. Foll, and D. Bose, J. Phys. III France, **4**, 2441 (1994).

[5] W. Ren, S. Bauer, S. Yilmaz, W. Wirges, and R. Gerhard-Multhaupt, J. Appl. Phys. **75**, 7211 (1994).

[6] C. C. Teng and H. T. Man, Appl. Phys. Lett., **56**, 1734 (1990).

[7] S. Bauer, W. Ren, S. Yilmaz, W. Wirges, W.-D. Molzow, R. Gerhard-Multhaupt, U. Oertel, B. Häussler, H. Komber, and K. Lunkwitz, Appl. Phys. **63**, 2018 (1993).

Physical aging after photo-induced or thermally assisted poling for enhancing the stability of polymeric dipole glasses

S. Bauer-Gogonea, S. Bauer, W. Wirges, R. Gerhard-Multhaupt
Heinrich Hertz Institut für Nachrichtentechnik
Einsteinufer 37, D-10587 Berlin, Germany
and
H. J. Wintle
Department of Physics, Queen's University
Kingston, Ontario, Canada K7L 3N6

Introduction

The thermal stability of the dipole orientation is a critical issue for poled polymers. Particularly for the newly developed photo-induced-poling (PIP) technique [1], it was shown that the dipole orientation is less stable than for thermally assisted poling (TAP) [2]. Physical methods to improve the thermal stability are thus highly desirable. Physical aging under applied field is known to significantly enhance the long-term stability of the dipole orientation [3]. Here, we study the improvement in the thermal stability of the dipole orientation achieved with physical aging under field after photo-induced and thermally assisted poling, using the recently introduced pyroelectric techniques (pyroelectric relaxation spectroscopy (PRS) and pyroelectric thermal analysis (PTA) [4]). In particular it is shown that two routes are possible to improve the thermal stability following PIP. One route is the use of high glass-transition polymers and PIP at a higher temperature, the other is physical aging under field after removing the pump light. The experimental results are discussed within the framework of a modified Narayanaswamy-Moynihan model. All the experiments were performed on P(S-MA)-DR1 side-chain polymers from Sandoz [5] (T_G of 140°C or 165°C).

Pyroelectric Effect in Poled Polymers

The pyroelectric effect describes the electric response of a material to a temperature change. In poled amorphous polymers, pyroelectricity arises mainly from the dipole density decrease upon thermal expansion. The experimental pyroelectric coefficient p is defined as the temperature derivative of the charge Q induced on the sample electrodes of area A during heating. In [6], a discontinuous polarization (Lorentz model) is combined with a reaction field (Onsager model). By including the effect of angle changes of the dipoles due to affine deformations as discussed in [7], we obtain:

$$p = \frac{1}{A}\frac{dQ}{dT} = \alpha_x\left(\frac{\epsilon_\infty + 2}{3} - \frac{2}{5}\right)P \qquad (1)$$

with the relative thermal expansion coefficient α_x and the relative unrelaxed dielectric constant ϵ_∞. Thus p is proportional to the frozen polarization P. However, we believe

that this treatment is an incompatible combination. The dipoles are frozen in a configuration that corresponds to the equilibrium at the poling temperature, whereas at the lower measuring temperature, only the electronic polarizability is involved. A distinction between these two regimes had previously been made, but we have recalculated the response using the self-consistent Onsager formulation for both the cavity containing the dipole and the exterior effective medium, and have found small differences in the results. Free (3D) or clamped (1D) expansion must also be allowed for [8]. In a first step, we have checked whether Eq. (1) is a useful approximation by measuring p with a quasi-static technique, α_x and ϵ_∞ by dielectric measurements, and P by TSD. The value of $p = 1.17\mu\mathrm{C/m^2\,K}$ for a poling field of $E = 40\,\mathrm{V}/\mu\mathrm{m}$ is in reasonably good agreement with Eq. (1), which predicts $p = 1.06\mu\mathrm{C/m^2\,K}$ from α_x, ϵ_∞, and P. This shows the usefulness of pyroelectric measurements for the characterization of the polar order in poled polymers. A more detailed discussion of pyroelectric effects in poled polymers will be published soon.

Photo-induced Poling (PIP)

In order to improve the thermal stability of the dipole orientation after photo-induced poling, we have adopted the following scheme: The polymer sample is heated at a constant rate to a temperature well below the glass-transition temperature of the polymer. Then the poling field is applied and the pump light is switched on. After switching the pump light off, the electric field is maintained for an extended period of time t_a, and then the sample is cooled to room temperature at the same rate. Subsequently, the thermal stability of the dipole orientation is investigated by PTA.

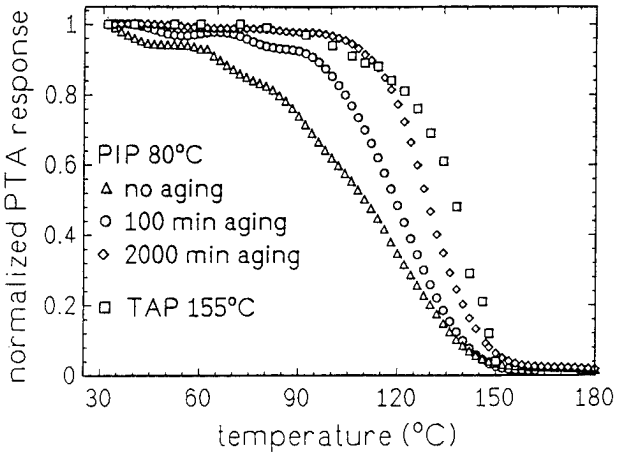

Fig. 1: PTA results for photo-induced poling (PIP) after different aging times.

Fig. 1 shows experimental results if photo-induced poling was performed at 80°C for a time of 120 min followed by different aging times t_a. In our in-situ pyroelectric measurements, we have found no significant increase of the pyroelectric signal during the aging period. This rules out any significant molecular motion at 80°C. From Fig. 1, it is obvious that aging significantly enhances the thermal stability after photo-induced poling. However, even after 2000 min of aging, the upper limit found with thermally

assisted poling (TAP) was not reached.

Yet another approach to increase the thermal stability of the dipole orientation after PIP is the use of a high-T_G polymer. This allows for PIP at higher temperatures while avoiding large thermal molecular motions. Fig. 2 shows the experimental results for a polymer film with a glass transition temperature of 165°C which was photo-induced poled at 110°C. It is obvious from Fig. 2 that in this case the thermal stability of PIP is superior to that of TAP of the lower-T_G polymer even without aging.

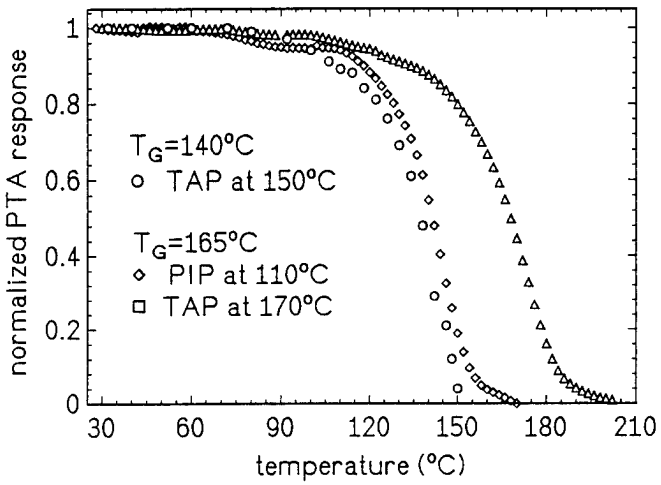

Fig 2: PTA results after PIP and TAP of the high-T_G polymer and after TAP of the low-T_G polymer .

Thermally Assisted Poling (TAP)

Physical aging under electric field can significantly enhance the thermal stability of the thermal orientation [3]. In order to deepen our understanding of the physical processes during aging, we have adopted the following scheme: first the polymer sample is poled ε , a temperature above T_G, then the film is quenched below T_G while the electric field is still applied for an extended period of time t_a. The dipole relaxation is monitored by the isothermal decay of the pyroelectric response. Fig 3 shows the experimental results after different aging times with enhanced thermal stability. For theoretical modeling, the Narayanaswamy-Moynihan (NM) model [9] was modified. The normalized polarization $P(t)$ and thus the pyroelectric coefficient $p(t)$ is:

$$P(t) = \exp[-(\int_0^t \frac{d\tilde{t}}{\tau(t_a, \tilde{t})})^{\beta}] \tag{2}$$

with a time-dependent mean relaxation rate $\tau(t_a, t)$ given by:

$$\tau = a\,(t + t_a)^{\gamma} \tag{3}$$

This model has only three parameters a, γ and β to fit all the different curves in Fig. 3. Fit and measurement agree reasonably well, and demonstrate that the thermal stability can be significantly enhanced by physical aging. However, even after 4000 min of aging, we have not reached the mean relaxation time τ for thermal equilibrium. Equally well, our decay curves can be fitted empirically by KWW-functions, with parameters which change according to the aging time, as proposed in [10]. It is tempting to assume that these fits represent the underlying aging dynamics, but this may not be the case because logically, the parameters would be changing continuously with time both before and after the field is removed (though perhaps at a different rate). The proposed model in Eq. (2) is a first trial to consider the continuous change of the relaxation rate as a function of time.

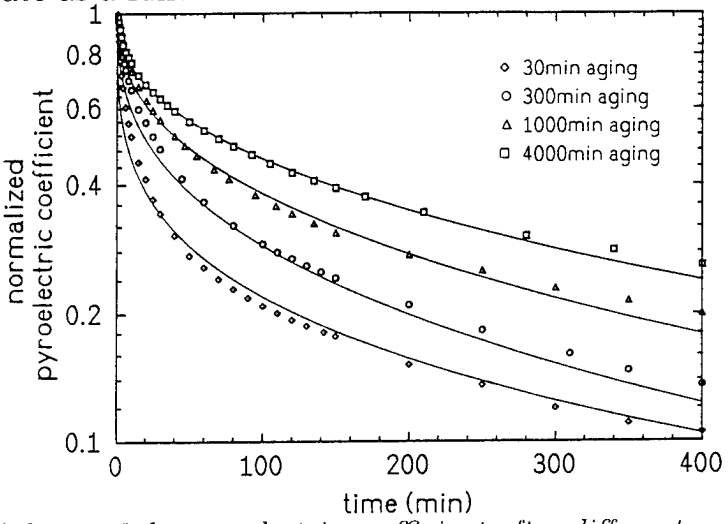

Fig 3: Isothermal decay of the pyroelectric coefficient after different aging times.

Conclusions

Pyroelectric techniques are useful for the analysis of dipole relaxation processes in poled polymers. Physical aging improves the thermal stability of PIP and TAP. The aging results can be well represented with a modified Narayanaswamy-Moynihan model.

References

[1] Z. Sekkat, and M. Dumont, Appl. Phys. B, **53**, 121 (1991).

[2] S. Bauer-Gogonea et al., J. Appl. Phys. **76**, 2627 (1994).

[3] H. T. Man and H. N. Yoon, Adv. Mat., **4**, (1992).

[4] S. Bauer at al., ACS Symposium Series, in press (1995).

[5] M. Ahlheim and F. Lehr, Macromol. Chem. Phys., **195**, 361(1994)

[6] F. I. Mopsik and M. G. Broadhurst, J. Appl. Phys., **46**, 4204 (1975)

[7] H.-J. Winkelhahn et al. , Appl. Phys. Lett., **64**, 1347 (1994)

[8] R. Hayakawa and Y. Wada in *Advances in Polymer Science* (Springer, Berlin, New York, 1973), **11**, 1.

[9] O. S. Narayanaswamy, J. Am. Ceram. Soc., **54**, 491 (1971) and C. T. Moynihan et al., Ann. N. Y. Acad. Sci., **279**, 15 (1976).

[10] H. S. Lackritz and J. M. Torkelson in *Molecular Nonlinear Optics*, J. Zyss (ed.), 339, Acad. Press (1994)

In situ RHEED observation of MBE growth of organic thin films

Tadashi Ishibashi, Shin'ichiro Tamura and Jun'etsu Seto
Sony Corporation Research Center, 174, Fujitsuka-cho, Hodogaya-ku, Yokohama-shi, 240, Japan
Telephone +81-45-353-6848, Fax.+81-45-353-6909

Masahiko Hara, Hiroyuki Sasabe and Wolfgang Knoll
Frontier Research Program, The Institute of Physical and Chemical Research (RIKEN), 2-1, Hirosawa,Wako-shi, 351-01, Japan, Telephone +81-48-462-1111 ex.6333, Fax.+81-48-465-8048

INTRODUCTION

Studies on molecular beam epitaxial growth for organic molecules (OMBE) have been attracting attentions as a new fabrication method for preparation of ultra-thin films of organic molecules. Molecular beam epitaxy (MBE) has been developed as a deposition technique for the controlled growth of atomically flat multilayer structures. Recently, this method has been applied to organic materials, while the mechanism of the growth has not been thoroughly understood compared to that of semiconductor. In this report, the growth mechanism of Lead Phthalocyanine (PbPc) thin films onto highly oriented pyrolytic graphite (HOPG) substrate by OMBE method was investigated using *in situ* refraction high energy electron diffraction (RHEED). RHEED has been widely used for *in situ* monitoring of the thin film MBE growth. The intensity of the RHEED specular beam spot oscillates according to the layer-by-layer growth[1]. In 1981, Joyce et.al. observed an oscillated phenomena of RHEED intensity with growth of semiconductor for the first time[2]. After that, a lot of work in the semiconductor field have been reported and developed. Although application for organic materials is expected, so far RHEED oscillation studies have only been reported for Copper Phthalocyanine (CuPc) on MoS_2 substrate[3]. Therefore, we explored the possibilities of using *in situ* RHEED observations to investigate the OMBE growth mechanism of PbPc on HOPG system.

EXPERIMENT

PbPc was grown on HOPG using an OMBE system (Vieetech Japan Co., Ltd.) in Frontier Research Program, RIKEN. This system is composed of a deposition chamber and a preparation chamber. The HOPG substrate was cleaved in air just before loading into the chamber and subsequently baked at 800 ℃ with a base pressure of about 10^{-6} Pa. PbPc was degased in a Knudsen-cell, which has a separate vacuum from the deposition chamber, at 100-150 ℃ for 8 hours before deposition. For the depositions, PbPc was evaporated from the Knudsen-cell at three different temperature, 260, 280 and 300 ℃ in the deposition chamber with a base pressure of about 10^{-7} Pa.

For the analysis of the growth mechanism, *in situ* RHEED observations were carried out before and during the deposition. The acceleration voltage was 10kV and the filament current was

10 μ A. In order to minimize the expected damage to the organic thin film by electron beam, each RHEED intensity was measured with 3 sec of electron beam exposure after 10 sec intervals. RHEED intensities and patterns on the screen were recorded by CCD camera system (DVS-3000, Hamamatsu Photonics K.K./).

The temperature dependence of the substrate for the changes of the RHEED specular beam intensity was observed at 0, 50 and 100 ℃. The temperature dependence of the PbPc evaporating speed during deposition was observed with the RHEED specular beam intensities at three different Knudsen-cell temperature, 260, 280 and 300 ℃.

For *ex situ*. characterization, scanning tunneling microscopy (STM) measurements were carried out at room temperature in air with NanoScope-II (Digital Instruments Inc.) using Pt-Ir tips, immediately after taking out from vacuum. These images were obtained in the constant current mode.

RESULTS AND DISCUSSION

Figure 1 shows a typical RHEED pattern of HOPG substrate. Figure 2 shows a RHEED pattern of oriented PbPc crystal thin films on HOPG. Considering the distance of 0.246nm for HOPG which was determined by diffraction measurement, the distance between PbPc molecules in the crystal thin films on HOPG substrate was 1.3-1.4nm determined by RHEED patterns.

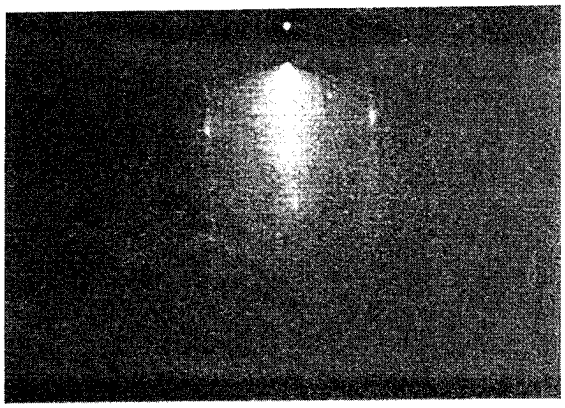

Fig.1 RHEED pattern of HOPG substrate before deposition.

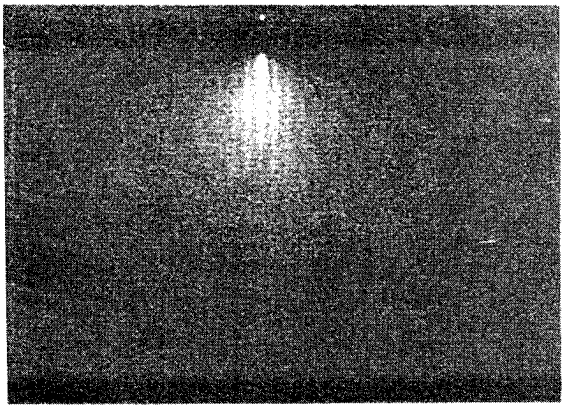

Fig.2 RHEED pattern of oriented PbPc crystal thin film deposited at 300℃ on HOPG substrate at 50℃ for 1 hour.

The change of RHEED specular beam intensity was observed as shown in Figure 3. In these figures, the shutter of Knudsen-cell was opened at 0 sec correspond to the start of the deposition. Just after opening the shutter, the intensity increased immediately. This result indicated the PbPc molecules covered the surface of HOPG, because that the scattering factor for electron beam of Lead, complex metal of PbPc molecules, was larger than that of carbon which is an element of the HOPG substrate. This phenomenon is a typical change of RHEED intensity by hetero-epitaxial growth. After the intensity reached a maximum, it decreased immediately, because that PbPc was producing islands on the substrate simultaneously with layer-by-layer growth, so that the flatness of the surface on the film and substrate was decreased. Thereafter the intensity was oscillated several periods, while the amplitude was decreasing very rapidly in this case. The

RHEED intensity changed after annealing the HOPG substrate covered PbPc thin film as shown in Figure 4. Clear oscillations in the RHEED intensity were observed for the first time in OMBE. The layer-by-layer growth of PbPc crystal thin film must have been the main process in this case, even though a gradual decrease in the amplitude was observed and island structure may grow simultaneously. These RHEED phenomena for organic material thin films were similar to the behavior observed in semiconductors[4].

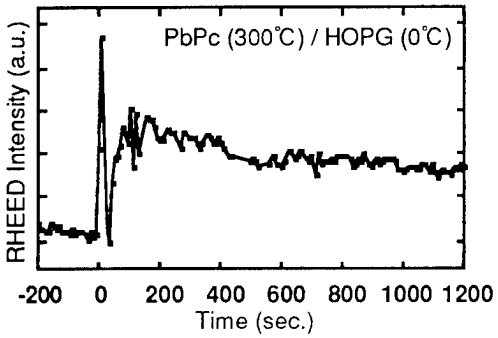

Fig.3(a) RHEED oscillation of specular spot from PbPc MBE growth at 300℃ on HOPG at 0℃.

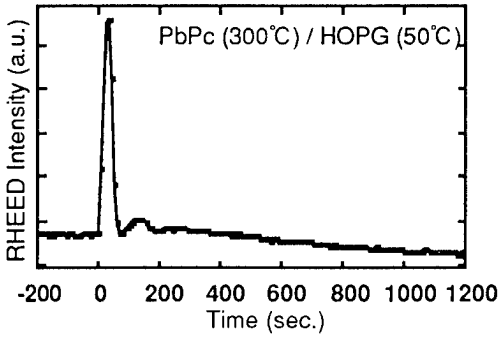

Fig.3(b) RHEED oscillation of specular spot from PbPc MBE growth at 300℃ on HOPG at 50℃.

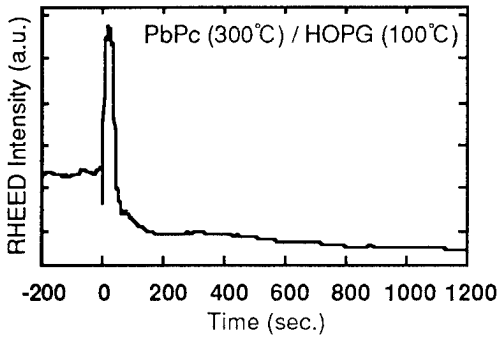

Fig.3(c) RHEED oscillation of specular spot from PbPc MBE growth at 300℃ on HOPG at 100℃.

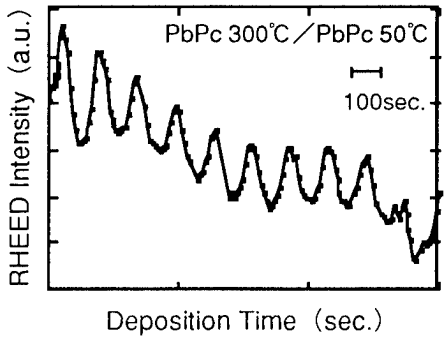

Fig.4 RHEED oscillation of PbPc Homo Growth on PbPc MBE crystal thin layer.

In order to investigate the morphology of the thin films, STM observation was carried out. STM image with area about 600nm×600nm of PbPc MBE crystal thin film on HOPG substrate is shown in Figure 5. In this figure, we can study the layer-by-layer grown PbPc along the step of HOPG and the simultaneously grown 3-dimensional PbPc. The RHEED oscillation decreased gradually in the case of the combination of layer-by-layer growth and 3-dimensional growth of PbPc as shown in Figure 5.

On the other hand, the change of RHEED intensity depended on the temperature of substrate as shown Figure 3(a), (b) and (c). About the first period of the oscillation which was corresponded to the growth time of the first layer, the case at 0 ℃ was the shortest, and the time of the period became longer with increasing the temperature of the substrate. These results indicated that growth rate at the interface were affected by the migration of PbPc molecules on HOPG substrate.

Furthermore, after the second period of the oscillations, the restoration of the intensity at the higher temperature of the substrate was larger than that at lower temperature. This result shows the ratio of the terrace of thin film grown at the lower temperature was larger than that at higher temperature.

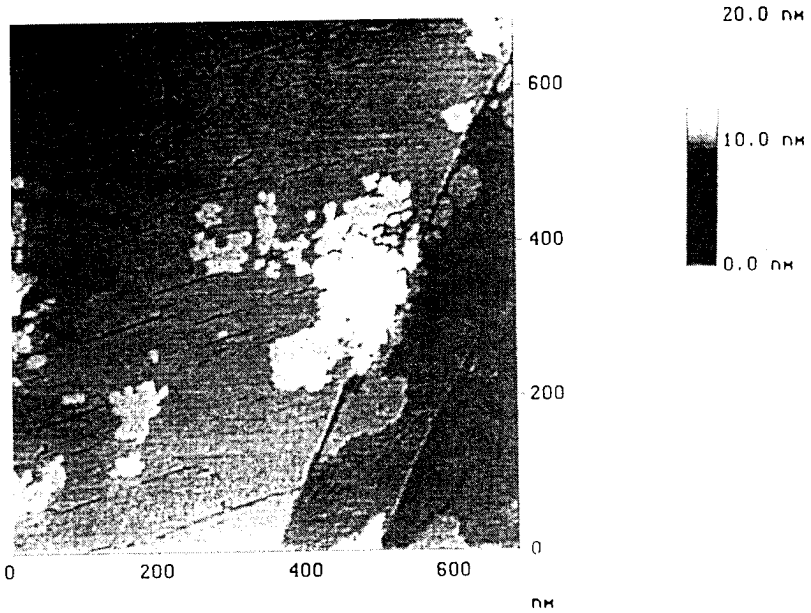

Fig.5 STM image of PbPc OMBE film on HOPG substrate, which shows the domains grown along the step of HOPG and PbPc islands.

CONCLUSIONS

The results of *in situ* RHEED observations indicated not only the structural factors but also the difference in the growth process. In the deposition of PbPc on HOPG, the growth was a combination of layer-by-layer growth and 3-dimensional nucleation, so that RHEED oscillations decreased rapidly. However, in the homo growths, the oscillation decreased gradually. These results were indicated that the PbPc growth onto HOPG was layer-by-layer growth with simultaneous 3-dimensional nucleations. In addition to that, *in situ* RHEED observations can be available for organic thin films and these results suggested the possibilities of preparing super-lattice structure of organic materials controlled by monolayer thickness using this method.

REFERENCE

[1] H.Tamada, IEEE J. Quantum Electron. QE-27, 502 (1991)
[2] J.J.Harris, B.A.Joyce and P.J.Dobson, Surf.Sci. 103, L90 (1981)
[3] M.Hara, H.Sasabe, A.Yamada and A.F.Garito, Jpn.J.Appl.Phys., 28, L306 (1989)
[4] J.Lee et.al.,Jpn.J.Appl.Phys., 32, 4889 (1993)

Structure and Properties of Fluoro-Aluminum Tetraphenyl-porphyrin (FAlTPP) Thin Films

Yuji Yakura[1,3], Rebecca Shia[3], Tomikazu Sasaki[2], Fumio Ohuchi[3]
[1] Sony Co. Research Center, 174 Fujitsuka-cho, Hodogaya-ku, Yokohama, 240 Japan
Telephone : (045)353-6849, FAX : (045)353-6907,
[2] Department of Chemistry, and [3] Department of Materials Science and Engineering, University of Washington, Seattle, WA 98195 U.S.A.
Telephone : (206)685-8272, FAX : (206)543-3100

Abstract

In an attempt to design molecular arrays with adjustable periodicity in two dimension, fluoroaluminum tetraphenylporphyrin (FAlTPP) molecules were synthesized and fabricated into thin film forms. This paper describes our preliminary results on structure and properties of FAlTPP thin films.

Introduction

Potential applications to molecular electronics and optics have led to an intense investigation on fabrication and characterization of ordered organic thin films. Fluoro-aluminum phthalocyanine (AlPcF) molecules are known to form a polymeric one-dimensional column with a straight $[\text{-Al-F-}]_n$ backbone, and exhibit unusual optical and conductivity properties. This is believed to be due to strong π–π interactions between macrocycles, as well as exciton couplings within the sandwich complex. The cofacially stacked AlPcF structure has been fabricated in thin film forms on KCl and KBr by means of molecular beam expitaxy (MBE) (ref.1).

Our interest has been centered around questions as to what unique electrical and optical properties can be obtained in thin film forms, if the distance between such one dimensional columns are controlled in two dimensions. Tetra-substituted metalloporphpyrins are an ideal molecular unit for the assembly of such two-dimensional array. Metal complexes of 5,10, 15, 20-tetracarboxyamide porphyrin can, for example, generate a two-dimensional tetragonal lattice structure with a periodicity of 13-14Å. The carboxyamide group will form inter-porphyrin hydrogen bonds, thus the periodicity of the porphyrin monolayer could be adjusted by inserting extended spacer groups between the carboxyamide group and the porphyrin ring.

In an attempt to demonstrate this concept, we have chosen fluoroaluminum tetraphenylporphyrin (FAlTPP) as a test molecule, because of its tendency to form a straight $[\text{-Al-F-}]_n$ backbone when they are stacked together in three dimension, and the potential adjustability of the molecular size by the structural modification of meso-substituents of porphyrin ring. This paper describes chemical synthesis of FAlTPP molecules and their fabrication into thin films. Preliminary results on structural and optical properties of thin films are discussed.

Experimental

In synthesis of FAlTPP molecules, meso-tetraphynylporphyrin was reacted with $AlCl_3$ in CS_2, forming chloro-aluminum tetraphynylporphyrin (ClAlTPP). The chlorine was ion-exchanged with OH in NaOH solution, yielding hydroxy-aluminum tetraphynylphorphyrin (HOAlTPP). The

HOAlTPP was then heated in a 48%HF solution for about 4 hours at 90°C, leading to FAlTPP after replacing OH by F. Synthesized FAlTPP molecules were placed in a small quartz boat inside the closed end of a quartz tube, which was evacuated and heated to sublimate the compound. This process purifies FAlTPP in the form of solid crystals.

FAlTPP thin films were fabricated by vacuum deposition from a simple Knudsen cell onto fused quartz substrates. Deposition was made under variou vacuum pressures varing from 10^{-6} torr to some 10s mtorr ranges. The substrate temperature was varied between 100 and 150°C. Several analytical techniques, including X-ray diffraction (XRD) and UV-visible spectroscopy, were used to characterized thin film structure and properties.

Results and Discussion

During the purification process, the sublimated materials were deposited on the inner wall of the quartz tubewith some distance away from the source. A glass microscope slide was placed at this location to collect the sublimated FAlTPPs. The FAlTPP crystals have two distinct shapes; needle-like and pyramid-like. The pyramid-like crystals were subjected to the three dimensional X-ray diffraction analysis to determine the crystal structure. Results are shown in Table 1.

Table 1: 3-D XRD analysis of FAlTPP Crystals

Empirical Formula	$C_{44}H_{28}AlFN_2$
Color	Dark Purple
Habit	Bipyramid
Crystal size (mm)	0.30 x 0.32 x 0.36
Crystal System	Tetragonal
Space Group	I4/m
Unit Cell Dimensions	$\underline{a}$ = 13.340(2) Å
	$\underline{c}$ = 9.780(2) Å
Volume	1740.4(9) $Å^3$
Formula weight	630.7
Density (calc.)	1.257 Mg/m^3
Absorption Coefficient	0.194 mm^{-1}

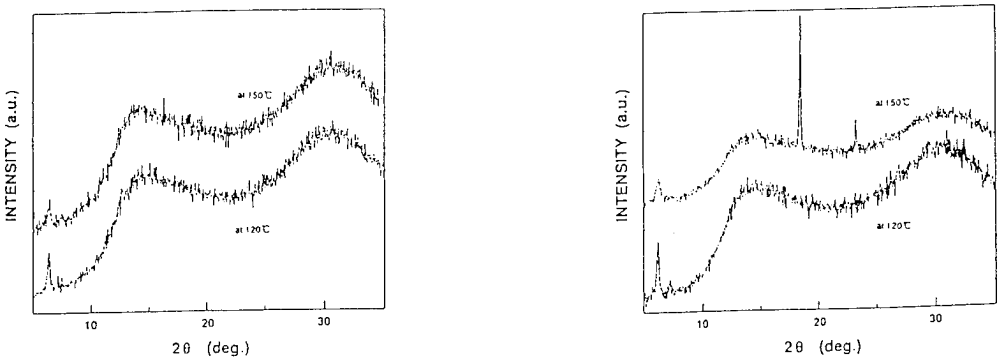

Figure 1. X-ray diffraction pattern in the vacuum condition under (a) 10^{-6} and (b) 10s mtorr.

The deposition condition strongly influences resultant thin film structures as determined by 2θ scan. Shown in Figure 1 compare four XRD spectra obtained from FAlTPP thin films with four different deposition conditions. Thin films fabricated under 10^{-6} torr range indicated a peak at 2θ=6.3° (13.9Å) in thin films deposited on the substrate of 120 and 150°C. The deposition conducted in some 10s mtorr range conditions exhibted very different behavior. This was done by breeding pure Ar gas into the vacuum chamber that was originally evacuated to 10^{-6} torr range. In these conditions, the substrate was placed right above the Kndsen source in order to collect the molecular flux from the source. Sharp reflections appeared in XRD spectra obtained from these specimens. Deposition at the substrate temperature of 150°C showed a strong peak at 2θ = 18.3°, corresponding the interspacing distance of 4.8Å, whereas the thin film deposited at 120°C exhibited a peak at 2θ =6.3° (13.9Å). Based on the crystal structure, the XRD results suggest the following molecular arrangement :

Deposition under 10^{-6} torr at T_S=120 and 150°C and 10s mtorr at T_S=120°C: FAlTPP thin film with $[\text{-Al-F-}]_n$ backbone lying parallel to the substrate. (figure 2(a))

Deposition under 10s mtorr at T_S=150°C: FAlTPP thin film with $[\text{-Al-F-}]_n$ backbone standing perpendicular to the substrate. (figure 2(b))

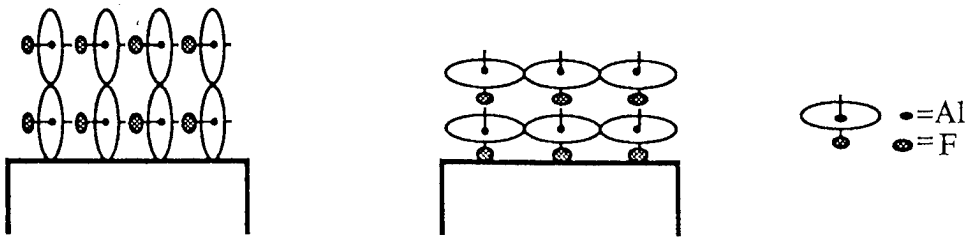

(a) (b)

Figure 2.

FAlTPP molecules have a tendency to cofacially stack together forming $[\text{-Al-F-}]_n$ backbones. This unique property has resulted an interesting observation during thin film formation. The mean free path of molecules under 10s mtorr vacuum conditions is estimated to be 0.5 cm, a several order of magnitude smaller than those at high vacuum conditions. It is therefore expected that the molecules sublimed from the Kundsen cell immediately collide each other in gas phase, forming clusters. This means the nucleation and growth of thin films under these conditions are significantly different from what is normally observed under high vacuum conditions. While the influence of pressures, in particular, in high pressure regimes, was not thoroughly studied, the present results indicate that the thin films are formed through condensation and re-arrangement of the clusters which are self-assembled into cofacially stacked molecular structure. During the re-arrangement over the substrate, temperature plays an important role. The data indicate that higher temperatures are required in order for molecular columns to stand up perpendicular to the substrate surface, otherwise cofacially stacked molecular units tend to lie down parallel to the surface. Depositions under high vacuum conditions have resulted random orientation of the molecules in the present case.

In UV-visible photoabsorption spectra, porphyrins are known to exhibit a strong Soret band absorption at peak around 400nm, while the Q bands around 600nm are weak. These features are

contrasted to those observed in phthalocyanines (high Q band and low soret band absorptions). In figure 3, UV-visible absorption spectra obtained from four specimens described above are shown. It is found that the characteristic features of Soret band absorption are dependent on the structural arrangement; for cofacially stacked macrocycle molecules. In the FAlTPP solution system in CCl_4, the Solet band appears at 413nm. However, the band of thin films deposited in the condition under 10s mtorr exhibited a broadened peak and shifted to blue. This fact shows that the molecules are cofacially stacking and supports the data of X-ray diffraction.

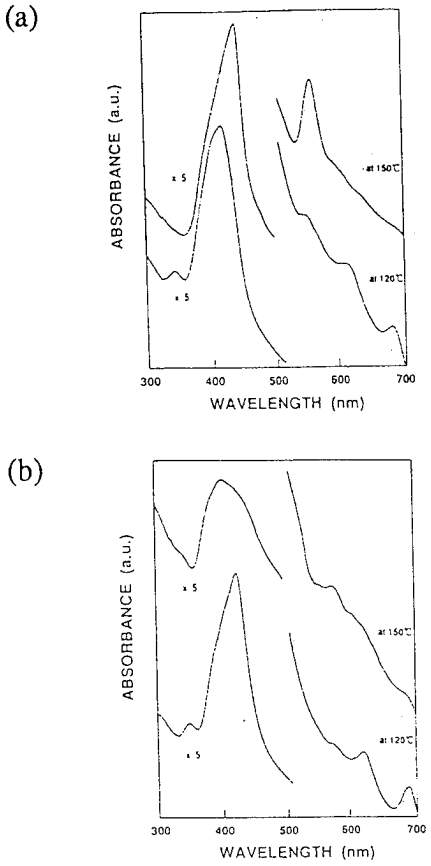

Figure 3. UV/vis spectra of FAlTPP thin films in the vacuum condition (a) 10^{-6} and (b) 10s mtorr.

Summary

Fluoroaluminum tetraphenylporphyrin (FAlTPP) molecules were synthesized and fabricated into thin film forms. Inherent nature to be self-assembled into cofacial stacking with $[\text{-F-Al-}]_n$ backbone straight has been utilize to control the thin film structure. Preliminary data indicate correlation between the molecular structure of thin films and the UV-visible absorption properties.

Acknowledgement

To SONY for partial finacial support.

References

[1]A. J. Dann, H. Hoshi and Y. Maruyama, *J. Appl. Phys.*,67(3), 1371 (1990).

OPTICAL NONLINEARITY OF CO-POLYMERS CAUSED BY CHARGE INJECTION

Barak Lavi and Garry Berkovic

Department of Materials and Interfaces

Weizmann Institute of Science

Rehovot 76100 Israel

Tel : + 972-8343423 Fax: + 972-8344138 e-mail : csberk@weizmann.weizmann.ac.il

We have shown [1] that asymmetric injection of electric charge into polymer-dye blends can induce second order nonlinear optical effects which are distinct from the more conventional mechanism of using electric fields to align the dye molecules. Using an "in-plane" geometry [1], charges can be injected into polymer-dye films causing symmetry breakage both parallel and perpendicular to the external field. The symmetry breakage perpendicular to the field results from the setting-up of a macroscopic charge gradient, while nonlinearity parallel to the field results from conventional dipolar alignment. Using high voltages but only moderate fields (2000 V across 2mm) charge injection effects can be stronger than dipolar alignment. It is believed that charged dimers and quadrupolar nonlinearities are responsible for the nonlinearity in a charge gradient [2].

In order to further investigate the charge injection mechanism for nonlinearity we have synthesized a series of methacrylate co-polymers with azo dye (Disperse Red 1 analog) in the polymer side chain. Polymers with variable dye concentrations of 2 - 80% have been synthesized (Figure 1).

Second harmonic generation (SHG) studies of charge injection effects in these polymers have been performed. Samples were subjected to a high voltage in our standard "in-plane" geometry [1] for

efficient charge injection. These results were compared to those obtained when the same copolymers were corona poled to create nonlinearity by dipolar alignment.

These studies have shown :

(1) Corona poling is much less efficient at room temperature than at the glass transition temperature (ca 120 °C) when the polymer is mobile. However, creation of nonlinearity via charge injection is most efficient at room temperature and its efficiency decreases as the temperature is increased (see Figure 2). The small shoulder in Figure 2 near the glass transition temperature (ca 120 °C) shows that dipolar alignment by the space charge field (created by the injected charges) can contribute only 5-10% of the total nonlinearity caused by charge injection.

(2) As a function of dye concentration in the copolymer, the nonlinearity caused by charge injection is maximal for 10% dye ; in corona poling nonlinearity increases with dye concentration to 60% (see Figure 3). The saturation of the former at low dye content can be understood since the number of injected charges is much less than the number of dye species ; these charges are distributed between monomer, dimer and higher aggregates of the dye. The decrease of nonlinearity above 10% dye reflects a decrease in the number of charged dye dimers due to production of larger dye aggregates which may be less NLO active than charged dimers, and from changes in the charge storage properties of the polymer.

References

[1] S. Yitzchaik, G. Berkovic and V. Krongauz, "Charge Injection Asymmetry: A New Route to Strong Optical Nonlinearity in Poled Polymers" *J. Appl. Phys.* 70 (1991) 3949.

[2] S. Yitzchaik, G. Berkovic and V. Krongauz, "Investigation of Two-Dimensional Optical Nonlinearity of 'in-plane' Poled Polymer Films" *Nonlinear Optics* 4 (1993) 265.

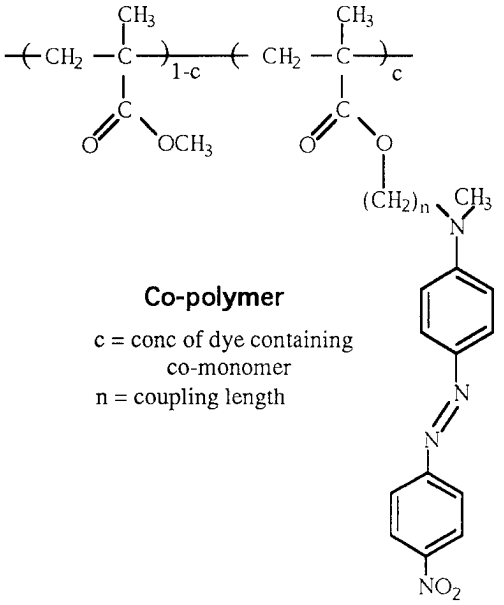

Figure 1. Methacrylate co-polymers containing an azo dye. Polymers were synthesized with c = 2, 10, 40, 60 and 80% dye concentration, and coupling lengths n = 2, 6, 10.

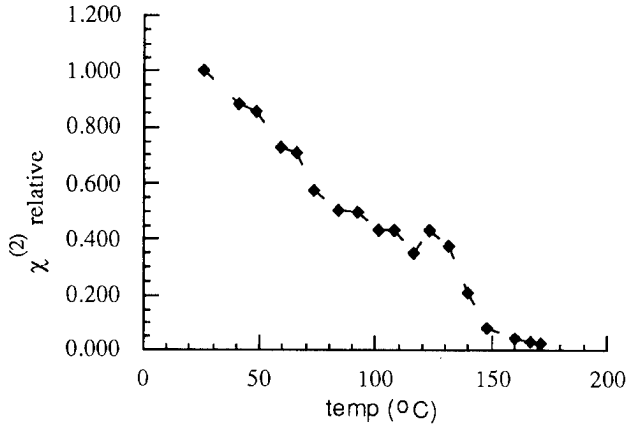

Figure 2. Dependence of nonlinearity induced by charge injection at various temperatures for copolymer with 10% dye and coupling length n=2.

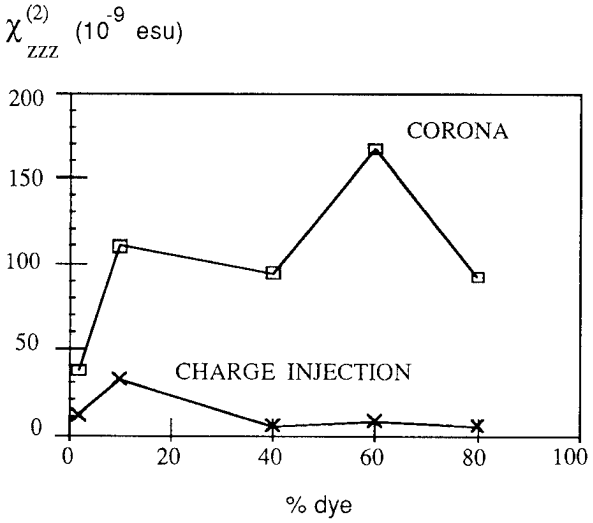

Figure 3. Comparison of nonlinearity created by charge injection and corona poling for various dye concentrations in the series with coupling length n = 6.

Fabrication of Out-of-Plane Branching Mirrors on Polymer Channel Waveguide

Manabu Kagami, Kazuo Hasegawa and Hiroshi Ito
Toyota Central Research and Development Laboratories, Inc.
41-1 Yokomichi, Nagakute, Aichi-gun, Aichi, 480-11, Japan
Tel. +81-561-62-6111 Fax. +81-561-63-5743

1. Introduction

Noncrystalline polymers are suitable as a low cost and high-power optical waveguide material because they have little optical damage. Optical waveguides with large core and high-Δ (LCHD) are effective for a high-power application, because of low power density and easy assembly. High optical power is necessary for driving an optical amplifier[1] or optical devices with nonlinear optical effects or light-to-heat conversion.[2] To couple these devices utilizing the waveguide, out-of-plane branching mirrors are useful (Fig. 1). These mirrors are also applicable to the coupling of optical fiber or OEIC chips[3] with the optical waveguide. A channel waveguide and the mirror are usually fabricated by different mask processes.[4] These complicated processes require precise mask alignment procedure. In this report, we propose a process of simultaneously fabricating out-of-plane branching mirrors and polymer channel waveguides from a slab structure by reactive ion etching (RIE).

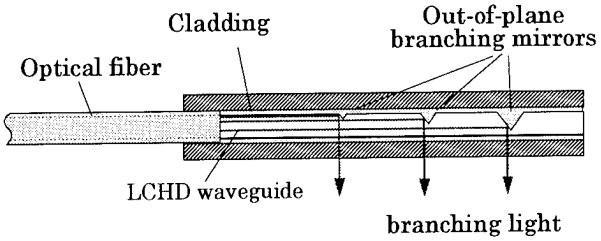

Fig. 1 Longitudinal-section of embeded LCHD channel waveguide with out-of-plane branching mirrors.

2. Fabrication

2.1 Laminate Coating

Undercladding (PFMA: poly-fluoroalkyl methacrylate) and core (PMMA: poly-methyl methacrylate) are laminated on a transparent quartz substrate by the dip-coating method. To obtain uniform and thick films we used a dip process in which multiple dipping was applied while turning upside down and controlled the film thickness by the drying-gas flow rate.[5] The thicknesses of the undercladding and core layer are 20 μm and 100 μm, respectively. Uniformity of the core layer is estimated to be 2.4 percent, except the region 6 mm from substrate edges.

2.2 O_2 RIE

RIE has both chemical and physical etching actions. Generally, the physical etching is made dominant to create a channel waveguide with vertical sidewalls. We have investigated a new method that relatively enhances the chemical etching just under the narrow slit of an etching mask, as shown in Fig. 2(a). Aluminum was used as a nonerodible mask, and the waveguide was defined pattern by normal photolithography. The reactive ion, which is accelerated in a space charge region, retards its speed while passing through the metal slit that is positively charged by ion bombardment. The slit reduces localized physical etching rate, thereby forming a triangular trench on the core surface. This shape (the depth ΔH and the base angle

θ) of the trench can be controlled by the slit width ΔL and RIE conditions. For example, the dependence of the shape on ΔL was measured (Fig. 2(b)). This experiment was carried out under the conditions shown in Table 1. It can be seen that a shallower and expanded trench is formed as ΔL reduces. This trench shape is important to define optical properties of an out-of-plane branching mirror. Figure 3 shows a SEM photograph of the trench when ΔL=10 μm. Sidewalls of the waveguide, of which ΔL is wide enough, are almost vertical (anisotropy $H/\Delta S$>10) and it is observed that recombinant species are stuck on the sidewalls. The relation between ΔL and θ can be controlled by the change of any parameter shown in Table 1.

Table 1. RIE Conditions

Etchant	O_2
Etching pressure	5 Pa
Power	0.16 W/cm^2
Frequency	13.56 MHz
Cathode temp.	25°C
Mask position	4 mm from cathode

2.3 Sidewall Flattening Process

In order to reduce the scattering loss an rough sidewalls, flattening treatment[5] of the ridged core was employed. This treatment is based on the core dissolution and PMMA coating by a solution-dip method. Figure 4 shows the out-of-plane branching mirror after the treatment. It was observed that a smooth surface was obtained, but the trench became shallow and has a wide base angle. The depth and base angle of the trench, corresponding to the branching ratio and reflecting directivity of the optical device, can also be controlled by the flattening conditions.

2.4 Device Assembly

Optical fiber was joined to the LCHD waveguide after a 2000-Å-thick aluminum film was evaporated on the trench. Graded-index multimode fiber with 100-μm core diameter, 140-μm cladding diameter and NA=0.28 was

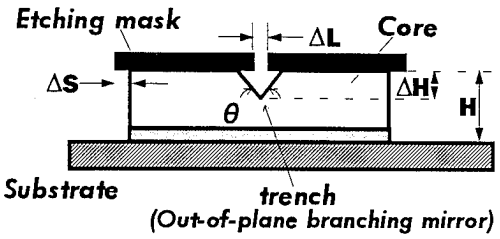

(a)

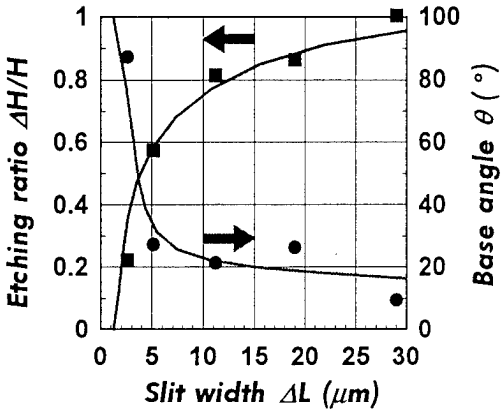

(b)

Fig. 2 Trench formation on PMMA film by O_2 RIE.

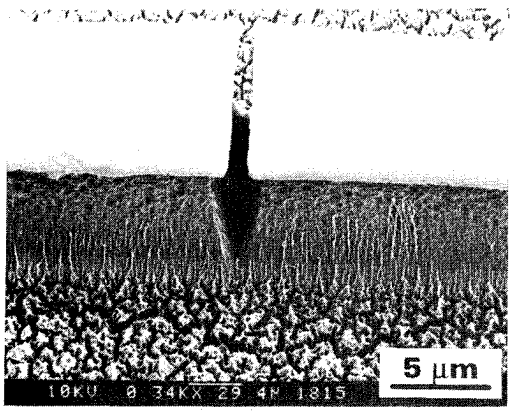

Fig. 3 Photograph of trench (out-of-plane branching mirror) after O_2 RIE.

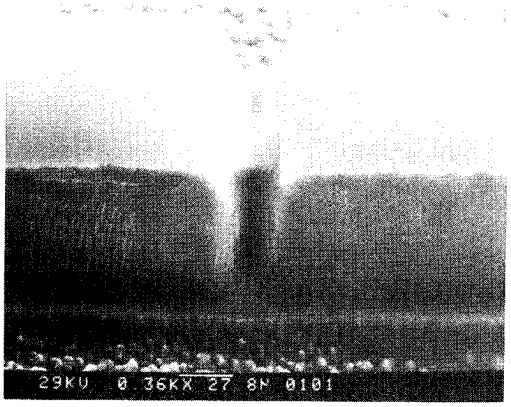

Fig. 4 Photograph of out-of-plane mirror after flattening treatment.

used as input fiber. Finally, the LCHD waveguide and the fiber were embedded in silicone resin to create a protected guide structure. The cured silicone resin also functioned as an overcladding. The refractive indices are summarized in Table 2. The propagation loss of the LCHD waveguide (Δ=5.4 %) is 1.4 dB/cm when the wavelength is 680 nm.

Table 2. Refractive Indices

Layer	Material	Index
Undercladding	PFMA	1.39
Core	PMMA	1.49
Overcladding	silicone resin	1.41

3. Optical Properties

Radiation patterns of the light reflected from out-of-plane branching mirrors were measured (Fig. 5). In the measurement, the light emitted from laser diode was coupled to the fiber in full-mode excitation using NA=0.28 focusing lens. It can be seen from both figures that the radiation peak points to the direction vertical to the substrate. Although, the incident light from the fiber has FWHM=33° mode distribution on far-field-pattern, the light radiated from the mirror is estimated to be about FWHM=80°. This difference is caused by the mode conversion in the waveguide and the curved mirror face shown in Fig. 4. Figure 6 shows a

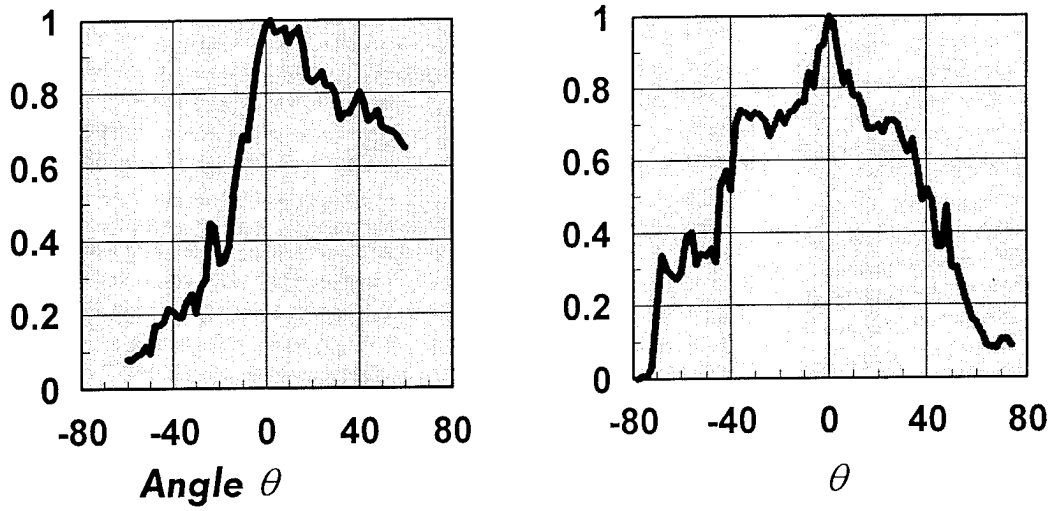

Fig. 5 Radiation pattern dependence on (a) θ_L: angle from vertical direction to longitudinal section, and (b) θ_T: angle from vertical direction to cross section.

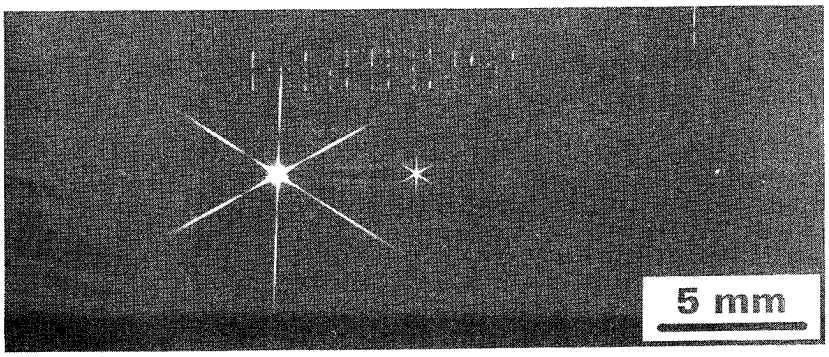

Fig. 6 Photograph of branching light reflected from out-of-plane branching mirrors.

photograph of the light radiated from out-of-plane branching mirrors. The light transmitted in the LCHD waveguide from the left of the photograph is reflected 15 percent at first mirror, and 8 percent of the remaining light is reflected at the downstream mirror. These branching ratios depend on the trench depth.

4. Conclusion

A new method of simultaneously fabricating LCHD optical waveguides and out-of-plane branching mirrors based on the RIE technique has been studied. This method utilizes the phenomenon that the physical etching is restrained just under the narrow-slitted etching mask. The shape of the mirror can be controlled by various parameters, such as the slit width, RIE conditions and flattening conditions. Consequently, this technique is applicable to the fabrication of micromachines as well as optical devices.

References

1. M. Wada and Y. Miyazaki, "Amplification characteristics of waveguide type optical amplifier using Nd doped garnet thin film," IEICE Trans. Electron., **E77-C**, 1138-1145 (1994).
2. H. Mizoguchi, M. Ando, T. Mizuno, T. Takagi and N. Nakajima, "Design and fabrication of light driven micropump," in Proceedings of the *Micro Electro Mechanical Systems*, W. Benecke and H. C. Petzold, eds. (Institution of Electrical Engineering, Piscataway, N.J., 1992), pp.31-36.
3. M. Dagenais, R. F. Leheny and J. Crow, ed., *Integrated Optoelectronics* (Academic Press, 1995), pp.627.
4. L. A. Hornak, ed., *Polymer for Lightwave and Integrated Optics* (Marcel Dekker, 1992), pp.250.
5. M. Kagami, H. Ito, T. Ichikawa, S. Kato, M. Matsuda and N. Takahashi, "Fabrication of large-core, high-Δ optical waveguides in polymers," Appl. Opt. **34**, 1041-1046 (1995).

Third-Order Nonlinear Optical Effects in Organic Nickel Complexes and Triarylmethyl Cations

Daniel R. Greve[#],Tommy Geisler[¤],Thomas Bjørnholm[#], Jan C. Petersen[*]

[#] CISMI,Department of Chemistry-Symbion, University of Copenhagen, Fruebjergvej 3, DK-2200 Copenhagen Ø, Denmark.

[¤] Institute of Physics, Aalborg University, DK-9220 Aalborg Øst, Denmark.

[*] Danish Institute of Fundamental Metrology, Anker Engelunds Vej 1, DK-2800 Lyngby, Denmark.

The second molecular hyperpolarizability, γ, has been determined at 1064 nm by Third-Harmonic Generation (THG) using the Maker fringe technique, for a family of triarylmethyl cations and for a familiy of organic Nickel complexes as guests in PMMA thin films. For the metal complexes it is a well established notion that the low-lying transition with ligand to metal charge transfer character is important for the nonlinear optical properties[1]. However, ambiguity arises due to large discrepancies between different measurements[2-5], as well as difficulties in assessing the exact contribution to γ of the ligand to metal charge transfer transition[2,6]. To assess the latter question by experimental means, we present here a comparison between a family of Nickel complexes, and triarylmethyl cations. The electronic structure of the triarylmethyl cations resemble that of the metal complexes in the sense that intramolecular charge transfer from the periphery to the central atom takes place upon excitation in the first electronic band. This is shown by semi-empirical PM3 calculations on the three members of the family shown in figure 1. For the amino substituted compound **1** the calculations reveal a significant charge transfer from the amino moiety to the central carbon atom. For the molecules **2** and **3** this effect decreases due to the less efficient donor substituents (**2**) or forced planarity (**3**) resulting in more delocalized electronic states both in the HOMO and the LUMO. The observed γ values (table 1) can be correlated with the PM3 calculations in the way that the greater the amount of charge

moved and the longer the spatial distance over wich it is moved, the greater is γ. The calculated static γ values, using the semi-empirical PM3/Finite-Field method follow the same trend although much smaller values are obtained.

From measurements of γ for the family of Nickel complexes shown in figure 2 (table 2) it is apparent that the oscillator strength of the NIR transition may vary by a factor of 3 without significantly changing the measured value of γ. This result is in good agreement with previous investigations of similar complexes[2]. A likely explanation of these observations is, that despite the large intensity of the transitions little charge is moved from the ligands to the metal[6,7] resulting in an insignificant direct contribution of this transition to γ.

REFERENCES :

1: See e.g. Nalwa, H. S., Appl. Organomet. Chem. 1991, 5, 349.

2: Bjørnholm, T.; Geisler, T.; Petersen, J. C.; Greve D.R.; Schiødt, N. C., Nonlinear Opics, in press.

3: Kafafi, Z.H.; Lindle,J.R.; Weisbecker, C.S.; Bartoli, F.J.; Shirk, J.S.; Yoon, T.H.; Kim, O.K., Chem. Phys. Lett. 1991, 179, 79-84.

4: Winter, C. S.; Oliver, S. N.; Manning, R. J.; Rush, J. D.; Hill, C. A. S.; Underhill, A. E., J. Mater. Chem. 1992, 2, 443.

5: Lindle, J.R.; Weisbecker, C.S.; Bartoli, F.J.; Pong, R.G.S.; Kafafi, Z.H., Mat. Res. Soc. Symp. Proc. Vol. 247, 1992, 277-282.

6: Schiødt N.C.; Sommer-Larsen, P.; Bjørnholm, T.; Folmer Nielsen, M.; J. Larsen J.; Bechgaard K., Inorg. Chem,. in press.

7: Herman, Z.S.; Kirchner, R.F.; Loew, G.H.; Mueller-Westerhoff, U.T.; Nazzal, A.; Zerner, M.C., Inorg. Chem. 1982, 21,46-56.

Figure 1

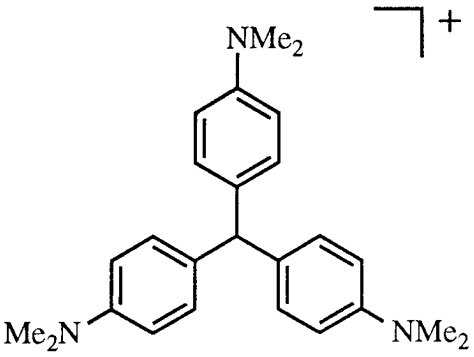

1

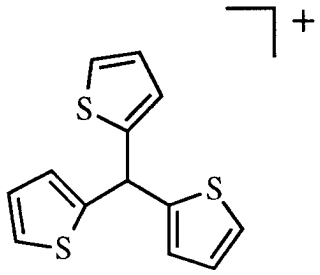

2

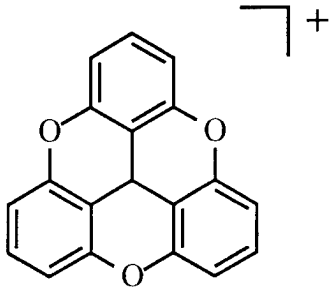

3

Table 1

#	λ_{max} / nm	ε / 10^4 $M^{-1}cm^{-1}$	$\langle\gamma\rangle$ / 10^{-34} esu	$\langle\gamma\rangle$ PM3-FF / 10^{-34} esu
1	597	11	20	5.0
2	472	4.4	10	0.25
3	470*	0.8*	<1	0.1

* : ref. 8.

Figure 2

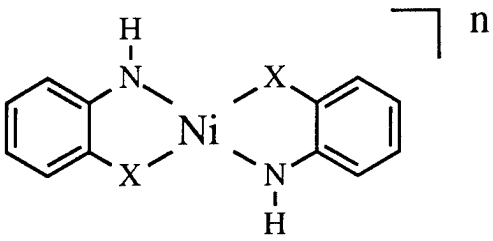

Table 2

#	n	X	λ_{max} / nm	ε / 10^4 $M^{-1}cm^{-1}$	$\langle\gamma\rangle$ / 10^{-34} esu
4	0	S	828	3.75	3.5
5	-1	S	950	1.36	4.0
6	0	Se	836	2.43	3.0
7	-1	Se	932	1.45	3.5

Design and Characterization of Phthalocyanine Thin Film Materials

Steven R. Flom, James S. Shirk, Richard G.S. Pong, F.J. Bartoli, Arthur W. Snow
U.S. Naval Research Laboratory, Washington, DC 20375
Young H. Chang† and Warren T. Ford
Oklahoma State University, Stillwater, OK 74078

INTRODUCTION

The phthalocyanines are a class of organic NLO materials that are of considerable interest both for their nonlinear optical[1] and their electrical properties.[2] The high nonlinearities, chemical stability, and the variety of molecular architectures that are possible make them promising materials for nonlinear optical applications. One application of these materials, optical limiters, already shows considerable promise.

An important advantage of organic NLO materials is the ability to form processable thin films. In the phthalocyanines this property must be specifically designed into the molecular structure. In this paper the design of phthalocyanines that form thin films of high optical quality and simultaneously maintain desirable NLO properties is reported. Specifically, we compare the optical response of thin films of a liquid phthalocyanine, a glassy phthalocyanine, and an amorphous film of a phthalocyanine that has a liquid crystalline phase. These films have several advantages over guest/host systems. Since our films are neat materials, they have high concentrations of the phthalocyanine moiety and consequently have large bulk nonlinear coefficients. Guest/host materials, when prepared with standard phthalocyanines, often have microscopic phase separations that can introduce undesirable optical losses due to light scattering.

EXPERIMENTAL APPARATUS

The picosecond experimental apparatus consists of a dye laser synchronously pumped by a mode-locked, doubled Nd/YAG laser. The dye laser output was amplified to provide 1.2 psec pulses with energies up to 1 mJ. For the degenerate four-wave mixing experiments, the output of the laser is split into three beams that are overlapped in the sample in the phase conjugate geometry. The phase conjugate signal intensity is measured as a function of the incident intensity and is fit to a cubic dependence. The resulting cubic coefficient is compared with that observed from CS_2 in the same apparatus. The time dependence of the phase conjugate signal is measured by delaying the arrival of the back pump beam. The polarization dependencies are measured by rotating $\lambda/2$ wave plates in the appropriate beams.

Z-scan and nonlinear absorption studies were also performed on the nanosecond time scale at several wavelengths between 532 nm and 650 nm using a spatially filtered Nd/YAG pumped dye laser.

RESULTS AND DISCUSSION:

Figure 1 shows the structure of the molecule Pb tetrakis (3-(N,N-bis(3-phenoxy-2-hydroxypropylether))aminophenoxy)phthalocyanine (PbPc(β-PGE)$_4$), one of the materials studied. Previous studies have used other peripheral substituents such as the cumylphenoxy (CP) group. In the solid state, however, PbPc(β-CP)$_4$ can have significant optical losses due to light scattering. Such scattering arises because of the propensity of such phthalocyanines to aggregate into anisotropic stacks. These stacks often lead to liquid crystal-like structures that are birefringent and form scattering domains in the solid. The PGE substituent is bulky, has an irregular symmetry and can form intermolecular hydrogen bonds on the periphery of the phthalocyanine. These structural features inhibit the formation of aggregates with a size sufficient to cause birefringence or optical scattering in the solid phase. However, the formation of smaller aggregates, such as dimers, can still occur.[3] Peripheral substitution also provides a means to control the morphology of the bulk material. PbPc(β-PGE)$_4$ has a glassy morphology at room temperature.

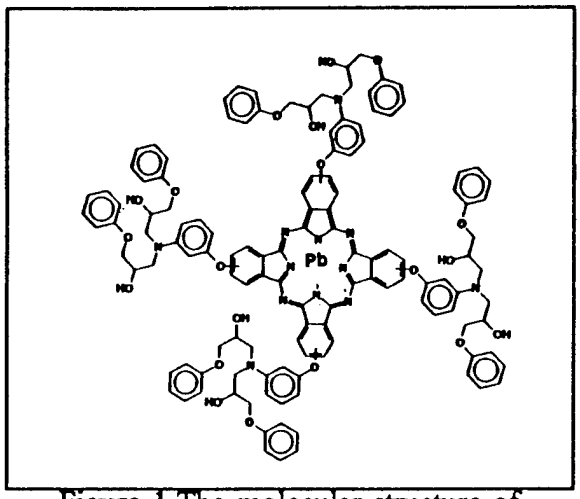

Figure 1 The molecular structure of PbPc(PGE)$_4$

The two other peripheral substituents we studied were a methoxy terminated polyethylene oxide (PEO) and the 2-ethylhexyloxy (EHO) group. The PEO group also inhibits extensive aggregation into macroscopic domains large enough to scatter light. The intermolecular interactions are sufficiently reduced so that PbPc(PEO)$_4$ is a liquid at room temperature. One difference between this and the glassy PGE material is the more extensive hydrogen bonding in the PGE substituent. The ethyl(hexyloxy) (EHO) substituent is more regular when compared to the other two substituents. PbPc(EHO)$_8$ has a more symmetric arrangement of the peripheral groups. It has been reported to give a liquid crystalline phase.[4] The EHO moiety has a branched chain that can inhibit stacking compared to a straight chain substituent. PbPc(EHO)$_8$ can be prepared in an amorphous phase that had good optical quality. The amorphous phase was used in this study.

The films were from 0.7 to about 2 μm thick. The linear absorption spectra are typical of a lead phthalocyanine. In each, there is a strong π-π^* transition, the Q band, peaked near

710 nm, with a vibronic shoulder near 650 nm. There is a window of low absorption from about 430 nm to 610 nm. The first absorption peak in the UV occurs at 370 nm. The position of the absorption maxima in each film was similar to that observed in $PbPc(CP)_4$ in a $CHCl_3$ solution,[5] however, the details of the band shape differ in the films. This may be due to different tendencies to form small aggregates and perhaps different supramolecular structures in the dimers and trimers.

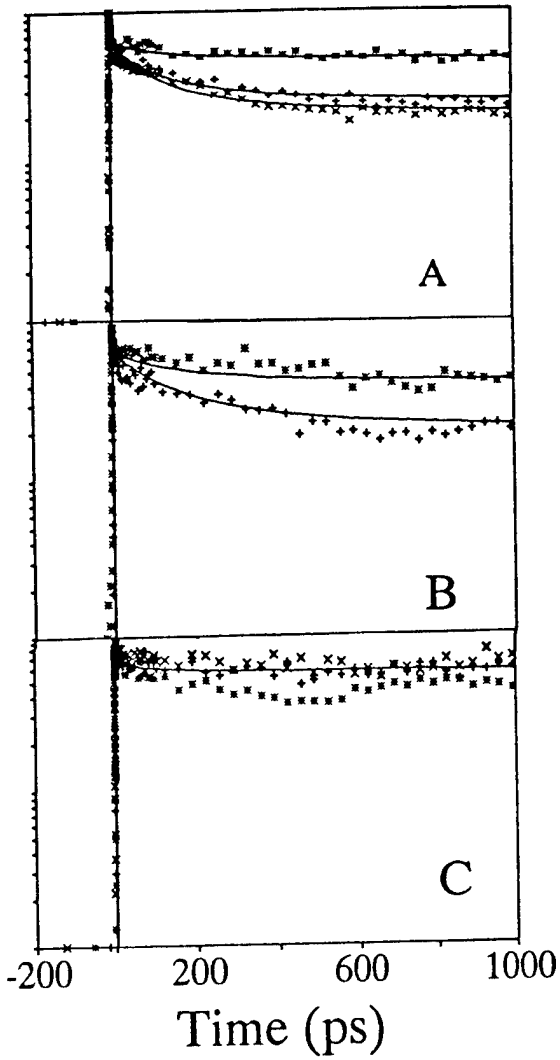

Figure 2 The temporal dependence of the DFWM signal (xxxx polarization)
A) $PbPc(EHO)_8$ excited with 0.7, 4.2 and 5.5 mJ/cm^2 from top to bottom
B) $PbPc(PEO)_4$ excited with 0.6 and 4.0 mJ/cm^2 from top to bottom.
C) $PbPc(PGE)_4$ excited with 0.4, 1.4 and 4.5 mJ/cm^2 from top to bottom

The nonlinear optical response of the neat thin films of these materials has been studied by degenerate four-wave mixing (DFWM), transient absorption, and nonlinear absorption. At visible wavelengths the nonlinear response is dominated by optical pumping. Nonlinear absorption at 590 nm shows that each of these materials is a reverse saturable absorber. The transmission through the sample decreases with increasing intensity. Transient absorption measurements for solutions of $PbPc(\beta\text{-}PGE)_4$ show that the excited state cross section exceeds that of the ground state over a considerable portion of the visible spectrum. The lifetime of this excited state is considerably longer than 1 ns. Similar lifetimes were found in solutions of $PbPc(\beta\text{-}CP)_4$. DFWM measurements for each material demonstrate that the magnitude of the picosecond nonlinear response, as measured by the effective $\chi^{(3)}/\alpha$ at 590 nm is approximately 8×10^{-14} esu-cm compared to ~6×10^{-14} esu-cm observed in $PbPc(\beta\text{-}CP)_4$ solutions. Ratios of the signal in the xyyx polarization to that in the xxxx polarization ranged from $(.13)^2$ to $(.16)^2$ near the ratio of $(.125)^2$ expected for optically pumping a degenerate transition such as the Q-band.

Figure 2 shows the temporal dependence of the DFWM signal in the xxxx polarization for the three thin films. The upper state lifetime, observed to be greater than 1 ns in

transient absorption experiments, is measured to be longer than 6 ns in these experiments for each film. The long upper state lifetime reported[6] for PbPc(β-CP)$_4$ solutions is preserved in these materials. Figure 2 also shows the fluence dependence of the dynamics of the DFWM signal in these materials. At times shorter than ~ 100 ps, a mild dependence of the excited state decay on the excitation fluence is seen with PbPc(β-EHO)$_8$ and PbPc(β-PEO)$_4$. In PbPc(β-PGE)$_4$, the fluence dependence becomes evident only after 100 ps. It is due to an acoustic response. The weak dependence of the excited state decay on fluence observed here contrasts with the stronger fluence dependence observed in polycrystalline metal-free phthalocyanine[7] and H_2Pc(β-CP)$_4$ films.[8] In the latter materials exciton-exciton annihilation is apparently more efficient than in the phthalocyanines described here.

CONCLUSIONS

The nonlinear optical responses of thin films of the three different lead phthalocyanines are similar. It is analogous to that reported for PbPc(β-CP)$_4$ in solution. In each, optical pumping dominates the nonlinear response at 590 nm. The principal difference between the films is a greater dependence of the excited state decay rate on fluence in the PbPc(β-PEO)$_4$ and PbPc(β-EHO)$_8$ films. The significance of these observations is that molecular engineering of the phthalocyanines has yielded single component thin films of good optical quality that possess the desirable linear and nonlinear optical properties previously reported in solutions.

REFERENCES

† Permanent address: Korea Institute of Advanced Technology, Taejon, Korea

1. J.S. Shirk, J.R. Lindle, F.J. Bartoli, Z.H. Kafafi, A.W. Snow, and M.E. Boyle, Intl J. Nonlin. Opt. Phys. 1, 699 (1992)

2. See for example: J. Simon and J.-J. Andre "Molecular Semiconductors", Springer-Verlag, Berlin (1985)

3. R.D. George, A.W. Snow, J.S. Shirk, S.R. Flom and R.G.S. Pong, Proc. Mat. Res. Soc. (in press)

4. W.T. Ford, L. Sumner, W. Zhu, Y.H. Chang, P-J. Um, K.H. Choi, P.A. Heiney, and N.C. Maliszewskij; New J. Chem. 18, 495, (1994)

5. J.S. Shirk, S.R. Flom, J.R. Lindle, F.J. Bartoli, A.W. Snow and M.E. Boyle; Proc. Mat. Res. Soc. 328, 661 (1994)

6. S.R. Flom, J.S. Shirk, R.G.S. Pong, J.R. Lindle, F.J. Bartoli, M.E. Boyle J.D. Adkins, and A.W. Snow; Proc. SPIE, 2143, 229 (1994)

7. B.I.Greene and R.R.Millard, Phys. Rev. Lett., 55, 1331 (1985).

8. S.R. Flom, J. S. Shirk, J. R. Lindle, F. J. Bartoli, Z. H. Kafafi, R.G.S. Pong and A.W. Snow; Proc. Mat. Res. Soc. 247, 271 (1992).

Optically Aligned Liquid Crystal Cells as Diffractive Optical Elements

T. Kosa and P. Palffy-Muhoray
Liquid Crystal Institute, Kent State University, Kent, OH 44242

T. Kosa, Liquid Crystal Institute, Kent State University, Kent, OH 44242.
tel.: (216) 672-4056, fax.: (216) 672-2796.

Conventional diffractive elements, such as gratings and zone plates, may be regarded as surfaces which are transparent in some regions and opaque in others. Their usefulness stems from the constructive interference of the transmitted light in certain regions of space. Here we propose another way to produce such constructive interference, by allowing light to pass through the originally opaque regions of the diffractive surface but with its polarization rotated by 90°. An interference pattern similar to that of the original surface is obtained, since orthogonal polarizations do not interfere.

Using liquid crystals, such a scheme can be implemented for polarized light. Because of their large birefringence, twisted nematics can efficiently rotate the polarization of light provided the twist pitch is longer than the wavelength. Diffractive elements utilizing this scheme can therefore be realized by nematic cells in which the director is uniform in some regions, and twisted through 90° in others.

The configuration of the nematic director in a cell is determined by surface interactions at the cell walls, and elastic effects in the bulk. If surface treatment causes the director to align in the plane of the walls in the same direction at both walls, the configuration in the cell is uniform. If the director aligns in the plane of the walls in perpendicular directions, a twisted configuration results. To realize the proposed diffraction scheme, the direction of surface alignment must be a function of position, at least on one wall.

In the past, mainly mechanical buffing of a thin polymer layer on the cell walls has been used to achieve surface alignment. Typically, the director aligns parallel to the rubbing direction. Recently, optical methods [1] have been developed to replace mechanical buffing, where polarized light is used to induce permanent director alignment at the surface. Using such optical buffing, spatially varying director orientation can be achieved at the surface with high resolution, and consequently, it is possible to construct nematic cells consisting of domains with either uniform or twisted configurations. We have constructed such devices, and report here on a zone plate utilizing this principle.

Dissolving a small amount of azo-dye (Aldrich Disperse Orange 3) in polyimide (DuPont PI-2555) creates a photosensitive alignment layer. We have spin-coated a solution of this mixture on glass, and using a polarized Ar^+ laser, wrote a zone plate pattern on one cell wall so that the resulting director orientation in one zone is perpendicular to the adjacent

one. The second cell wall was spin coated with undyed polyimide, and was mechanically buffed.

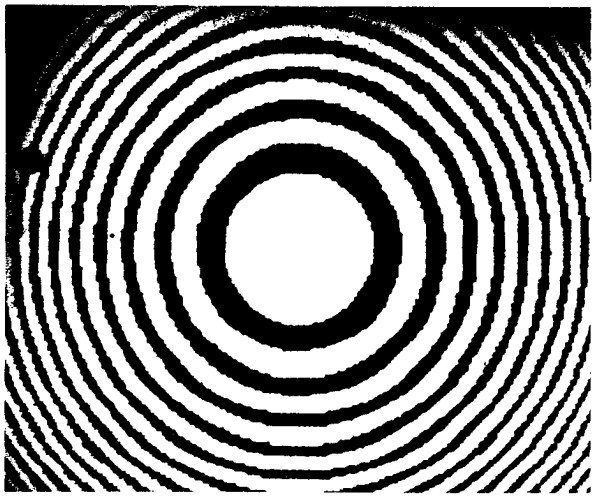

Fig. 1a.: Cell between crossed polarizers. Bright regions indicate twisted configuration.

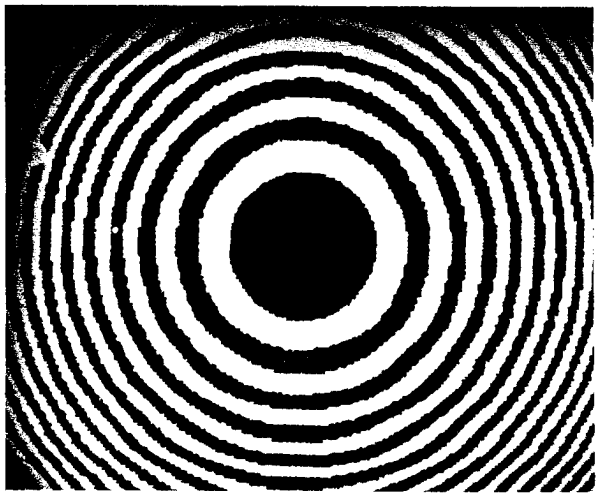

Fig. 1b.: Cell between parallel polalrizers. Dark regions indicate twisted configuraton.

The cell was then assembled, and filled with the nematic liquid crystal E7 (BDH). In regions of the cell where the surface alignment is parallel the director is uniform, in regions where it is orthogonal, the configuration is twisted. A photograph of the cell between polarizers is shown in Fig. 1.

We have studied the diffraction efficiency of our zone plate with both He-Ne and Ar lasers. A key feature of this mechanism is that both polarizations interefere constructively at the focal point. We note that, in spite of some similarities, our device fundamentally differs from the Fresnel lens of Patel *et al.* [2], which does not rotate polarization. In addition to zone plates, other diffractive elements, such as and gratings, are feasible. Furthermore, the refraction can be made switchable if glass coated with an electrically conducting material (such as ITO) is used, since a sufficiently large applied voltage causes the director to align perpendicular to the plates. The electrooptic response will be reported elsewhere.

Switchable liquid crystal diffractive devices exploiting the mechanism demonstrated here may be useful in a variety of applications.

References

[1] P.J. Shannon, W.M. Gibbons and S.T. Sun, *Nature*, **368**, 532, 1994

[2] J.S. Patel and K. Rastani, *Opt. Lett.***16**, 532, 1991

Nonlinear Optical Anisotropy of Highly Oriented Poly(*p*-Phenylene Benzobisthiazole)Langmuir-Blodgett Films

Liming Wang, Tatsuo Wada, Tomoyuki Yuba*, Masaaki Kakimoto*,
Yoshio Imai* and Hiroyuki Sasabe

Frontier Research Program, The Institute of Physical and Chemical Research (RIKEN), Hirosawa 2-1, Wako, Saitama 351-01, JAPAN

**Department of Organic and Polymeric Materials, Tokyo Institute of Technology, Meguro-ku, Tokyo 152, JAPAN*

INTRODUCTION

Poly(*p*-phenylene benzobisthiazole) (PBT) has received a strong attention as a nonlinear optical (NLO) material because of its large, ultrafast NLO response[1] and inherently superior physical and chemical properties[2]. However, the material is difficult to process into thin film with good optical quality, which hindered the detailed and accurate NLO studies. In order to improve optical quality, the PBT Langmuir-Blodgett (LB) films were fabricated via a novel precursor route. The PBT LB films show not only improved optical quality but also highly in-plane oriented molecular packing. Because the π-electrons are delocalized along the polymer chain direction, the highly oriented packing of the polymer chains results in linear and NLO anisotropy properties. Therefore, in-plane anisotropy measurement of optical third-harmonic generation (THG) is one of the powerful tools to elucidate the packing arrangement in LB films of one-dimensional conjugated system.

EXPERIMENTAL

The chemical structure of PBT is shown in Figure 1. The PBT LB films used in this study were prepared through their precursor films by LB technique[3] with the surface pressure of 30, 40 and 50

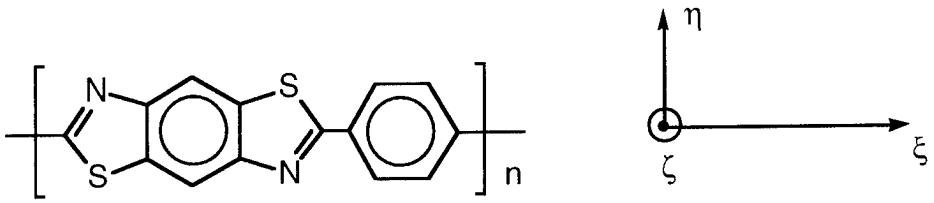

Figure 1 Chemical structure of PBT and molecular coordinate.

mN/m, respectively. The refractive index and the birefringence of the films were measured by the anisotropy Brewster angle determination at four wavelengths. The detail of the method will be published elsewhere.

The NLO anisotropy properties of the PBT LB films concerning the non-resonant THG was evaluated by measuring the non-resonant third-harmonic susceptibilities $\chi^{(3)}$ as a function of the azimuth φ at a fundamental wavelength of 1907nm, where φ is defined as the angle of dipping direction with respect to the polarization of the incident light. At each φ, a Maker fringe was measured and the value of $\chi^{(3)}$ was calculated with a fused silica plate as a reference ($\chi^{(3)}_{\text{fused silica}}=1.4\times10^{-14}$ esu)[4].

RESULTS AND DISCUSSIONS

The $\chi^{(3)}$ dependence on azimuth φ is shown in Figure 2. The third-order optical susceptibility tensor $\chi'^{(3)}_{XXXX}$ in the laboratory framework is related to the $\chi^{(3)}_{ijkl}$ components as follows:

$$\chi'^{(3)}_{XXXX}=\chi^{(3)}_{xxxx}\cos^4\varphi+\chi^{(3)}_{yyyy}\sin^4\varphi+6\chi^{(3)}_{xxyy}\sin^2\varphi\cos^2\varphi. \qquad (1)$$

The experimental data were fitted by Eq.(1) as shown in Figure 2. The $\chi^{(3)}_{xxxx}$, $\chi^{(3)}_{yyyy}$ and $\chi^{(3)}_{xxyy}$ values for the three samples are listed in Table I. The highly oriented anisotropy of molecular packing comes from the preferential alignment of the long chain molecules along the dipping direction[5,6].

If we assume that the PBT molecule is a perfect one-dimensional π-conjugated system with a cylindrical symmetry along its long axes and the PBT polymer chains are aligned with a Gaussian type orientational distribution function:

$$F(\phi,\theta,\psi)=\exp\left[-(\theta/\theta_0)^2\right], \qquad (2)$$

the macroscopic third-order susceptibility $\chi^{(3)}_{ijkl}$ can be expressed by the microscopic second hyper-polarizability $\gamma_{\xi\xi\xi\xi}$ by the following equation[7,8]:

$$\chi^{(3)}_{xxxx}=N\gamma^*_{\xi\xi\xi\xi}\frac{\int_0^\pi d\theta\sin\theta\cos^4\theta\exp\left[-(\theta/\theta_0)^2\right]}{\int_0^\pi d\theta\sin\theta\exp\left[-(\theta/\theta_0)^2\right]},$$

$$\chi^{(3)}_{yyyy} = \frac{3}{8} N\gamma^*_{\xi\xi\xi\xi\xi} \frac{\int_0^\pi d\theta \sin^5\theta \exp\left[-(\theta/\theta_0)^2\right]}{\int_0^\pi d\theta \sin\theta \exp\left[-(\theta/\theta_0)^2\right]},$$

$$\chi^{(3)}_{xyyx} = \chi^{(3)}_{xyxy} = \chi^{(3)}_{xxyy} = \chi^{(3)}_{yyxx} = \chi^{(3)}_{yxyx} = \chi^{(3)}_{yxxy}$$
$$= \frac{1}{2} N\gamma^*_{\xi\xi\xi\xi\xi} \frac{\int_0^\pi d\theta \sin^3\theta \cos^2\theta \exp\left[-(\theta/\theta_0)^2\right]}{\int_0^\pi d\theta \sin\theta \exp\left[-(\theta/\theta_0)^2\right]},$$

$$\chi^{(3)}_{xyxx} = \chi^{(3)}_{xxyx} = \chi^{(3)}_{xxxy} = \chi^{(3)}_{xyyy} = \chi^{(3)}_{yxxx} = \chi^{(3)}_{yyyx} = \chi^{(3)}_{yyxy} = \chi^{(3)}_{yxyy} = 0, \quad (3)$$

where $\gamma^*_{i'j'k'l'} = f^{3\omega}_{i'i'}\gamma_{i'j'k'l'}f^{\omega}_{j'j'}f^{\omega}_{k'k'}f^{\omega}_{l'l'}$, f's are components of the local-field correction tensor for anisotropic media, N is the number of molecules per unit volume, θ is the angle of the individual polymer chain with respect to the dipping direction as defined by Eular angle. The parameter θ_0 is related to the standard deviation as $\sigma = \theta_0/\sqrt{2}$ and $\theta_0 \to 0$ means a perfect uniaxial alignment of the chains.

Table I : Measured values of susceptibility tensor components and molecular packing parameters for PBT LB films.

sample	surface pressure (mN/m)	$\chi^{(3)}_{xxxx}$	$\chi^{(3)}_{yyyy}$ ($\times 10^{-12}$ esu)	$\chi^{(3)}_{xxyy}$	θ_0	$N\gamma^*_{\xi\xi\xi\xi}$	$N<\gamma>$ ($\times 10^{-12}$ esu)
PBT-1	30	8.3	0.67	0.52	0.56	13	2.6
PBT-2	40	11	1.5	0.91	0.56	18	3.6
PBT-3	50	17	2.0	1.5	0.56	27	5.4

The measured data were fitted again by using Eqs.(1) and (3) with θ_0 and $N\gamma^*_{\xi\xi\xi\xi\xi}$ as adjustable parameters, which are given in Table I. The azimuth dependence of $\chi^{(3)}$ values was well fitted as shown by the dotted line in Figure 2. The value of $N\gamma^*_{\xi\xi\xi\xi\xi}$ indicates the maximum $\chi^{(3)}$ that is accessible if the polymer chains are perfect aligned. The $\chi^{(3)}$ value for a random molecule distribution ($N<\gamma>$ in Table I) is only one fifth of $N\gamma^*_{\xi\xi\xi\xi\xi}$ value. With the sample PBT-3 as a example, for a perfect alignment ($\theta_0 \to 0$), the maximum $\chi^{(3)}$ could be 27×10^{-12} esu, while for the material with molecules randomly distributed ($\theta_0 \to \infty$), $\chi^{(3)}$ would be only about 5.4×10^{-12} esu. On the other hand, the fact that θ_0 value remained the same (θ_0=0.56) for all the films and only $N\gamma^*_{\xi\xi\xi\xi\xi}$ varied indicates the molecular orientational distribution state did not changed, only the molecule packing became more condensed when surface pressure increased.

CONCLUSIONS

THG measurements on PBT LB films show that the molecules were highly oriented by the precursor fabrication route. The components of $\chi^{(3)}$ tensor of the 50mN/m LB film are $\chi^{(3)}_{xxxx} = 17\times10^{-12}$ esu and $\chi^{(3)}_{yyyy} = 2.0\times10^{-12}$ esu. The anisotropy can be explained well by a Gaussian distribution function of the PBT polymer chains with a standard deviation $\sigma = 0.40$. In the surface pressure range 30~50mN/m, the surface pressure did not influenced on the alignment degree of the polymer chains, but the molecular packing density.

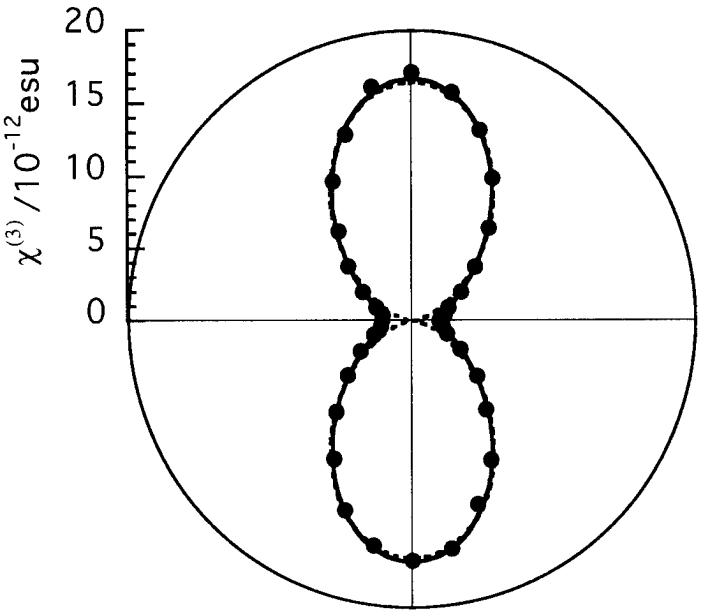

Figure 2 A polar plot of $\chi^{(3)}$ dependence on the angle of the dipping direction with respect to the polarization of the light for the PBT LB films fabricated with the surface pressure of 50 mN/m. The solid and dotted lines are the theoretical fitting according to Eq.(1), and Eq.(3), respectively.

REFERENCES

1. H. Vanherzeele, J. S. Meth, S. A. Jenekhe and M. F. Roberts, J. Opt. Soc. Am., B**9**, 524 (1992).
2. M. F. Roberts and S. A. Jenekhe, Chem. Mater., **5**, 1744 (1993).
3 T. Hattori, K. Kagawa, M. Kakimoto and Y. Imai, Polym. J., **26**, 930 (1994).
4. T. Wada, S. Yamada, Y. Matsuoka, C. H. Grossman, K. Shigehara, H. Sasabe, A. Yamada and A. F. Garito, in *Nonlinear Optics of Oganics and Semiconductors*, T. Kobayashi (Ed.), Springer Proc. in Physics, **36**, 292 (1989).
5. D. Neher, S. Mittler-Neher, M. Cha, G. Stegeman, F. W. Embs, G. Wegner, R. D. Miller and C. G. Willson, in *Nonlinear Optical Properties of Organic Materials IV*, Proc. SPIE, **1560**, 335 (1991).
6. K. Kamiyama, M. Era, T. Tsutsui and S. Saito, Jpn. J. Appl. Phys., **29**, L840 (1990).
7. K. Y. Wong and A. F. Garito, Phys. Rev., A**34**, 5051 (1986).
8. L.M. Wang, T. Wada, T. Yuba, M. Kakimoto, Y. Imai and H. Sasabe, Mol. Cryst. Liq. Cryst. (1995) (in press).

Investigation of the Stability of Electro-Optic Dyes

Lixia Zhang, Priya Calamegham, Carl W. Dirk
Department of Chemistry
The University of Texas at El Paso
El Paso, Texas 79968
Tel (915)747-5964

Susan Ermer
Lockheed Research and Development Division
Tel (415)424-3131

R. J. Twieg
IBM Almaden Research Center
Tel (408)927-1630

Recent progress in organic electro-optic materials has lead to organic polymer devices that can modulate broad band visible light at frequencies which will permit the simultaneous transmission of thousands of real-time television signals down a single optical fiber. The intent is to manufacture modulator device structures which are incorporated directly on the same semiconductor chip which supplies both the electronics and power for the modulation process. Doing this requires polymers and electro-optic dyes that can withstand the processing conditions typical for semiconductor devices. The lowest temperature conditions available are about 350°C. We are presently involved in a collaborative project in conjunction with IBM Almaden Research Laboratories and Lockheed Corporation, in attempting to discover the decomposition temperatures of existing electro-optic dyes and conducting the analysis of the relationship between the decomposition temperatures and the molecular structures.

The importance of this research is that we hope to determine a quantitative structure property relationship (QSPR) which will guide the design of new electro-optic dyes with higher thermal stability.

The method used for the thermal analysis is Differential Scanning Calorimetry (DSC). The melting point and decomposition temperature of each compound was measured.

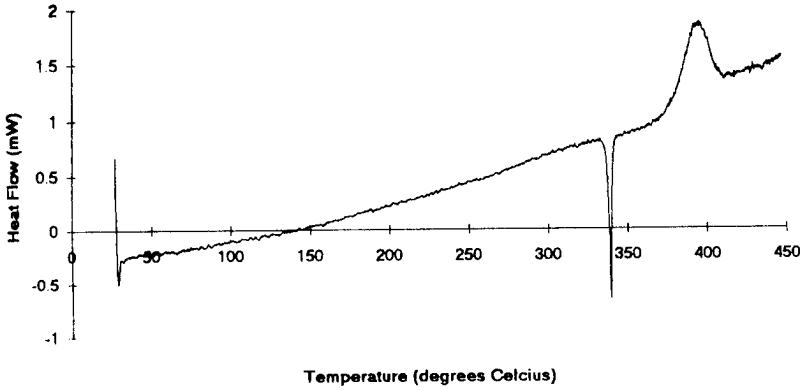

Fig 1 Typical DSC Plot

For the QSPR analysis, we use the empirical formula (referred to as the zero-order connectivity) and the first-order connectivities (defined below) to correlate the decomposition temperatures. For example:

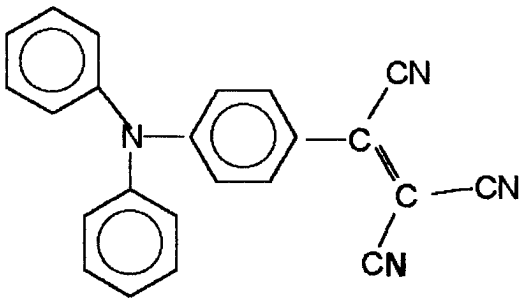

empirical formula

number of carbon	**23**
number of nitrogen	**4**
number of hydrogen	**14**

first-order connectivities

NCCC (nitrogen attached to three other carbons) 1

NC (nitrogen in the cyano group which is connected to only one atom--carbon) 3

etc.

Our present results are listed below:

(1) The variations in the molecular structures have a great effect on the thermal stability. For example compounds that have phenyl groups are more stable than those with non-aromatic groups.

(2) There are good correlations between the molecular structures and the decomposition temperatures. Thus, the use of non-structural parameters may be avoided in predicting decomposition temperatures from test structures.

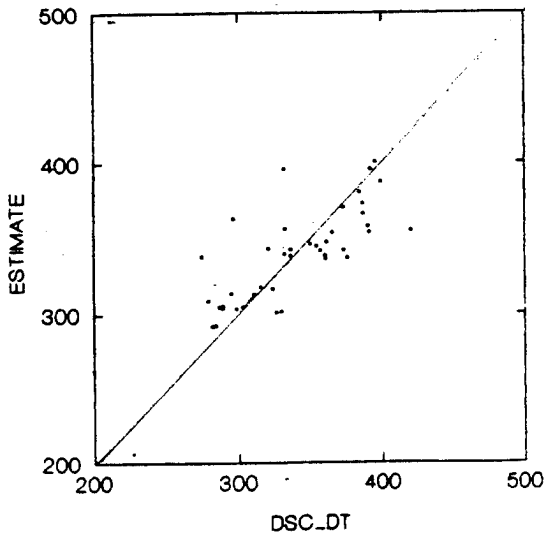

Fig 2 Correlation using empirical formula only (R=0.748)

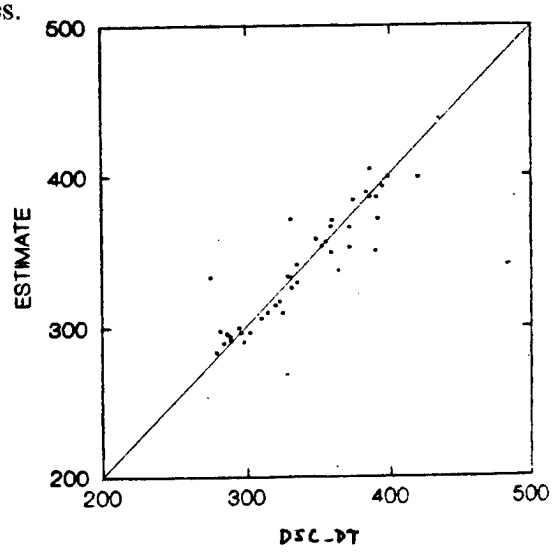

Fig 3 Correlation using first-order connectivities (R=0.916)

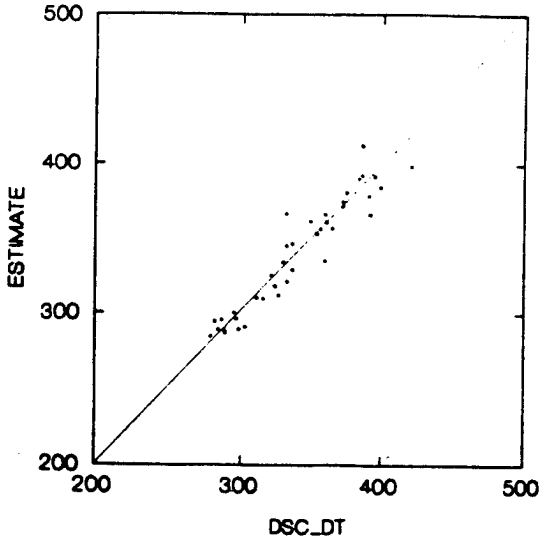

Fig 4 Correlation using selected first-order of connectivities and number of atoms (R=0.952)

(3) The correlation coefficient increases as we use higher level of descriptors.

(4) After further studies using QSPR, we should be able to predict the structures of compounds that will result in higher non-linear-optical properties with higher thermal stability. Our results suggest that significant improvements in thermal stability should be possible.

REFERENCES

1. Carl W. Dirk, Multi-institution consortium proposal submitted to the office of Naval Research.
2. R. D.Miller, K. M. betterton, D. M. burland, V. Y. Lee, C. R. Moylan, R. J. Twieg, C. A. Walsh, W. Volksen, SPIE, Vol. 2042, **354**

Nonlinear Optical Properties of Self-Assembled Mainchain Polymer Films

W.N. Herman and J.A. Cline, *U.S. Navy, NAWCAD, MS07, Warminster, PA 18974* (phone: 215-441-1135)
J.M. Hoover, A. Chafin and G.A. Lindsay, *U.S. Navy, NAWCWD, China Lake, CA 93555*
K.J. Wynne, *Office of Naval Research, Arlington, VA 22217*

We report second harmonic generation measurements on multilayers of two interleaved mainchain polymers fabricated by Langmuir Blodgett (LB) deposition. LB processing[1] offers advantages over electric-field poling in that it can be done at room temperature (hence the *kT* Brownian motion is much less) without the strong electric fields that can lead to film damage during corona poling. Mainchain polymers are inherently more stable than sidechain polymers because both ends of the chromophore are attached to the backbone of the polymer, whereas only one end of the chromophore is attached to the backbone in a sidechain polymer, and the other end is dangling free at one of the interfaces of each monolayer. Furthermore, only mainchain polymers that contain the chromophore in a head-to-head (syndioregic) configuration can have the chromophores ordered normal to the plane of the film by hydrophilic/hydrophobic forces. This is because a mainchain polymer containing chromophores in a heat-to-tail configuration will probably have all of the chromophores lying on the water, in the plane of the film with opposing dominant hyperpolarizability components.

The chemical structures of the polymers incorporating amphiphilic molecules[2] used in building up the ABAB... multilayer films are shown in Figure 1. Spreading solutions of polymer A (0.49 mg/mL) and polymer B (0.653 mg/mL) were prepared using spectroscopy grade chloroform. These solutions were used to spread films on pure water at 23°C. A dual-compartment Langmuir-Blodgett trough (Nima Model TKB 2410A) was used to prepare multilayer films. The trough was cleaned with chloroform and filled with pure water (18 MO, Millipore Milli-Q system). The polymer A and B solutions were spread by dropping 80 μL of each onto the water in compartments A and B of the trough (about 500 cm^2, each compartment). The films in each compartment were allowed to dry for several minutes and then compressed at a rate of about 20 cm^2/min. until a surface pressure of 20.0 mN/m was obtained. The compressed films were aged at 20 mN/m for about 20 min. to allow densification of the monolayers.

A 24-layer film was fabricated on a hydrophobic microscope slide through the use of a dipper mechanism which transported the substrate down through the interface in compartment A (with polymer A) and up through the interface in compartment B (with polymer B) at a rate of about 2 mm/min. The dipping direction was across the narrow dimension of the slide. Hydrophobic glass was prepared by conditioning in a refluxing nitrogen atmosphere of hexamethyldisilazane (HMDS) for about 30 minutes. The change in surface area of each compartment was monitored as the transfer of the film from the interface to the substrate was made at constant surface pressure.

The experimental setup for observing second-harmonic generation from these films is shown in Figure 2. The sample was positioned at the waist of a focused (100 mm lens)

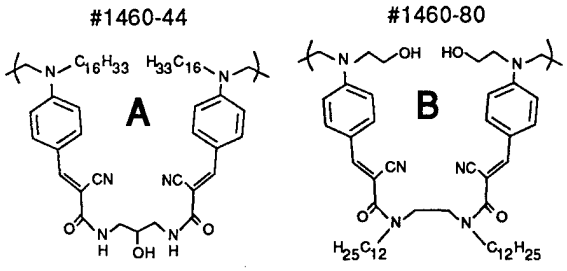

Figure 1. Chemical structure of syndioregic main-chain polymers A and B.

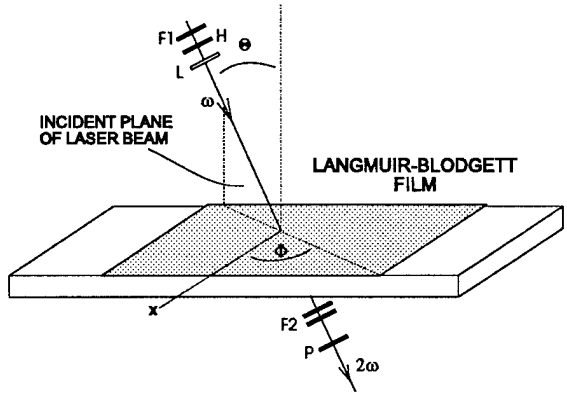

Figure 2. Transmission SHG configuration: Angle of incidence Θ = 56°, azimuthal angle Φ, IR pass filter (F1), half-wave plate (H), 100 mm lens (L), IR blocking filters (F2), and polarizer (P).

fundamental beam (1064 nm) produced by a Q-switched Nd:YAG laser. The pulse width was 150 ns and the repetition rate 1 kHz. The fundamental beam was polarized inside the laser cavity and a half-wave plate was used to control the polarization of the beam incident on the sample. The second-harmonic signal was detected by a Hamamatsu R928 photomultiplier tube in conjunction with a Stanford Research SR250 boxcar averager, which was operated using active baseline subtraction. To account for laser power fluctuations, the fundamental was monitored along with the second harmonic in order to normalize the second harmonic signal. The sample was mounted on a computer-controlled Oriel rotation stage and data was collected by computer at 5° increments of the azimuthal angle Φ. The angle of incidence of the laser beam was fixed at $\Theta = 56°$.

Complete 360° SHG scans were recorded for each of six different polarization combinations of the fundamental and detected second harmonic. The s-s (s-polarized fundamental with detection of the s-polarized component of the 2nd harmonic) and the p-s combinations were very small and in the noise of the detection system. The results of the remaining four combinations — p-p, 45°-p, s-p, and 45°-s — are shown in Figure 3. Prior SHG measurements[4] for a monolayer of polymer A on water resulted in s-s second-harmonic generation that was comparable in magnitude to the p-p and s-p data. For reference, an additional azimuthal scan at a 45° angle of incidence was made on an X-cut quartz crystal using a p-p combination. The solid lines in Figure 3 are the theoretical fits to the data using the theory of Ref. 3, which includes the effect of reflections of the second harmonic. Making use of the absence of s-s SHG, a minimal set of nonzero SHG d-coefficients permitting simultaneous fits to all the data sets is given by

$$d = \begin{pmatrix} 0 & 0 & 0 & d_{14} & d_{31} & 0 \\ 0 & 0 & 0 & d_{32} & d_{14} & 0 \\ d_{31} & d_{32} & d_{33} & 0 & 0 & d_{14} \end{pmatrix} \qquad (1)$$

which appears to be monoclinic, class 2. The symmetry, however, can be shown to be $mm2$ by performing a rotation transformation. Since $d_{36} = d_{25} = d_{14}$, rotation through an angle Ω about the z-axis, with $\tan 2\Omega = 2d_{14}/(d_{31} - d_{32})$, transforms the d-tensor to

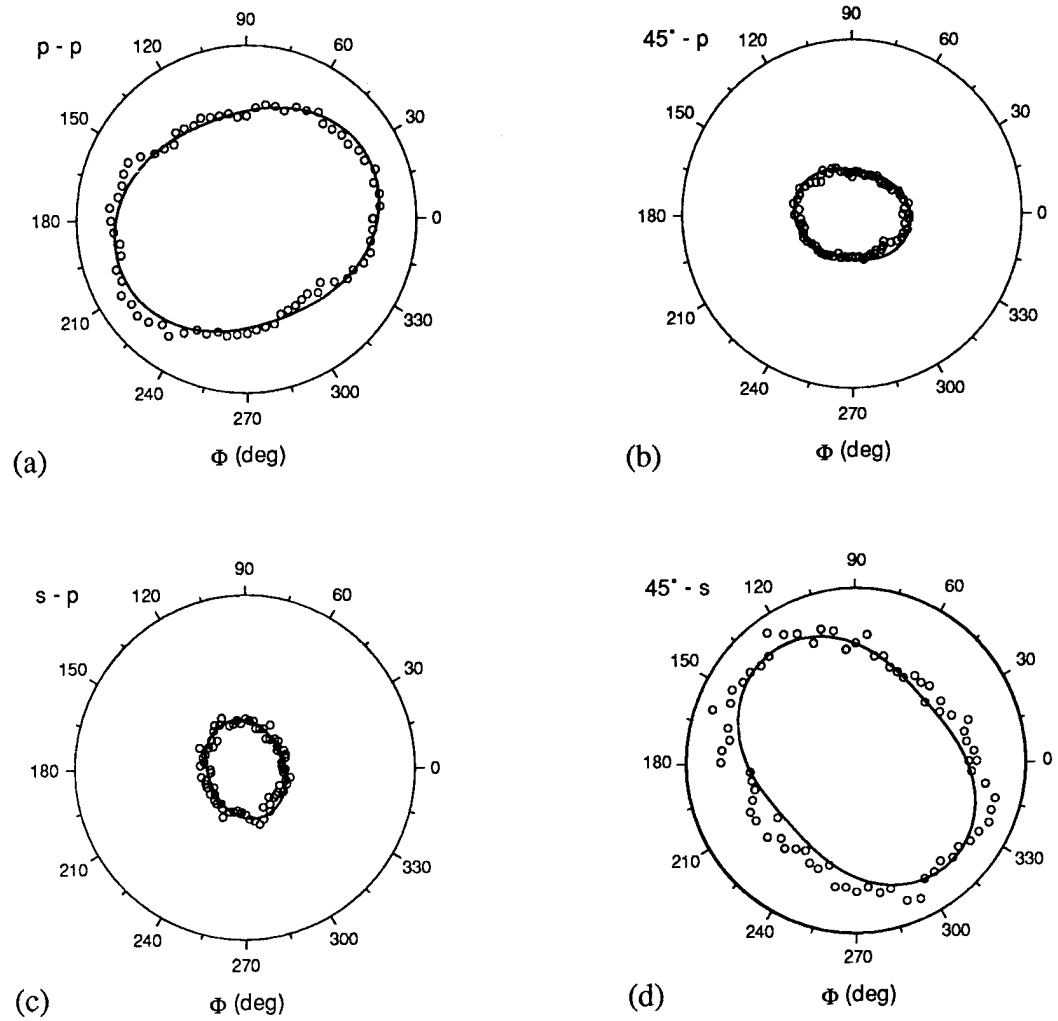

Figure 3. SHG (arbitrary units) as a function of azimuthal angle for a fixed angle of incidence of 56° for the fundamental laser beam . The radial maximum for (a) p-p and (b) 45°-p is 0.4, while for (c) s-p and (d) 45°-s the maximum is 0.1.

$$\tilde{d} = \begin{pmatrix} 0 & 0 & 0 & 0 & \tilde{d}_{31} & 0 \\ 0 & 0 & 0 & \tilde{d}_{32} & 0 & 0 \\ \tilde{d}_{31} & \tilde{d}_{32} & \tilde{d}_{33} & 0 & 0 & 0 \end{pmatrix} \tag{2}$$

where

$$\begin{aligned} d_{31} &= \tilde{d}_{31}\cos^2\Omega + \tilde{d}_{32}\sin^2\Omega\ , & d_{32} &= \tilde{d}_{31}\sin^2\Omega + \tilde{d}_{32}\cos^2\Omega\ , \\ d_{14} &= (\tilde{d}_{31} - \tilde{d}_{32})\sin\Omega\cos\Omega\ , & d_{33} &= \tilde{d}_{33}\ . \end{aligned} \tag{3}$$

For the data in Fig. 3, the transformation angle is Ω=20°, which corresponds to the deviation of the long axis of the p-p oval (Fig. 3a) from the dipping direction (the x-direction). Note that, unlike the case of a poled polymer film, $\tilde{d}_{32} \neq \tilde{d}_{31}$. The effective d-coefficients for the

polarization combinations shown in Fig. 3 are

$$d_{eff}^{p-p} = t_{1p}^2 t_{2p}[\tilde{d}_{33}(s_2c_1 + c_2s_1) + f(\Phi)(s_1c_1^2 + 2c_2s_1c_1)],$$

$$d_{eff}^{s-p} = t_{1s}^2 t_{2p} s_2 g(\Phi), \qquad d_{eff}^{45-s} = t_{1p}^2 t_{2s} s_1 c_1 h(\Phi) + t_{1p} t_{1s} t_{2s} s_1 g(\Phi), \tag{4}$$

$$d_{eff}^{45-p} = \tfrac{1}{2}(d_{eff}^{p-p} + d_{eff}^{s-p}) + t_{1p} t_{1s} t_{2s}(s_2c_1 + c_2s_1)h(\Phi),$$

where

$$\begin{aligned} f(\Phi) &= \tilde{d}_{31}\cos^2(\Phi-\Omega) + \tilde{d}_{32}\sin^2(\Phi-\Omega), \\ g(\Phi) &= \tilde{d}_{31}\sin^2(\Phi-\Omega) + \tilde{d}_{32}\cos^2(\Phi-\Omega), \\ h(\Phi) &= \frac{(d_{31}-d_{32})}{2}\sin[2(\Phi-\Omega)], \end{aligned} \tag{5}$$

the t's are transmission coefficients for the (1) fundamental and (2) second-harmonic, and $s_m = \sin(\Theta_m)$, $c_m = \cos(\Theta_m)$, m=1,2, where Θ_1 and Θ_2 are the angles of refraction of the fundamental and second-harmonic, respectively, in the film.

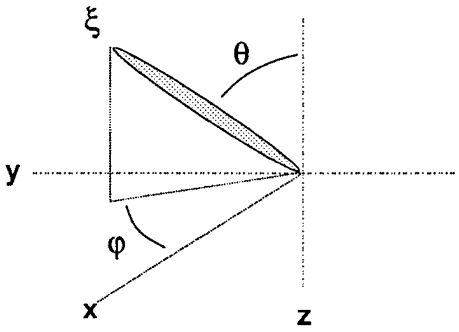

Figure 4. Relation of long molecular axes ξ to sample coordinates.

For a chromophore with a single dominant hyperpolarizability component $\beta_{\xi\xi\xi}$ along the charge transfer axes ξ, shown in Fig. 4, the structure of $\tilde{d}$ in Eq.(2) dictates[5] that the odd azimuthal moments, $<\cos^3\varphi>$, $<\cos\varphi\sin^2\varphi>$, $<\cos\varphi>$, $<\sin^3\varphi>$, $<\cos^2\varphi\sin\varphi>$, and $<\sin\varphi>$, are zero, leaving

$$\begin{aligned} \tilde{d}_{33} &\propto <\cos^3\theta>\beta_{\xi\xi\xi}, \\ \tilde{d}_{31} &\propto <\cos\theta\sin^2\theta><\cos^2(\varphi-\Omega)>\beta_{\xi\xi\xi}, \\ \tilde{d}_{32} &\propto <\cos\theta\sin^2\theta><\sin^2(\varphi-\Omega)>\beta_{\xi\xi\xi}, \end{aligned} \tag{6}$$

where θ is the polar tilt angle and φ is the azimuthal angle of the charge transfer axes. These results are consistent with a model having the polymer chains aligned Ω=20° to the long axis of the substrate with chromophore pairs in the chain arranged in a zig-zag conformation.

Helpful discussions with Dr. L. Michael Hayden are gratefully acknowledged. This work was supported by the Office of Naval Research.

References

1. G.G. Roberts, Langmuir-Blodgett Films (Plenum Press, New York, 1990).
2. J.M. Hoover, R.A. Henry, G.A. Lindsay, S.F. Nee, and J.D. Stenger-Smith, in Organic Materials for Nonlinear Optics III, G.J. Ashwell and D. Bloor, eds., (Royal Society of Chemistry, 1993), p.40.
3. W.N. Herman and L.M. Hayden, *J. Opt. Soc. Am.* **B12**, 416(1995).
4. J.M. Hoover, M.D. Seltzer, J.D. Stenger-Smith, A.P. Chafin, R.A. Hollins, and R.A. Henry, *Polymer Preprints* **35**, 266(1994).
5. See, *e.g.*, M.B. Feller, W. Chen, and Y.R. Shen, *Phys. Rev.* **A43**, 6778(1991).

Defeating the Nonlinearity-Transparency Tradeoff

Christopher R. Moylan, I-Heng McComb, and Robert J. Twieg

IBM Almaden Research Center, Dept. K13, 650 Harry Road, San Jose, California 95120

(408) 927-1287, (408) 927-2100 (fax)

Susan Ermer, Steven M. Lovejoy, and Doris S. Leung

Lockheed Research and Development, 3251 Hanover Street, Palo Alto, CA 94304

(415) 424-3131, (415) 354-5795 (fax)

In order to be truly useful, nonlinear optical chromophores must have large molecular nonlinearities, high thermal decomposition temperatures, and low absorption coefficients at the application wavelengths. Yet it has been empirically observed that tradeoffs exist between nonlinearity and each of the other qualities (thermal stability and transparency). The ultimate success of organic nonlinear optical materials depends upon whether these tradeoffs can be defeated.

It has been shown recently[1] that the nonlinearity-thermal stability tradeoff can be evaded for a small but growing class of compounds. Chromophores with diarylamino donor groups and cyanovinyl acceptor groups exhibit both impressive nonlinearities and high decomposition temperatures. The challenge that remains is to defeat the nonlinearity-transparency tradeoff.

According to the two-level model of Oudar and Chemla,[2] that is impossible. The zero-frequency molecular hyperpolarizability can be expressed as a function of λ_{max} in two equivalent ways:[3,4]

$$\beta_0 = \frac{3\mu_{ge}^2 \Delta\mu \lambda_{max}^2}{h^2 c^2} = \frac{9e^2 f \Delta\mu \lambda_{max}^3}{8\pi^2 c^3 h m_e} \qquad (1)$$

In this expression, $\Delta\mu$ is the difference between the ground and excited state dipole moments, μ_{ge} is the transition dipole between the ground and excited states, f is the oscillator strength, and e and m_e are the charge and mass of the electron. Because f tends to increase with λ_{max}, log-log

plots of β_0 vs. λ_{max} typically[5-8] have slopes of about 6.5. β_0 is therefore usually a very strong function of λ_{max} How, then, can this tradeoff be avoided?

Since the two-level model indicates that β_0 is at least a quadratic function of the absorption maximum wavelength, the optimum strategy is to find a class of compounds that are not well-described by the two-level model. The symmetric, "lambda-shaped" dicyano-4*H*-pyran compounds based on DCM laser dye and first synthesized by Ermer and coworkers[9] appear to be such a class. We have characterized DCM and five of its derivatives using the EFISH technique, and find all of the derivatives to be more nonlinear than their absorption maxima would imply.

The first reported lambda-shaped chromophores[10] were simply dimers of aniline derivatives, designed to crystallize in a noncentrosymmetric fashion for frequency-doubling purposes. The DCM analogues, referred to as DADx by Ermer et al., feature two electron donor moieties attached to a single acceptor. In this respect, they are most analogous to the triarylimidazole (lophine) chromophores and their derivatives.[6] The key difference between the dicyanopyrans and the lophines is that the DAD compounds are truly symmetric (C_{2v}), whereas the lophines are not.

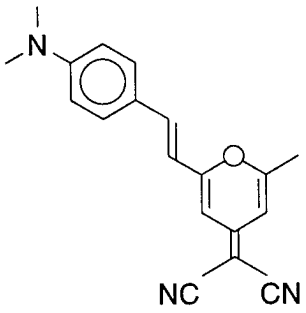

DCM

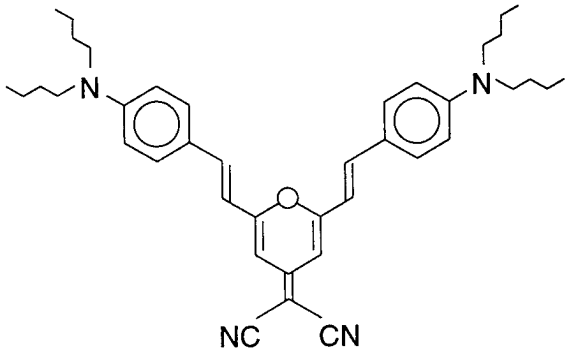

DADB

DCM and its symmetric dibutylamino analogue DADB are shown above. As one might expect, DADB is somewhat red-shifted (1200 cm^{-1}) and has a higher dipole moment (12.6 vs. 10.2 debye). The increase in β_0 is greater than expected (more than a factor of 2), and estimation of f from the uv/vis spectrum suggests the cause. The experimental oscillator strength of the first transition of DCM is 0.71; for DADB, it is 1.36. Evidently, the absorption near 496 nm re-

presents transitions to two low-lying excited states close to each other in energy. If each of these states contributes to β, nonlinearity has been increased with no sacrifice in transparency.

To check this hypothesis, we have performed semiempirical calculations (DZDO) on the simple amino derivative of DADB. We find that there are indeed two charge-transfer excited states, shown below. Interestingly, the cyanomethylene moiety does not function as an electron acceptor at all in the first excited state, and only minimally in the second excited state. The pyran ring is where most of the electron density goes in the transition from the ground state to either of these excited states.

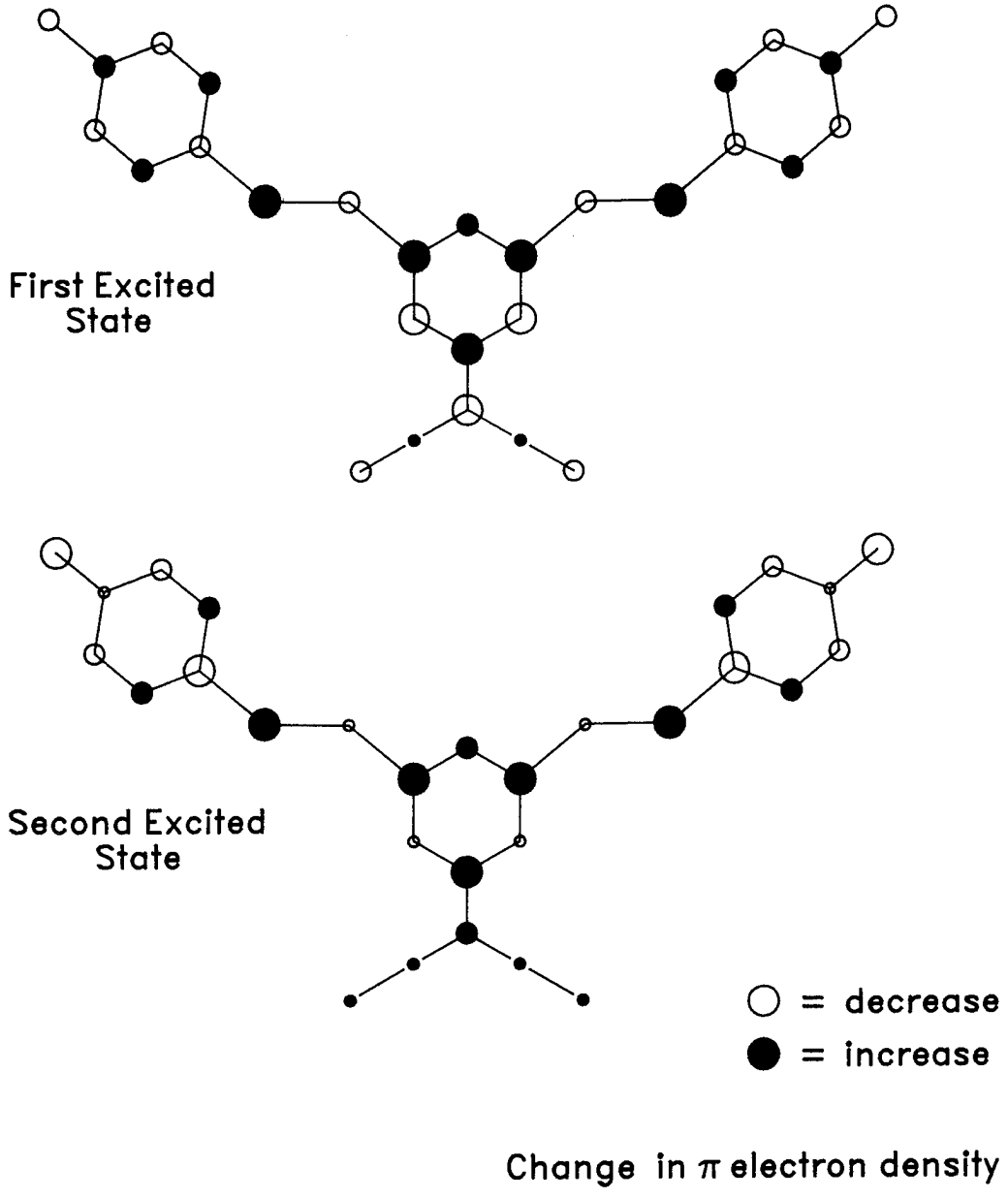

All of the DAD compounds exhibit apparent oscillator strengths greater than 1.0, and several of them (DADIH, DADCH, and DADTB, prepared by Ermer and coworkers[11]) clearly show multiple peaks in the lowest-energy absorption bands. We believe that all of the symmetric DAD compounds have two excited states that contribute to β, and therefore do not follow the two-level model, since it assumes that only one excited state is important. Since these compounds do not follow the model, they are not bound by its restrictions. They do have stronger λ_{max} dependences than single excited state chromophores do, but their nonlinearities are approximately twice as large as the others for any given λ_{max}, so that they do not need to be red-shifted as much (by changing donor groups) in order to achieve a given hyperpolarizability.

References

1. C.R. Moylan, R.D. Miller, R.J. Twieg, and V.Y. Lee, submitted for publication.
2. J.L. Oudar and D.S. Chemla, *J. Chem. Phys.* **1977**,*66*,2664-8.
3. C.R. Moylan, *J. Chem. Phys.* **1993**,*99*,1436-7.
4. C.R. Moylan, R.J. Twieg, V.Y. Lee, S.A. Swanson, K.M. Betterton, and R.D. Miller, *J. Am. Chem. Soc.* **1993**,*115*,12599-600.
5. R.D. Miller, C.R. Moylan, O. Reiser, and C.A. Walsh, *Chem. Mater.* **1993**,*5*,625-32.
6. C.R. Moylan, R.D. Miller, R.J. Twieg, K.M. Betterton, V.Y. Lee, T.J. Matray, and C. Nguyen, *Chem. Mater.* **1993**,*5*,1499-508.
7. C.R. Moylan and C.A. Walsh, *Nonlin. Opt.* **1993**,*6*,113-21.
8. R.D. Miller, V.Y. Lee, and C.R. Moylan, *Chem. Mater.* **1994**,*6*,1023-32.
9. S. Ermer, D.S. Leung, S.M. Lovejoy, J.F. Valley, and M. Stiller, in *Organic Thin Films for Photonic Applications Technical Digest, 1993*, (Optical Society of America, Washington, DC, 1993), vol. 17, pp 50-3.
10. H. Yamamoto, S. Katogi, T. Watanabe, H. Sato, and S. Miyata, *Appl. Phys. Lett.* **1992**,*60*,935-7.
11. S. Ermer, S.M. Lovejoy, and D.S. Leung, submitted for publication.

The Efficiency and Time-Dependence of Luminescence in a High Electron Affinity Conjugated Polymer

I.D.W. Samuel[1], G. Rumbles[2], C.J. Collison[2], B. Crystall[2], S.C. Moratti[3], A.B. Holmes[3] and R.H. Friend[1]

1 *Optoelectronics Group, Cavendish Laboratory, Madingley Road, Cambridge, CB3 0HE, U.K., telephone 44 1223 337287, fax 44 1223 353397*

2 *Department of Chemistry, Imperial College, South Kensington, London, SW7 2AY, U.K.*

3 *University Chemical Laboratory, Lensfield Road, Cambridge, CB2 1EW, U.K.*

Measurements of luminescence in conjugated polymers give insight into their photophysics and the operation of electroluminescent devices. The same excited state, the singlet exciton is believed to be responsible for both photoluminescence and electroluminescence. Excitons decay by a combination of radiative and non-radiative processes, and the relative rate of these processes determines the luminescence efficiency. An important feature of conjugated polymers is the possibility of chemical tailoring to realise desired properties. A recent innovation has been the development of high electron affinity polymers made by cyano substitution of members of the poly(arylene vinylene) family [1]. The increased electron affinity improves the performance of light-emitting-diodes by facilitating electron injection.

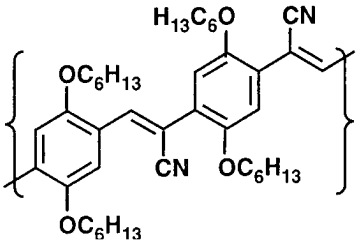

CNPPV

We report here measurements of photoluminescence efficiency and time-dependence in a cyano substituted derivative of poly(*p*-phenylene vinylene), CNPPV (shown above), and we compare and contrast measurements in solutions and films. Time-resolved measurements were made by time-correlated single photon counting with a time-resolution of 50 ps. Luminescence quantum efficiencies were measured in solution, using Rhodamine 101 in ethanol as a reference standard, and in films using an integrating sphere.

The luminescence quantum yield of CNPPV in toluene solution was 0.52±0.05, which is one of the higher values observed for a conjugated polymer. We have studied how time-resolved luminescence measurements depend on the excitation wavelength. For excitation at 557 nm, in the tail of the absorption, we find that the decay of the luminescence is dominated by a component with a time constant of approximately 800 ps. Shorter wavelength excitation leads to a more complicated decay. We consider that this difference arises because longer-wavelength excitation excites only the most-conjugated regions of the sample, whereas shorter wavelengths excite regions of the sample with a range of conjugation lengths.

In thin films the absorption and especially the luminescence spectra are red-shifted with respect to the solution spectra. The luminescence quantum yield of films was measured to be 0.33±0.05 for excitation at 514 nm. The time-resolved measurements once again show a simpler decay for excitation in the tail of the absorption, and the luminescence decay is dominated by a single exponential with a time constant in the range 5.5-5.9 ns. The decay of the luminescence is faster at shorter wavelength, and we believe that this is due to the migration of excitons. The luminescence is even longer-lived at low temperature.

The most striking result is that the decay of the luminescence is slower in the film than in solution. This is the opposite of what was observed in the related polymers MEHPPV and PPPV, and the measured lifetime is approximately twenty times longer than the lifetime in films of MEHPPV and poly(p-phenylene vinylene), PPV[2-4]. Combining the measured lifetimes and quantum yields implies that the natural radiative lifetime is 1.6 ns in solution and 17 ns in the film. We will discuss the implications of this result, and possible explanations for it.

REFERENCES

1 N.C. Greenham, S.C. Moratti, D.D.C. Bradley, R.H. Friend, and A.B. Holmes, Nature **365**, 628 (1993)

2 I.D.W. Samuel, B. Crystall, G. Rumbles, P.L. Burn, A.B. Holmes, and R.H. Friend Synthetic Metals **54**, 281 (1993)

3 U. Lemmer, R.F. Mahrt, Y. Wada, A. Greiner, H. Bässler, and E.O. Göbel, Appl. Phys. Lett. **62**, 2827 (1993)

4 I.D.W. Samuel, B. Crystall, G. Rumbles, P.L. Burn, A.B. Holmes, and R.H. Friend, Chem. Phys. Lett. **213**, 472 (1993)

Anisotropic Self-Alignment of Supramolecular Amylose Inclusion of Chromophores for Second-Order Nonlinear Optical Materials

Oh-Kil Kim and Ling-Siu Choi
Chemistry Division, Naval Research Laboratory, Washington, DC 20375-4325,
Phone: (202) 767-2088, Fax: (202) 767-0594

He-Yi Zang, Xue-Hua He and Yan-Hua Shih
Dept. of Physics, University of Maryland Baltimore County, Baltimore, MD 21228,
Phone: (410) 455-2558, Fax: (410) 455-1072

Anisotropic alignment of nonlinear chromophores and their dipolar stability are the key issues[1] of nonlinear optical (NLO) materials. Poling is a usual means in guest-host systems to bring about such an alignment[2-4]. Since poling is carried out around the glass transition temperature(T_g) of hosts[5], and the temporal stability of chromophores depends primarily on T_g values of hosts, matrix materials for high-temperature stability are required to have high T_g such as with polyimides. However, the high-temperature poling causes problems in nonlinear chromophores, such as bleaching[6-7], decomposition[8,9] or loss of dipolar alignment[10], unless they have very high decomposition temperatures. Also, a related problelm is a plasticizing effect[8,11] of chromophores which lowers the T_g of the matrix with increasing chromophore concentration.

A unique approach we have made avoids the need of poling for chromophore orientation, because poling occurs spontaneously in the process of solid thin-film formation. The material system is based on a supramolecular inclusion complexation of a nonlinear dye (guest) with a helical amylose (host). Amylose is a linear chain polysaccharide consisting of α-1,4-glucosidic units. Once included, the guest molecule is stretched out along the helical axis of the host cavity and rigidified by loss of conformational freedom, as indicated by an enhanced fluorescence emission[12] such that the host amylose controls the complex conformation and solubility, providing the guest with thermal shielding. The uniqueness of this molecular material is that dry amylose has virtually no T_g that contributes a great deal to the dipolar stability. In addition, since the supramolecular complex of amylose has a rigid-rod struscture, above a critical concentration[13] the complex molecules form a liquid crystal phase or self-ordering of parallel molecular alignment in solution. This will lead to an ordered structure of the amylose complex in the solid state.

We chose a low molecular-weight amylose (M_n=4,100) to make a soluble and yet film-forming complex because inclusion complexes of high-molecular weight amylose are insoluble[14]. Among hemicyanine dyes, 4-[4(dimethylamino)styryl]-1-docosylpyridinium bromide, $DASPC_{22}$ is chosen for nonlinear dye because of its large molecular nonlinearity, strong hydrophobicity and the molecular length scale that is most suitable to allow only one chromophore to be incorporated into the host cavity to form a 1:1 complex. Amylose-$DASPC_{22}$ complex is prepared in a DMSO-H_2O mixture and then, subjected to purification

and freeze-dried to separate as a soluble solid. Optically transparent solid thin-films are made by casting an aqueous solution on the glass substrate to give various thickness (0.1 - 12 μm). The supramolecular inclusion brought about a significant increase[15] in the thermal stability of the chromophore (ca. 30 °C increase in the decomposition temperature).

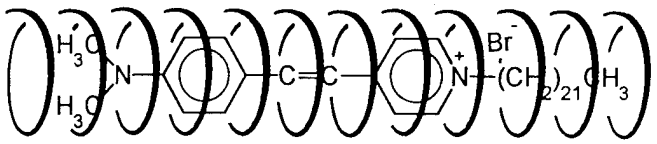

Supramolecular Amylose-DASPC$_{22}$ Inclusion Complex

The second harmonic (SH) signal of the thin film was measured with a Spectro-Physics Q-switched Nd:YAG laser (λ = 1064 nm, a fundamental wavelength) at pulse width of 10 ns and repetition rate of 10 Hz. A y-cut quartz crystal plate was used as the reference. The intensity at SH wavelength (532 nm) is monitored. We observed a signal at 532 nm, and from the intensity the $\chi^{(2)}$ value is determined to be 1 to 4 x 10^{-9} e.s.u., depending on film samples (0.1-12 μm). Since no poling is applied to the sample and $\chi^{(2)}$ of the glass substrate is zero, the $\chi^{(2)}$ value obtained is due to the sole contribution from the anisotropicity of the supramolecular chromophore in the solid state.

For the cast film, there are two different interfaces: one end is in contact with air and the other end is with glass substrate. When the incident light of 1064 nm enters the film sample from the glass-film interface, the intensity of SH signal generated by the bulk layer will undergo a destructive interference, if the film thickness is larger than the coherent length of the material. Another factor attenuating the SH signal is the absorption which depends on the absorption coefficient of the material. For the sample we study, the coherent length is 2.12 μm. Since the film color is red (λ_{max} =496 nm), a strong absorption occurs at 532 nm. The absorption coefficient at 532 nm is 0.55 μm^{-1}.

Figure 1a shows SH signal intensity versus incident angle from the normality to the glass substrate for the sample with 6 μm thickness. It exhibits two maximum peaks at the incident angles of +52.5° and -52.5°. Due to the coherent length and the absorption coefficint of the sample, the second harmonic light generated by the bulk supramolecular inclusion except a thin layer of 2.12 μm close to the glass substrate can not be detected. The maximum SH signal detected is thus generated by the thin layer of the supramolecular chromophore which is anisotropically aligned. Figure 1b exhibits two other maximum peaks at the incident angles of 180+52.5° and 180-52.5° in SH versus incident angle from the normality to the glass substrate. Due to the same reason, only the supramolecular layer close to the air-film interface contributes to the SH signal detected when the incident light enters the sample through the glass substrate. This indicates that supramolecules close to the air-film interface are also in anisotropic alignment. Such observations lead to the conclusion that the polar order in the supramolecular solid thin-films is extended from the glass surface to the air interface in a long range order.

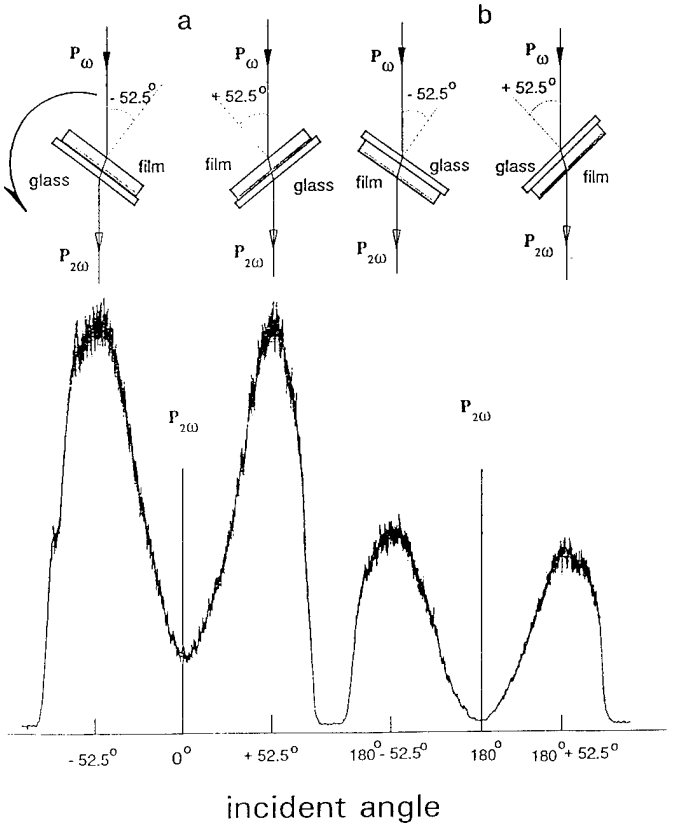

Fig. 1. Measured Maker fringes of an amylose-DASPC$_{22}$ supramolecular films of 6.0 μm thickness, showing angular dependence of SH signal intensities.

Depending on the direction of incident light, the SHG intensities at 52.5° and -52.5° are stronger than those at 180+52.5° and 180-52.5°. The ratio of the corresponding intensities is 2 to 1. This indicates that the polar order of supramolecules close to the glass-film interface is larger than that close to the air-film interface. However, with decreasing film thickness the polar orders become nearly identical between the two near-interface layers, suggesting a long-range anisotropic polar order in the entire film.

Regarding the temporal stability of $\chi^{(2)}$, we found that at room temperature, it remained unchanged for at least 1200 hrs. A further measurement of the SHG signal from the film at 90 °C in air for 100 hrs showed no change in the $\chi^{(2)}$ (Fig.2) within the experimental error (4% for SHG signal). These results clearly indicate an exceptional thermal stability of the supramolecular inclusion. An important contribution to the stability is due to H-bonding that laterally binds the rigid-rod supramolecular helices in the alignment.

In conclusion, a long-range anisotropic self-alignment of chromophores is observed in sloid thin films made from aqueous solutions of supramolecular inclusion complexes with helical amylose. The rigid-rod supramolecules are aligned almost perpendicularly to the substrate. Nonlinear susceptibility $\chi^{(2)}$ of the films measured to be 1 to 4 x 10^{-9} e.s.u., depending on the film thickness. They show an exceptionally high temporal stability; no decay in the $\chi^{(2)}$ at 90 °C for 100 hrs.

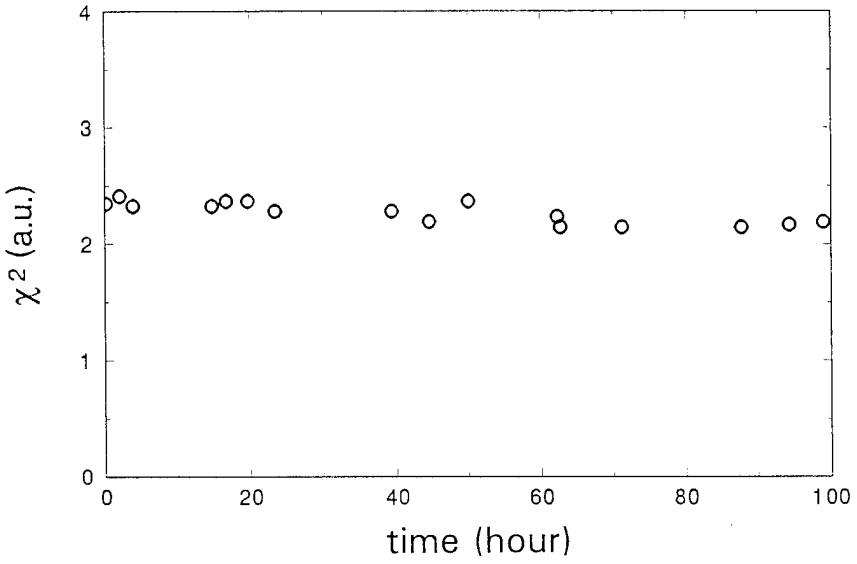

Fig. 4. Temporal stability of an amylose-DASPC$_{22}$ supramolecular film of 6.0 μm thickness at 90 °C.

References

1. D. J. Williams, Angew. Chem. Inter. Ed. Engl. 23, 690(1984).
2. G. R. Meredith, J. G. Van Dusen and D. J. Williams, Macromolecules, 15, 1385(1982).
3. K. D. Singer and A. F. Garito, J. Chem. Phys. 75, 3572(1981).
4. M. A. Mortazavi, A. Knoesen, S. T. Kowel, B. G. Higgins and A. Dienes, J. Opt. Soc. Am., B6, 733(1989).
5. K. D. Singer, J. E. Sohn and S. J. Lalama, Appl. Phys. Lett., 49, 248(1986).
6. J. W. Wu, J. F. Valley, S. Elmer, E. S. Binkley, J. T. Kenney, and R. Lytel, Appl. Phys. Lett. 59, 2213(1991).
7. R. J. Jeng, Y. M. Chen, A. K. Jain, J. Kumar, S. K. Tripathy, Chem. Mater. 4, 1141(1992).
8. S. F. Hubbard, K. D. Singer, F. Li, S. Z. D, Cheng and F. W. Harris, Appl. Phys. Lett. 65, 265(1994).
9. M. Staehelin, C, A, Walsh, D. M. Burland, R. D. Miller, R. J. Twieg and W. Volksen, J. Appl. Phys., 73, 8471(1993).
10. S. E. Barry and D. S. Soane, Appl. Phys. Lett. 58, 1134(1991).
11. J. Valley, J. Wu, S. Ermer, M. Stiller, E. S. Binkley, J. T. Kenney, G. F. Lipscomb and R. Lytel, Appl. Phys. Lett. 60, 160(1992).
12. O.-K. Kim and L.-S. Choi, Langmuir, 10, 2842(1994)
13. P. J. Flory in "Advances in Polymer Science 59; Lquid Crystal Polymers I (H. Gordon and N. A. Plate, eds), Springer-Verlag, Berlin, New york (1984), pp. 1-36.
14. G. Wulff and S. Kubik, Carbohydr. Res. 237, 1(1992) and Makromol. Chem.,193, 1071(1992).
15. Will be published elsewhere.

Structural and solvatochromic studies of a series of chromophoric TCNQ derivatives with large second order nonlinearities.

Marek Szablewski*, Philip Thomas*, Graham Cross* and Jacqueline Cole#

Department of Physics,Department of Chemistry#, University of Durham, South Rd, Durham DH1 3LE, U. K. Tel. +44 191 3743909, FAX +44 191 3743749*

As a result of our discovery of a novel reaction of TCNQ with triethylamine[1] which led to the synthesis of DEMI (structure I, fig. 1)[2], we have prepared a range of similar adducts of TCNQ with tertiary ethyl amines (structures I - VII). All of these adducts have similar structural components, a dicyanomethanide group separated from an electron deficient amino moiety by an aromatic/quinoidal ring and a "conjugated" π system. The spectral properties of these species are therefore very similar, comprising a broad charge transfer band with very little absorption to either side of it, in fact a "blue window" centred on 460 nm (fig. 2, below). As a result of their charge separated ground state, these molecules have large theoretical $\mu\beta(0)$ products, indicative of a high second order nonlinearity. The molecular figure of merit, $\mu\beta(0)$ has been calculated for I as -17,500 x 10^{-48}esu. Three TCNQ adducts prepared by conventional reactions of TCNQ with secondary amines[6] are included (IIX - X) for comparison purposes. The $\mu\beta(0)$ product of X has been determined[7] to be -840 x 10^{-48} esu, assuming a calculated μ of 3.5 D. This material is however extremely insoluble and therefore difficult to work with.

Theoretical models such as those of Meyers et al[3] in which the microscopic polarisabilities are calculated as a function molecular environment predict 'cross-over' behaviour between neutral and charge separated ground states. Using the notion of a classical reaction field as a model for the environment, molecules may be stabilised in their charge separated ground states at sufficiently high field. In typical plots of this berhaviour, zwitterionic molecules lie to the 'right hand side' of the cyanine limit, a point where α and γ are maximised and β goes to zero. Experimentally, one might easily identify this character by the negative solvatochromism of molecules within certain limits:-a shift in the position of the charge transfer band in the uv/vis spectrum to shorter wavelengths with an increase in solvent reaction field.

The charge separated or zwitterionic ground state has been indicated in a number of the structures I to VII by crystallographic studies[4,5]. These do however emphasise the inadequacy of using conventional Kekule structures to represent such species. It has been found that the presence of the residual cyano group (not part of the dicyanomethanide group), is necessary for the retention of some quinoidal character. The species IIX, for example, has no such group and has only a small quinoidal contribution. The negative solvatochromism displayed by this species and species X

(table 1) supports such a postulation. The extra cyano group in structure III extends the conjugated system with respect to the otherwise iso-structural compound I, resulting in a molecule which is less quinoidal than I. The bond linking the skeletal N to the adjacent carbon atom in the conjugated system in each case has been found to be more characteristic of a double bond than a single bond - the greater the localisation of the positive charge on the N atom the shorter the C-N bond. This counteracts the quinoidal nature of the system, which if perfect would result in a single C-N bond.

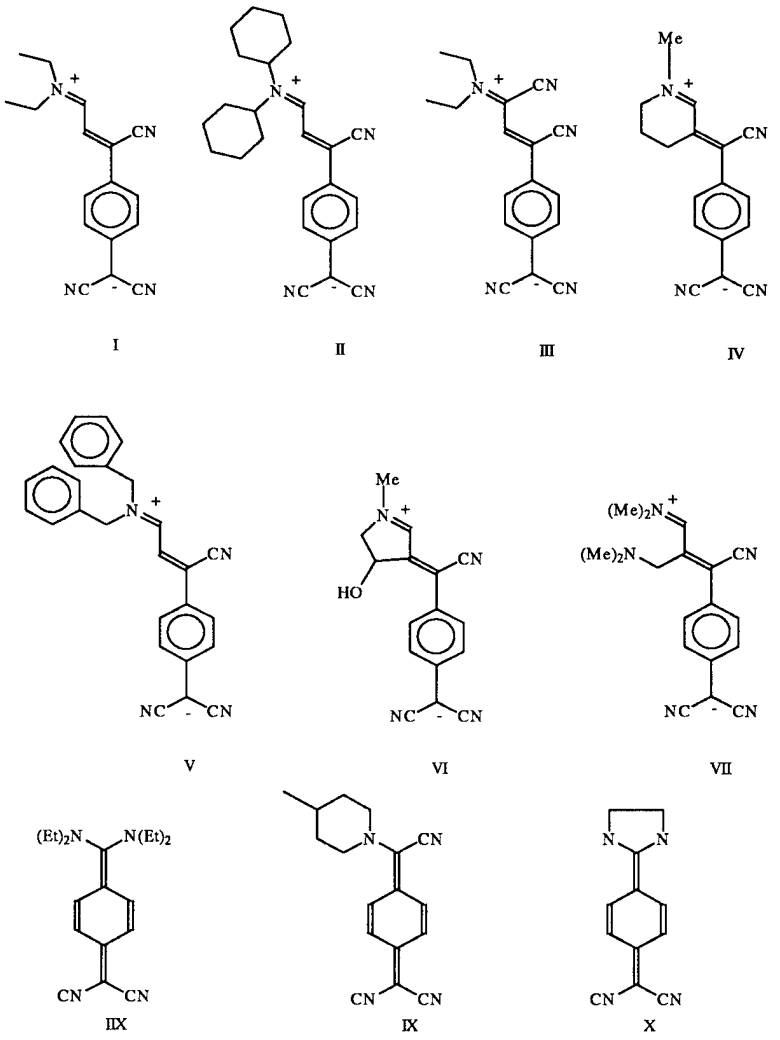

Figure 1: TCNQ amino adducts referred to in the text

Because of their highly dipolar nature, the zwitterionic molecules readily form associated dimer pairs. Such dimerisation can be observed as a departure from the expected Beer-Lambert law behaviour expected in a plot of concentration vs. absorbance. Molecules I and IV have been found to exhibit dimerisation while even at low concentrations in polar solvents such as MeCN and DMF whilst II in dichloromethane does not appear to dimerise. The presence of dimers along with insolubility, hampers progress in determining dipole moments and in experimentally determining $\mu\beta$ by EFISH.

The spectral characteristics of the charge separated species are extremely sensitive to the environment in which the molecule is located. This is very well illustrated by comparing solution uv/vis spectra of I in MeCN and PhCl (fig. 2). The PhCl spectrum of I shows three distinct peaks at 612, 657, and 720 nm with a shoulder on the short wavelength side of the band. The band at approximately 657nm is solvatochromic to a degree whilst the longest wavelength band displays negative solvatochromism over a given range of solvent environments (see Table 1).

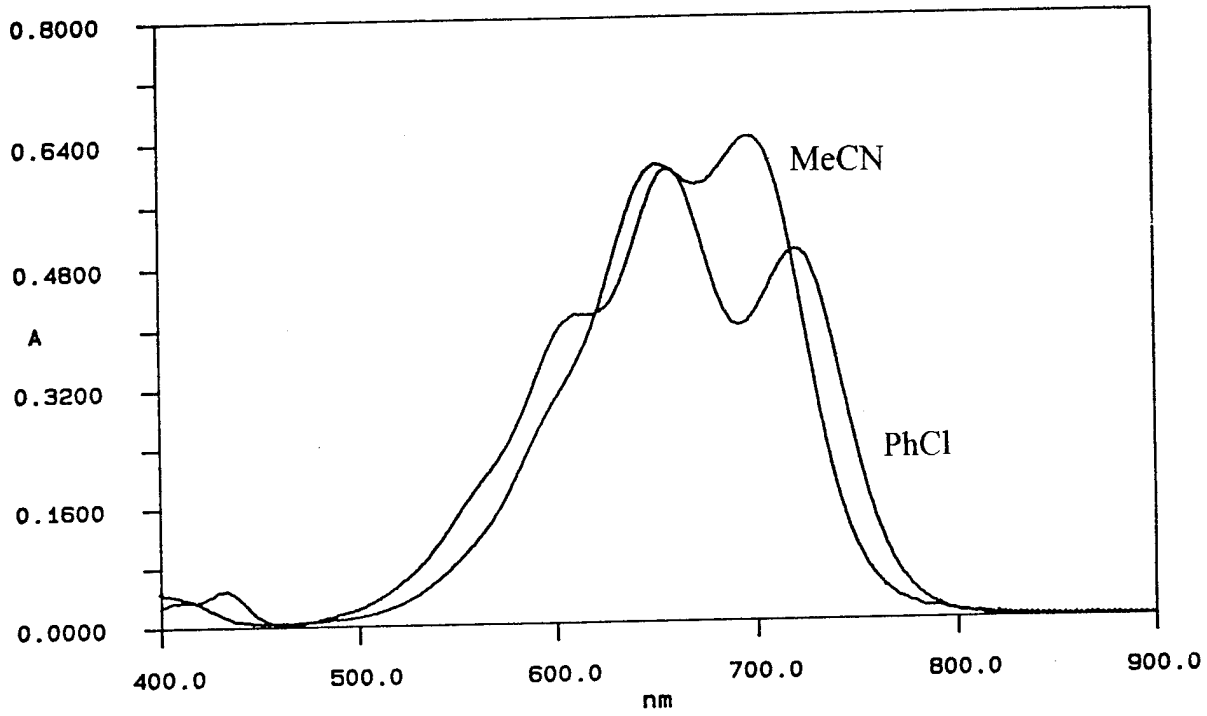

Figure 2: uv/vis absorption spectra of I in MeCN and PhCl

Table 1 demonstrates the negative solvatochromic trend expected for charge separated species. Reaction field, R, for a given solvent system is used as a measure of environment and is defined as follows:-

$$R = \left[\frac{4}{3}\pi N\mu\left(\frac{2\varepsilon-2}{2\varepsilon+n^2}\right)\left(\frac{n^2+2}{3}\right)\right]$$

where N = number density, μ = dipole moment, ε = dielectric constant and n = refractive index.

Solvent	R (au x 10^4)	I	II	IV	VI	IX
Toluene	2.4	702	716	724	-	
1,4 Diox.	3.9	711	720	712	716	
$(Et)_2O$	13.1	701	716	710	-	559
$CHCl_3$	18.5	717	726	719	722	
PhCl	22.8	722	728	722	726	571
DCM	27.8	720	725	719	722	570
THF	32.3	719	723	708	723	
EtOH	49.0	703	709	671	703	
TMUrea	53.4	708	717	689	709	
$(Me)_2CO$	62.2	705	712	688	707	565
DMF	78.4	693	708	665	697	
DMSO	111.5	670	702	662	668	574
MeOH	114.8	688	700	652	693	
MeCN	117.9	698	705	680	702	565

Table 1: Position of the lowest energy absorption band versus reaction field, R, in solution for some TCNQ amine adducts

From table 1, the trend of negative solvatochromism can clearly be seen in species I, II, IV,and VI. Over the range of solvents studied the conventional monosubstituted TCNQ adduct IX does not exhibit any significant solvatochromism. The effect is greatest with IV (μ = 45 D in DMF), then with VI, while the effect is smallest with II , which has a much smaller dipole moment of 21 D measured in DMF solution. Anomalies occur in the general trend. For example, protic solvents such as alcohols tend to cause a much greater shift than is expected.

The dipole moment of I has been determined as 34 D in PMMA films and 45 D in DMF solution.

Acknowledgment : We wish to thank the EPSRC for funding this work.

References

1. M. Szablewski, *J.Org.Chem.*, **59**, 1994, 954.
2. M. Szablewski, G.H. Cross, J.C. Cole, *Polymer Preprints*, **35**, 1994, 174.
3. F.Meyers, S.R.Marder, B.M.Pierce, J.L.Bredas, *J.Am.Chem.Soc.* **116**, 1994, 10703
4. J.C. Cole, J.A.K. Howard, G.H. Cross, M. Szablewski, *Acta Cryst.C.*,
5. J.Cole, J.A.K.Howard, G.H.Cross, M.Szablewski, M.Farsari, *Acta Cryst. B*, in preparation
6. W.R. Hertler, H.D. Hartzler, D.S.Acker, R.E. Benson, *J.Am.Chem .Soc*, **84**, 3387
7. S.J. Lalama, K.D. Singer, A.F. Garito, K.N. Desai, *Appl.Phys.Lett*, **39**, 1981, 940

Photobleaching in Side Chain NLO Polymers

Manfred Eich, Hanno Beisinghoff, Hubertus Feix, W. Görtz, Jan Vydra

German Telekom Research Center, FZ 324 e, P.O. Box 10 00 03, 64276 Darmstadt, FRG
Phone: +49-6151-83-3742, Fax: +49-6151-83-4960
E-mail: eich@vmxa.fz.telekom.de

We carried out photobleaching experiments on thin films of azo chromophore functionalized side chain polymers at different wavelengths in the UV and visible sprectral regions. Photobleaching alters the polymer layer due to two different mechanisms: In the first place, bleaching results in lowering of the index of refraction by destruction of the highly polarizable NLO chromophore electronic π system and thus shifting the absorption band. Secondly, as a result of outgassing of molecular fragments and ablation, the polymer layer thickness is significantly reduced. Both effects strongly depend on the wavelength spectrum of the bleaching source and in addition exhibit remarkably different time responses. Limiting the wavelength spectrum the proper way we were able to either concentrate on chromophor modification alone or on both chromophor modification and thickness modification. This allows us to tailor the resulting geometrical profile of channel waveguides as well as the index difference to the surrounding cladding. Figure 1 (left) shows an AFM-micrograph of the geometrical dimensions of the top surface of a channel waveguide photobleached in a NLO-sidechain polymer as described. A very smooth profile (Figure 1 right side) is realized with a rms-value of the surface roughness of only 0.3 nm. In addition to the modification of the surface topography, the refractive index in the bleached region of the polymer is shifted by up to 10^{-2}.

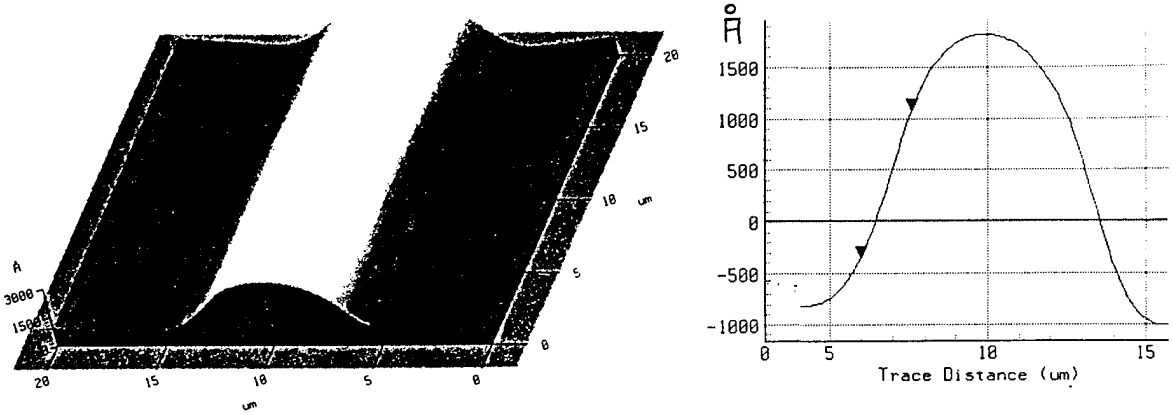

Figure 1: Surface topography by AFM of photobleached waveguide (left)
Height profile of top surface (right)

Since during bleaching the intensity decay within the film strongly depends on the optical density and hence on the wavelength, the resulting index depth profile was studied as a function of bleaching time and bleaching wavelength. Prism coupling was used as experimental technique and data was analyzed applying the WKB method. Experimental results are interpreted in terms of a theoretical model that describes the time dependent evolution of the index profile. In addition, results on waveguide loss dependence on bleaching parameters will be presented.

Enhanced Photo-oxidative Stability and Nonlinear Optical Response of a Dialkoxy-Substituted Poly-Phenylenevinylene through C_{60} Addition

H. W. Sarkas, S. R. Flom, F. J. Bartoli and Z. H. Kafafi
U.S. Naval Research Laboratory, Washington, D.C. 20375
Phone: (202) 767-9529
Facsimile: (202) 404-8114
E-Mail: KAFAFI@CCF.NRL.NAVY.MIL

The conjugated polymer poly-phenylenevinylene (PPV) and its derivatives have been the subject of numerous nonlinear optical[1] and light-emitting diode[2] studies. These polymers can photobleach in the presence of oxygen and the photo-oxidation can modify their optical properties.[3] For instance, it was recently shown that the nonexponential photoluminescence decay of this polymer is caused by exciton quenching at defects.[4] One type of defect has been identified as carbonyl groups formed on the polymer chain as a result of photo-oxidation.[3] The present work explores the effect of C_{60} doping on the photo-oxidative stability and the nonlinear optical (NLO) response of a derivative of PPV called poly-[2-methoxy,5-(2'-ethylhexyloxy)-p-phenylenevinylene] (MEH-PPV). Photoinduced electron transfer from the excited state of MEH-PPV to C_{60} has been reported to occur on a subpicosecond time scale.[3] By direct excitation into the tail of the π-π^* transition of MEH-PPV, one may be able to access this charge transfer state, stabilize MEH-PPV against photo-oxidation, and enhance the NLO properties of the composite material.

Composite films of C_{60} and MEH-PPV were fabricated by spin coating from xylene solutions. Optical absorption spectra were measured using a Perkin Elmer Lambda 9 spectrophotometer. The C_{60}, MEH-PPV, and C_{60}/MEH-PPV film thicknesses were determined from interference fringe patterns in the transparent near-infrared region. Figure 1 shows absorption spectra of films of C_{60}, MEH-PPV, and several C_{60}/MEH-PPV composites. The spectra of the composite materials resemble those of C_{60} and MEH-PPV. There is no spectroscopic evidence for the formation of a ground-state charge-transfer complex between C_{60} and MEH-PPV. The UV absorption bands associated with C_{60}, vary monotonically with concentration but are narrower and blue shifted relative to those observed in the pure C_{60} film.

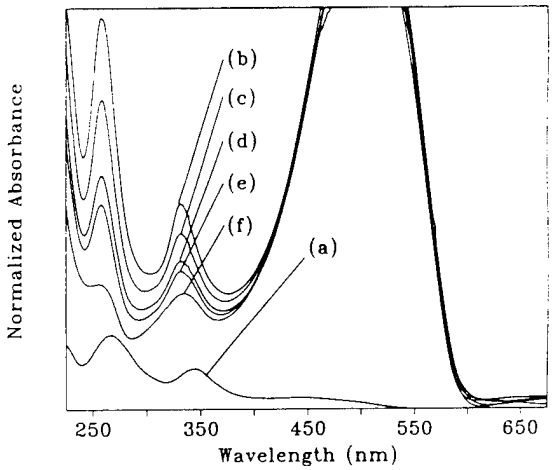

Figure 1. The absorption spectra of films of (a) C_{60} (spectrum is off-set for clarity), C_{60}/MEH-PPV with compositions (weight ratios) of C_{60}:MEH-PPV=40:60 (b), 30:70 (c), 20:80 (d), 10:90 (e), and (f) MEH-PPV.

However, these peaks are strikingly similar in position and width to those measured for solutions of C_{60}. The spectral resemblance between the C_{60} features in liquid solutions of C_{60} and C_{60}/MEH-PPV solid films is an indication that C_{60} is dispersed in the composite film.

The photooxidation study was carried out *under extreme conditions* where thin films of MEH-PPV and C_{60}/MEH-PPV were exposed to the output of an Ar^+ laser (514.5 nm line) at a total irradiance of 20 mW/cm^2 in an 800 Torr atmosphere of pure O_2.

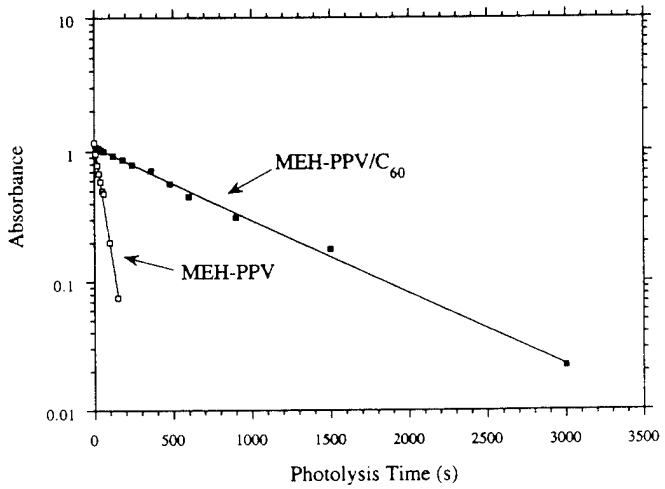

Figure 2. The absorbance at 540 nm of MEH-PPV and C_{60}/MEH-PPV (225 nm thick) composite plotted as a function of photolysis time. Photolysis was conducted at 514.5 nm close to λ_{max} of MEH-PPV absorption, in an O_2 (800 Torr) atmosphere.

Figure 2 shows the absorbance at 540 nm for a MEH-PPV film and a C_{60}/MEH-PPV composite film of similar thicknesses plotted as a function of irradiation time. The decay in the absorption band due to the π-π^* transition in MEH-PPV appears to follow first-order kinetics for both films. The decay rate is more than an order-of-magnitude smaller for the composite film relative to that of the pure MEH-PPV film. Hence the presence of the fullerene tends to stabilize MEH-PPV against photo-oxidation.[7]

Degenerate four-wave-mixing (DFWM) experiments were conducted on films of C_{60}, MEH-PPV, and C_{60}/MEH-PPV using 1.2 ps (FWHM) laser pulses with energies up to 1 mJ at 590.5 nm. A detailed description of the experimental set-up using the phase conjugate geometry has been recently described.[6] Measurements were performed in a dry nitrogen atmosphere as well as in an ambient atmosphere. MEH-PPV was found to be easily photo-oxidizable in air, and more than an order-of-magnitude variation in $\chi^{(3)eff}_{xxxx}$ was measured for the two forms of the polymer. A $\chi^{(3)eff}_{xxxx} = 5.2 \times 10^{-10}$ esu was measured for C_{60} in a dry nitrogen atmosphere. This value is not altered by the presence of oxygen, as was demonstrated earlier,[6] in which $\chi^{(3)eff}_{xxxx}$ measured for a C_{60} film doped with O_2 was almost identical to that of pure C_{60}. Table 1 gives the measured linear and NLO properties of C_{60}, MEH-PPV and C_{60}:MEH-PPV films.

Table 1. Linear and Nonlinear Optical Properties of C_{60}:MEH-PPV Films at 590.5 nm.

C_{60}:MEH-PPV x:y (weight %)	n	α_0 cm^{-1}	$\lvert\chi^{(3)eff}_{xxxx}\rvert$ 10^{-10} esu	$\lvert\chi^{(3)eff}_{xxxx}\rvert/\alpha_0$ 10^{-13} esu-cm
0:100	2.3	7700	66	8.6
0:100*	(2.3)	10,600	3.5	0.33
10:90	2.29	8700	100	11
20:80	2.27	11000	120	11
30:70*	2.26	8500	65	7.6
40:60*	2.23	7000	61	8.7
100:0	2.04	9800	5.2	0.53

* indicates that experiments were performed in a normal atmosphere.

The index of refraction for the composite films is calculated on the basis of a volume average. The linear absorption coefficients α_0 listed in Table 1 are the experimental values, uncorrected for interference fringe patterns and/or scattering. The most striking result in the table is the large difference in $\chi^{(3)eff}_{xxxx}$ of MEH-PPV measured in dry nitrogen versus air. The photo-oxidized form exhibits an order-of-magnitude smaller NLO coefficient. This result is not surprising since photo-oxidation is expected to shorten the conjugation length and disrupt the delocalization of π electrons along the polymer chain. While the values of $|\chi^{(3)eff}_{xxxx}|$ for the C_{60}:MEH-PPV composites measured in dry N_2 are larger than that of MEH-PPV, a trend cannot be established yet for the series since the NLO responses of the composites with higher C_{60} concentrations were measured in air. A complete concentration study of the NLO properties of C_{60}:MEH-PPV composites in the presence and absence of O_2 is in progress.

In conclusion, MEH-PPV photo-oxidation is markedly slowed down by C_{60} doping, and its large NLO response is preserved. The third order optical susceptibilities of the composite films are markedly greater than that of C_{60}, with more than an order-of-magnitude increase in the figure of merit $|\chi^{(3)eff}_{xxxx}|/\alpha_0$. The origin of the large NLO response of the composite films and its dependence on C_{60} concentration will be discussed. Results on the nonlinear transmittance of these materials and the dynamics of the fluence-dependent NLO response will be also given.

References

1. J. Swiatkiewicz, P. N. Prasad, F. E. Karasz, M. A. Druy, and P. Glatkowski, Appl. Phys. Lett. 56, 892 (1990).

2. J. H. Burroughes, D. D. C. Bradley, A. R. Brown, R. N. Marks, K. Mackay, R. H. Friend, P. L. Burn, and A. B. Holmes, Nature 347,539 (1990).

3. F. Papadimitrakopoulos, M. E. Galvin, H. H. Kim, K. Konstadinidis, T. M. Miller, and E. A. Chandross, Chem. Mater. 6, 1563 (1994).

4. M. Yan, L. J. Rothberg, F. Papadimitrakopoulos, M. E. Galvin, and T. M. Miller, Phys. Rev. Lett. 73, 744 (1994).

5. N. S. Sariciftci, L. Smilowitz, A. J. Heeger and F. Wudl, Science, 258, 1474 (1993).

6. S. R. Flom, F. J. Bartoli, H. W. Sarkas, C. D. Merritt, and Z. H. Kafafi, Phys. Rev. B, 51, 11376 (1995).

7. H. W. Sarkas, W. Kwan, S. R. Flom, C. D. Merritt, and Z. H. Kafafi (to be published).

Preparation, Optical Spectroscopy, and Fluorescence of Molecular Organic Composites for Light-Emitting Diodes

Harry. W. Sarkas, Charles D. Merritt, and Zakya H. Kafafi
U.S. Naval Research Laboratory, Washington, DC 20375
Phone: (202) 767-9529
Facsimile: (202) 404-8114
E-mail: KAFAFI@CCF.NRL.NAVY.MIL

Electroluminescence from small organic molecules has been known for some time. Thirty years ago, Helfrich and Schneider reported blue-violet electroluminescence in anthracene with an external quantum efficiency as high as 8%.[1] This quantum efficiency is much better than that for the best polymer-based light-emitting diode (LED) reported to date.[2] In spite of the superior quantum efficiency of molecular-based electroluminescent devices, no major progress was achieved until fairly recently when Tang and VanSlyke reported the first low-voltage organic LED with an external quantum efficiency of 1% (number of photons per electron).[3] The emitting layer in this device consists of a thin layer of the metal complex, tris (8-hydroxyquinolinato) aluminum (AlQ_3). Later, Littman and Martic showed an enhancement in the electroluminescence quantum efficiency of AlQ_3 by doping it with the highly fluorescent laser dyes, Coumarin 540, Coumarin 343, and DCM.[4] The paper focuses on a new class of organic composites consisting of highly fluorescent guest molecules dispersed in AlQ_3. The electronic and optical properties of organic nanostructures based on these materials are studied, as functions of the luminescent center concentration, via optical and fluorescence spectroscopies. Photoluminescence quantum yields are measured and used to probe the efficiency of energy transfer between host and guest molecules.

Composite films of 5,6,11,12-tetraphenylnapthacene (rubrene) or 9,10-bis (phenylethynyl) anthracene (BPEA) in AlQ_3 were prepared by vacuum deposition. Guest and host materials were codeposited from resistively heated furnaces onto sapphire substrates maintained at room temperature while under high vacuum (~1×10^{-8} Torr) at total deposition rates of 2-4 Å/s. Film thicknesses and compositions were determined and controlled using quartz crystal microbalances. Fluorescence spectra of the films were recorded in-situ by imaging the emission 1:1 onto the slit of an f/4 Jobin-Yvon HR320 spectrograph, using an EG&G OMA III with an SIT detector. The 325 nm line of a He-Cd laser was used as the excitation source. Absorption spectra were recorded ex-situ using a Perkin-Elmer Lambda 9 Spectrophotometer.

Figure 1 shows the optical spectra for thin (~350 Å) films of rubrene, AlQ_3, and rubrene/AlQ_3 composites. The peak at 306 nm is associated with rubrene and increases monotonically with rubrene concentration. The inset in Figure 1 shows a plot of the composite

film absorbances at this wavelength as a function of guest molecule molar concentration. This plot shows that Beer's law is obeyed for all the composites, indicating that they are well-behaved solid solutions.

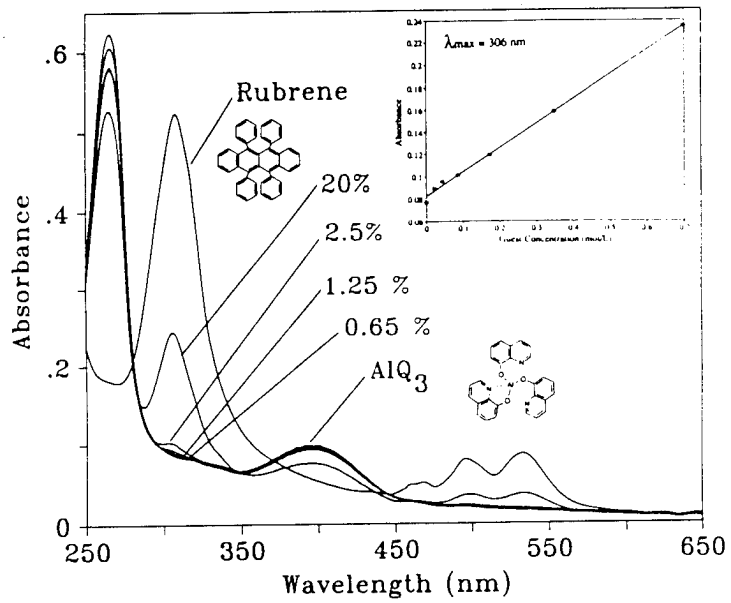

Figure 1. Optical spectra for thin films of rubrene, AlQ_3, and rubrene/AlQ_3 composites.

Figure 2 shows the fluorescence spectra for thin films of rubrene, AlQ_3, and rubrene/AlQ_3 composites. The fluorescence of the composite films is significantly enhanced relative to that of either AlQ_3 or rubrene in the solid state. In contrast to the AlQ_3 film which yields green emission, the rubrene and rubrene/AlQ_3 composites emit yellow-orange light. The composite materials exhibit fluorescence spectra that closely resemble that of rubrene in solution, indicating relatively efficient energy transfer from the host to the guest molecules. At high rubrene concentrations (>5 mol %), a quenching of the fluorescence quantum yield was observed for these composite materials.

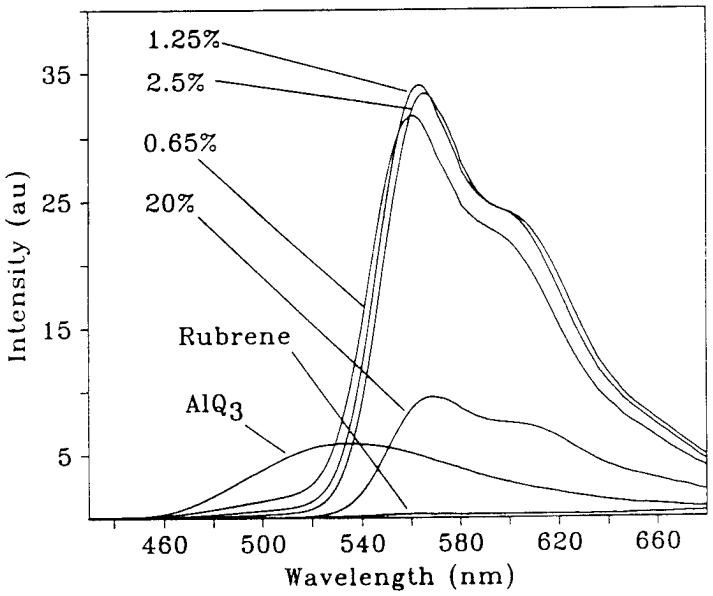

Figure 2. Fluorescence spectra for films of rubrene, AlQ_3, and rubrene/AlQ_3 composites.

Figure 3 shows optical spectra for thin (~350 Å) films of BPEA, AlQ_3, and BPEA/AlQ_3 composites. The broad features from 420-500 nm are associated with BPEA and increase monotonically with BPEA concentration. This result suggests that these composites are also well-behaved solid solutions.

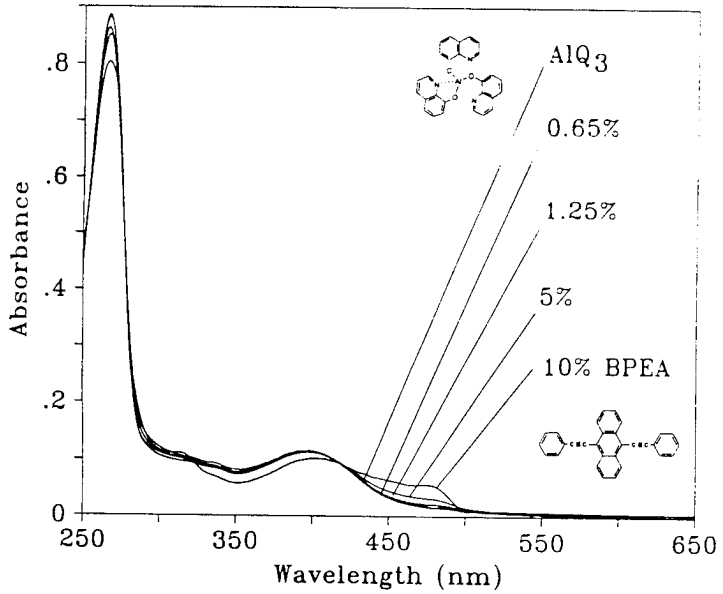

Figure 3. Optical spectra for thin films of BPEA, AlQ_3, and BPEA/AlQ_3 composites.

Figure 4 shows fluorescence spectra for thin films of BPEA, AlQ_3, and BPEA/AlQ_3 composites. The fluorescence of the composite films is again enhanced relative to that of either AlQ_3 or BPEA in the solid state. At low concentrations, the average wavelength of emission is blue shifted relative to that of either AlQ_3 or BPEA in the solid state. The fluorescence spectra of the composites having low guest concentration are similar to that of BPEA in solution. This is

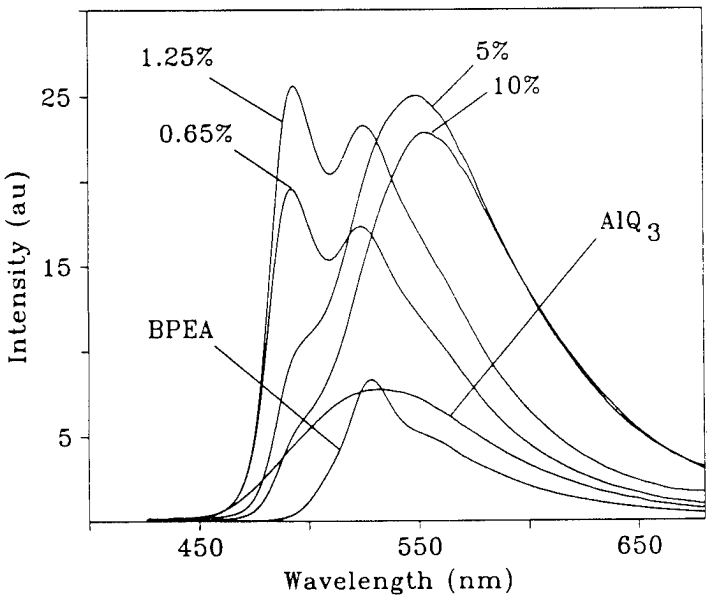

Figure 4. Fluorescence spectra for films of BPEA, AlQ_3, and BPEA/AlQ_3 composites.

again indicative of relatively efficient energy transfer between host and guest molecules. In addition, this observation implies that, at these low concentrations, the BPEA guest molecules are well-isolated and dispersed in the AlQ_3 matrix. As the BPEA concentration is increased, the photoluminescence spectra begin to red shift. Interestingly, for the highest concentrations examined, the average wavelength of emission is red shifted even relative to that of either the host or guest materials in the solid state. Figure 5 shows the photoluminescence quantum yields (Φ) for thin films of AlQ_3 and BPEA/AlQ_3 composites, relative to that of AlQ_3 (Note also that Φ[BPEA] = 0.68 Φ[AlQ_3]). Enhancements in the fluorescence yields of the composite films are observed, and these persist even at high concentrations.

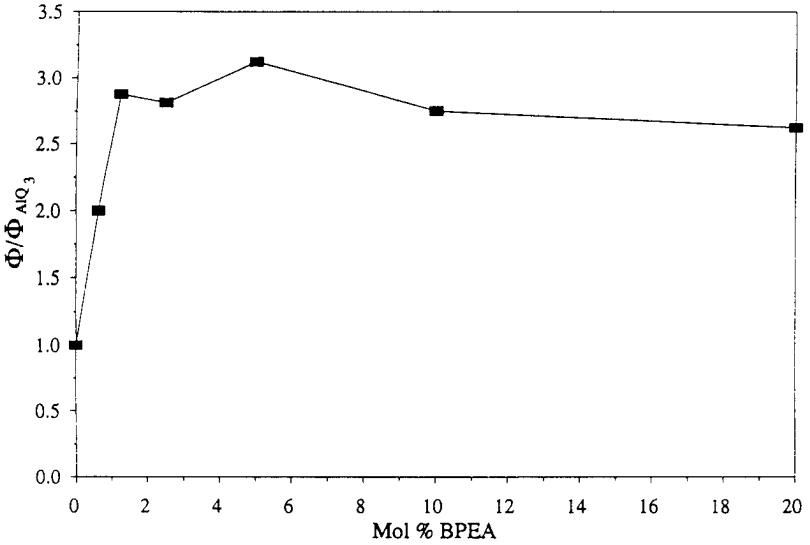

Figure 5. Relative photoluminescence quantum yields (Φ) for thin films of AlQ_3 and BPEA/AlQ_3 composites as a function of BPEA conentration.

In summary, results on two representative organic composites for light-emitting diodes were presented. Composite materials with high guest concentrations and of high optical quality were prepared by high vacuum deposition. Tunability of the emission wavelength (as a function of guest molecule concentration) was demonstrated for BPEA/AlQ_3 composites. The photoluminescence quantum yields of the composite films were significantly enhanced even at high dopant concentrations (20%). Work is in progress to fabricate LEDs based on these materials and evaluate their performance.

References

1. W. Helfrich and W. G. Schneider, Phys. Rev. Lett. 14, 229 (1965).
2. N. C. Greenham, S. C. Moratti, D. D. C. Bradley, R. H. Friend, and A. B. Holmes, Nature 365, 628 (1993).
3. Tang and S. A. VanSlyke, Appl. Phys. Lett. 51, 913 (1987).
4. Littman and P. Martic, J. Appl. Phys. 72, 1957 (1992).

Two Beam Coupling in a Photorefractive Polymer Waveguide

Dan Kokron, Stephen M. Evanko, L. Michael Hayden
University of Maryland Baltimore County
Department of Physics
5401 Wilkens Ave., Baltimore, MD 21228
(410)455-3199, hayden@umbc.edu

Photorefractive polymers have attracted a great deal of attention since they were first reported[1] in 1991. Since then, four wave mixing (FWM) diffraction efficiencies have increased from 10^{-5} to near unity[2] in films on the order of 100 μm thick. Two beam coupling gains have also seen dramatic increases.[3] These enhancements are mostly due to improvements in the materials and their processing. For example, it has been found that by substantially reducing the glass transition temperature of the polymer composite, a significant orientation of the nonlinear optical (NLO) chromophores in these composites can be achieved. The orientational enhancement[4] gives rise to a large modulation of the linear birefringence which in turn gives a stronger photorefractive (PR) effect. In this work, we report on a new application for these PR polymer composites.

The polymer composite used in this study was made from a mixture of the photoconducting polymer poly(*N*-vinylcarbazole) (PVK), a sensitizing agent 2,4,7-trinitro-9-fluorenone (TNF), an NLO chromophore 4-Nitrophenyl-2-pyrrolidinemethanol (NPP), and a plasticizing agent 9-ethylcarbazole (ECZ). The materials were dissolved in a 4:1 solution of toluene and cyclohexanone to produce an overall mixture by weight of PVK:TNF(1.3%):NPP(30%): ECZ(20%). All materials were obtained from the Aldrich Chemical Co. The waveguides were multilayered structures consisting of a 3-5 μm thick bottom buffer layer of poly(acrylic acid) (PAA) which was spin coated onto indium tin oxide (ITO) coated glass, followed by a ~15μm thick layer of the PR polymer, which was occasionally overcoated with another layer of PAA. The PR layer was applied with a knife edge technique. An electric field was applied to the film by suspending a corona wire about 1 cm above the surface of the film while grounding the ITO surface. Typically, the potential required to reach the onset of corona was about 5-7 kV, during which 2-5 μamps of current were drawn. Since we were not able to measure the applied field directly during the corona charging, we estimated the field by monitoring the change in the peak absorbance with and without the field applied in a spectrophotometer. The field was derived from the measured order parameter and knowledge of the dipole moment of NPP.[5] Using this method we estimate that the maximum applied field was about 140 V/μm.

The optical setup is depicted in Figure 1. The pump beam was laterally incident on the guided wave structure. With both input and output prisms in place, the angle of incidence of the pump could be varied from -10° to 10°. The signal beam was launched via the input prism at the appropriate coupling angle. Using the configuration as shown in Figure 1 we found that the output beam could be increased when the pump beam illuminated the waveguide. However, we also found that an output signal beam could be observed when only the pump was present. Since the output signal, when only the pump was present, was only slightly smaller than the output signal obtained when the input signal was also present, we chose to study the former situation first. Specifically, the data presented here is for the case where only the pump beam was present. As a result, we removed the unneeded input prism to allow the range of incident pump angles to be increased to -10° to 70° (negative pump angles of incidence refer to the case where the pump is propagating in the opposite direction to the guided wave). The presence of the output signal beam is due to waveguide two beam coupling (WTBC). The "signal" beam is derived from light that is scattered from the intense pump into one of the allowed guided modes. This very weak beam then interacts with the pump beam over the length of the pump (~5 mm in this case) and writes a grating. Subsequently, the pump beam then diffracts off the PR grating and into the

waveguide. In effect, in a PR waveguide, an external pump beam can create its own input grating coupler. This effect was originally observed in 70-100 μm thick slabs of $BaTiO_3$ by Fischer et. al.[6]

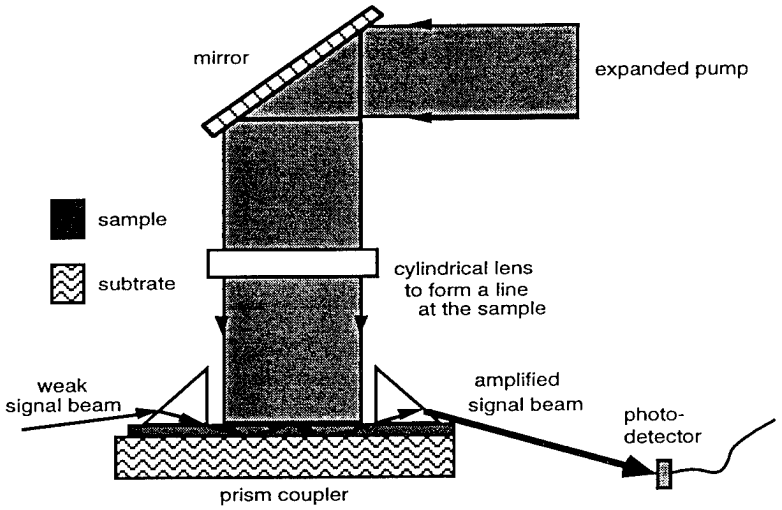

Figure 1. Close-up view of waveguide two beam coupling (WTBC) with the pump at normal incidence.

In order to confirm that our material was photorefractive, we measured the photoconductivity, electro-optic coefficient, and asymmetrical two beam coupling gain in non-waveguide structures. The electro-optic coefficient was found to be 5 pm/V at 710 nm with an applied field of 40 V/μm. We also measured a TBC gain coefficient $\Gamma = 5.8\ cm^{-1}$ at 710 nm with an applied field of 62 V/μm. The results of our waveguide experiments are presented in Figures 2-5 below. Figure 2 shows the dependence of the output signal power on the angle of incidence of the pump beam.

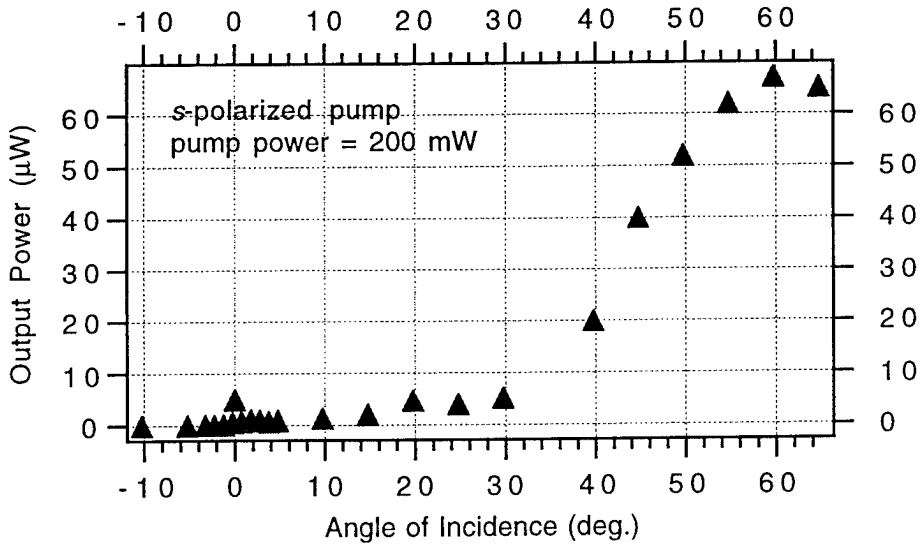

Figure 2. Power of the outcoupled signal beam as a function of the angle of incidence of the pump at 750 nm. At normal incidence the pump was 2 mm long and 0.2 mm wide.

The growth in output power at higher angles of incidence can be explained by the increase in the projection of the grating wavevector along the poling direction and by an increase in the interaction length at more oblique angles. Figure 3 shows the relationship between the input pump power and the output signal power as the pump power is varied. The total amount of output light is less in Figure 3 due to two effects. First, the data shown in Figure 3 were taken on a different portion of the film that exhibited more loss and second, we have also observed a slow decrease in the output at a steady input, possibly due to bleaching.

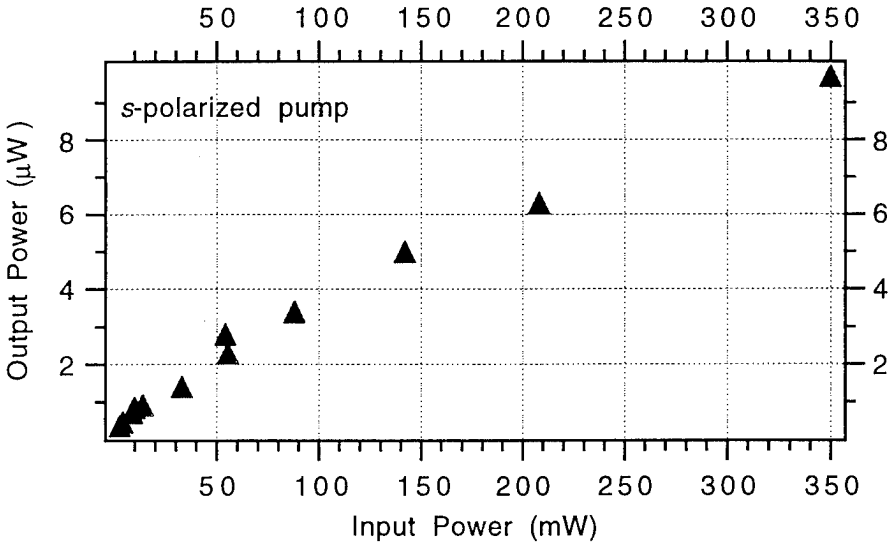

Figure 3. Dependence of the output signal power as a function of the pump power at 750 nm and an incident angle of 65°.

While a slight bend is seen in the curve of Figure 3, by plotting the ratio of output to input (Figure 4) the effect is more readily seen.

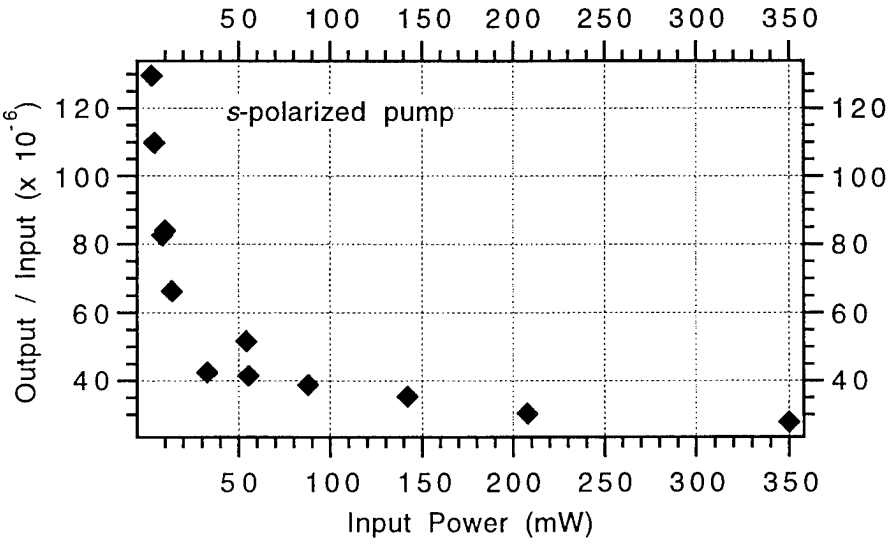

Figure 4. Ratio of power coupled out of the waveguide to the power incident on the slab as a function of the pump power at 750 nm and an incident angle of 65°.

We do not have an explanation for this saturation effect as yet, but speculate that it is due to the grating being washed out to some degree at the higher pump powers. Finally, in Figure 5 we show the relationship between the grating growth time and the input pump power. For this test, we defined the growth time as the time after the pump was incident on the slab, with the field already applied, until the output signal grew to 90% of its final maximum value. Clearly, the buildup of the grating was faster at the higher pump powers. In fact, at a pump power of 2 mW, the grating took nearly 10 seconds to build up while a grating was formed in less than one second for only 22 mW of pump power. When the corona field is not applied, no output signal is observed for any pump power or angle of incidence. Further, removal of the field while a grating is present causes the output signal to decay to zero in a few seconds.

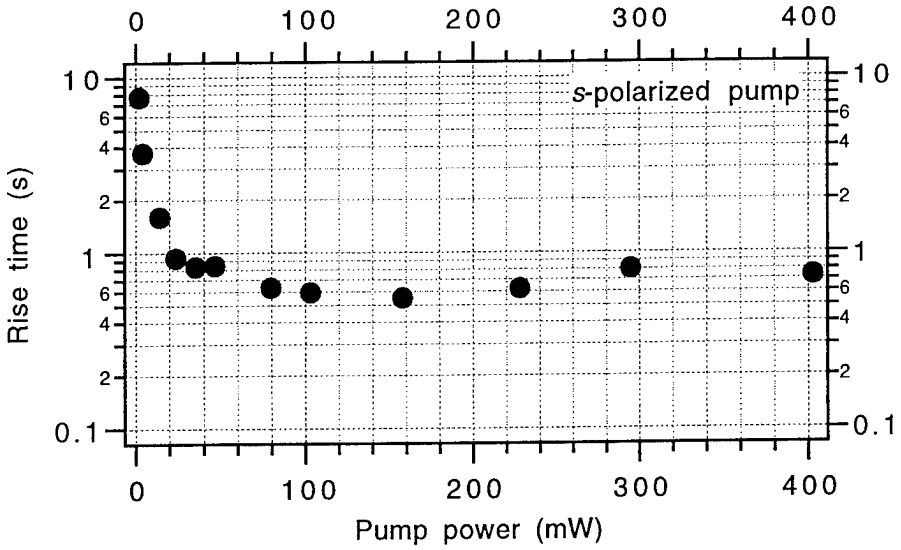

Figure 5. Grating growth time as a function of input power at 750 nm and an angle of incidence of 60°.

In summary, we have observed that a guided wave can be launched in a PR polymer slab waveguide by laterally pumping the slab. The efficiency is improved at higher angles of incidence. We are currently working on quantifying the gain experienced by existing guided signal beams and the effects on their mode structure.

The support of the National Science Foundation (Grant # ECS-9224795) is gratefully acknowledged.

References

1 S. Ducharme, J. C. Scott, R. J. Twieg, and W. E. Moerner, *Phys. Rev. Lett.* **66**, 1846 (1991).

2 K. Meerholz, B. L. Volodin, Sandalphon, B. Kippelen, and N. Peyghambarian, *Nature* **371**, 497 (1994).

3 M. Orczyk, B. Swedek, J. Zieba, and P. Prasad, *J. Appl. Phys.* **76** 4995 (1994).

4 W. E. Moerner, S. M. Silence, F. Hache, and G. C. Bjorkland, *J. Opt. Soc. Am. B* **11**, 320 (1994). See also reference 2.

5 R. H. Page, M. C. Jurich, B. Reck, A. Sen, R. J. Twieg, J. D. Swalen, G. C. Swalen, G. C. Bjorklund, and C. G. Willson, *J. Opt. Soc. Am. B* **7**, 1239 (1990).

6 B. Fischer and M. Segev, *Appl. Phys. Lett.* **54**, 684 (1989).

GROWTH OF THIN SINGLE CRYSTALLINE FILMS OF m-NITROANILINE AND THEIR NONLINEAR OPTICAL CHARACTERIZATION

A. Leyderman and M.Espinosa

Physics Department
University of Puerto Rico
Mayaguez, PR 00680

During the last decade, efforts have been focused on optimizing electro-optic coefficients as well as on search for a reliable configuration of electro-optic devices. There have been reported a few configurations of optical waveguides made from organic material.[1-6] To our best knowledge, there was no indication that structures fabricated were suitable for device fabrication. In the following, we give description of a method used for fabrication of thin single crystalline organic films. We call it plate-guided (PG) method, and have applied it to grow thin films of numerous organic compounds. In this communication, we report fabrication of *meta*-nitroaniline (*m*NA) thin single crystalline films and their nonlinear optical properties. Data on other compounds will be published elsewhere.

In the PG method , thin single crystalline film is grown between two plates made of high quality quartz. One of the plates is deepened at the center for the thickness of the crystal, with the diameter of ca. 10 mm. The recess is surrounded by a groove for the remnant of the substance. The second plate serves as a lid. The cell is filled out by a substance which is recrystallized by heating at a hot plate to obtain a homogeneous material distribution. Thereafter, the cell is positioned into a heat exchange chamber in which the temperature is achieved by a liquid heat carrier from a temperature circulator. The chamber is placed onto a polarizing microscope stage with two translational and one angular (azimuthal) freedom of motion for observation and control of single crystal growth. The material is recrystallized to obtain a single crystal seed. Manipulating the temperature of the cell one can grow a single crystal of a large size. Thus, grown crystal is packed between plates preventing its evaporation and mechanical damaging. Such an arrangement allows one to study the orientation, thickness and surface quality of the crystal. Thin single crystal films of thickness ranging from less than 1 to ca. 500 μm, were grown from a seed formed during recrystallization.

m-NA crystal belongs to the space group $Pbc2_1$ (point group *mm*2), melts at 112°C, and has a well developed gliding system which includes crystallographic plane (010) and direction [001].[7,8] It is a negative biaxial crystal belonging to the *class 13* of Hobden's classification.

At the first stage of growth from a seed, the crystal had an arrow-like shape, and as our observation revealed, with longer side aligned perpendicular to the larger in the plane of the crystal refraction index. For the m-NA crystal, this is also the largest refraction index of the crystal. These observations confirm data of Carenco *et al.*[8] and Suhara *et al.*[4] By manipulating the temperature gradient one can observe the seed to orient along the temperature gradient. Additional spikes formation prevented by manipulating the rate of growth. Despite observed high asymmetry of growth rate, we were able to grow large area high quality crystalline films. The crystal of the large size is readily reproduced.

The SHG studies of *m*-NA were conducted by Bergman and Crane,[9] and Carenco *et al.*[8] According to these studies, phase matching conditions in *m*-NA crystal were observed in the cone of directions about the optic axis only for processes involving fundamental waves of parallel polarization (type I).

A traditional experimental setup for the SHG measurements was used.[8] A Quantel Q-switched Nd:YAG laser (1064 nm) with 10 Hz pulse repetition rate was used as a fundamental source. The crystal was preliminary oriented using a polarizing microscope, and placed onto a honiometer head with its plane perpendicular to the incident beam. The polarization of the incident beam was rotated by a double-Fresnel rhomb, and setup either parallel or perpendicular to the *c*-axis. The generated second harmonic was focused by a lens onto a diode detector and observed and measured by a Tektronix model 7704A oscilloscope. The SH intensity as a function of angle rotation along n_β-axis is shown in the Figure 1. The principal cleavage plane of single crystalline films coincide with the $n_\gamma n_\beta$-plane of optical indicatrix, and the crystal was initially

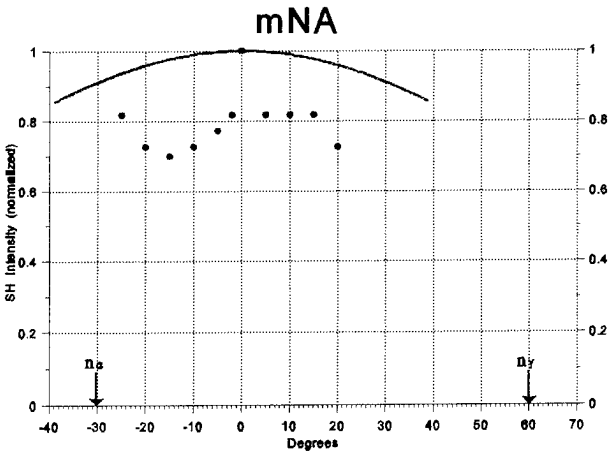

Fig. 1. Second Harmonic Intensity generated by *m*-NA crystal.

positioned on the stage with the n_γ axis to be horizontal, and the n_β one to be vertical. Rotating the crystal along vertical axis, one might find its orientation with the maximum intensity of the SH thus defining the direction of matching conditions. The intensity of the second harmonic was measured *vs.* azimuthal rotation angle (along axis n_β) and around the n_γ axis (tilting). The result is significant in defining the orientation of the crystal for the most efficient nonlinear performance.

We observed discrepancy between the experimental and theoretical SH intensity angular distributions. One might suggest that it is due to the scattering of light by the cell and film as well as absorption by the crystal. Our preliminary results on such compounds as Vanillin which is transparent in the visible region, revealed less scattering. We noticed increase in the SH generated by thin films with the thickness decreasing from 5 to 1 μm. The coherence length for the *m*-NA at 1,064 μ varying in the range from l_{32}= 16 to l_{33} = 3.9 μm,[8] and one must assume that the SHG by very thin films is due to the Čerenkov mechanism. The SH intensity generated through the Čerenkov mechanism is observed under the condition $n_{eff} > n_j$, where n_{eff} and n_j are effective indices of refraction for the film and cell materials, respectively.

References:

1. Itoh, H., Hotta, K., Takara, H., and Sasaki, K. Appl. Opt. **25,** 1491 (1986).
2. Sasaki, K., Kinoshita, T., and Karasawa, N. Appl.Phys.Lett. **45**, 333 (1984).
3. Tomaru, S., Kawachi, M., and Kobayashi, M. Opt. Commun. **50**, 154 (1984).
4. Suhara, T., Suetomo, K., Hwang, N.H., and Nishihara, H. IEEE **3**, Photonics Technology Letters, 241 (1991).
5. Stegeman, G.I., Seaton, C.T., Chilwell, J., and Smith, S.D. Appl. Phys,Lett. **44**, 830 (1984).
6. Vach, H., Seaton, C.T., Stegeman, G.I., and Khoo, I. Opt.Lett. **9**, 238 (1984).
7. Skapski, A.C., and Stevenson, J.L., J.Chem.Soc., Perkin Trans. **2**, p.1197-1200(1973).
8. Carenco, A., J.Jerphagnon, and A.Perigaud. JCP **66**(8), p.3806-3813 (1977).
9. Bergman, J., and Crane, G.R. JCP **66** (8), 3803 (1977)

Recent Progress in Polymer Electroluminescence: Electron Transport Polymers and Microcavity Devices

D. O'Brien[1,2], M.S. Weaver[1,2], M. Pavier[1,2], A. Bleyer[1,2], D.G. Lidzey[1,2], S.J. Martin[1,2], A. Tajbakhsh[2], M.A. Pate[3], Sun Meng[4], T.A. Fisher[1], T. Richardson[1,2], T.M. Searle[1], M.S. Skolnick[1] and D.D.C. Bradley[1,2*]

[1]Department of Physics & [2]Centre for Molecular Materials, University of Sheffield, Hicks Building, Hounsfield Road, Sheffield S3 7RH

[3]Department of Electronic and Electrical Engineering, University of Sheffield, Mappin Street, Sheffield S1 3JD

[4]Department of Macromolecular Science, Fudan University, Shanghai 200433, China

* tel: +44-114-276 8555 ext 4575, fax: +44-114-272 8079,
e-mail: D.Bradley@Sheffield.ac.uk

We present results concerning the design, synthesis and characterisation of new electron transport polymers and the fabrication and operation of polymer microcavity LEDs.

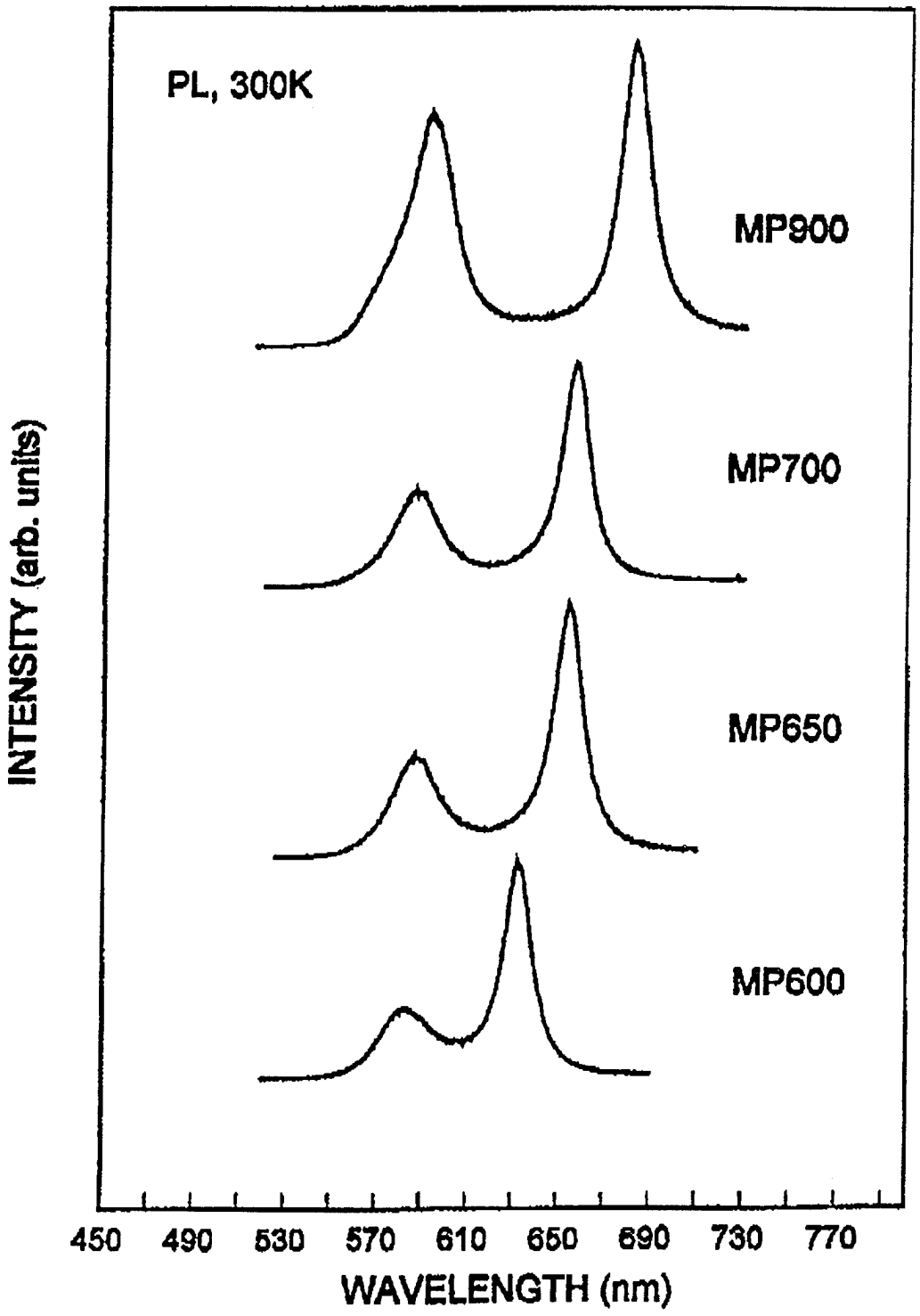
PL, 300K
MP900
MP700
MP650
MP600
INTENSITY (arb. units)
450
490
530
570
610
650
690
730
770
WAVELENGTH (nm)

Chi-electric Relaxation: Frequency Domain Chromophore Dynamics in Nonlinear Optical Polymers

J.A. Cline and W.N. Herman
U.S. Navy, NAWCAD, MS07, Warminster, PA 18974
phone: 215-441-2472

The orientational stability of nonlinear optical chromophores in polymer systems has been the subject of extensive research.[1-8] A new experimental method of observing chromophore dynamics has been developed. The method is similar to dielectric relaxation measurements where the linear polarization of the material is induced by a sinusoidal electric field. However, this new method probes the orientation of just the chromophores through second harmonic generation (SHG). This method is unique because it yields information about chromophore dynamics in the frequency domain, whereas the bulk of the work is done in the time domain. The method is dynamic and the chromophores are in steady-state motion in response to a time varying electric field, as opposed to studies such as Boyd *et al.*[4] where measurements are made with a static electric field. A description of the experimental method and a discussion of the results follows.

The polymer samples were prepared by blading a solution of DR1 and PMMA on ITO coated glass and vacuum baking to yield a film 5 microns thick and 10% by weight DR1. The polymer film was sandwiched by another blank piece of ITO glass, and bonded under compressive stress (approx. 6.0×10^5 N/m^2) and heat (140 °C) for 16 hours. The sandwich was then annealed at 140 °C for two hours to relieve any residual stresses or ordering from the bonding process. In order to evenly control the temperature, the polymer-ITO sandwich was mounted in a custom oven that had electrical leads for applying voltages to both halves of the polymer-ITO sandwich and windows for simultaneous measurement of SHG.

The data was collected by applying a sinusoidal voltage (400 V p-p) of fixed frequency to the polymer samples, while in real time the second harmonic, fundamental, and electric field signals were collected by a series of analog to digital conversions (ADCs). Typical raw data for the electric field and second harmonic normalized by the fundamental are shown in Figure 1. A complete set of data, usually 16 cycles, was collected for each frequency. The SHG was initiated with a Q-switched Nd:YAG laser operating a 1.064 microns, with a pulse width of 150 nsec and a repetition rate of 800 Hz. Since both the magnitude and phase relation of the data is desired, the timing of the data acquisition was important. The boxcar is updated only when the laser fires, thus a simultaneous reading of the three signals at a random time can cause an error since the second harmonic signal could correspond to an electric field value of an earlier time. Therefore, it was necessary to trigger the ADC conversions synchronously with the pulses from the Nd:YAG laser to ensure that all signals correspond to the same point in time. SHG data is typically collected by using the boxcar to average over many samples to improve the signal to noise ratio. However, in this case averaging would distort the signals, so the boxcar was set for no averaging, and multiple waveform cycles were collected to increase the signal to noise. The available frequency window was limited on the high frequency side by the laser repetition rate, and on the low side by collection time convenience.

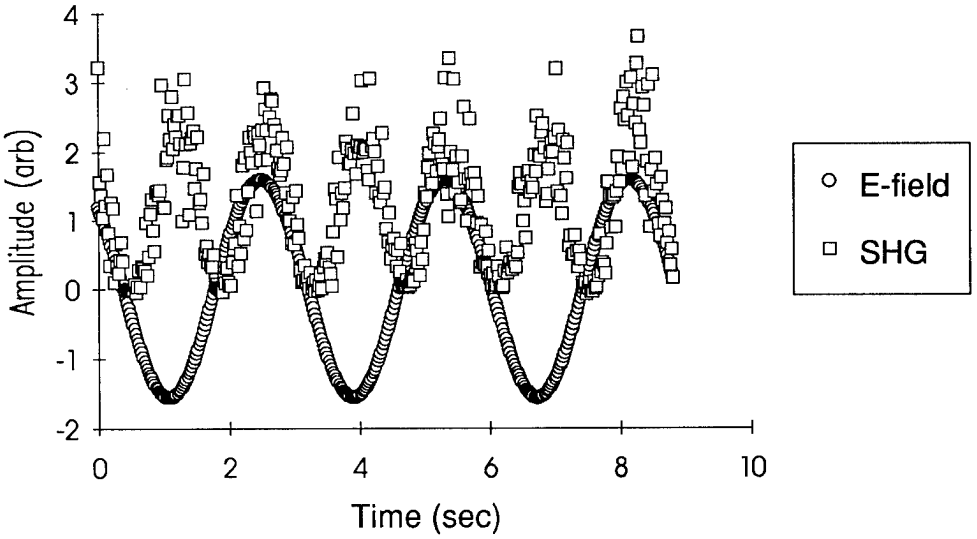

Figure 1. Plot of typical raw data showing both the applied electric field and the SHG signal normalized by the fundamental signal.

The goal of the data analysis is to describe the response of the chromophore alignment, responsible for SHG, with respect to the stimulating electric field. The analysis is similar to linear dielectric relaxation measurements, in which one is interested in the polarization response of the material with respect to the applied electric field. The two effects will be similar since the orientation of the molecules contribute to both. However, the SHG response will depend on only the properties of the chromophores, whereas the linear dielectric response is a combined response of the polymer-chromophore system. For a polymer system with a single dominant hyperpolarizability element β_{333} and second-hyperpolarizability element γ_{3333}, the effective $\chi^{(2)}$ in the presence of an applied electric field is given by,[4]

$$\chi^{(2)}_{zzz} = N f_z^2(\omega) f_z(2\omega)\left[\beta_{333}\left\langle\cos^3\theta\right\rangle + \gamma_{3333} f_z^0 E_\Omega \left\langle\cos^4\theta\right\rangle\right], \quad (1)$$

where the response of $\chi^{(2)}$ to the applied electric field, E_Ω, is through the orientational averages $\langle\cos^3\theta\rangle$ and $\langle\cos^4\theta\rangle$, and θ is the angle between the charge transfer axis and the electric field. For a system of unconstrained dipoles in thermal equilibrium, the averages can be described by a Boltzman distribution. In this case, the orientational averages for a static field E can be approximated[9] by $\langle\cos^3\theta\rangle \approx a/5$ and $\langle\cos^4\theta\rangle \approx 1/5$, when $a \equiv \mu f^0 E/kT << 1$. For a time varying field E_Ω, however, the third-order term involving γ_{3333} in Eq. (1) depends explicitly on E_Ω and is in phase with the applied field, while the second-order term involving β_{333} depends implicitly on E_Ω through $\langle\cos^3\theta\rangle$ and can lag the applied field.

To quantify the response of $\chi^{(2)}$ to the applied electric field, an approach similar to dielectric response is adopted.[10] Let the applied field E_Ω be represented by,

$$E_\Omega = E_0 \sin \Omega t. \tag{2}$$

Since $\chi^{(2)}$ is assumed to vary linearly with the applied electric field, we can represent $\chi^{(2)}$ by,

$$\chi^{(2)} = \chi_0^{(2)} \sin(\Omega t - \delta) = \chi_0^{(2)} (\sin \Omega t \cos \delta - \cos \Omega t \sin \delta). \tag{3}$$

There is an in-phase component and a 90 degrees out of phase component with magnitudes given by,

$$\begin{aligned} \chi_{in}^{(2)} &= \chi_0^{(2)} \cos \delta, \\ \chi_{out}^{(2)} &= \chi_0^{(2)} \sin \delta, \end{aligned} \tag{4}$$

respectively. These components can be determined from the raw data by using a least squares method to fit $A\sin(\Omega t+\phi_s)$ to E_Ω and $B\sin^2(\Omega t+\phi_r)$ to the SHG intensity, which is proportional to the square of $\chi^{(2)}$. Then $\chi_0^{(2)}/E_0$ is proportional to the square root of B, divided by A, and $\delta = \phi_s - \phi_r$. The results for $\chi^{(2)}{}_{in}/E_0$ and $\chi^{(2)}{}_{out}/E_0$ are shown in Figs. 2 and 3, respectively. The curves qualitatively look very similar to dielectric relaxation data. In both figures, the effect of lower temperature is to shift the curves to the left toward lower frequency. In the out of phase component data, there are two peaks in the frequency window, one for the 95°C curve and one for the 107°C. The corresponding in-phase curves go through transitions that qualitatively look similar to typical linear dielectric relaxation data.

The third-order contribution to the effective $\chi^{(2)}$ is electronic in nature and the magnitude should not decrease in the frequency range of our experiment. In addition, since third-order contributions can respond so quickly, they should be entirely in phase with the electric field at these frequencies. From Fig. 2 we can see that at either high frequency, or equivalently low temperature, the in-phase component approaches a nonzero lower bound. This lower bound can

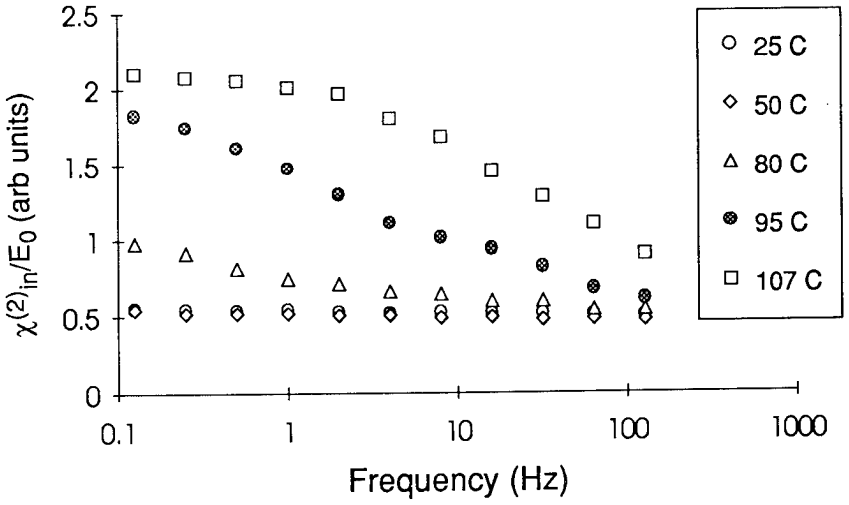

Figure 2. Behavior of the in-phase component, $\chi^{(2)}{}_{in}/E_0$, versus frequency.

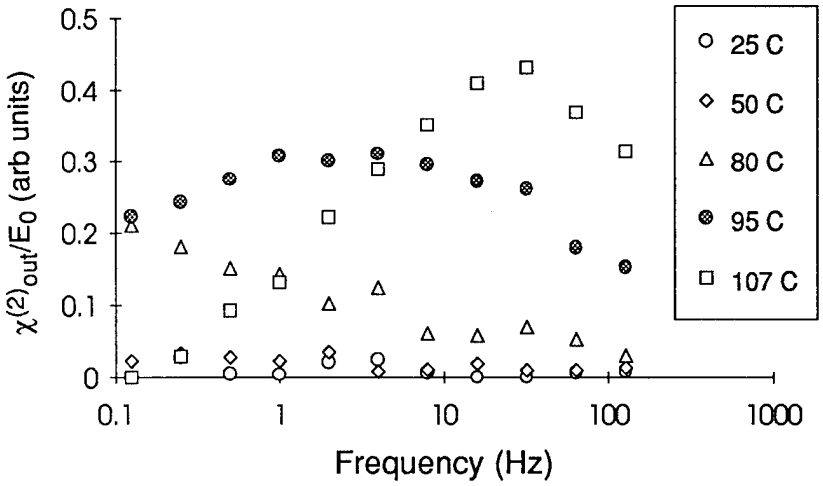

Figure 3. Behavior of the out of phase component, $\chi^{(2)}_{out}/E_0$, versus frequency.

be attributed to a combination of third-order contributions and elastic second-order contributions from chromophore orientations that happen on time scales less than 10^{-2} sec (100 Hz). Dhinojwala *et al.*[6] argue that for DR1/PMMA the response is purely third-order for time scales less than 10^{-2} sec. If this is correct, then the nonzero lower bound is purely a third-order effect, and the magnitude is approximately 20% of the largest effective $\chi^{(2)}$ found at the highest temperature and lowest frequency. It should be noted that this number is larger than what is found in the literature[6] because third-order contributions are typically compared to second-order contributions from a sample allowed sufficient time to reach maximum orientation. In our case we would have to let the system orient on time scales much longer than the present 10 sec (.1 Hz).

Interpretation of the data in light of various models[2,4,6,8] and other issues, such as charge injection, will be discussed.

References

1 H.L. Hampsch, J.M. Torkelson, S.J. Bethke, and S.G. Grubb, J. Appl. Phys. **67**, 1037 (1990).
2 M.G. Kuzyk, R.C. Moore, and L.A. King, J. Opt. Soc. Am. B **7**, 64 (1990).
3 W. Kohler, D. Robello, P.T. Dao, C.S. Willand, and D.J. Williams, J. Chem. Phys. **93**, 9157 (1990).
4 G.T. Boyd, C.V. Francis, J.E. Trend, and D.A. Ender, J. Opt. Soc. Am. B **8**, 887 (1991).
5 K.D Singer and L.A. King, J. Appl. Phys. **70**, 3251 (1991).
6 A. Dhinojwala, G.K. Wong, and J.M. Torkelson, Macromolecules **26**, 5943 (1993).
7 M. Stahelin, C.A. Walsh, D.M. Burland, R.D. Miller, R.J. Twieg, and W. Volksen, J. Appl. Phys. **73**, 8471 (1993).
8 L. Liu, D. Ramkrishna, and H. S. Lackritz, Macromolecules **27**, 5987 (1994).
9 D.J. Williams, in *Nonlinear Optical Properties of Organic Molecules and Crystals*, D.S. Chemla and J. Zyss, eds. (Academic, New York, 1987), Vol. 1 Chap II-7.
10 A.R. Blythe, *Electrical Properties of Polymers* (Cambridge University Press, New York, 1979).

PREPARATION OF HIGH QUALITY THIN FILMS. SHG PROPERTIES OF Y-TYPE LB FILMS PREPARED BY USING MOVING-WALL TYPE LB DEPOSITION SYSTEM

M. Talukder, S. Fujita*, T. Watanabe*, G. Lindsay, and S. Miyata*
Naval Air Warfare Center Weapons Division
China Lake, California, USA

* Tokyo University of Agriculture and Technology
Higashi Koganei, Tokyo, Japan
January 19, 1995

OBJECTIVE:

The purpose of the present research program is to prepare high quality thin films using Moving Wall type LB trough, which are expected to exhibit an efficient second harmonic generation.

BACKGROUND:

Recently, nonlinear optical organic materials have been extensively investigated due to their large optical non linearity and ultra fast response time. Second order nonlinear optical phenomena require the lack of inversion symmetry in a medium. Therefore control of molecular alignment becomes a very important issue. Langmuir-Blodgett (LB) technique is a good candidate to form noncentrosymmetric structure by the number of dipping of monolayer films on the water surface with maintaining molecular orientation. In order to obtain highly efficient second harmonic generation (SHG), not only increase the order parameter but also reducing optical defects in the Langmuir Blodgett film is required. Recently moving-wall type LB trough was developed by Miyata et. al., (1-3) which can transfer rigid polymeric monolayer without deforming the molecular orientation on the water surface. The thin films deposited by moving wall type LB trough show a strong in plane anisotropic structure, together with optical quality. In this project we will concentrate on the preparation of high quality thiin films of accordion type main chain polymer using moving-wall type LB trough for frequency doubling.

EXPERIMENTAL:

MATERIALS: The sample used in the present experiment is a typical accordion polymer which was synthesized by Lindsay et. al.. 1,3- Diamino-2-hydroxypropane was condensed with cyanoacetate to produce which is finally condensed in a Knoevengel polymerization to give polymer XIV.

POWDER SHG EFFICIENCY: The powder SHG efficiency was examined to confirm the spontaneous polarization in the bulk sample. The accordion polymer was irradiated with Nd:YAG laser (1064 nm). The sample did not show any SHG.

THIN FILM PREPARATION: The accordion polymer was dissolved in chloroform (0.455 mg/ml) to give a clear solution. Precautions were taken not to expose the polymer and the solution to light during the storage and operation conditions

Π-A CURVE: The solution was spread on water and the pressure-area curves were measured using moving-wall type LB trough.

LB FILM DEPOSITION: The Y-type LB films were prepared by using moving-wall type trough. The glass substrate was made hydrophobic by silination with hexamethyldisilizane. The accordion polymer was deposited on the glass substrate at a surface pressure of 20 mN/m. Y-type films were prepared by depositing a number of bilayers.

SHG MEASUREMENT OF LB FILMS: The SHG intensity was measured according to the Maker-Fringe technique. The dipping direction corresponds to the rotation axis. The accordion polymer films were irradiated with Nd:YAG laser (1064 nm). The source used in this study is a Quantel Q-switched Nd:YAG laser emitting 1.064μm. The energy of the emerging pulses is than 0.2 mJ and their duration 10 ns in Q-switched regime at a repetition rate of 10 Hz. The fundamental beam is p-polarized and the second harmonic beam is s-polarized. The sample holder can be rotated by a stepping motor. The harmonic beam emerging from the samples detected after filtering by a photomultiplier and subsequently displayed.

X-RAY MEASUREMENTS: In order to investigate the polymer LB films orientation , wide angle x-ray spectrum of the LB films was measured. There were no peaks in the x-ray spectrum. This phenomenon is not well understood However, the supra molecular or special intermolecular structure might have been formed, by which the LB films showed SHG without antyorientation in unlplaner form.

UV ABSORPTION: UV-vis absorption spectra of polymer XIV are shown in figure. Spectrum, transmission through 12 monolayers of polymer XIV on hexamethyldisilizane treated glass is similar to spectrum B in parallel to the main chain. It appears that the orientation of chromophores is randomly distributed for the intermolecular structure of the LB film system.

TEMPORAL STABILITY OF SHG: The LB film was heated from room temperature to about 100°C. Also the LB film was heated to 100°C and the SHG was measured at different times to study the stability with time. The

hysteresis of SHG intensity during cooling was investigated to study the relaxation effect.

POLING OF LB FILMS: The LB films investigated for temporal stability was cooled and SHG of the sample was measured. The sample was again heated to 70°C and 90°C separately, and poled separately to observe the effect of temperatures on the poling of the film. A noncentrosymmetric structure of polymer films for SHG was induced by corona poling. A sharp tungsten needle at high static potential was used as the positive electrode, and vacuum evaporated aluminum layer on backside of the slide glass was used as the ground electrode. The distance between the needle tip to the film surface was about 1 cm. The poling temperature was 90°C and 70°C which were selected according to the Tg of the polymer about 80°C.

RESULTS AND DISCUSSION:

The accordion polymer XIV (Figure 1) was irradiated in powder form with laser to show the second harmonic generation. It was expected that the frequency doubling of Nd:YAG laser light would give green light (532 nm). However, no green light was observed. It is assumed that the polymer does not have the self assembly characteristics in the bulk form.

The pressure-area isotherm curve (Figure 2) was obtained by spreading the polymer solution on water (Table 1). The film was compressed to 40 mN/m of pressure before collapsing. The occupied area of monolayer is 75 A^2/monomer is smaller than that of LB films prepared by conventional LB trough. The stability of monolayer (Figure 3) was examined by keeping a surface pressure at 20 mN/m. A number of different y-type layers were easily prepared (Figure 4).

A strong SHG was observed as shown in Figure 5, which suggests that even y-type LB films possess the noncentrosymmetric structures without poling. The origin of this SHG is not known. But, it is apparent that there are definitely some conformational changes of polymer chains occurred during deposition using moving wall type LB trough. The monolayers are spatially distributed or arranged in such a way that there are some kind of intra or intermolecular orientations of dipoles in the overall multimolecular structure. It is also noted that SHGs were observed in p-p, p-s, s-s, and s-p orientations ((Figure 6).. However, p-polarized fundamental beam and p-polarized SHG light gave the strongest SHG .

The temporal stability was investigated from room temperature to 100°C The SHG intensity gradually decreased with increasing temperature until about no SHG intensity at about 92°C, which corresponds to approximately the glass transition temperature of the polymer (Figure 7). The heat treated LB polymer film was then poled at 70°C and 90°C to regenerate SHG. SHG was observed for both cases (Fifures 8-9). However, the intensity of SHG for 92°C is higher than that for 70°C. The difference may be explained by the relative easiness of the mobility of the dipole chromophores at both temperatures. At 92°C the mobility of the chromophore was easier, as a result the molecular orientation is better than that at 70°C. Other experimens such as uv-vis absorption spectra of polymer XIV, x-ray, etc. were carried out to further investigate the material.

SUMMARY:

Y-type thin films of syndioregic polymer XIV, prepared by moving wall type LB trough gave strong SHG. The result suggests that even y-type LB films possess the noncentrosymmetric structures without poling. It is apparent that there are definitely some conformational changes of polymer chains occurred during deposition using moving wall type LB trough. Further studies are needed to fully explain the SHG phenomena of y-type films.

REFERENCES:

1. Hl. Kumehara, T. Kauga, T. Watanabe, and S. Miyata, Thin Solid Films, 178 (1989) 175-182

2. T. Kasuga, H. Kumehara, T. Watanabe, and S. Miyata. Thin Solid Films, 178 (1989) 183-189

3. H. Kumehara and S. Miyata, Nn Kagaku Kaishi, 12 (1987) 2330

4. G.A. Lindsay, J.D. Stengersmith, R.A. Henry, J.M. Hoover, R.A. Nissan, "Main Chain Accordion Polymers for Nonlinear Optics", Macromolecules, 26,6075(1992)

5. J.D. Stenger-smith, R.A. Henry, J.M. Hoover, G.A. Lindsay, M.P. Nadler, R.A. Nissan, "Main-Chain Syndioregic, High- Glass Transition Temperature polymer for Nonlinear Optics: Synthesis and Characterization", J. Polym. Sci, Part A, 31, 2899(1993)

Tuesday, September 12, 1995

Symposium on Displays Based on Organic Thin Films I

(Joint with OSA Annual Meeting)

TuA 8:00am–9:30am
Holladay Room

Peter Palffy-Muhoray, *Presider*
Kent State University

Electroluminescence from conjugated polymers

Richard Friend

Cavendish Laboratory

Madingley Road

Cambridge CB3 0HE, UK

e-mail: rhf10@cam.ac.uk

Conjugated polymers can be processed as thin films, and can be used as the emissive or charge-transport layers in thin-film electroluminescent diodes. I will discuss the present understanding of the operation these devices, including the improvement to the efficiency that can be produced by the use of heterojunction devices.

Current Conduction and Electroluminescence Mechanisms in Molecular Organic Light Emitting Devices.

S.R. Forrest, P.E. Burrows, Z. Shen and V. Bulovic,
Advanced Technology Center for Photonics and Optoelectronic Materials (ATC/POEM)
Department of Electrical Engineering
C436 Equad, Olden Street,
Princeton University
Princeton NJ 08544
Phone: 609-258-4204 Fax 609-258-1954

D.M. McCarty and M.E. Thompson,
Advanced Technology Center for Photonics and Optoelectronic Materials (ATC/POEM)
Department of Chemistry
Frick Building, Washington Road,
Princeton University
Princeton NJ 08544
Phone: 609-258-6623

Electroluminescence (EL) from vacuum deposited organic molecular heterojunction (HJ) devices can potentially yield red, green and blue light at levels of brightnesses and efficiencies adequate for viable flat panel displays[1]. However, to date, there has been little detailed analysis of the origin of EL and the current conduction mechanisms in these novel devices. The spatial distribution of EL in HJ devices using tris-(8-hydroxyquinoline) aluminum (Alq_3) as the light emitting layer has been measured and shown to occur within a few hundred Ångstroms of the organic HJ.[2] This was assigned to excitons created at the organic HJ subsequently diffusing into the bulk organic layer before radiatively recombining. Charge *injection* mechanisms in such structures, however, were not elucidated. In polymeric OLEDs, tunneling[3] into the conduction bands of the organic material has been invoked to explain the observed current-voltage (I-V) and EL characteristics. However, given the low carrier mobilities characteristic of many organic materials and the difficulties in measuring and interpreting band offset data, the validity of simple band structure and tunneling models remains unclear.

In this paper, we model the temperature-dependent current-voltage (I-V) characteristics of Alq_3-based OLEDs, and show that the data are consistent with space-charge-limited current injection in an insulator with a large trap distribution with an exponential energy distribution below the Alq_3 lowest unoccupied molecular orbital (LUMO). In this picture, current conduction is limited by the *intrinsic bulk* properties of the organic layer. Using the measured temperature dependence of the Alq_3 photoluminescence (PL) quantum efficiency, we further show that the temperature dependence of the EL quantum efficiency is consistent with the radiative recombination of trapped charge. This model correctly predicts the room temperature quantum efficiency of EL generation.

We have previously shown[4] that at high injection currents, the filling of traps below the electron quasi-Fermi level results in the current being governed by the density and energy distribution of the traps. An analytical expression relating the current to voltage in this trapped-charge-limited (TCL) regime is obtained by assuming a continuous exponential energy distribution of traps , so that the density of traps at energy E is given by:

$$N_t(E) = \left(\frac{N_t}{kT_t}\right)\exp\left(\frac{E - E_c}{kT_t}\right), \qquad ...(1)$$

where N_t is the total trap density, E_c is the Alq_3 LUMO energy and $T_t = E_t/k$, where E_t is the characteristic trap energy and k is the Boltzmann constant. Then, assuming the electron current in Alq_3 dominates[5]:

$$J_{TCL} = N_C \mu_n q^{(1-m)} \left[\frac{\varepsilon m}{N_t(m+1)}\right]^m \left(\frac{2m+1}{m+1}\right)^{(m+1)} \frac{V^{(m+1)}}{d^{(2m+1)}}, \qquad ...(2)$$

where $m = T_t/T$, ε is the permittivity, T is the temperature, d is the thickness of the Alq_3 layer, μ_n is the electron mobility and Nc is the density of states at the LUMO.

Figure 1 shows the I-V characteristics of a device with 270Å of preferentially hole-conducting TPD and 550Å of Alq_3 (open symbols) at temperatures ranging from 120 K to 300 K. The inset shows the variation of m with 1/T, which is fit by a straight line corresponding to E_t = (0.15 ± 0.02) eV. It has previously been determined that $\mu_n = 5 \pm 2 \times 10\text{-}5$ cm^2/Vs at room temperature[6]. Using this value, and taking into account the temperature dependence of the electron mobility, we fit the data as shown in Fig. 1 (solid lines). The fit to the data over a

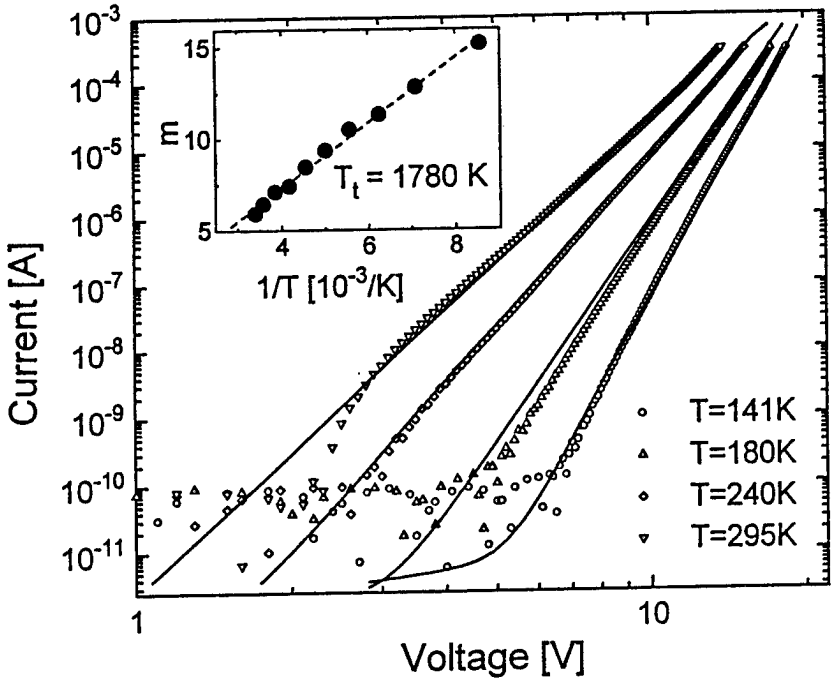

Figure 1: Temperature dependence of OLED I-V characteristics, with fits to the model discussed in the text. Inset shows the variation of m with temperature.

wide range of temperature and six decades of current is excellent. From the fit, we find Nt = 3 x 10^{18} cm^{-3} and Nc = 1 x 10^{19} cm^{-3}. The fact that N_c and N_t are roughly equal (and within two orders of magnitude of the density of molecular sites) suggest that each conduction electron is self-trapped on an Alq_3 molecule.

We further propose that EL is the result of recombination of electrons in the filled trap states with holes in the Alq_3 highest occupied molecular orbital (HOMO, at energy Ev), via an intermediate Frenkel-like exciton state. To investigate this hypothesis, we show in Fig. 2 the EL quantum efficiency, η_{EL}, at a constant device current of 50μA (solid symbols) as function of temperature. The upper inset in Fig. 2 shows a proposed energy level diagram for the Alq_3 layer, illustrating the recombination process along with the electron and hole quasi Fermi levels, F_n and F_p, under high forward injection. Since holes, of density p(x), are minority carriers in Alq_3, the recombination rate is limited by the density of holes, p(x), where x is the distance from the MgAg (injecting) electrode. Using the model of Shockley, Read and Hall,[7] we can obtain an equation for the steady state EL flux, $\Phi_{EL}(T)$:

$$\Phi_{EL}(T) = \eta_{PL}(T) p(d) \mu_p E(d), \qquad \ldots(3)$$

where η_{PL} is the PL quantum efficiency of Alq_3, p(d) and E(d) are the hole density and electric field respectively at the TPD/Alq_3 interface. The lower inset in Fig. 2 shows the measured temperature dependence of η_{PL}. Using this data and the same values of N_t, N_c and μ_p derived from the I-V data, we fit the temperature dependence of η_{EL}, shown by the solid line in Fig. 2. Thus, the same exponential trap distribution responsible for limiting the current conduction in OLEDs can be used to correctly predict both the shape and magnitude of the temperature dependence of EL.

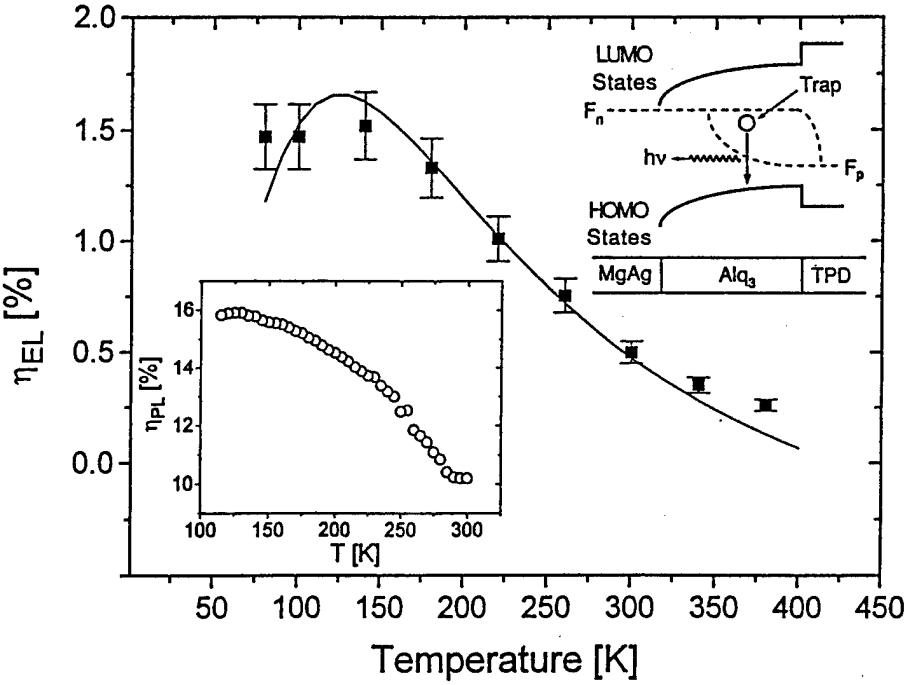

Figure 2: Dependence of El efficiency on temperature (open circles) and fit to the TCL model (broken line). Insets show the energy levels in the Alq3 layer (top) and the temperature dependence of PL (bottom).

Since the emission from these materials results from a trapped Frenkel exciton, the nature of the emitting species can be determined from calculations carried out on single molecules. We use a semiempirical calculational method (intermediate neglect of differential overlap developed by Zerner, ZINDO) to elucidate the influence of molecular structure on the traps, and hence on the color of EL. Using atomic coordinates for Alq3 from crystallographic data, we use ZINDO to show that, in Alq3, the filled π orbitals are located on the phenoxide side of the quinolate ligand and the unfilled π^* orbitals on the pyridine side of the quinolate. The phenoxide π system corresponds to the highest energy filled state, and is the likely site of the trapped hole. Conversely, the pyridyl system is the lowest energy vacant state, making it the likely site of the

Molecule	Peak PL Wavelength
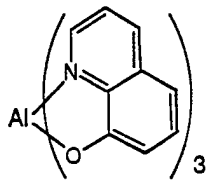	520 nm
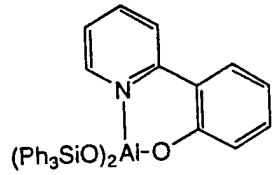	450 nm

Table 1: Influence of molecular structure on peak PL wavelength.

trapped electron. Recombination is therefore from localized states on a single quinolate ligand, consistent with the picture of a Frenkel exciton. ZINDO calculations of the cationic and anionic states of Alq3 to show that molecular reorganization in the presence of a charge carrier results in self trapping with approximately the same energy as that calculated from the I-V characteristics. Furthermore, chemical modification of the quinolate ligands results in shifts in the wavelength of EL, which can be accurately modelled and predicted by ZINDO. As an example, we show in Table 1 a modification to the Alq3 structure which results in bright blue emission.

We acknowledge ARPA, American Biomimetics and Hewlett-Packard for their support of this work.

1. C.W. Tang and S.A. VanSlyke, Appl. Phys. Lett. **51**, 913 (1987).
2. C.W. Tang, S.A. VanSlyke and C.H. Chen, J. Appl. Phys. **65**, 3610 (1989).
3. I.D. Parker, J. Appl. Phys. **75**, 1656 (1994).
4. P.E. Burrows and S.R. Forrest, App. Phys. Lett. **64**, 2285 (1993).
5. M.A. Lampert and P. Mark, *Current Injection in Solids*, Ch.4, Academic Press, New York (1970).
6. C. Hosokawa, H. Tokailin, H. Higashi and T. Kusumoto, Appl. Phys. Lett. **60**, 1220 (1992).
7. W. Shockley and W.T. Read, Phys. Rev. **87**, 835 (1952).

Double Heterostructure and Multiple Quantum Well Organic Light Emitting Diodes for Flat Panel Displays

Dirk Ammermann, Achim Böhler, Christoph Rompf, and Wolfgang Kowalsky
Insitut für Hochfrequenztechnik, Technische Universität Braunschweig
Postfach 3329, D-38023 Braunschweig, Germany
Phone: +49-531-391-2461 Fax: +49-531-391-5841

Introduction

Multilayer organic light emitting diodes (OLEDs) have recently been intensively studied [1,2] for future applications in large-area flat panel color displays. The principle of operation is similar to that of inorganic light emitting diodes (LEDs). Holes and electrons are injected from opposite electrodes into the organic layer sequence and recombine generating singlet excitons that decay radiatively. The emission layer consists of highly fluorescent organic dye molecules sandwiched between separate hole and electron transport layers. This multilayer structure allows to achieve bright electroluminescent emission in the visible spectral region at low driving voltages. We discuss the growth and characterization of high brightness double heterostructure diodes in the green spectral region and present results obtained from organic multiple quantum well light emitting diodes.

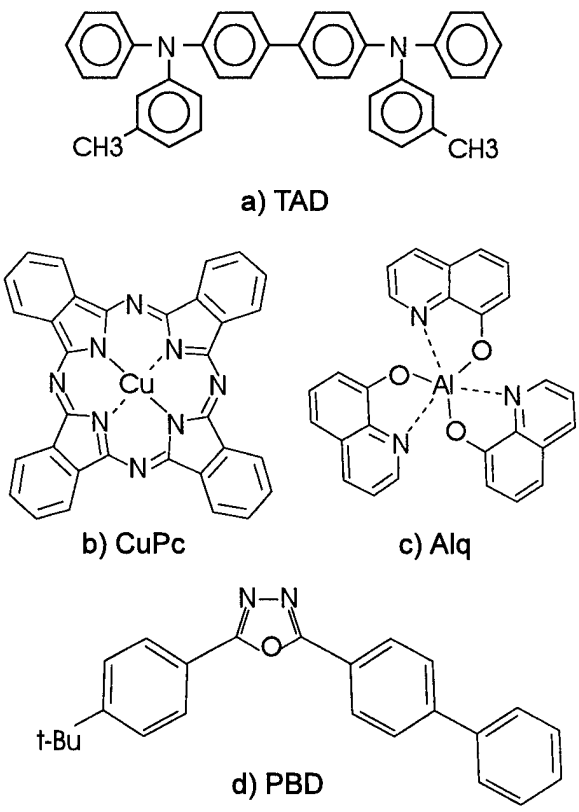

Fig.1: Molecular structures of a) TAD, b) CuPc, c) Alq, and d) PBD.

Growth and Preparation of Organic Light Emitting Diodes (OLEDs)

Transparent ITO (tin-doped indium oxide) coated glass slides with a sheet resistance of 120 Ω/□ are used as substrate. Thin organic films are grown by the organic molecular beam deposition technique under ultrahigh vacuum conditions at a base pressure of about 10^{-9} Torr [3,4]. Varying the substrate temperature allows to control the morphology of the deposited layers. Low substrate temperatures are obtained by cooling with liquid nitrogen. Growth rates as low as 25 - 80 Å/min tend to yield smooth or even crystalline thin films and improved optical and electrical properties of the organic layers.

Fig. 1 shows the molecular structures of the organic source materials used for the electroluminescent devices described here. Preferentially hole transporting behavior is observed for CuPc (copper phthalocyanine) and TAD (N,N'-diphenyl-N,N'-bis(3-methylpheny)-1,1'-biphenyl-4,4'-diamine) whereas Alq (tris-(8-hydroxychinoline) aluminum) and PBD (2-(4-biphenylyl)-5-(4-tert-butylphenyl)-1,3-4-oxadiazole) serve as electron transport layer. The metal chelate com-

plex Alq is also well known for its high fluorescence yield in the green spectral region. TAD, CuPc, and PBD are commercially available, Alq is synthesized by adding hydroxychinoline to a solution of $Al(OH)_3$ in water.

The top electrode consists of a vacuum deposited 200 nm thick Mg layer reinforced by a 200 nm Ag protection layer. Circular, 2 mm diameter metal contacts are defined by a shadow mask.

Double Heterostructure OLEDs

The device structure of a double heterostructure organic light emitting diode is schematically shown in Fig. 2. An Alq emission layer is sandwiched between the CuPc hole transport and the PBD electron transport layer. Electrons injected from the low work function Mg-Ag top contact and holes injected from the wide-gap ITO electrode are transferred to the emission layer and recombine generating singlet excitons that decay radiatively. The simple band theory model of the double heterostructure device depicted in Fig. 2 suggests the advantages of the multilayer structure: The overlap of the electron and hole densities is enhanced, contact recombination is impeded, and the carrier recombination is confined within the emission layer. Moreover, generated singlet excitons also decay radiatively within the Alq layer without being quenched at the electrodes.

Emission in the green spectral region at a peak wavelength of λ=530 nm and a half width of about 80 nm is achieved under cw-operation at room temperature and normal ambient conditions. Fig. 3 shows the detected optical output power-current (P-I) characteristic of an optimized double heterostructure device. The optical output power is measured with a large area Si photodetector. A maximum value of 270 µW is obtained for a layer sequence of 30 nm CuPc, 80 nm Alq, and 30 nm PBD. The dependence of Alq layer thickness on the relative quantum efficiency of the double heterostructure OLED is shown in Fig. 4. However, only a small fraction of the generated radiation contributes to the detected optical signal due to total reflection at the organic-glass and glass-air interfaces and absorption in the CuPc layer. In addition, the aperture of the Si photodetector limits the detected optical output power to about 75 % of the total optical emission

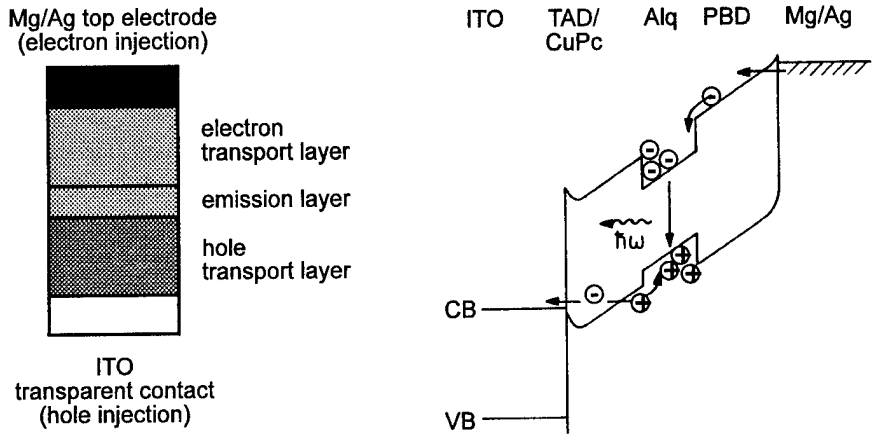

Fig. 2: Device structure and band model of a double heterostructure organic light emitting diode (OLED).

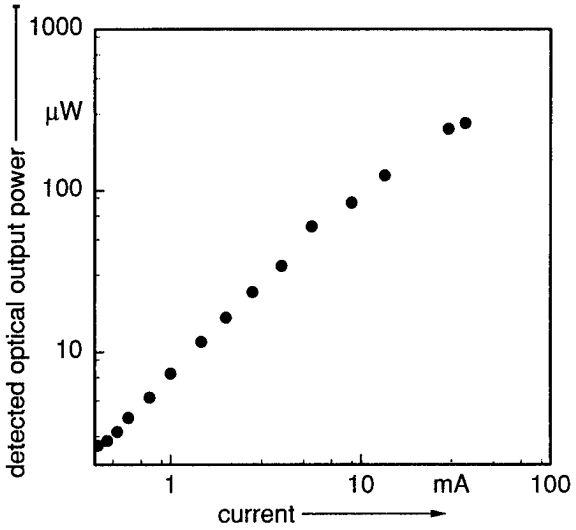

Fig. 3: P-I characteristic of a double heterostructure organic light emitting diode (OLED).

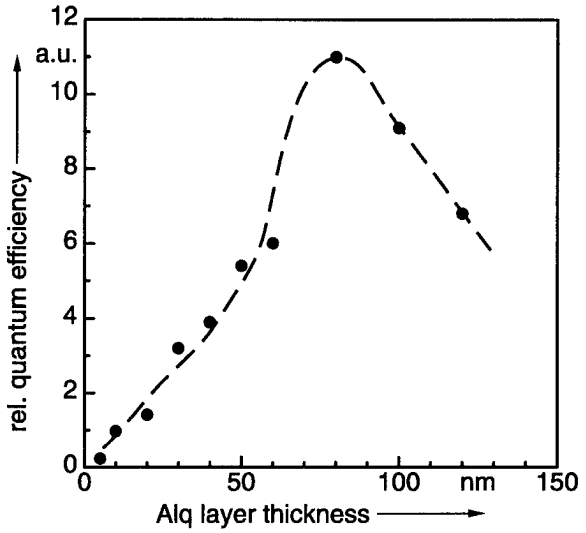

Fig. 4: Relative quantum efficiency of a double heterostructure OLED as a function of the Alq layer thickness.

through the glass substrate. Taking into account an overall optical efficiency of 8.4 %, the estimated internal quantum efficiency of the device is about 5.5 %, compared to an internal quantum efficiency of a single layer and single heterostructures OLEDs of only 0.03 % and 0.4 %, respectively [5].

Multiple Quantum Well OLEDs

Organic light emitting diodes consisting of three, only several molecular monolayers thin Alq emission films (*quantum wells*) sandwiched between PBD electron transport layers (*barriers*) are schematically shown in Fig. 5. The device structure stems from inorganic multiple quantum well (MQW) structure, however, the underlying principle is different.

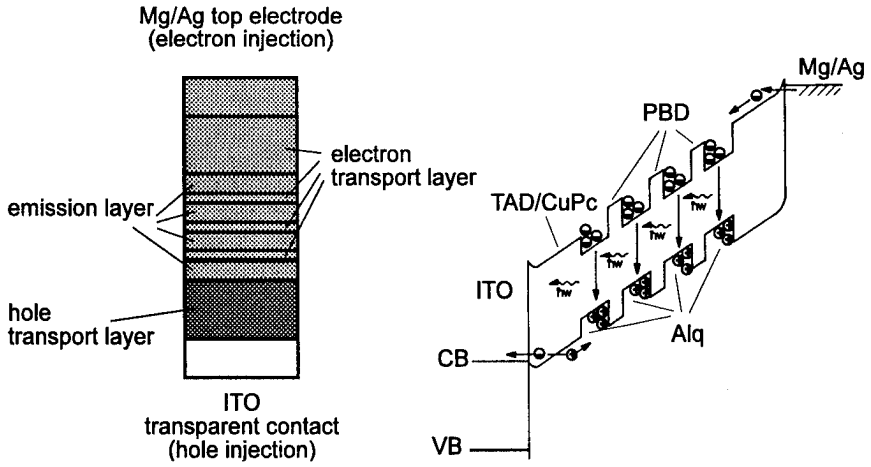

Fig. 5: Device structure and band model of a multiple quantum well organic light emitting diode (MQW-OLED).

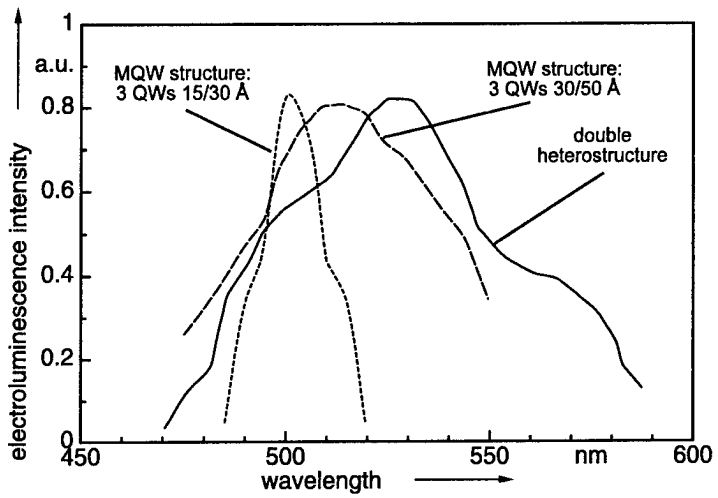

Fig. 6: Emission spectra of MQW-OLEDs as a function of Alq well/PBD barrier width.

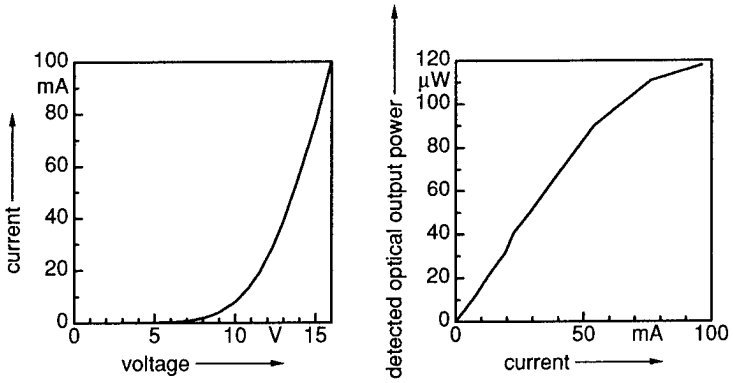

Fig. 7: I-V and P-I characteristics of MQW-OLEDs.

The electroluminescent emission spectra of MQW-OLEDs as a function of Alq well/PBD barrier width are shown in Fig. 6. The blue shift of the peak emission energy of the 15/30 Å MQW-OLED amounts to about 140 meV compared to the double heterostructure device. In addition, a spectral narrowing of the emission is observed. The peak wavelength shift may be attributed to a disturbance of the Alq well molecular environment by PBD barrier molecules. A more detailed investigation is currently prepared.

The current-voltage and optical output power-current characteristics of MQW-OLEDs are in good accordance with results obtained for double heterostructure devices. The turn-on voltage of about 10 V is mainly determined by the organic layer thickness. Carrier transport is trap or space charge limited [6]. An estimated internal quantum efficiency of 1 % can be derived from the P-I characteristic.

Conclusions

Double heterostructure organic light emitting diodes (OLEDs) for the green spectral region were successfully fabricated and show an optimized maximum optical output power of 0.3 mW and an estimated internal quantum efficiency of 5.5 %. Multiple *quantum well* OLEDs allow to continuously detune the emission wavelength from λ=530 nm to λ=500 nm.

References

[1] C. W. Tang, S. A. VanSlyke, and C. H. Chen, J. Appl. Phys. **65** (1989), p. 3610.
[2] S. Saito, T. Tsutsui, M. Era, N. Takada, C. Adachi, Y. Hamada, and T. Wakimoto, Proc. SPIE **1910** (1993), p. 212.
[3] S. R. Forrest and Y. Zhang, Phys. Rev. B **49** (1994), p. 11297.
[4] D. Ammermann, C. Rompf, and W. Kowalsky, Jpn. J. Appl. Phys. **34** (1995), p. 132.
[5] C. Rompf, D. Ammermann, and W. Kowalsky, Mater. Sci. Technol. (1995), accepted for publication.
[6] P. E. Burrows and S. R. Forrest, Appl. Phys. Lett. **64** (1994), p. 2285.

Highly Scattered Optical-Transmission Polymer for the Liquid Crystal Display Backlight

Akihiro Horibe, Megumi Izuhara, Eisuke Nihei, Yasuhiro Koike

Faculty of Science and Technology Keio University

3-14-1 Hiyoshi, Kohoku-ku, Yokohama 223, Japan

Phone : +81-45-563-1141 Ext.3454

Fax : +81-45-562-7625

Introduction

In LCD application, it was thought that transparent polymer materials were necessary for optical-transmission media of light sources. Therefore, for conventional edge-light type backlight systems which have lamps on one or both edges, transparent PMMA homopolymer plate has been used as a waveguide. And, it was believed that a transparent PMMA homopolymer plate as a waveguide was indispensable. However, this conventional system has not given satisfied luminance.

In this paper, a new concept, the highly scattered optical-transmission (HSOT) polymer, is proposed as a new light source medium. The HSOT polymer materials were prepared by the polymerization of MMA including a small amount of polymer with a different refractive index (ex. polystyrene (PSt), polybenzyl methacrylate (PBzMA), poly2,2,2-trifluoroethyl methacrylate (P3FMA)).

The Vv light scattering from polymer glass is correlated to specified microscopic heterogeneity having the correlation function of $\gamma(r)$ as written by[2)]

$$V_V = \left(\frac{4\langle \eta^2 \rangle \pi^3}{\lambda_0^4} \right) \int_0^\infty \frac{r^2 \sin(vsr)}{vsr} \gamma(r)\, dr \qquad (1)$$

where λ_0 is the wavelength of the incident light, $v = (2\pi n) / \lambda_0$, $s=2\sin(\theta_{sca} / 2)$, n the refractive index of the medium, θ_{sca} a scattering angle, $\langle \eta^2 \rangle$ a mean square of the dielectric constant fluctuation in the medium.

Provided that the HSOT polymer consists of phases A and B, then

$$\langle \eta^2 \rangle = \phi_A \phi_B \left(n_A^2 - n_B^2 \right)^2 \qquad (2)$$

$$\gamma(r) = \exp(-r / a) \qquad (3)$$

where ϕ_A and ϕ_B are volume fractions of phases A and B, and n_A and n_B are the refractive indices of phases A and B, respectively. A symbol "a" is a correlation length expressed by $a=(4V/S)\phi_A\phi_B$, V is a total volume, and S is a total area of the interface between phases A and B.

The above relationship indicates that an increase in the size of heterogeneous structure strengthens the forward scattering intensity. The calculated result is shown in Figure 1.

Application to the LCD Backlight

Figure 2 shows the luminance angular dependence from the surface of the HSOT polymer plate including a small amount (0.2-0.4wt%) of P3FMA, PBzMA, or PSt (These are 4 inches LCD backlights which have two lamps on both edges.). In this figure, θ (differ from θ_{sca} in the equation (1)) means the angle between scattering direction and the normal of the surface. The better solubility with PMMA, the smaller the size of the heterogeneous structure. The HSOT back-light system including PBzMA which has a good solubility with PMMA has small heterogeneous structures (submicron correlation length). Therefore, as can be seen from Figure 1, the incident light is scattered in a wide range of angles, providing a high luminance in the vertical direction of the surface (Figure 2 (c)). On the other hand, the HSOT back-light system including P3FMA which has a large correlation length (a few microns) in PMMA has almost uniform luminance in the wide angle (Figure 2 (a)) because the forward scattering is dominant and two lamps are located at both edges of the HSOT plate.

All conventional edge-light type backlight systems have consisted of a transparent PMMA plate as a waveguide and surrounding light-controlling devices (such as diffuser film and dot printing etc.). Our proposal is to use only the HSOT polymer plate without other light-controlling devices used in conventional backlight systems.

The conventional LCD backlight which has two lamps placed at both edges of the waveguide plate (transparent PMMA) is shown in Figure 3 (a). The complicated dot printing pattern is necessary at the bottom of the PMMA-waveguide plate to obtain uniform luminance. Further, a diffuser film is indispensable to hide the dot printing pattern. On the other hand, the backlight system consisting of one HSOT polymer plate which is equivalent to (a), is shown in (b).

Results and Discussion

Although the thickness of the HSOT polymer plate is constant, the luminance is almost uniform all over the surface of plate. It is suggested that the high-order scattering would make the luminance from the surface uniform. This scattering phenomenon inside the HSOT polymer was exactly confirmed by the Monte Carlo simulation[3] using Mie scattering. The calculated result is shown in Figure 4 (a), in which a laser beam is injected to the HSOT polymer from the left-hand side. Figure 4 (b) shows this experimental result. It is recognized that the luminance on the right side is almost uniform. These figures show that the HSOT polymer has a bright and uniform luminance because of the homogenization effect of the high-order scattering.

Table 1 summarizes the comparison of luminance between the conventional (Figure 3 (a)) and the HSOT (Figure 3 (b)) backlight systems. The intensity of illumination from the backlight system using the HSOT polymer plate is about 50% brighter than that of the commercially available one. Further, the color temperature of the former is about 7500K which is higher than the color temperature of the latter by 700K. Figure 5 shows the comparison of the luminance between the conventional backlight (with dot printing pattern, diffuser film, and prism film)(A) and the HSOT backlight (only with prism film)(B) with using the same cold fluorescent lamp on upper edge. This result suggests that the conventional concept that the transparent materials are necessary for transmission media of light source should be carefully reviewed.

Conclusion

For optical-transmission media of light source, it has been believed that a transparent waveguide such as PMMA has been indispensable.
We propose a new concept, the HSOT polymer, as a new light source medium. The incident beam is effectively converted to the homogeneous illumination from the HSOT polymer during transmission of light. The luminance from the HSOT polymer plate is more than 50% brighter than that of the conventional PMMA plate system.

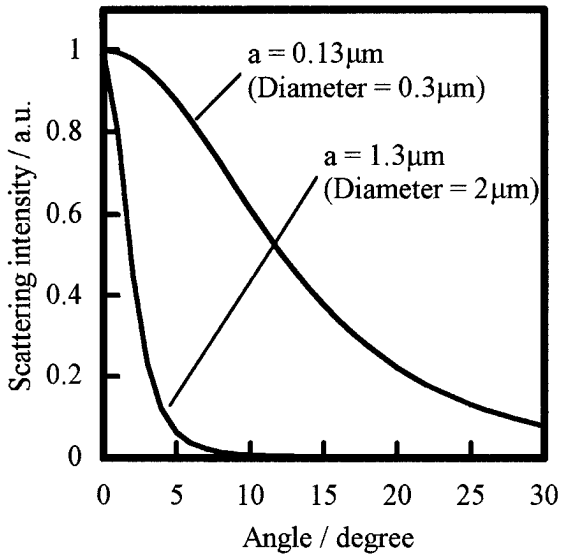

Figure 1. Angular dependence of scattering intensity.

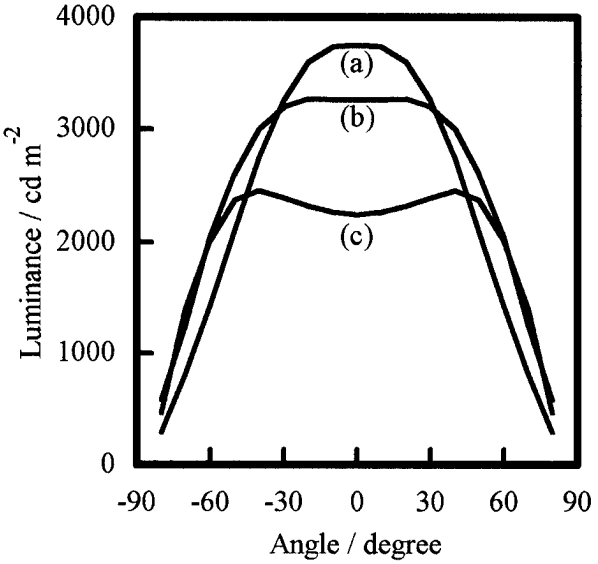

Figure 2. Angular dependence of luminance of backlight devices consisting of HSOT polymer plate.
(a) PMMA / PBzMA
(b) PMMA / PSt
(c) PMMA / P3FMA

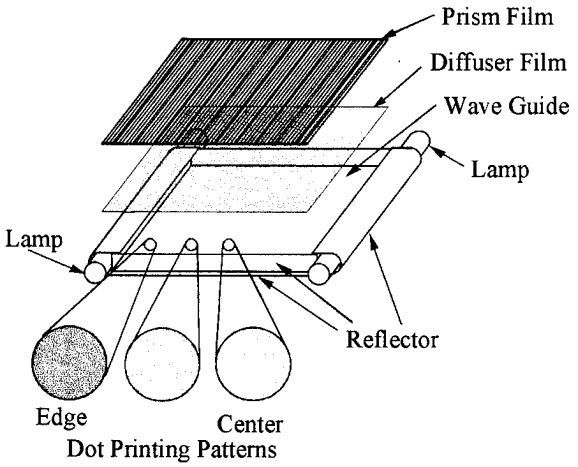

(a) Conventional system

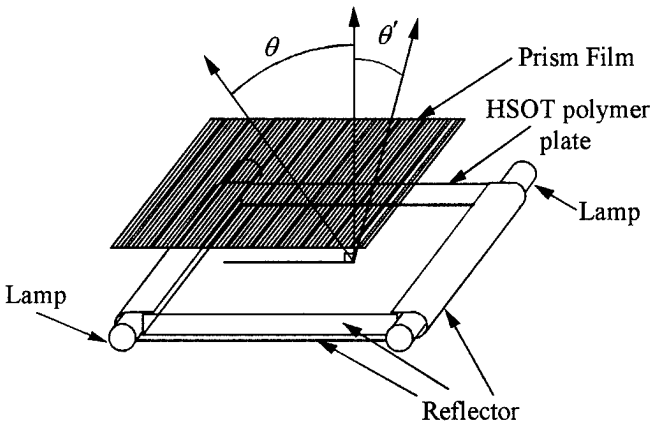

(b) HSOT system

Figure 3. The diagram of the backlight systems.

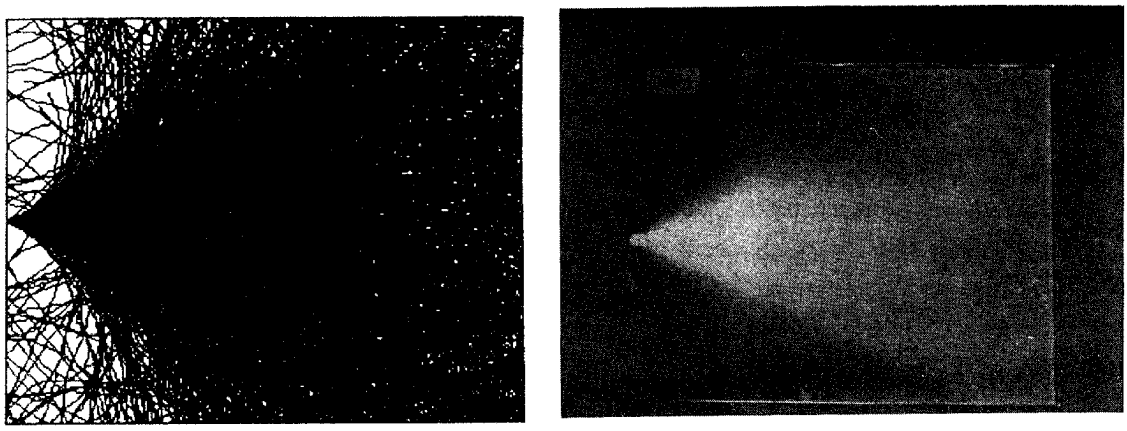

(a) Calculated result (b) Experimental result

Figure 4. High-order scattering in the HSOT polymer.

Table 1 Luminance and correlated color temperature of backlight systems.

Polymer plate	Luminance ($cd\ m^{-2}$)	Normalized luminance (%)	Color temperature (K)
Conventional	4498	100	6750
PMMA/P3FMA	6826	152	6800
PMMA/PBzMA	6758	151	7800
PMMA/PSt	6739	150	7700

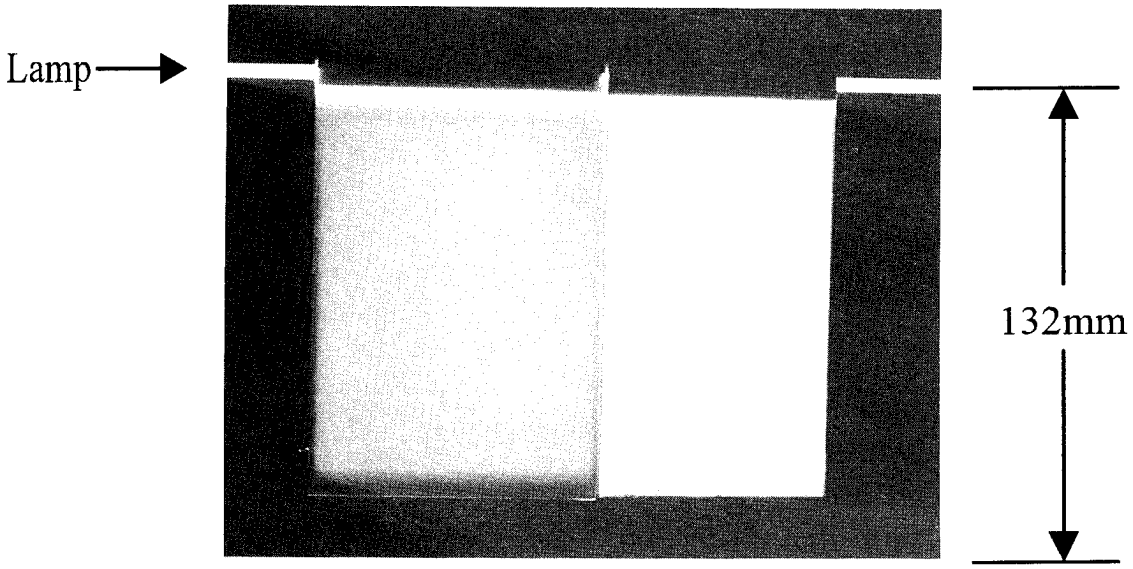

(A) (B)

Average of luminance 806cd/m^2 1583cd/m^2

Figure 5. Photograph of conventional (A) and new HSOT (B) backlights.

References

1. Y. Koike, S. Matsuoka, H. E. Bair, Macromolecules, p.4807 (1992).
2. P. Debye et al., J. Appl. Phys., p.679 (1957).
3. J. Briton, B. Maheu, G. Grehan, G. Gousbet, Part. Part. Syst. Charact., p.52 (1992)

Tuesday, September 12, 1995

Symposium on Displays Based on Organic Thin Films II

(Joint with OSA Annual Meeting)

TuC 9:45am–11:15am
Holladay Room

Stephen R. Forrest, *Presider*
Princeton University

Optical Alignment of Liquid Crystal Displays and Devices Via Polarized Light

Wayne M. Gibbons, Paul J. Shannon, and Shao-Tang Sun
Alliant Techsystems, Research Center, 500 Hercules Road, Wilmington, DE 19808
Phone:(302) 995-3825
Fax:(302) 995-4102

The optical alignment of liquid crystals provides spatial and angular control of the local liquid crystal director.[1-3] This is achieved by properly designing photosensitive polymer alignment layers. These photosensitive alignment polymers are illuminated with polarized light which alters the bulk and surface properties of the polymer. The liquid crystal molecules adjacent to the alignment polymer interact with the altered polymer and align accordingly. The long range interaction of the liquid crystal molecules transfers the aligned state at the interface to the bulk of the liquid crystal layer. Since the alignment polymer itself is altered, the liquid crystal remains aligned after the illumination is terminated. With the proper design of the alignment material, the process is reversible allowing for the potential of real-time write/re-write control of the local liquid crystal director.

We will discuss the use of optical alignment as a non-contact method to align liquid crystal displays and devices. Liquid crystal displays and devices require uniform alignment of the liquid crystal molecules in the absence of an electric field.[4] The resulting birefringence of the aligned liquid crystals give the desired passive optical properties of the device. Under the influence of an electric field, the local alignment direction is changed and, as a result, the local birefringence changes.[5] The changes in birefringence are used to modulate the phase and/or amplitude of the light passing through the device.

In general, the uniform alignment of the liquid crystals is achieved by mechanical buffing. Here, a cloth is rubbed unidirectionally across an alignment polymer which is subsequently placed adjacent to the liquid crystal molecules when the device is fabricated. The rubbed alignment polymer interacts with the liquid crystal causing it to align along the rub direction. By its nature, mechanical buffing typically has low spatial resolution, creates static electricity which can damage certain liquid crystal devices, and is a source of contamination (e.g., dust). These issues subsequently limit the type and yield of liquid crystal devices that can be manufactured using mechanical rubbing techniques. Optical alignment techniques overcome these limitations of mechanical buffing.

To replace mechanical buffing with optical alignment in liquid crystal displays, issues such as the pretilt angle, the uniformity of the liquid crystal alignment, the dielectric properties, and color of the optically controlled alignment polymer all need to be addressed. Other issues of importance are the optical energy density requirements to align the liquid crystals and, the optical and thermal stability of the optical alignment polymer.

The pretilt angle is the angle the liquid crystal molecules align relative to the plane of the alignment layer. In active matrix liquid crystal displays (AMLCDs), the pretilt angle must be uniform across each pixel and along the same direction for all the pixels in the display to get good electro-optical performance.[6] Desired pretilt angles range from 4-6

degrees for AMLCDs, but often values of 2-4 degrees are considered acceptable. We have optically generated pretilt angles that range from 0 to 10 degrees depending on the alignment material and the processing conditions. Usually, we observe a degradation in liquid crystal alignment uniformity with the higher pretilt values.

Early optical alignment materials developed by us contained azo chromophores which gave films that were slightly colored. For liquid crystal displays, this was considered undesirable. We have subsequently developed colorless optical alignment polymers that uniformly align liquid crystals. These systems are being investigated for use in AMLCDs.

The dielectric properties of the optical alignment polymer are important for the electro-optical performance of AMLCDs. In particular, switching times and voltages, and the voltage holding ratio are measured to see if the alignment materials meet the requirements of AMLCDs. Voltage holding ratios measure the alignment polymers ability to maintain the voltage on the liquid crystal during one refresh cycle of the display. Typically, it is desired that the value be at $\geq$95% of the initial applied voltage during the time between refresh of the pixels. Conductivities of the alignment polymer must be low and the alignment polymer must not contaminate the liquid crystal with impurities that will decrease the resistivity of the liquid crystal.

Optical energy density requirements must be low enough to allow a reasonable throughput of the devices during manufacturing ($\geq$ 1 substrate/minute) but at the same time high enough to prevent realignment during normal operating conditions. We have found that the optical alignment of liquid crystals demonstrate a thresholding behavior which can prove advantageous for the manufacturing of devices. The thermal stability of the alignment polymer must have a short term stability in excess of the maximum temperature excursion of subsequent process steps, and a long term stability in excess of the maximum storage temperature of the display.

The high resolution of the optical alignment process allows for the development of the next generation liquid crystal displays and devices difficult to manufacture using existing alignment techniques. Multi-domain liquid crystal displays utilize multiple alignment directions within a single pixel to improve viewing angle characteristics of the display. Although this can be achieved with standard mechanical buffing techniques, it involves a multi-step process that is time consuming and difficult to implement. Optical alignment can greatly simplify the process. We are investigating this application for our alignment polymers.

Other applications for liquid crystals enabled by optical alignment include diffractive optical elements[3], holograms, and optical memory storage media. Issues different from those involving displays must be addressed for these applications. However, the similarity in requirements allows one to leverage the development effort for liquid crystal displays.

References:

1. Gibbons, W.M., Shannon, P.J., Sun, S.T. & Swetlin, B.J. *Nature* **351**, 49-50 (1991).

2. Shannon, P.J., Gibbons, W.M. & Sun, S.T. *Nature* **368**, 532-533 (1994).

3. Gibbons, W.M. & Sun, S.T. *Appl. Phys. Lett.* **65**, 2542-2544 (1994).

4. Cognard, J. *Molec. Cryst. Liq. Cryst.* **51**, 1-77 (1982).

5. DeGennes, P.G. & Prost, J. *The Physics of Liquid Crystals* (Clarendon, Oxford, 1993).

6. O'Mara, W.C. *Liquid Crystal Flat Panel Displays* (Van Nostrand Reinhold, New York, 1993).

TN and GH-LCDs Fabricated by Non-Rubbing Techniques and an Overview of LCDs in Japan

S.Kobayashi, Y.Iimura, T.Saitoh, H.Suzuki, T.Hashimoto*, T,Sugiyama*, and K.Katoh*

Faculty of Technology, Tokyo University of A&T, Koganei, Tokyo 184, Japan

*) Stanley Electric Co., Ltd., Yokohama Kanagawa 225, Japan

Abstract

Amorphous TN(twisted by 90°) and amorphous highly twisted chiral nematic (N*)(twisted by 300°) are utilized for fabricating TN and GH-LCDs, respectively, and furthermore, photopolymer films are utilized for fabricating TN-LCD and hybrid aligned N-LCD. These NLC alignment techniques are non-rubbing techniques and they make it possible to overcome the disadvantages of current rubbing technique. An overview of LCDs in Japan is also given.

1. Introduction

Nowadays, TN and STN-LCDs are widely utilized as useful information displays. Currently, they are manufactured using rubbing technique which is done by buffing or rubbing LC alignment layers (such as polyimide films) with fabrics such as nylon cloths. This rubbing process generates dusts and static electric charges that degrades manufacturing environment and damages thin film switching devices for active matrix LCDs.

There are several non-rubbing techniques, among them we devised the formation of amorphous TN structure and the unidirectional alignment of NLC with pretilt angle using photopolymer films.

2. Experimentals and results

2.1 Amorphous TN-LCD

An NLC doped with a chiral agent to give 90° twist is filled into a cell at the isotropic state, where the inner surfaces of the cell are covered with un-rubbed polyimide films, and then the NLC is cooled down to room temperature. The NLC medium formed in this way consists of twisted columns whose diameter is comparable to the thickness of LC layers (5μm). The director of the NLC molecules are almost continuous in the boundaries between columns are almost continuous, but no coherence existist between two distant columns. For this structure, the medium is called amorphous (a) TN medium. This a-TN-LCD medium is shown to be useful to fabricated a TN-LCD featuring uniform viewing angle and an excellent grayscale capability. These behaviors are fully described fully in the literature. [1]

2.2 Amorphous N*-GH-LCD

In 1974, White and Taylor devised a guest host LCD using highly teisted NLC as a host medium to enhance the optical absorption by dichroic dye molecules.[2]

Recently the authors established an idea to use a-N* medium with 300° twist for GH-LCD.[3]

The results are splendid imagination our exception. As shown in Fig.1, the EO performance of a-N*-GH-LCD (with 300° twist) exhibits hysteresis free and the free from the stripe domains; both of them appear in a mono-domain White-Taylor type GH-LCD with the same 300° twist.

Resently, by using a developed black dye, we obtaied a result better data than those shown in Fig.1, the obtained reflectivity at 10V is 45°% due to the polarizer free and the obtained contrast retio is 8:1; these apecifications are almost the same as those of news papers.

2.3 TN-LCD with quartered subpixels fabricated by using a photopolymer

As a preliminary research, we adoped a photopolymer, polyvinylcinnamate (PVCi) which first reported by Schadt etal.[4]

We devised a way to generate a pretilt angle by performing the combination of double exposure and slanted illumination of UV light on the PVCi films.[5]

Fig.2 shows a microphotograph of a part of a matrix TN-LCD whose pixels are divided into four parts that promises a uniform viewing angle and a good grayscale capability. As is shown in Fig.2, the position of reverse tilt disclinatious is completely controlled.

The research on other photopolymer materials is now underway and the results will be published elsewhere.

2.4 Hybrid N-LCD with dual subpixels

Using the combination of photopolymer films and an NLC alignment agent for homeotropic alignment, we fabricated a hybrid N-LCD operated in tunable birefringence mode. By dividing each pixel into two parts and by adopting an optical compensation films, it is possible to fabricate a N-LCD showing wide viewing angle, an excellent grayscale capability, and a high speed response.

3. An overview of LCDs in Japan

The amount of sale of LCD by Japanese manufactures will reach 10B$ in 1995. The motive force for LCD manufacturing is to produce displays for personal computers, AV imstruments, and car navigation. Some detailed investements for LCDs and some new technologies are introduced and discussed.

References

1. Y.Toko et al, J.Appl.Phys.74(1993)2071.

2. D.L.White and G.N.Taylor, J.Appl.Phys.45(1974)4718.

3. H.Koimai et al 1995 SID Digest 26(1995)699.

4. M.Schadt et al, Jpn.J.Appl.Phys. 31(1992)2155.

5.T.Hashimoto et al 1995 SID Digest 26(1995)877.

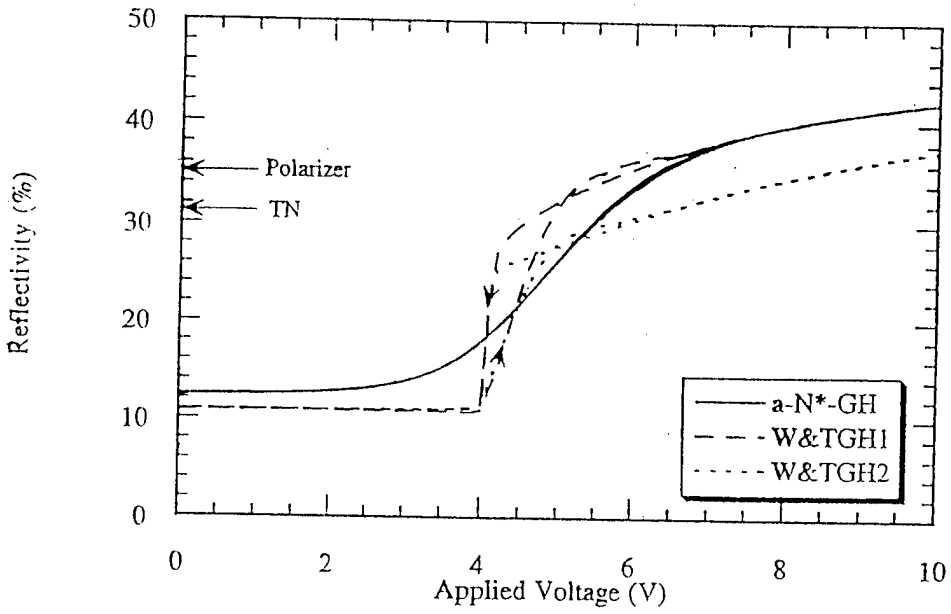

Figure 1 Reflectivity of various LCDs versus applied voltage.

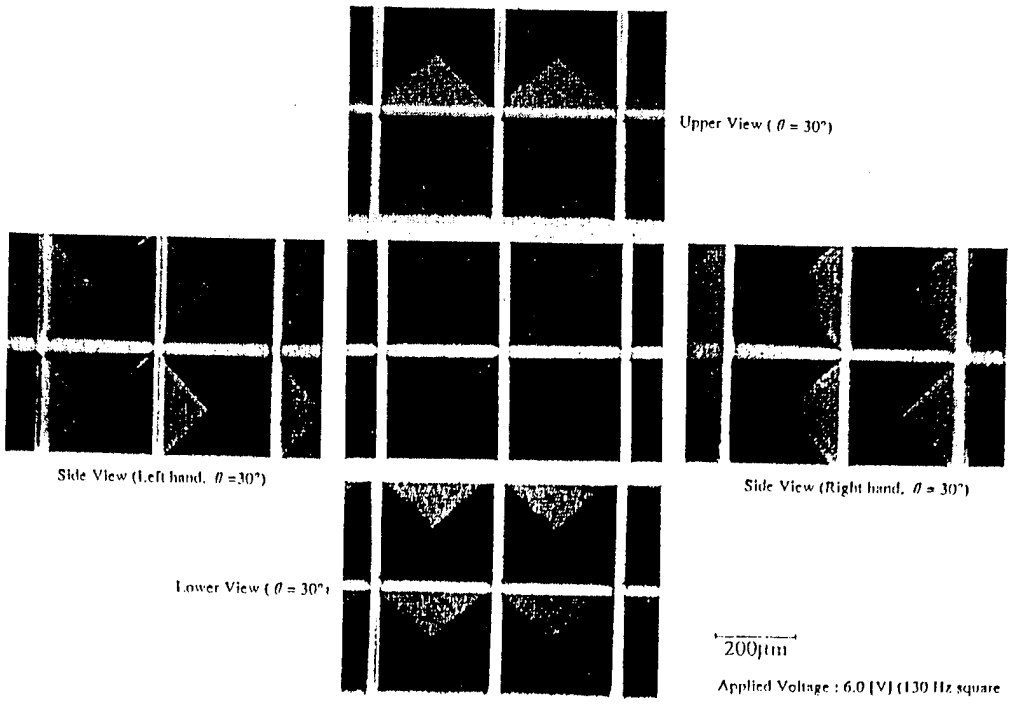

Figure 2 Microphotographs of a part of dot-matrix TN-LCD with QSPs fabricated using UV irradiated PVCi films showing a pretilt angle. Photos are taken from five different directions.

ELECTROLUMINESCENCE FROM ORGANOMETALLIC THIN FILMS

R. A. Campos, I. Kovalev, N. Wakili, Y. Guo and T. Skotheim
Moltech Corporation, 25 East Loop Road, Stony Brook, New York 11790

INTRODUCTION - Efficient electrical conversion into a wide range of optical wavelengths as well as low fabrication costs are some of the attractions of organic thin films which drive the use of these materials for flat-panel display applications [1]. Since the pioneering work of Tang and VanSlyke in 1987 [2], the organometallic material tris-(8-hydroxyquinoline)-aluminum (ALQ) has been the focus of intense research. This compound electroluminesces in the green region of the spectrum over a broad spectrum peaked near 520 nm. Although ALQ microcavity architectures can provide narrowband emissions at select wavelengths [3], the resulting brightnesses in the blue and red regions are limited by the decreasing spectral content in the tails of the ALQ emission spectrum.

An alternative approach is to employ organic materials, such as organometallic complexes of the rare earths, which by their own nature provide narrowband spectral emissions. In previous work we have explored the suitability of trivalent europium for electroluminescence device applications [4]. The $^5D_0$-$^7F_2$ transition of this atom provides a sharp (~ 40 nm bandwidth) line emission near 610 nm, which is perceived as orange-red in color. In this report we compare the performance of the complex (1,10-phenanthroline)-tris-(4,4,4-trifluoro-1-(2-thienyl)-butane-1,3-dionate)-europium (III) [Eu(TTFA)(P)] with that of ALQ in device architectures containing the diamine hole transport material TPD (N,N'-diphenyl-N,N'-bis-(3-methylphenyl)-1,1'-biphenyl-4,4'-diamine), an indium-tin-oxide (ITO) anode, and an aluminum cathode.

EXPERIMENTS - Figure 1 shows the chemical structures of the organic materials and the architecture of the electroluminescence cells used in this work. ALQ was obtained commercially from TCI America, while TPD and Eu(TTFA)(P) were synthesized in house starting from Aldrich reagents. The substrates are 1-inch-square pieces of Balzers soda lime float glass coated with a 110-nm thick layer of ITO providing 30 Ω sheet resistance. After etching in acid, the ITO-coated substrate is washed in toluene for degreasing and placed in an ultrasonic cleaner for 20 minutes in toluene and 20 minutes in acetone. It is then dried in a vacuum oven and promptly loaded into the vacuum chamber at 25 cm from the sources.

The thermal evaporations for both organics (~ 0.2-0.5 nm/sec) and metals (~ 0.8-1.0 nm/sec) were carried out inside a Harris Environmental Systems dry room with relative humidity < 2% using a diffusion-pumped vacuum system cooled by liquid nitrogen, providing typical base pressures of $\leq 10^{-7}$ Torr. The layer thicknesses were monitored *in vacuo* via an Inficon XTM/2 instrument using density estimates from pressed pellets of the organic

materials. The organic film thicknesses were measured via a Veeco/Sloan Dektak[3] surface profiler and found to be on average within 2 nm of the corresponding XTM/2 values.

The aluminum cathode was evaporated in a separate vacuum run through a 0.005-inch thick molybdenum mask capable of patterning contacts for four electroluminescence cells. Each contact is composed of a 5-mm square pad which is clipped to the external driving circuit; these pads are connected via a 1 mm channel to a smaller 3-mm square pad which defines the emission region.

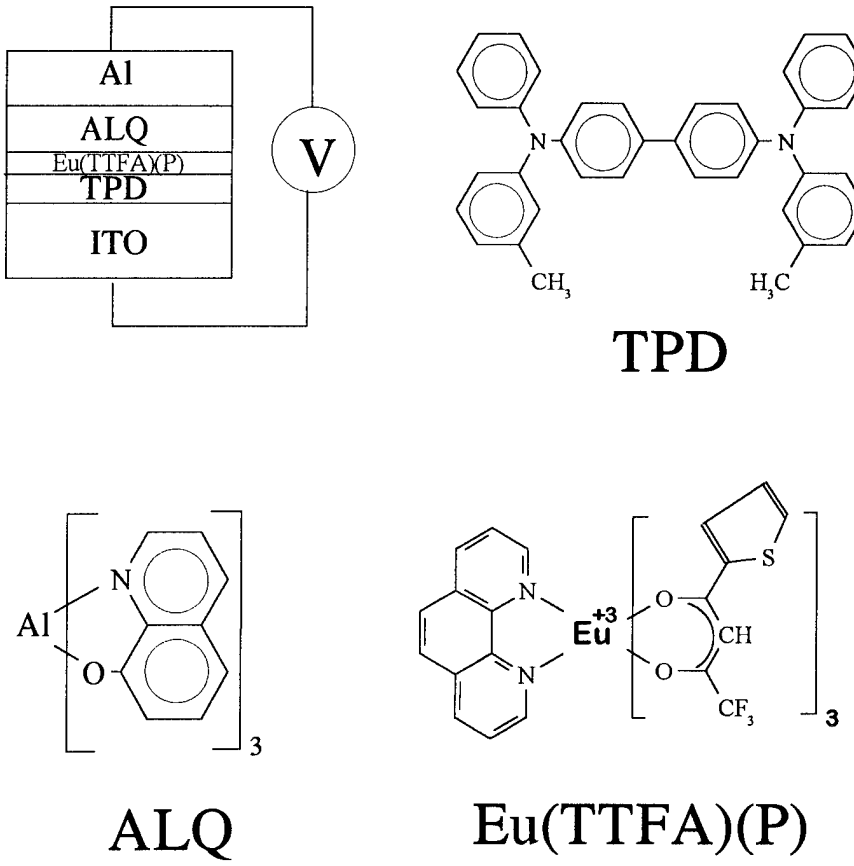

FIGURE 1 - Shows the chemical structures of the organic materials used in our electroluminescence cells, and the layered architecture of these devices.

The finished electroluminescence cell is then transferred to a VAC glove box that provides a controlled neutral argon atmosphere for testing. The cell bias is applied via an HP E3611A dc power supply and a Keithley 175A autoranging multimeter is used for current measurements. Cell luminances are determined under dark conditions through the plexiglass front end of the glove box with a Minolta LS-110 luminance meter and a closeup lens defining a 1.3 mm diameter focal region from a distance of 345 mm. The plexiglass has a transmittance > 90% through the visible spectrum.

DISCUSSION - ALQ has dual specificity as an emitter as well as an electron transport material. Tang *et. al* demonstrated the utility of placing a thin emitter layer (*e.g.*, ALQ itself doped with organic dyes such as DCM for broadband red emission) between TPD and ALQ for multicolored electroluminescence [5]. Tsutsui *et. al.* recently utilized this particular strategy to obtain red emission from a 12 nm layer of a modified Eu(TTFA)(P) complex sandwiched between TPD and ALQ, and a magnesium-silver cathode [6].

In Figure 2 we present electrical and optical data for TPD/ALQ electroluminescence cells with and without a sandwiched layer of Eu(TTFA)(P). The cell structures are ITO // TPD (30 nm) / ALQ (57 nm) // Al (76 nm) and ITO // TPD (31 nm) / Eu(TTFA)(P) (5 nm) / ALQ (50 nm) // Al (81 nm), where the double slash (//) delineates separate runs in the vacuum system. By varying the layer thickness of Eu(TTFA)(P) from 3 to 22 nm we have determined that a 5 nm layer of the material provides the optimal performance.

The luminance-voltage data for these cells are shown in Fig. 2(a). The inclusion of the europium layer (black dots) has clearly raised the turnon voltage relative to ALQ (gray dots) by 6 V, indicating the presence of an additional barrier to carrier injection that is contributed by the europium layer. Both cells, however, demonstrate similar power-law behavior of high order, which are suggestive of trap-modified space-charge limited conduction [7]. Straight-line fits to the double logarithmic plots of Fig. 2(a) yield optical power laws of +14.4 and +16.6 for the cells with and without the europium layer, respectively. The luminance decay data at fixed voltage for these cells indicates similar behavior as a function of time: inverse power laws of magnitude -0.6 and -0.84, respectively [Fig. 2(d)].

We have seen no indication of green electroluminescence in this europium cell, suggesting an exciton confinement to 5 nm. This is in agreement with multilayer studies by Tang *et. al.*[5]. From the luminance-current density data of Fig. 2(b), we note a significant improvement in electrical to optical conversion from our earlier studies of Eu(TTFA) dispersed in the hole transporting polymer poly-(methylphenylsilane), shown by the unshaded white dots. Our results are comparable to the electroluminescence data from the europium cell reported by Tsutsui [6] (shown by the black triangle).

A continued study of europium complexes will determine whether additional improvements in optical conversion can be achieved with this class of materials. *We acknowledge support from the National Science Foundation via contract number III-9208591.*

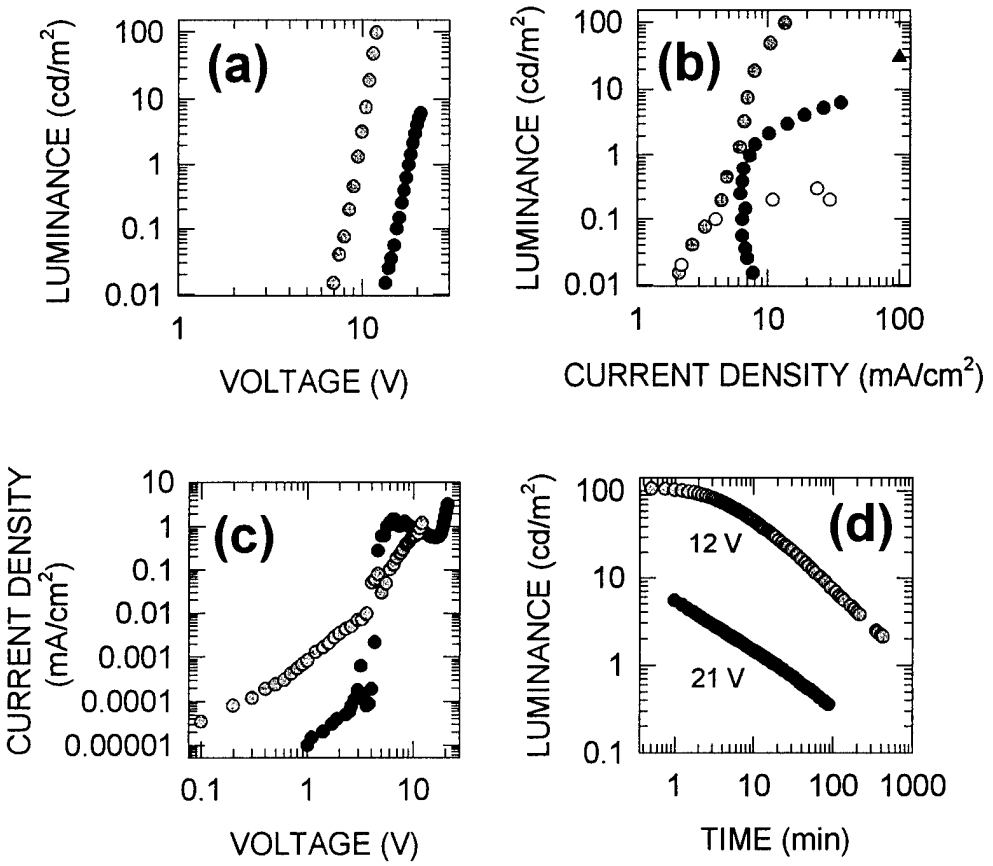

FIGURE 2 - (a) Luminance-voltage, (b) luminance-current density, (c) current density-voltage and (d) luminance-time characteristics for electroluminescence cells composed of ITO//TPD/ALQ//Al (gray dots) and ITO//TPD/Eu(TTFA)(P)/ALQ//Al (black dots). The white dots and the black triangle in part (b) are electroluminescence data for europium abstracted from References 4 and 6.

REFERENCES

[1] S. R. Forrest, P. E. Burrows and M. Thompson, "Organic emitters promise a new generation of displays," *Laser Focus World* (February 1995) p. 99.

[2] C. W. Tang and S. A. Van Slyke, *Appl. Phys. Lett.* **51**, 913 (1987).

[3] A. Dodabalapur, L. J. Rothberg and T. M. Miller, *Appl. Phys. Lett.* **65**, 2308 (1994)

[4] J. Kido, K. Nagai, Y. Okamoto and T. Skotheim, *Chem. Lett.* 1267 (1991); J. Kido, K. Nagai and Y. Okamoto, *J. All. Comp.* **192**, 30 (1993).

[5] C.W. Tang, S.A. Van Slyke and C.H. Chen, *J. Appl. Phys.* **65**, 3610 (1989).

[6] T. Tsutsui, N. Takada, S. Saito and E. Ogino, *Appl. Phys. Lett.* **65**, 1868 (1994).

[7] P.E. Burrows and S.E. Forrest, *Appl. Phys. Lett.* **64**, 2285 (1994).

Accelerated Degradation Studies of MEH-PPV*

H.B. Radousky, A. D. Madden, K. Pakbaz, T. W. Hagler,
H. W. H. Lee, H. E. Lorenzana, G. A. Fox, and P. R. Elliker
Lawrence Livermore National Laboratory, Livermore, CA 94551, USA;

MEH-PPV is of interest due to its potential use as the active element in electroluminescent devices.[1] The usefulness of these devices is limited at the present due to a variety of degradation mechanisms.[2-3] We have studied one class of degradation in MEH-PPV using photoluminescence (PL).

MEH-PPV, which normally has a reddish color, is well known to show photobleaching problems. The photobleaching can be greatly accelerated by exposure to laser light while in air. For example, shining 457 nm light of relatively low intensity (20 μW over a 100 micron diameter spot) on the MEH-PPV causes the photoluminescence to decrease by a factor of two within a few seconds of exposure, and to show a nearly complete bleaching of the material within 30 minutes. We also observe a strong shift of the PL spectra to the blue, which is consistent with a shortening of the effective conjugation length.[4-5]

The degradation rate in MEH-PPV was observed to be strongly influenced by sample thickness, oxygen exposure during preparation and spin casting, laser power, as well as the oxygen environment during the measurement. The measurements were performed using a sample chamber which could be maintained under vacuum, or filled with specific gases. The oxygen content was controlled by introducing premixed gases with 0.1%, 0.3% and 0.8% oxygen in nitrogen, as well as pure oxygen.

MEH-PPV which was spin coated in a nitrogen environment, as well as measured in vacuum, showed no measurable photo-chemical degradation. This is illustrated in Figure 1, which compares the reduction of the PL peak with time for this sample measured in vacuum

and in air. For MEH-PPV films spin coated in air, we find that degradation occurs even when measured in vacuum.

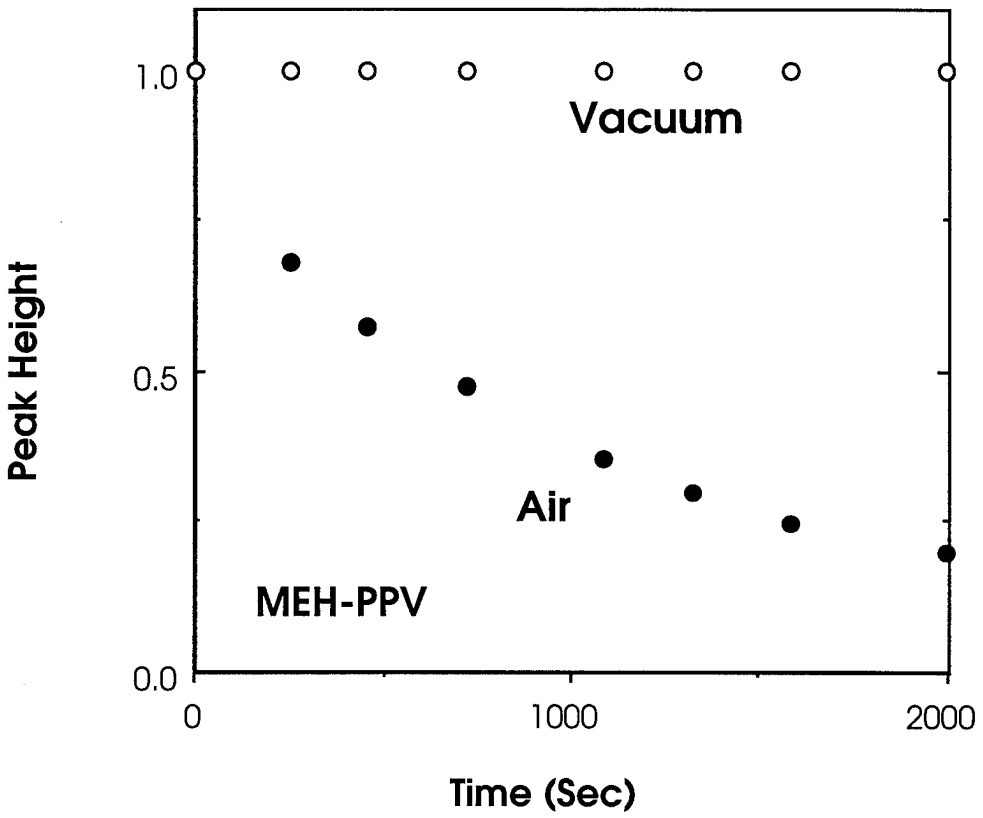

Figure 1 - Decrease in the PL peak height for a MEH-PPV film which was spin-coated under nitrogen.

References

1. D. D. C. Bradley, Synthetic Metals, 54, 401 (1993).
2. M. Yan, L. J. Rothberg, F. Papadimitrakopoulos, M. E. Galvin and T. M. Miller,
Phys. Rev. Lett., 73, 744 (1994).
3. H. Antoniadis, L. J. Rothberg, F. Papadimitrakopoulos, M. Yan and M. E. Galvin, Phys. Rev. B 50, 14911 (1994).
4. K. Pakbaz, C. H. Lee, A. J. Heeger, T. W. Hagler and D. McBranch, Synthetic Metals, 64, 295 (1994).
5. T. W. Hagler, K. Pakbaz and A. J. Heeger, Phys. Rev. B 49, 10968 (1994).

Work at LLNL was performed under USDoE contract no. W-7405-ENG-48.

Tuesday, September 12, 1995

Chromophores I

TuD 1:30 pm-3:30 pm
Holladay Room

Charles Y.-C. Lee, *Presider*
U.S. Air Force Office of Scientific Research

EXPERIMENTAL AND THEORETICAL STUDIES OF NONLINEAR OPTICAL CHROMOPHORES

M. Ahlheim,[a] J.-L. Brédas,[b] M. Barzoukas,[c] P. V. Bedworth,[d] Y. Cai,[e] C. Dehu,[b] M. Blanchard-Desce,[f] A. Fort,[b] Z. Hu,[d] A. K.-Y. Jen,[e] S. R. Marder,[d,g] F. Meyers,[b,d] J. W. Perry,[d,g] C. Runser,[c] M. Staehelin,[a,h] and B. Zysset[a]

a: Sandoz Huningue S. A., Avenue de Bale, F-68330 Huningue, France.

b: Université de Mons-Hainaut, Place du Parc 20, B-7000 Mons, Belgium.

c: IPCMS, 23, rue du Loess, F-67037, Strasbourg Cedex France.

d: The Beckman Institute, California Institute of Technology, Pasadena, CA 91125.

e: ROI Technologies, Monmouth Junction, New Jersey 08852.

f: Ecole Normale Supérieure, 24 rue Lhomond 75231 Paris Cedex 05, France.

g: The Jet Propulsion Laboratory, California Institute of Technology, Pasadena, CA 91109.

h: Institute of Physics, University of Basel, Klingelbergstrasse 82, 4056 Basel, Switzerland.

We have described how the first hyperpolarizability, β, varies as a function of ground-state polarization and bond length alternation, BLA.[1] Previously, our predictions of this relationship were derived by examining an prototypical push-pull polyene under the presence of static homogenous electric field.[1] In order to develop a more realistic understanding of how real molecules behave in solution, we have now examined both p-nitroaniline and the push-pull polyene 1,1-dicyano-6-dibutylamino-hexatriene at the Hartree Fock *ab initio* level on the basis of an expanded Self Consistent Reaction-Field approach to simulate solvents with dielectric constants up to 37.5. The calculations were carried out using both spherical and elliptical cavities and taking into account multipole interactions up to 2^6 poles. Predictions were compared to Hyper-Rayleigh Scattering (HRS) results determined by Persoons *et al.* As had been shown earlier,[2] the second-order NLO response of 1,1-dicyano-6-dibutylamino-hexatriene exhibits a peak as a function of solvent polarity, which was confirmed by the HRS measurements. Interestingly, we found that this peaked behavior of β as a function of solvent dielectric constant was predicted only when an elliptical cavity and the up to $l = 6$ pole contributions were taken into account, but was not observed when the calculations employed either an elliptical cavity and a

dipole (l = 1) approximation, or a spherical cavity with up to l = 6 pole contributions. These results suggest that it is possible to model the geometric and electronic structure of polarizable molecules using a Self Consistent Reaction-Field approach, but it is necessary to build into the calculations mechanisms to account for the subtleties of the molecular charge distributions, not taken into account within a simple dipole approximation.

In our continuing attempts to develop structure property relationships and to identify highly nonlinear molecules, we have synthesized several chromophores containing the [3-(dicyanomethylidenyl)-2,3-dihydrobenzothiophen-2-ylidenyl-1,1-dioxide acceptor in Figure 1. The compounds incorporating this acceptor have large β, even in comparison to compounds with the very strong acceptor N, N'-diethylthiobarbituric acid (series **2[n]**)[3] as measured by electric field induced second harmonic generation, (EFISH), in chloroform, with 1.907 μm fundamental radiation. For example, compound **5** below had a $\mu\beta = 13{,}500 \times 10^{-48}$ esu. In comparison, compound **4** had a $\mu\beta = 640 \times 10^{-48}$ esu.

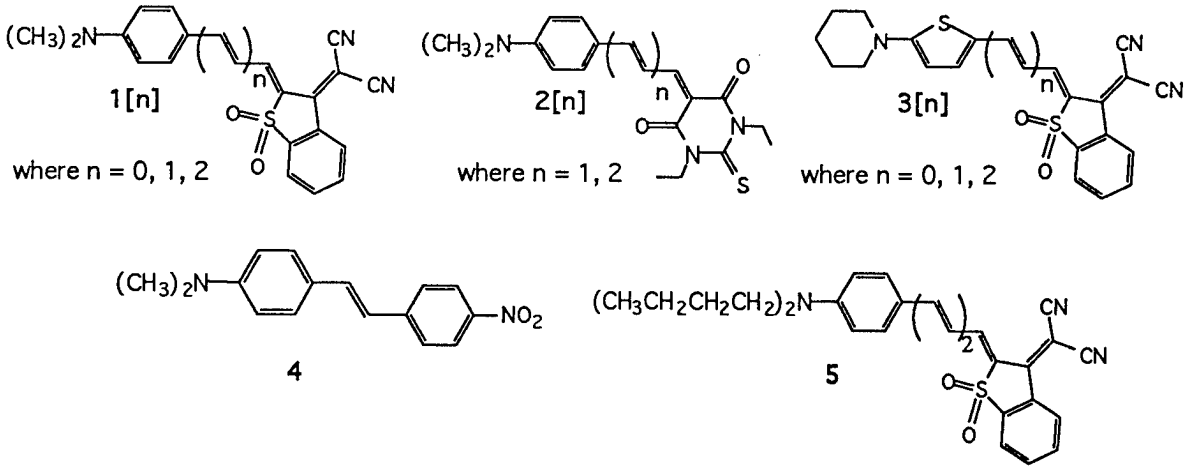

Figure 1. Molecular structure of donor-acceptor polyenes.

A polycarbonate (PC) film containing 20 weight percent of **5** was spin coated onto an indium tin oxide coated slide and a thin film of gold was deposited on top of the polymer as the second electrode. The chromophore-PC composite was poled at 80°C with an applied field of 150 V/μm. After cooling the sample to ambient temperature, the electro-optic coefficient was determined at 1.313 μm using modulated ellipsometry.[4] This resulted in a r_{33} value of 55 pm/V for the polymer, substantially larger than any value reported previously. Measurements as a function of the static phase shift between s and p waves showed that the electro-optic coefficient had essentially no (< 1%) imaginary component. A sample kept at room temperature showed an

initial decay of the electro-optic coefficient to 85% of initial value 100 hours after poling and gave the same value after 300 hours. Nonetheless, we expect that the low glass transition temperature of the polymer (approximately 80°C) will preclude its use in commercial devices. The initial electro-optic coefficient is roughly twice that of lithium niobate, demonstrating that organic poled polymers based upon highly nonlinear chromophores can have electro-optic coefficients far in excess of this technologically important inorganic crystal at a telecommunication wavelength. We are currently exploring derivatives related to **5** which may have both large $\mu\beta$ products and improved thermal stability, relative to **5**, such that they can be incorporated into a polymer with a higher T_g than the polycarbonate used in this study. Preliminary results suggest that chromophores as nonlinear as **5**, but which can be poled at temperatures approaching 200°C can be synthesized.

The results we have obtained therefore demonstrate that it is possible to design and synthesize molecules that have not only large nonlinearities, but also sufficient solubility, and stability, such that a highly active electro-optic polymer can be fabricated. While much additional work must be done before commercially viable electro-optic polymers with such large r_{33} values become available, these results validate the concept that organic polymers can have substantially larger optical nonlinearities than inorganic crystals.

References:

(1) Meyers, F.; Marder, S. R.; Pierce, B. M.; Brédas, J. L. *J. Am. Chem. Soc.* **1994**, *116*, 10703.

(2) Bourhill, G.; Brédas, J. L.; Cheng, L.-T.; Marder, S. R.; Meyers, F.; Perry, J. W.; Tiemann, B. T. *J. Am. Chem. Soc.* **1994**, *116*, 2619-2620.

(3) Marder, S. R.; Cheng, L.-T.; Tiemann, B. G.; Friedli, A. C.; Blanchard-Desce, M.; Perry, J. W.; Skindhøj, J. *Science* **1994**, *263*, 511-514.

(4) Teng, C. C.; Man, H. T. *Appl. Phys. Lett.* **1989**, *56*, 1734-1736.

New Polymers for Second-Order Nonlinear Optics

G. Lindsay, J. Stenger-Smith, A. Chafin, R. Hollins, L. Merwin, R. Yee, R. Nissan, M. Nadler, R. Henry, K. Wynne[1], P. Ashley[2], L. Hayden[3], W. Herman[4], Research & Technology Div., Code 474220D, U.S. Navy, China Lake, CA 93555; [1]Office of Naval Research, [2]U.S. Army Missile Command, Redstone Arsenal, AL 35898-5248; [3]Department of Physics, University of Maryland Baltimore County, Baltimore, MD 21228; [4]Avionics Div., Code 5052, U.S. Navy, Warminster, PA 18974-0591

Progress on mainchain syndioregic polymers for $\chi^{(2)}$ applications is reported. An electro-optic coefficient, r_{33}, of 8.5 pm/V @ 1.3 microns and loss of < 1 dB/cm was measured in a Mach-Zehnder interferometer waveguide fabricated by parallel plate electrode poling and photobleaching. This EO film has been stable at ambient room temperature for many months, and the long term thermal stability is estimated to be ≥125°C if protected from UV radiation and air. Preliminary results on the preparation of a series of related polymers designed for low temperature fabrication of $\chi^{(2)}$ thin films will be reported.

In order to achieve the highest degree of thermal and temporal stability of $\chi^{(2)}$ properties in a polymeric thin film, the nonlinear optical (NLO) chromophores must be chemically attached to the polymer. Dissolving chromophores in a host polymer lowers the glass transition temperature of the polymer, and the chromophores diffuse out of the polymer at high temperatures, and present a potential health hazard to operators handling the films. In addition to meeting the synthetic challanges of chemically attaching the chromophore to the polymer, one must also design the polymer to withstand the processing time/temperature requirement.

The accordion polymer. Promising results on a syndioregic mainchain NLOP system[1] encouraged us to pursue waveguide measurements in a Mach-Zehnder interferometer fabricated from Polymer A (shown below). Polymer A has syndioregic mainchain α-cyano-cinnamamide chromophoric units bridged with *trans*-cyclohexyl and *o*-xylyl units, and has a glass transition temperature of about 200° to 205°C.

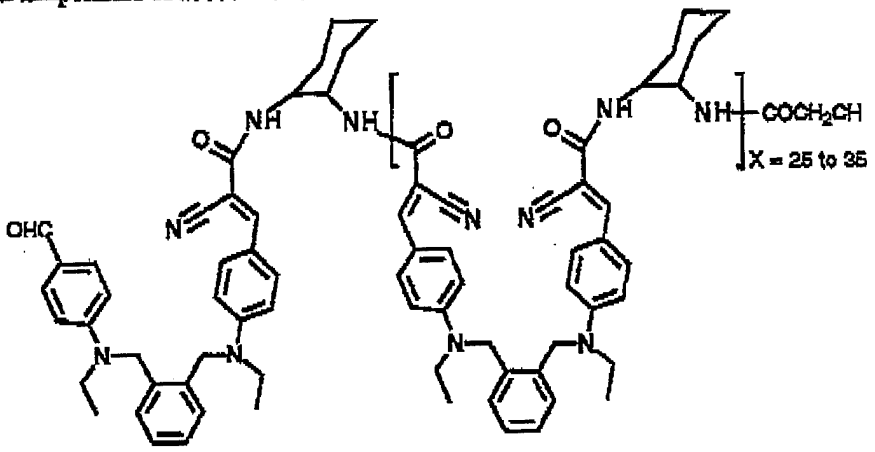

Other versions of this polymer were synthesized, and depending on molecular weight, configuration of the cyclohexane ring, and substituents on the amine donor, the glass transition temperature ranged from 173° to 212°C. The dependence of glass transition temperature (Tg) upon number-average molecular weight (Mn) and chemical structure is shown below.

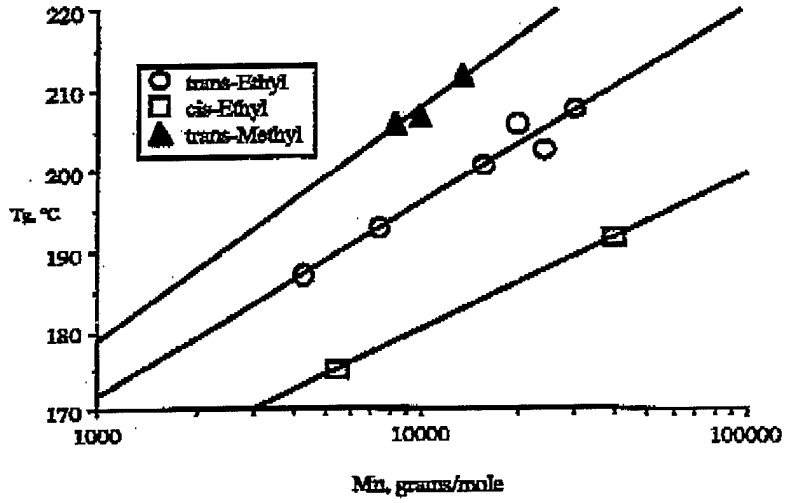

In the caption of this plot, *trans-* and*cis-* and refer to the particular isomer of the cyclohexyl ring, and Ethyl and Methyl refer to the alkyl substitment on the amine nitrogen. Tg was measured by DSC in nitrogen at 10°C/min. The *cis*-ethyl and *trans*-methyl versions of this polymer were dropped from further consideration because of their lower solubility and lower stability.

Optical Measurements on Polymer A. Due to exposure to UV and visible light during poling at 200°C, preliminary measurements on Polymer A showed unexpectedly low nonlinear optical properties[2]. Subsequently, it has been found that poling Polymer A in the dark gives superior results which are in line with expectations based on the calculated molecular hyperpolarizability.[3] Shown below are refractive index dispersion measurements:

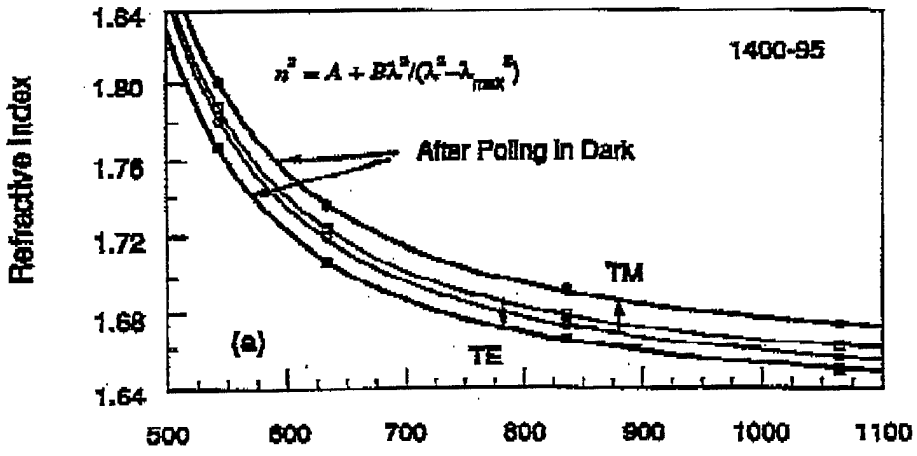

For these index measurements, bladed thin films of polymer A were baked in vacuum above the glass transition temperature to remove residual solvent. Laser light was prism-coupled into the films, before and after poling. Refractive indices at the four wavelengths were fit to a single-oscillator Sellmeier equation (λ_{max} = 400 nm was obtained from the UV-VIS spectra).[4] The unpoled films showed very little birefringence ($n_{TM} - n_{TE} = -0.002$), where as corona-poled films showed a large birefringence ($n_{TM} - n_{TE} = 0.03$).

The nonlinear optical d-coefficients ($2d = \chi^{(2)}$) were measured by second harmonic generation (using a Q-switched Nd:YAG laser). Using a computer-fit to an expression[5] for the second-harmonic power (using the measured refractive index and thickness data), and assuming Kleinman symmetry (since the UV-VIS spectra indicated negligible absorption at 532 nm) we obtained $d_{33} = 30 \pm 5$ pm/V with $d_{31}/d_{33} = 0.35$. No correction was made for absorption.

To generate index of refraction data for the design and fabrication of a buried waveguide, several 1.4-micron thick films were made by spin casting a solution of polymer A on a glass substrate. Prism coupling was used to excite the guided modes at wavelengths of 1.32 and 0.859 microns. An unbleached film and a film bleached at room temperature for 4 hrs with a UV light source (17 mw/cm @360 nm in air) were prepared. Loss measurements and index values based on measurements of n_{eff} are shown below.

Bleach time(hours)	@ 1.32 μm: n	loss(dB/cm)	@ 0.859 μm: n	loss(dB/cm)
0	1.608 ±0.002	<1	1.666 ±0.005	3.3
4	1.605 ±0.002	<1	1.614 ±0.005	3.3
Δn	0.003		0.052	

A Mach-Zehnder optical intensity modulator was constructed with polymer A as the core layer (2.3 μm thick) of a three layer stack. The cladding material (3.5 μm thick) used was UV curable polymer (Norland NOA81). A gold ground plane formed the lower electrode along with a patterned gold layer for the upper electrode. Channel waveguides were formed by photobleaching with a 5 μm wide mask. Poling was accomplished using the device electrodes with an average field of 107 V/μm at 200°C. The device was overcoated with a polymer layer and cut/polished for end fire coupling. The measured EO coefficient was found to be 8.5 pm/V and has remain stable at room temperature for many months.

Stability measurements. In order to gain insight into the stability of NLO activity in the poled polymer films, solid-state nuclear magnetic resonance (NMR) was used in an attempt to measure the temperature dependence of specific molecular motions in a sample of polymer A powder (unpoled). Relaxation of nuclear magnetic order for a given site in a molecule takes place via small local magnetic field fluctuations caused by molecular motions or exchange processes. The NMR spin-lattice relaxation time (T_1), spin-lattice relaxation in the rotating frame ($T_{1\rho}$), and resonance line widths (T_2) can provide relative indications of molecular motion on the megahertz, kilohertz, and hertz timescales respectively[6]. There was no significant change in T_1, $T_{1\rho}$ or line width for polymer A from room temperature to 110°C (the limit of the instrument).

In another stability test, poled films of polymer A were placed on a hot stage in a setup designed to measure the second-harmonic decay during isothermal aging. With the temperature maintained at 125 °C, p-polarized light at 1047 nm from a diode-pumped Nd:YLF laser was incident on the sample at an angle of incidence of 52 degrees. A slow decay of d_{eff} as a function of time was noticed with the room lights off. The absorbance at λ_{max} in the UV-VIS absorption spectrum shows a concurrent slow decrease in air at 125°C in the dark which is indicative of a chemical degradation (not a loss of chromophore alignment).

When the room lights were turned on and a fluorescent desk lamp was used to illuminate the film from a distance of about 1 foot , at 125°C in air, a fast decay mechanism was observed, probably due to attack by UV-generated singlet oxygen. After 24 hrs at 175 °C in a nitrogen blanket in the

dark, there was no perceptible change in the UV-VIS nor in the infrared fingerprint (FTIR) spectrum of polymer A. Hence, films should be sealed from air if used above about 100°C, and protected from UV light at any temperature. When exposed to light in air at 150°C, the FTIR spectra exhibited an appreciable change in the methylenes (carbonyl formation) attached to the anilino nitrogen after less than one hour. This chemical reaction bleaches and blue-shifts the charge transfer band, thus effecting a large change in index of refraction, which is useful in the fomation of channel waveguides.

Design and Synthesis of Mainchain Syndioregic Polymers for LB Deposition

Previously, it has been shown that syndioregic mainchain polymers can be designed for Langmuir-Blodgett deposition of second-order nonlinear optical films.[7] Now it has been shown that multilayer films may be generated from complementary pairs of these polymers by the LB technique at room temperature, and that the as-deposited films exhibit second-harmonic generation without poling. Readers are referred to a companion paper in this conference on this topic for further information on optical characterization of the LB films ('Nonlinear Optical Properties of Self-Assembled Mainchain Polymer Films,' by W.N. Herman, et al.)

Acknowledgements

Financial support of the Office of Naval Research - Engineering Materials & Physical Science & Technology Division, and the Advanced Research Projects Agency - Microelectronics Technology Office is gratefully acknowledged.

Reference

1 Stenger-Smith, J. D.; Henry, R. A.; Hoover, J. M.; Lindsay, G. A.; Nadler, M. P.; and Nissan, R. A.; *J. Poly. Sci. Part A: Chem. Ed.*, **1993**, 31, 2899.

2(2) (a) Lindsay, G. A.; Stenger-Smith, J. D.; Henry, R. A.; Nissan, R.A.; Merwin, L.H.; Chafin, A.P.; Yee, R.Y.; Herman, W.N.; and Hayden, L.M.; *Organic Thin Films for Photonic Applications*, ACS/OSA Technical Digest Series, **1993**, 17, 14; (b) Herman, W.N; Hayden, L.M.;Brower, S.;Lindsay, G. A.; Stenger-Smith, J. D.; and Henry, R. A.; *Organic Thin Films for Photonic Applications*, ACS/OSA Technical Digest Series, **1993**, 17, 18.

3 J. D. Stenger-Smith, *et al.*, in *Polymers for Second-Order Nonlinear Optics*, G. A. Lindsay and K. D. Singer, Eds., Am. Chem. Soc. Advances in Chemistry Series, in press.

4 Ulrich, R.; and Torge, R.; *Applied Optics* **1973**, 12, 2901.

5 Hayden, L. M.; Sauter, G. F.; Ore, F. R.; P.L. Pasillas, Hoover, J. M.; Lindsay, G. A.; and Henry, R. A.; *J.Appl. Phys.* **1990**, 68, 456.

6 "*Spectroscopy of Polymers*, Chapter 10", Koenig, J. L., NMR Relaxation Spectroscopy of Polymers, American Chemical Society, American Chemical Society, Washington, D. C. **1992**

7 G. A. Lindsay, J. D. Stenger-Smith, R. A. Henry, J. M. Hoover, R. A. Nissan, K. J. Wynne, *Macromolecules* **1992**, 25, 6075.

HIGH PERFORMANCE CHROMOPHORES AND POLYMERS FOR E-O APPLICATIONS

Alex K-Y. Jen*[1], Varanasi Pushkara Rao[1], Tian-An Chen[1], Yongming Cai[1], Kevin J. Drost[1], Yue-Jin Liu[1], J. T. Kenney[1], Robert M. Mininni[1], Peter V. Bedworth[2], Seth R. Marder[2], Larry Dalton[3]

1. ROITechnology, Optical Materials Division, 2000 Cornwall Rd., Monmouth Junction, NJ 08852
2. The Beckman Institute, California Institute of Technology, Pasadena, CA 91109
3. Loker Hydrocarbon Institute, University of Southern California, Los Angeles, CA 90089

Thermally And Chemically Stable NLO Chromophores Derived From the 1,1-Dicyanovinyl Electron Acceptor

Although tricyanovinylated thiophene derivatives have been demonstrated to possess large molecular nonlinearities, their use in practical electro-optic devices utilizing high temperature processing conditions is somewhat limited by the low thermal stability ($T_d \approx 250$ °C) of the tricyanovinyl group. Furthermore, the tricyanovinyl group is very sensitive to many polar solvents which are commonly employed in the curing and processing of polyimide based electro-optic materials. For this reason, we modified some of the highly active tricyanovinyl derivatives with the objective of achieving tradeoffs among many useful properties such as thermal stability, molecular nonlinearity, and stability to solvent and acid-base environments.

We discovered that a modification which involves the replacement of the cyano group on the vinylcarbon-2 of the 1,1,2-tricyanovinyl acceptor with aromatic rings, produces high thermal stability and excellent chemical stability. However, such a modification is found to significantly reduce the molecular nonlinearity. To optimize molecular nonlinearity in thermally and chemically stable systems, we developed several symmetrical 1,1'-dicyanovinyl NLO chromophores. Two examples of such systems are shown in Table I.

Compounds 1, 2 were synthesized using a simple one-step sequence from the corresponding tricyanovinyl compounds (Scheme 1). Lithiation of compounds 3 and 4 with n-BuLi, followed by quenching with tricyanovinyl derivatives 5 and 6, respectively, resulted in compounds 1 and 2. They possess significantly blue shifted absorption (~ 100 nm) relative to the corresponding tricyanovinyl derivatives. This feature makes them attractive and suitable candidates for electro-optic devices which operate at 830 nm. The $\beta\mu$ values obtained for compounds 1 and 2 are lower than those of the corresponding tricyanovinyl compounds. However, considering the better solubility properties 1 and 2 possess, reasonably high r_{33} values can be obtained by optimizing their concentrations in polymer matrices. The thermal decomposition temperatures obtained from an adiabatic heating process (10 °C/min) in a DSC pan revealed their high thermal stability behavior (>325°C). Another unusual feature demonstrated by these compounds is stability to strong bases. For example, treatment with alcoholic KOH results in no chemical change in these compounds, while the majority of organic compounds including tricyanovinyl derivatives readily decompose under these conditions. Thermal stability studies carried out on guest/host based polyimide thin-films indicate that compounds 1 and 2 do not decompose at temperatures as high as 275-300 °C.

Thermally Stable Poled Polyquinoline With Very Large Electro-optic Response

In this paper, we report our new approach to achieving both very large electro-optic activity and long-term thermal stability by incorporating a highly active heteroaromatic chromophore into a rigid rod, high temperature polyquinoline.

The earlier results of design and synthesis of NLO chromophores from Enichem and Dirk et.al revealed that using the five-membered heteroaromatic rings as conjugated structures strongly enhance the first order nonlinear optical hyperpolarizability(β). The heteroaromatic chromophore dietheyl-amino-tricynovinyl substituted cinnamyl thiophene (RT-9800) was employed as dopant in polyquinoline . As reported earlier, this compound demonstrates exceptionally large second order nonlinearity. The μβ value (9800 x 10^{-48} esu), the product of molecular dipole moment and microscopic second order susceptibility, of this compound measured at 1.907 μm using electric field induced second harmonic generation (EFISH) is approximatedly 15 times larger than that of diethylamino-nitrostilbene (DANS), which is a commonly used chromophore in second order nonlinear optical material development.

Polyquinolines are ideal polymer materials for device fabrication because they are mechanically strong, easily processed into low optical loss thin films, and thermally stable up to 500-600°C. Polyquinolines are very soluble in common organic solvents, such as NMP, cyclopentanone, DMAC, etc. The polymer solution can be spin-coated easily onto substrates such as glass and silicon wafers to form thin films. The chromophore RT-9800 is readily dissolved in the polyquinoline/cyclopentanone solution at a 20% by weight content of chromophore relative to the polyquinoline. Further increase of the weight fraction of the chromophore may result in aggregation of the dye. Very good quality thin films (2-4 μm) were obtained by careful spin-coating the filtered (through a 0.2 μm microfilter) polymer solution onto an indium tin oxide (ITO) glass substrate. After being soft baked at 110°C for a few minutes, the films were kept in a vacuun oven for several days at 120°C to remove the residual solvent. A thin layer of gold was then deposited onto the film by sputtering (Desk II, Denton Vacuum). The original glass transition termperature (Tg) of PQ is 265°C, however, after doped with 20 wt% of RT-9800, the Tg dropped to ~180°C due to plasticization. The film was poled at 180°C for 5 minutes in Argon with an applied electric field of around 0.8 MV/cm. The poling field was removed after the chromophore/polyquinoline film was slowly cooled to room temperature.

The electro-optic response of the poled RT-9800/polyquinoline film was measured using an ellipsometric technique similar to that described by Teng and Man. In order to minimize the contribution due to resonant enhancement, the electro-optic coefficient (r_{33}) was measured at a wavelength of 1.3 μm. For a 20 wt % RT-9800/polyquinoline film poled at 0.8 MV/cm, an r_{33} value of 45 pm/V was achieved. This nonresonant r_{33} value was not only much larger than most of the organic and polymeric nonlinear optical materials, but also exceeds that of $LiNbO_3$, the standard inorganic electro-optic material. Considering the relatively low poling field (less than 1 MV/cm), a higher electro-optic coefficient can be expected if the processing environment can be further improved.

In addition to good electro-optical properties, the ultimate implementation of poled polymer materials in photonic devices requires that the electro-optic activities of the poled films be stable over a long time period at elevated temperatures. In order to test the thermal stability of the poled film, the electro-optic coefficient r_{33} was measured after the sample film was heated isothermally at 80°C over a period of 2000 hours. The results are shown in Figure 2. Except for an initial decay of about 40% in the first 100 hours, there is little relaxation of the electro-optic activity at a temperature of 80°C. The orientational relaxation phenomena of the electro-optic activity can be empirically described by Kohlrausch-Williams-Watts (KWW) stretched exponential function

$$r_{33}(t) = r_{33}(0)\exp[-(t/\tau)^{\beta}]$$

where τ is the characteristic time of relexation and β is a constant between 0 and 1, describing the deviation from the ideal exponential decay process. In fitting our data with this approach,

we plotted ln[-ln($r_{33}(t)/r_{33}(0)$)] against ln(t). From the intercept and slope of the fitting line, we obtain a value of $\beta = 0.085$ and the characteristic time constant $\tau = 1{,}000{,}000$ hours.

Another alternative for fitting the experimental data is to employ a sum of two exponential functions

$$r_{33}(t)/r_{33}(0) = r_1 \exp(-t/\tau_1) + r_2 \exp(-t/\tau_2).$$

where $r_1 + r_2 = 1$

Here, τ_1, the "short" characteristic relaxation time is related to the orientational relaxation, and τ_2, the "long" characteristic relaxation time, which is more temperature sensitive, is related to the diffusion of the dipole moments in the polymer matrix. We fit our data (Figure 1) using both the "KWW" stretched exponential function (dotted line) and the bi-exponential functions (solid line) using a least-square routine. Since the bi-exponential form produces a better fit result, the "fast" and "slow" characteristic relaxation time approach is a good approximation to describe the complicated, multiplicity of relaxation behavior of the electro-optic activities in this poled polymer thin film. The "short" relaxation time τ_1 and "long" relaxation time τ_2 extracted from the bi-exponential fitting are 20 hours and 40,000 hours, respectively. The corresponding values of r_1 and r_2 from the curve fitting are 0.41 and 0.59 respectively.

In summary, very large electro-optic activity (45 pm/V) and long-term thermal stability at 80°C for more than 2000 hours can be achieved by incorporating heteroaromatic chromophores with exceptionally large second-order nonlinearities into rigid-rod, high temperature polyquinoline. The experimentally measured r_{33} value agrees relatively well with the theoretical prediction based on EFISH measurements and a two-level model. The long term thermal stability of the electro-optic activity was demonstrated and maintained 26 pm/V at 80°C over a period of more than 2000 hours. A bi-exponential function fits our electro-optic relaxation data slightly better than the (KWW) stretched exponential function.

We gratefully acknowledge the partial support by the US Air Force Office of Scientific Research (AFOSR) under Contract F 49620-94-C-0064

Scheme 1

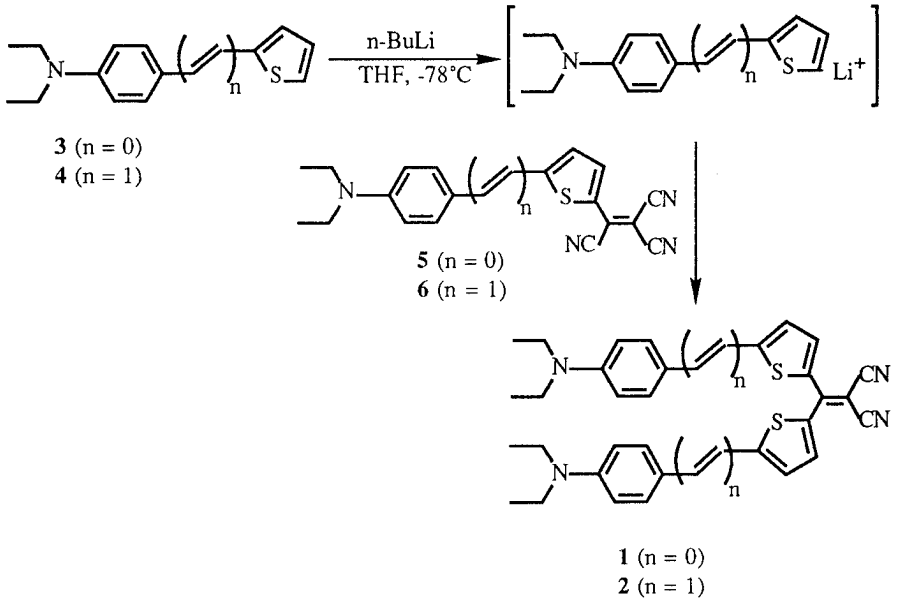

3 (n = 0)
4 (n = 1)

5 (n = 0)
6 (n = 1)

1 (n = 0)
2 (n = 1)

Table 2: Thermally and Chemically Stable Nonlinear Optical Chromophores

	Compound	λ_{max} (nm)	$\beta\mu\ 10^{48}$ (esu)
2	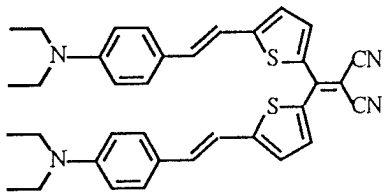	566	2463
1	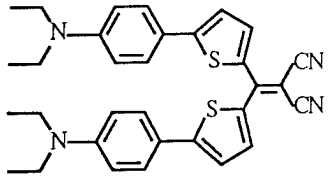	543	1300

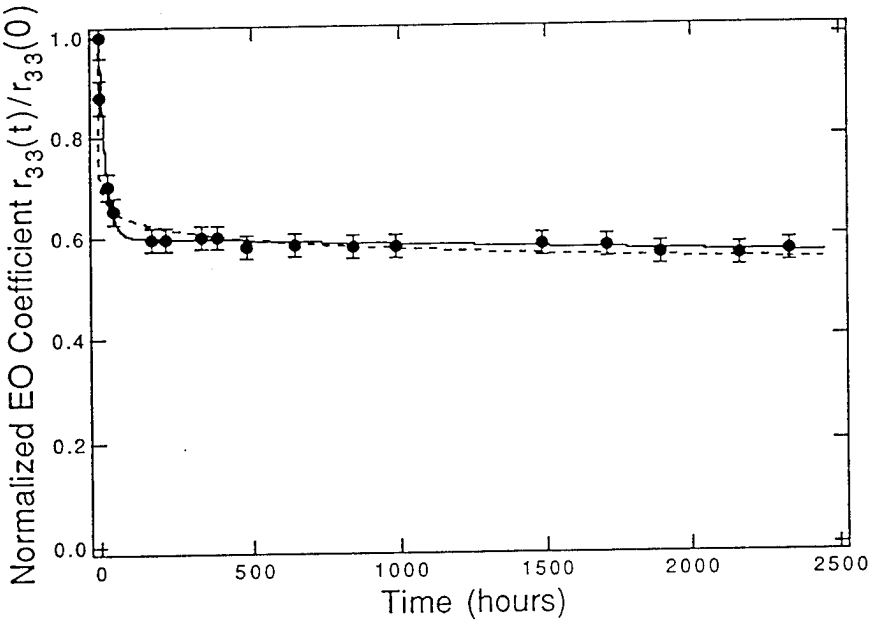

Figure 1. Normalized electro-optic coefficients of RT9800/polyquinoline at 80°C. The data points are the experimental values. The dotted line is "KWW" stretched exponential function fitting and the solid line is a bi-exponential function fitting.

Polyurethane based polymers with improved stability of electrooptic properties

J.Zieba, C.-K. Park, B. Swedek and P.N. Prasad
428 NSM Complex, Department of Chemistry, The State University of New York at Buffalo, Buffalo, NY 14260-3000
phone# (716)645-6800 ext.2089 fax# (716)645-6945

Kwang-Sup Lee
Department of Macromolecular Science, Han Nam University, Taejon 300-791, Korea

Ki-Jeong Moon and Hong-Ku Shim
Department of Chemistry, Korea Advanced Institute of Science and Technology, Taejon, 305-701, Korea

INTRODUCTION

In the presented work we have investigated the basic chemical and optically nonlinear properties of two types of polyurethane based second order active nonlinear polymers.
The polymers were designed to enhance both the values of their nonlinearity (expressed in terms of the macroscopic second harmonic susceptibility $\chi(2)$ and electrooptic coefficient r_{33}) and the temporal stability of poled alignment.

In the part of our work devoted to material formulation we have revisited the two basic concept about tayloring NLO polymers; crosslinkable NLO polymers and polymers with NLO active units in the side groups. The first of the polymers described here (Structure I) presents a thermosetting structure in which poly-[phenyl isocyanate)-co-formaldehyde], a liquid polymer and 4-[[N-(2-hydroxyethyl)-N-methylamino]phenyl]-4'[(6-hydroxyhexyl)sulfonyl]azobenzene, which is the second order chromophore, undergo a very efficient cross-linking reaction when electrically poled at elevated temperature. This design of this system was driven by the expectation that the use of a crosslinking agent in the form of an amorphous liquid polymer along with an NLO chromophore possesing two highly reactive hydroxy groups on the opposite ends of its long molecular dipole axis will produce a highly uniform and rigid structure without affecting the optical quality of the final material. Furthermore, a polymer with one cross-linking site located on every single of its structural repeat unit should allow a very high doping level with the second-order chromophore which, in turn, is expected to increase material's nonlinearity and the glass transition temperature, T_g, of polymer I after the thermosetting reaction is accomplished.

The second material (Structure II) presents an polyurethane-like main chain polymer with covalently attached side groups containing the NLO chromophore in form of a hemicyanine dye ionic structure. In this system an extensive formation of hydrogen bonds between urethane linkages is expected to increase the rigidity of the polymeric structure and to restrain the molecular motion leading to a randomization of the previously aligned dipoles of NLO active molecules. Additionally, the use of the bulky and "softer" tetraphenylborate counterion in the hemicyanine moiety promotes higher nonlinearities of the hemicyanine based NLO chromophores. Also it is expected to reduce the ionic mobility in strong electric field during electric poling and slow down the process of aligned dipoles relaxation occuring after the removal of the electric field.

MATERIAL PREPARATION

The chemical structure of material I is shown in Fig. 1. It was obtained by combining, prior to the casting of the films, equimolar quantities of isocyanate groups contained in poly[(phenyl isocyanate)-*co*-formaldehyde] and hydroxy groups present in 4-[[N-(2-Hydroxyethyl)-N-methylamino]phenyl]-4'-[(6-hydroxyhexyl)sulfonyl]azobenzene.

The final polymeric structure was formed during a thermally induced crosslinking raction which was controled by following the disappearance of the isocyanate -C=N- streching band of the crosslinking agent at 2270 cm^{-1} in the IR spectrum.

The second material was synthesized by using the step growth polymerization technique in a reaction between E-N-Buthyl-4-[2-[4-bis(2-hydroxyethyl)-aminophenyl]ethyl]pyridinium tetraphenylborate and 2,4-tolyene diisocyanate.

Figure 1

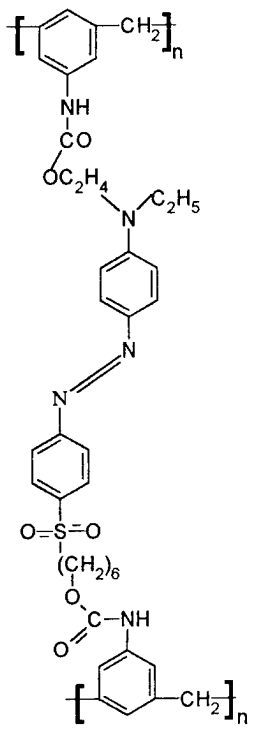

Structure I

Figure 2

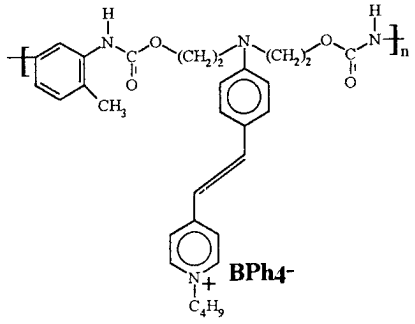

Structure II

These materials were processed into thin films by spin casting onto ITO covered glass substrates. In order to improve the adhesion between the polymers and the ITO surface, it was modified by a 10 minutes long exposure to a RF discharge. After drying, the polymeric fims were poled in corona discharge produced electric field ranging between 1.5-4.5 Vcm^{-1}.

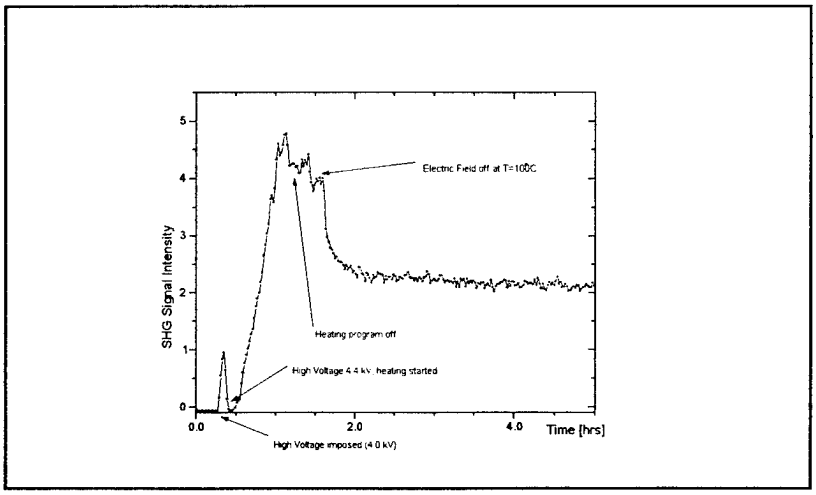

Figure 3

RESULTS

In Fig. 3 a typical *in situ* poling profile of the crosslinkable polymer is shown. One can see that imposing the elctric field at the room temperature immediately introduces a nonlinearity into our material which is followe by observation of the SHG signal. It decays after few minutes, which is due to the build-up of a space charge field that cancels out the externally imposed fileld. When heating begins, the SHG signal reapears and then increases until it reaches an stable plateau. When the temperature is lowered to 100°C and the electric field is removed a sharp drop in the SHG signal intensity is observed. We explain it as a fast thermal randomization of that fraction of the NLO chromophore which has not been stabilized by the cross-linking reaction. After this fast decay in the SHG signal intensity it reaches a very stable level. This SHG activity of a poled and highly crossliked film can be retained unchanged for a period of over three months of storage at a temperature of 100°C.

This materials posses also, beyond the extended temporal stability, a very high degree of optical second-order nonlinearity. Using the angular dependence technique and a Y-cut quartz crystal with a d_{11} coefficient of 0.81×10^{-9} esu as a reference a $\chi^{(2)}$ value of 3×10^{-7} esu was obtained at the fundamental wavelength of 1064 nm. Additionally, an electrooptic coefficient r_{33} of 29.8 pmV^{-1} was measured at 632.8 nm using the ellipsometric technique. It should be noted that those values possess signifficant contribution of a resonance induced enhancement. When we shift λ to longer wevelengths the r_{11} changes as follows:

λ(measurement) [nm]	**r_{11} [pmV^{-1}]**
632.8	**29.8**
687	**18.1**
823	**13.2**

In case of our second polymer with the NLO chromophore designed as hemicyanine moieties incorporated into polymer's side groups even higher values of second order nonlinearity were accesible; by optimizing the poling process parameters, such as temperature, humidity, time,

electric fileld, a $\chi^{(2)}$ value of 5×10^{-7} esu was obtained. We consider this high nonlinearity to be the effect of utilizing the ionic structure of the NLO chromophore and its extremely high doping level. In this material we also observed extended temporal stability of the poled alignment, comparing to similar materials utilizing other types of polymers in their main chain. This fact is in a good agreement with our expectations regarding the possible stabilizing effect of the hydrogen bridge formation between neighbouring polyurethane chains.

It should be noted that the crosslinked NLO polymer exhibits a well defined and rather narrow region of glass transition temperatures around 142°C. In Fig. 4 a rapid decay in the SHG signal can be seen when temperature reaches 150° C. In the case of the polyurethane-hemicyanine structure a broader T_g transition region was detected around the tempearture of 121°C. Consequently, no clear cut-off behaviour of the thermally induced decay of the poled alignment was observed on this material; the SHG signal decreases gradually in a temperature range between 125°C and 175°C.

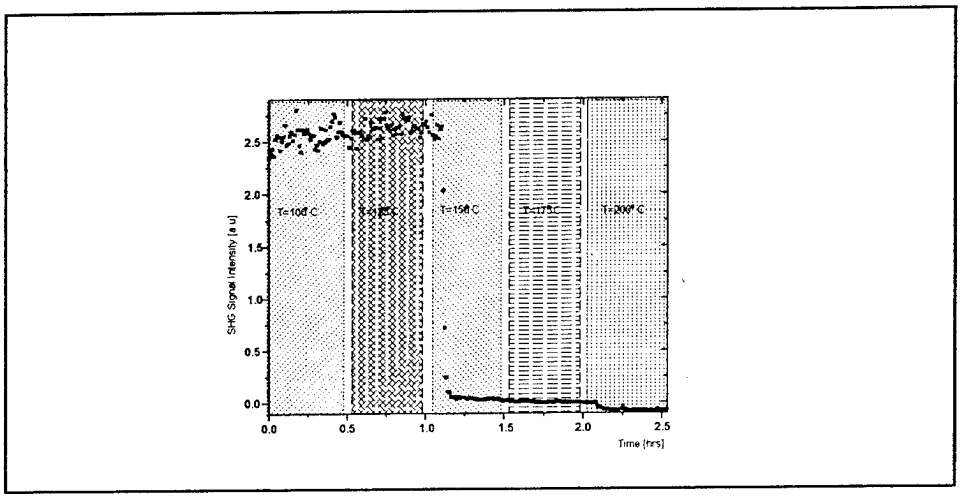

Figure 4

CONCLUSIONS

1. High spatial density and uniformity of cross-linking reaction sites promotes the formation of optically active and stable nonlinear polymers.

2. The hemicyanine structure of a side group NLO chromophore, applied in conjuction with a bulky and soft counterion and attached, with a high doping ratio, to a polyurethane main chain produces a material which can be poled efficiently, producing a very high second order nonlinearity with extended temporal stability.

Design and Synthesis of Soluble Thermally Stable Nonlinear Optical Chromophores Based on the Dicyanomethylenepyran Moiety

Steven. M. Lovejoy, Susan Ermer, and Doris S. Leung

Lockheed Missiles and Space Company, Inc., Research and Development Division
Organization 93-50, Building 204, 3251 Hanover Street, Palo Alto, CA 94304-1191
Telephone: (415) 424-2580, FAX: (415) 354-5795

Carl W. Dirk, Priya Kalamegham, and Lixia Zhang

University of Texas, El Paso, Department of Chemistry, El Paso, TX 79968-0513
Telephone: (915) 747-7560, FAX: (915) 747-5748

Christopher R. Moylan

IBM Almaden Research Center, 650 Harry Road, San Jose, CA 95120-6099
Telephone: (408) 927-1287, FAX: (408) 927-2100

For several years we have been developing polyimide-based electro-optic materials based on commercially available components. In 1992, we described a proof-of-principle all-polyimide triple stack Mach-Zehnder modulator using DCM (4-(dicyanomethylene)-2-methyl-6-(p-dimethylaminostyryl)-4*H*-pyran) in Amoco Ultradel 3112 polyimide as the active core layer with Amoco Ultradel 4212 polyimide cladding layers.[1] During the course of our work we found that some commercial preparations of DCM contained a significant amount of a less soluble, more thermally stable impurity which we identified as the bis condensation product arising from the synthesis of DCM itself.[2] This impurity, DAD, and several analogs were synthesized, and their physical and NLO properties were investigated.[3] Figure 1 shows the synthetic scheme used for their preparation.

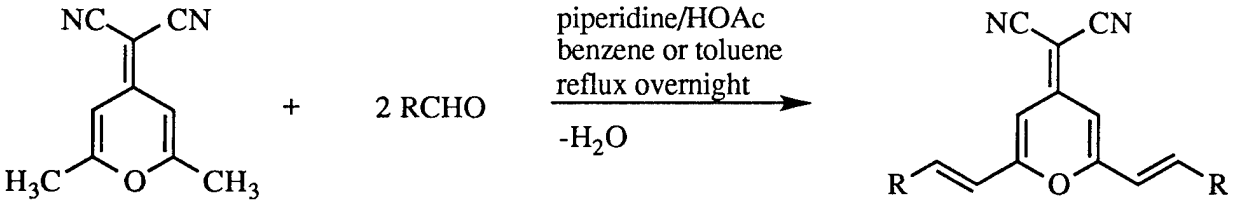

Figure 1. Generic DAD analog synthetic scheme.

In general, the DAD analogs can be prepared by refluxing two or more equivalents of the appropriate aldehyde and (2,6-dimethyl-4*H*-pyran-4-ylidene)propanedinitrile together overnight in benzene or toluene using piperidine and glacial acetic acid as catalysts while removing the generated water with a Dean-Stark trap. After cooling the reaction solution, the precipitated

crude analog is filtered and/or flash chromatographed and recrystallized to give the pure compound.

While the early DAD analogs demonstrated thermal stability equaling or exceeding 330 °C in air or nitrogen as evidenced by thermogravimetric analysis and they exhibited very low absorption at device operating wavelengths (830 nm, for example), their low solubility in organic solvents rendered EFISH measurements and reasonable loading levels in polyimides and their polyamic acid precursors impossible or unreliable. Synthetic efforts were made to solubilize the DAD analogs by increasing the length of the alkyl portion of their donor amine moieties. The physical properties and EFISH measurement values of this series of much more soluble DAD analogs and the standard DCM for comparison are shown in Table I. Melting points (mp) were determined by differential scanning calorimetry (DSC) at a scan rate of 20 °C/minute. Visible absorption maxima were obtained in chloroform. Molar extinction coefficients (ε, units of $M^{-1}\cdot cm^{-1}$) times 10^{-4} are given in parentheses. The EFISH measurements were performed at 1.907 microns in chloroform.

Table I. Physical properties and EFISH results of soluble DAD analogs and DCM

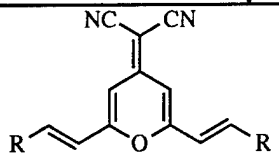 R=	Acronym	mp (°C)	λ_{max} (nm) in $CHCl_3$	μ (D)	$\beta_{1.907}$ (10^{-30} esu)	$\mu\beta_{1.907}$ (10^{-30} esu·D)
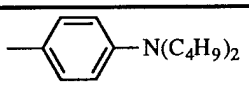	DADB	258	496 (7.70)	12.6	197	2480
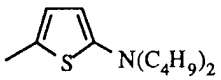	DADTB	216	526 (7.16) 586 (5.68)	13.1	215	2830
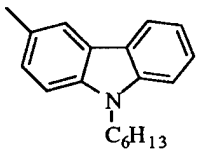	DADCH	229	458 (9.15)	10.7	106	1130
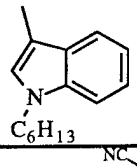	DADIH	198	456 (6.90)	11.9	70.8	842
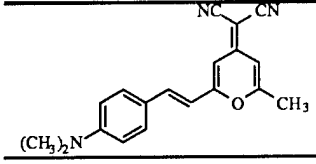	DCM	227	468 (3.85)	10.2	88.8	904

The DAD analogs do not appear to be well described by the two-level model as all of the compounds are more nonlinear than their absorption maxima would indicate. Moylan et al.[4] give a possible explanation of this observation and have performed semi-empirical calculations (DZDO) on DADB to test their hypothesis.

Table II gives the thermal properties of the DAD analogs by four different methods. The first three are standard thermogravimetric (TGA) and DSC methods run at 20 °C/minute while the fourth employs a sealed quartz capillary and are recorded at 5 °C/minute. In this method decomposition temperatures are identified as the peak of the exotherm rather than the onsets as these seem to be more reproducible. All four methods show that the soluble DAD analogs are thermally stable as neat, crystalline solids at least to 300 °C and higher. Their thermal stability and nonlinear optical activity in cured polyimides is now under investigation .

Table II. Thermal properties of soluble DAD analogs and DCM

Acronym	TGA Onset temperature of weight loss in N_2 (°C)	TGA Onset temperature of weight loss in air (°C)	DSC Decomposition temperature (°C) (IBM)	Sealed tube DSC Decomposition temperature (°C) (UTEP)
DADB	387	371	348	373
DADTB	347	not determined	300	not determined
DADCH	432	413	412	392
DADIH	411	364	392	378
DCM	311	291(in pure O_2)	332	331

Experimental

All organic chemicals were purchased from Aldrich Chemical Company and were used as received. DCM was obtained from Exciton (Dayton, OH). The syntheses of DADB, DADCH, and DADIH have been described previously.[5] (2,6-dimethyl-4*H*-pyran-4-ylidene)propanedinitrile was prepared according to Woods.[6] Melting points (mp) were determined in capillary tubes on a Mel-Temp II capillary melting point apparatus utilizing a digital thermometer and are uncorrected. Proton nuclear magnetic resonance (^{1}H NMR) spectra were obtained at room temperature (RT) on a Varian XL-300 NMR spectrometer using deuterated dimethylformamide (DMF-d_7) as solvent and tetramethylsilane (TMS) as an internal reference. Chemical shifts are reported in parts per million (ppm). Fourier transform infrared (FT-IR) spectra were measured on a KVB/Analect RFX300 FT-IR spectrometer. Ultraviolet-visible (UV-vis) spectra were obtained on a Varian Cary 5E spectrometer. Elemental microanalyses were performed by Desert Analytics (Tucson, AZ).

(2,6-Bis(2-(5-(dibutylamino)thien-2-yl)ethenyl)-4*H*-pyran-4-ylidene)propanedinitrile (DADTB). A solution of 5-dibutylamino-2-thiophenecarboxaldehyde (1.38 g, 5.76 mmol, prepared in very low yield from 5-bromo-2-thiophenecarboxaldehyde, dibutylamine, anhydrous potassium carbonate, and Aliquat 336 in DMSO at 110 °C for three days), (2,6-dimethyl-4*H*-pyran-4-ylidene)propanedinitrile (0.4976 g, 2.89 mmol), piperidine (2 mL), and glacial acetic acid (1 mL) in benzene (100 mL) was refluxed for 22 hours using a Dean-Stark trap. The reaction solution was cooled to RT and roto-evaporated. Hexane was added to the solid which was filtered and re-dissolved in dichloromethane. The organic solution was washed with water and brine, dried with anhydrous magnesium sulfate, filtered through a short bed of flash silica, and roto-evaporated. The crude solid was recrystallized from ethyl acetate/hexane to give the product as green crystals, 1.12 g (63%): mp 209-210 °C; ^{1}H NMR (DMF-d_7) δ 0.96 (t, J = 7.1 Hz, 12 H, four CH_3), 1.31-1.45 and 1.61-1.72 (two m, 8H each, eight aliphatic CH_2), 3.42 (t, J = 7.3 Hz, 8 H, four NCH_2), 6.06 and 7.28 (two d, J = 4.2 Hz, 2H each, four thiophene ring CH), 6.41 and 7.89 (two d, J = 15.4 Hz, 2H each, four trans double bond CH), 6.58 (s, 2H, two pyran ring CH); FT-IR (KBr) 2192 and 2177 cm^{-1} (CN stretch); UV-vis λ_{max} (NMP) 434 nm (ε = 2.68 X 10^4), 533 nm (ε = 6.96 X 10^4), 608 nm (ε = 5.22 X 10^4); Anal. Calcd for $C_{36}H_{46}N_4OS_2$: C, 70.32; H, 7.54; N, 9.11; S, 10.43. Found: C, 70.21; H, 7.57; N, 9.03; S, 10.50.

References

[1]Ermer, S.; Valley, J.F.; Lytel, R.; Lipscomb, G.F.; Van Eck, T.E.; Girton, D.G. *Appl. Phys. Lett.* **1992**, *61(19)*, 2272-2274.

[2]Ermer, S.; Valley, J.F.; Lytel, R.; Lipscomb, G.F.; Van Eck, T.E.; Girton, D.G.; Leung, D.S.; Lovejoy, S.M. In *Organic and Biological Optoelectronics*, Rentzepis, P.M., Ed.; Proc. SPIE 1853; Society of Photo-Optical Instrumentation Engineers: Bellingham, WA, 1993; pp 183-192.

[3]Ermer, S.; Leung, D.; Lovejoy, S.; Valley, J.; Stiller, M. In *Organic Thin Films for Photonic Applications Technical Digest, Volume 17*; Optical Society of America: Washington, DC, 1993; pp 50-53; Ermer, S.; Girton, D.G.; Leung, D.S.; Lovejoy, S.M.; Valley, J.F.; Van Eck, T.E.; Cheng, L.-T. *Nonlinear Optics* **1994**, in press; Ermer, S.; Lovejoy, S.M.; Leung, D.S. In *Polymeric Thin Films for Photonic Applications*, Lindsay, G.A. and Singer, K.D., Eds.; ACS Symposium Series; American Chemical Society: Washington, DC, 1995; in press.

[4]Moylan, C.R.; McComb, I-H.; Twieg, R.J.; Ermer, S.; Lovejoy, S.M.; Leung, D.S., this volume.

[5]Ermer, S.; Lovejoy, S.M.; Leung, D.S. In *Polymeric Thin Films for Photonic Applications*, Lindsay, G.A. and Singer, K.D., Eds.; ACS Symposium Series; American Chemical Society: Washington, DC, 1995; in press.

[6]Woods, L.L. *J. Am. Chem. Soc.* **1958**, *80*, 1440-1442.

Tuesday, September 12, 1995

Chromophores II

TuE 4:00 pm-6:00 pm
Holladay Room

Susan P. Ermer, *Presider*
Lockheed Research and Development Division

PERMANENT ALL OPTICAL POLING OF AN OCTUPOLAR DYE

Joseph Zyss and Ifor Samuel*
France Télécom-CNET-Centre Paris B-Laboratoire de Bagneux
Département d'Electronique Quantique et Moléculaire
196, Avenue Henri Ravera, 92225 BAGNEUX, FRANCE

Céline FIORINI, Fabrice CHARRA and Jean-Michel NUNZI
Commissariat à l'Energie Atomique, Leti/Technologies Avancées
DEIN-SPE, Groupe Composants Organiques, Centre d'Etudes de Saclay
91191 GIF-SUR-YVETTE Cedex, FRANCE

present adress: Cavendish Laboratory, Cambridge, UK*

The predominant class of molecular systems considered so-far towards applications in the realm of quadratic nonlinear optics has been derived from the all-pervading "molecular diode" template as exemplified by paranitroaniline-like molecules. The underlying basic paradigm consists in the dipolar anchoring of an interacting couple of electron donor and acceptor groups to a conjugated π electron linkage[1]. The virtue of such a configuration is to provide a significant electronic charge displacement in the ground state which is further enhanced upon directional optical excitation towards the charge-transfer level. This basic mechanism has been confirmed by nearly two decades of experiments in solutions, crystals and polymer media with the two-level quantum model providing solid theoretical support[2]. Both the Electric Field Induced Second Harmonic (EFISH) experiment and the current poled polymer technology essentially depend on the existence and magnitude of a strong ground state dipole μ contributing to the $\boldsymbol{\mu}.\mathbf{E}$ coupling potential between individual molecules and the externally applied dc poling field **E**.

This perspective has been recently broadened[3,4] by the proposition of multipolar systems for nonlinear optics, initially based on the recognition of the full tensorial nature of β_{ijk} which is reflected in the following irreducible decomposition[5]:

$$\beta = \beta_{J=1} \oplus \beta_{J=3} \qquad \text{Eq.1}$$

where $\beta_{J=1}$ and $\beta_{J=3}$ stand respectively for the dipolar and octupolar contributions to β. Non dipolar non centrosymmetric systems, such as abide to trigonal (e.g.D_{3h}) or tetraedral (e.g.T_d) symmetries are indeed compatible with a non-zero β tensor which is then reduced to its $\beta_{J=3}$ component. The absence of dipole moment precludes however the traditional utilization of an electric field dipolar coupling scheme for measurement as well as material fabrication purposes. Following the recent revival of the pionneering Harmonic Light Scattering experiment by Maker[6], systematic measurements in solution of octupolar molecules and ions have been performed in a non-coherent regime[7]. This method permits to by-pass the poling constraint imposed in the coherent regime at the price of a linear dependance of the harmonic intensity in terms of the number of scattering units. Such experiments have permitted to confirm the validity of the octupolar molecular engineering scheme and pointed-out the relevance of propeller-shaped chiral organo-metallic molecules displaying octupolar β's of the order of 800 10^{-30} esu in the non-resonant regime[8]. Permanent macroscopic orientation of octupoles had nevertheless remained an unsettled issue, so far obscuring perspectives towards the actual use of octupolar systems in materials and devices.

We will report the first application of a general all-optical scheme to achieve a significant level of octupolar order in a prototype guest-host system where the guest octupolar

system, namely the Ethyl Violet triphenylmethane dye, is embedded in a standard tetrametoxysilane polymeric sol-gel matrix. A purely optical technique, based on a non-classical six-wave mixing holographic process with multifrequency fields is being used[9-11]. The method is based on two essential properties of the time averaged tensorial product $F_{ijk}=<(E_i^{2\omega})^*\otimes E_j^{\omega}\otimes E_k^{\omega}>$ where $\mathbf{E}^{\omega}$(resp. $\mathbf{E}^{2\omega}$) stand for the fundamental (resp. harmonic) field coherently shining the medium to be oriented: firstly, F is non vanishing as opposed to the time average of individual ω or 2ω field components and moreover, contains both dipolar and octupolar irreducible components with a decomposition that parallels that of the β tensor. Orientation of molecules in a self-phase-matched structure with a non-vanishing macroscopic second-order susceptibility $\chi^{(2)}$ can thus be achieved for both dipolar and octupolar species. In the case of octupoles, such an orientation had been achieved so-far only in a transient picosecond regime in solution[12].

In the present permanent orientation process, the source is a Q-switched mode-locked Nd^{3+}-YAG laser delivering 25-ps pulses at 1064 nm while the coherent second-harmonic writing beam is obtained by frequency doubling in a KDP crystal. The seeding process consists of simultaneous irradiation of the sample by the two coherent co-propagating beams at ω and 2ω. Seeding is periodically interrupted for probing the light-induced non-centrosymmetry by second harmonic generation from the sole fundamental beam while the harmonic beam is temporarily filtered-out by a RG 630 Schott filter. The sample is a 1.3 μm thick film of a silica-gel matrix doped with the octupolar Ethyl-Violet triphenylmethane dye. The absorption is peaking at 580 nm with an optical density of 0.5 at 532 nm.

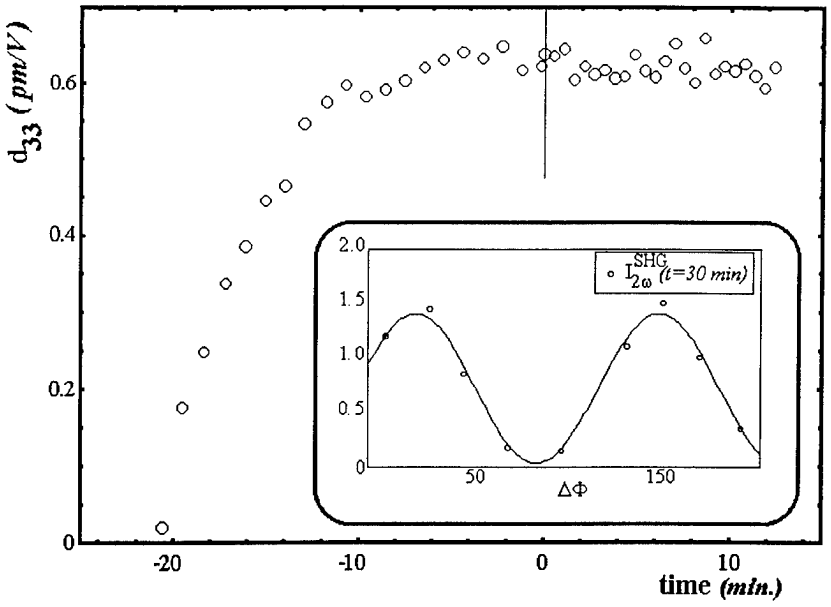

Fig.1: *Experimental build-up (at negative times) and free evolution (at positive times) of the photoinduced d_{33}. The inset represents the dependence of the second-harmonic intensity with respect to the relative phase $\Delta\Phi$ between the ω and 2ω beams. The continuous line corresponds to the theoretical fit.*

Fig.1 shows the real-time growth of the light-induced $\chi^{(2)}$. The energy in each beam is of the order of 700 μJ for the fundamental beam and 2μJ for the second-harmonic with beam diameters at the sample location of 600 μm and 400 μm respectively. Both beams are vertically polarized with the generated second-harmonic analyzed in the direction parallel to that of the excitation. As shown in the inset of **Fig.**1, the relative phase $\Delta\phi$ between the ω and

2ω beams strongly influences the efficiency of the light-induced orientation process according to the following equation:

$$\chi^{(2)} = \left\| (E^{\omega})^2 E^{2\omega^*} \right\| \cos(\Delta\Phi + \Delta kz) \exp(-\frac{\alpha}{2} z) \qquad \text{Eq.2}$$

Resolution of the propagation equation[13] leads to a periodic pattern of the harmonic intensity dependence with respect to ΔΦ as shown in the inset. A realistic coherence length of 6 μm is infered from fitting the periodic pattern with its theoretical expression, in good agreement with Kramers-Krönig relations. An optimal dephasing of 25° is found by tilting a BK7 plate with known thickness and index dispersion. The growth dynamics plotted in **Fig.**1 is obtained in the optimal dephasing configuration and is similar to that already observed in the case of DR1[14]. Saturation at a maximal value of $d_{33}=\chi^{(2)}/2=0.6$ pm/V is obtained after a few minutes and no significant decay observed over a few tens of minutes following the termination of the seeding process. Whereas a sequence of photoinduced "*Trans/Cis/Trans*" photoizomerization processes and associated volume shrinkage have been invoked in the case of the diazo-benzene DR1 species to account for molecular reorientation, the precise photochemical process attached to the octupolar photoexcitation of Ethyl Violet is more likely to be associated to orientationally selective breaking and subsequent rearrangement of chromophore-polymer bonds.

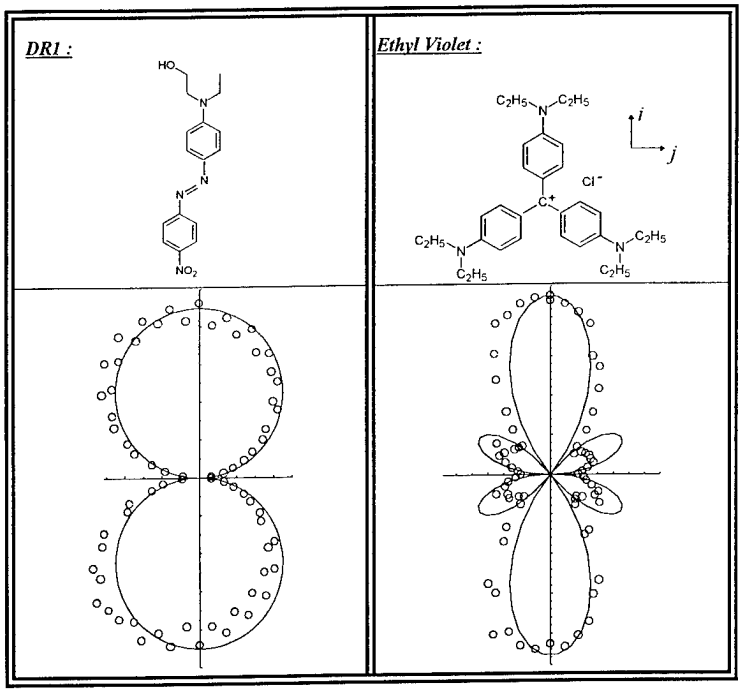

Fig.2: *Molecular structures of the uniaxial DR1 molecule and of the octupolar Ethyl Violet with polar plots of the harmonic intensity as a function of the angle δ between seeding and reading polarizations. The continuous lines correspond to the theoretical dependence as from Eqs.5 and 6.*

Of particular interest is the symmetry analysis of the radiated harmonic signal when varying the angle δ between the reading direction Δ and the seeding polarization. The nonlinear susceptibility along Δ, with both the incoming E^{ω} and outgoing $E^{2\omega}$ fields polarized along Δ, is given by the following statistical averaging:

$$\chi^{(2)} = \int_{\Omega} N(\Omega)\beta_{\Delta\Delta\Delta} d\Omega \qquad \text{Eq.3}$$

where $\beta_{\Delta\Delta\Delta}(\Omega) = (\Delta.\boldsymbol{i})(\Delta.\boldsymbol{j})(\Delta.\boldsymbol{k})\beta_{ijk}$ and N(Ω) depends only on the sole θ and ψ Euler angles between laboratory and molecular reference frames. The cartesian expression of the molecular β tensor is given, in the case of an octupolar molecule, by:

$$\beta(-2\omega;\omega,\omega) = \beta_{iii}(i\otimes i\otimes i - i\otimes j\otimes j - j\otimes i\otimes j - j\otimes j\otimes i) \qquad \text{Eq.4}$$

In the case of a uniaxial molecule of the DR1 type, the β tensor is limited to the first "diagonal" term of this expansion. After adequate expansion in Y_{lm} spherical harmonics of N(Ω) and β up to l=3 and application of orthogonality relations as from Eq.3, the following expressions can be established respectively for octupolar and uniaxial molecules:

$$\chi^{(2)}_{\Delta\Delta\Delta} \propto \left(\frac{5}{14}\sqrt{\frac{4\pi}{7}}A_{30} + \frac{4}{7}\sqrt{\frac{2\pi}{105}}A_{32}\right)\left(\cos^3\delta - \frac{3}{5}\cos\delta\right) \qquad \text{Eq.5}$$

$$\chi^{(2)}_{\Delta\Delta\Delta} \propto \left(\sqrt{\frac{4\pi}{7}}A_{30}\right)\left(\cos^3\delta\right) + \frac{3}{5}\left(\sqrt{\frac{4\pi}{3}}A_{10} - \sqrt{\frac{4\pi}{7}}A_{30}\right)(\cos\delta) \qquad \text{Eq.6}$$

As can be seen from the polar plots in **Fig.**2, the latter uniaxial case, corresponding to DR1, is amenable to a purely bi-circular cos δ dependence, as would be strictly the case for a purely dipolar system (e.g. $\beta=\beta_{J=1}$). The signature of the octupolar symmetry (e.g. Ethyl Violet) is clearly revealed by a more elongated shape with additional lateral lobes.

In conclusion, octupolar symmetry, as revealed by optical poling at the macroscopic level is confirmed in the prototypical case of Ethyl Violet. The use of octupolar molecules in conjunction with the all-optical poling technique enlarges perspectives towards the design of devices for frequency conversion. New symmetries of the induced $\chi^{(2)}$ can be tailored from the interplay of photochemically sensitive multipolar systems with adequately polarized writing beams.

1- J.Zyss, I.Ledoux and J.F.Nicoud p.129 in *Molecular Nonlinear Optics, Materials, Physics and Devices* J.Zyss Ed. (Academic Press, Boston, 1994)
2- J.L.Oudar, J.Chem.Phys.67,466(1977)
3- J.Zyss, Nonlinear Optics 1,3(1991)
4- J.Zyss, J.Chem.Phys. 98,6583(1993)
5- J.Jerphagnon, D.S.Chemla and R.Bonneville, Adv.Phys. 27,609(1978)
6- P.D.Maker, Phys.Rev.A1,923(1970)
7- J.Zyss and I.Ledoux, Chem.Rev. 94,77(1994)
8- C.Dhenaut, I.Ledoux, I.D.W.Samuel, J.Zyss, H.Bourgault and H.Le Bozec, Nature 374,339(1995)
9- N.B.Baranova and B.Y.Zel'dovitch, JETP Lett 45,716(1987)
10- F.Charra, F.Devaux, J.M.Nunzi and P.Raimond, Phys.Rev.Lett. 68,2440(1992)
11- C.Fiorini, F.Charra and J.M.Nunzi, J.Opt.Soc.Am.B 11,2347(1994)
12- J.M.Nunzi, F.Charra, C.Fiorini and J.Zyss, Chem.Phys.Lett. 219,349(1994)
13- C.Fiorini, F.Charra, J.M.Nunzi and P.Raimond, Nonlinear Optics, to be published
14- F.Charra, F.Kajzar, J.M.Nunzi, P.Raimond and F.Idiart, Opt.Lett. 18,941(1993)

Potentials of Ionic Organic Chromophores for Second-Order Nonlinear Optical Thin Film Materials

H. Nakanishi, X.-M. Duan, S. Okada, H. Oikawa, and M. Matsuda

Institute for Chemical Reaction Science, Tohoku University,
2-1-1 Katahira, Aoba-ku, Sendai 980-77, Japan.
Tel, +81-22-217-5643; Fax, +81-22-217-5645.

1. Introduction

Organic second-order nonlinear optical materials, in competition with inorganic materials, must fulfill the conditions of both large susceptibilities and short cut-off wavelength, together with processability, mechanical strength, chemical, thermal and temporal stabilities. Enormous numbers of conjugated compounds have already been investigated. Almost all of them are, however, electrically neutral molecules, and do not conquer the trade-off issues between susceptibility and cut-off wavelength. Ionic organic compounds have been investigated little for this purpose, even though they generally have several advantages as follows. In the case of single crystals, alignment of the ionic chromophore can be controlled into a polar structure by changing the counter ions [1-3]. Thus, there is no need to modify the chemical structure of the chromophore itself after having determined the ionic species with large hyperpolarizability (β). Mechanical properties, especially hardness, of the ionic crystals are better than those of neutral crystals. In addition, high melting point and/or thermal stability is also expected. In the case of poled-polymers as well some of these advantages must be exemplified.

One of the major reasons why ionic organic compounds have not been investigated is that the assessment of β values of ionic species has been impossible until the recent discovery of the hyper Rayleigh scattering (HRS) method [4-6]. The HRS method is a powerful tool for the evaluation of β of not only neutral molecules but also ionic and/or octupolar species since it requires no static electrical field under measurement conditions. Thus in our recent study, we used this method to

evaluate the β values of a series of stilbazolium derivatives [7]. Very recently, we examined the ionic species having cut-off wavelengths shorter than 300 nm: i.e. the β values of *p*-toluenesulfonate anion [8] and its related ions were determined.

In this paper, we demonstrate that they are potential candidates to break the above-mentioned trade-off problem.

2. Experimental

Chemical structures of the compounds used in the present study are shown in Fig. 1. They were dissolved in methanol for the measurement of HRS and absorption spectra. Concentrations of the solutions were 10^{-4}-10^{-2} M for the HRS measurement and 6.5×10^{-5} M for absorption spectra. The cut-off wavelength (λ_{co}) was determined from the 99% transmittance of 2.4×10^{-2} M methanolic solution. A Q-switched Nd:YAG laser operated at 1064 nm with 10 ns pulse width and 10 mJ energy per pulse was used as the fundamental beam of HRS. The intensity of HRS observed at 532 nm was measured as a function of the intensity of the incident fundamental beam for the solutions at various concentrations. The β value of the solute was calculated, using β of the solvent as a known value; 6.9×10^{-31} esu [4] was used for methanol. The experimental setup and the calculation procedure of the β values, including the absorption correction, were previously reported in detail [4-7].

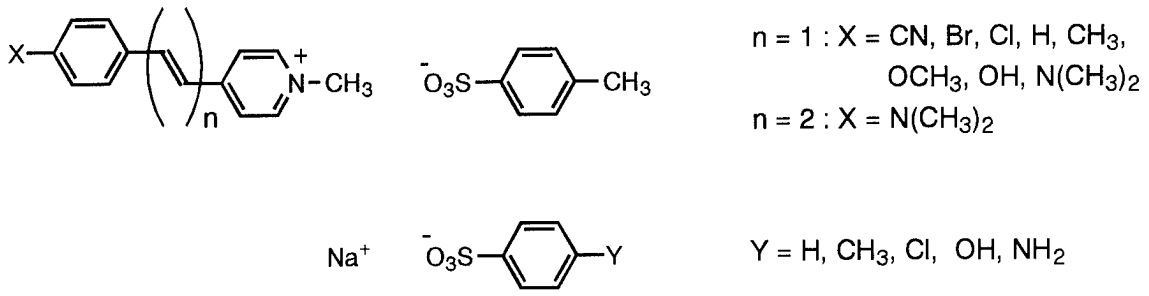

Fig. 1. Chemical structures of stilbazoliums and benzensulfonates.

3. Results and Discussion

Table 1 summarizes the absorption data and β values of stilbazolium cations (with *p*-toluenesulfonate anion). The β value of *p*-nitroaniline (*p*NA), obtained by us under the same experimental conditions, is also listed in Table 1. In order to make fair comparison, apart from the different degrees of resonance effects, β_∞ values at the nonresonant wavelength are also calculated on the basis of two-level model and are listed in the right-most column of Table 1. It is seen that compared with *p*NA, many stilbazolium derivatives with shorter cut-off wavelength give 3-10 times larger β value. Especially interesting are the halogen-substituted compounds which give quite large β values at the short cut-off wavelengths. Butadienyl derivative gives far larger β value though the cut-off is shifted to longer wavelength. These moieties must be useful for EO materials.

Table 1. Absorption data and β values of stilbazolium cations

Compound		λ_{co} (nm)	λ_{max} (nm)	ε_{max}	β_{1064} ($\times 10^{-30}$ esu)	β_∞ ($\times 10^{-30}$ esu)
n	-X					
1	-CN	390	335	39000	150±20	60
1	-Br	410	348	35000	305±60	160
1	-Cl	410	346	38000	290±60	150
1	-H	410	347	25000	190±40	100
1	$-CH_3$	425	361	23000	280±60	130
1	$-OCH_3$	470	381	26000	360±80	150
1	-OH	480	391	28000	390±80	160
1	$-N(CH_3)_2$	600	474	35700	2200±500	370
2	$-N(CH_3)_2$	635	492	37000	5500±1000	610
*p*NA			381		39±5	16

Table 2. Absorption data and β values of benzenesulfonate anions

Compound -Y	λ_{co} (nm)	λ_{max} (nm)	ε_{max}	β_{1064} ($\times 10^{-30}$ esu)	β_{∞} ($\times 10^{-30}$ esu)
-H	273	217	8600	15±4	12
$-CH_3$	280	222	12300	22±6	17
-Cl	298	226	9900	10±3	8
-OH	314	252	14100	17±4	12
$-NH_2$	317	253	15900	19±5	14

Table 2 lists up the absorption data and β values of sodium *p*-toluenesulfonate (*p*TSNa) and related compounds. It turns out that these ions (in methanol) have β values similar to that of *p*NA irrespective of very short cut-off wavelengths, i.e. shorter than 300 nm. The neutral derivative of *p*TSNa, say methyl *p*-toluenesulfonate gives the β value of about half of *p*TSNa. It suffices to say that the present results indicate the possibility of realizing ionic crystals with almost the same *d* constant and FOM as well-known MNA, together with short cut-off like inorganics. Thus, π-conjugated organic ions are concluded to be worth investigating as potential chromophores for second-order nonlinear optics, irrespective of single crystals or poled polymers.

References

[1] G. R. Meredith, *ACS Symp. Ser.*, **233**, 27 (1983).
[2] H. Nakanishi, H. Matsuda, S. Okada, and M. Kato, *Proc. MRS Int. Mtg. Adv. Mater.*, **1**, 97 (1989).
[3] S. R. Marder, J. W. Perry, and W. P. Schaefer, *Science*, **245**, 626 (1989).
[4] K. Clays and A. Persoons, *Phys. Rev. Lett.*, **66**, 2980 (1991).
[5] K. Clays and A. Persoons, *Rev. Sci. Instrum.*, **63**, 3285 (1992).
[6] K. Clays, A. Persoons, and L. D. Maeyer, *Adv. Chem. Phys.*, **85**, 455 (1994).
[7] X.-M. Duan, S. Okada, H. Nakanishi, A. Watanabe, M. Matsuda, K. Clays, A. Persoons, and H. Matsuda, *Proc. SPIE*, **2143**, 41 (1994).
[8] X.-M. Duan, S. Okada, H. Oikawa, H. Matsuda, and H. Nakanishi, *Jpn. J. Appl. Phys.*, **33**, L1559 (1994).

ORIENTATION OF THE DISPERSE RED 1 CHROMOPHORE ALONG THE POLAR AXIS IN FERROELECTRIC LIQUID CRYSTALS

David M. Walba,* Peter L. Cobben,* Daniel J. Dyer,* Uwe Müller,* Renfan Shao,† and Noel A. Clark†

*Department of Chemistry and Biochemistry, †Department of Physics, and Optoelectronic Computing Systems Center, University of Colorado, Boulder, Colorado 80309 USA

Organic thin films with large second order nonlinear susceptibility $\chi^{(2)}$ are of potential utility in fast integrated electro-optic modulators. Ferroelectric liquid crystals (FLCs), possessing a thermodynamically stable polar structure, and therefore non-zero $\chi^{(2)}$ with infinite "thermal stability," combined with good processibility on semiconductor substrates, seem to provide an excellent approach to creation of $\chi^{(2)}$ thin films. Indeed, we have outlined in detail an approach for achieving useful $\chi^{(2)}$ values in FLCs by orientation of the p-nitroaniline unit along the FLC polar axis. [1] This approach was later shown to afford an FLC glass with $\chi^{(2)}$ values on the order of 5 pm/V. [2] However, to be most useful for fabrication of integrated electro-optic modulators, $\chi^{(2)}$ values on the order of 50 pm/V are required.

In order to achieve $\chi^{(2)}$ values of this magnitude, organic functional arrays possessing donor-conjugating spacer- acceptor units of extended length relative to p-nitroaniline must be oriented along the FLC polar axis. An example of such an extended NLO chromophore is the p-dialkylamino-p'-nitroazobenzene unit found

in the classic NLO dye disperse red 1 (DR1). The DR1 chromophore possesses a molecular second order susceptibility β on the order of ten times larger than that of p-nitroaniline. Orientation of such a "two ring" unit along the polar axis of an FLC, however, seems a difficult task since "long" functional arrays typically orient along the director.

Herein we report a class of FLCs wherein the DR1 chromophore is oriented along the polar axis. Thus, based upon our model for the molecular origins of the polar structure occurring in FLCs, in combination with the excellent precedent that dimer structures possessing two side by side mesogenic units can provide smectic phases, [3] azo dyes of type **1** were designed. Two examples of this system are illustrated in

Figure 1. While compound **1a** possesses only a monotropic A* phase, utilization of linoleic acid-derived achiral tails [4] provided an enantiotropic A* phase for **1b**. Interestingly in the context of NLO, compound **1b** shows the orthogonal smectic B* phase below the A* and a large electroclinic effect which is relatively insensitive to temperature.

In order to gain evidence for the structure of the smectic phases of compounds **1** polarized light spectroscopy was carried out. In neat samples and in mixtures compound **1b** showed a maximum visible absorption in parallel-aligned smectic A* cells when in the input light was polarized along the polar axis and a minimum absorption along the director. In "dilute" smectic A* mixtures, where the absorbence was appropriate for the spectrometer, a good fit with the expected form of the curve ($A=a+b\cos^2\theta$) was obtained, as indicated in

Figure 3. The observed dichroic ratio of 2.1 provides a calculated value of 66° for the angle between the

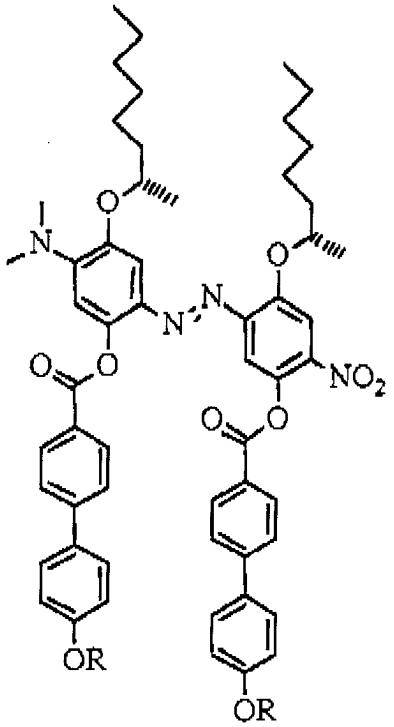

1a; R = n-Decyl; Phase sequence:
X ← <25 — A* ← 99-97 — I

1b; R = (*Z*,*Z*)-9,12-Octadecadienyl;
Phase sequence:
X ← <25 — S_B ← ≅40 — A* ← 67 — I
X — 72 → A* — 74 → I

Figure 1. Structure and phase sequence of new FLCs.

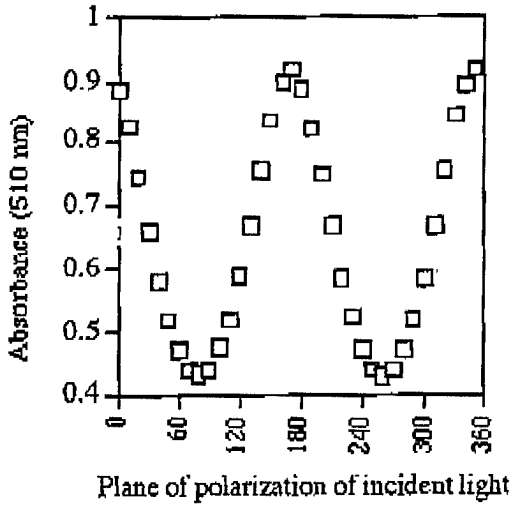

Figure 2. Absorbence as a function of incident angle (rubbing direction 90°).

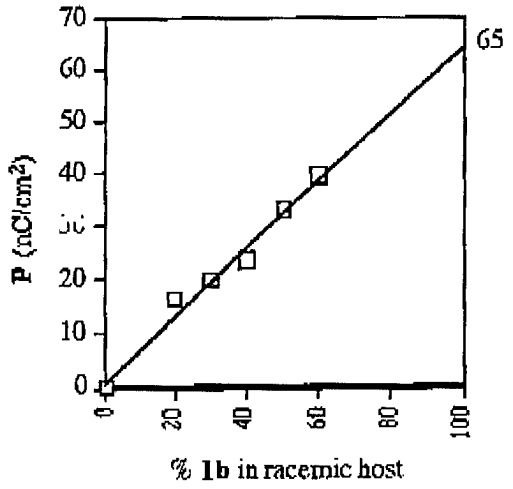

Figure 3. Polarization as a function of concentration for C* mixtures of **1b**.

SELF-ASSEMBLY APPROACHES TO ORGANIC SECOND-ORDER NONLINEAR OPTICAL THIN FILM MATERIALS

GEORGE K. WONG*, WEIPING LIN, HAITIAN ZHOU, DAVID HAHN, PAUL M. LUNDQUIST, Department of Physics and the Materials Research Center, Northwestern University, Evanston, IL 60208 USA

WENBIN LIN, STEPHEN B. ROSCOE, SHLOMO YITZCHAIK, TOBIN J. MARKS*, Department of Chemistry and the Materials Research Center, Northwestern University, Evanston, IL 60208 USA

There is much current interest in molecule-based nonlinear optical (NLO) materials because they offer attractions such as large nonresonant response, ultrafast response times, low dielectric constants/losses, intrinsic tailorability.[1] Although considerable progress has been made in the fabrication of organic NLO materials in recent years, particularly in the areas of poled glassy polymers[2,3] and Langmuir-Blodgett films[4], significant synthetic challenges have impeded the realization of optimum materials.[1,2] These challenges include maximizing chromophore hyperpolarizability and number density as well as maximizing the degree and thermal/temporal stability of induced microstructural acentricity. An attractive and intuitively superior alternative to the above approaches [2-4] is a covalent self-assembly[5] process in which acentric chromophoric superlattices[6] are built up in a layer-by-layer fashion.[6,7] We report here a new topotactic self-assembly approach to the preparation of robust chromophoric architectures with high structural regularity and large nonlinear optical response.

The present approach to acentric chromophoric superlattices utilizes the sequential repetition of three layer-building steps (Figure 1). The progress of the assembly process is

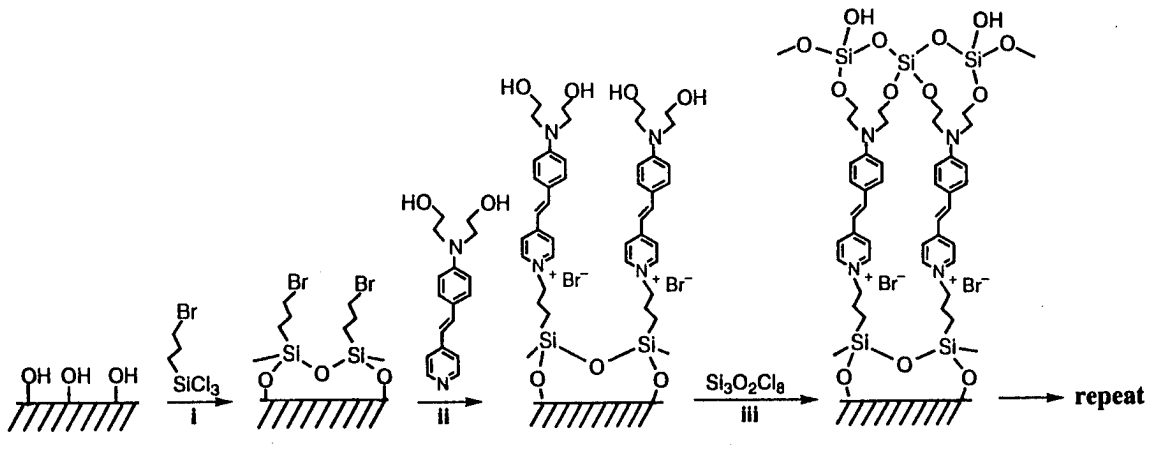

Figure 1. Scheme for the covalent self-assembly of chromophoric superlattices.

monitored by X-ray photoelectron spectroscopy (XPS), advancing aqueous contact angle (θ_a) measurements, transmission optical spectroscopy, polarized second harmonic generation (SHG;

λ_0 = 1064 nm), and specular X-ray reflectivity (XRR). A clean, hydroxylated surface (e.g., SiO_2 or single crystal silicon) is first treated with a solution of 3-bromopropyltrichlorosilane (step i), which introduces a bromoalkyl functionality on the surface. The presence of the bromoalkyl functionality is evident from the Br 3d XPS spectrum which shows a single peak at 70.4 eV, a binding energy characteristic of a bromoalkane. This structural model is further supported by an appropriate hydrophobic change in θ_a (15°(SiO_2) → 75°) and XRR thickness of ~ 10 Å.

An NLO-active layer of stilbazolium chromophore can be self-assembled onto the bromoalkyl-functionalized surface via the quaternization of the pyridine nitrogen and can be effected in either of two efficient topotactic modes (step ii). In the first, a thin layer (~ 1000 Å) of the stilbazolium chromophore precursor, 4-(N,N-hydroxyethyl)aminostilbazole, is spin-coated on the bromoalkyl-functionalized surface, followed by brief heating *in vacuo* to effect quaternization and removal of excess reagent (130°C/0.4 torr). Alternatively, the precursor vapor can be passed over the heated substrate in a chemical vapor deposition (CVD) process. The course of the quaternization/assembly is verified by the appearance of the Br 3d signal at 68.0 eV as a result of the formation of Br^- and the appearance of two N1s signals at 399.5 and 401.6 eV for the amino and pyridinium nitrogen, respectively. The self-assembly of the 4-(N,N-hydroxyethyl)aminostilbazolium chromophore results in an appropriate hydrophilic change in θ_a (75° → 50°), an increased thickness to ~30 Å in the XRR, and most importantly, an extremely large SHG response from the anchored, high-hyperpolarizability stilbazolium chromophore, $\chi^{(2)}_{zzz}$ = 7 x 10^{-7} esu. Angular-dependent SHG measurements reveal an average tilt angle of the chromophore β_{zzz} direction of 40 ± 3° from the surface normal, in good agreement with earlier results.[6]

In order to adapt this monolayer self-assembly technique to the construction of chromophoric multilayers, the surfaces terminated with 4-(N,N-hydroxyethyl)aminostilbazolium chromophore are treated with octachlorotrisiloxane (step iii). This treatment provides lateral structural stabilization/planarization via interchromophore crosslinking and "regenerates" a (hydroxylated) substrate for the subsequent iterative superlattice assembly process. The course of this step can be ascertained from the expected hydrophilic change in θ_a (50 → 17°), and the additional thickness detected in the XRR (~ 7Å).

The degree to which this scheme produces a regular superlattice microstructure without loss of acentricity (randomization of chromophore orientation) and diminution of SHG efficiency, was investigated as a function of the number of added layers (steps i-iii) by XRR, transmission optical spectroscopy, and SHG. The superlattice thicknesses calculated from the XRR data (Figure 2A) show a smooth, monotonic increase as a function of the total number of assembled layers, consistent with a high degree of structural regularity. From the minima in the X-ray reflectivity data, the interlayer spacing of 36 ± 1Å can be calculated.

Further evidence for the build-up of regular superlattice layers with uniform chromophore orientation comes from the linear dependence of the 480 nm stilbazolium chromophore HOMO → LUMO longitudinal charge-transfer excitation absorbance on the number of assembled layers (Figure 2B). A final test of the present superlattice regularity comes from the SHG response as a function of the number of layers. Because the film thicknesses are small compared to the wavelength of the incident light, the intensity of the SHG light from a regular structure

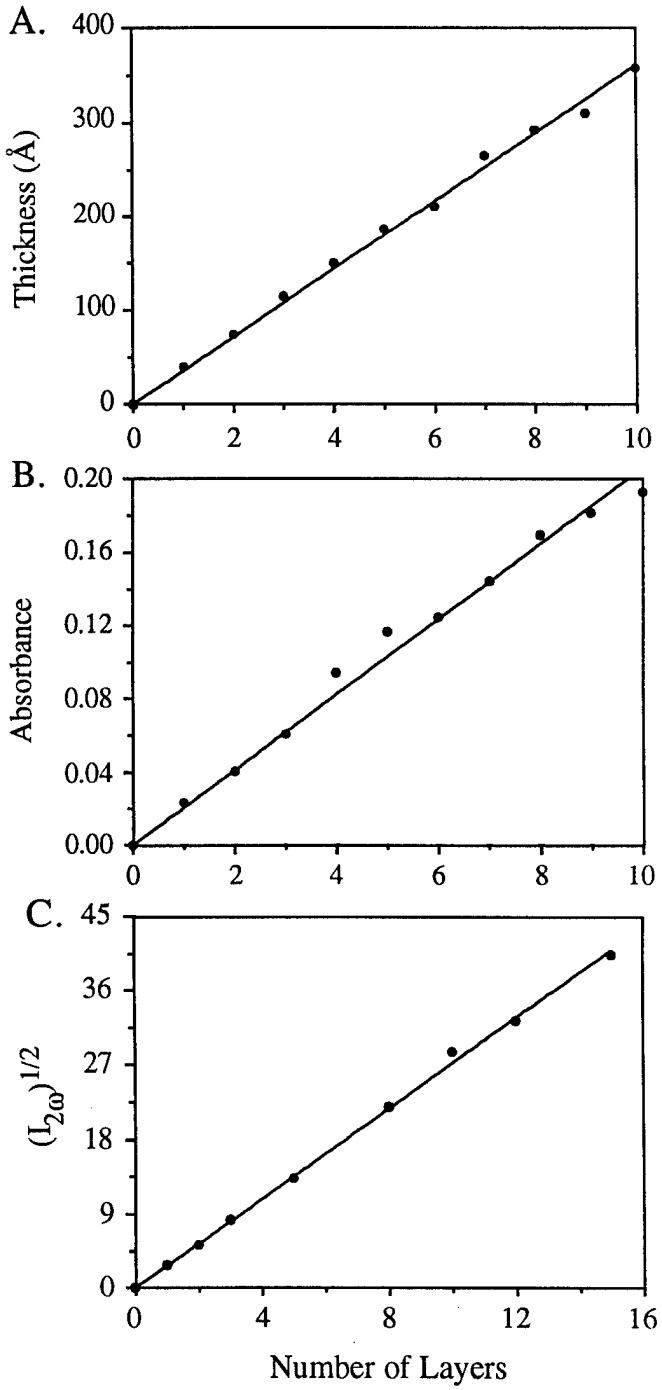

Figure 3.
A. Specular X-ray reflectivity-derived thicknesses for the chromophoric self-assembled superlattices of Figure 1 plotted against the number of layers.
B. Transmission optical absorbance at 480 nm versus the number of layers for the chromophoric superlattices of Figure 1.
C. Square root of the 532 nm second harmonic generation intensity for the chromophoric superlattices of Figure 1 plotted versus the number of layers.

should scale quadratically with the number of layers. The observed linear dependence of the square root of the second harmonic response on the number of layers (Figure 2C) indicates both structural regularity in layer thicknesses as well as uniform alignment of the chromophore molecules. From the slope, $\chi^{(2)}_{zzz} \sim 5 \times 10^{-7}$ esu (~200 pm/V) can be deduced; this level of frequency doubling efficiency rivals or exceeds those under the same conditions of the most efficient poled polymers and Langmuir-Blodgett films reported to date.[1,2]

Interestingly, the SHG response of the self-assembled monolayers grown on the native oxide of a Si(111) substrate by this topotactic approach is strikingly different from that of the films grown with the conventional solution deposition method.[6b,c] In contrast to the films grown with the conventional solution deposition method, the "topotactic" films do not show a 3-fold structure when they are rotated about the surface normal. The presence of this pattern in the former case is attributed to the structural order in the silicon lattice, while its absence in the "topotactic" films could be due to different packing in these denser films.

In summary, these results demonstrate an expeditious and likely generalizable molecular synthetic route to robust, intrinsically acentric and structurally regular, self-assembled superlattices exhibiting very large second-order nonlinear optical responses. We are currently pursuing device fabrication with these chromophoric superlattices and are extending these novel synthetic approaches to the preparation of other artificial multimolecular assemblies.

We thank the NSF-MRL Program (Grant DMR 9120521) through Northwestern University Materials Research Center and AFOSR (Contract 93-1-0114) for support of this research. We would also like to thank Professor Pulak Dutta, Mr. Amit Malik, Ms. Mary K. Durbin, and Mr. Andrew G. Richter for collaboration in X-ray reflectivity measurements.

REFERENCES

1. D.M. Burland, Optical Nonlinearities in Chemistry, Chem. Rev., **94** (1994) and references therein.
2. T.J. Marks, M.A. Ratner, Angew. Chem. Int. Ed. Engl., **34**, 155 (1995) and references therein.
3. D.M. Burland, R.D. Miller, Chem. Rev., **94**, 31 (1994).
4. (a) G.J. Ashwell, P.D. Jackson, W.A. Crossland, Nature, **368**, 438 (1994). (b) T.L. Penner, H.R. Matschmann, N.J. Armstrong, Ezenyilimba, D.J. Williams, Nature, **367**, 49 (1994).
5. (a) A. Ulman, An Introduction to Ultrathin Organic Films, (Academic Press: New York, 1991), Part 3. (b) S.R. Wasserman, Y.-T. Tao, G.M. Whitesides, Langmuir, **5**, 1074 (1989). (c) M. Pomerantz, A. Segmuller, L. Netzer, J. Sagiv, Thin Solid Films, **132**, 153 (1985). (d) G. Cao, H.-G. Hong, T.E. Mallouk, Acct. Chem. Res., **25**, 420 (1992).
6. (a) D. Li, M.A. Ratner, T.J. Marks, C. Zhang, J. Yang, G.K. Wong, J. Am. Chem. Soc., **112**, 7389 (1990). (b) S. Yitzchaik, S.B. Roscoe, A.K. Kakkar, D.S. Allan, T.J. Marks, Z. Xu, T. Zhang, W. Lin, G.K. Wong, J. Phys. Chem., **97**, 6958 (1993). (c) S.B. Roscoe, S. Yitzchaik, A.K. Kakkar, T.J. Marks, W. Lin, G.K. Wong, Langmuir, **10**, 1337 (1994).
7. (a) H.E. Katz, G. Scheller, T.M. Putvinski, M.L. Schilling, W.L. Wilson, C.E.D. Chidsey, Science, **254**, 1485 (1991). (b) H.E. Katz, W.L. Wilson, G. Scheller, J. Am. Chem. Soc., **116**, 6636 (1994).

Photochemical Stability and Performance of Second Order Nonlinear Optical Chromophores and Polymers

R. J. Twieg, V. Y. Lee, R. D. Miller, C. R. Moylan, W. Volksen
IBM Research Division, Almaden Research Center
650 Harry Road, San Jose, California 95120-6099
Telephone: (408) 927 1630 Fax: (408) 927 3310

A. Knoesen, R. A. Hill, D. R. Yankelevich
Department of Electrical and Computer Engineering,
University of California, Davis, California 95616
Telephone: (916) 752 8023 Fax: (916) 752 8428

The performance of $\chi^{(2)}$ poled polymer nonlinear optical media is influenced by numerous intrinsic materials properties as well as the specific conditions of subsequent processing and use of the materials. The origins of microscopic optical nonlinearity have now become much better understood and some highly optimized nonlinear optical chromophores have been prepared. The processing to create polar thin polymer films containing these chromophores by application of an electric field is also now much better optimized. Once the polar order is created the influence of temperature (thermal history) on its magnitude has also been studied in great detail and much progress has been made on design of materials with enhanced temporal stability of poled order. In conjunction with this latter effort chromophores with enhanced thermal stability were identified to permit use of high glass transition temperature media.

The cumulative influence of the light propagating through the optically nonlinear media on performance (ultimately in a device environment) has been studied only very superficially. In fact, given the scope and depth of study on the other durability issues the indifference to optical damage is surprising. It appears to be of strategic interest now to evaluate the photostability of those materials which have evolved with optimized nonlinear and thermal stability properties to ensure that they also simultaneously possess adequate photochemical stability for practical applications.

Interaction of the active NLO media with the propagated light results in damage and losses by mechanisms which are only presently not well understood.[1,2] The propagated light may be a fundamental frequency (as in the case of an electro-optic modulator) or a fundamental and harmonic frequency (as in the case of a waveguide

or thin film used for harmonic generation). Our own interest in the photochemical stability of NLO media comes not only from the demands of the electro-optic modulator area but also from yet another application of poled thin polymer films for ultrashort pulse second harmonic generation (USP-SHG).[3,4] In this application the polymer films are not employed as a waveguide but instead the thin film is probed transversely by short (10 fs) optical pulses with very large energy densities. The short interaction length minimizes pulse broadening by processes such as group velocity mismatch. Because of this requirement for very short interaction lengths chromophores with large nonlinearities and transparency at the high energy side of the CT-band ("blue window") are essential so that anomalous dispersion enhancements (ADPM) might also be utilized. The very high energy densities involved also place special demands on the optical stability of the nonlinear media.

The class of chromophores we have pursued most aggressively for USP-SHG are derivatives of tricyanovinylaniline (TCVA) because they are relatively easy to prepare and are known to have large nonlinearities and dipole moments.[5] Additionally, these materials have intense charge transfer bands which are well separated from the higher energy electronic transitions providing the "blue window" at the harmonic wavelength. Tricyanovinyl acceptor groups have found increasing use in electro-optic chromophores[6,7] and comprehensive assessment of the photostability and thermal stability of this structure is now warranted. It is anticipated that these efforts to study the photochemical degradation of the ultrashort pulse media will be relevant to related degradation problems in the electro-optic waveguides.

The TCVA chromophores have been evaluated as guests in polymethylmethacrylate (PMMA) and in Ultem® polyimide (PI). The PMMA and Ultem® are loaded to about 5 wt% with TCVA chromophore and poled at 80° and 200° respectively. The TCVA chromophore has also been studied covalently attached to a polyimide backbone. The particular sidechain PI utilized (Poly(PhTCV)) has approximately a 50% loading (the tricyanovinyl group is randomly distributed on the pair or pendent triphenylamine groups attached to the benzidine) and is also poled at 200°.

Thin films of the TCVA containing polymers are irradiated with a 100 fsec 80 MHz modelocked Ti-sapphire laser centered at 800 nm and focused to a diameter of $48\mu m$ with peak power density of 3 GW/cm^2. The decay in the SHG intensity at about 400 nm correlates only with optical damage alone since an electric field is sustained on the samples to inhibit orientational decay of the bulk polar order. The first studies were performed in a PMMA host with a range of guest TCVA molecules which differed only in identity of the groups on the amine donor and significant photochemical

degradation was found for all these compositions. More recent studies have kept the chromophore structure relatively constant as a diphenylaminotricyanovinylaniline (PhTCV) or derivative and have also been run in a polyimide media.

The differences in photochemical stability between the PMMA and PI samples are very intriguing. As is clearly evident from Figure 1 the PI samples are much more stable than the PMMA samples. In the case of the PMMA samples the dependence of the decomposition rate on the atmosphere is large while in the case of both PI samples there is no detectable difference between decomposition rates in pure nitrogen and air. Between the two PI samples the side chain system is somewhat more stable than the guest host system. The reasons for the remarkable stability and insensitivity to oxygen of the TCVA chromophores in PI versus PMMA are not yet known nor is it known whether this result is general for other types of chromophores. However, it is now becoming evident that both the polymer medium and the chromophore must be considered in evaluation of net photochemical stability and that the manipulation of polymer structure may play an influential role in the enhancement of photochemical stability just as its manipulation has already proved so effective for the enhancement of thermal and bulk polar order stability.

REFERENCES

1. M. A. Mortazavi, H. N. Yoon, C. C. Teng, J. Appl. Phys., **74**, 4871 (1993)
2. M. Mortazavi, K. Song, H. Yoon, I. McCulloch, Amer. Chem. Soc. Polym. Prepr., **35(2)**, 198 (1994)
3. D. R. Yankelevich, A. Dienes, A. Knoesen, R. W. Schoenlein, C. V. Shank, IEEE J. Quantum Elec., **28**, 2398, (1992).
4. A. Dienes, E. Sidick, R. A. Hill, A. Knoesen, Chapter 35 in "Second-Order Nonlinear Optical Polymers", G. A. Lindsay, K. D. Singer, Eds., American Chemical Society, in press.
5. H. E. Katz, K. D. Singer, J. E. Sohn, C. W. Dirk, L. A. King, H. M. Gordon, J. Amer. Chem. Soc., **109**, 6561 (1987).
6. A. K.-Y. Jen, V. Rao, K. J. Drost, K. Y. Wong, M. P. Cava, J. Chem. Soc. Chem. Commun., 2057 (1994).
7. R. D. Miller, D. M. Burland, M. Jurich, V. Y. Lee, C. R. Moylan, R. J. Twieg, J. Thackara, T. Verbeist, W. Volksen, C. A. Walsh, Chapter 20 in "Second-Order Nonlinear Optical Polymers", G. A. Lindsay, K. D. Singer, Eds., American Chemical Society, in press.

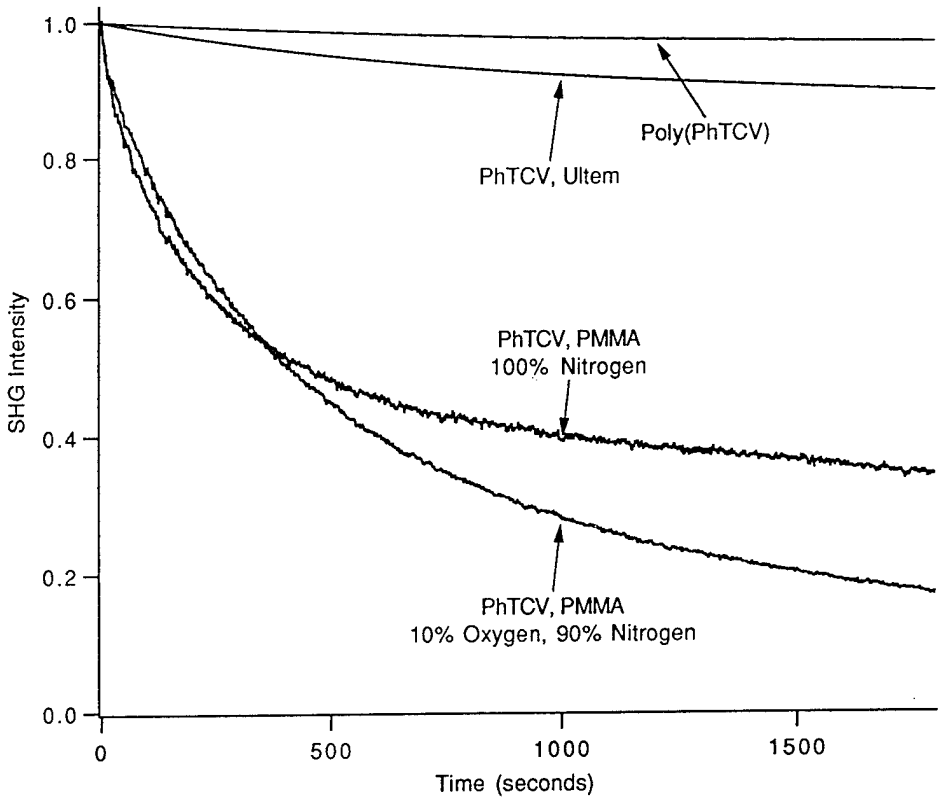

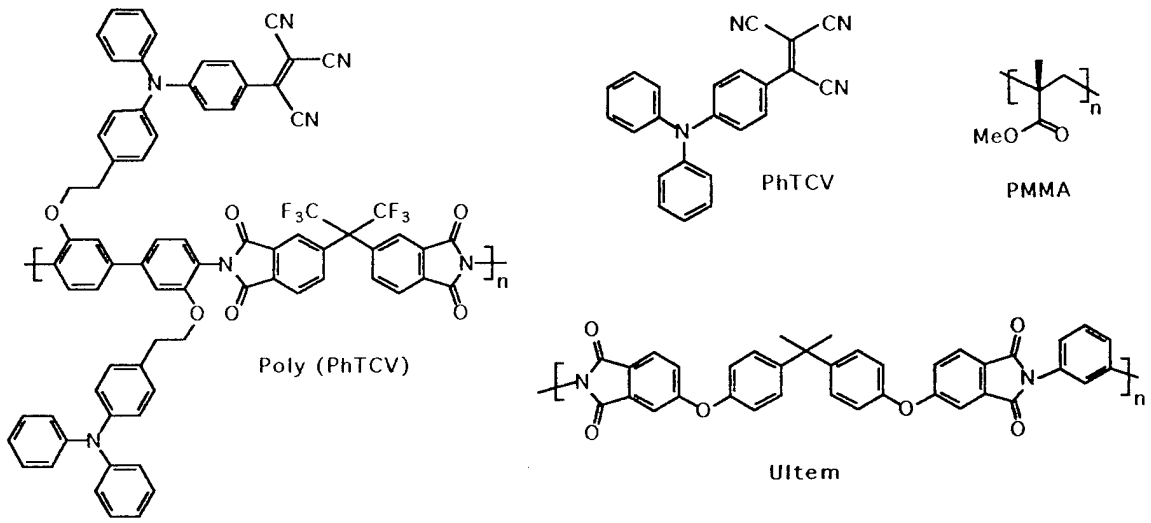

Figure 1. Photochemical Damage of USP-SHG Compositions and Chemical Structures of the Chromophore and Polymers. The SHG intensity for all samples diminishes as a function of dose of radiation. For the guest-host samples in PMMA the damage induced decay is substantial and dependent on the composition of the atmosphere about the sample. In the case of the samples in PI the stability is dramatically improved and decay in pure nitrogen or 90% nitrogen-10% oxygen cannot be differentiated. The sidechain polyimide Poly(PhTCV) has the best photochemical stability.

Wednesday, September 13, 1995

Active Devices I

WA 8:00 am-10:00 am
Holladay Room

Tony Ticknor, *Presider*
Akzo Nobel Electronic Products

Electro-optic Polymer Waveguide Devices - Materials, Fabrication, and Applications

William H. Steier
Department of Electrical Engineering
University of Southern California
Los Angeles, CA 90089-0483

This presentation will include a discussion of three of the promising areas where electro-optic polymers have unique advantages (i) high bandwidth traveling wave external optical modulators operating at millimeter wave frequencies (>30 GHz), (ii) monolithic integration of EO polymers with VLSI electronics for high speed opto-electronics, and (iii) photonic sensing and measuring, without metal electrodes, of electro-magnetic fields.

The status of current polymer millimeter wave modulators will be compared to $LiNbO_3$ modulators from the standpoint of extending the operating range to 100 GHz and from the modulator power drive requirements. The issues of stabilizing and linearizing the modulators will be reviewed. We will briefly review the status of our millimeter wave modulator work and review the future prospects.

The unique advantages and the current problems of integrating EO polymers with pre-fabricated Si and GaAs electronic circuits will be reviewed. Some of the issues to be addressed include protection of the electronics during polymer poling, interconnections between the EO devices and the driving electronics, and conservation of wafer real estate. Potential applications and some selected examples of the integration will be presented. Some novel concepts for low cost packaging and fiber connections to the EO devices will be presented.

The prospect of using photonics to sense and measure electro-magnetic fields and the advantages of polymers in this application will be discussed. Some of the potential applications include measurement of radar antenna patterns and environmental monitoring of E field levels.

Following this review of the potential applications of EO polymers, we will review the various techniques for the fabrication of polymer EO devices. The difficult problem of designing a traveling wave device which combines an optical waveguide and a millimeter wave structure and the sometimes conflicting requirements of each will be discussed. Various dry etch techniques for creating buried channel waveguides and the potential optical losses will be reviewed. The often troubling issues of finding compatible cladding material for both corona and in-plane electrode poling will be addressed.

To complete the presentation, we will discuss some future applications of arrays of polymer switches and modulators for such diverse applications as tunable wavelength filtering and ultra-high speed A to D conversion.

Progress Toward Practical Polymer Electro-Optic Devices

Susan Ermer, William W. Anderson, Timothy E. Van Eck, Dexter G. Girton,
James A. Marley, Alex Harwit, Steven M. Lovejoy and Doris S. Leung,
Lockheed Research and Development Division, Department 93-50, Building 204
3251 Hanover St., Palo Alto, CA 94304
(415) 424-3131, fax: (415) 354-5795
ermer@lmsc.lockheed.com

ABSTRACT

High speed analog and digital switching has been demonstrated in a polymer Mach-Zehnder modulator with a voltage-length product of 13 V-cm. Materials and process optimization will enhance this performance. Anisotropic V-groove etching for fiber attachment provides a path to low-cost packaging of these improved devices.

PROJECTED EO PERFORMANCE: POLYMERS AND LITHIUM NIOBATE

Until recently it seemed that the natural RF-optical velocity matching in polymer modulators would enable them to reach frequencies far in excess of those available from lithium niobate modulators, for which there are already several commercial sources. Recent advances in lithium niobate technology have resulted in velocity-matching by lifting more of the electric field into air to increase the RF velocity [1,2]. All reports of this approach have involved using the vertical electric field rather than the normally-used horizontal field, which causes longer field lines and higher driving voltage. As a result, the reported voltage-length product ($V\pi L$) is 12.5 V-cm. The voltage-length product of the 15% DCM/4212 M-Z modulator described in this paper is nearly identical, and there is still room for a huge improvement in the polymer electro-optic coefficient through use of higher ß chromophores, increases in loading level, and improvement in poling efficiencies. Thus, while high modulation speeds can be reached with lithium niobate modulators, it seems likely that high-speed polymer modulators will surpass them in the voltage-length product, which is a critical figure of merit for applications.

50 GHz ANALOG DEMONSTRATION

One of the long-cited promises of polymer materials for integrated optics is the natural RF-optical velocity match that enables very high frequency modulation[3,4] with an impedance-matched traveling wave drive electrode. The electro-optic response of such a device has been measured from 10 MHz to 50 GHz, using the two-tone technique described previously by Girton et al., in which the RF signal on one arm of the Mach-Zehnder interferometer differs from that on the other arm by a small fixed frequency, and the signal at the difference frequency is measured. The optical wavelength was 830 nm, the active length was 2.6 cm, and the DC half-wave voltage was 5 V. The measured two-tone high-frequency response is shown in Figure 1. The distortions in the frequency response are probably due to electric field discontinuities at the interface between the 18 µm wide microstrip electrode and the 100 µm wide center post of the microwave connector, which could be corrected by an electrical transition from the connector to the microstrip. A one-tone measurement would be half as sensitive to this type of distortion.

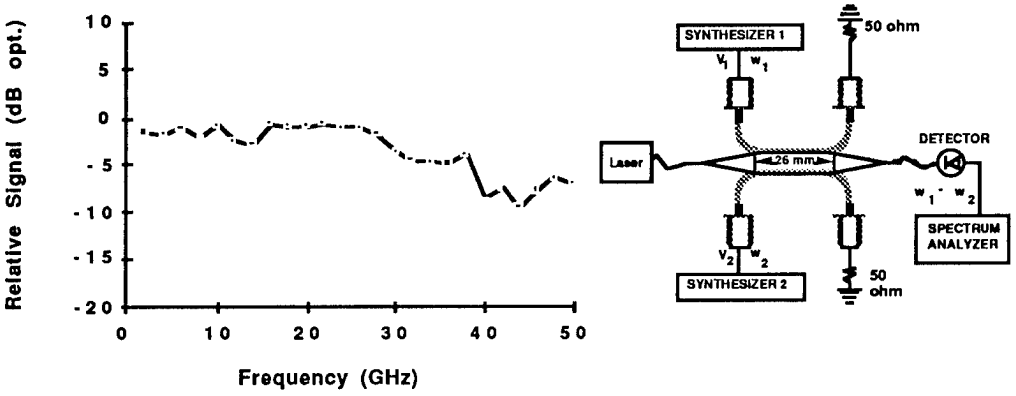

Figure 1. 50 GHz switching observed in two-tone experiment (set up shown at right)

HIGH SPEED DIGITAL DEMONSTRATION

Mach-Zehnder modulators were tested at high speed using an Anritsu ME523 bit error rate tester (BERT) to evaluate their digital switching characteristics. The BERT system was used to drive one microstrip electrode using a pseudorandom bit pattern at a clock rate of 900 MHz, the maximum clock rate for this system. The modulated light output was detected by the receiver portion of the BERT system while a sampling oscilloscope monitored this output, resulting in an "eye-pattern". For these tests a laser diode with $\lambda = 980$ nm was used as the laser source since the optical detector in this system peaks at 1300 nm and was not sensitive at 830 nm. A photograph of an eye-pattern from the oscilloscope at a clock rate of 900 Mb/s is shown in Figure 2 together with the test set-up. The device performance corresponded to a BER of 10^{-12}, with an eye-pattern showing clear transitions between on and off. These transitions were likely faster than observed by the sampling oscilloscope, which was limited by a 600 MHz bandwidth. The noise in the signal was caused by laser amplitude fluctuations, and this noise made it difficult to obtain long term BER data. The actual polymer modulator performance is expected to be significantly above the equipment limitations.

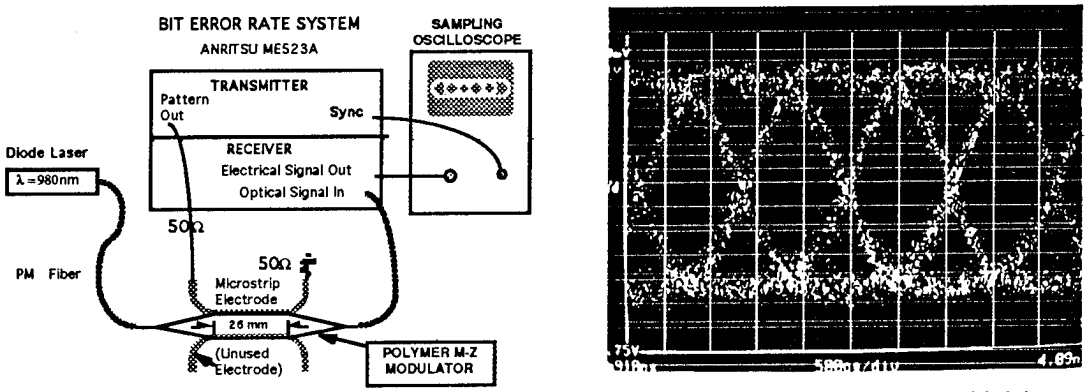

Figure 2. BERT set-up (left) and Eye-pattern of polymer M-Z modulator at 900 MHz (right).

DEVICE FABRICATION AND PERFORMANCE

The triple-stack Mach-Zehnder modulators used for the tests described above were constructed on a Si wafer using EO polymer materials with a layout and cross-section as shown in Figure 3 (a) and (b). Using a previously described process and DCM-based core material system[5] with acrylate cladding layers,[6] the polymer layers were fabricated by spin coating, and the channel waveguide was defined by photobleaching. Microstrip electrodes were built 4 μm thick by gold plating and end faces were prepared by sawing. The resulting 2.6 cm device had a switching voltage of 5 V, resulting in a voltage-length product of 13 V-cm.

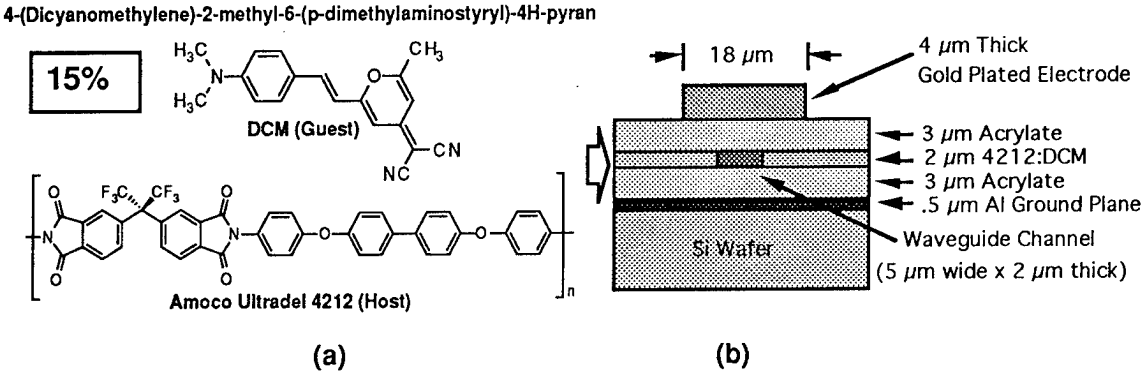

Figure 3. Core Components (a) and Dimensions (b) of Mach-Zehnder Modulator

MATERIALS AND PROCESS IMPROVEMENTS

Performance of polymer EO modulators will improve with use of more effective materials and improvements in the poling process. We have previously described a series of lambda-shaped donor-acceptor-donor (DAD) compounds structurally related to DCM. These chromophores exhibit greater thermal stability than DCM, and are readily

synthesized.[7] All of these compounds are derivatives of the structure shown below in Figure 4a. DADB and DADOH (Figure 4b,c) are processible compounds which can be loaded in polyimides at levels beyond that obtainable using DCM.

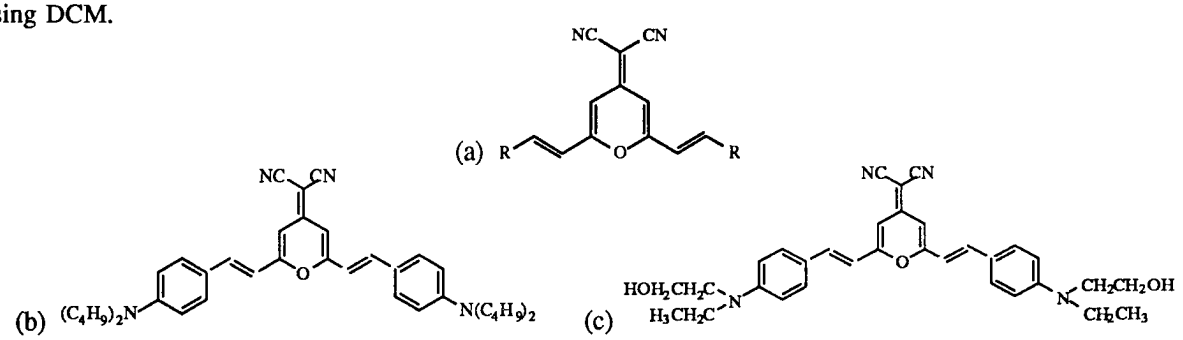

Figure 4. Generic structure of DAD series (a) with structures of DADB (b) and DADOH (c)

The DAD-series compounds are exceptionally transparent[8] for their relatively high hyperpolarizabilities.[9] Moylan ascribes this effect to the presence of two-charge transfer states which contribute to ß, allowing higher nonlinearity without the red-shifted λ_{max} commonly seen in other chromophores which follow the two-level model.[10] The DAD-type compound nonlinearities are generally higher than the corresponding DCM values (ß = 89 x 10^{-30} esu, ßo = 63.3 x 10^{-30} esu, μ = 10.2 D.)[11] For comparison, the DADB values are: ß = 197 x 10^{-30} esu; μ = 12.6 D. DADOH μ and ß values would be expected to be similar, and its dual hydroxyl (-OH) groups enable covalent attachment to a large variety of polymers. Along with higher loading levels of more active chromophores, poling optimization improves device performance. We are currently investigating current flow during the poling process in order to optimize poling in triple-stack EO polymer devices.[12]

LOW-COST PACKAGING USING SILICON V-GROOVE TECHNOLOGY

The major cost components of electro-optic component technologies are (1) the cost of component fabrication and (2) the cost of packaging or coupling one component to another or to the fiber optic transmission medium. The low cost of making polymer devices results from using small quantities of polymer materials fabricated on top of substrates such as Si or GaAs, while employing the same equipment that is used to build ICs. In addition, polymer waveguide structures can be easily fabricated directly on top of circuitry previously built into these substrates. The dominant cost is that associated with interfacing an electro-optic device with the fiber transmission medium since sub-micron transverse positioning tolerances and sub-degree angular alignment are required to reduce coupling losses below 1 dB. The fiber optic connector technology has been developed around the precise control of anisotropic wet etching of single crystal Si. Since polymer based electro-optic devices can be fabricated on single crystal Si substrates, this established connector technology is available for passive alignment of components to fibers (Figure 5). Etching in single-crystal Si is anisotropic, so that V-groove depth is determined by the width W (as shown in Figure 6) which can be defined precisely using lithographic techniques. This has been demonstrated using silica waveguides fabricated on Si substrates with sub-dB loss per connection.[13]

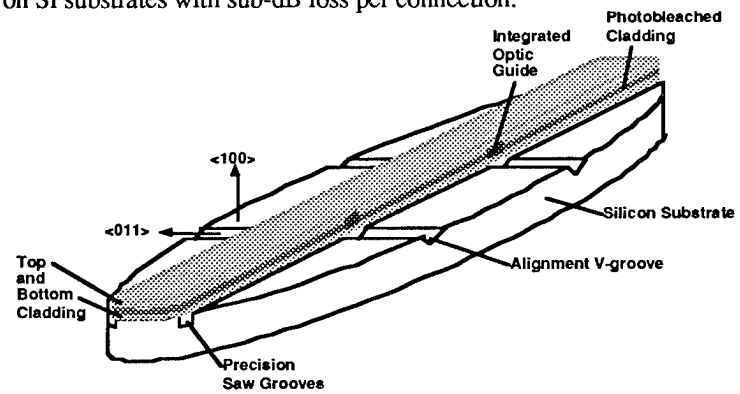

Figure 5. Use of V-grooves to align fibers to waveguides

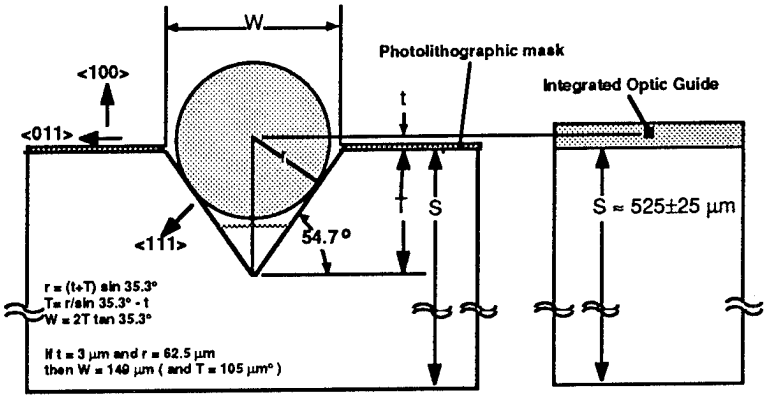

Figure 6. Anisotropic etching of crystalline Si to produce V-grooves

SUMMARY

High-speed analog and digital switching have been demonstrated in polymer electro-optic devices. Achieving these switching speeds in lithium niobate devices requires increasing the driving voltage, which in turn increases the voltage-length product (VπL). Even with a relatively modest chromophore loading level of 15% by weight DCM, a device with a switching voltage just under 5 V and VπL = 13 V-cm has been produced. This value should be easily reduced with improved chromophore activity and loading coupled with greater poling efficiencies. Anisotropic etching of Si V-grooves will allow precise positioning of fibers to waveguides, enabling low-cost packaging of these devices.

ACKNOWLEDGMENTS

This work was supported by Lockheed Independent Research and Development Funds. We appreciate the support of Wright Laboratory Materials (WL/MLPO) and Solid State Electronics (WL/ELOT) Directorates for the development of improved materials and processes which will enhance performance and utilization of active polymer EO devices.

REFERENCES

[1]K. Noguchi, H. Miyazawa and O. Mitomi, Electronics Letters, 30, 949-951 (1994).

[2]G. K. Gopalakrisnan, et al., J. Lightwave Technology, 12, 1807-1818 (1994).

[3]D. G. Girton, S. L. Kwiatkowski, G. F. Lipscomb, and R. S. Lytel, Appl. Phys. Lett. 58, 1730-1732 (1991).

[4]C. C. Teng, Appl. Phys. Lett. 60, 1538-1540 (1992).

[5]S. Ermer, J.F. Valley, R. Lytel, G.F. Lipscomb, T.E. Van Eck, D.G. Girton, "DCM-Polyimide system for triple-stack poled polymer electro-optic devices,"*Appl. Phys. Lett.* **1992**, *61*, 2272-2274.

[6]D.G. Girton, W.W. Anderson, J.F. Valley, T.E. Van Eck, L.J. Dries, J.A. Marley and S. Ermer, "Electro-Optic Polymer Mach-Zehnder Modulators; High Speed Analog and Digital Considerations," to appear in proceedings of Washington D.C. ACS meeting, August 1994.

[7]S. Ermer, J.F. Valley, R. Lytel, G.F. Lipscomb, T.E. Van Eck, D.G. Girton, D.S. Leung, and S.M. Lovejoy, in Organic and Biological Optoelectronics, P.M. Rentzepis, ed., Proc. SPIE **1853**, 183-192 (1993).

[8] S. Ermer, S.M. Lovejoy and D.S. Leung, "Design and Synthesis of Thermally Stable Chromophores with Low Absorption at Device Operating Wavelengths," to appear in proceedings of Washington D.C. ACS meeting, August 1994.

[9] S. M. Lovejoy, D.S. Leung, Carl W. Dirk, Priya Kalamegham, Lixia Zhang, and Christopher R. Moylan, "Design and Synthesis of Soluble Thermally Stable NLO Chromophores Based on the Dicyanomethylenepyran Moiety," this proceedings volume.

[10]C. R. Moylan, I.-H. Mc-Comb, R.J. Twieg, S. Ermer, S.M. Lovejoy and D.L. Leung, " Defeating the Nonlinearity-Transparency Trade-off," this proceedings volume.

[11]C. R. Moylan, R.J. Twieg, V.Y. Lee, R.D. Miller, W. Volksen, J.I. Thackara, and C.A. Walsh, Proc. SPIE **2285**,17-30 (1994).

[12]D.G. Girton, W.W. Anderson, J.A. Marley, T.E. Van Eck, and S. Ermer, "Current Flow in doped and undoped electro-optic polymer films during poling," this proceedings volume.

[13]M. F. Grant, R. Bellerby, S. Day, G. J. Cannell and M. Nelson, "Self-Aligned Multiple Fibre Coupling for Silica-On-Silicon Integrated Optics," EFOC/LAN 91, 269-272 (1991)

Incorporation of Thermally Stable Nonlinear Optical Polymers into Electrooptic Devices

D.M. Burland, R.G. Devoe, M.C. Jurich, V. Y. Lee, R. D. Miller, C.R. Moylan, J. I. Thackara, R. J. Twieg, T. Verbiest and W. Volksen

IBM Research Division, Almaden Research Center
650 Harry Road, San Jose, CA 95120-6099
Telephone: 408-927-2426; Fax: 408-927-3310

In order to be useful in practical nonlinear optical(NLO) devices such as high speed optical switches and modulators, several key properties of electrooptic(EO) polymers must be optimized: the polymer's electrooptic response must be sufficiently large, the response must be stable at all temperatures that the polymer will experience in processing and in operation and the attenuation of light in the polymer by scattering and by absorption must be low. For the specific applications of on-chip and chip-to-chip active optical interconnects, the thermal stability requirements are particularly severe. During the processes of microprocessor die attachment and hermetic packaging, the EO polymer will experience temperatures of >300°C for several minutes[1]. We have investigated the potential and limitations of electrooptic polymers under these severe thermal conditions, proceeding from the identification of NLO chromophores with high intrinsic molecular hyperpolarizabilities[2], incorporation into thermally stable polymers[3][4], and fabrication into electrooptic switches and devices[5].

A class of NLO chromophores containing diarylamino donor substituents with substantial optical nonlinearity and high thermal stability has been described[2]. For example, the thermal stability of the diarylamino modification of the dye Disperse Red 1 (DR1) has a decomposition temperature of 393°C as measured by differential scanning calorimetry (DSC), compared to a value of 309°C for DR1 itself. This greatly enhanced stability of diphenylamino substituted chromophores over their dialkyl aminophenyl substituted analogs is a surprising, but quite general, phenomenon. Recently, these thermally stable chromophores have been chemically incorporated into polyimides resulting in EO polymers with exceptional thermal stability and reasonable optical nonlinearity as measured by the EO coefficient $r = 5-10$pm/V (1.3μm). An example of this thermal stability is shown in Figure 1 where the thermal stability of two polymers

based on the chromophore DR1 are compared[3]. The thermal stability is followed by monitoring the absorbance at the absorption maximum of the lowest energy electronic transition (the charge transfer band) as a function of time at 275°C. The polymer containing the diaryl substituted side chain group is clearly more stable at this temperature. Polyimides in which the electron donor

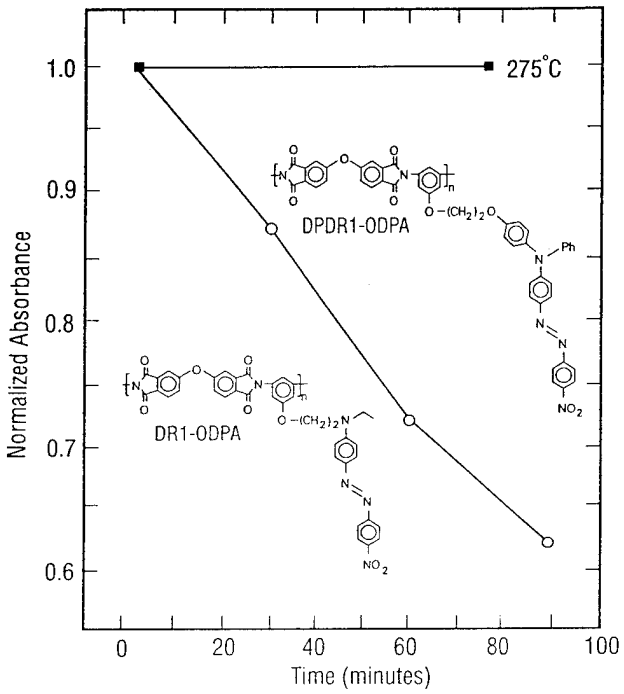

Figure 1

group of the chromophore is incorporate directly into the polymer backbone without any flexible connector functionality have also been prepared and evaluated[4]. One such EO polyimide has a glass transition temperature of 350°C, shows less than 5% loss of optical nonlinearity over 2000sec. at 250°C and less than 15% loss at 300°C over a comparable time period.

The next step in evaluating these highly stable EO polyimides is to attempt to fabricate a prototype device[5]. For such a device the balanced bridge[6] or Mach-Zehnder[7] switch geometry was chosen in order to take advantage of the reduced device length afforded by this design when compared with a more conventional directional coupler switch[8]. Both device designs are shown in Figure 2; the conventional switch in (a) and the Mach-Zehnder switch in (b). Switches were fabricated using the well studied polymer PMMA-DR1 and a modification of the

diaryl substituted chromophore containing polymer shown in Figure 1, in which the dianhydride used to form the polyimide was changed to hexafluorisopropylidene diphthalic anydride[3]. This polymer known as 6FDA-DPDR1 has a T_g of 228°C. The buffer layer material used with the

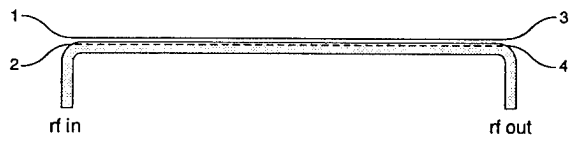

(a)

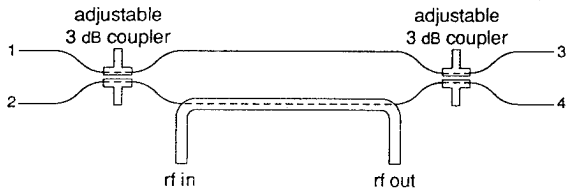

(b)

Figure 2

PMMA-DR1 devices was a UV cured acrylate polymer. This polymer could not be used with the 6FDA-DPDR1 which had to be poled at 220°C. The acrylate buffer layer begins to chemically decompose at temperatures above 200°C. A siloxane-imide copolymer with a bisazide cross linking additive was used as the buffer layer material for the 6FDA-DPDR1 devices.

EO polymer conductivity is a problem when one attempts to fabricate EO devices that must be poled at temperatures exceeding 200°C. For lower poling temperatures, it is not difficult to find a buffer layer whose conductivity is greater than that of the EO layer. Thus nearly all of the poling voltage can be dropped across the middle EO polymer layer in the three layer sandwich configuration used, resulting in the highest degree of poling. Above 200°C, the conductivity of buffer layer and EO layer are nearly equal for a broad range of buffer layer materials and several polyimides. This means that only about 1/3 of the externally applied voltage is actually dropped across the buffer layer substantially limiting the degree of poling. The mechanism of this

enhanced high temperature conductivity along with poling strategies to circumvent the problem are currently under investigation.

Figure 3 shows the performance of the Mach-Zehnder switch fabricated from PMMA-DR1 at an operating wavelength of 1.32μm . The measured extinction ratios in both the cross and the bar switching states were on the order of 30dB for both input ports.

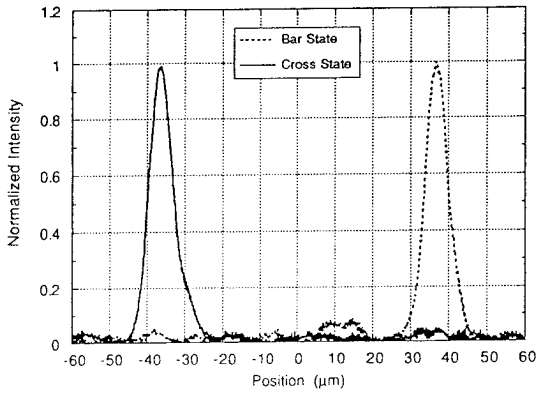

Figure 3

REFERENCES

[1] R. Lytel, G.F. Lipscomb, J.T. Kenney and E.S. Binkley in **Polymers for Lightwave and Integrated Optics**, L.A. Hornak,ed. (Marcel Dekker, NY, 1992) p.433.

[2] C.R. Moylan, R.J. Twieg, V.Y. Lee, S.A. Swanson, K.M. Betterton and R.D. Miller, *J. Am. Chem. Soc.* **115**, 12599 (1993).

[3] T. Verbiest, D.M. Burland, M.C. Jurich, V.Y. Lee, R.D. Miller and W. Volksen, *Macromolecules*, in press.

[4] T. Verbiest, D.M. Burland, M.C. Jurich, V.Y. Lee, R.D. Miller and W. Volksen, *Science*, in press; R.D. Miller, D.M. Burland, M.C. Jurich, V.Y. Lee, C.R. Moylan, J.I. Thackara, R.J. Twieg, T. Verbiest and W. Volksen, *Macromolecules*, in press.

[5] J.I. Thackara, J.C. Chon, G.C. Bjorklund and D.M. Burland, to be published.

[6] V. Ramaswmay, M.D. Divino and R.D. Standley, *Appl. Phys. Lett.* **32**, 644 (1978)

[7] S.K. Korotky, *IEEE J. Quant. Elec.* **QE-22**, 952 (1986).

[8] H.F. Taylor, *J. Appl. Phys.* **44**, 3257 (1973).

60 GHz Electro-optic Modulation by Polymer Waveguide Phase Modulators

Wenshen Wang, Datong Chen, and Harold R. Fetterman
Electrical Engineering Department
University of California, Los Angeles, CA 90095
Tel: (310)206-9457
Fax: (310)206-9497

Yongqiang Shi, James H. Bechtel
TACAN corporation
2330 Faraday Ave., Carlsbad, CA 92008
Tel: (619)438-1010
Fax: (310)438-2412

Srinath Kalluri, William H. Steier, and Larry R. Dalton
Electrical Engineering Department and Chemistry Department
University of Southern California, Los Angeles, CA 90089-0483
Tel: (213)740-4415
Fax: (213)740-8684

Organic nonlinear optical (NLO) materials have the potential to become very important for making photonic devices that are inexpensive to produce, capable of being integrated with other electronics, and suitable for ultrahigh frequency broadband operation [1]. 40 GHz electro-optic (E-O) modulation from a Mach-Zehnder intensity modulator has been demonstrated with thermal plastic polymers [2]. We have reported fabrication of traveling wave E-O phase modulators using a thermally cross-linked NLO polymer, PUR-DR19 [3, 4]. Our devices have exhibited good temporal stability and optical power handling capability, and were tested up to 40 GHz [5]. In this paper, we report our new measurement results up to 60 GHz obtained with an optical heterodyne detection technique. This is the highest modulation frequency reported so far for polymer E-O modulators.

Our devices have a three-layer stack structure with buried straight channel optical waveguide, integrated with a 50 Ω gold microstrip line circuit on top of the waveguide. A fused silica microscope slide covered with a gold ground-plane was used as the substrate, and commercial polyurethane was used for the cladding layers. Corona poling and thermal cross-linking were performed in the same temperature ramp. The channel optical waveguide structure was defined using standard photolithography and oxygen reactive ion etching on the poled and cross-linked polymer layer. An etching depth of 0.6 μm and waveguide width of 8 μm were chosen as a compromise between the mode quality and waveguide loss. The end surfaces of the device were cut with a dicing saw and carefully polished for end-fire coupling. Two Wiltron V launchers were used for coaxial component connections.

The devices typically have about a 13 dB optical insertion loss with a pair of 20× microscope

objectives, and on-off ratios of better than 13 dB in the polarization modulator configuration. We have used up to 30 mW of input optical power at 1.319 μm wavelength for 24 hours to test the device durability , which is equivalent to an optical power density of about 10^5 W/cm^2 inside the waveguide. No change in half-wave voltage was observed within our experiment error. Optical power levels from 10 to 20 mW have frequently been used for system alignment , and up to 40-50mW were used for short times in other measurements where high signal to noise ratios are desired. We have devices that are made of films poled 2 years ago and have been under test from time to time for over 12 months in ambient conditions. No change in half-wave voltage was observed for these devices. Shorter wavelengths, however, do cause nonlinearity relaxation at the same or even lower power levels. More systematic investigations of device damage threshold and mechanism are under way, and we will report the results elsewhere.

The device frequency response was obtained initially up to 40 GHz with direct detection using fast photodetectors and external microwave mixers in a polarization modulator configuration. For higher frequency measurements, where our commercial photodetectors and microwave mixers start to degrade, we used an optical heterodyne technique to directly observe the phase modulation signal [6,7]. The experiment setup is shown schematically in Fig. 1. Two Lightwave Electronics diode pumped Nd:YAG lasers at 1.319 μm were used for the measurement. The beam of the first laser was end-fired coupled in and out of the modulator through microscope objectives. Using a beam sampler, the second laser was aligned co-linearly with the phase modulated output light from the modulator to a low frequency detector. The photo current excited in the detector, for small signal modulation, has a term that can be written as:

$$i_d \sim (I_1 I_2 P)^{1/2} \sin[(\Delta\omega-\Omega)t+\Delta\phi]$$

where $_{I1, I2}$ are the laser intensities, P the driving microwave power, $\Delta\omega$ the laser frequency difference, Ω the modulation frequency, and $\Delta\phi$ the slow varying phase difference between the laser beams. This is the signal to which the low frequency photodetector would respond and that was displayed on the spectrum analyzer.

Since the frequency difference of the lasers, $\Delta\omega$, can be tuned close to the modulation frequency by adjusting the crystal temperatures and the cavity lengths, the detected signal at $\Delta\omega$-Ω can be a very low frequency. The flexibility of the detection frequency alleviates the requirement of very high frequency photodetectors, and permit us to choose a convenient detection frequency. 500 MHZ was chosen in our measurement. The second laser, acting as a local oscillator, can significantly enhance the detection sensitivity. We were able to observe the phase modulation signal up to 60 GHz with a clear signal above the noise level using driving microwave power less than 0.1% of that required for π phase shift and moderate optical power into the modulator (Fig. 2). Using this technique, we have measured the frequency response of our polymer modulator from 40-60 GHz (Fig. 3), limited by our microwave source which was a semiconductor quadrupler. There is no

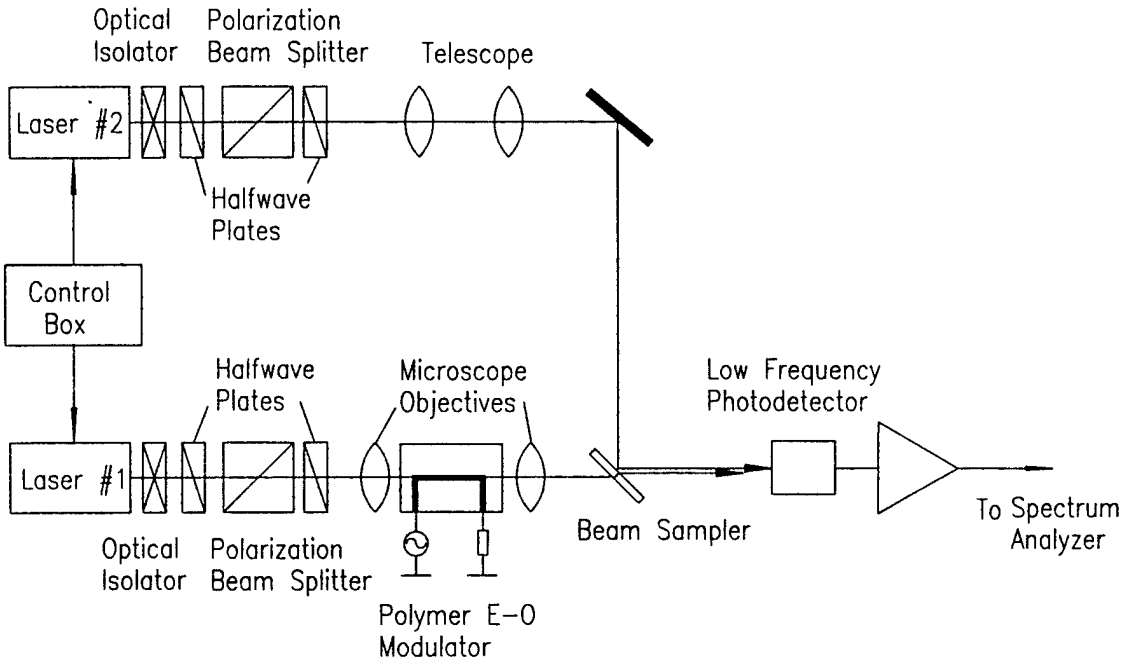

Figure 1. The experiment setup for optical heterodyne detection of the polymer E-O phase modulator.

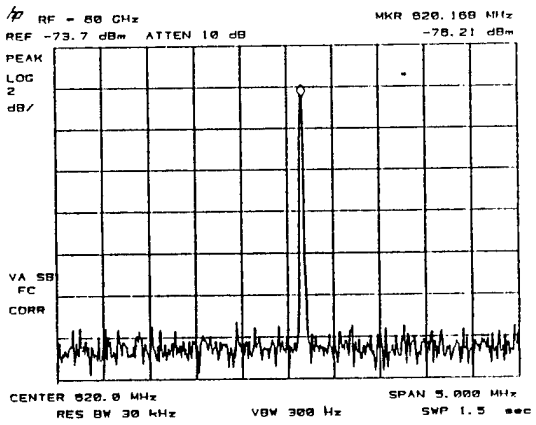

Figure 2. The optical heterodyne down converted 60GHz modulation signal.

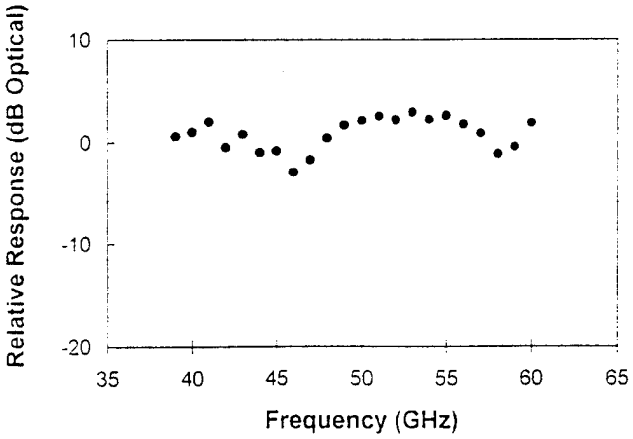

Figure 3. The frequency response of the polymer modulator from 40-60GHz.

identifiable rolling off at high frequencies other than resonances resulting from the mismatch between the microstrip line and the coaxial transitions. This indicates that there are no fundamental material difficulties for polymer devices with simple planar circuit structures to reach very high frequency performance, well into the millimeter wave range. Using a superstrate layer, even better velocity match could be expected, requiring only one more polymer layer spin-cast.

In conclusion, we have demonstrated up to 60 GHz E-O modulation from polymer traveling wave E-O modulators made of PUR-DR19. Our results showed that high frequency performance can be achieved with simple planar circuit structures, indicating polymer E-O modulators have the potential to be the future inexpensive high performance component for fiber millimeter wave links. Optical heterodyne detection has been validated as a powerful tool for millimeter wave modulator characterization. The cross-linked polymer demonstrated good temporal stability and durability at high optical power densities. Current efforts are to extend our device frequency response to 94 GHz using microwave transitions between waveguide and coplanar circuit. Further investigation of novel broadband microwave circuit designs is also under way. This project has been supported by National Center for the Integrated Photonic Technology (NCIPT) and Air Force Office of Scientific Research.

References:

[1] R. Lytel, *Proc. SPIE*, 1216, **30** (1990).

[2] C. C. Teng, *Appl. Phys. Lett.*, **60**, 1538 (1992).

[3] Y. Shi, W. H. Steier, P. M. Ranon, W. Wang, D. Chen, and H. R. Fetterman, *Organic Thin Films for Photonic Applications Technical Digest* 1993.

[4] W. Wang, D. Chen, H. R. Fetterman, Y. Shi, W. H. Steier, and L. R. Dalton, *Appl. Phys. Lett.*, **65**, 929 (1994).

[5] W. Wang, D. Chen, H. R. Fetterman, Y. Shi, W. H. Steier, and L. R. Dalton, to be published in *IEEE Photon. Technol. Lett.*.

[6] W. Wang, D. Chen, H. R. Fetterman, Y. Shi, and W. H. Steier, *CLEO '95, Baltimore, Maryland*, paper CthI39, May 1995.

[7] T. S. Tan, R. L. Junggerman, S. S.Elliott, *IEEE Trans. Microwave Theory Tech.*, **37**, 1217 (1989).

Wednesday, September 13, 1995

Active Devices II

WB 10:30 am-12:30 pm
Holladay Room

William H. Steier, *Presider*
University of Southern California

Integration of Nonlinear Optical (NLO) Polymer Waveguides with Indium Gallium Arsenide p-i-n Photodiodes

Jeffrey S. Cites
AEgis Research Corporation
6703 Odyssey Dr., Suite 200
Huntsville, AL 35806
Phone: (205) 922-0802 FAX: (205) 922-0904

Paul R. Ashley
Weapons Sciences Directorate
Research, Development, and Engineering Center
U.S. Army Missile Command
AMSMI-RD-WS-CM
Redstone Arsenal, AL 35898-5248
Phone: (205) 876-7484 FAX: (205) 842-2507

Richard P. Leavitt
U.S. Army Research Laboratory
2800 Powder Mill Rd.
Adelphi, MD 20783-1197
Phone: (301) 394-2042 FAX: (301) 394-2103

I. Introduction

The integration of optoelectronic functions on a common substrate can offer significant advantages in terms of size, weight, cost, and performance over traditional hybrid approaches. Given the advantages of NLO polymers over other material systems for integrated photonics applications (flexible fabrication, low dielectric constant, etc.) [1,2], it is advantageous to develop a processing technology for the integration of polymer waveguide devices on an active semiconductor substrate. The approach reported here allows for optimization of the semiconductor for source, detector, and electronic circuit functions, while relying on a flexible, multilayered spin-cast fabrication technology for passive waveguide and electro-optic modulator functions. Among those applications which may benefit from this integration are sensors such as the fiber optic gyroscope[3]. Reported here is the integration of NLO polymer waveguides with InGaAs p-i-n photodiodes on an InP substrate for operation at 1.3 μm, with special emphasis placed on the use of existing low-cost, low-risk fabrication processes.

II. Design and Fabrication

Figures 1, 2, and 3 show the top, side, and end views, respectively, of the waveguide/detector structure, where the photobleached polymer waveguide interacts with an etched trench in the lower cladding to exhaust light from the waveguide mode in the direction of the detector. A C-shaped electrode then collects the photocurrent. Figures 2 and 3 show that the optical confinement due to the photobleaching and the trench boundary is maintained inside the interaction region. The gold photobleaching mask is left in place after the fabrication to provide additional vertical confinement. The optical signal is free to radiate downward into the InGaAs detector layer to be absorbed.

The p-i-n photodiode detectors were grown by molecular beam epitaxy (MBE) on an n-doped (~$5x10^{18}/cm^3$) InP substrate, consisting of the following four layer structure: a 0.2 μm thick n-type $In_{0.52}Al_{0.48}As$ layer ($1x10^{17}$), an undoped 2.0 μm thick $In_{0.53}Ga_{0.47}As$ detector layer (residual p-type: $5x10^{15}$), a 0.2 μm thick p-type $In_{0.52}Al_{0.48}As$ layer ($1x10^{17}$), and a 0.02 μm thick p-type $In_{0.53}Ga_{0.47}As$ cap layer (~$1x10^{18}$). Channel detectors were formed by patterning self-aligned Cr/Au/Cr electrodes (10 / 200 / 50 nm) and chemically etching to a depth of 0.35 μm using a 1:1:9 solution of H_3PO_4:H_2O_2:H_2O at room temperature.

The polymer waveguide stack was fabricated next by spin casting a 4.5 μm thick lower cladding of Norland NOA-81 optical epoxy followed by reactive ion etching of the detector trenches in an argon/oxygen atmosphere. The polymer waveguide core material was Dow Chemical TP31, a nonlinear thermoplastic whose electro-optic properties have been previously reported in detail[4]. The polymer was spin cast to a thickness of approximately 3.0 μm. The upper cladding was applied in the similar manner as the lower cladding with a thickness of 3.5 μm. Next, 6.0 μm wide waveguide photobleaching masks were applied by gold evaporation (75 nm), photolithography, and reactive-ion etching in argon. The devices were then bleached for four hours at a UV power density of 17.2 mW/cm^2. Finally, vias were opened in the polymer stack by reactive-ion etching in argon/oxygen to permit access to the detector electrode bonding pads. An array of eight detectors were fabricated with channel lengths varying from 32 μm to 4.096 mm in a binary progression.

III. Device Characterization

A 1.3 μm laser diode was end-fire coupled to the devices. Photocurrent was measured as a function of detector length, optical input power, bias voltage, and polarization. Control waveguides fabricated adjacent to the integrated detector waveguides were used to determine coupling efficiencies and responsivities. Responsivity is defined here as the ratio of generated photocurrent to optical power coupled into the channel waveguide in units of amps/Watt. Coupling efficiency is defined as the percentage of optical power that is lost from the polymer waveguide in the interaction region, not necessarily the amount which propagates through or is absorbed by the the detector.

Figure 4 displays the coupling efficiency and responsivity of the detectors as a function of detector length (log scale) for a coupled input optical power of 3.7 μW. It can be seen from the coupling efficiency plot that this geometry is extremely efficient at exhausting the light from the channel waveguide, with approximately 90% out-coupling for an interaction length of only 100 μm. For detector lengths greater than 1 mm the coupling efficiency peaks at 98.5% and is noise-limited by the background light level of the planar waveguide. The responsivity plot in Figure 4 shows a trend of increasing response with detector length, with a sharp rise to nearly 0.1 A/W in the vicinity of 50 μm. The rapid rise in responsivity and the corresponding rise in coupling efficiency near 50 μm can be explained by considering a Gaussian beam diffracting in a half-space from the waveguide aperture. Therefore, a minimum interaction length exists for any significant detector response. The responsivity approaches 0.2 A/W for a length of 4 mm. This relatively low responsivity is limited by the detector design in which the p-cap is removed in the active region by chemical etching. Surface normal illumination measurements on the same detectors yielded similar responsivities. Responsivities measured with separately fabricated mesa devices at normal incidence exhibited much higher values. Polarization data was collected on the 1.024 mm detector and it showed a factor of 3.5:1 higher responsivity for TM polarization compared to TE polarization. This is easily explained by the ratio of the Fresnel reflection coefficients, given the refractive indices of 1.66 and 3.58 for the polymer and

InGaAs, respectively, and the spread of incident angles ($75° < \theta < 90°$ with respect to the surface normal) obtained from Gaussian beam diffraction.

Photodiode responsivities as a function of bias voltage were measured for the 1.024 mm detector for biases ranging from 0V to -2V. The responsivity was observed to increase linearly with reverse bias from 0.155 A/W at 0V to 0.198 A/W at -2V. Calculations show that the diode should be fully depleted near 0V, but since the p-cap was removed, the fringing field that is primarily responsible for carrier collection will increase steadily with bias voltage, enhancing responsivity.

IV. Conclusion

In conclusion, NLO polymer waveguides have been successfully integrated with InGaAs p-i-n detectors and operated at 1.3 μm. Optical coupling efficiencies over 98% and responsivities greater than 0.2 A/W were observed. Polarization sensitivity was observed due to differences in TE and TM reflection coefficients at the surface of the detector. Improvements to detector design as well as applications will be discussed at the meeting.

The authors wish to thank R.J. Gulotty of Dow Chemical for supplying the NLO polymer material.

---

[1] P.R. Ashley, "Overview of EO polymeric devices and fabrication," *Proc. SPIE,* **2290**, 114 (1994).

[2] R. Lytel, "Integration of EO polymers in optoelectronic devices," *Proc. ACS National Meeting - Polymer Preprints*, **35**, No. 2, 156 (1994).

[3] P.R. Ashley and R.J. Gulotty, "EO polymeric devices for fiber optical gyroscope applications," *Proc. ACS National Meeting - Polymer Preprints*, **35**, No. 2, (1994).

[4] R.J. Gulotty, D.J. Brennan, M.A. Chartier, J.K. Gillie, A.P. Haag, K.A. Hazard, M.N. Inbasekaran, P.R. Ashley, and T.A. Tumolillo Jr., *Organic Thin Films for Photonic Applications OSA Technical Digest,* **17**, 6 (1993).

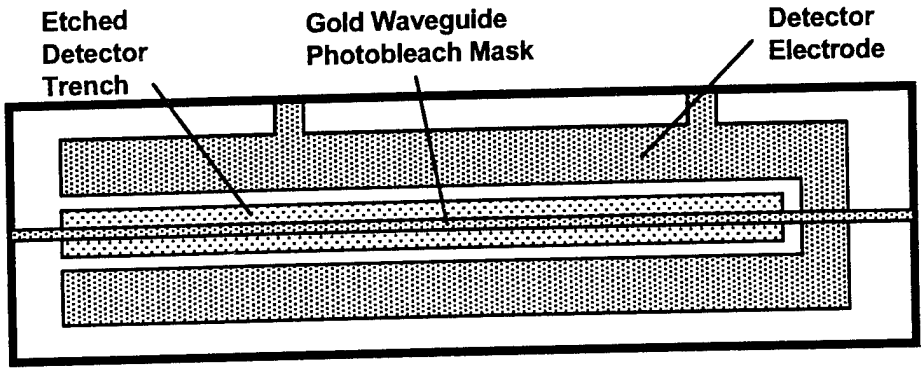

Figure 1. Top view of integrated waveguide/detector.

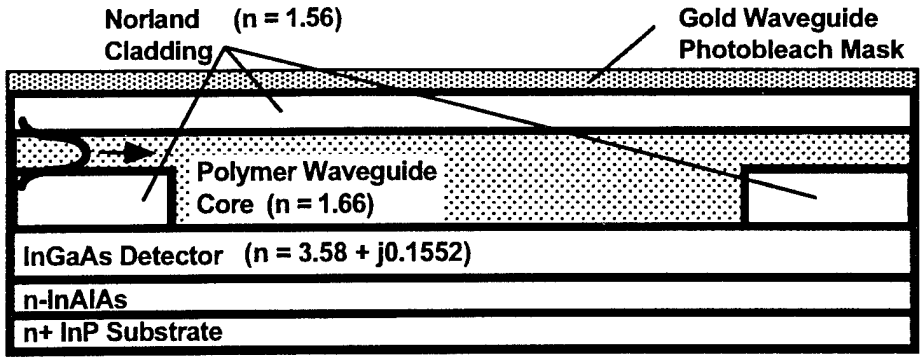

Figure 2. Side view of detector interaction region.

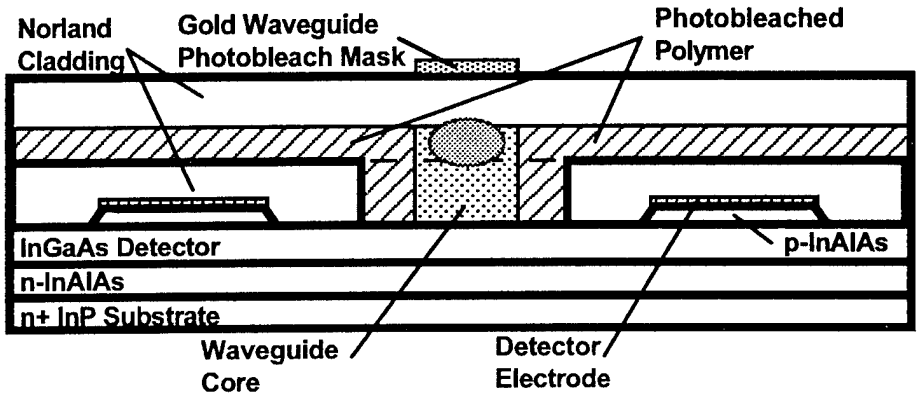

Figure 3. End view of detector interaction region.

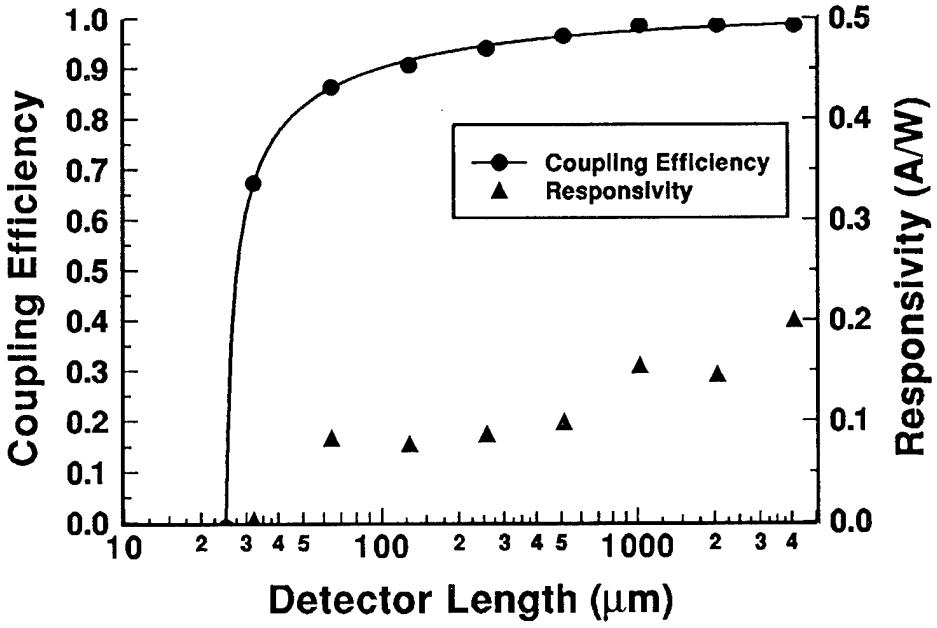

Figure 4. Coupling efficiency and responsivity versus detector length.

Arrays of Flip-Chip Mounted, Surface-Illuminated, Crystalline-Organic Optoelectronic Modulators on Glass Substrates

D. Yap
Hughes Research Laboratories, Malibu, CA 90265 (310-317-5360)
P.E. Burrows and S.R. Forrest
Princeton University, Princeton NJ 08544

INTRODUCTION

Thin films of organic molecular crystals are promising optoelectronic materials. Some of these crystalline organic materials can have very high optical nonlinearities. Conventional optoelectronic devices are usually formed on crystalline semiconductor substrates such as GaAs, InP or silicon which have a good lattice match with the optoelectronic material. In contrast, by using the ultrahigh vacuum process of organic molecular-beam deposition (OMBD), the crystalline organic materials can be deposited on highly lattice-mismatched substrates without generating defects.[1] Thus, devices can potentially be fabricated on a variety of substrates such as glasses, semiconductors, ceramics and polymers. This feature enables selection of the substrate to be based on considerations such as microwave or thermal properties, manufacturability or cost rather than being limited by the substrate's lattice match. Furthermore, it opens the door to a variety of new applications that require conformally embedded optoelectronic modules or large-area sheets of optoelectronic devices.

We have developed procedures based on conventional processes used in fabricating III-V semiconductor devices and circuits for fabricating the crystalline organic optoelectronic devices. We demonstrate these procedures by fabricating arrays of surface illuminated modulators on glass substrates. The modulators have an active layer that consists of the organic molecule 3,4,9,10-perylenetetracarboxylic dianhydride (PTCDA).Simple electronic and optical structures have been demonstrated in the past using PTCDA.[2,3] These structures were made primarily for characterization of the organic material and often involved non-standard or imprecise fabrication processes. The devices reported herein demonstrate the application of present state-of-art fabrication approaches to the crystalline organic devices. Due to the ability to fabricate devices with micron-level tolerances, the procedures developed afford for the first time an opportunity to realize a wide range of sophisticated organic device structures. The fabrication approach described can be applied to other organic materials and extended to more complicated optoelectronic circuits based on the crystalline organic materials; it finally makes feasible the integration of crystalline organic devices with III-V optoelectronic circuits.

MODULATOR STRUCTURE AND OPERATION

The basic structure of the surface illuminated modulator is shown in Figure 1. The modulator consists of an active region shaped like a circular mesa. The mesa is comprised of three layers. Two electrical contact layers sandwich a layer of PTCDA. The top electrical contact consists of thin

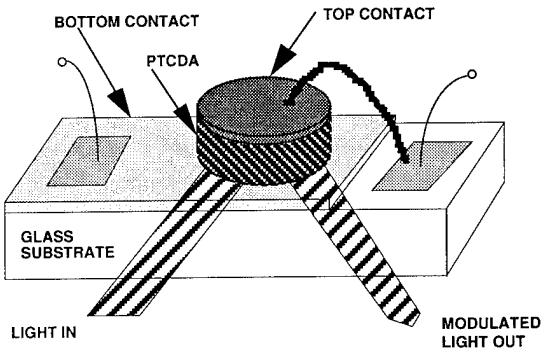

Figure 1. Illustration of basic crystalline-organic modulator structure.

films of nickel and gold, for the devices made. The bottom layer, in this case indium-tin oxide (ITO), extends beyond the mesa to form a pad for addressing the device. An electrical connection links the top contact layer to another pad adjacent to the mesa. The modulator is formed on a glass substrate. In normal operation, light to be modulated by the device enters from the back or substrate side. The light passes through the transparent ITO layer and the PTCDA layer, reflects off the top contact metal, and exits through the back side. Both the ITO and Ni/Au form electrically conducting (ohmic) interfaces with the PTCDA. Thus, current passes through the mesa when an electrical signal is applied. The injected electrical carriers in the PTCDA act to modify the optical refractive index as well as increase the optical absorption.

Arrays of 1×4, 1×8 and 2×8 modulators have been fabricated. Figure 2(a) shows an SEM photograph of a 2×8 array. Each modulator of the array can be addressed individually. It has one individual contact pad and shares the second contact pad with all of the other elements of the array. Figure 2(b) shows the back view of the modulator array, as seen through the glass substrate. The circular active regions can be seen clearly. These modulators have a mesa diameter of 60 μm.

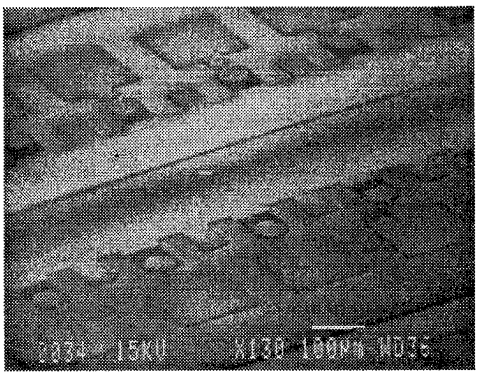

(a)

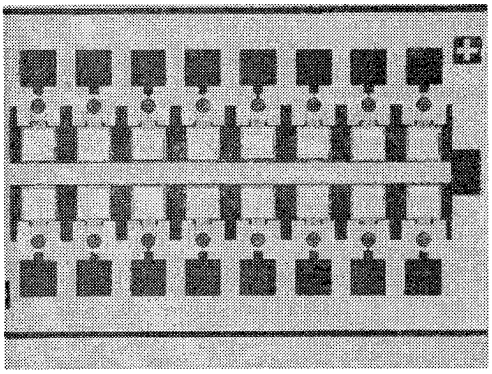

(b)

Figure 2. Photographs showing the (a) top side and (b) back side of a 2×8 array of crystalline-organic surface-illuminated modulators.

MODULATOR ARRAY FABRICATION

For the crystalline-organic devices to be suitable for high-volume optoelectronic applications, it is important that they be fabricated using conventional processing techniques. Several key issues were considered in developing the fabrication procedure for the modulators. These issues relate to chemical exposure and processing temperature. Some crystalline organic materials such as PTCDA are hydrophilic. Thus, for long-term stability, the crystalline organic materials should be encapsulated by an impermeable film. Such encapsulation is also needed to protect the crystalline organic material from attack by chemicals used in the device fabrication processes. For example, common positive-photoresist developers attack PTCDA. Also, PTCDA absorbs common organic solvents such as acetone and can swell or delaminate when immersed in baths of these solvents. Thus in fabricating the modulator arrays, a silicon nitride coating is deposited to encapsulate the PTCDA before any photolithography or metal liftoff step. Encapsulation is also useful for protecting the PTCDA from solder fluxes that may be used in hybrid integration or packaging. Another area of concern is the processing temperatures. The maximum processing temperature is limited by the decomposition of the organic material. PTCDA has a sublimation temperature of approximately 400°C. Thus, we have limited our process steps to temperatures below 300°C. Any steps requiring higher temperature, such as some processes for depositing ITO, are done before the PTCDA film

is deposited. In addition, mounting of the modulator arrays is done using low temperature solders such as Pb/Sn or In.

The procedure for fabricating the crystalline-organic modulator arrays is described next. It is based on standard semiconductor dry-processing methods. To fabricate the modulators, first, an ITO contact layer is deposited on a cleaned glass substrate. The ITO can be deposited by either sputtering or evaporation. Next, a layer of PTCDA is deposited at -190°C by OMBD. Films of Ni/Au (or Ti/Au) for the top contact are then deposited on the crystalline organic layer. Both ITO and Ni/Au form ohmic contacts to the PTCDA without the need for a high-temperature anneal. The subsequent processing steps involve the patterning and etching of the Ni/Au, PTCDA and ITO layers to form the active modulator mesa and the connections to the contact pads. When necessary, a film of silicon nitride is deposited before a photolithography step to encapsulate the PTCDA and protect it from the conventional photoresist developers and solvents. The nitride is deposited at temperatures of 200-300°C by a conventional plasma-enhanced chemical vapor deposition (PECVD) system. Etching of the silicon nitride, the Ni/Au, the PTCDA and the ITO layers are done by dry processes such as reactive ion etching (RIE) and ion-beam milling. The photolithographically patterned photoresist layers serve as the initial masks. To minimize the parasitic resistance of the device, the contact pads as well as the connection between the top contact and its pad are formed by plating a thick (>1 μm) layer of Au. The plating ensures that the connection to the top contact adequately traverses the physical step of the mesa and is preferred over depositing the interconnection by a lift-off process.

Figure 3 shows an SEM photograph of an etched mesa, with the top-contact, PTCDA and bottom-contact layers labeled. A sequence of dry etching steps were used to etch through the nitride, top-contact metals and the PTCDA but stop at the ITO layer. Figure 4 shows an SEM photograph of a completed modulator. Evident in the photo is the plated Au of the pads, the top contact and its interconnection. The extension of the ITO layer beyond the mesa is also evident.

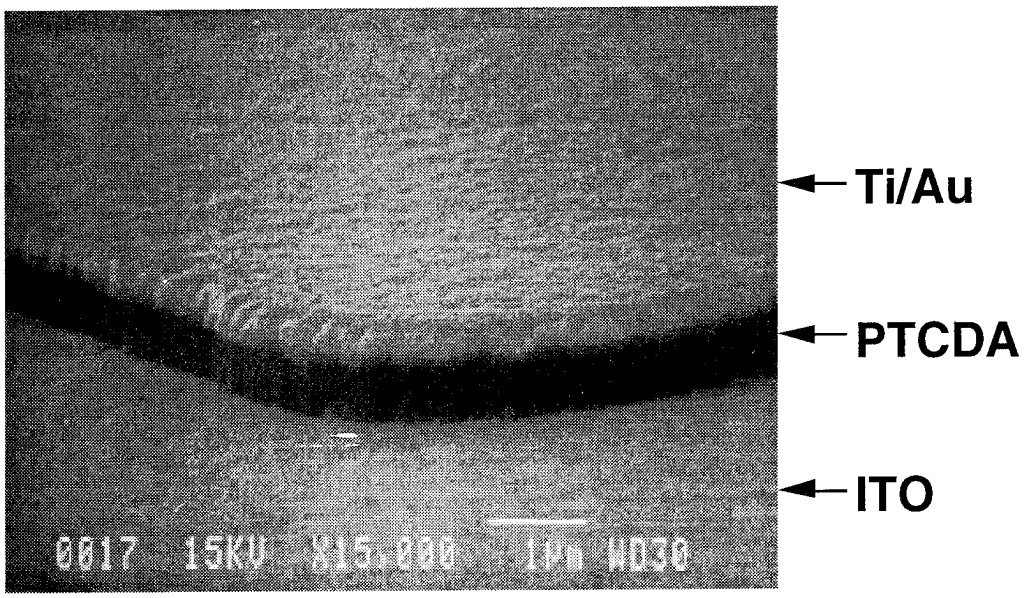

Figure 3. Dry etched mesa of the crystalline organic modulator.

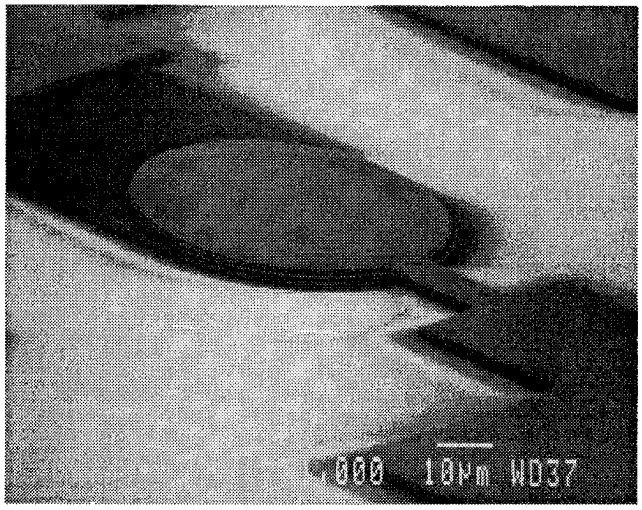

Figure 4. Crystalline organic modulator with Au plated interconnections and pads.

The electrical current-voltage characteristics of the modulators, shown in Figure 5, indicates the presence of conducting interfaces at both the PTCDA/ITO and the PTCDA/Ni interfaces. The current through the present devices is limited to a maximum value of 15 to 20 mA because of the finite current-carrying capability of the ITO layer. In order to measure the optical characteristics of the modulators, they were mounted in a flip-chipped manner onto another substrate that contains pads for electrical probing or contacting. Additional electrical and optical results will be reported at the presentation.

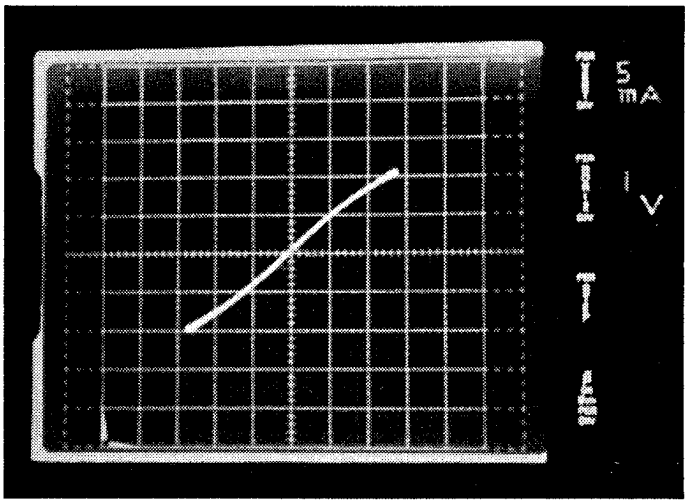

Figure 5. Electrical current-voltage characteristic of crystalline organic modulator.

REFERENCES

1. S.R. Forrest, P.E. Burrows, E.I. Haskal and F.F. So, Phys. Rev. B, **49**, 11309-11321 (1994).
2. V. Prabhakar, S.R. Forrest, J.P. Lorenzo and K. Vaccaro, IEEE Photonics Tech. Lett., **2**, 724-726 (1990).
3. D.Y. Zang and S.R. Forrest, IEEE Photonics Tech. Lett., **4**, 365-368 (1992).

LIGHT INDUCED SPATIAL MODULATION OF SECOND-ORDER OPTICAL NONLINEARITY VIA A PHOTOCONDUCTING LAYER

Rami Cohen and Garry Berkovic

Department of Materials and Interfaces

Weizmann Institute of Science

Rehovot 76100 Israel

Tel : + 972-8343423 Fax: + 972-8344138 e-mail : csberk@weizmann.weizmann.ac.il

Poling organic polymers containing hyperpolarizable dye species can produce high second-order nonlinearities. One limitation for application to second harmonic generation is the difficulty to achieve phase matching. A solution may be periodic spatial modulation of the nonlinearity to achieve quasi phase-matching [1].

We demonstrate a means for spatial control of $\chi^{(2)}$ by light using a bilayer film structure. One layer is a conventional NLO polymer-dye and the other is photoconductor - we have used [2] poly vinylcarbazole : trinitrofluorenone (PVK:TNF) as shown in Figure 1. Each layer is about 1 μm thick, over an area of several cm^2. Light from a mercury lamp passes through a mask to irradiate part of the sample, creating charge carriers in the illuminated area of the photoconductor. The corona source can pole the NLO polymer, and also leads to injection of charge from the photoconductor into the NLO layer.

Application of the corona field with simultaneous illumination of part of the film leads to different $\chi^{(2)}$ in the dark and irradiated areas of the film. A typical experimental result is shown in Figure 2. Several factors are responsible for the different responses from these two regions :

(a) A different electric field created by the corona in the two regions due to a drop of resistivity in the illuminated photoconductor

(b) Charge injection from the photoconductor to NLO layer in the illuminated region, which can lead to $\chi^{(2)}$ even at room temperature when samples cannot be poled [3]

(c) Photoassisted poling [4] of certain dyes (e.g. azo dyes such as Disperse Red 1) in the illuminated regions

We show how the interplay of these factors can be varied (by annealing, changing temperature, changing the dye etc.) to control the contrast between $\chi^{(2)}$ in the dark and illuminated areas of the film. An extension to periodic spatial modulation of $\chi^{(2)}$ should be possible by illuminating with crossed laser beams to form a grating structure - periodicities of the order of 20 μm required for quasi-phase matching are clearly achievable.

References

[1] M.A. Mortazavi and G. Khanarian, "Quasi-phase-matching frequency doubling in periodic polymeric structures", Opt. Lett. 19 (1994) 1290.

[2] R. Cohen and G. Berkovic, "Creation of Second-Order Nonlinearity in Polymers by Light induced Asymmetric Charge Injection" *Opt. Lett.* 14 (1994) 1025.

[3] S. Yitzchaik, G. Berkovic and V. Krongauz, "Charge Injection Asymmetry: A New Route to Strong Optical Nonlinearity in Poled Polymers" *J. Appl. Phys.* 70 (1991) 3949.

[4] Z. Sekkat and M. Dumont, "Photoassisted Poling of Azo Dye doped Polymeric Films at Room Temperature", *Appl. Phys. B* 54 (1992) 486.

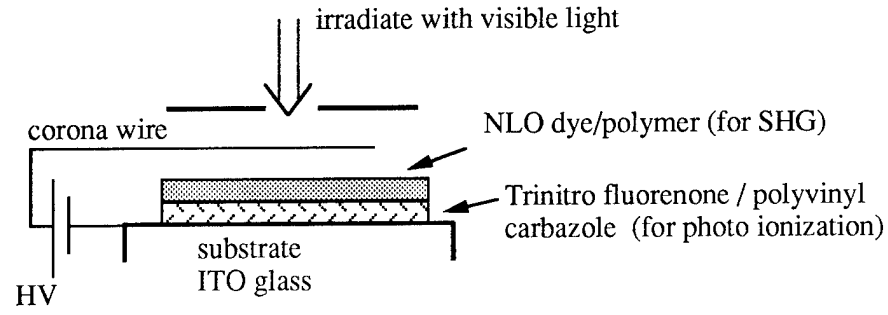

Figure 1. Set-up for production of spatially modulated $\chi(2)$ in a bilayer structure of a photoconductive film and NLO polymer film. Each film in the bilayer is 1-2 μm thick and area approx 2cm x 2cm..

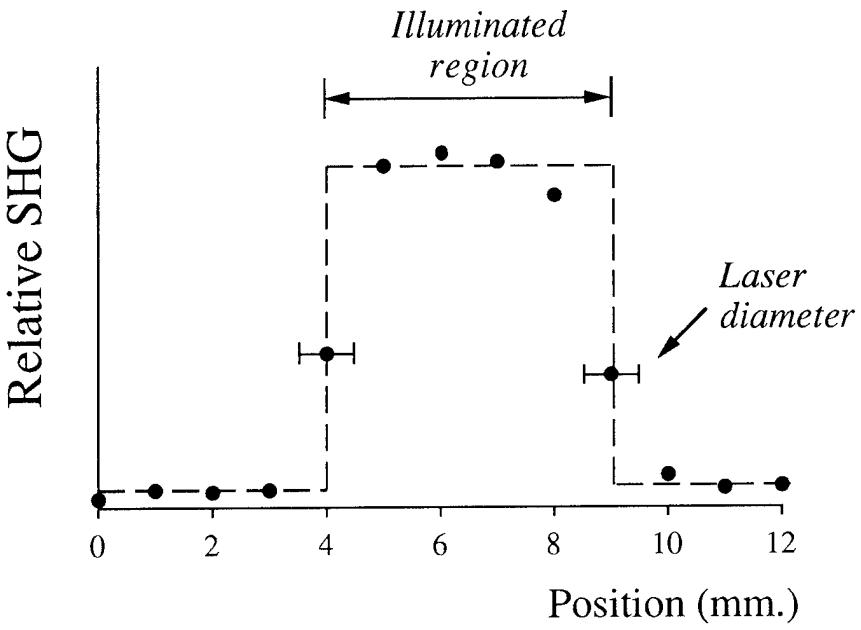

Figure 2. Typical resultant spatial distribution of optical second harmonic generation scanned across thefilm. In this example, the experiment was conducted at room temperature, and the NLO film is a blend of 2% of the dye DANS in PMMA. The material in the dark region cannot be poled efficiently, and a very sharp contrast between dark and lit regions results.

Miniature Integrated Optical Wavelength Analyzer Chip

R. E. Kunz and J. Dübendorfer

Paul Scherrer Institute, Badenerstrasse 569, CH-8048 Zurich, Switzerland
Telephone: +41 1 492 63 50 Telefax +41 1 491 00 07

1. Introduction

Measuring or monitoring the spectrum of narrow-band light sources such as lasers is an important application of spectrometers. The conventional spectrometer types are typically based on converting the angular light distribution emerging from wavelength-dispersive elements such as prisms or diffraction gratings into a spatially varying intensity distribution either in a free-space [1] or planar [2] arrangement.

In this paper, we report on a novel type of integrated optical (IO) spectrometer which basically consists of a coated thin plate through which a collimated beam of the light to be analyzed is transmitted. By means of a chirped grating coupler, a portion of the incident power is diffracted into a planar waveguide at a wavelength-dependent position. This approach achieves the wavelength-to-position conversion in one step directly at the waveguide grating, neither requiring an angular dispersion nor an imaging function. Therefore, it lends itself to the realization of compact miniature integrated optical wavelength analyzer (MIOWA) modules.

The working principle and the most important theoretical fundamentals are presented in Section 2. In Section 3, the feasibility of this approach for monitoring changes in the mode spectrum of a diode laser is demonstrated. Experimental results are reported and discussed for a replicated MIOWA chip based on a polycarbonate substrate.

2. Theoretical Fundamentals

Figure 1 shows an example of a MIOWA chip whose essential parts are two chirped waveguide grating pads G_1 and G_2. An on-chip degree of freedom is provided by the spatially varying grating periodicity $\Lambda(y)$, resulting in a spatial variation of the resonance condition for maximum power coupled into the waveguiding film F. The working principle is based on creating an 'IO light pointer' IOLP [3] by illuminating the complete

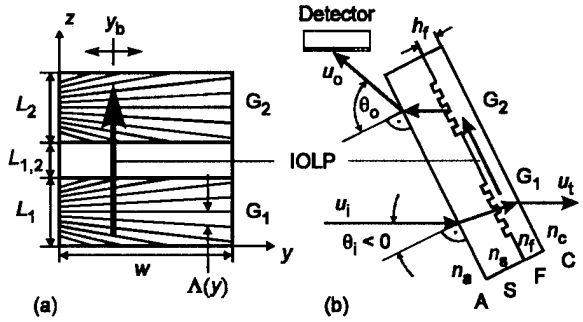

Fig. 1. Working principle of a MIOWA chip based on a dual chirped grating pad structure. Top view (a) and cross-section (b) schematically show the grating patterns and layers.

grating pad G_1 by the collimated input beam u_i, incident at a fixed angle θ_i. The IOLP is a guided beam with finite lateral extent, propagating at a position y_b for which the grating coupler resonance condition is fulfilled. For a monochromatic input beam, a change of its wavelength λ is converted into a change of the pointer position $y_b(\lambda)$ which represents an *on-chip measuring variable*. If the input beam is polychromatic, an ensemble of shifted IOLPs at the wavelength-dependent positions $y_b(\lambda)$ is generated, whose superposition gives rise to a spatial variation $I(\lambda)$ of the intensity emerging from the output pad G_2 at an exit angle θ_o. This intensity distribution, which is a measure for the spectral composition of the input beam, is directed by pad G_2 onto a photodetector (cf. Fig. 1b). This approach results in an extremely simple and compact readout arrangement, since neither any off-chip optical parts nor additional space is required for analyzing the exit beam u_o. An additional advantage is that the MIOWA chip can be designed to introduce only negligible distortions on the transmitted beam u_t.

In order to derive the most basic theoretical fundamentals, we consider the special case of a collimated monochromatic (laser) beam u_i, exhibiting changes of its wavelength λ which are to be measured. Figure 1b shows a typical MIOWA chip with a waveguiding film F (thickness h_f,

refractive index n_f) deposited on a substrate S with refractive index n_s. The refractive indices of the ambient (A) and cover (C) media are denoted by n_a and n_c, respectively. Only the most basic properties are treated here, making use of the thin grating approximation and the theoretical expressions presented in [4]. By means of the effective refractive index N, the waveguide dispersion relation can be expressed in a convenient form (cf. Eq. (1) in [4]). Taking the derivative by λ then yields the effective index dispersion $dN/d\lambda$. Since we consider the example of monitoring the mode spectrum of a laser source within a small spectral range of a few nm only, we can obtain simple yet meaningful mathematical expressions by neglecting the physical refractive index dispersion, i.e. by assuming the refractive indices n_a, n_s, n_f and n_c not to depend on the wavelength. This approximation leads to a compact expression for the effective index dispersion as

$$N' \equiv \frac{dN}{d\lambda} = -\frac{\varepsilon_{ef}}{N \cdot \lambda} \cdot \left(1 + \frac{F \cdot \lambda}{2\pi \cdot h_f}\right)^{-1} \quad (1)$$

with

$$F = n_f^{2\not p} \cdot \left[\frac{\left(q_{fs} \cdot N^2 - \varepsilon_{ef}\right)^{-\not p}}{\sqrt{\varepsilon_{es}}} + \frac{\left(q_{fc} \cdot N^2 - \varepsilon_{ef}\right)^{-\not p}}{\sqrt{\varepsilon_{ec}}} \right] \quad (2)$$

where

$$q_{fc} \equiv \left(n_f / n_c\right)^2;\ q_{fs} \equiv \left(n_f / n_s\right)^2 \quad (3)$$

$$\varepsilon_{ef} \equiv n_f^2 - N^2;\ \varepsilon_{ec} \equiv N^2 - n_c^2;\ \varepsilon_{es} \equiv N^2 - n_s^2 \quad (4)$$

and

$$\not p = 0 \text{ (for TE modes), } 1 \text{ (for TM modes).} \quad (5)$$

The wavelength of light in air is denoted by λ.

Upon illumination of the whole input grating pad by a collimated beam at a fixed angle of incidence θ_i, the photons are coupled into the waveguide at a position $y = y_b(\lambda)$ where the value $\Lambda(y)$ of the grating periodicity satisfies the grating coupler resonance condition for the effective index value $N(\lambda)$ obtained from the dispersion relation (cf. Eqs. (3, 10, 27) in [4]). This leads to a wavelength-dependent "resonant grating periodicity"

$$\Lambda = \Lambda(\lambda) = m_g \lambda / \left[N(\lambda) - n_a \sin\theta_i\right] \quad (6)$$

where m_g denotes the grating diffraction order. For simplicity, we assume a linear periodicity chirp

$$\Lambda = \Lambda_0 + g_\Lambda \cdot y \quad (7)$$

where g_Λ is the chirp gradient and Λ_0 is the periodicity at position $y = 0$. This leads to the MIOWA chip characteristic

$$y = y_b(\lambda) = \left[\Lambda(\lambda) - \Lambda_0\right] / g_\Lambda . \quad (8)$$

Again taking the derivative by λ, we obtain a simple expression for the sensitivity of the wavelength analyzer chip in terms of the linear dispersion

$$y' \equiv \frac{dy}{d\lambda} = \left(\frac{dy}{d\Lambda}\right) \cdot \left(\frac{d\Lambda}{d\lambda}\right) = \frac{\Lambda}{\lambda \cdot g_\Lambda} \cdot \left(1 - \frac{N' \cdot \Lambda}{m_g}\right). \quad (9)$$

Figure 2 shows the MIOWA chip characteristic, i.e. the variation of the light pointer position y_b versus the wavelength λ, which has been calculated based on Eq. (8). The parameter values correspond to the ones for the example presented in Section 3. For this MIOWA chip, the linear dispersion, i.e. the slope of the $y_b(\lambda)$ characteristic, is $y' = 0.607$ mm/nm for the TE_0 mode and $y' = 0.634$ mm/nm for the TM_0 mode.

Since no angle-to-position conversion is needed, no optical imaging function is required and hence, no quantities such as effective focal length [1] or Rowland circle diameter [2] appear in Eq. (9) for the linear dispersion, in contrast to the case of conventional spectrometers.

As can be seen from Eq. (6), the angle of incidence θ_i is a suitable parameter for setting the working point of the MIOWA chip. Thus, the same chip can be used for applications at very different wavelength regions just by mounting it at different angles with respect to the input beam. Furthermore, the angle θ_i provides the possibility to use the same chip for different polarizations.

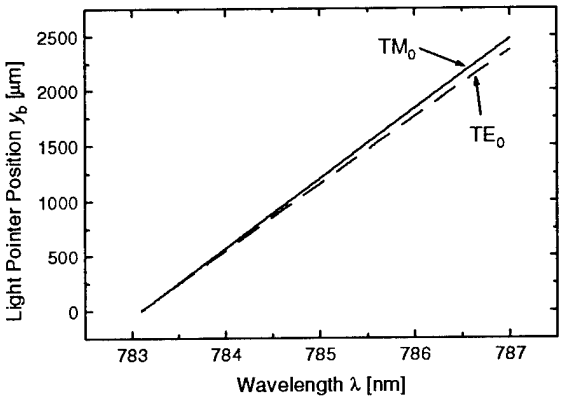

Fig. 2. Calculated characteristics showing the IO light pointer position y_b versus the wavelength λ of the input light beam for TE_0 and TM_0 guided modes.

This is illustrated by the characteristics shown in Fig. 2, where we have achieved the same wavelength $\lambda_0 (y_b = 0, \Lambda_0)$ for TE and TM polarization just by setting the angle of incidence to $\theta_i = -14.9°$ for the TE_0 mode and $\theta_i = -31.5°$ for the TM_0 mode.

As an alternative, MIOWA chips can also be realized based on other types of on-chip degrees of freedom. One such possibility is to use chips with a gradient effective index [3,4] for creating the IO light pointer.

3. Experimental Results and Discussion

Figure 3 shows the arrangement used for characterizing the MIOWA chip in a laser mode spectral analyzer application. The collimated beam of a diode laser (Sharp, LT026MD0, $\lambda \approx 785$ nm) is transmitted through the transparent substrate (polycarbonate, refractive index $n_s = 1.571$) and the dielectric waveguide grating. In this example, the chip was mounted in air, hence $n_a = n_c = 1.0$. The performance of the chip was investigated by coupling the transmitted beam u_t into a fiber for measuring its center wavelength λ_s by a commercial spectrometer (Ando AQ 6312B).

The feasibility of using chirped grating coupler chips for sensing applications was investigated by fabricating various sensor pads with different grating periodicities and chirps simultaneously on a 50x50 mm^2 sized polycarbonate sheet. Only one specific example, namely a dual grating sensor pad with design parameters $w = 2785$ µm, $L_1 = L_2 = 790$ µm, $L_{1,2} = 400$ µm (cf. Fig. 1) is considered here.

The waveguide was fabricated by depositing a thin TiO_2 film on the replicated polycarbonate substrate [5]. The only reason that we have chosen a hard dielectric film with a high refractive index is that we use this kind of waveguide also for other purposes such as refractometry and chemical sensing [4-7]. For an improved device, a cover layer with refractive index n_c could be applied on the waveguiding film F to render the chip insensitive to environmental disturbances by humidity and dust.

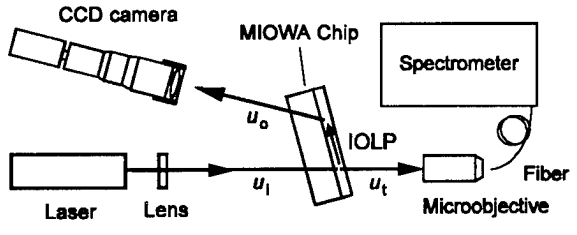

Fig. 3. Experimental setup for characterizing the MIOWA chip.

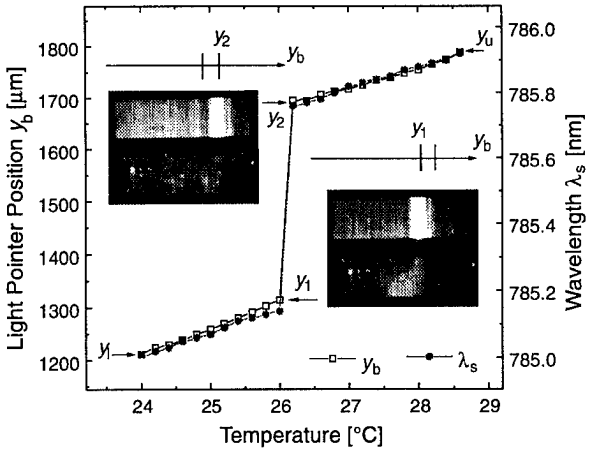

Fig. 4. Experimental results for wavelength analyzer chip. Comparison between the position y_b (□) of the light pointer and the wavelength λ_s (●) of the diode laser versus its case temperature. The insets show micrographs of the light distribution emerging from the MIOWA output pad taken by the CCD camera.

The waveguide parameters were determined in situ by means of an additional uniform grating pad using the procedures described in [5-7]. For the waveguide, a thickness $h_f = 159.9$ nm and a refractive index $n_f = 2.349$ were obtained.

Figure 4 shows the variation of the light pointer position y_b and the wavelength λ_s of the diode laser upon changing its case temperature T. The input pad G_1 was illuminated by the collimated diode laser beam (TM polarization) at an angle $\theta_i \approx -31.5°$. The emerging light distributions ($\theta_o \approx 7.2°$) were recorded by a CCD camera and then fitted with Gaussian curves to obtain the IOLP positions $y_b(T)$. In the insets of Fig. 4, the light pointer can be clearly seen as a bright bar on the output grating G_2. An additional white light illumination, with a filter (Schott RG9) to block the visible wavelengths, was used to show the pads themselves.

Forcing a mode hop of the diode laser by increasing its temperature to $T > 26°C$ produced a drastic increase of the light pointer position by $\Delta y_b = y_2 - y_1 = 381.2$ µm corresponding to a measured wavelength change $\Delta\lambda_s = 0.62$ nm.

The parameters for the grating pad G_1 have been calibrated by requiring the resonant periodicities at the lower and upper wavelengths λ_l and λ_u to be $\Lambda_l(y_l) = \Lambda(\lambda_l)$ and $\Lambda_u(y_u) = \Lambda(\lambda_u)$, respectively (cf. Eqs. (6) and (7)). This yields $\Lambda_0 = 352.8$ nm and $g_\Lambda = 8.766 \cdot 10^{-7}$. The output pad G_2 was also linearly chirped, the parameters being $\Lambda_0 = 499.9$ nm and $g_\Lambda = 1.724 \cdot 10^{-6}$. The gratings were 5 nm deep.

A linear dispersion $y' = 0.634$ mm/nm has been determined for this chip. To evaluate the chip performance, the values of the wavelengths at the 24 different temperatures, according to the data points in Fig. 4, have been determined based on the chip characteristic (Eq. (8)). The comparison of these values with those measured by the spectrometer resulted in a root mean square (rms) wavelength deviation of 0.012 nm. This represents the accuracy and resolution for monochromatic light sources. The corresponding values for broadband radiation depend on the detailed spectrum and are currently under investigation.

With one single chip, widely separated wavelength regions can be measured, since the angle of incidence θ_i is an appropriate parameter for setting the spectral working point of the MIOWA chip. As an example, we have successfully used the same chip for wavelengths in the visible as well as in the near infrared. A striking observation is to visually follow the changes in the mode spectrum of laser diodes upon changes of their operating parameters just by imaging the MIOWA chip light pointer with a video camera.

Calculations have shown that the above mentioned approach works for a very wide class of waveguides. Therefore, many different technologies and materials can be applied for fabricating MIOWA chips. Examples are chips based on semiconductor, glass or polymer [8] waveguides.

4. Conclusions

A novel integrated optical chip suitable for realizing compact miniature wavelength analyzers with a high linear dispersion is presented. The chip can perform the whole task of converting the spectrum of an input beam into a corresponding *spatial* irradiance distribution without the need of an imaging function. The most basic theoretical fundamentals for modelling the performance of this chip have been derived.

The feasibility of this approach was experimentally demonstrated by monitoring the changes in the mode spectrum of a laser diode upon varying its case temperature. Comparing the results with simultaneous measurements by a commercial spectrometer yielded an rms wavelength deviation of 0.012 nm.

An essential advantage besides its extreme compactness is that it can be used as part of a transmissive plate or window for the beam whose optical spectrum is to be measured or monitored (spectral beam sampling). A major aspect, besides the reduction of size and complexity, is the large potential for cost reduction offered by the suitability of these chips for low-cost mass production by replication.

The microoptical spectrometer chip presented here has very attractive features for applications such as on-line monitoring of laser mode spectra, finding and controlling the optimal operating conditions and stabilizing the wavelength of narrow band light sources.

References

[1] M. C. Hutley, *Diffraction Gratings* (Academic Press, London, 1982).

[2] K. R. Poguntke, J. B. D. Soole, "Design of a Multistripe Array Grating Integrated Cavity (MAGIC) Laser," J. Lightwave Technol., Vol. 11, 2191 - 2200 (1993)

[3] R. E. Kunz, "Gradient Effective Index Waveguide Sensors," Sensors and Actuators B, Vol. 11, 167-176 (1993).

[4] R. E. Kunz and L. U. Kempen, "Miniature Integrated Optical Sensors," Proc. SPIE, Vol. 2068, 69-86 (1994).

[5] R. E. Kunz, J. Edlinger, P. Sixt and M. T. Gale, "Replicated Chirped Waveguide Gratings for Optical Sensing Applications," Sensors and Actuators A, Vol. 47, 481-485 (1995).

[6] R. E. Kunz, C. L. Du, J. Edlinger, H. K. Pulker and M. Seifert, "Integrated Optical Sensors Based on Reactive Low-voltage Ion-plated Films," Sensors and Actuators A, Vol. 25, 155-159 (1991).

[7] R. E. Kunz, J. Edlinger, B. J. Curtis, M. T. Gale, L. U. Kempen, H. Rudigier, and H. Schütz, "Grating Couplers in Tapered Waveguides for Integrated Optical Sensing," Proc. SPIE, Vol. 2068, 313-325 (1994).

[8] L. Baraldi, R. E. Kunz and J. Meissner, "High-precision Molding of Integrated Optical Structures," Proc. SPIE, Vol. 1992, 21-29 (1993).

Photomechanical Multistability and Logic in a Polymer Optical Fiber

D. J. Welker and M. G. Kuzyk

Department of Physics, Washington State University, Pullman, Washington 99164-2814

phone: 509-335-4672 fax: 509-335-7816

Optical multistability and optical logic both operate on the principle that light can interact with itself through an intensity dependent refractive index. More precisely, an intensity dependent phase shift is responsible. This implies that multistability can originate in both a refractive index change or a physical path-length change within a material. While the refractive index mechanism has been routinely studied, the implications of the length change mechanism has been largely ignored. In this contribution, we show that an intensity dependent length change can be used to build a new class of devices. In particular, we show that mechanical and optical multistability in a polymer optical fiber Fabry-Perot interferometer can be used in the design of a mesoscale all-optical vibration suppressor and an optical positioner.

Figure 1 shows three possible designs of the all-optical photomechanical vibration suppressor. Figure 1a shows the design in which we have demonstrated multistability. The ends of a multimode poly(methyl methacrylate) (PMMA) polymer optical fiber are cut with a razor blade to form a beveled end. The fiber end thus acts as a retroreflector. Due to spread of the light rays, some of them are reflected while others are transmitted out of the fiber. The fiber ends so prepared thus act as partial reflectors that form a Fabry-Perot cavity. The fiber is doped with the azo dye DR1 to increase its absorbance at 670nm, the wavelength of the

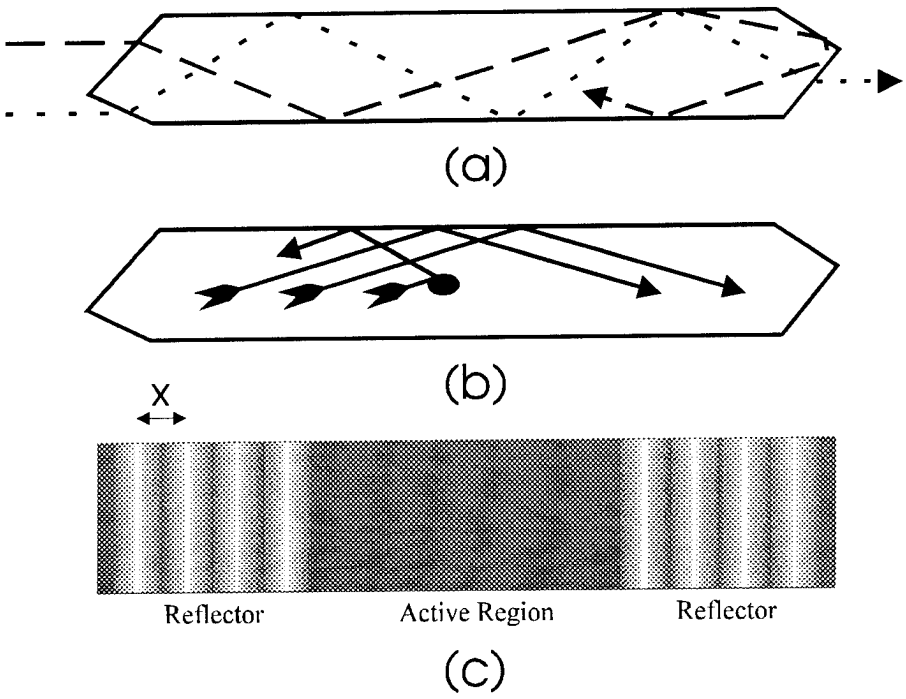

Figure 1: Three methods for defining reflectors in a fiber, a) retroreflector, b) impurity site, c) refractive index grating.

laser diode source. The intensity of the light inside the interferometer depends on the round trip optical path length in the cavity. A change in either the refractive index or the length results in a change in optical path which causes a change in the cavity intensity. Because the fiber is slightly absorbing at the laser wavelength, a change in the cavity intensity will result in a change in its temperature. Through photothermal heating, then, both the fiber's length and refractive index can change. In our dye-doped PMMA polymer, the phase shift due to a photothermal length change (as calculate from the coefficient of thermal expansion) is about half as large as the change in phase due to a refractive index change. Any measured phase change thus contains both contributions.

The Fabry Perot cavity acts as a length stabilizer (i.e. a vibration suppressor) because it is inherently a feedback system: the length of the fiber is a function of the intensity inside the fiber while the intensity is a function of fiber length. When the fiber is in thermal equilibrium with the laser source, that is - its cooling rate is balanced by the energy added by the laser, it will resist changes in its length. For example, if the system is tuned so that

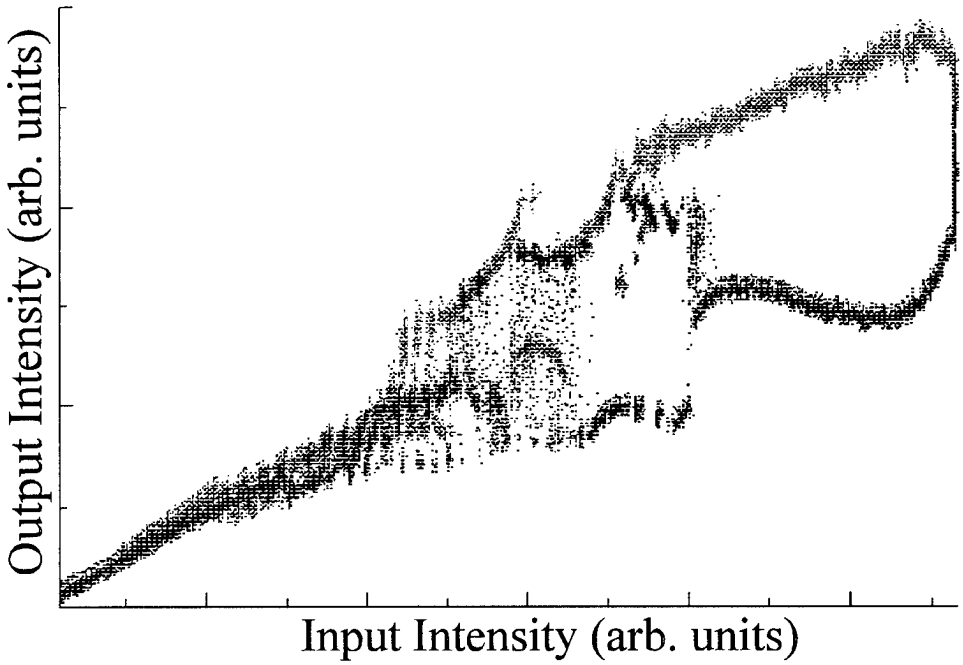

Figure 2: Input intensity versus output intensity for an MPU.

a decrease in the length results in an increase in the intensity within the fiber, a decreased length will result in photothermal heating, thus restoring the fiber to its equilibrium length. The operation of this miniature fiber device works analogously to the bulk device that we have previously demonstrated.[1, 2]

In the previous bulk device demonstration, we found that for a fixed input laser intensity, the fiber length could occupy a series of stable lengths. This an example of multistability. Because the length state of a fiber Fabry-Perot cavity determines the transmitted intensity, the system should also exhibit optical bistability. We have therefore performed measurements of the fiber's output intensity as a function of input intensity.

Figure 2 shows the output versus the input intensity of a 2cm PMMA fiber of 100μm diameter that is doped with 0.1% DR1 dye. A diode laser as 670nm acts as the light source. The input intensity is ramped up at a uniform rate until the laser diode reaches its maximum intensity. The laser is then ramped down at a uniform rate. There are several interesting features of the data. First, hysteresis is clearly evident. Furthermore, there appear to be several stable branches for a fixed input intensity. At lower power, there is clear evidence of

chaotic behavior. All of these observations are consistent with a feedback system.

It is interesting to speculate about the new classes of devices that are made possible by these mesoscopic photomechanical units (MPU). Because they act both as an optical logic unit (the output intensity is a nonlinear function of input intensity) and a photomechanical unit, they offer the possibility of making smart composite materials in which the embedded MPUs detect stress and react accordingly through the photomechanical effect. Figure 1b shows an MPU in which an impurity site acts as an additional reflector while Figure 1c shows reflectors that are made from a refractive index grating. Such gratings can be formed with photobleaching techniques. It is thus possible to make a series of MPUs in a single fiber. This would allow for a high degree of interconnection, in which the state of each MPU would be determined by the states of all other units. Because each unit's state depends on both its mechanical state, and, the light intensity within, an association of units could be designed to respond collectively to external stimuli. This would make possible such applications as smart skins that act as vibration or acoustic suppressors.

In summary, we have demonstrated a mesoscale polymer fiber Fabry-Perot interferometer that is optically and mechanically multistable; and, offers the possibility of high levels of integration. This work was supported by the Army Research Office.

References

[1] D. J. Welker and M. G. Kuzyk, Proc. of ICIM'94, 1308, Technomic Press, Lancaster (1994)

[2] D. J. Welker and M. G. Kuzyk, Appl. Phys. Lett. **64**, 809 (1994).

Vertical Integration of Polymer Electro-Optic Devices on Electronic Circuits

Srinath Kalluri, Antao Chen, Mehrdad Ziari and William H. Steier
Department of Electrical Engineering, University of Southern California
Los Angeles, CA 90089-0483
Tel: (213) 740-4408, Fax: (213) 740-8689

Zhiyong Liang and Larry R. Dalton
Chemistry Department, University of Southern California
Los Angeles, CA 90089

Datong Chen and Bahram Jalali and Harold R. Fetterman
Department of Electrical Engineering, University of California - Los Angeles

A major topic of research in the opto-electronics field over the last decade has been the integration of photonic devices with electronic circuits. The major hurdle here is the fabrication incompatibility of the different material systems required for electronics and photonics. Most integrated photonic devices with applications in fiber communications are fabricated from compound semiconductors (lasers, modulators, detectors) or from crystalline dielectrics (modulators). On the other hand Si electronics (or GaAs for high speed) are highly developed and available through semiconductor foundries. To integrate this well developed electronics technology with conventional photonics technology has required techniques like flip chip bonding, epitaxial liftoff, solder bump technology and other forms of hybrid integration.

Polymer electro-optic materials offer many advantages over conventional materials for opto-electronic integration. The devices are relatively easy to fabricate, the processing technology is compatible with semiconductor processing, and they can be fabricated directly onto preprocessed semiconductor circuitry. Many polymers such as photoresists, polyimides, epoxies, silicones and spin on glasses are commonly used in semiconductor processing. The integration of electrooptic polymers with high speed integrated electronics to achieve high speed opto-electronics is a promising approach.

Polymer-semiconductor integrated opto-electronics has potential applications in several areas such as linearized optical modulators for CATV and microcell wireless systems and as integrated smart switching nodes for high bandwidth optical communication systems. There is good potential for this approach to lower the cost of opto-electronic devices and circuits. However to achieve this integration there are several technical issues that must be addressed. Among these are the issues of planarizing the wafers as a base for low loss optical waveguides, protecting the electronics during polymer poling, interconnects between the electronic and photonic layers, packaging and hermetic sealing.

As a first step towards the monolithic integration of active polymer devices on Si electronics we have built an EO phase modulator on top of planarized VLSI circuitry. Since the Si circuits were fabricated before the polymer electro-optic devices, the various thermal cycling steps involved in the electronics fabrication process take place before the deposition of the active polymer layer, thus avoiding problems with the thermal stability of the nonlinearity. However, in the normal fabrication of electronic devices the various etchback, diffusion and metalization steps leave the surface topology of the Si circuitry very non-planar. Acceptable optical substrates, on the other hand, need a high degree of surface uniformity to permit fabrication of low optical loss passive and active waveguide devices. Therefore, the first step in the integration is to planarize the various step heights of the VLSI circuit. We deposited a 4.5μm thick layer of the thermosetting polymer PC3-

6000 (Futurrex) as the planarizing layer. The sample was then heated in air on a 200 °C hot plate to cure the material. At these temperature the material also re-flows from the peaks to the troughs which further smoothens out the surface topology.

To test the quality of this "optical substrate" we made optical loss measurements on polymer slab waveguides prepared on the planarized substrates. Surface non-uniformity is expected to increase scattering loss. We evaluated scattering losses using the streak method. For comparison purposes, we fabricated slab waveguides on optically smooth Si substrates with 4 μm of thermally grown SiO_2 lower cladding. Our results indicate that the scattering loss on planarized substrate is low and comparable to the optically smooth Si/SiO_2 substrate waveguide. Figure 1 shows a photograph of the in-coupled and out-coupled light for a slab waveguide on the planarized substrate.

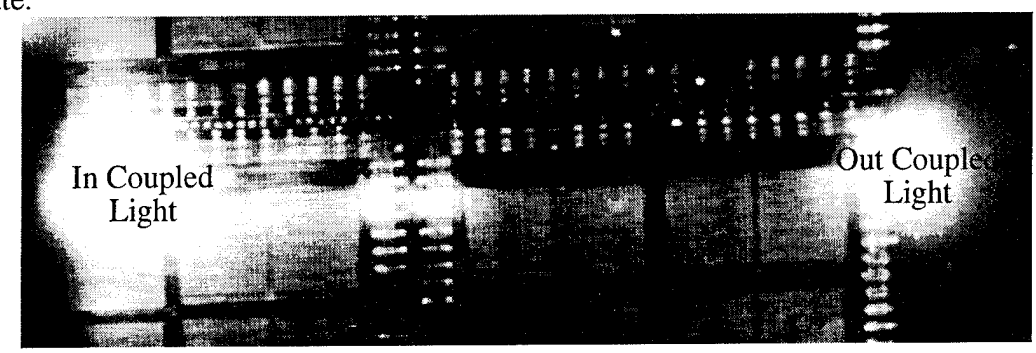

Figure 1: Waveguiding on Planarized Substrate

The fabrication sequence for a slab phase modulator is shown in Figure 2. On the planarized substrate, we first evaporated a 0.2μm layer of gold on which a lower epoxy cladding layer of index, n (1.06μm) ~ 1.55) and thickness 5-6 μm thick was spin coated and cured. Next a DR-19 dye containing EO guiding layer, PURDR19, (n (1.06μm) ~ 1.67, thickness ~ 1.4μm) was deposited and corona poled. Next, a thin 0.1 μm to 0.2 μm polysiloxane spin on glass (SOG, n (633) =1.42) layer was spin coated. This material when cured has excellent etch resistance to O_2 RIE and can therefore be used as an etch stop for subsequent processing.

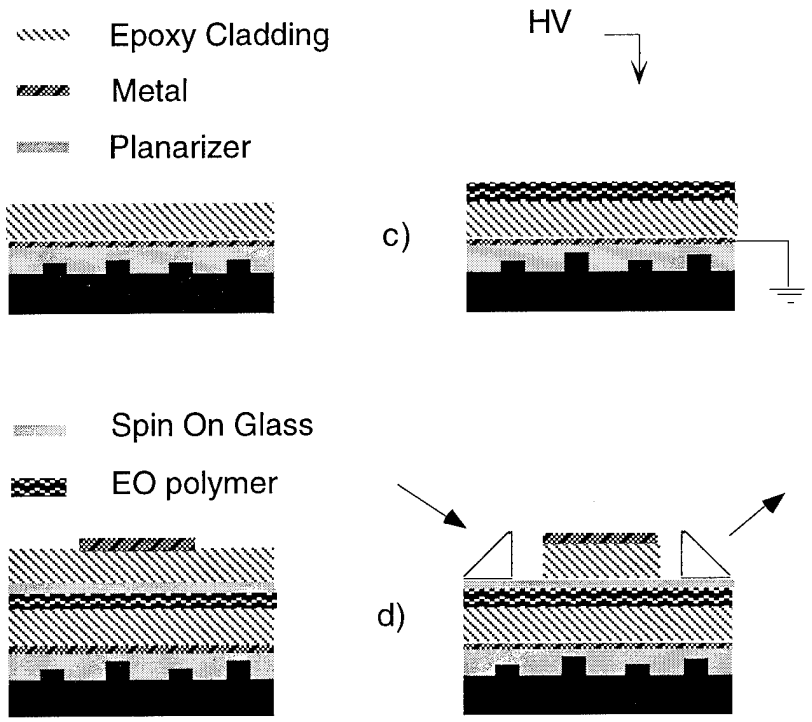

Fig. 2: Fabrication of Slab Modulator

Normally, this material cures at 200 °C; such a high temperature, however, would cause relaxation of the molecular alignment of the poled EO layer. An alternate method for preparing this layer is to O_2 RIE etch off all the organic species contained in the organosilicon SOG. The SiO_2 species that remain on the surface after the etch are highly solvent and O_2 RIE resistant. The plasma etching parameters used were 200 mTorr O_2 pressure, 150 Watts power, etch times of 15-20 minutes. Other than the room temperature processing, one advantage of this kind of "curing" is its insensitivity to the processing parameters. Once the organic species are removed subsequent etching has little effect on either the SOG etch stop or the underlying polymer layers. On top of the spin on glass layer, an upper cladding of 6 μm thick epoxy was spun and cured at room temperature.

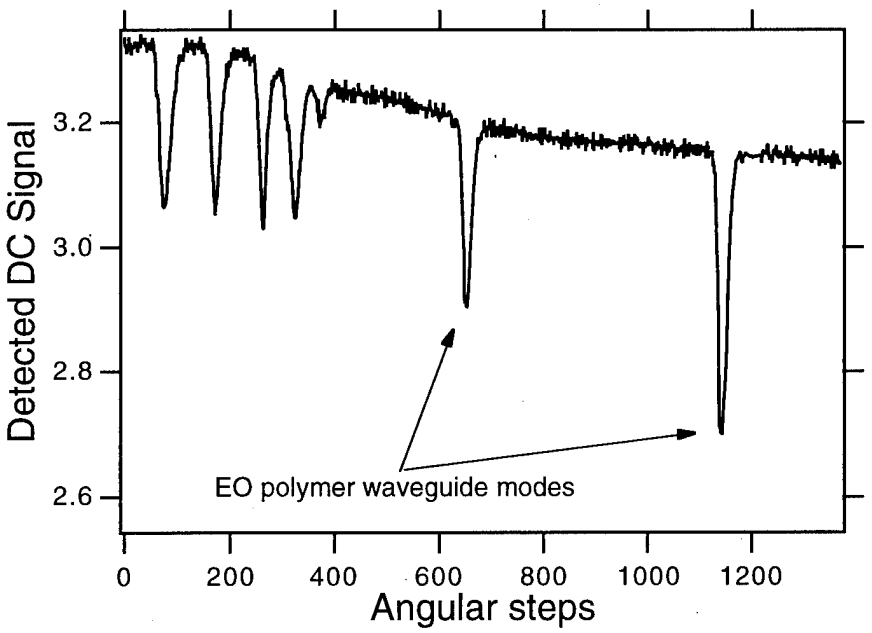

Figure 3: Mode dips for device obtained by using attenuated total reflection (ATR)

The final layer was a shadow masked, 1 cm wide, 0.2 μm thick evaporated Au electrode. Since it is not possible to prism couple through 6μm of upper cladding, the epoxy on either side of the metal electrode was O_2 RIE etched. Here the metal electrode acts as the etch mask and the SOG serves as an etch stop. The TE waveguiding mode dips measured using attenuated total reflection (ATR) for the finished device are shown in figure 3. The two mode dips at angular steps greater than 600, correspond to the two modes of the epoxy/PUDR19/SOG-epoxy composite waveguide. An additional advantage compared to say a metal etch stop layer is that the SOG is essentially an optical material and therefore unlike a metal does not contribute to optical loss. Thus this material need not be removed. Performance measurements of this phase modulator will be presented. Fabrication of single mode channel phase modulators with the potential for better confinement and lower loss are also underway.

The wafer on which we performed the integration was obtained from aborted fabrication runs. Therefore, any degradation of the electronics during the poling and modulator fabrication process could not be determined. To explicitly test the charge and temperature sensitivity of electronic circuits to the poling and fabrication process we subjected several GaAs MESFETs to various aspects of the fabrication process. One sample was first coated with the planarizing polymer and then cured and reflowed at 200 °C for half hour. A water soluble polymer PAA was spun on the planarized substrate. Next, a 0.1μm Cr layer was vacuum evaporated, and a 1μm layer of photoresist was spun and dried. This photoresist layer serves as a dummy electro-optic polymer. The metal layer acts both as a ground plane for subsequent poling and as a shielding layer for the underlying electronics. A corona poling profile typical for most of our device polymers; 140 °C for 45 min. and needle voltage of 6kV was used to simulate the poling conditions. The substrate was then immersed in deionized water for approximately 2-3 hours. The water dissolves the water soluble PAA and thus permits easy removal of the metal and photoresist layers. The substrate was

then transferred to a RIE chamber where the planarizing polymer was etched off in an oxygen plasma. The plasma etching parameters were: 150 W RF power, 200 mTorr O_2 pressure, and 15 minutes etch time. These parameters are more than adequate for the etching requirements of normal polymer waveguide fabrication.[1] Figure 4 shows the I-V characteristics of the MESFET devices on this substrate and demonstrates that there was no degradation after the poling process.

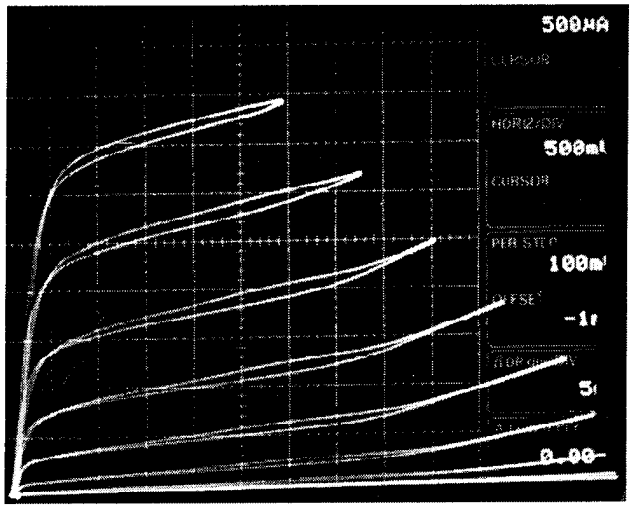

Figure 4: I-V characteristics of GaAs MESFETdevice after annealing and poling

These experiments demonstrate in principle that the integration of polymer electro-optic modulators on Si electronics is possible. The next step in the integration process is to fabricate polymer phase and amplitude modulators on working electronic circuitry. Thus schemes to provide interconnection pathways between the electronics and photonics layers and other packaging aspects must be worked out in order to demonstrate a self contained chip in which the underlying electronics perform some useful function in either driving or imposing functionality to the optical modulator integrated above. Experiments that deal with these issues are in progress.

References:

[1]. W. H. Steier, Y. Shi, P. M. Ranon, C. Xu, B. Wu and L. R. Dalton, "Waveguide photonic devices made from thermally crosslinked second-order nonlinear optical polymers," in Nonlinear Optical Properties of Organic Materials VI (San Diego, 1993), Vol. 2025, pp. 535-546.

C_{60}:Electron Donor Nanocomposites and Multilayer Structures for Nonlinear Optics

Harry W. Sarkas and Zakya H. Kafafi
U.S. Naval Research Laboratory, Washington, DC 20375
Phone: (202) 767-9529
Facsimile: (202) 404-8114
E-mail: KAFAFI@CCF.NRL.NAVY.MIL

Since the development of preparative scale syntheses of the fullerenes, [1] we have examined the nonlinear optical (NLO) properties of C_{60} in the solid state.[2-4] Following the characterization of solid films of pure C_{60}, we have explored means of altering the optical and NLO properties of this molecule via chemical modification including photopolymerization, oxygen doping, and the creation of charge transfer (CT) complexes in both the ground and excited states. [5-7] Studies on solutions of C_{60} with the electron donor, N,N,N′,N′-tetramethyl-1,4-phenylene-diamine (TMPD) revealed the formation of a 1:1 CT complex where C_{60} acted as the acceptor. NLO studies conducted on solutions of C_{60}/TMPD at 675 nm (near the λ_{max} of the CT absorption) showed a great enhancement in the third-order optical susceptibility, $\chi^{(3)}_{xxxx}$, of the complex relative to C_{60}. Direct optical excitation in the CT band accessed higher-lying excited states with larger absorption cross-sections than the ground state, which contributed to the enhanced NLO response observed for the TMPD:C_{60} complex.[5]

Since this initial effort, we have started to prepare C_{60}-based CT complexes in the solid state by high vacuum deposition, and explore their linear and NLO properties. More recently, we have reported on the synthesis of a solid state composite of C_{60} and 5,10, 15,20-tetraphenyl-21*H*,23*H*-porphine (TPP). The resultant TPP:C_{60} CT complex was characterized by visible-near infrared absorption spectroscopy. Nonlinear transmittance conducted at 590.5 nm near one of the broadened TPP vibronic bands showed that the TPP:C_{60} CT complex acts as a reverse saturable absorber. Degenerate four-wave mixing (DFWM) studies performed at the same wavelength showed a large contribution to the real part of $\chi^{(3)}_{xxxx}$.[6]

The formation of these CT complexes results in weak ground state absorptions. Since C_{60} has been shown to act as a stronger electron acceptor in the excited state than in the ground state,[8] the composite materials tend to have larger absorption cross sections in their excited states than in their ground states. This condition can give rise to an enhanced nonlinear optical response.

We have also prepared and spectroscopically characterized films of C_{60} with electron donor materials that have been assembled as organic multilayer structures (OMLS). Recently, Agranovich has predicted significant enhancements in both the second and third-order optical susceptibilities for these types of structures owing to exciton confinement and interfacial effects.[9,10] In addition, Zakhidov and Yoshino have predicted novel electronic properties for organic multilayer structures due to interactions at the interfaces which can be exploited for some device applications.[11]

High optical quality films of C_{60} with the electron donors: N,N,N′,N′-tetramethyl-1,4-phenylene-diamine (TMPD), N,N′-bis-(3-methylphenyl)-N,N′-bis-(phenyl)benzidine (TPD); 5,10, 15,20-tetraphenyl-21*H*,23*H*-porphine (TPP); 5,6,11,12-tetraphenylnapthacene (rubrene) were prepared by high vacuum deposition. Nanocomposite films having 1:1 molar ratios were prepared by codeposition. Both C_{60} and the electron donor material were codeposited from resistively heated furnaces at total deposition rates of 6-10 Å/s onto sapphire substrates maintained at room temperature while under high vacuum (~1×10^{-9} Torr). Film thicknesses and compositions were controlled using quartz crystal microbalances. Multilayer structures of C_{60} with TPD, TPP, or rubrene were prepared by depositing alternating layers of C_{60} and a given electron donor material under comparable conditions. Optical characterization of these materials was carried out ex-situ by recording optical spectra using a Perkin-Elmer Lambda 9 Spectrophotometer. Film thicknesses for all materials were determined by examining interference fringe patterns in the near-infrared regions of the spectra where the films are transparent.

Figure 1 shows the optical spectra of one micron thick films of C_{60}, TPD, and a 1:1 molar TPD:C_{60} composite. The spectra of the pure materials have been scaled to reflect the amount of each material in the composite. The broad absorption in the TPD:C_{60} composite spectrum appearing to the red of the absorptions in the C_{60} spectrum is attributed to the formation of a CT complex.

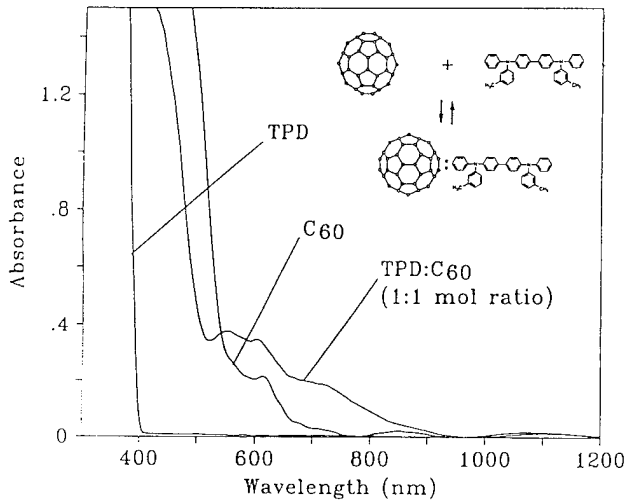

Figure 1. Absorption spectra for films of C_{60}, TPD, and TPD:C_{60} (1:1) on sapphire.

The optical absorption spectra for two organic multilayer structure (OMLS) films of C_{60} and TPD are presented in Figure 2, along with the spectrum for a film of pure C_{60}. As indicated on the figure, one of these films was fabricated by depositing 250 alternating 40 Å thick layers of C_{60} and TPD, while the other was prepared by depositing 125 alternating 80 Å thick layers, with total thicknesses of 1μm. The spectra of both OMLS materials show broad, weak absorptions similar to that seen for the composite material. The appearance of these features is indicative of

charge transfer at the interfacial regions. In addition, the weaker C_{60} absorption at 430 nm of the 40 Å OMLS is consistent with the expectation of significantly less free C_{60} (ie., a larger fraction of C_{60} interacting at the interfaces) in this film.

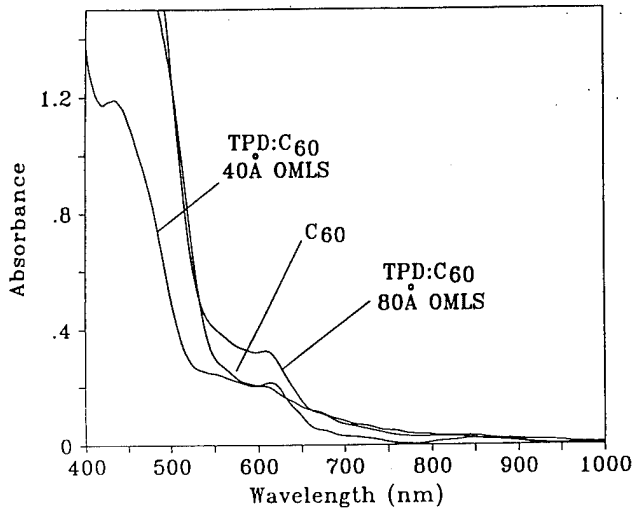

Figure 2. Absorption spectra of C_{60}, and OMLS films of TPD and C_{60} on sapphire.

Figure 3 shows the optical spectra of one micron thick films of C_{60}, rubrene, and a 1:1 molar rubrene:C_{60} composite. The spectra of the pure materials have again been scaled to reflect the amount of each material in the composite. The broad absorption in the rubrene:C_{60} composite spectrum appearing to the red of the absorptions in the C_{60} spectrum is attributed to the formation of a CT complex. In addition, the peak at 537 nm in the composite spectrum is associated with the π–π^* absorption of rubrene and is red-shifted by ~7 nm relative to the pure material. An OMLS structure comprised of 250 alternating 40 Å layers of C_{60} and rubrene has also been prepared and specroscopically characterized. The optical spectrum of this film also reveals some degree of charge transfer at the interfaces.

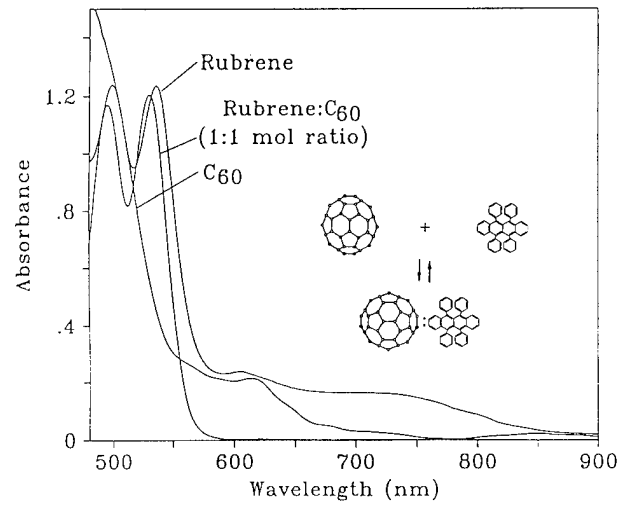

Figure 3. Absorption spectra of C_{60}, rubrene, and rubrene:C_{60} (1:1) on sapphire.

The preparation, spectroscopic, and NLO characterization of TPP:C_{60} nanocomposites has been reported previously.[6] More recently, we have prepared an OMLS film of these materials by depositing alternating 40 Å thick layers to a total thickness of 400 nm. The optical spectrum for this film, together with scaled spectra of C_{60} and TPP are shown in Figure 4. The OMLS spectrum shows a broadening of the Q-band vibronic features associated with TPP relative to the pure material. Also, these features fall on top of the absorption tail of another spectral feature in the OMLS spectrum. Work is currently underway to further characterize these systems, examine their film morphology, and investigate their NLO properties.

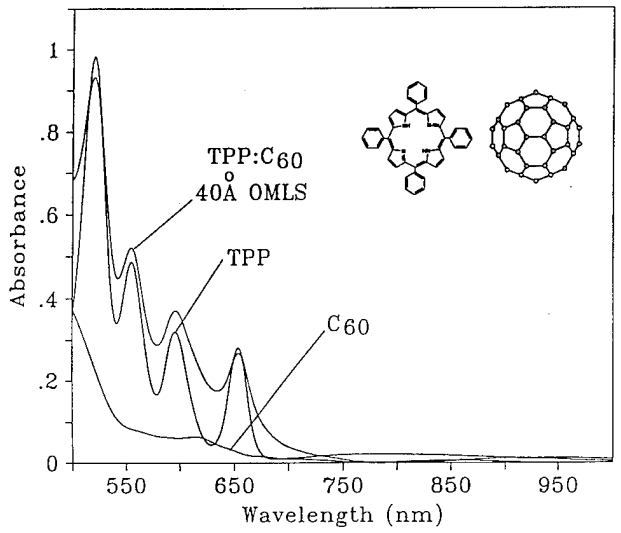

Figure 4. Absorption spectra for films of C_{60}, TPP, and a TPP:C_{60} OMLS on sapphire.

References

1. W. Krätschmer, L. D. Lamb, K. Fostiropoulos, and D. R. Huffman, Nature (London) 347, 354 (1990).
2. S. R. Flom, R. G. S. Pong, F. J. Bartoli, and Z. H. Kafafi, Phys. Rev. B 46, 15598 (1992).
3. J. R. Lindle, R. G. S. Pong, F. J. Bartoli, and Z. H. Kafafi, Phys. Rev. B 48, 9447 (1993).
4. F. P. Strohkendl, R. J. Larsen, L. R. Dalton, R. W. Helwarth, H. W. Sarkas, and Z. H. Kafafi, SPIE 2284, 78 (1994).
5. S. R. Flom, R. G. S. Pong, F. J. Bartoli, and Z. H. Kafafi, Mol. Cryst. Liq Cryst. 256, 289 (1994).
6. S. R. Flom, H. W. Sarkas, R. G. S. Pong, C. D. Merritt, F. J. Bartoli, and Z. H. Kafafi, SPIE 2284, 134 (1994).
7. S. R. Flom, F. J. Bartoli, H. W. Sarkas, C. D. Merritt, and Z. H. Kafafi, Phys. Rev. B 51, 11376 (1995).
8. N. S. Sariciftci and, A. J. Heeger, Int. J. Mod. Phys. B 8, 237 (1994).
9. V. M. Agranovich, Phys. Lett. A 183, 395 (1993).
10. V. M. Agranovich, Physica Scripta T49, 700 (1993).
11. A. A. Zakhidov and K. Yoshino, Synth. Met. 64, 155 (1994).

Photo excitation stability and bias voltage stability of electro-optic polymer modulators for broadband analog transmission systems

Yongqiang Shi, David J. Olson, James H. Bechtel
TACAN Corporation, 2330 Faraday Ave., Carlsbad, CA 92008
Tel: (619) 438-1010, Fax: (619) 438-2412

Srinath Kalluri, William H. Steier
Department of Electrical Engineering, University of Southern California, Los Angeles, CA 90089-0483
Tel: (213) 740-4415, Fax: (213) 740-8684

Wenshen Wang, Datong Chen, Harold R. Fetterman
Department of Electrical Engineering, University of California, Los Angeles, CA 90095
Tel: (213) 206-9457, Fax: (213) 206-9497

Broadband analog transmitters are an important part of many information delivery systems. Nonlinear optical (NLO) polymer devices have shown a great potential of playing a major role in ultra-wide bandwidth analog transmission systems due to the low dielectric constant, flexibility of processing, compatibility with semiconductor technology, and high nonlinearities. The general requirements for polymer modulators used in an externally modulated broadband transmission system were briefly discussed previously.[1] In this summary, we will focus on two practical issues for polymer modulators used in an externally modulated analog transmission system: the photo excitation stability and the quadrature bias voltage stability of electro-optic(EO) polymer modulators. The photo excitation stability is directly related to the signal-to-noise ratio of the analog signal link, device life-time, and processing conditions. The bias voltage stability will affect the fidelity of the transmitted analog signal. Using a thermally crosslinkable polyurethane with Disperse Red 19 side groups(PUR-DR19), we have tested the performance and the stability of EO polymer devices.

1. Photo excitation stability

In many applications such as second-harmonic generation in NLO polymer waveguides, guided wave EO modulators, and Fabry-Perot resonator modulators, the active polymer materials often carry an intense optical beam. The photo excitation stability monitors the characteristics of NLO polymer materials or polymer device performances at different optical power levels and different optical wavelengths. At a designated working wavelength, the photo excitation stability also determines the optical power handling capability of the device or the material.[2]

It was reported that the linear and nonlinear optical properties of the poled polymer materials will change significantly under the exposure of ultra-violet, visible, or even near infrared beams.[2-4] Recently, we have conducted a systematic study on the nonlinearity relaxation of the poled polymer thin films as a function of the exposure dosages at optical wavelengths from 543 nm to 1320 nm. For the optical wavelengths near or within the absorption band of PUR-DR19 material, we have employed an EO grating defined on a thin film poled by corona discharge.[5] A waveguide set-up was used to monitor the device stability at 1320 nm wavelength. In our measurement, the polymer samples were monitored over a total exposure fluence of approximately 12 orders of magnitude, as shown in Figure 1. This measurement revealed several important facts in a poled NLO polymer film. First, as the exposure wavelength approaches peak absorption wavelength($\lambda_{max}\approx$470 nm), the relaxation of the EO coefficient becomes faster and faster. At 670 nm, a 30 % EO coefficient decay requires an exposure fluence of ~2×10^5 J/cm^2 while the same decay needs only ~3 J/cm^2 at 543 nm, corresponding to a change of

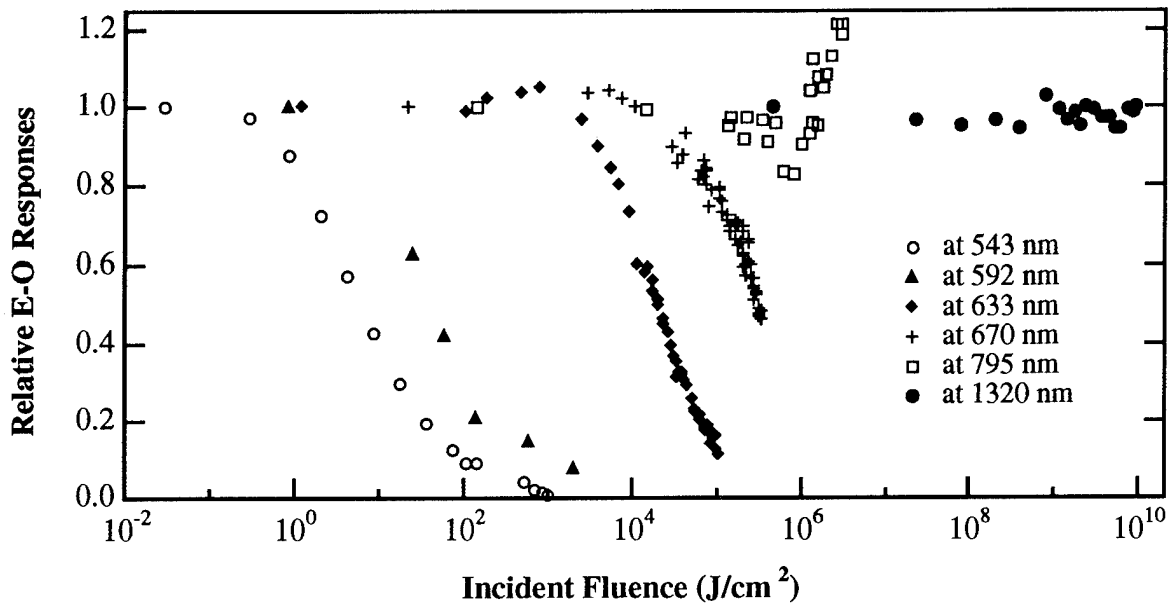

Fig. 1 The normalized EO response as a function of incident fluence at different wavelengths. The 1320 nm response curve was converted from half-wave measurement using a waveguide modulator. Responses at other wavelengths were measured from an etched EO grating modulator.

approximately 5 orders of magnitude. Second, the relaxation of material's nonlinearity due to photo excitation can take place at a wavelength far away from λ_{max}. In the case of PUR-DR19, this decay in nonlinearity was clearly seen at 670 nm wavelength which is ~200 nm longer than λ_{max}. The decay in EO response is attributed to the photoinduced randomization of the NLO chromophore alignment. Third, at near infrared wavelengths from 795 nm to 1320 nm, no clear trend of the decay in EO responses was observed. These wavelengths can be considered as the "first-order" safe working range if we ignore the second harmonic beam generated by an intense incident beam.

During the measurement of the half-wave voltage of the waveguide modulator at 1320 nm wavelength, we have simultaneously monitored the stability of the waveguide output power at the quadrature bias point. The total laser power incident onto the coupling lens was 25~30 mW and ~10 mW was coupled into the waveguide with 10 μm^2 cross section. As shown in Figure 2 with the normalized output power as a function of the total incident fluence, the waveguide output remains relatively stable without any obvious trend of decay. The experimental results indicate a good photo excitation stability of PUR-DR19 waveguide devices at 1320 nm wavelength and the experiment incident intensity level.

2. Quadrature bias voltage stability

A good commercial analog multi-channel(~80 channels) transmission system usually requires a composite second order (CSO) harmonic distortion below -65~-70 dBc. Taking an 80 channel (6 MHz/channel) AM analog transmitter as an example, tens of second order components fall into either high or low frequency ranges in the transmission band. When the modulator is biased exactly at the quadrature point of the transfer function, the CSO of the transmission system is minimized. However, if the bias point is off the quadrature point, the CSO will increase significantly. Therefore, in order to improve the transmitted signal quality, the bias point of the EO modulator must be maintained at the quadrature point of the sinusoidal transfer function.

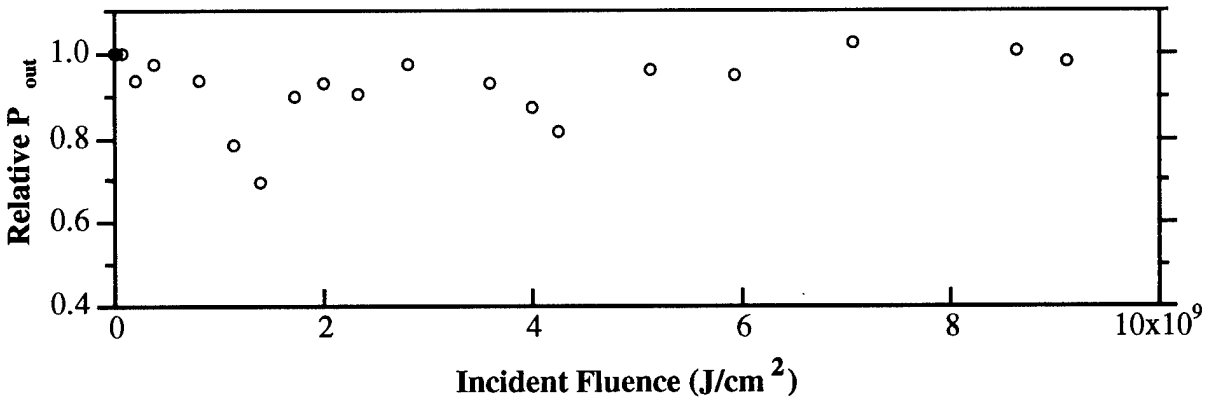

Fig. 2 The waveguide modulator output power at quadrature bias point as a function of the 1320 nm incident fluence.

The bias point of an EO modulator depends on many factors. Taking interference type modulators such as Mach-Zehnder and polarization modulator as examples, the bias point depends mainly on the beam path differences which can be affected by the driving RF power, the temperature fluctuation, and the externally applied electric field. Due to the constant and slow changes of the environment conditions, the bias point is also constantly and slowly drifting. This drift has been well-documented in $LiNbO_3$ modulators.[6] Recently, we have studied the bias point drifting phenomenon in EO polymer waveguide modulators. In our experiment, a polarization modulator made of PUR-DR19 was used. An external Babinet-Soleil compensator was used to first bias the modulator at an arbitrary bias point. The AC modulation voltage and the DC bias control voltage was combined by a bias-tee. With a triangular wave voltage connected to the AC port to over-modulate the device, the DC voltage was adjusted to the quadrature bias point where the output waveform was symmetric. When the DC voltage was applied, the bias point immediately jumped to a new position, indicating the fast index change due to the EO effect. A slow process, on the order of minutes, was also observed to accompany the fast index change. The initial few adjustments usually had overshoot effect, which can be damped by slow voltage ramping rather than step increase of voltage adjustment. A typical short-term "tuning" curve of a PUR-DR19 modulator is shown in Figure 3. The data from Figure 3 shows that the bias voltage for the quadrature point in the testing modulator is traceable. One can fine-tune the applied voltage to obtain an appropriate bias point within a given voltage range. From Figure 3, the total bias voltage change, including those induced by misalignment of the incident beam due to vibration, is approximately 25% of the half-wave voltage of the modulator over a period of ~7 hours, corresponding a 6.5°/hour drifting rate. However, with improved input coupling techniques such as fiber attachment, we can eliminate the discontinuities during the measurement induced by mechanical vibration or misalignment. Then the drifting rate is expected to be slower.

In practical applications, the bias voltage will be limited within a pre-determined range to avoid using a power supply with very wide voltage range. Therefore, when the bias voltage shifts to a high voltage range, the power supply will automatically switch the voltage down by $2V_\pi$, since the transfer function has a periodicity of $2V_\pi$. The whole switching process involves the establishment of a new equilibrium in the material which may result in unstable responses of the system. We have also monitored this voltage down switching process in our set-up, as shown in the inset of Figure 3. Except for the first few minutes after switching, stable quadrature bias voltage was observed. An interesting phenomenon was that the bias voltage change was only a fraction of $2V_\pi$, indicating that there were other factors contributing to the device's phase shift in addition to the EO effect. This phenomenon is attributed to the electric field induced slow re-orientation of the chromophores in the polymer matrix. The contribution depends on the amount

of the chromophores available to the re-orientation process. This also explains why the half-wave voltage measured using DC voltage is usually smaller than that measured by an AC method. In our experiment, the thermoset polymer(PUR-DR19) device showed a much better bias point stability compared with a separate thermoplastic polymer device, although their glass transition temperatures were similar.

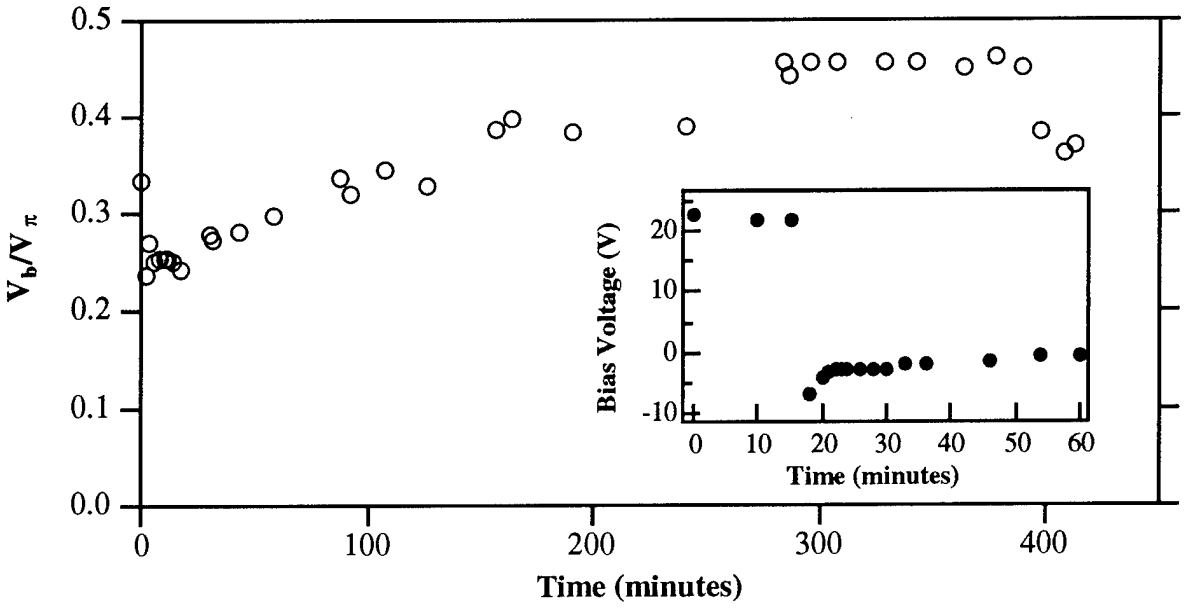

Fig. 3 The normalized bias voltage change as a function of testing time. The inset shows the bias voltage stability after a voltage switching for 2π phase change.

In conclusion, the photo excitation stability was studied in a typical NLO polymer PUR-DR19. The bias voltage stability was also tested in a PUR-DR19 waveguide modulator. The polymer thin film showed a good photo excitation stability at near infrared wavelengths, but the nonlinearity decayed when exposed to visible light. The stable bias point at an applied voltage makes it possible to design an automatic bias control circuit to minimize second order distortion.

This work was supported by Air Force Office of Scientific Research.

References:

1. Y. Shi, W. J. Swarford, J. H. Bechtel, S. Kalluri, W. H. Steier, W. Wang. D. Chen, H. R. Fetterman, *Polymer Preprints*, **35**, 223 (1994).
2. M. Mortazavi, H. Yoon, C. Teng, *J. Appl. Phys*, **74**, 4871 (1993).
3. G. L. J. A. Rikken, C. J. E. Seppen, S. Nijhuis, E. W. Meijer, *Appl. Phys. Lett.*, **58**, 435 (1991).
4. Y. Shi, W. H. Steier, M. Chen, L. Yu, L. R. Dalton, *Appl. Phys. Lett.*, **60**, 2577 (1992).
5. Y. Shi, J. H. Bechtel, S. Kalluri, W. H. Steier, C. Xu, B. Wu, L. R. Dalton, *Proc. SPIE*, **2285**, 131 (1994).
6. H. Nagata, J. Nayyer, in *Integrated Photonics Research*, Vol. 7 1995 Technical Digest Series (Optical Society of America, Washington DC, 1995), p. 290.

Wednesday, September 13, 1995

Symposium on Data Storage I
(Joint with OSA Annual Meeting)

WGG 1:30pm–3:30pm
Holladay Room

George I. Stegeman, *Presider*
University of Central Florida

Photorefractive Polymers for Holographic Optical Storage

W. E. Moerner, C. Poga, Y. Jia, R. J. Twieg

IBM Research Division, Almaden Research Center
K13/D2, 650 Harry Road, San Jose, California 95120-6099
Telephone: 408-927-2426, Fax: 408-927-2100

In the past few years, a new class of polymeric materials for photonic applications has appeared called *photorefractive* (PR) polymers. Photorefractivity is defined as modulation of the index of refraction in an electro-optic material by internal electric fields produced by optical redistribution of charge carriers; hence it must not be confused with the more standard local mechanisms of index change such as photochromism, excited state population, heating, etc. When a material shows the required properties of charge generation, transport, trapping, and dependence of the index of refraction upon the internal electric field, it can be tested for photorefractivity by observation of asymmetric energy transfer (two-beam coupling) between two laser beams in the material.

Until very recently, all materials showing the PR effect were inorganic crystals. In principle, such materials can be used for many optical processing, holographic, optical limiting, phase conjugation, and storage applications, but to date, no widespread applications have attained practicality, partly because of the difficulty and expense of growing and doping the required low-symmetry inorganic crystals. The potential application currently driving new materials development involves holographic optical storage, where a large number of 2-dimensional pages of digital information are stored in the PR material by multiplexed volume holography.

Polymers exhibiting the photorefractive (PR) effect have attracted interest since their first discovery in 1990 [1] because this new class of photorefractive materials offers potentially large improvements in photorefractive figures of merit due to the low dielectric constant of these materials. They also possess other advantages over inorganic materials, such as compositional flexibility and ease of sample preparation and processability. For some performance parameters, the newest PR polymers are beginning to be competitive with the conventional inorganic crystals. This talk reviews the basics of photorefractivity, the formulation and testing of photorefractive polymers, the materials issues most relevant for holographic optical storage applications, and the classes of PR polymers which have shown the most promise for holographic optical storage to date. For

a broader review of PR polymers in general, see Ref. [2].

The materials requirements for holographic optical storage applications may be grouped into several areas: writing, reading, multiplexing, and miscellaneous. For writing holograms, fast response (short writing time) at an easily achieved writing intensity is essential. (Exact values for the required speed depend upon the specific type of storage system, laser available, etc.)

For reading, samples must have (i) large dynamic range (large saturation Δn), (ii) large thickness (for largest diffraction efficiency), and (iii) high optical clarity (low scattering, no crystallization, bubbles, or striations). Taken together, the need for fast response and large Δn mean that the sensitivity should be high, where the sensitivity S_{n1} is the Δn per unit absorbed energy per unit volume. In order to achieve the largest amount of multiplexing of holograms in the same volume, the samples should have large thickness (narrow Bragg readout), and low crosstalk between holograms.

Additional miscellanous, but extremely important requirements are (i) long dark lifetime, (ii) absence of fatigue and/or bleaching, (iii) the ability to tolerate high electric fields, (iv) and temperature insensitivity.

It becomes immediately obvious that high sensitivity and the need for high signal-to-noise ratio during readout are somewhat contradictory requirements, since reading involves irradiation of the sample with a uniform reference beam, and that this uniform irradiation would act to erase the previously written gratings. For this reason, many workers in the inorganic field are concentrating on achieving nondestructive reading by some form of thermal or electrical fixing, or by inventing new photon-gated writing mechanisms. Two-color writing mechanisms were demonstrated some years ago for write-once holography[3] and for optical storage schemes based on persistent spectral hole-burning[4].

At present, no material, inorganic or organic, meets all these requirements simultaneously. However, proofs-of-principle that many of the requirements can be met within the class of PR polymers have been identified in recent research. For example, long interaction lengths can be achieved by configuring the PR polymer in stacked layers, forming a stratified volume holographic optical element[5].

Considering materials with long dark lifetime and high optical clarity, an important proof-of-principle is provided by PR polymers based on the dual-function-dopant concept described by Silence et al. [6]. A suitable binder polymer (such as PMMA) is doped in high concentration with chromophores that provide both optical nonlinearity as well as charge transport, such as 1,3-dimethyl-2,2-tetramethylene-5-nitrobenzimidazoline (DTNBI), and

in low concentration with a sensitizer such as C_{60}. Materials in this class have shown[6] the following useful properties: (a) quasi-nondestructive reading at sufficiently low reading intensity, (b) enhancement of diffraction efficiency and patterning by optical trap activation, and (c) long dark lifetime (ca. 4 days). In addition, the optical quality of these materials is quite good, with bidirectional transmissive distribution function (BTDF) values of $3x10^{-3}$ per unit solid angle at 30° from the forward direction. However, in a digital data recording experiment in which a holographic image with 64 kbits of data was recorded with a 1 minute writing time at ~10 mW/cm^2 writing intensity, only a low contrast could be achieved. The inability of the stored hologram to overcome the scattered light at the detector occurred as a result of the low sensitivity of this material, which is approximately $6x10^{-8}$ cm^3/J.

Turning to the requirement for high sensitivity, the best results to date have been achieved with PR polymers based on charge-transporting host polymers doped with nonlinear optical (NLO) chromophores in high concentration and with a sensitizer in low concentration. For example, the first material to show net two-beam-coupling gain was composed of the photoconducting polymer poly(N-vinylcarbazole) (PVK), doped with the optically nonlinear chromophore 3-fluoro-4-N,N diethylamino-β-nitrostyrene (FDEANST) and sensitized for charge generation with 2,4,7 trinitro-9-fluorenone (TNF) [7]. The high performance of this class of PR polymers is due to an orientational enhancement mechanism[8], which operates for materials with glass transition temperature near the operating temperature, and which allows the polarizability anisotropy of the molecule to contribute to the diffraction as well as the molecular hyperpolarizability.

Recently, high-density holographic recording experiments were performed with the IBM Holographic Optical Storage Tester (HOST) which was developed for the ARPA-sponsored Photorefractive Information Storage Materials (PRISM) consortium. We used a variant of the PVK:FDEANST:TNF material in which the chromphore is liquid at room temperature and in which C_{60} acts as the sensitizer[9]. As the sensitivity of this material is almost 100 times higher than that for the PMMA-based dual-function-dopant material, the contrast of the recorded image is much higher, in the range 10-20, as shown in Figure 1 below. However, due to dark conductivity, the dark lifetime of the hologram was only on the order of 10 s, so multiplexing of holograms was not possible. Nevertheless, the images shown in this figure, which were obtained in collaboration with the IBM HOST team, represent the highest resolution image recording in a PR polymer to date.

While these demonstrations of proofs-of-principle are useful, it is clear that further development of PR materials for holographic optical storage applications is required, in

order to obtain all of the required performance characteristics in the same material.

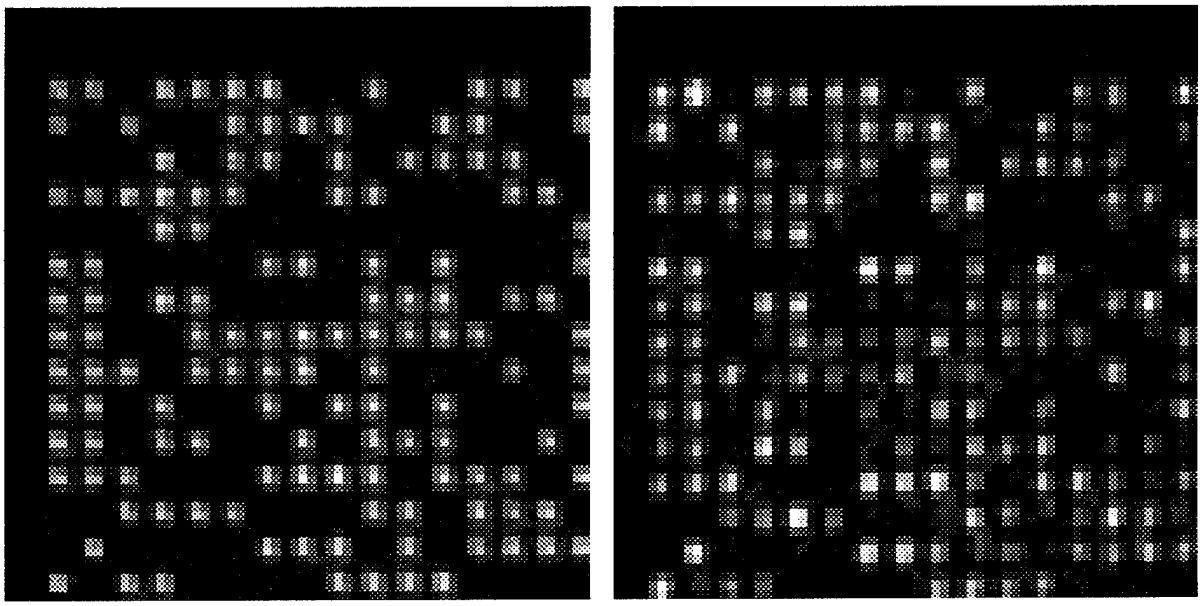

Figure 1: Small portion of 64 kbit data image: (left) transmitted through sample, (right) reconstructed hologram, 6 ms reading time.

REFERENCES

1. S. Ducharme, J. C. Scott, R. J. Twieg, and W. E. Moerner, *Phys. Rev. Lett.* **66**, 1846 (1991).
2. For a review, see W. E. Moerner and S. M. Silence, *Chem. Revs.* **94**, 127 (1994).
3. G. C. Bjorklund, C. Bräuchle, D. M. Burland, and D. C. Alvarez, *Opt. Lett.* **6**, 159 (1981).
4. W. E. Moerner, W. Lenth, and G. C. Bjorklund, Ch. 7 of *Persistent Spectral Hole-Burning: Science and Applications*, W. E. Moerner, ed., Topics in Current Physics Vol. 44 (Springer, Berlin, Heidelberg, 1988), pp. 251-307.
5. J. J. Stankus, S. M. Silence, W. E. Moerner, and G. C. Bjorklund, *Opt. Lett.* **19**, 1480 (1994).
6. S. M. Silence, J. C. Scott, J. J. Stankus, W. E. Moerner, C. R. Moylan, G. C. Bjorklund, and R. J. Twieg, *J. Phys. Chem.* **99**, 4096 (1995).
7. M. C. J. M. Donckers, S. M. Silence, C. A. Walsh, F. Hache, D. M. Burland, W. E. Moerner, and R. J. Twieg, *Opt. Lett.* **18**, 1044 (1993).
8. W. E. Moerner, S. M. Silence, F. Hache, and G. C. Bjorklund, *J. Opt. Soc. Am. B* **11**, 320 (1994).
9. C. Poga, Y. Jia, R. J. Twieg, and W. E. Moerner, to be published.

High Efficiency Photorefractive Polymers

B. Kippelen, K. Meerholz, B. L. Volodin, Sandalphon, and N. Peyghambarian
Optical Sciences Center - University of Arizona
Tucson AZ 85721
Tel: (520) 621-4341 Fax: (520) 621-9610

The processibility and structural flexibility of *photorefractive polymers* give them an important technological potential and have driven intensive research efforts to improve the performance of this new class of PR materials. Since the first proof of principle of photorefractivity in a polymer [1], numerous PR polymeric materials have been synthesized by using different approaches [2], but significant performance improvement was obtained by using the photoconductive polymer poly(N-vinylcarbazole) (PVK) as the composite host and by doping it with nonlinear optical molecules referred to as chromophores [3,4]. In plasticized PVK-based polymer composites doped with the chromophore 2,5-dimethyl-4-(p-nitrophenylazo)anisole) (DMNPAA) [4], we recently demonstrated [5] that PR polymeric materials can exhibit light-induced refractive index modulation amplitudes as high as $\Delta n = 7 \times 10^{-3}$ at 1 W/cm^2 writing intensity, and applied field of 90 V/μm. As shown in Fig.1, such a high index modulation leads to complete diffraction and periodic energy transfer between the probe and diffracted beams in four-wave mixing (FWM) experiments and also, to net gain coefficients in excess of 200 cm^{-1} in two-beam coupling (TBC) experiments [5]. These results demonstrate that PR polymeric materials can reach performance levels that are competing with those of the best inorganic crystals, but with better processing capabilities.

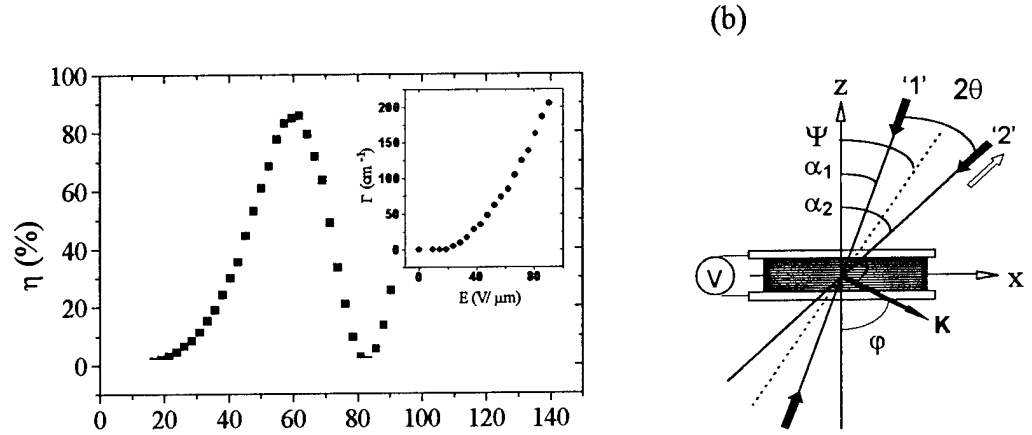

Fig.1: (a) Electric field dependence of the diffraction efficiency for a p-polarized reading beam and of the coupling gain coefficient for p-polarized beams (inset). (b) Slanted geometry used for these experiments ($2\theta = 22°$, $\psi = 60°$).

In this paper, we investigate guest/host polymeric composites that have a glass transition temperature T_g close to or even below room temperature and discuss the origin of their high efficiency. The performance of 105-μm-thick samples of the polymer composite DMNPAA:PVK:ECZ:TNF sandwiched between two transparent conducting electrodes, is evaluated by means of FWM and TBC experiments, and by independent frequency-dependent electro-optic characterization that clearly identifies several contributions to the total refractive index changes. Our results show that the so-called *orientational enhancement* mechanism [6] is responsible for the high efficiencies. A schematic representation of our low T_g PR polymeric material and the chemical structure of its constituents are shown in Fig.2. The polymer PVK (33% wt.) plays the role

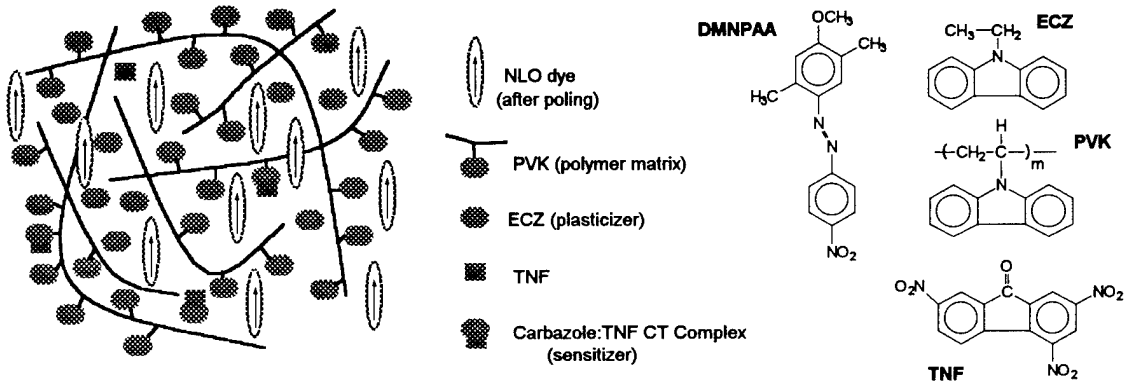

Fig.2: Schematic representation of the photorefractive polymeric material and chemical structure of its constituents

of binder and provides the photoconducting properties needed for the build-up of a space-charge through hole transport. The small amount (1% wt.) of the strong acceptor TNF (2,4,7-trinitro-fluorenone) that is added, provides photosensitivity at the working wavelengths of 633 and 675 nm by forming a charge-transfer (CT) complex with the carbazole moieties. The NLO chromophores DMNPAA (50% wt.) are responsible for the field-induced refractive index changes. N-ethylcarbazole (ECZ) monomers are added (16% wt.) in order to lower the T_g of the composite and to allow the orientation of the NLO chromophores by the total dc electric field which is the superposition of the external field $\mathbf{E}_{ext}$ and the internal space-charge field $\mathbf{E}_{sc}$. As a result, the degree of orientation of the chromophores is periodically changing both in amplitude and direction. It is well-known [7] that the degree of orientation of rod-like NLO chromophores determines the magnitude of the second-order susceptibility tensor elements of the material and changes its linear susceptibility tensor elements as well, leading to birefringence. In the oriented gas model, where the average orientation of the molecules is described by Maxwell-Boltzmann distribution functions, and in the low poling field limit, the second-order susceptibility $\chi^{(2)}_{ZZZ}$ and the change in linear susceptibility $\Delta\chi^{(1)}_{ZZ}$ along the Z-axis of the sample, can be approximated by:

$$\chi^{(2)}_{ZZZ} = N F^{(2)} \beta \langle \cos^3 \theta \rangle \approx N F^{(2)} \beta \frac{\mu E_T}{5kT} \quad (1)$$

$$\Delta \chi^{(1)}_{ZZ} = N F^{(1)} \Delta\alpha \left(\langle \cos^2 \theta \rangle - 1/3 \right) \approx N F^{(1)} \Delta\alpha \frac{2}{45} \left(\frac{\mu E_T}{kT} \right)^2 \quad (2)$$

where N is the density of NLO chromophores, $F^{(2)}$ and $F^{(1)}$ are local field correction factors, β is the first hyperpolarizability of the chromophore along its main axis, θ is the angle between the molecular axis and the symmetry Z-axis of the sample determined by the direction of the poling field, μ is the permanent dipole moment of the chromophore in the matrix, $\Delta\alpha$ is the linear polarizability anisotropy of the molecule, and kT is the thermal energy. In low T_g polymers, the effect of a spatially varying orientation of the molecules has several consequences [6]: (i) the electro-optic contribution is doubled compared to a spatially uniform poled polymer, (ii) a new contribution due to the modulation of the linear susceptibility contributes to the total refractive index modulation, (iii) gratings with higher-order grating vectors are created in the material.

The change in sign of the beam-coupling gain coefficient observed in TBC experiments [5] when the polarization of the interacting beams is changed from "s" to "p" indicate that the contribution from the linear susceptibility is much stronger than the electro-optic contribution. This behavior can be explained by the different polarization anisotropy of the two effects:

$$\Delta n^{(1)}_{\perp} = -1/2 \Delta n^{(1)}_{//} \quad (3)$$

$$\Delta n^{(2)}_{\perp} = +1/3 \Delta n^{(2)}_{//} \quad (4)$$

where the indices // and $\perp$ refer to the directions parallel and perpendicular to the poling direction, respectively. In the slanted geometry shown in Fig.1b, $\Delta n_{//} = \Delta n^{(1)}_{//} + \Delta n^{(2)}_{//}$ is the dominant contribution for p-polarized beams, while for s-polarized beams the total refractive index change is given by $\Delta n_{\perp} = \Delta n^{(1)}_{\perp} + \Delta n^{(2)}_{\perp}$, which according to Eqs. (3) and (4) can be rewritten as $\Delta n_{\perp} = -1/2 \Delta n^{(1)}_{//} + 1/3 \Delta n^{(2)}_{//}$. Thus, a measured ratio $\Delta n_p / \Delta n_s < 0$ clearly indicates that the linear contribution is stronger than the electro-optic one. This conclusion is confirmed by the results obtained from frequency-dependent ellipsometric experiments where ac and dc fields are applied simultaneously to the sample. The field-induced refractive index changes in the sample modify the relative phase of the s and p-components of a linearly polarized laser beam (polarized at 45°) resulting in light transmission through the crossed analyzer placed after the sample [8]. The intensity modulated at the frequency of the ac field is detected with a lock-in amplifier. At the highest frequencies, only the dc field is poling the sample. The ac field component is changing too rapidly to affect the orientation of the molecules. In the high frequency limit, the detected signal is due to the electro-optic contribution only, if Kerr effects are

neglected. In contrast, at low frequencies, the ac field component is influencing the orientation of the chromophores leading to doubled electro-optic activity and to an additional contribution due to the change in linear susceptibility as for the steady-state photorefractive diffraction efficiency. As shown in Fig.3, the significant difference in response observed between the low and high frequency limits confirms that the modulated birefringence plays a major role.

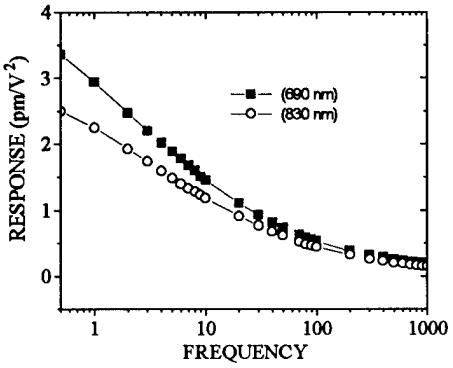

Fig.3: Frequency-dependence of the effective refractive index change measured at two different wavelengths in DMNPAA:PVK:ECZ:TNF samples.

Our results demonstrate that the efficiency of low T_g polymers is not limited by the electro-optic properties of the chromophore and can be drastically improved by taking advantage of the orientational enhancement mechanism. A new figure of merit $Q = N\left(\Delta\alpha\,\mu^2 + \beta\,\mu\right)$ can be defined for optimizing chromophores as dopant for low T_g photorefractive polymers. Time-resolved and intensity-dependent FWM mixing experiments performed in our materials demonstrate also their good sensitivity ($S = 0.03\,cm^3/J$). Examples of applications including holographic storage, real-time interferometry [9], and optical correlation [10] have been demonstrated and will be presented.

Acknowledgments:

This research has been supported by NSF (# ECS-9408810) and AFOSR (# F49620-93-1-0199). B. K. is also at CNRS, on leave from IPCMS, France.

References:

[1] Ducharme S. et *al.*, *Phys. Rev. Lett.* **66**, 1846 (1991).
[2] Moerner W. E. and S. M. Silence, *Chem. Rev.* **94**, 127 (1994); and references therein.
[3] Donckers M. C. J. M. et *al.*, *Opt.Lett.* **18**, 1044 (1993).
[4] Kippelen B. et *al.*, *Electron. Lett.* **29**, 1873 (1993).
[5] Meerholz K. et *al.*, *Nature* **371**, 497 (1994).
[6] Moerner et *al.*, *J. Opt. Soc. Am. B* **11**, 320 (1994).
[7] Wu J. W., *J. Opt. Soc. Am. B* **8**, 142 (1991).
[8] Teng C. C. and Man H. T., *Appl. Phys. Lett.* **56**, 1734, (1990).
[9] B. L. Volodin et *al.*, to appear in *Opt. Eng.* (1995).
[10] C. Halvorson et *al.*, *Opt. Lett.* **20,** 76 (1995).

PHOTOINDUCED BIREFRINGENCE, HOLOGRAPHIC SURFACE GRATINGS AND PHOTOREFRACTIVE PROPERTIES OF AZO POLYMERS

Mei Sing Ho[1], Chris Barrett[2], Paul Rochon[2] and Almeria Natansohn[1]

[1]Department of Chemistry, Queen's University, Kingston, Ontario, K7L 3N6
[2]Department of Physics, Royal Military College, Kingston, Ontario, K7K 5L0, CANADA

Azo polymers are the subject of an impressive number of publications in the recent literature, due to a variety of possible applications. The main area of interest is in their nonlinear optical (NLO) properties, and azo-containing polymer films have been synthesized, poled and their second harmonic generation and waveguide properties have been investigated. The publication pace on this subject is considerable, and it would be impossible to summarize the most important trends. The general directions of the research are related to improved thermal stability and especially to methods to increased stability of orientation of the azo chromophores. Polyimides and/or crosslinked polymers are the preferred methods to achieve these goals.

There is much more to azo polymers than just nonlinear optical properties. Photoisomerization has been known for a long time, and the photochromism has been proposed as a recording method. The cis isomer is very unstable in all azoaromatic compounds, hence the feasibility of such a recording is very low. As a consequence of photoisomerization, however, the azoaromatic groups are moving within the polymer film and orienting perpendicular to the light's polarization direction. This order/disorder transition can be used to store digital information, but it is inherently slow, since it requires at least a few trans-cis-trans isomerization cycles per azo group. The literature on this subject is also growing rapidly.

More recently, azo compounds have been used as the NLO groups in photorefractive polymers, and the photochemical orientation due to polarized light is used to enhance the photorefractive effect in some polymer films. This use takes advantage of both the NLO and photoisomerization properties of azobenzene group.

We will show in this presentation that both these properties **plus** a third one: surface grating production on polymer films, can be used to obtain almost any active element in a potential photonic device, making azobenzene-containing polymers probably the most versatile materials for photonic applications.

Photoinduced Birefringence

It is well known that dichroism and birefringence can be induced in either amorphous or liquid crystalline or semicrystalline polymer films. If the polymer is amorphous, the induced birefringence can reach levels of 0.1 and is achieved in a few hundred of milliseconds. The saturation level decays to

a lower level upon termination of the write beam, and this level of the photoinduced birefringence is stable for a very long time (four years have been verified in our laboratory). For liquid crystalline and semicrystalline polymers, the level of orientation is obviously much higher, thus greater photoinduced birefringence can be achieved, but the process is much slower[1].

Our recent investigations have been limited to amorphous high-Tg polymers with the scope of understanding the relation between the polymer structure and its optical storage properties. We have proposed a biexponential fit for both the photoinducing birefringence process and the relaxation upon termination of the write beam[2]. The biexponential equations can be used to compare various polymers and the results indicate that the volume of the azo group plays a relatively minor role in orientation, while the polarity is extremely important[3].

Other studies on copolymers clearly showed that the polarity of the neighboring group plays a crucial role in the mobility of the azobenzene groups. This was revealed studying cis-trans thermal isomerization kinetics[4], and photoinduced birefringence in copolymers[5,6,7]. An in-situ orientation study was performed by monitoring infrared dichroism while the "writing" process took place. The results clearly show different types of alignment of the azobenzene groups in homopolymers as compared with copolymers[8].

Surface gratings

When subjecting an azo-containing polymer film to an interfering pattern generated by two light beams, a volume diffraction grating can be obtained based on variations of the refractive index induced by the orientation of the azobenzene groups. The diffraction efficiency of such a grating is very small, usually below 1%. However, continuous illumination, preferably with circularly polarized light, produces an unexpected motion of polymer molecules to form a fairly deep surface grating[9-11]. An atomic force microscope image of such a surface is presented in Figure 1. The depth, tilt and period of the gratings can be adjusted by modifying the two light beams, the material and/or the exposure time. For the grating shown in Figure 1, with a depth below 100 nm, the diffraction efficiency is 12%, but values as high as 42% and depths of about 1 μm have been obtained.

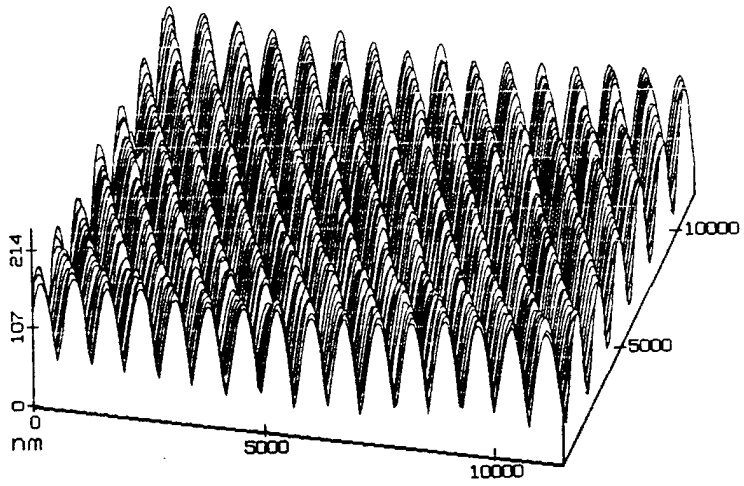

Figure 1. Diffraction gratings inscribed on a copolymer containing 25 mol% azo structural units.

Carbazole-containing polymers: single-unit photorefractive polymers

Azo groups are being used to provide the necessary nonlinear optical properties of photorefractive polymers[12]. Apart from the NLO component, a a photoconductive component is necessary, and the traditional route has been to work with a photoconductive polymer with the NLO component added to the composition. In the example above, a third component was necessary to lower the glass transition temperature of the film in order to allow for poling at a reasonable temperature. Alternatively, both the photoconductive and the NLO sites could be attached to the same polymer by chemical bonds[13].

In fact, the two sites can be linked together into a single monomer unit if a photoconductive moiety is being made part of the azo group. The most obvious moiety would be carbazole, which is a known photoconductor in the UV region. When poly(N-vinylcarbazole) was used in photorefractive polymers, a charge transfer complex with an electron acceptor was usually prepared by addition of an appropriate electron accepting compound, sensitizing the mixture in the visible range of the spectrum. Binding carbazole in such a way that its nitrogen would be the electron-donor substituent on the azobenzene group avoids the requirement of sensitization in the visible region, since the absorbance maximum of the resulting compound is well above 400 nm. The formula of the proposed structural unit is presented below:

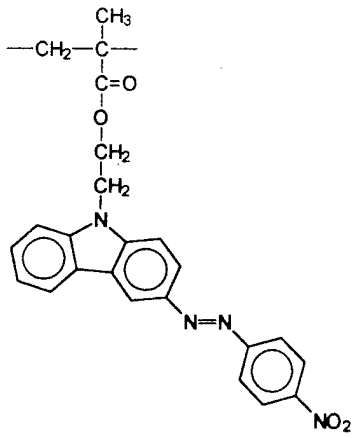

Such a polymer has a Tg of 160°C[14] and decomposes at 260°C. Its maximum absorbance in film form is at 428 nm. Birefringence can be induced on the polymer film to a level of 0.09, at a relatively fast rate (equivalent exponential rate constant of 2.7 s^{-1}), and 90% of the photoinduced birefringence is conserved in the film at room temperature for an indefinite length of time. This polymer is also amenable to surface gratings inscription, by the procedure described[10], and diffraction efficiencies of 25% are easily obtained.

The most interesting feature of this polymer, however, is the fact that it is photorefractive. To obtain two-beam coupling gains, the polymer film has to be poled first, and poling can be performed at room temperature, taking advantage of the motion induced by the trans-cis-trans isomerization cycles of the azobenzene groups. Illumination with a polarized laser can be performed in an electric field, producing not only directional alignment, as in

photoinduced birefringence, but polar alignment as well. Then, two-beam coupling gains can be measured on the photorefractive film. A normalized beam-coupling energy-transfer coefficient of $\Gamma = 5500\ cm^{-1}$ before absorption losses is observed on a fairly thin film. Absorption losses are 11,000 cm^{-1}.

Potential for devices

Stable birefringence can be locally induced and erased on a polymer film made of an azobenzene-containing polymer at a very high resolution. The birefringence can be used as a memory bit, or can be used for waveguide purposes. A "printed circuit" of waveguides can in principle be drawn on such a polymer film. At the points of incidence with a light beam coming from outside the film, the surface grating can be used to couple the external beam into and out of the polymer film. Such a surface grating can be obtained by exclusive optical means and its efficiency and direction of guiding are adjustable. Such a grating can also be erased, although local heating would be required for erasing. Finally, by local poling on films with photorefractive properties, optical switches can be obtained. In principle, such an integrated circuit can be changed at will using only optical means.

Azo-containing polymers show such a wide range of useful properties that their serious investigation has probably only begun.

References

1. A. Natansohn, P. Rochon, M. Pézolet, P. Audet, D. Brown and S. To, *Macromolecules*, 27, 2580 (1994).
2. M. S. Ho, A. Natansohn and P. Rochon, *Macromolecules*, submitted.
3. M. S. Ho, A. Natansohn, C. Barrett and P. Rochon, *Can. J. Chem.*, in press.
4. C. Barrett, A. Natansohn and P. Rochon, *Macromolecules*, 27, 4781 (1994).
5. D. Brown, A. Natansohn and P. Rochon, *Macromolecules*, submitted.
6. M. S. Ho, A. Natansohn and P. Rochon, *Macromolecules*, submitted.
7. X. Meng, A. Natansohn, C. Barrett and P. Rochon, in preparation.
8. M. Pézolet and T. Buffeteau, in preparation.
9. P. Rochon, J. Mao, A. Natansohn and E. Batalla, *Polym. Prepr. (ACS)*, 35(2), 154 (1994).
10. P. Rochon, E. Batalla and A. Natansohn, *Appl. Phys. Lett.*, 66, 136 (1995).
11. D. Y. Kim, S. K. Tripathy, L. Li and J. Kumar, *Appl. Phys. Lett.*, 66, 1166 (1995).
12. K. Meerholz, B. L. Volodin, Sandalphon, B. Kippelen, N. Peyghambarian, *Nature*, 371, 497 (1994).
13. Z. Peng, Z. Bao and L. Yu, *J. Amer. Chem. Soc.*, 116, 6003 (1994).
14. M. S. Ho, C. Barrett, J. Paterson, A. Natansohn and P. Rochon, *J. Amer. Chem. Soc.*, submitted.

High Efficiency Photorefractive Polymer with Immunity to Crystallization

C. Poga, R. J. Twieg, and W. E. Moerner
IBM Research Division, Almaden Research Center
K13/801, 650 Harry Road, San Jose, California 95120-6099
Telephone: 408-927-1682, Fax: 408-927-3310

In the few years since the first report of a photorefractive (PR) organic polymeric material [1], much research has been done [2] to improve the material characteristics in order to meet the requirements necessary for applications such as holographic optical storage. A potentially useful polymeric system would combine a wide variety of properties in the same material, such as high diffraction efficiency, long dark lifetime, fast response, excellent optical clarity, just to name a few.

Meerholz, et al. [3] reported that the photorefractive polymeric composite composed of 50 wt % 2,5-dimethyl-4-(p-nitrophenylazo)anisole (DMNPAA), 33 wt % poly(N-vinylcarbazole) (PVK), 16 wt % N-ethylcarbazole (ECZ) and 1 wt % 2,4,7-trinitro-9-fluorenone (TNF) shows diffraction efficiency approaching 100% and high two-beam coupling gain coefficients. Subsequent study [4] shows that this composition, despite its outstanding performance, presents problems concerning optical quality. Samples made from this composition tend to crystallize on time scales varying from hours to weeks depending on the sample fabrication. The irreproducibility of this composite, which is due to the high loading level (50 wt %) of the nonlinear optical chromophore, also results in large variations of the measured PR properties from sample to sample. For example, various samples show about a factor of 5 variation in maximum index of refraction change Δn, or equivalently, a factor of 25 variation in steady-state diffraction efficiency for equal thicknesses.

In this contribution we describe a new PR polymeric material consisting of 40 wt% of the nonlinear optical chromophore β-methyl-β-nitro-3-fluoro-4-N,N-diethylaminostyrene (FDEAMNST), 59.8 wt % of the photoconductive polymer PVK, and 0.2 wt % C_{60} for charge generation. The FDEAMNST chromophore is liquid at room temperature, a property which allows higher loading levels without inducing crystallization. The samples have very good optical quality; for example, the scattering behavior as measured by the bidirectional transmissive distribution function (BTDF), is of the order of 10^{-2} per unit solid angle at 30^{o} from the forward direction. At the experimental wavelength of 676 nm, the absorption coefficient is $\alpha \approx 17.8\ cm^{-1}$. The dc photoconductive properties were measured using illumination from a Kr^{+} laser. The dark conductivity was measured to be $\sigma_{dark} \approx 6.7 \times 10^{-14}\ (\Omega\text{-cm})^{-1}$ which was ohmic over the field range 0.5 - 2.5 V/

μm. The specific photoconductivity at 5 V/μm was $\sigma_{ph} \approx 5.1 \times 10^{-13}$ $(\Omega\text{-cm})^{-1}/(W/cm^2)$. This value for σ_{ph} is smaller than that observed for the related PVK:FDEANST:TNF material [5], possibly due to the difference in sensitizer.

To study the hologram formation behavior, the diffraction efficiency of a p-polarized probe beam was measured using our standard four-wave mixing geometry [6] in which the bisector of the two writing beams (each of intensity 1 W/cm^2 unless otherwise noted) is tilted 45^o with respect to the sample normal and the external crossing angle between the writing beams is 30^o. The steady-state diffraction efficiency reaches 9.4 % for a 250μm thick sample in an applied electric field of 40 V/μm. The corresponding change of the index of refraction is 3.2×10^{-4} and the photorefractive sensitivities[2] at 40 V/μm were found to be $S_{n1}=9.48 \times 10^{-3} cm^3/KJ$, $S_{n2}=0.168 cm^2/KJ$, $S_{\eta 1}=3.6 \times 10^{-4} cm^2/mJ$, $S_{\eta 2}=6.4 \times 10^{-3} cm/mJ$, which compare favorably to iron-doped $LiNbO_3$. The electric field dependence of the index of refraction change Δn is shown in Figure 1 and is quadratic as expected[2]. The sensitivities are correspondingly larger by at least a factor of 4 at 60 V/μm.

The lifetime of the stored gratings in the dark was ~ 10 s at 40 V/μm, too short for holographic storage applications. Study of the dark conduction process and modification of this composition to add deep traps are subjects of future work.

The growth rate of the index of refraction change (measured by the inverse of the refractive index growth time τ^{-1}) is expected to increase linearly with incident light intensity in the simplest one-carrier model of photorefractivity. However, as in some inorganic crystals, sublinear behavior is often observed in PR polymers [2] presumably due to the presence of shallow traps. Figure 2 shows the grating growth rate as a function of writing beam intensity for the PVK:FDEAMNST:C_{60} system. The fit to the data is a power law with exponent 0.65.

Finally, the electric field dependence of the inverse response time τ^{-1} is presented in Figure 3. Although the data do not span a large enough interval to state conclusively, the fast increase in growth rate is suggestive of the field dependence of the Onsager theory of geminate recombination, reflecting the importance of the charge generation step in determining the PR speed.

In conclusion, we have fabricated a new PR polymer containing a liquid nonlinear optical chromophore which is immune to crystallization, and which shows high diffraction efficiency and fast response. To date, numerous samples have been stored at room temperature without loss of optical quality. In separate work, high contrast, high resolution holographic images have been stored in this material [7]; however, the dark lifetime must be improved for practical storage applications.

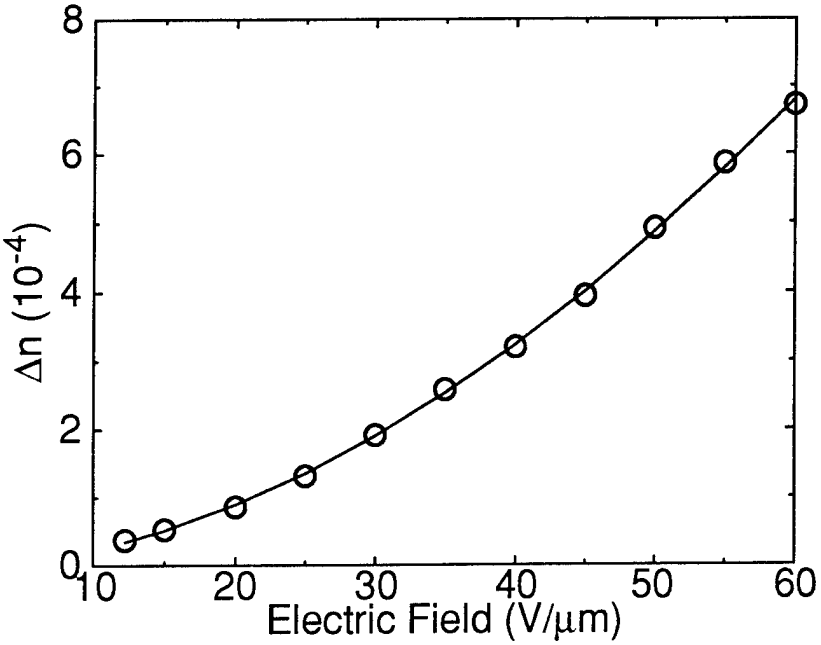

Figure 1. Δn vs. applied electric field; solid curve, quadratic fit.

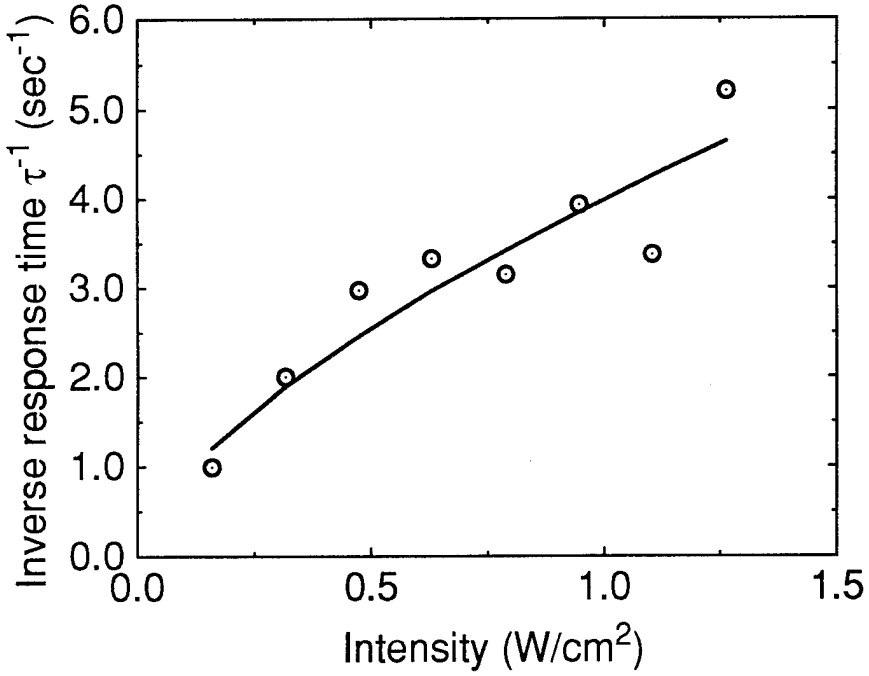

Figure 2: Inverse response time as a function of intensity at 40 V/μm with power law fit.

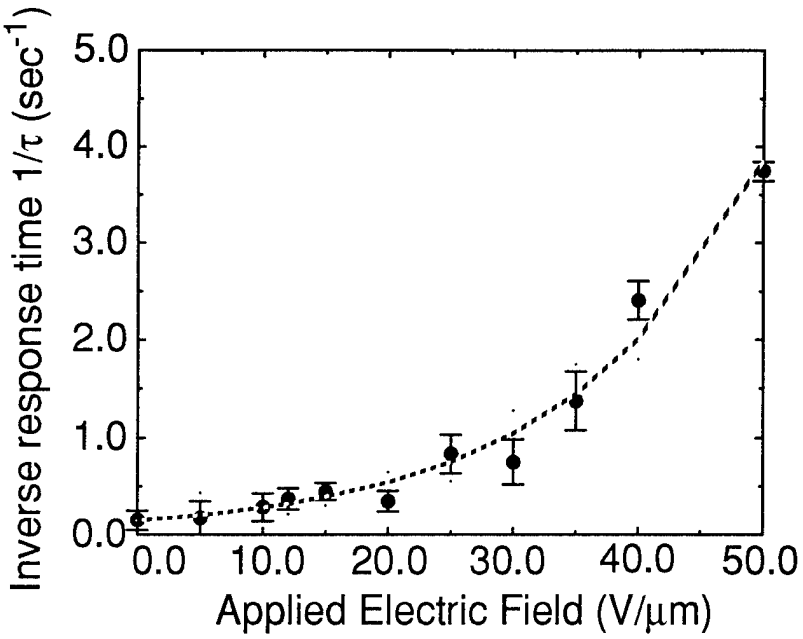

Figure 3: Growth rate at 1 W/cm^2 as a function of applied electric field with exponential fit.

References

1. S. Ducharme, J. C. Scott, R. J. Twieg, and W. E. Moerner, *Phys. Rev. Lett.* **66**, 1846 (1991).
2. For a review, see W. E. Moerner and S. M. Silence, *Chem. Rev.* **94**, 127 (1994).
3. K. Meerholz, B. L. Volodin, Sandalphon, B. Kippelen, and N. Peyghambarian, *Nature* **371**, 497 (1994).
4. C. Poga, J. J. Stankus, R. J. Twieg, and W. E. Moerner, to appear in *Proc. SPIE* (1995).
5. M. C. J. M. Donckers, S. M. Silence, C. A. Walsh, F. Hache, D. M. Burland, W. E. Moerner, and R. J. Twieg, *Opt. Lett.* **18**, 1044 (1993).
6. W. E. Moerner, C. A. Walsh, J. C. Scott, S. Ducharme, D. M. Burland, G. C. Bjorklund, and R. J. Twieg, *Proc. SPIE* **1560**, 278 (1991).
7. W. E. Moerner, Y. Jia, C. Poga, and R. J. Twieg, Invited paper presented at this conference.

Two-photon absorption based optical recording in organic planar waveguide

Ram Piyaket, Ilkan Cokgor, Frederick B. McCormick, Sadik Esener
Department of Electrical and Computer Engineering
University of California, San Diego
9500 Gilman Drive, Mail code 0407
La Jolla, CA 92093-0407
Tel: (619) 534-8155, Fax: (619) 534-1225
E-mail: rpiyaket@ucsd.edu

Alexander S. Dvornikov, Peter M. Rentzepis
Department of Chemistry
University of California, Irvine
Irvine, CA 92717

Introduction

Two-photon absorption based three-dimensional (3-D) memories have been investigated and demonstrated over the last years, providing potentials for high memory densities and parallel access for fast data rates. Figure 1 illustrates the basic principle by which information is stored and retrieved in these 3-D memories. Two photons with appropriate combined energy (for example, λ = 1064 and 532 nm) are introduced into the memory and are absorbed simultaneously by the memory material which consists of spirobenzopyran (SP) in a PMMA host matrix).[1] The simultaneous absorption of the two photons by the photochromic molecule results in a bond dissociation transforming it into a new form with different properties, including the absorption spectrum as shown in Fig. 1. These two different molecular forms are defined as the non-written and written forms of the memory. When properly excited, the new molecular form emits fluorescence which can be detected during the read-out process. The peak fluorescence occurs at 660 nm.

Two addressing schemes are used to record and read data in 2-photon 3-D memories: orthogonal beam addressing (OBA), in which two orthogonally propagating beams are used to address any bit in the memory; and the counter-propagating pulse addressing (CPPA) where two ultrafast (femtosecond) pulses propagating collinearly in opposite directions are used to address any bit inside the memory. Both schemes permit the memory to be accessed randomly. In addition, optical beams in each addressing scheme can be arranged such that a single bit (bit-oriented), a series of bits (line-oriented), or a plane of bits (page-oriented) can be accessed at a time.[2]

In previous work, 3-D memory devices were investigated using SP doped polymers only in bulk form. In this paper, we discuss the possibility of implementing two-photon absorption based three-dimensional memories in an array of waveguides using the counter-propagating pulse addressing scheme. We will refer to this implementation scheme as a microchannel 3-D memory to distinguish it from bulk 3-D memories.

Microchannel 3-D memory with CPPA

The performance of two-photon memories can be greatly affected by the internal structure of the storage medium. Consider, a fiber bundle where the core of each fiber is a material sensitive to

two-photon absorption. Then, each bit can be recorded in a predetermined position along each fiber by CPPA addressing. Similarly readout can be carried out by interrogating each bit position along each fiber by CPPA addressing using two infrared beams

The addressing in a CPPA memory is accomplished by delaying one of the pulses such that the two pulses will intersect each other at different locations in the memory. The orthogonal addressing architecture provides a simple means to access the information stored in a bulk 3-D memory cube. However, there are several aspects of the counter-propagating pulse addressing, especially in a waveguide structure, that may have an advantage over the orthogonally addressed scheme.

First, since the 2-photon microchannel 3-D memory with CPPA employs waveguides to guide the light along the channel, it eliminates the requirement for a variable focusing mechanism to access the proper information plane, which may limit the access time of the OBA architecture to milliseconds. The pulse delay operation required in CPPA addressing can on the other hand be achieved much faster, in microseconds.[3] Second, the waveguide approach may potentially improve the collection efficiency of the fluorescent light emitted by the written bits during read-out. Third, since two-photon absorption process varies quadratically with the light intensity, the efficiency of the two-photon writing process may be enhanced in the waveguide structure due to the small diameter of the channels. Finally, when retrieving a data plane with OBA, illumination with a single addressing beam from one side causes fluorescence non-uniformity along the data plane since the addressing beam is absorbed as it propagates from one side of the material to the other.[4] This problem is totally eliminated in the CPPA approach since the wavelengths of the two addressing pulses can be chosen such that they lie outside the absorption band of the written material. Only in the plane where two pulses intersect does the two-photon absorption take place, resulting in spatially uniform fluorescence.

Experimental demonstration of memory waveguide

In order to investigate the merits and limitations of this new approach, we fabricated planar waveguides using fused-quartz microscope slides (n = 1.468) as the substrate. A solution of SP in PMMA (14 mg/ml) was spin-coated onto the slide. The film thickness was measured as 3 μm. We coupled light into this planar waveguide structure by using a prism coupling technique. Figure 2(a) shows light at λ = 632.8 nm being guided by a waveguide memory. The functions of the memory have been preliminarily demonstrated by single-photon writing of the film with UV light. Erasing in the waveguide memory is accomplished by coupling of an optical beam at 514.5 nm into the film. The fluorescence from the written material can also be observed during erasure since the excited wavelength also lies in the absorption band of the written molecules. Figure 2(b) shows the single-photon written material with a white line indicating part of the material which was erased by the coupled 514.5 nm beam.

Studies of the memory material in waveguide form

The use of this memory material in a waveguide form introduces two important effects that are directly related to the index of refraction of the memory material. These effects are pulse broadening, caused by dispersions, and inter-channel propagation delay caused by differences in refractive indices of written and non-written forms of the material. Pulse broadening in the memory leads to the limitation on memory capacity since in CPPA the bit size is directly proportional to the width of the addressing pulses. Pulse broadening associated with chromatic

dispersion can be calculated from the dispersion parameter ($d^2n/d\lambda^2$) obtained directly from the dispersion curve (Fig. 3). While modal dispersion can also cause pulse broadening in multi-mode waveguides, we plan to use single mode waveguides eliminating this dispersion mechanism. Other forms of dispersion such as waveguide dispersion, or profile dispersion are negligible under our assumptions. The interchannel propagation delay may cause shifting of bit locations in different channels during a recording process and may also cause a reduction of fluorescent intensity during the read-out operation. Also, when the practical capacity of the memory is to be calculated, the value of this propagation delay should be taken into account to obtain a more realistic quantity. Fresnel reflection loss is another effect that may result from the index difference when light goes from one region containing written bits to the other regions containing non-written bits and vice versa. Figure 3 shows the plot of the measured index of refraction versus the wavelength for the written and non-written forms of the memory material. The anomalous region seen in the curve of the written material corresponds to the absorption peak of a written material.

The pulse broadening can be calculated from the curve shown in Fig. 3. The broadening of a 100 fs pulse at λ = 450 and 900 nm (two possible addressing wavelengths) are 30 fs and 4 fs, respectively. In order to study the effect of index variations in the memory, we assume that half of the material is written on average in one channel, the delay calculated is then compared with the value obtained from the channel with no written regions. For 1-cm long channels, the propagation delay is approximately 58 fs at λ = 450 nm. If the bit size is taken to be equal to the width of a 100 fs pulse, the value suggests that the delay of the pulse is not negligible and can cause a significant shifting of the recording plane. Hence data encoding may be necessary to ensure low interchannel delay. Finally, the reflection coefficient due to the index break is given by $(n_2 - n_1)/(n_2 + n_1)$ = 0.033 % at λ = 450 nm and 0.037 % at λ = 900 nm, which should introduce less than 12% loss in a 1-cm long microchannel memory.

Conclusions

We have discussed the potential of implementing a 2-photon absorption based optical storage in a waveguide made from an organic material. Several merits and limitations of this approach have been investigated and described. Preliminary demonstration of the memory functions in a planar waveguide is presented. In order to further investigate the potential of this approach, we are investigating several fabrication methods for incorporating microchannels in the structure of the memory material.

References

1. D. A. Parthenopoulous, P. M. Rentzepis, "Three dimensional optical memory," Science 245, 843 (1989).
2. J. E. Ford, *et al.*, "Write/read performance in 2-photon 3-D memories," SPIE Proceedings 2026-60, San Diego CA, July 11-16, 1993.
3. R. Piyaket, *et al.*, "Programmable ultrashort optical pulse delay using an acousto-optic deflector," accepted for publication in Applied Optics, Information Processing issue.
4. I. Cokgor, *et al.*, "System issues in 2-photon absorption based 3-D optical memories," Optical Computing, Vol:10, 1995 OSA Tech. Dig. Series, pp.: 222-224.

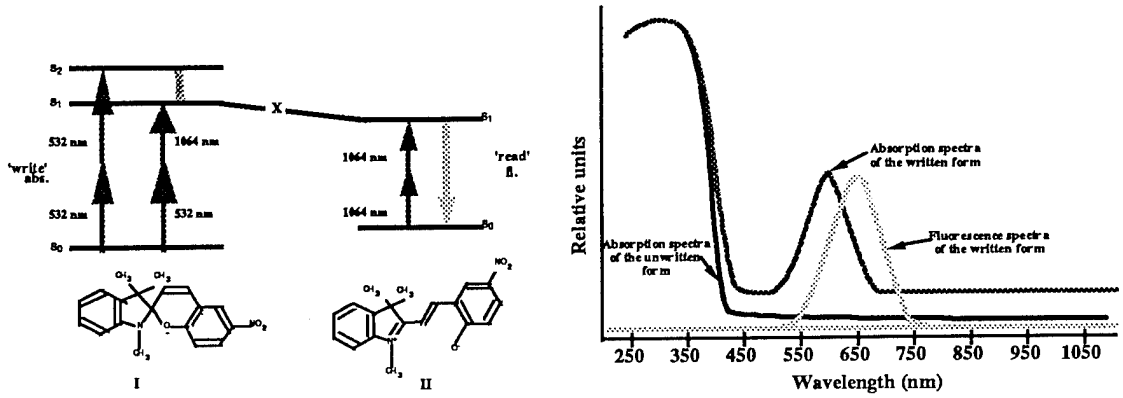

Figure 1 Fundamental concept of the 2-photon 3-dimensional memory and the material absorption spectrum.

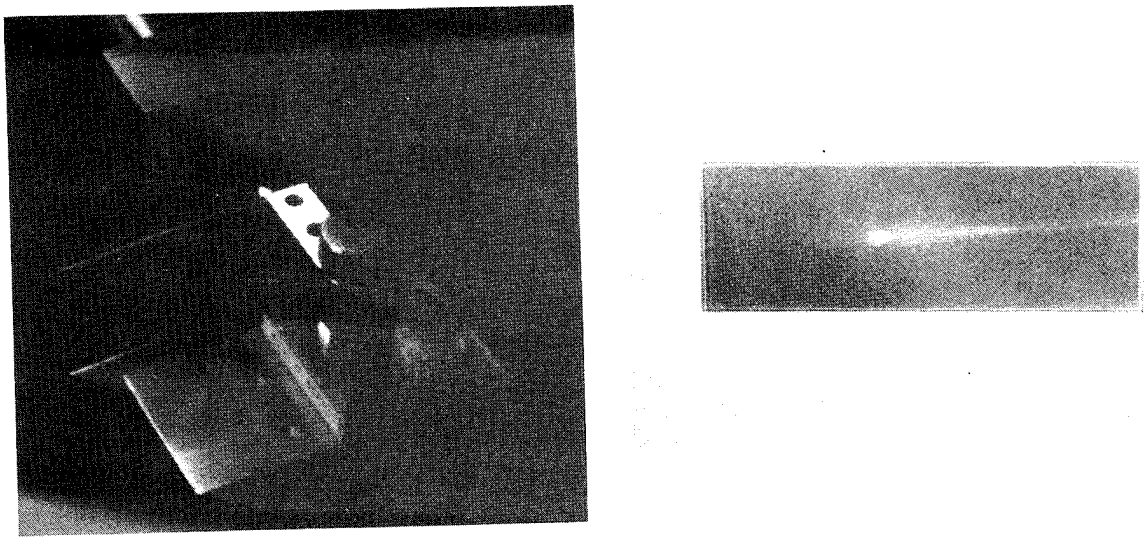

(a) (b)

Figure 2 Demonstration of (a) light being guided, and (b) single-photon writing and erasure in two-photon memory planar waveguide.

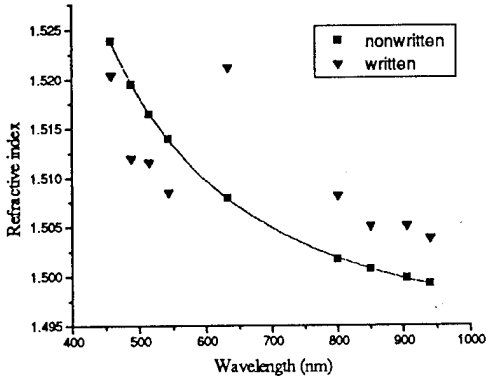

Figure 3 Refractive index versus wavelength of written and non-written forms of the memory material

Wednesday, September 13, 1995

Symposium on Data Storage II
(Joint with OSA Annual Meeting)

WTT 4:00pm–5:45pm
Holladay Room

W. E. Moerner, *Presider*
IBM Almaden Research Center

Liquid Crystalline Polymer Based Optical Data Storage

Nico Maaskant
Akzo Nobel Electronic Products BV
PObox 9300, 6800 SB Arnhem, The Netherlands
tel. +31-85-662309, fax +31 -85-664505

Introduction

Still some 90% of all information is stored on paper. But, the storage and distribution of information in an "electronic" format is rapidly growing and will play an ever increasing important role in the way our society will cover its information needs.

Data storage, the trends

Within the electronic data storage market, the following trends can be observed

- a switch from tape to disk
- a switch from magnetic to optical
- a continuing increase in areal density (number of bits per square inch)
- steady price drop

The success story of the CD-ROM is a nice example of these trends: the CD-ROM is optical, it is a disk format, a high density CD-ROM will be introduced shortly, prices have dropped while volumes have raised accordingly (see Figure 1)

Figure 1: CD-ROM drives
price and volume trend

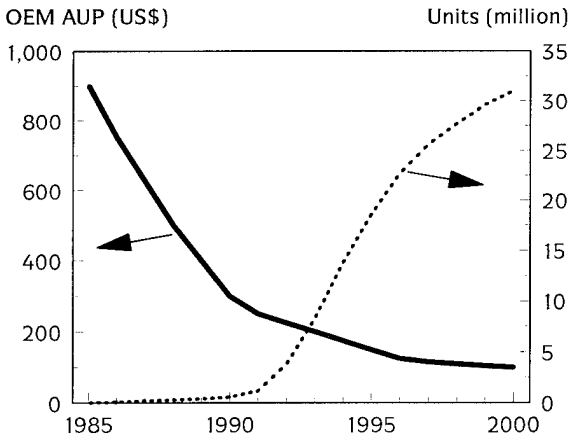

Liquid Crystalline Polymer (LCP) Optical Data Storage

Optical data storage is part of the photonic polymers program of Akzo Nobel Electronic Products. In this program unique, proprietary (liquid crystalline) side chain polymers are developed for data storage, solid state optical switches, and optical films for polarization and phase retardation.

By choosing side chain polymers, a maximal flexibility in tailoring the physical properties of the materials to the application needs is obtained. Within the "three building block" concept of side chain polymers the side chains contain the optical active groups, the back-bone is mainly responsible for physical properties as temperature stability, solubility and mechanical properties, while spacer groups can be used for fine tuning of physical properties and the de-coupling of back-bone and functional groups.

LCPs are very well suited for optical data storage. By changing the orientation of the liquid crystalline side groups, the optical properties will change accordingly, e.g. a change in reflectivity, polarization or transparency.

An Example: thermal rewritable film

A thermal re-writable film consists of an ultra-thin (typically 5 µm) layer of a LCP coated on a plastic substrate, and protected by a thin, transparent coating.

The LCP used in these thermal re-writable film can be present in two solid, optically different states: the nematic phase and the isotropic phase. In the nematic phase, the LCP is opaque (non-transparent); in the isotropic phase, the material is transparent.

The nematic phase is characterized by a relatively high degree of orientation of the liquid crystalline side groups. This orientation is not homogeneous throughout the whole film; small domain are formed each with a certain orientation of the director. Incident light is scattered mainly by the boundaries between the individual domains, causing an opaque appearance.

The LCP can be "switched" from the nematic to the isotropic phase (and vice versa) by simply heating the material above its clearing temperature (Tc). If the LCP is subsequently cooled down fast, the transparent, isotropic phase is obtained. By cooling down more slowly the opaque, thermodynamically preferred nematic phase is obtained. Below the glass transition temperature (Tg) the orientation is "frozen in" and cannot change anymore.

These type of thermal rewritable films can find applications in data storage (e.g. rewritable microfiches), magnetic/smart card systems (acting as a display), reusable overhead sheets and message signs.

Figure 2: Principle of thermal rewritable film

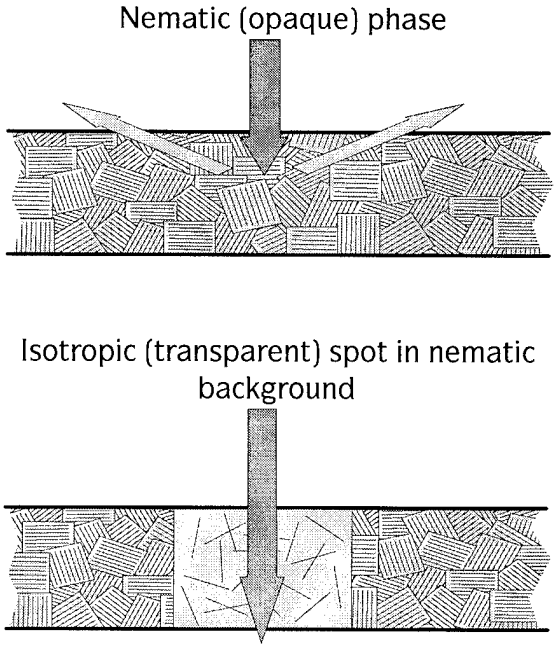

Figure 3: Effect of Cooling Speed on Optical Properties

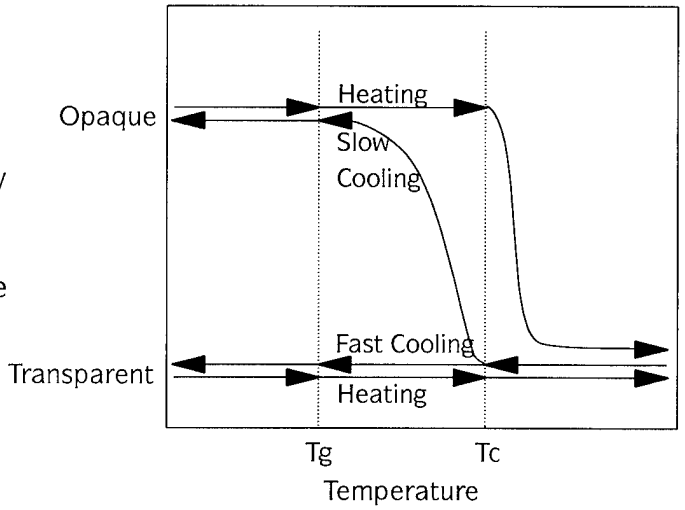

Photochromic Diarylethenes for Erasable Optical Memory.

Masahiro Irie
Institute of Advanced Material Study, Kyushu University
Kasuga-Koen 6-1, Kasuga, Fukuoka 816, Japan
Tel. +81-92-573-9611 Fax. +81-92-573-8671

Photon-mode optical recording offers advantages over magnet-optic or phase change recording, which utilizes light as a heat source for recording, with regard to resolution, speed of writing, and multiplex recording capability. One of the candidates for the photon-mode recording media is organic photochromic media(1). Although much effort has been made in this field in the past, the photochromic materials still await practical application. The limitation is due to the lack of suitable materials which fulfill the requirements for the reversible recording media(2). The requirements for the use are:

1. Archival storage capability.
2. Low fatigue (write/erase cycles can be repeated many times).
3. High sensitivity at diode laser wavelengths and rapid response.
4. Non-destructive readout capability.
5. High contrast even if the thin film thickness is thin.

We recently developed a new type of fatigue resistant and thermally stable photochromic compounds, diarylethenes with heterocyclic rings. The coloration/decoloration cycles can be repeated more than $5x10^4$ times (1,3) and both isomers are stable for more than 3 months at 80°C(2).

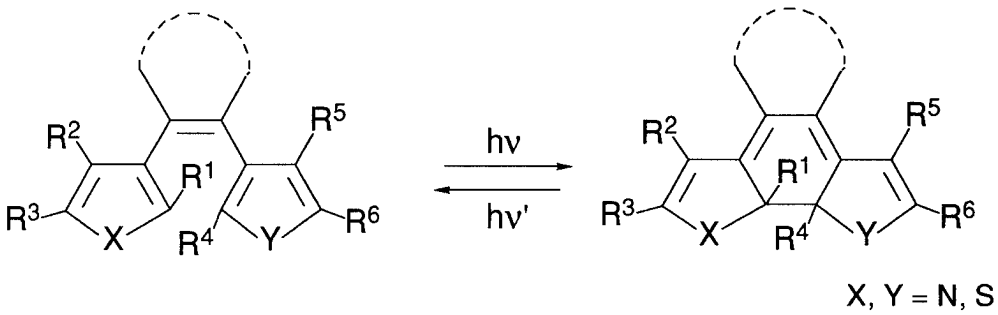

For practical application, other properties 3, 4 and 5 are also equally required. The response time of our photochromic compounds was measured by a pico-second laser photolysis method to be a few pico-second in both coloration/decoloration processes (4). In general, photochromic media have not readout stability. A property that is indispensable to the practical use is a gated photochromic reactivity. We developed photochromic media with a reaction threshold (5,6,7), in which the photochromic reactions is suppressed at room temperature, while it occurs at higher temperature, and reading more than 10^6 times without destroying the memory was achieved(5). In order to obtain high contrast even in the thin film (less than 300 nm)

the compounds should have high absorption coefficients and reactivity in the bulk. We recently found some of diarylethenes undergo photochromic reactions in the crystal phase. These compounds can be used as sensitive thin film memory media. This lecture reports on our approach to gain access to a photochromic thin films which fulfill all of the requirements for erasable optical memory media.

References

1. M.Irie, "Photoreactive Materials for Ultrahigh Density Optical Memory" M. Irie ed., Elsevier Sci. (1994) p 1
2. M.Irie, Jpn. J. Appl. Phys., 28-3 (1989) 215
3. M.Hanazawa, R.Sumiya, Y.Horikawa, M.Irie, J. Chem. Soc. Chem. Commun., (1992) 206
4. H.Miyasaka, S.Arai, A.Tabata, T.Nobuto, N.Mataga, M.Irie Chem. Phys. Lett., 230 (1994) 249
5. F.Tatezono, T.Harada, Y.Shimizu, M.Ohara, M.Irie, Jpn. J. Appl. Phys. 32 (1993) 3987
6. M.Irie, O.Miyatake, K.Uchida, T.Eriguchi, J. Am. Chem. Soc. 116 (1994) 9894
7. M.Uchida, M.Irie, J. Am. chem. Soc. 115 (1993) 6442

Photochromic Azo-Polymer Structures for Photonic Applications

Z. Sekkat[1], J. Wood[1], Y. Geerts[2], M. Büchel[1], E. F. Aust[1], R. D. Miller[3], and W. Knoll[1,4].

1 Max-Planck-Institut für Polymerforschung, Ackermannweg 10, 55128 Mainz, Germany.

2 Massachusetts Institut of Technology, Department of Chemistry, Cambridge, MA 02139.

3 IBM Research Division, Almaden Research Center, 650 Harry Road, San Jose, California 95120-6099.

4 Frontier Research Program, The Institute of Physical and Chemical Research (RIKEN), Wako, Saitama 351-01, Japan.

In the past few years azo-dye containing polymeric films have been the subject of intensive investigations because of their possible application in the areas of optoelectronics, photonics and optical signal processing[1-3]. The trans⇔cis isomerization of azobenzene derivatives in bulk polymer films has been used for producing polarization hologramms[1a], optical channel waveguides[1b], writing-erazing optical memories[1c], and second order nonlinear-optical effects[2]. Langmuir-Blodgett-Khun (LBK) multilayer assemblies of azobenzene containing polymeric materials have been used for all-optical modulation[3a], optical image recording[3b], and molecular switching[3c]. However, despite this activity, the Weigert effect that is the induction of photochemical birefrengence or dichroism in certain materials, on irradiation with polarized light, has rarely been reported for organized molecular structures, or in azobenzene containing polymeric films. Here, we report on dichroism that has been induced in a monomolecular layer of azo-silane molecules self assembled on a quartz glass substrate. The Weigert effect is studied in an azo-polyglutamate polymer for spun-cast polymer films and for LBK multilayer assemblies. It will be particularly emphisized that in contrast to the LBK structures, efficient photoselection can be achieved in the spun-cast films. Finally, photoisomerization of the push-pull azo-dye Disperse Red 1 (DR1) molecule, will be shown to create an appreciable alignment of DR1 chromophores chemically attached to the side chains of a high T_g (about 210 °C) rigid main chains polyimide polymer. This may be used to help poling this kind of polymers for second order nonlinear-optical effects.

Azobenzene derivatives have two geometric isomers, the "trans" and the "cis" forms (Figure 1a). The photoisomerization reaction begins on elevating molecules to electronically excited states after which nonradiative decay brings them back to the ground state in either the "cis" or "trans" forms. The ratio of cis/trans states is dependant on the quantum yield of the appropriate isomerization reaction. As the azobenzene trans isomer is generally more stable than the azobenzene cis isomer (the energy barrier at room temperature is about 50 $kJmol^{-1}$), molecules in the cis form may relax back to the trans form by one of two mechanisms: 1) a spontaneous thermal back reaction or 2) a reverse cis⇒trans photoisomerization cycle. As a complete cis⇒trans thermal back reaction requires several hours at room temperature, the cis isomer can be considered as stable on a time scale of minutes.

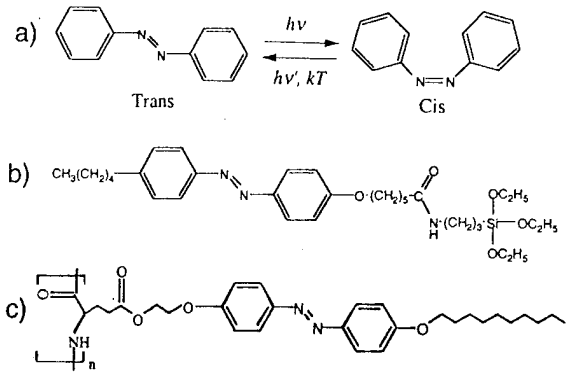

Figure 1.

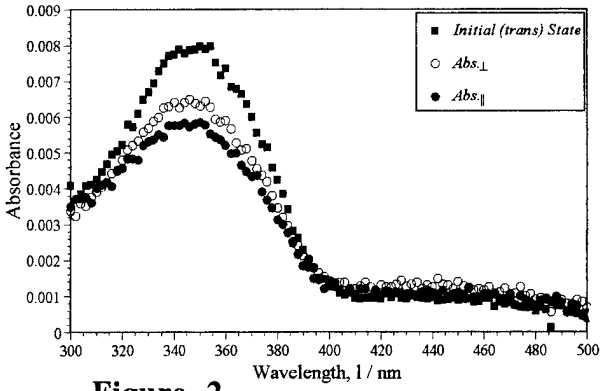

Figure 2.

The molecular structures of respectively 4-(6-carboxy-(3-amidopropyl)triethoxysilane)-4'-pentylazobenzene and poly-(5-(2-(4-(4-decyloxyphenylazo)phenoxy)ethyl)-L-glutamate), henceforth referred to as the azo-silane and the azo-polyglutamate, are given in Figure 1b) and c).

In the azo-polyglutamate molecules the main chain is coiled into an α-helix that is stabilized by hydrogen bonds, thus forming a rigid rod with the side chains pointing to the outside. This is a type of the so-called "hairy rod" polymers which are well suited for constructing multilayer structures by the Langmuir-Blodgett-Kuhn technique. Spectroscopic characterization of such azobenzene-type molecules is usually performed by the observation of a low energy band in the visible region of the absorption spectrum, and a high energy in the *UV* region. Photoisomerization of the azobenzene units was induced by *UV* light (360 nm) for the trans⇒cis reaction and by visible light (blue, 450 nm) for the cis⇒trans back isomerization. The irradiating light source was a high pressure mercury lamp (Oriel, 200 W) with a glass filter for *UV* light and an interference filter for blue light. At these wavelengths the lamp power was adjusted to 2 mW/cm^2. A Hewlett Packard UV-vis diode array spectrometer (model 8452A) was used to record linearly polarized absorption spectra of the reference and azo-polymer substrates. A self-built sample holder enabled us interchange the reference and azo-polyme substrates without altering sample position or orientation. Dichroism measurements were performed by irradiating the samples with a linearly polarized UV light, and immediately recording absorption spectra with the probe light polarization parallel ($Abs_{//}$) and perpendicular ($Abs_{\perp}$) to the initial UV polarization. Ambient red light conditions were employed to avoid the influence of the room light on the isomerization reaction.

Figure 2 shows the dichroism observed in our self-assembled azo-silane layer. These spectra were obtained after 3 minutes irradiation with linearly polarized UV light . It is clear that the absorption, $Abs_{\perp}$, of the probe light, linearly polarized perpendicular to the initial UV light polarization, is higher than the absorption, $Abs_{//}$, recorded with the probe light linearly polarized parallel to the initial UV light polarization. Identical spectra were recorded for both $Abs_{//}$ and $Abs_{\perp}$ prior to UV irradiation (only $Abs_{\perp}$ shown), demonstrating that the monolayer was optically isotropic at that time. The UV induced dichroism could be erased on irradiation with unpolarized blue light (2 min.) upon which the initial spectra for both $Abs_{//}$ and $Abs_{\perp}$ were recovered. Further irradiation with linearly polarized UV light restores the initial dichroism, and successive cycles of UV (linearly polarized) / blue (unpolarized) irradiation have shown that this dichroism can be written/erased and rewritten without any fatigue over several cycles. Additionally the sign of this dichroism could be switched from positive to negative (and back again) by rotating the polarization of the UV irradiating light. Dichroic spectra ($Abs_{//}$ and $Abs_{\perp}$) recorded immediately after 3 minutes irradiation with linearly polarized UV light and, subsequently, after 2 hours relaxation in the dark (spectra not shown), show that the spectra from the relaxed sample have been shifted to higher absorbance, due to the thermal back reaction, but that the initial dichroism was retained. We believe that this "smart communication" between light polarization and an ultrathin photochromic layer may be useful for anisotropically altering the structural and/or optical properties of ultrathin supramolecular structures containing azobenzene molecules.

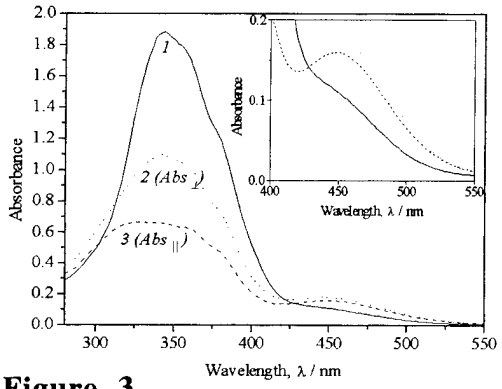

Figure 3.

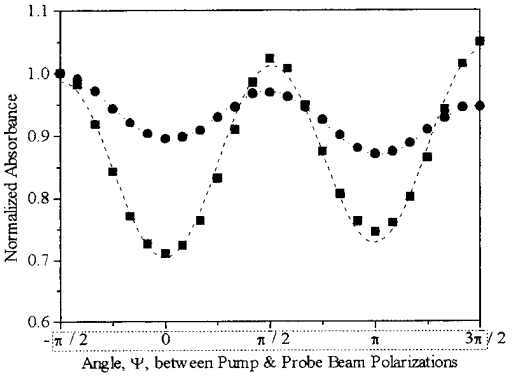

Figure 4.

Similar dichroism experiments have been performed on spun-cast azo-polyglutamate films. Figure 3 shows the dichroism observed in a spun-cast azo-polyglutamate layer. These spectra were obtained after 35 minutes irradiation with linearly polarized UV light. It can be clearly seen that the absorption, $Abs_{\perp}$ (2), is higher than the absorption, $Abs_{//}$ (3). Identical spectra (1) were recorded for both $Abs_{//}$ and $Abs_{\perp}$ prior to UV irradiation (only $Abs_{\perp}$ shown), demonstrating that the sample was optically isotropic at that time. These findings are true for the trans absorption band in the UV region around 360 nm; and also for the cis absorption band in the visible region around 450 nm (see the inset in Figure 3). This clearly shows that both the trans and cis azomolecules are preferentially distributed perpendicular to the initial UV polarization, and unumbigiously demonstrates that the cis isomer aligns perpendicular to the initial UV polarization within the trans⇒cis isomerization. Irradiation with unpolarized blue light does not eraze this dichroism, because only the cis isomer has significant absorption in the blue region around 450 nm, and consequently, the trans molecules can not be exited and reoriented. The in-plane isotropy in the both trans and cis molecular distributions can be restored only after successive unpolarized UV and blue light irradiations. However, the initial spectra of a freshly prepared sample prior to irradiation is not restored by this procedure because a net out of plane orientation of the azomolecules remains. Heating the azo-polyglutamate sample at 80 °C for 30 minutes and 14.5 hours failed to eraze the UV irradiation induced dichroism in the sample. At this temperature the sample is still at least 50 °C below the glass transition temperature (T_g > 130 °C) of the polymer, and molecular movement in polymeric material is governed by the difference between the operating temperature T and the T_g of the polymer; in other words the smallest the difference $T-T_g$ the highest the molecular movement.

In Figure 4 we have plotted the absorbance of linearly polarized probe light (at 360 (■) and 450 (●) nm) at various angles, Ψ, between the polarizations of probe and UV lights. Sinusoidal behaviour is clearly shown and unambigiously demonstrates the photoselection in both trans and cis molecular distributions. As in Figure 3 the highest absorption for both trans and cis distributions is observed when the probe and irradiation beams have perpendicular polarizations. The small drift in this absorption data results from the amount of time required to perform this experiment (e.g. 25 minutes). During this time there is a small, but noticeble, amount of cis⇒trans thermal recorvery. The dotted curves on Figure 4 are theoretical fits that vary with a law in cosine square of Ψ with an amplitude that decays in accordance with the cis⇒trans thermal back reaction.

LBK azo-polyglutamate optical waveguides have been prepared by the vertical dipping method, and investigated by the waveguide spectroscopy technique. Figure 5 shows the evolution of in-plane (n_x, n_y) and out of plane (n_z) refractive indices of the 0.37 μm thick azo-polyglutamate LBK structure, under successive UV and blue unpolarized light irradiation cycles. The mean refractive index ($n=(n_x+n_y+n_z)/3$) is also reported in this figure. In all the columns of figure 5 (labelled New, UV and B, and corresponding, respectively, to the LBK structure before any irradiation, and after UV and blue light irradiations) a small and persistant in-plane anisotropy (n_y-n_x) can be noted between the dipping direction y, and the direction x perpendicular to it. This is due to the LBK film deposition process where the flow orients the rods parallel to the transfer direction. In the columns labelled New and B, the out of plane refractive index is much higher than the in-plane refractive indices (n_z-$n_{x,y} \approx 0.14$; where $n_{x,y}$ is the in-plane mean refractive index), and means that the side chains with the azobenzene in the trans form are highly oriented, and point out perpendicularly to the plane of the substrate leading to a highly optically anisotropic LBK structure. This orientation is due to the structure of the monolayer at the air/water interface on the through that is conserved by transfer. When the LBK film is exposed to the UV light n_z decreases significantly ($\delta n_z \approx 0.1$), and n_x and n_y increase both by nearly the same amount (see columns UV in figure 5). This shows, that the LBK structure is nearly optically isotropic when the azo units are in the cis form, because the polarizibility of the azobenzene molecules breaks down as a consequence of the change in their electronical and structural properties that is induced by the trans to cis photoisomerization. This can be seen also at the value of n (the mean refractive index), which is not conserved after the UV irradiation (see columns UV in Figure 5). The order parameter of this LBK structure changes drastically by an order of magnitude under succesive UV and blue

light irradiations. In contrast to the spun-cast film, the LBK film does not show any phototselection under irradiation with polarized light, an effect that can be due to a subtle manner of reorientation imposed to the azo units by the LBK deposition process.

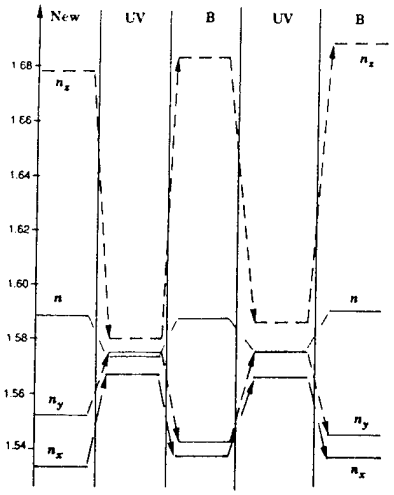

Figure 5.

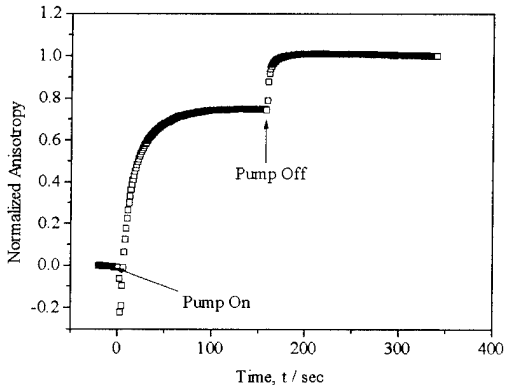

Figure 6.

The weigert effect has been extensively studied in polymer films containing push-pull azo-dye chromophores such as DR1; here we offer experimental evidence for efficient alignment that has been induced by means of photoisomerization of DR1 chromophores chemically linked to a high T_g (210 °C) rigid main chain polyimide polymer film (DR1-polyimide). Figure 6 shows the dynamics of this photoinduced alignment in a 0.8 μm thick DR1-polyimide observed under linearly polarited light irradiation. The irradiation light source was a 532 nm frequency doubled diode laser (70 mW/cm^2), and the photoinduced anisotropy was studied by means of waveguide spectroscopy. The moments of turning the irradiating light on and off are indicated by arrows on the figure. We can see that when the irradiating light beam is turned off at the photostationary state, cis molecules relax back to the trans molecules, and an appreciable and stable alignment has been induced in this film. Room temperature Photo-Electro Poling[2] of this DR1-polyimide has been performed by applying a dc poling field during the photoisomerization process. The induced polar order is appreciable and stable as has been demonstrated by using the electro-optic pockels effect from an attenuated total reflection electro-optical modulation set up. This shows that the isomerization process is able to allow the DR1 chromophores a certain mobility at a temperature that is at least 180 °C below the glass transition temperature of this DR1-polyimide polymer. This may be important for poling this kind of polymers for final applications.

(1) a) T. Todorov, L.Nicolova, and N. Tomova, Appl. Opt. **23**, 4309 (1984); b) Y. Shi, W. H. Steier, L. Yu, M. Shen, and L. R. Dalton, Appl. Phys. Lett. **58**, 1131 (1991); **59**, 2935 (1991); c) Z. Sekkat, and M. Dumont, Synthetic metals **54**, 373 (1993); SPIE Proceeding **1774**, 188 (1992); R. Loucif-Saibi, K. Nakatani, J. A. Delair, M. Dumont, and Z. Sekkat, Chem. Mater. **5**, 229 (1993); P. Rochon, J. Gosselin, A. Natanson, and S. Xie, Appl. Phys. Lett. **60**, 4 (1992).
(2) Z. Sekkat, and M. Dumont, Appl. Phys. B. **54**, 486 (1992); Mol. Cryst. Liq. Cyrs. Sci. Technol. - SecB: Nonlinear Optics, **2**, 359 (1992). Z. Sekkat, and W. Knoll, J. Opt. Soc. Am. B. **5**, 1 (1995).
(3) a) M. Sawodny, A. Schmidt, M. Stamm, W. Knoll, C. Urban, and H. Ringsdorf, Polym. Adv. Technol. **2**, 127 (1991); b) W. Hickel, G. Duda, G. Wegner, and W. Knoll, Makromol. Chem. Rapid Commun., **10**, 353 (1989); c) T. Seki, M. Skuragi, Y. Kawanishi, Y. Suzuki, T. Tamaki, R. Fukuda, and K. Ichimura, Langmuir, **9**, 211 (1993).

Azobenzene side chain polymer films for optically induced holographic surface relief gratings

D. Y. Kim, Lian Li, J. Kumar, and S. K. Tripathy
Center for Advanced Materials
University of Massachusetts Lowell, Lowell, MA 01854
Phone: (508) 934-3788 Fax: (508) 458-9571

Introduction

Recently we have observed the formation of large amplitude and stable surface relief gratings directly produced on epoxy-based nonlinear optical polymer films with Disperse Orange 3 azobenzene side groups.[1] The surface relief gratings were produced upon exposure to an interference pattern of polarized laser beams at modest intensities without any subsequent processing steps. Very similar results of the formation of the surface relief gratings were also independently reported on an acrylate polymer with Disperse Red 1 azobenzene side groups by Rochon *et al.*[2] A surface modulation depth of more than 1000 Å has been observed. The intensities of the writing beams were well below the power required for ablation of the polymer. The gratings could be erased by heating the polymer above its glass transition temperature (T_g) and the writing and erasing cycles could be repeated. While it was already known that irradiation of a polarized laser beam could result in orientation of the azobenzene groups leading to birefringence in the polymer film,[3-7] such a large surface change on the polymer film solely due to the alignment of molecules was not expected and seems to have its origins due to new optically induced processes which have not been explained so far. Large scale molecular motion and volume change due to reorientation seemed to be occurring simultaneously.

This new direct process of surface relief grating formation has considerable significance from both technological and polymer physics points of view. It provides several advantages over other conventional surface grating formation processes such as photoresist development, laser ablation techniques and a process using thermoplastic photoconductor materials.[8-10] Since the amplitude of the surface variation is large and the relief gratings can be conveniently recorded on the polymer films, such polymers may have significant potential applications for optical devices and optical elements. Optically induced large nondestructive periodic volume change of the high T_g polymer film evokes questions about the mechanism of this process.

In order to understand the mechanism of this novel process, the structure of the polymer should be simplified and modified to identify the role of each of the structural elements - polymer backbone and chromophore side groups. Especially the structure of the chromophore side groups is considered to be critical to the process. We report here the detailed investigation of the surface relief grating formation in polymers with various chromophore side groups. The effects of important structural and optical parameters on the process are investigated and possible mechanisms are discussed.

Results and Discussion

Epoxy based polymers were synthesized from diglycidyl ether of bisphenol A and selected chromophores by the procedure described previously.[11] The chemical structures of the polymers are presented in Fig. 1. All the polymers synthesized were amorphous. Optical quality polymer films were prepared by spin coating of filtered polymer solutions in 1,4-dioxane (5% w/w) on clean microscope glass slides. The typical thickness of the polymer films was approximately 0.6 μm. The spin coated polymer films were optically isotropic when viewed between two crossed polarizers. All the polymer films showed high absorption at 488 nm and absorption at 633 nm was negligible. Therefore, an Ar^+ laser at 488 nm was used as the writing beam and a He-Ne laser at 633 nm was chosen as the reading beam.

We confirmed the polarized light induced birefringence in the films of the azobenzene containing polymer PDO3 and PNA by exposure of a plane polarized Ar^+ laser beam at 488 nm. The polarized laser beam induced the preferred orientation of the azobenzene side groups in the direction perpendicular to the polarization of the writing beam through well established trans-cis-

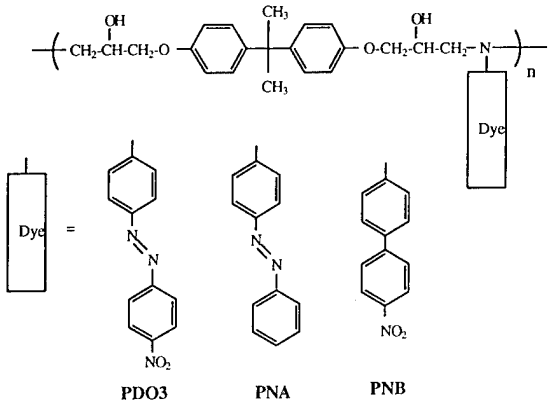

Fig. 1. Chemical structures of epoxy based polymers.

trans isomerization steps,[3-7] which consequently induced birefringence in the amorphous polymer films. The induced birefringence values were in the range of 10^{-2}. These birefringence values were in the same range of those reported from other azobenzene containing amorphous polymers.[6] However, as expected, optically induced birefringence was not observed in case of the polymer PNB which has biphenyl side groups.

Holographic gratings were recorded by a simple interferometric apparatus at wavelength of 488 nm from an Ar^+ laser with intensities ranging from 5 to 70 mW/cm^2. Grating formation was monitored with a low power unpolarized He-Ne laser beam at 633 nm by measuring the power of the +1 order diffracted beam in the transmission or reflection mode. The surface relief gratings were optically created on azobenzene containing PDO3 and PNA polymer films by exposure to an interference pattern of the laser beams at 488 nm. It is apparent that strong electron donor-acceptor structure of the chromophore was not a critical requirement for the surface grating formation. Fig. 2 shows a typical three dimensional view of the surface relief gratings on a PDO3 film observed from atomic force microscope (AFM). In this case, a *p*-polarized Ar^+ laser beam at 488 nm with an intensity of 50 mW/cm^2 was exposed for 30 minutes. Very regularly spaced sinusoidal surface relief structures with large surface modulation depth (>1300 Å) were observed. There was no regular structural periodicity on the surface of the polymer films before exposure to laser beams. Therefore, it is clear that the interfering polarized laser beams produced the surface relief structures. In case of the biphenyl side group polymer PNB, neither surface grating nor refractive index grating was observed. When it is considered that the polymer PNB has the same backbone as PDO3 and PNA, it is apparent that the presence of azobenzene side groups which can undergo trans-cis photoisomerization is a critical structural requirement for the surface deformation process.

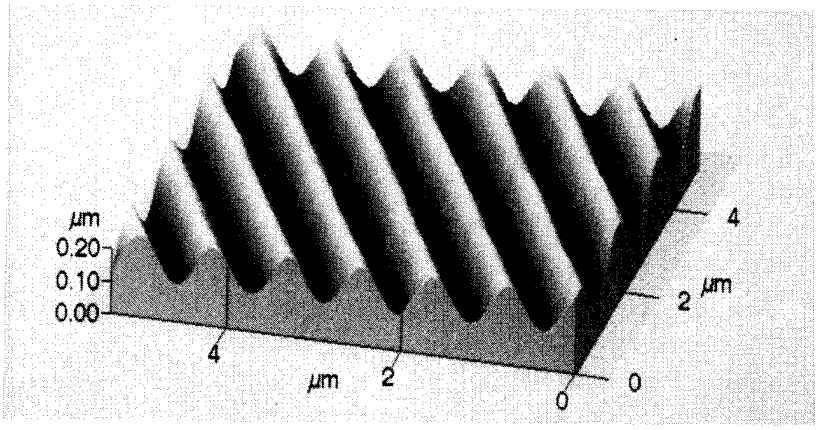

Fig. 2. AFM three dimensional view of the grating produced on the PDO3 film.

The diffraction efficiency was monitored during the writing process in order to trace the grating formation process. The grating formation process could be divided into three stages according to the slope of the diffraction efficiency curve. In the first stage which is the early stage continuing less than 3 minutes, the diffraction efficiency sharply increased. In the second stage, the diffraction efficiency increased almost linearly with a lower rate than the first stage. Finally the rate became much slower and reached saturation at the third stage. The distinction between the first and second stage was apparent when low intensity light was used for the writing. Fig. 3 shows the diffraction efficiency curve of the PDO3 film in an early stage exposed to relatively low intensity light. When the laser beam was turned on, the diffraction efficiency increased rapidly and reached 0.04 % in about 3 minutes. Then the diffraction efficiency decreased, which may indicate the presence of a transition stage, and again started increasing in the second stage. The diffraction efficiency of 0.04 % was close to the value expected from 10^{-2} of the birefringence. And no surface change at the first stage was observed during AFM scan. Therefore it is apparent that the first stage of the grating formation is due to the well established photoinduced birefringence of the azobenzene groups. The transition stage between the first and the second stage highly depended on the intensity of the writing beam. With low intensity exposure, slight decrease of the efficiency was observed. One possible explanation is that migration of polymer chains which causes the surface change partially cancels index modulation due to chromophore orientation. The development of the surface relief structure is responsible for the slow increase of the diffraction efficiency in the second stage. In the final stage a diffraction efficiency as large as 15 % could be obtained in the transmission mode.

The polarization state of the writing beams significantly influenced on the process. When the PDO3 film was exposed to *p*-polarized beams, diffraction efficiencies higher than an order of magnitude were observed than the film exposed to *s*-polarized beams. Although the light intensity absorbed by the polymer in both cases is comparable, the surface modulation and consequently the diffraction efficiencies are considerably different. Since the polymer is isotropic before exposure we believe that the *p*-polarized light cycles more number of azo moieties through a trans-cis-trans cycle than the *s*-polarized light which has no component of the electric field normal to plane of the polymer film.

Thermal effect due to light absorption might contribute to the process because the polymer films have high absorption of the writing beams. To study the thermal effects, PDO3 polymer films were exposed to the writing beams with different intensities while keeping the same fluence of the total light energy. The polymer films which were exposed to the beams with

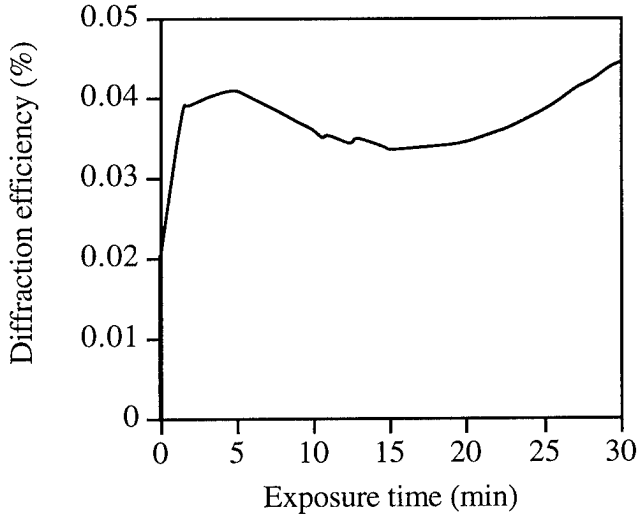

Fig. 3. Diffraction efficiency of the PDO3 polymer film as a function of time when exposed to laser beams with an intensity of 12 mW/cm^2 at 488 nm.

higher intensity showed substantially larger surface deformation leading to higher diffraction efficiency than the film exposed to low intensity light. Therefore, a certain amount of thermal effect resulting from absorption of light seems to contribute to the surface deformation process or at least accelerate the process. A spatial variation of temperature resulting from the interference of the writing beams could make polymer molecules mobile and promote the macro scale molecular migration even though the T_g of the polymer is much higher than the ambient temperature. However, a thermal effect alone cannot explain the dependence of grating amplitude on the writing beam polarization. Although the thermal effect does play a significant assistive role it is not the driving force for the grating formation process.

The effect of the grating spacing on the surface modulation was investigated. The samples were exposed to the same fluence and intensity of light and writing beams were turned off well before the grating efficiency saturated. The samples with grating spacing ranging from 3 to 0.35 μm were easily made. As the spacing became smaller from 3 to 0.8 μm, the amplitude of surface modulation was increased. However, the surface modulation heights dropped for samples with spacings shorter than 0.8 μm. If we assume that material migration rate remains constant at a fixed incident intensity, we could explain the increase in the amplitude of the relief gratings when the period changes from 3 to 0.8 μm. However the sharp drop in the diffraction efficiency at short periods clearly shows that the behavior is more complicated perhaps involving thermal effects as discussed earlier.

Conclusions

Holographic surface relief gratings with large surface modulation depth were directly produced on the polymer films containing azobenzene side groups. The orientation of the azobenzene groups was induced first and was followed by the surface deformation process. The azobenzene side groups which are capable of trans-cis photoisomerization are responsible for the surface deformation process. Strong electron donor-acceptor structure of the chromophores was not a critical requirement for the surface relief grating formation. The surface deformation process depends on the polarization state of the writing beams. Therefore, the process is related to the optically induced orientation of the azobenzene groups. Also we demonstrated that thermal effect due to light absorption is also involved in the process although it is not the dominant factor.

References

1. D. Y. Kim, L. Li, J. Kumar, and S. K. Tripathy, *Appl. Phys. Lett.*, **66**, 1166 (1995).
2. P. Rochon, E. Batalla, and A. Natansohn, *Appl. Phys. Lett.*, **66**, 136 (1995).
3. T. Todorov, L. Nikolova, and N. Tomova, *Appl. Opt.*, **23**, 4309 (1984).
4. M. Eich, J. H. Wendorff, B. Reck, and H. Ringsdorf, *Makromol. Chem., Rapid Commun.*, **8**, 59 (1987).
5. U. Wiesner, M. Antonietti, C. Boeffel, and H. W. Spiess, *Makromol. Chem.*, **191**, 2133 (1990).
6. A. Natansohn, P. Rochon, J. Gosselin, and S. Xie, *Macromolecules*, **25**, 2268 (1992).
7. D. Y. Kim, L. Li, R. J. Jeng, J. Kumar, M. A. Fiddy, and S. K. Tripathy, *SPIE proc.*, **1853**, 23 (1993).
8. L. F. Johnson, G. W. Kammlott, K. A. Ingersoll, *App. Opt.*, **17**, 1165 (1978).
9. H. Philips, D. Callahan, R. Sauerbrey, G. Szabo, and Z. Bor, *App. Phys. Lett.*, **58**, 2761 (1991).
10. T. C. Lee, *App. Opt.*, **13**, 888 (1974).
11. B. K. Mandal, R. J. Jeng, J. Kumar, and S. K. Tripathy, *Makromol. Chem., Rapid Commun.*, **12**, 607 (1991).

Photoinduced Refractive Index Changes in PMMA Films Including a Photochromic Fugide

S. Morino, T. Yamazaki, S. Machida, T. Yamashita and K. Horie
Department of Chemistry and Biotechnology, Graduate school of Engineering, University of Tokyo, Hongo 7-3-1, Bunkyo-ku, Tokyo 113, Japan

Tel. 81 3 3812-2111 Ex. 7289
Fax. 81 3 5802 3327

Introduction

Photochemical reactions such as photochromic reactions, photodegradation and photocrosslinking, change optical properties of the samples during their reactions, and are applicable for optical memories, optical switching devices, and so on[1~3].

In this study, we discuss optical switching devices making use of photoinduced refractive index changes during photochromic reactions. In order to reduce the switching energy of such switching devices, photoinduced refractive index change should be large, which can be obtained at the wavelength near absorption bands which appear/disappear during photochromic reactions. However the use of such wavelength region is limited by absorption losses of switched light due to photochromic dyes, and also by photochromic reactions due to the switched light. Therefore, the wavelength of switched light should be optimized in relation to these absorption bands.

We will report the results of measurements for photoinduced refractive index changes and its wavelength dispersion during photoisomerization. The minimum switching energy for optical switching devices using photochromic dyes is also estimated.

Measurements of photoinduced refractive index change during photochromic reactions

Samples are PMMA films containing a fulgide, FG540 ((*E*)-α-2,5-dimethyl-3-furylethylidene(isopropylidene)succinic anhydride). The chemical structure of FG540 is shown in Figure 1. Samples were casted from dye/polymer solutions onto fused silica substrates with a barcoater, and dried under vacuum at room temperature for one day. Concentration of the dye is 0.248 *mol/l*. Thickness of films are about 3.6 μm.

Refractive indices were measured by using prism coupling technique. To avoid the photoisomerization caused by refractive index measuring light, the power of the measuring

beam is reduced to 5 μW, and incident beams were irradiated for only 0.6 s per one measurement.

Light sources used in these measurements are a line selectable tunable He-Ne laser (REO LSTP-1010, λ = 543 *nm*, 594 *nm*, 604 *nm*, 612 *nm*, 633 *nm*), Ar^+ laser pumped ring dye laser (Dye: DCM, 633 ~ 690 *nm*), and Ar^+ laser (488 *nm*).

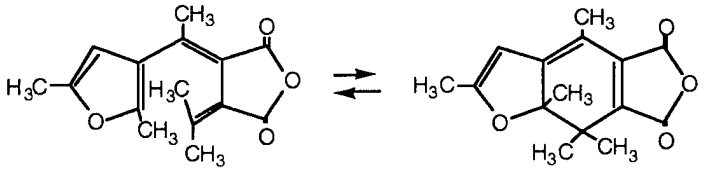

Figure 1. The chemical structure and the phtooisomerization of FG540

Refractive indices were measured before and after photoirradiation. The light source for the photochromic reaction is a Hg lamp with a UVD-36A filter (Toshiba). Figure 2. shows the absorption spectra before and after the photochromic reaction. Conversion of photoisomerization was calculated to be 0.90 by using molar extinction coefficient of FG540[4]. Figure 3 shows the refractive indices before and after photoisomerization. In order to obtain the continuous wavelength spectra of refractive indices, Kramers-Kronig transformation was carried out. Absorption spectra measured for 200 ~ 800 *nm* were used for this transformation, and other absorption bands for vacuum ultra-violet (VUV) and infrared (IR) regions were assumed as follows. Absorption bands in IR wavelength region is simplified just as one absorption band because it is very far from the wavelength region of our interest (500 *nm* ~ 700 *nm*). Those in VUV region were simplified to be two absorption bands. One

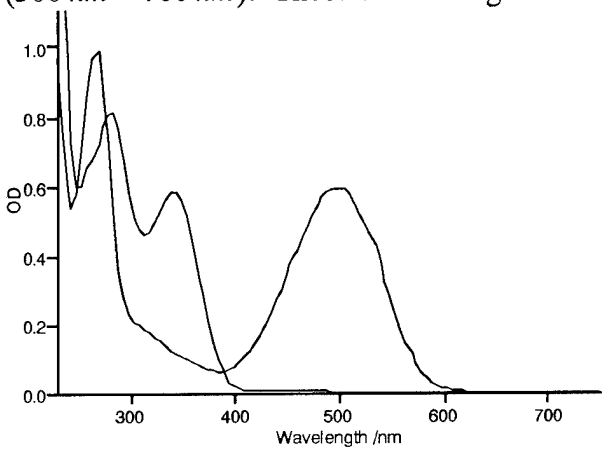

Figure 2. Absorption spectra of PMMA film including FG540 before and after photo-irradiation. Fine line is for unirradiated samples, Bold line is for irradiated sample.

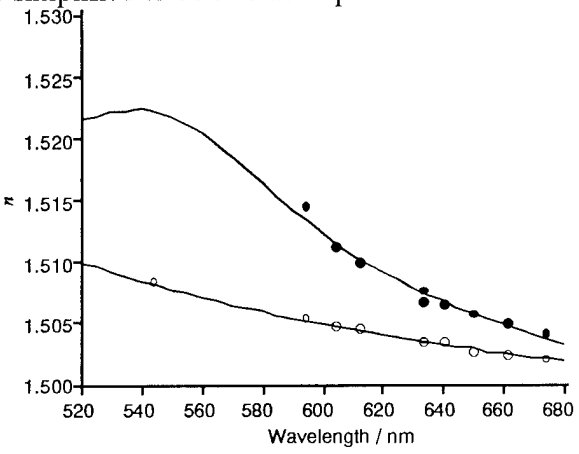

Figure 3. Refractive indices of PMMA films including FG540 before and after irradiation. Open circles are for the unirradiated sample, filled circles are for the irradiated sample.

is assumed to locate at very short wavelength (< ca. 150 *nm*), and is treated as a constant. The other was assumed to locate at the wavelength region between 150 *nm* and 200 *nm*. Parameters for these absorption bands were determined by L.S.F. method by using the measured refractive indices. The results are also shown in Figure 3 with solid lines, andfit well with the measured refractive indices, though absorption bands in VUV and IR wavelength region have been much simplified.

Estimation of the minimum switching energy of optical switching devices with FG540

As is mentioned in the introductory section, one should optimize the wavelength of the switched light in relation to the absorption band. In this section, we propose the way of the optimization. Here, we consider the optical switching devices like a Mach-Zehnder type one consisting of channel waveguides.

At first, the light to be switched should be transmitted through the waveguide including FG540. The minimum requirement of transmittance, $T_{\min}$, shown in eqs 1 derived from the Lambert-Beer's law as shown eqs (1),

$$T = 10^{-\varepsilon c (100 L_{\max})} \tag{1}$$

where $L_{\max}$ [m] is the acceptable maximum optical path, ε [$l/cm \cdot mol$] is the mole extinction coefficient, c [mol/l] is the mole concentration of FG540.

Normalized refractive index change, δN, for photoisomerization corresponding to 100% conversion and reduced concentration are given by eqs (2).

$$\delta N = \frac{\delta n}{x\, c} \tag{2}$$

where x is for the fractional conversion of photoisomerization, δn for the photoinduced refractive index change. In this equation, we have assumed that the photoinduced refractive index change is proportional to both conversion and mole concentration of the chromophore, which is roughly satisfied[1,2,5,6].

Available retardation, ϕ [rad], is defined by eqs 3,

$$\phi = k\, \delta n\, L_{\max} = -\frac{2\pi x\, \delta N(\lambda)}{100\, \lambda\, \varepsilon(\lambda)} \log T_{\min} \tag{3}$$

where$k$ [rad/m]is the wavenumber. The ϕ represents the available retardation under the limitation subscribed by eqs 1.

Figure 4 shows the wavelength dependence of ϕ by putting $T_{\min} = 0.9$ and $x = 1$ for the FG540/PMMA system. On one hand ϕ should be larger than π to switch the state, and on the other hand photoinduced refractive index change increses for the wavelength nearer to abosorption band. Therefore, 624 *nm* is the optimized wavelength the light to be switched.

Next, we calculated the minimized switching energy. The cross-section,S $[m^2]$, of a channel waveguide composing the optical switch is assumed to be $3\times3\,\mu m^2$, and the ratio of effective refractive index change to photoinduced refractive index change is assumed to be

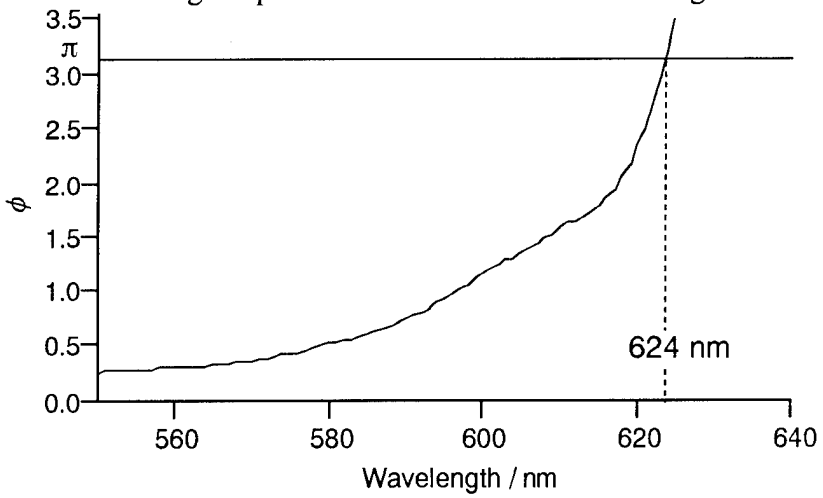

Figure 4. Wavelegnth dependence of the available retardation for FG540/PMMA

unity. Then the minimum switching energy , E $[J]$, can be calculated from eq 4,

$$E = \frac{cL_{\max} S}{1000} \frac{hC}{\lambda} N_A \frac{1}{\Phi} \qquad (4)$$

where h $[m{\bullet}s]$ is the Planck constant, C $[m/s]$ is the velocity of the light, N_A is the avogadro number, and Φ for the quantum efficiency for photoisomerization of FG540. The value of $cL_{\max} = 1.1$ $mol{\bullet}m/l$ is obtained for the optimized wavelength of $\lambda = 624$ nm. By using $\Phi = 0.20$ [4] together with these valuse, the minimum switching energy, E, was calculated to be 170 nJ. Further results with detailed discusssion will be given at the time of presentation.

References

1. S. Morino, S. Machida, T. Yamashita, and K. Horie, *J. Phys. Chem.*, in press.

2. S. Morino, T. Watanabe, Y. Magaya, T. Yamashita, and K. Horie, T. Nishikubo, *J. Photopolym. Technol. Sci.*, **7**, 121(1994)

3. F. Ebisawa, M. Hoshino, and K. Sukegawa, *Appl. Phys. Lett.*, **65**, 2919(1994)

4. H. Dürr, H. Bounas-Laurent, eds., "Photochromism, Molecules and Systems", Elsevier, Amsterdam(1990)

5. Th. Lückemeyer and H. Franke, *Polym. Eng. Sci.*, **31**, 912 (1991)

6. Th. Lückemeyer and H. Franke, *Appl. Phys.* **A 55**, 41 (1992)

Thursday, September 14, 1995

Characterization

ThA 8:00 am-10:00 am
Holladay Room

George I. Stegeman, *Presider*
University of Central Florida

Spatial and Temporal Orientational Correlations Between Nonlinear Optical Chromophores Probed by Femtosecond Hyper-Rayleigh Scattering

Koen Clays, Marvin Wu, and André Persoons

Laboratory of Chemical and Biological Dynamics,
Center for Research in Molecular Electronics and Photonics,
Department of Chemistry, University of Leuven,
Celestijnenlaan 200D, B-3001 Leuven, Belgium

Tel.: +32/16/32.75.08
Fax.: +32/16/32.79.82

After designing and synthesizing a new candidate molecule for nonlinear optical (NLO) applications, the molecular hyperpolarizability of this molecule has to be experimentally determined. This measurement at the microscopic level can be performed in an isotropic solution using hyper-Raleigh scattering (HRS).[1] For a second-order NLO application, the individual molecules have to be assembled in a macroscopically non-centrosymmetric fashion. The efficiency of a phase-matched second-order NLO process is highly dependent on the length over which the coherent nonlinear interaction can be maintained. In artificially ordered systems, such as poled polymers and Langmuir-Blodgett films, this length is much more determined by the length over which the local order is constant than by the coherence length, calculated from the bulk refractive indices at fundamental and second-harmonic wavelength. A measurement scheme to determine the degree of spatial correlation between the chromophores would therefore be instrumental in the development of reliable and reproducible devices.

Since the introduction of HRS as a measurement technique for the first hyperpolarizability (second-order polarizability) of molecules in solution,[1,2] the importance of fluctuations in the orientational distribution was realized.[3] For isotropic solutions, at the molecular level, a combination of the spatial and temporal fluctuations causes the instantaneous and local deviations from macroscopic centrosymmetry, which allows the observation of a second-order HRS signal. The intensity of the scattered light can then be related to a value for the first hyperpolarizability of the molecules in solution.

The development of femtosecond (Titanium-sapphire based) HRS[4] was instrumental for the study of spatial and temporal orientational correlations. The continuous-wave (cw) femtosecond laser has a much higher repetition rate than the Q-switched nanosecond laser normally used for HRS (82 MHz versus 10 Hz). The smaller pulse separation time (12 nsec) is a prerequisite to extend temporal correlation studies in solution to the sub-microsecond time domain. For the spatial correlations in solids, the somewhat lower peak power (on the order of 100 kWatt) associated with the cw laser is compensated by the much higher repetition frequency. This results in at least the same signal-to-noise ratio, but without radiation damage to the solid samples.

In a correlation measurement, the intensity of the HRS signal is recorded as a function of time for temporal correlations or as a function of position for spatial correlations. Since HRS is a second-order NLO process, it is sensitive to centro-symmetry: any fluctuation in centrosymmetry of the NLO chromophore arrangement will show up as a fluctuation in HRS signal. The decay of the autocorrelation function of this fluctuating signal is characterized by a correlation length or time. The correlation length indicates the degree of spatial correlation between the chromophores in the solid state. The correlation time is determined by the rotational diffusion coefficient in solution.

Reproducible runs of HRS signal as a function of position have been obtained for a) a commercial frequency doubling crystal (KTP); b) a thin Langmuir-Blodgett (LB) film of 10 layers of 2-docosylamino-5-nitropyridine (DCANP); and c) a sample with *para*-nitroaniline (*p*NA) dispersed in a solid poly (methylmethacrylate) (PMMA) matrix. These three typical macroscopic ensembles, single-crystallinity with a high degree of orientational order, an LB film with micro-domain formation and a macroscopically isotropic, centrosymmetric, unpoled, polymeric sample were expected to show different fluctuations in HRS signal as a function of position. Figure 1 shows the spatial fluctuations of the HRS signal for the three different types of macroscopic ensembles. The corresponding autocorrelation curves are shown in Fig. 2. The difference in degree of spatial correlation is evident. The approximately constant intensity of the scattered second harmonic from the single crystal results in the highest degree of correlation. Only the entrance and exit surface of the crystal are polished. Nonuniform grinding or local defects may cause the small intensity variations. A much longer spatial correlation has been observed for the LB film. In Langmuir-Blodgett deposition, the amphiphilic properties of the molecules are used to induce molecular ordering. There is virtually no spatial correlation to be observed between the randomly oriented chromophores dispersed in an unpoled polymer matrix. All correlation is lost within the spatial resolution of the set-up.

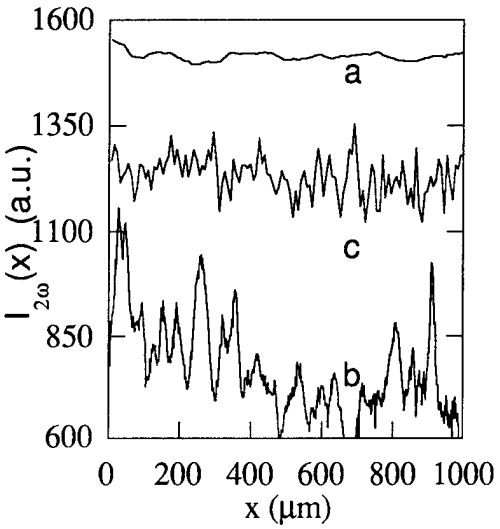

Fig. 1. Intensity of the HRS signal as function of position x for a) KTP crystal; b) DCANP LB film; c) pNA in PMMA.

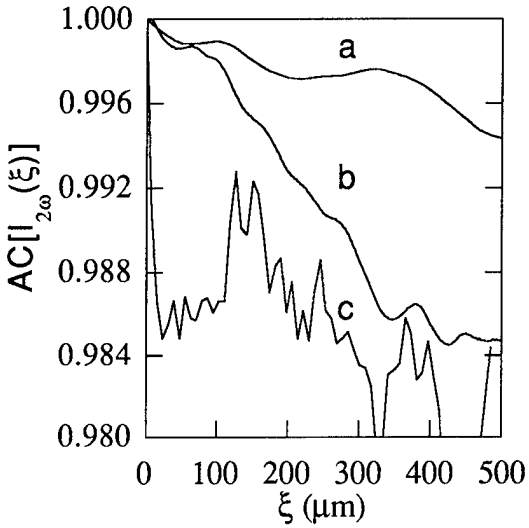

Fig. 2. Autocorrelation of the HRS intensity as a function of displacement ξ for a) KTP crystal; b) DCANP LB film; c) pNA in PMMA.

Experimental aspects determining the spatial resolution with femtosecond pulses will be addressed. The number of data taken is still limited, especially when comparing the acquisition and autocorrelation function calculation in real time for temporal correlation study, as in quasi-elastic light scattering (QELS).

The study of the fluctuations in the HRS signal as a function of time for isotropic solutions is the second-order variant of QELS. In linear dynamic light scattering, the fluctuations in scattered light intensity are caused by density fluctuations, governed by translational diffusion. The correlation time is then determined by the translational diffusion coefficient. This coefficient can be linked to the hydrodynamic radius of the scattering particle through the Stokes-Einstein relation. Because of symmetry, fluctuations in the second-order scattered light intensity are related to rotational fluctuations. The rotational correlation time can then be linked to the hydrodynamic volume of the NLO chromophore.

The optical part of the experimental set-up that is used for the quasi-elastic nonlinear light scattering (QENLS) is basically the same as described for HRS measurement with femtosecond pulses.[4] The output of the photomultiplier is now fed to a discriminator, counter and autocorrelator. The build-up of the autocorrelation function can be followed in real time. The autocorrelator has a minimal sample time of 10 nsec. The temporal resolution is determined by the pulse repetition frequency of the laser (12 nsec). After checking the quadratic dependence of the intensity of the detected second-

order scattered light (Figure 3 shows this dependence for a solution of crystal violet, 10^{18} cm^{-3} number density in glycerol), the correlation experiment is run at maximum fundamental intensity. The resulting autocorrelation function is shown in Fig. 4, together with a fit to a single-exponential decay. The resulting orientational correlation time of (2.14 ± 0.05) μsec is in good agreement with what is expected for the volume of the crystal violet molecule in the viscosity of glycerol (13.2 Poise) at room temperature.

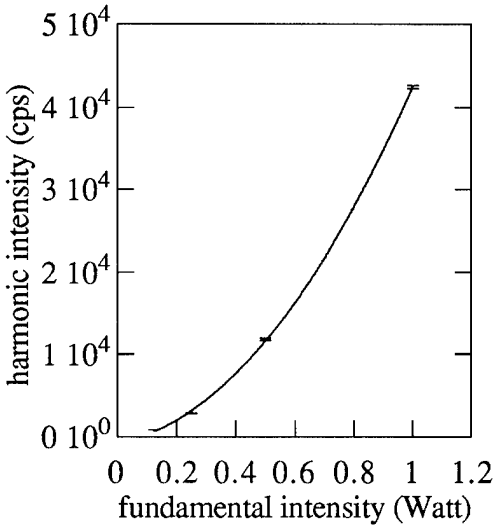

Fig. 3. Intensity of the HRS signal as a function of fundamental intensity (data-points and fitting to quadratic function).

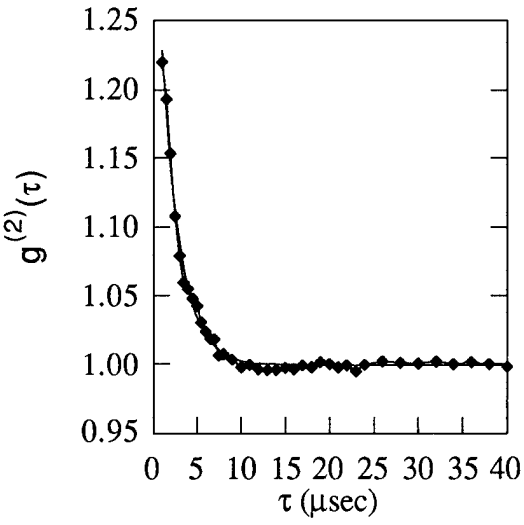

Fig. 4. Autocorrelation of the HRS intensity as a function of time τ (second-order nonlinear intensity autocorrelation function $g^{(2)}(\tau)$; datapoints and fitting to single-exponential decay.

Experimental aspects of QENLS, such as the trade-off between number of counts and coherence volume, and the influence of relaxation oscillations from the solid-state Titanium-sapphire laser, will be addressed.

In conclusion, second-order nonlinear optics in general can take advantage of the high peak power that is available in femtosecond pulses. We have shown two examples of new fields that have become accessible. In particular, hyper-Rayleigh scattering, as an incoherent nonlinear optical measurement technique, can reveal a lot of information about spatial correlation in solid samples and temporal dynamics in solution.

References:
1. K. Clays and A. Persoons, *Phys. Rev. Lett.* **66**, 2980 (1991).
2. K. Clays and A. Persoons, *Rev. Sci. Instrum.* **63**, 3285 (1992).
3. K. Clays, A. Persoons and L. De Maeyer, in *Modern Nonlinear Optics, Part 3* (Ed: M. Evans and S. Kielich, John Wiley & Sons, Inc.,) pp. 455 (1994)
4. K. Clays and A. Persoons, *Rev. Sci. Instrum.* **65**, 2190 (1994).

MEASUREMENTS OF FIRST HYPERPOLARIZABILITIES β: ANOMALOUS HYPER-RAYLEIGH SCATTERING RESULTS

Marinus C. Flipse, Roel de Jonge, Richard H. Woudenberg
Akzo Nobel Central Research, PO Box 9300, 6800 SB, The Netherlands
Telephone: (31)85663613 Fax: (31)85665272
Albert W. Marsman, Cornelis van Walree, Leonardus W. Jenneskens
Debeye Institute, Department of Physical Organic Chemistry, Utrecht University, Padualaan 8, 3584 CH Utrecht, The Netherlands
Telephone: (31)30533128 Fax: (31)30534533

The large optical nonlinearities, the accessibility of molecular engineering, and the intriguing physics of quadratic nonlinear optics made both chemists and physicists explore the field of organic chromophores for nonlinear optics. Furthermore, the potential of polymers derived from these nonlinear optical chromophores for applications within telecommunications led to a considerable interest from industry.
The applicability of highly nonlinear optical polymers facilitates the development of optical waveguiding structures for use as integrated optical components [1]. Key parameters for the design of these materials are properties such as refractive index, optical absorption, and optical nonlinearity. Part of our research for new polymers for nonlinear optical applications is devoted to the optimization of the first hyperpolarizability β of the chromophores. However, the lack of a simple technique to measure the first hyperpolarizability β of the chromophores considerably hampered the search for better chromophores. Until recently, electric field-induced second-harmonic generation (EFISH) [2,3] was the standard characterization technique which was used for a large number of polar chromophores. However, in part due to the complexity of this technique, a large scatter of the β-values can be found in literature [4].
The feasibility of the hyper-Rayleigh scattering (HRS) method to characterize quadratic molecular nonlinearities was explored by Clays et al.[5]. The experimentally relatively simple HRS technique offers a number of advantages compared to EFISH. Besides the well-known polar chromophores, HRS also allows the study of ionic and apolar chromophores.
This paper deals with anomalous results obtained with the HRS method. Some fluorescent and non-fluorescent well-known π-conjugated chromophores were characterized and the origin of the anomaly with the EFISH results will be discussed.

Scattering of second-harmonic light can be observed in isotropic solutions when the light of a high peak-power pulsed laser is focused in a solution [6]. The first hyperpolarizability β_c of the chromophore (c) can be determined relative to β_s of the solvent (s)[5], by measuring the second-harmonic scattering efficiency $S_{2\omega}$ of a concentration series. The scattering efficiency is given by

$$S_{2\omega} = g[N_c\beta_c^2 + N_s\beta_s^2]I_\omega^2$$

where g is a geometry factor, N the number of scattering centers, and I_ω the intensity of the harmonic light. The geometry factor can be estimated by measuring the pure solvent, provided that β_s is known.

Our HRS set-up is essentially identical to the set-up described by Clays et al.[7]. As a representative example, the results of a HRS experiment for 4-N,N-dimethylamino-4'-nitrostilbene in chloroform is presented in Figure 1. The data of four chromophores (pNA, MNA, MONS, and DANS) are listed in Table 1. All measurements were done using chloroform ($\beta_s = -0.49*10^{-30}$ esu [8]) as the solvent.

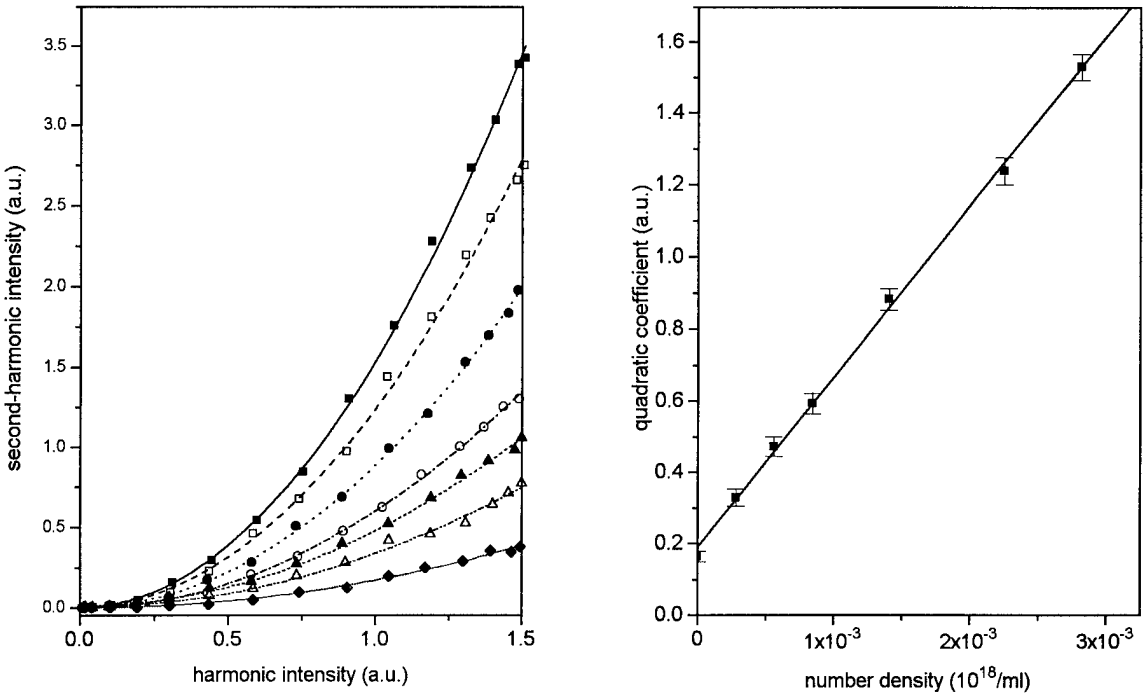

Figure 1 *a) Quadratic dependency of the scattered second-harmonic light for a concentration series of DANS in chloroform. b) Quadratic parameter $g(N_s\beta_s^2+N_c\beta_c^2)$ versus number density N_c of the chromophore. The geometry factor g can be obtained by measuring the pure solvent. The slope of the line gives β_c^2.*

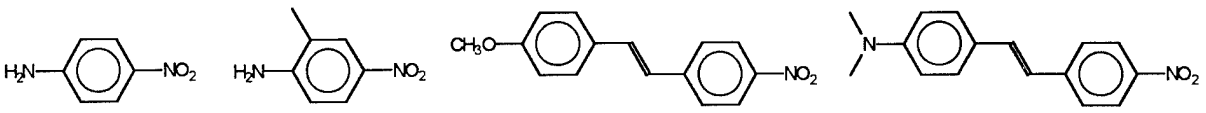

pNA MNA MONS DANS

	λ_{max} nm	β_{HRS} 10^{-30}esu	$\beta_{HRS}(0)$ 10^{-30}esu
pNA	347	34	17
MNA	353	52	26
MONS	370	337	153
DANS	437	2209	597

Table 1 *Absorption maximum (λ_{max}), first hyperpolarizability (β_{HRS}), first hyperpolarizability corrected for resonance enhancement $\beta_{HRS}(0)$*

Although the β_{EFISH} data for these compounds are not unambiguous, it can be concluded that the β_{HRS} values for pNA and MNA are relatively close to the values measured with EFISH at 1064 nm [9,10]. However, β_{HRS} for MONS is approximately 4 times larger [11] and β_{HRS} for DANS is 5 to 8 times

larger [3,12] than the related β_{EFISH} values. For other standard π-conjugated chromophores, even larger differences between β_{HRS} and β_{EFISH} were observed [13].
This discrepancy can not be attributed to either a solvent effect or to the fact that for β_{EFISH} the projection of β on the ground state dipole moment is measured, whereas for HRS several β components will contribute to β_{HRS}. Especially for MONS and DANS, β_{HRS} and β_{EFISH} will be dominated by a single component of the β-tensor along he ground state dipole moment of the molecule.
To account for the high β_{HRS}-values, we were prompted to search for a different process generating photons at the second-harmonic wavelength. Note that focusing of high peak-powers in a chromophore solution may give rise to different nonlinear optical processes. Here we show that multi-photon absorption followed by fluorescence at the second-harmonic wavelength is observed in the case of fluorescent chromophores during the HRS experiment. To this end, the band-pass filter and the photomultiplier in the HRS set-up were replaced by a monochromator and an optical multichannel analyzer in order to determine the multi-photon absorption induced fluorescence spectrum. These spectra are shown in Figure 2a for MONS and DANS in chloroform. It should be stipulated that they closely resemble the single-photon fluorescence spectra of MONS and DANS. Note that at 532 nm no significant contribution from the HRS signal is discernible.
The nature of the fluorescence process in the case of MONS was checked by using different band-pass filters in the HRS set-up spanning the single-photon fluorescence band of the chromophore. A quadratic dependency even below 532 nm was observed at all band-pass transmission wavelengths (Figure 2b). The fluorescence below 532 nm can on the analogy of single-photon fluorescence be considered as anti-Stokes fluorescence [14].

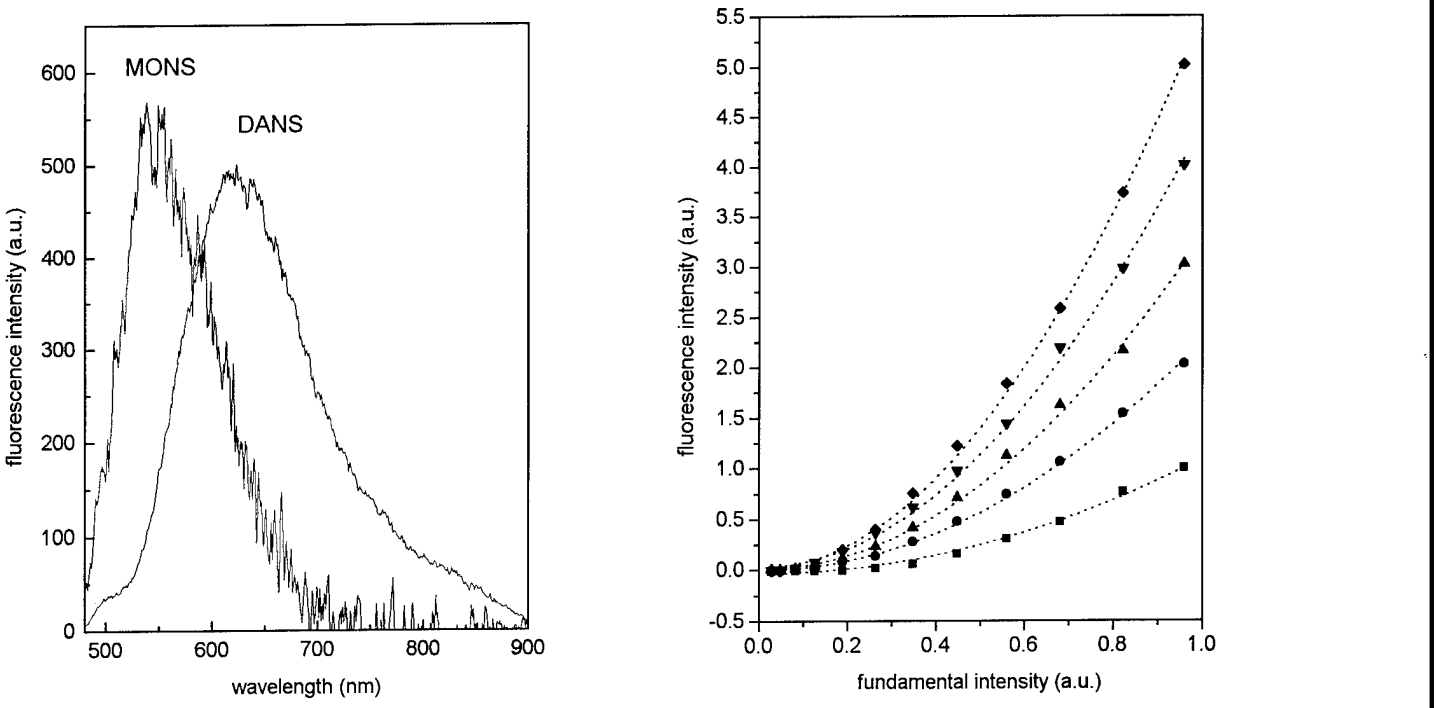

Figure 2 *a) Two-photon absorption induced fluorescence spectra of MONS and DANS in chloroform. Excitation wavelength: 1064 nm. b) Fluorescence intensity at different wavelengths of MONS in chloroform. 480 nm (■), 500 nm (●), 532 nm (▲), 560 nm (▼), 600 nm (◆). The intensity of each curve is not scaled with respect to the absolute fluorescence intensity. Excitation wavelength: 1064 nm.*

In conclusion, we have shown that for some well-known quadratic nonlinear optical chromophores (MONS and DANS), that the HRS method at 1064 nm is not a suited method to determine the first hyperpolarizability β. For the HRS method, two-photon absorption induced fluorescence will be a fundamental problem which has to be solved for the study of the numerous organic chromophores which show fluorescence near the second-harmonic wavelength. If fluorescence at the second-harmonic wavelength occurs, then the magnitude of β_{HRS} measured will be mainly determined by the characteristics of the band-pass filter in the experimental set-up. HRS at longer wavelengths to avoid two-photon absorption will considerably complicate the experiment, since scattering efficiency, resonance enhancement and detector sensitivity will be reduced at longer wavelengths. Furthermore, an increase of the harmonic intensity will be limited by the occurrence of optical breakdown in the solution. For chromophores which do not show two-photon fluorescence at the second-harmonic wavelength, like pNA and MNA, the HRS technique is a relatively simple method to fully characterize their quadratic nonlinearity.

References

[1] Polymers for Lightwave and Integrated Optics: Technology and Applications, edited by L.A. Hornak, Marcel Dekker Inc., New York (1992)

[2] B.F. Levine, and C.G. Bethea, *J. Chem. Phys.*, **63**, (1975), 2666

[3] J.L. Oudar, *J. Chem. Phys.*, **67**, (1977), 446

[4] R.A. Huijts, J.N. Louwen, and L.W. Jenneskens, *Trends in Chem. Phys.*, **2**, (1992) 39

[5] K. Clays, and A. Persoons, *Phys. Rev. Lett.*, **66**, (1991), 2980

[6] R.W. Terhune, P.D. Maker, and C.M. Savage, *Phys. Rev. Lett.*, **14**, (1965), 681

[7] K. Clays, A. Persoons, *Rev. Sci. Instrum.*, **63**, (1992), 3285

[8] F. Kajzar, I Ledoux, and J. Zyss, *Phys. Rev. A*, **36**, (1987), 2210

[9] J.L. Oudar, and D.S. Chemla, *J. Chem. Phys.*, **66**, (1977), 2664

[10] B.F. Levine, C.G. Bethea, C.D. Thurmond, T.T. Lynch, and J.L. Bernstein, *J. Appl. Phys.*, **50**, (1979), 2523

[11] R.A. Huijts, and G.L.J. Hesselink, *Chem. Phys. Lett.*, **156**, (1989), 209

[12] G.R. Moehlmann, C.P.J.M. van der Vorst, R.A. Huijts, and C.T.J. Wreesman, *Proc. SPIE*, **971**,(1988), 252

[13] to be published

[14] C.A. Parker, Photoluminescence of Solutions, Elsevier Publishing Company, Amsterdam, (1968), 424

Evanescent Wave Surface Enhanced Raman Scattering from Organic Molecules Bonded to "Optical Chemical Benches"

Wenbo Xu and Mark P. Andrews
Department of Chemistry, McGill University
801 Sherbrooke St. West
Montréal, Québec H3A 2K6
Canada
andrews@omc.lan.mcgill.ca
Tel. 514-398-4459 FAX 514-398-3797

I. Introduction

Our interest is in using molecular self-assembly (MSA) techniques to develop hybrid functional organic/inorganic thin film materials for applications in spectroscopy, optics and photonics.[1,2,3] MSA can be seen as a convergent methodology for combining the "bottom up" techniques of molecular chemistry with the "top down" techniques of nanoscale device fabrication.

Methods for characterizing thin films derived by MSA include advancing contact angle measurement, infra-red reflection-absorption, X-ray photoelectron, attenuated total reflection spectroscopies, and scanning probe microsopy. Molecular monolayers present special challenges to each of these techniques, and these are well documented in the literature.[4] Ideally, one would like to probe the structure of the molecular interface of an optical device directly, *in situ*, without damage to the fragile adlayer, and in a variety of environments that are actual or simulated operating conditions. Such information is crucial to assess the stability of these ultrathin self-assembled films to optical damage and other kinds of environmental perturbations encountered under real device operating conditions. As described in this paper, our strategy is to co-opt a passive optical circuit (waveguide) into behaving simultaneously as an autoscopic structure that reveals chemical and structural information about an interface deposited by MSA. To do this, we use MSA protocols to prepare "integrated optical chemical benches". The concept is illustrated in

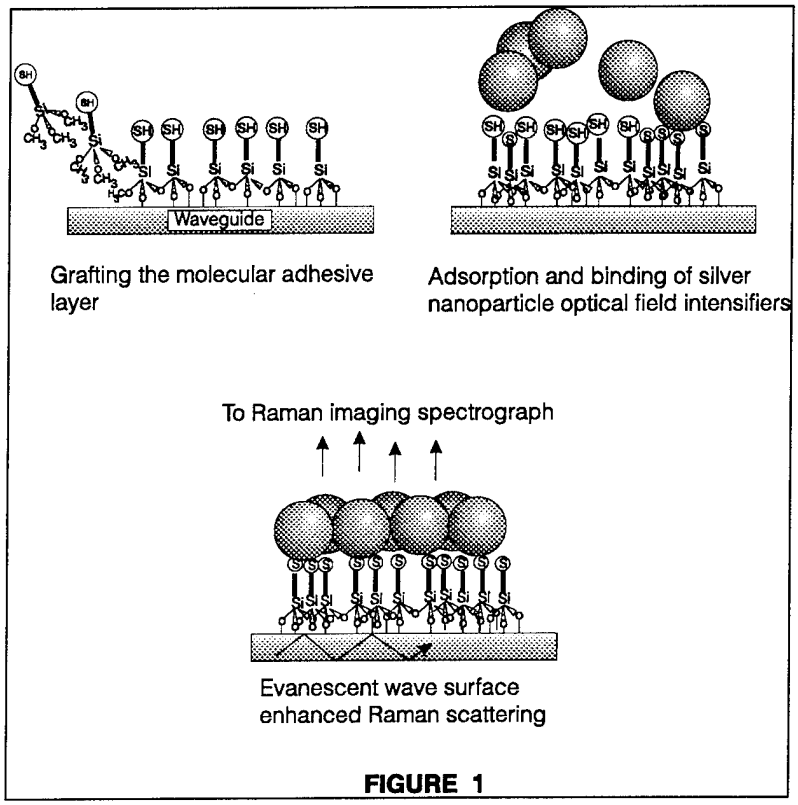

FIGURE 1

Figure 1, which depicts the sequential deposition of different kinds of layers onto a silica waveguide. Our experiments take advantage of the chemical selectivity of bifunctional surface active compounds for optical components (waveguide surfaces) and adventitious species - colloidal metal particles.[2] The principle here is to use metal nanoparticles of silver, for example, as field intensifiers to magnify optical field effects (Raman scattering) at interfaces.[1,2] In this paper, we describe applications of a hybrid waveguide heterostructure that provides an unusal glimpse of the vibrational properties of molecular scale, sub-monolayer organic thin films grafted onto optical waveguides. The new technique of evanescent wave surface enhanced Raman spectroscopy (EWSERS) is described in the limiting case in which metal nanoparticles are chemically attached to an organic film of molecular dimensions. Bound, sub-Rayleigh limit metal particles enhance Raman scattering (SERS) at the metal-organic molecule-waveguide interface. A flow cell arrangement is described that is used to generalize the technique to permit study of molecular grafts that do not chemisorb colloidal metals. In this case, flowing silver hydrosol provides optical field enhancement sufficient to observe high quality Raman spectra of molecules in fluid environments on waveguides in matters of seconds.

II. Experimental

The experimental configuration for the evanescent waveguide Raman experiment is shown in Fig. 1. Grafting and polycondensation of organothiol terminated mercaptobenzylltrimethoxysilane (MBTMS) was achieved by refluxing thick silica waveguides in toluene solutions of MBTMS. Thiol functionalities were used in experiments where it was desirable to bind the colloid to the waveguide surface to give a robust heterostructure. Grafting was achieved in a similar manner with 1-(trichlorosilyl)-2-(*p,m*-chloromethylphenyl)ethane. In this case, a flow cell (Figure 2) was placed atop the waveguide and sealed against a gasket derived from medical grade silicone rubber. The incident laser beam (514.5 nm, Ar^+) was launched into the waveguide through a high refractive index prism. As the guided light propagates along the waveguide, the evanescent field penetrates from the waveguide across the organic monolayer and into the flow cell. Because water has a higher refractive index than air, the evanescent field penetrates more deeply into the flow cell, improving the sensitivity of the Raman signal through an increase in the incident power at the molecular film. The function of the silver hydrosol is to provide an extra enhancement at the waveguide/organic molecule inter-face through the SER effect. We speculate that as silver colloid solution flows over the organic layer, nanoparticles enter the field of the evanescent wave which excites dipolar surface plasmon modes in the particles, effectively focusing and magnifying the laser field near the grafted organic overlayer. The result is enhanced Raman scattering at the interface. Unaggregated silver colloid did not give a SER signal from the flow cell. Sodium

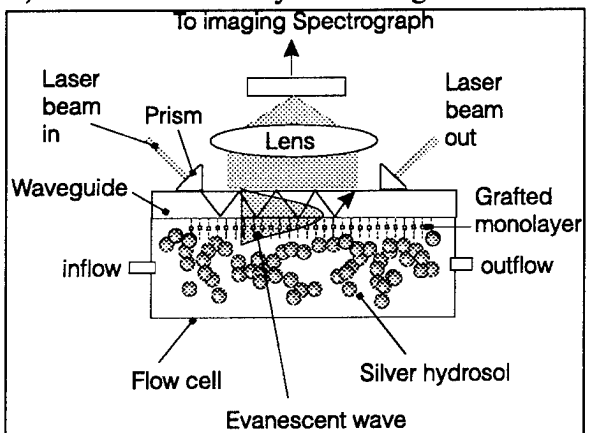

Figure 2

chloride was used to promote Ag colloid aggregation to initiate the SER response. The guided light was adjusted by changing the incident angle of the laser beam at the prism hypotenuse. It was found that the highest sensitivity was obtained when the light was guided as close as possible to the solution interface. The 514 nm line of a Coherent Argon ion laser was used to excite SERS. The waveguide streak was focused through near-diffraction limited collection optics, a holographic Bragg filter and onto the slit of a THR 640 spectrograph equipped with a holographic grating (1800 grooves/mm). Dispersed light was captured with a liquid nitrogen-cooled 1152 x 298 pixel CCD detector.[1] Laser power was kept at 200 mw.

III. Results and Discussion

Figure 3 shows the Raman spectrum derived from MBTMS at the chemically bonded silver adlayer/waveguide interface in the sampling configuration given in Figure 1. Insert (a) in Figure 3 locates the SH stretching mode in unreacted, neat MBTMS at 2572 cm^{-1}. This mode, and the symmetric stretching mode of the terminal methyl groups of the methoxysilane portion of the moecule, disappear after grafting to the waveguide (loss of ν_s CH_3) and adsorption and binding of silver (loss of ν_{SH}). Insert (b) in Figure 3 implies that loss of the ν_{SH} mode is definitive for binding Ag colloid through the sulfur terminus, whereas loss of the band associated with ν_s CH_3 indicates the grafting and polycondensation of MBTMS at the waveguide surface in the vicinity of the bound Ag is complete. The remaining features of the spectrum are assigned in the Figure. We have elected not to subtract the background signal from the waveguide in order to emphasize the enhancement of the spectral information at the interface, despite submonolayer coverage by MBTMS and the fact that most of the laser light is confined to the guide.

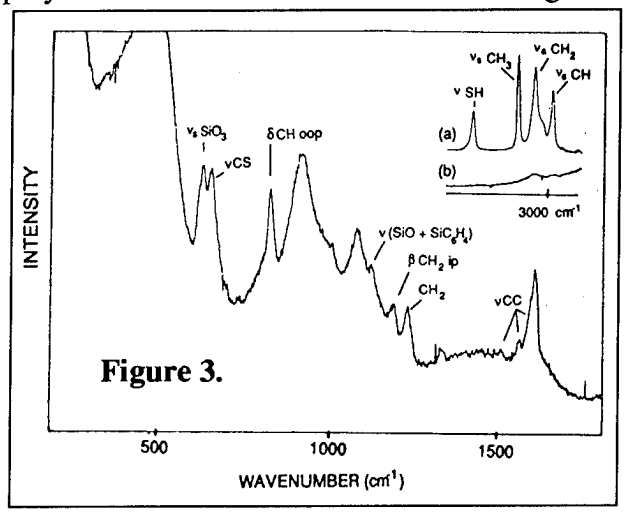

Figure 3.

Figure 4a. shows the Raman spectrum collected from a waveguide that had been conjugated with with 1-(trichlorosilyl)-2-(*p,m*-chloromethylphenyl)ethane and embedded in an air-filled flow cell. The only peaks detected are those from the glass waveguide itself. A five minute integration time was used for acquisition. When aggregated silver hydrosol was subsequently flowed over this surface, the Raman signal from the graft was easily detected. This is confirmed in Figure 4b, where the data was acquired with only 20 seconds of detector integration time. Note that the background Raman from the glass waveguide contributes substantially less to the spectrum, which indicates the highly localized nature of the electromagnetic field near the metal colloid/graft interface.

IV. Conclusion

We have described a new technique of evanescent wave surface enhanced Raman spectroscopy for probing vibrational properties of organic molecules grafted onto optical

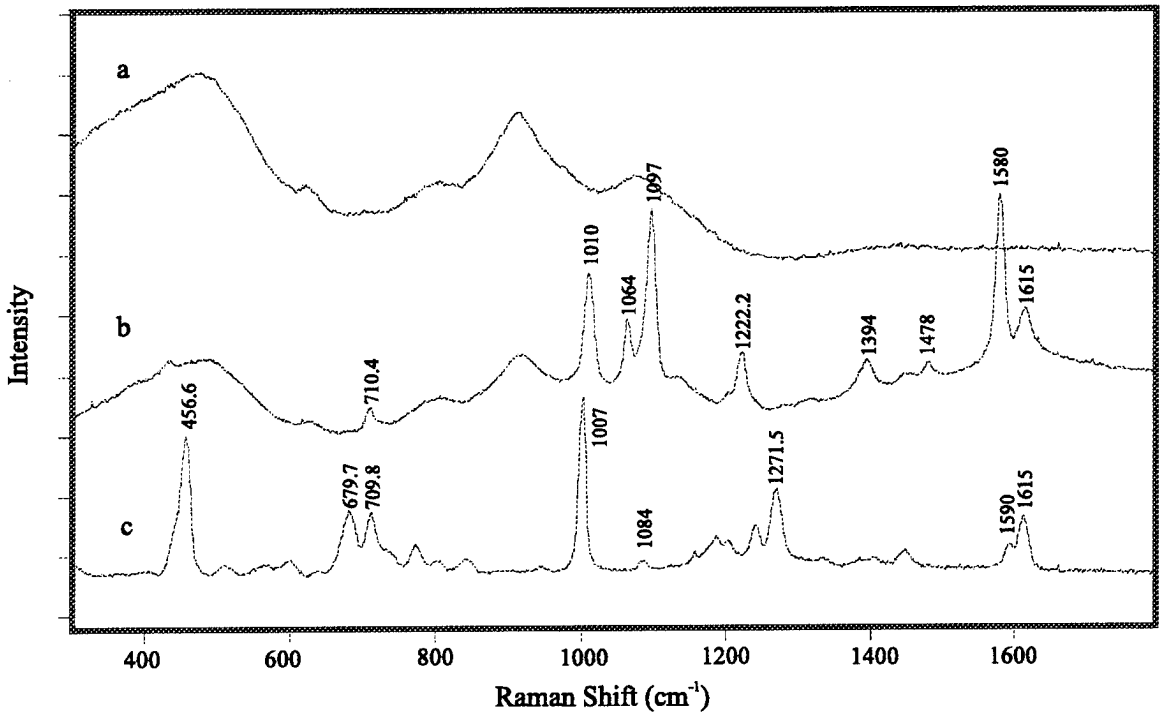

Fig. 4. (a) Raman spectrum of glass waveguide with grafted 1-(trichlorosilyl)-2-(*p,m* chloromethyl-phenyl)ethane when the flow cell is empty. Laser power, 200mw; acquisition time, 5 minutes. (b) same as in (a) but flow cell is filled with aggregated silver hydrosol. Laser power, 200mw; acquisition time, 20second. (c) Raman of neat 1-(trichlorosilyl)-2-(*m,p* chloromethylphenyl)ethane.

waveguides. Methods of molecular self assembly were used to convert optical waveguides into "chemical benches" for studying ultrathin organic films. The technique is fast, nondestructive, and imposes little restriction of the type of organic molecule that can be studied in this kind of configuration. Currently we are extending this technique to other *in situ* studies of interfacial processes related to the structure and stability of optical interfaces.

References

[1]. Andrews, M. P.; Kanigan, T.; Xu, W.; Kuzyk, M. G. *Integrated Optics Waveguide Spectroscopy of Self-Organizing Polymers and Fractal Composites*. SPIE. **1994**, *2042*, 366.

[2]. Xu, W.; Andrews, M. P., *J. Am. Chem. Soc.*, submitted for publication

[3]. Xu, W.; Andrews, M. P., *Langmuir*, submitted for publication.

[4]. See for example, Ullman, A. "An Introduction to Ultrathin Organic Films: From Langmuir Blodgett to Self-Assembly", Academic Press, New York, 1991.

A Two Slit Electrooptic Coefficient Measurement Technique and Efficient In-Plane Poling of Polymer Thin Films

Sean Garner, Srinath Kalluri, Mehrdad Ziari and William H. Steier
Department of Electrical Engineering, University of Southern California
Los Angeles, CA 90089-0483
Tel: (213) 740-4408, Fax: (213) 740-8689

Yongqiang Shi
TACAN Corporation, 2330 Faraday Ave., Carlsbad, CA 92008

Zhiyong Liang and Larry R. Dalton
Chemistry Department, University of Southern California
Los Angeles, CA 90089

Several techniques are in use for the characterization of the electrooptic properties of poled polymer thin films. Of these, three techniques - 1) extrapolation of electrooptic coefficient from second-harmonic generation data 2) attenuated total reflection (ATR)[1] and 3) ellipsometry[2,3] - are favored for their convenience and accuracy. However, these methods are mainly used for material characterization and it is difficult to adopt them for measurements of the material nonlinearity in certain practical device structures such as those poled in-plane by coplanar electrodes. The new technique that we will present here - a two slit interference modulation measurement - is capable of measuring the electrooptic coefficient for both material and device characterization. Moreover, in this method, waveguiding is not required and both the real and the imaginary parts of either r_{13} or r_{33} coefficients can be measured independently.

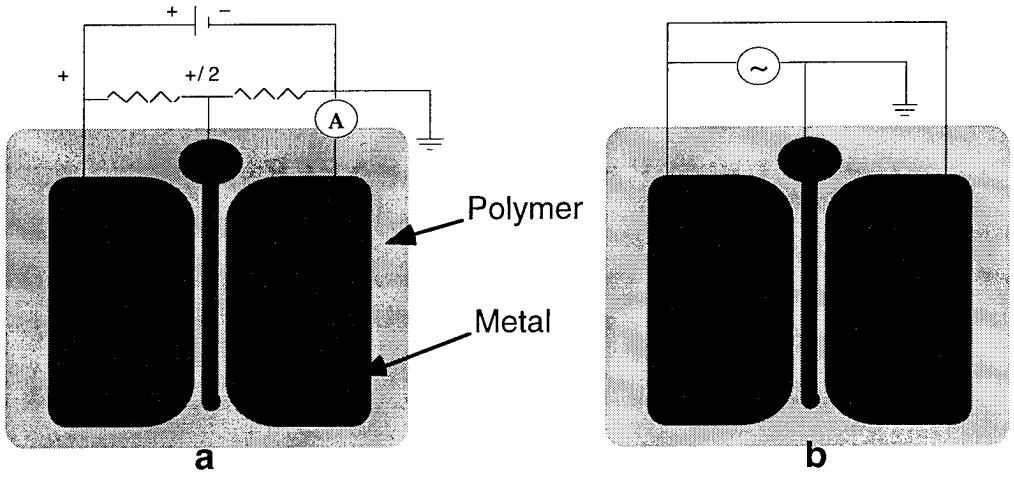

Figure 1. Sample geometry: poling and measurement. a) Two arm poling b) Push-pull modulation

The sample geometry is shown in figure 1. Samples were prepared photolithographically. A 0.2μm thick chrome layer was evaporated on an insulating and transparent quartz substrate. Two

10 μm wide thin slits with a center to center separation of 90μm between them were photolithographically defined and wet etched in the metal. After some initial calibration of the lithographic steps, measurement samples were easily and repeatably fabricated. Electro-optic polymer films 0.8 μm to 1.5 μm thick were subsequently spun to cover both slits and dried. A thick passive, non-electrooptic buffer layer such as polystyrene was often spun on top of the EO layer to prevent electrostatic breakdown through air and allow for higher poling fields. Samples were poled by applying DC fields as high as 150V/μm to 180V/μm across one slit. For push-pull modulation experiments, a voltage divider circuit was used to pole equally across both slits (Figure 1a). Push-pull modulation doubles the modulation efficiency and is useful for practical device geometries such as the Mach-Zenhder modulator and will be discussed shortly.

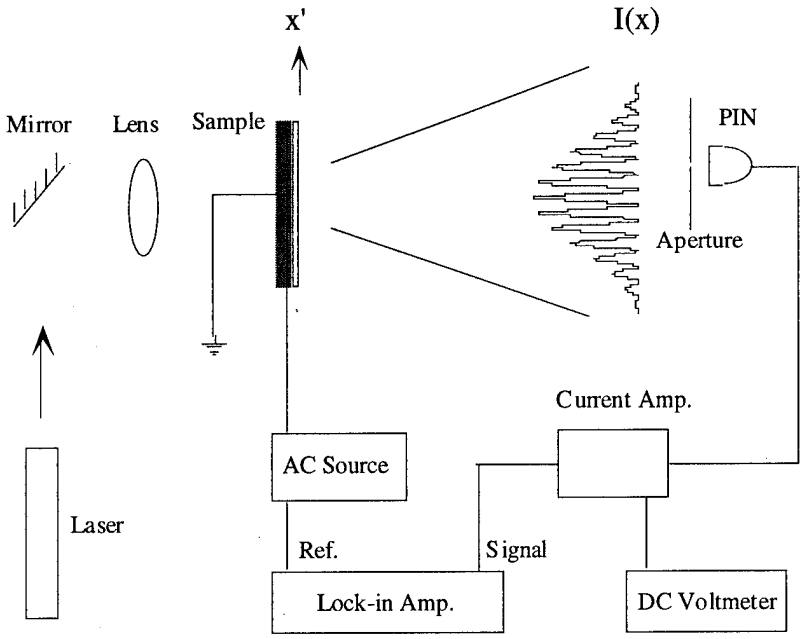

Figure 2: Two Slit Measurement Set-Up

The measurement set-up is shown in figure 2. Polarized light propagates normal to the film and through the two parallel and coplanar electrodes. This metalized pattern also functions as a double-slit aperture and the resulting interference pattern is sensitive to the relative phase changes between the slits and can shift by inducing an electrooptic index change through one or both slits. For measurement purposes, we apply an ac field across one slit only and monitor the shift in the interference pattern using a small detector (relative to pattern width) and lock-in detection. For samples poled across both slits (and in the same direction), the measurement ac voltage is applied across both slits and push-pull modulation is achieved by keeping the ac field across one slit exactly opposite in direction with respect to the field across the other slit (Figure 1b). Thus when the field induced index change associated with the EO effect across one slit is positive, the index change across the other slit is negative and the total effective index change is twice what it would be if only one slit were used.

Measurements were made at three different wavelengths: 632 nm, 1.06 μm and 1.3 μm. The dispersion of the r_{33} coefficient for a sample poled at 150 V/μm is shown in Figure 3. These

measurements were made in the push-pull configuration. The filled circles represent the experimental data points and the curve shows the two level model extrapolation of the measured value of the r coefficient at 632 nm to longer wavelengths. The measured and extrapolated values are quite close.

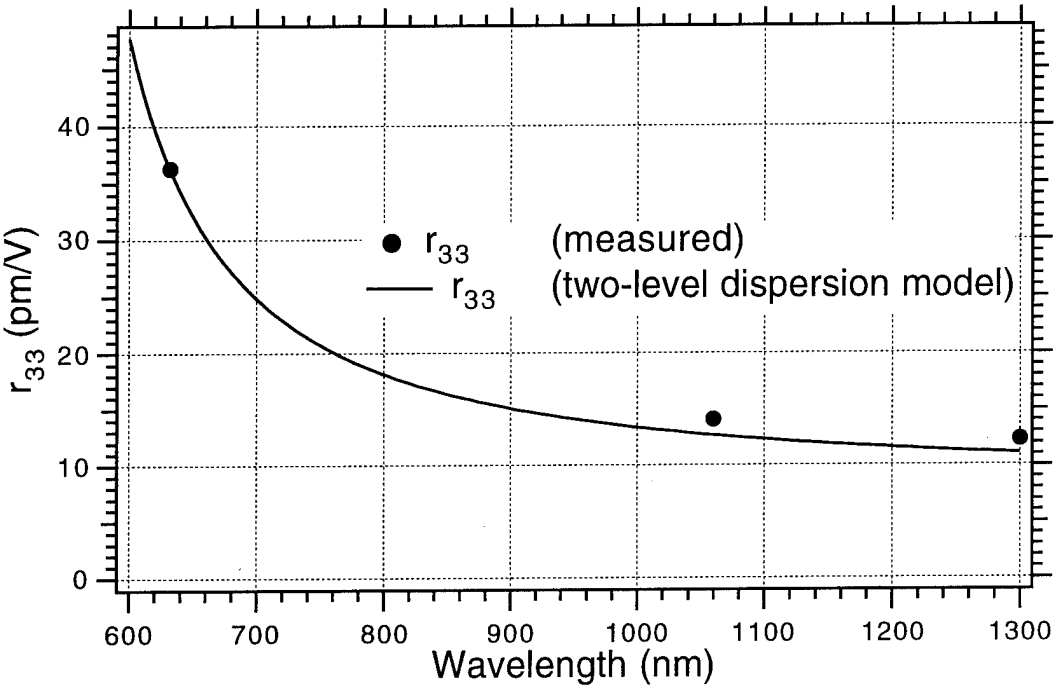

Figure 3: Dispersion of the r coefficient

Poling fields as high as 178V/μm were applied across each slit. The measured r_{33} at 1.3 μm for this poling field was 12.5 pm/V. This value agrees quite closely with our previous measurements of the best corona poled samples using other techniques such as external Mach-Zenhder measurements and extrapolation of second harmonic generation results.[4] The relationship between the poling field and the measured r_{33} coefficient is shown in figure 4. The relationship is linear as expected. Since we do not yet see a saturation of the r coefficient with this method of poling, perhaps larger nonlinearites are possible with higher poling fields.

In summary, there are several advantages to this poling and measurement technique. The real and imaginary parts of r_{33} and r_{13} coefficients can be independently measured by choosing an input polarization either perpendicular or parallel to the slits. In situ poling measurements can be easily made by applying a small AC field along with the DC poling field. Moreover, push-pull poling and modulation schemes that effectively double the modultion efficiency can be easily implemented.

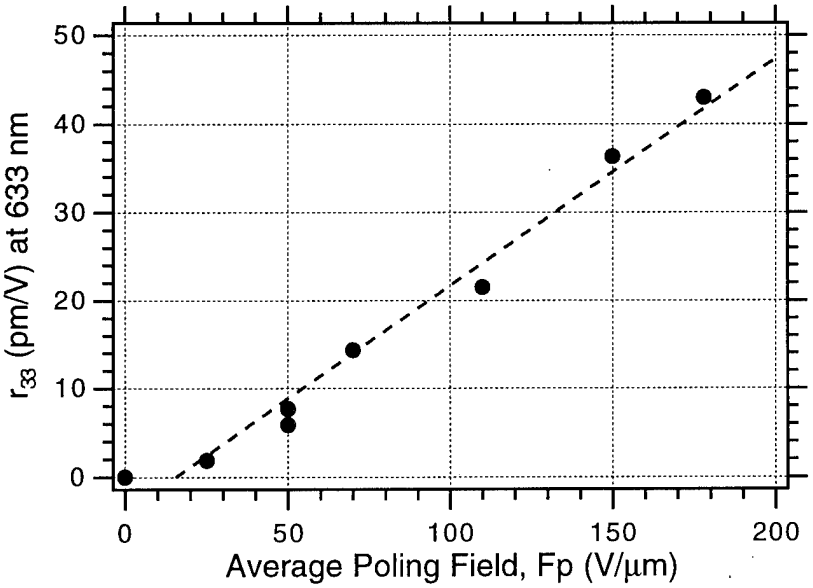

Figure 4: r vs. strength of poling ield

This method can also be used to monitor the nonlinearity at various stages in the device fabrication process by probing a "testing" window on a small area of the substrate. Measurement results that illustrate some of these advantages and other details like the choice of buffer layer, etc. will be discussed.

References:

[1]. V. Dentan, Y. Lévy, M. Dumont, P. Robin and E. Chastaing, "Electrooptic properties of a ferroelectric polymer studied by attenuated total reflection," *Optics Communications* **69,** 379-383 (1989).

[2]. C. C. Teng and H. T. Man, "Simple reflection technique for measuring the electro-optic coefficient of poled polymers," *Appl. Phys. Lett.* **56,** 1734-1736 (1990).

[3]. Y. Lévy, M. Dumont, E. Chastaing, P. Robin, P. A. Chollet, G. Gadret and F. Kajzar, "Reflection method for electro-optical coefficient determination in stratified thin film structures," *Mol. Cryst. Liq. Cryst. Sci. Technol. B (Nonlinear Optics)* **4,** 1-19 (1993).

[4]. Y. Shi, W. H. Steier, M. Chen, L. P. Yu and L. R. Dalton, "Thermosetting nonlinear optical polymer: polyurethane with disperse red 19 side groups," *Appl. Phys. Lett.* **60,** 2577-2579 (1992).

Optical Response of a Chiral Molecule and Circular Dichroism in Second-Harmonic Generation

Jeffery J. Maki, Martti Kauranen, Thierry Verbiest, and André Persoons
Laboratory of Chemical and Biological Dynamics and
Center for Research on Molecular Electronics and Photonics
University of Leuven
Celestijnenlaan 200 D
B-3001 Heverlee, Belgium
32-16-32.71.71
32-16-32.79.82 FAX

Surface second-harmonic generation has been found experimentally and theoretically to be capable of detecting chirality of a surface and of discriminating between the two enantiomers of a chiral molecule.[1,2] We calculate the second-order nonlinear optical response of a chiral molecule using a simple classical model and calculate the circular dichroism in second-harmonic generation from a thin film of chiral molecules.

I. Classical Model of the Optical Response of a Helical Molecule

Inspired by previous classical models of the linear-optical response of chiral molecules,[3-5] we model the optical response of a chiral molecule by taking the molecule to be a helix. The

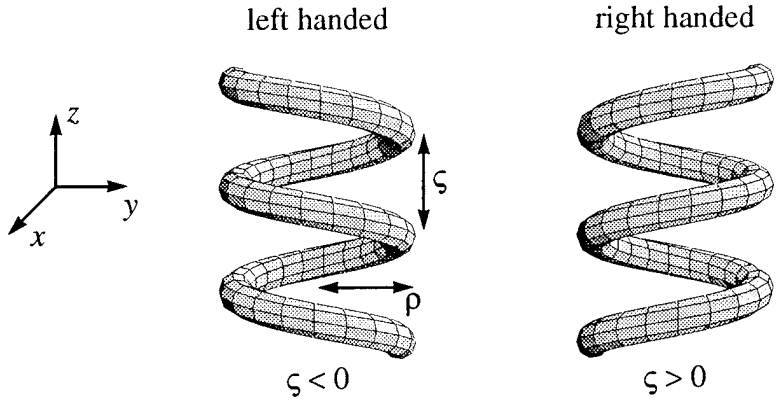

Fig. 1. Left- and right-handed helixes of radius ρ and pitch ς.

position of an electron bound to a helical path orientated along the z-axis (as shown in Fig. 1) is

$$\mathbf{r} = \hat{\mathbf{x}}\rho\cos\varphi + \hat{\mathbf{y}}\rho\sin\varphi + \hat{\mathbf{z}}\frac{\varsigma}{2\pi}\varphi \tag{1}$$

and the motion of the electron is always in the +/– tangential direction

$$\hat{\mathbf{t}} = (-\hat{\mathbf{x}}\rho\sin\varphi + \hat{\mathbf{y}}\rho\cos\varphi + \hat{\mathbf{z}}\frac{\varsigma}{2\pi})/L\,, \tag{2}$$

where $L = [\rho^2 + \varsigma^2/4\pi^2]^{1/2}$. The motion of the electron gives rise to both an electric-dipole moment and, in particular, a magnetic-dipole moment, because of the windings of the helical path. We calculate the second-order nonlinear optical response owing to both the electric- and magnetic-dipole moments using an extension of the classical model of Lorentz for an atom.[6] The restoring force is taken to be $\mathbf{F}_{\text{restoring}} = -m\omega_o^2\mathbf{r} - am(\mathbf{r}\cdot\hat{\mathbf{t}})\mathbf{r}$, where a is the anharmonicity parameter that changes sign between the two enantiomers. The driving force on the electron is taken to be both that due to the electric field and that due to the magnetic-induction field as given by Faraday's law for a current carrying loop. The resulting differential equation for φ is

$$\ddot{\varphi} + 2\gamma\dot{\varphi} + \omega_o'^2\varphi + b\varphi^2 = \frac{e}{mL^2}(E_x\rho\sin\varphi - E_y\rho\cos\varphi - E_z\frac{\varsigma}{2\pi}) + \frac{e\rho}{2mcL^2}(\dot{B}_x\frac{\varsigma}{2\pi}\sin\varphi - \dot{B}_y\frac{\varsigma}{2\pi}\cos\varphi + \dot{B}_z\rho)\,, \tag{3}$$

where $\omega_o'^2 = \omega_o^2\varsigma^2/4\pi^2L^2$ and $b = a\varsigma^4/16\pi^4L^3$.

We solve Eq. (3) using perturbation theory, where the electromagnetic field is assumed to be a plane wave oscillating at an angular frequency ω. The second-order nonlinear optical response is found by taking the portion of the electric-dipole moment $\mathbf{p} = -e\mathbf{r}$ and magnetic-dipole moment $\mathbf{m} = -\frac{e}{2mc}(\mathbf{r}\times m\dot{\mathbf{r}})$ that oscillates at 2ω. The result can be expressed up to first-order in the magnetic interaction by

$$p_i = \beta_{ijk}^{eee}E_jE_k + \beta_{ijk}^{eem}E_jB_k \text{ and } m_i = \beta_{ijk}^{mee}E_jE_k\,. \tag{4}$$

Many elements of β_{ijk}^{eee}, β_{ijk}^{eem}, and β_{ijk}^{mee} are nonvanishing and many originate from the magnetic interaction. For brevity of the remaining discussion, however, we shall only consider the elements of electric origin. Two important and illustrative elements allowed by the chirality of the molecule, which change sign between the two enantiomers, are

$$\beta_{xyz}^{eee} = \frac{e^3\rho^2\varsigma}{4\pi m^2L^4D^2(\omega)} \quad \text{and} \quad \beta_{yzx}^{eee} = \frac{e^3\rho^2\varsigma}{4\pi m^2L^4D(\omega)D(2\omega)}\,, \tag{5}$$

where $D(\omega) = \omega_o'^2 - \omega^2 - i2\omega\gamma$. We can thus see the dependance upon the pitch ς and radius ρ of the helical molecule. Another important element, which is not chiral and does not change sign between the two enantiomers, is

$$\beta_{yyz}^{eeee} = \frac{be^3\rho^2\varsigma}{2\pi m^2 L^4 D^2(\omega) D(2\omega)} . \tag{6}$$

For an isotropic distribution of these helixes standing on a surface, two of the many resulting components of the second-order surface susceptibility tensor are

$$\chi_{xyz}^{eeee} = \frac{N}{2}(\beta_{xyz}^{eeee} - \beta_{yzx}^{eeee}) \quad \text{and} \quad \chi_{xxz}^{eeee} = \frac{N}{2}\beta_{yyz}^{eeee} , \tag{7}$$

where N is the number density (cm^{-2}) of helixes on the surface.

II. Surface Second-Harmonic Generation from Chiral Materials

In a completely general manner, the generated second-harmonic electric field from a surface can always be expanded in terms of the three possible bilinear combinations of the *s* and *p* components of the fundamental electric field. The specific form of the expression derived by Maki *et al.* [7] (presented here ignoring Fresnel reflections at the interfaces) is

$$E_j(2\omega) = \frac{i4\pi\omega}{c\cos\theta}[f_j E_p(\omega) E_p(\omega) + g_j E_s(\omega) E_s(\omega) + h_j E_s(\omega) E_p(\omega)] , \tag{8}$$

where j is *s* or *p* and θ is the angle of incidence of the fundamental light. For circularly polarized fundamental light, the ratio $E_p(\omega)/E_s(\omega)$ is $\pm i$, where right-handed light is $+i$ and left-handed light is $-i$. The intensity of the *s* or *p* component of the second-harmonic light for circularly polarized fundamental light is

$$I_j(2\omega) = \frac{32\pi^3\omega^2}{c^3\cos^2\theta}|-f_j + g_j \pm ih_j|^2 I^2(\omega) . \tag{9}$$

The functional dependence of the coefficients f_j, g_j, and h_j upon the susceptibilities χ^{eee}, χ^{eem}, and χ^{mee} is a primary result of Ref. 7. In the limit of only electric-dipole response and again ignoring Fresnel reflections at the interfaces,

$$f_s = 2\chi_{xyz}^{eeee}\sin\theta\cos\theta , \quad g_s = 0 , \quad \text{and} \quad h_s = 2\chi_{xxz}^{eeee}\sin\theta . \tag{10}$$

The measured second-harmonic-generation circular dichroism in the s-component of the second-harmonic light is predicted to be

$$\Delta I_s^{\text{SHG-CD}} = I_s^{\text{left}} - I_s^{\text{right}} = -a \frac{\rho^4 \varsigma^6}{L^{11}} \frac{2N^2 e^6}{\pi^3 c^3 m^4} \frac{\gamma \omega^3}{|D(\omega)|^4 |D(2\omega)|^2} \frac{\sin^2\theta}{\cos\theta} I^2(\omega) \qquad (11)$$

assuming the functional forms of the susceptibilities for a thin film of chiral molecules are those given by Eqs. (7). The frequency dependence of this electric-dipole circular-difference effect is illustrated in Fig. 2.

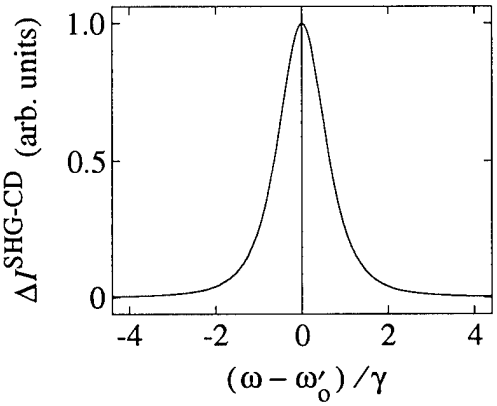

Fig. 2. Variation with angular frequency ω of the electric-dipole contribution to the circular dichroism of the *s*-polarized component of second-harmonic generation from a chiral surface.

III. Conclusions

We have calculated the second-order optical response for a chiral molecule using a simple classical model. The macroscopic response is related to the possible structural properties of the chiral molecular building blocks of an actual thin film. This might be important in interpreting the chirality observed in biological membranes and macromolecules (e.g., proteins and DNA). We have also used the calculated susceptibility tensors to make an explicit prediction of the frequency dependence of circular dichroism in second-harmonic generation from a chiral surface.

References

[1] T. Petralli-Mallow, T. M. Wong, J. D. Byers, H. I. Yee, and J. M. Hicks, J. Phys. Chem. **97**, 1383 (1993).
[2] M. Kauranen, T. Verbiest, J. J. Maki, and A. Persoons, J. Chem. Phys. **101**, 8193 (1994).
[3] P. Drude and M. Boll, *Précis D'Optique* (Gauthier-Villars, Paris, 1912), Vol. 2, Ch. 8.
[4] W. Kuhn, Zeits. f. Physik. Chemie **B20**, 325 (1933).
[5] D. L. Jaggard, A. R. Mickelson, and C. H. Papas, Appl. Phys. **18**, 211 (1979).
[6] H. A. Lorentz, *The Theory of Electrons* (Dover, New York, 1952).
[7] J. J. Maki, M. Kauranen, and A. Persoons, Phys. Rev. B **51**, 1425 (1995).

Linearly and Circularly Polarized Probes of Second-Order Optical Activity of Chiral Surfaces

Thierry Verbiest[1], Martti Kauranen[1], Jeffery J. Maki[1], M.N. Teerenstra[2], A.J. Schouten,[2] R.J.M. Nolte[3], and André Persoons[1]
[1]University of Leuven
Laboratory of Chemical and Biological Dynamics
Celestijnenlaan 200 D, B-3001 Heverlee,Belgium
Tel : +32-16-32.71.71
Fax : +32-16-32.79.82
[2]Laboratory of Polymer Science, University of Groningen
9747 AG Groningen, The Netherlands
[3]Department of Organic Chemistry, University of Nijmegen,
6525 ED Nijmegen, The Netherlands

It was recently observed experimentally that second-harmonic generation (SHG) from chiral surfaces is sensitive to the handedness of the incoming fundamental light. This phenomena is called nonlinear optical activity[1,2]. We have subsequently developed a theory of SHG from chiral surfaces that includes contributions of electric- and magnetic-dipole transitions to the surface nonlinearity. The theory can be used to explain the experimental results very well[3-5].

The intensity of the SH light generated by a surface can always be expressed in the general form :

$$I(2\omega) = \left| fE_p^2(\omega) + gE_s^2(\omega) + hE_p(\omega)E_s(\omega) \right|^2 \qquad [1]$$

where $E_p(\omega)$ and $E_s(\omega)$ refer to the p- and s-polarized components of the fundamental field. For circularly-polarized excitation ($E_s = \pm iE_p$), the second-harmonic intensity is then of the form :

$$I(2\omega) = |f + g \pm ih|^2 I^2(\omega) \qquad [2]$$

were the upper (lower) sign corresponds to right-handed (left-handed) circularly-polarized excitation. The coefficients f,g and h are combinations of the different susceptibility (electric-dipole and magnetic-dipole) components and are different for the reflected and transmitted s- and p-polarized components of the SH field. From these equations it is clear that circular-difference effects (i.e different SH response to left-handed and right-handed circularly-polarized fundamental light) can only occur when a phase-difference exists between the coefficient h and the two other coefficients (f and g). Furthermore, depending on the SH signal measured, (f + g) and h are nonvanishing only for chiral surfaces and hence a circular-difference effect can occur only for chiral surfaces.

Eq. 1 also implies that for the case of ±45° linearly polarized incident light ($E_s = \pm E_p$), the intensity of the SH field is :

$$I(2\omega) = |f + g \pm h|^2 I^2(\omega) \qquad [3]$$

In contrast to the previous case (circularly-polarized excitation), difference effects for ±45° linear excitation (linear-difference effects) will occur even if there is no phase-difference between h and the other coefficients. Hence, the circular- and linear-difference effects are complementary in studying chiral effects. The difference effects observed with circularly-polarized incident light are due to the imaginary (real) part of h combined with the real (imaginary) part of (f + g), while difference-effects observed with linearly-polarized excitation arise from the real (imaginary) part of h combined with the real (imaginary) part of (f + g).

Both circular- and linear-difference effects were studied experimentally in Langmuir-Blodgett films of a chiral polymer (a poly(isocyanide) functionalized with a nonlinear optical chromophore). These polymers form rigid-rod helices on a water surface and can be easily transferred to a solid substrate by means of the Langmuir-Blodgett method. The sample used consisted of 18 layers of z-type deposited chiral poly(isocyanide). Infrared light from a Q-switched and injection-seeded Nd:YAG laser (1064 nm, 10 ns pulses, 50 Hz) was used as the fundamental beam and was incident at the sample at an angle of 45°. The polarization of the fundamental beam was continuously varied by a rotating a half-wave or a quarter-wave plate and the intensity of the second harmonic (p- or s-polarized) was recorded in reflection and transmission. Sufficient polarization purity of the experiment was verified by making sure that no difference effects (circular or linear) were observed in the second-harmonic intensity generated from achiral samples.

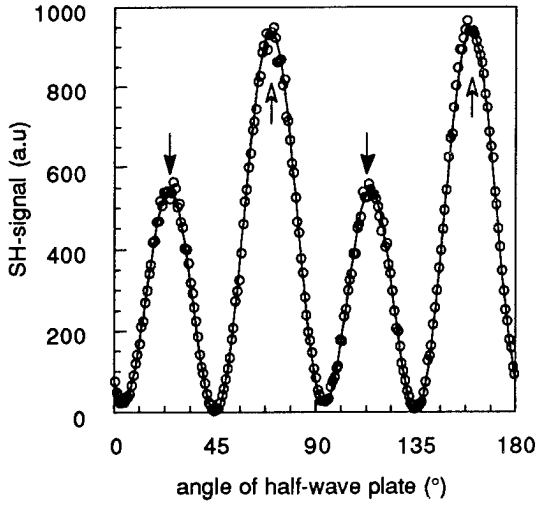

Fig. 1a : transmitted SH-signal (s-polarized) vs. the rotation angle of the half-wave plate. Black (white) arrows indicate +45° linear (-45° linear) polarization. Open circles represent the experimental data, solid line is the theoretical fit.

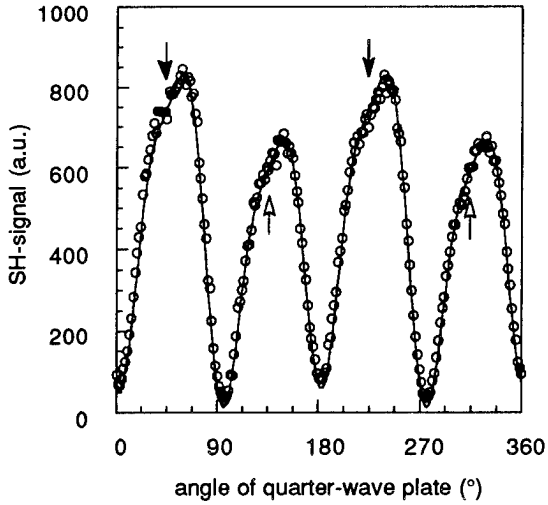

Fig. 1b : transmitted SH-signal (s-polarized) vs. the rotation angle of the quarter-wave plate. Black (white) arrows indicate right-handed (left-handed) circular polarization. Open circles represent the experimental data, solid line is the theoretical fit.

For the case of the chiral poly(isocyanide) sample, both circular- and linear-difference effects were observed in the SHG generated by the sample. The results for circular and linear excitation and s-polarized transmitted signal are shown in Fig. 1a and Fig. 1b, respectively. A preliminary fit between the results of Fig. 1a (b) and Eq. 2 (Eq. 3) was obtained in the limit in which the coefficient g was assumed to vanish. The fits are also shown in Fig. 1a and b and have been determined using the following relative values of the coefficients f and h : h = 1.0, f = -0.137 - i0.0887 (h = 1.0, f = -0.155 - i0.0576), for linearly (circularly) polarized excitation. It is evident from Fig. 1a and b that the experimental results can be explained very well using our theoretical model. We expect that the remaining small discrepancy between the f coefficients for the two cases can be accounted for by including the coefficient g that can only be nonvanishing in the presence of significant magnetic contributions to the surface nonlinearity.

We believe that these results are very interesting because i) they indicate that one does not necesarily need circulary-polarized excitation to study chiral effects in thin films by SHG and ii) the complementarity of both techniques opens up new ways of studying the chirality of biological membranes and surfaces.

References

1. T. Verbiest, M. Kauranen, A. Persoons, M. Ikonen, J. Kurkela, and H. Lemmetyinen, *J. Am. Chem Soc.* **116**, p. 9230, 1994

2. T. Petralli-Mallow, T.M. Wong, J.D. Byers, H.I. Yee, and J.M. Hicks, *J. Chem. Phys.* **97**. p. 1383, 1993

3. M. Kauranen, T. Verbiest, J. J. Maki, and A. Persoons, *J. Chem. Phys.* **101**(9), p. 8193, 1994

4. J. J. Maki, M. Kauranen, and A. Persoons, *Phys. Rev. B* **51**, p. 1425, 1995

5. M. Kauranen, T. Verbiest, E.W. Meijer, E.E. Havinga, M.N. Teerenstra, A.J. Schouten, R.J.M. Nolte, and A. Persoons, *accepted for publication in Advanced Materials*

Thursday, September 14, 1995

SHG Devices

ThB 10:30 am-12:15 pm
Holladay Room

Gerd Marowsky, *Presider*
Laser-Laboratorium Göttingen, Germany

The Effect of Poling Induced Polymer Film Deformation on Second-Harmonic Generation in Periodically Poled Polymer Channel Waveguides

M. Jäger, G.I. Stegeman
CREOL, University of Central Florida
12424 Research Parkway, Orlando, FL 32826
Tel. (407) 658-3927
Fax (407) 658-3955

W. Brinker, S. Yilmaz, S. Bauer
Heinrich-Hertz-Institut für Nachrichtentechnik Berlin
Einsteinufer 37, D-10587 Berlin, Germany
Tel. +30-31002-356
Fax +30-31002-213

W.H.G. Horsthuis, G.R. Möhlmann
Akzo Nobel Electronic Products
Arnhem, The Netherlands

Second-harmonic generation (SHG) in waveguides has been important for years as a method of obtaining a compact, coherent blue light source. Recently, this field has received new attention due to the possibility of using cascaded $\chi^{(2)}$-effects for all-optical switching, spatial solitons etc. Because some polymers have exhibited large second order non-linearities after poling, there has been a growing interest in using these materials for waveguide SHG. Besides high d-coefficients, polymers offer easy processing and are a cheap alternative to inorganic crystals. In this paper we report the fabrication of periodically poled polymer channel waveguides, the deformation of the waveguide under the electrode fingers during poling, and the demonstration of SHG by quasi-phase-matching in a channel waveguide made of 4-dimethylamino-4'-nitrostilbene (DANS) side-chain polymer.

Quasi-phase-matching (QPM), in which the d-coefficient is periodically modulated[1], e.g. by periodical poling[2,3], bleaching[3,4] or laser ablation[5] appears to be ideal for polymeric waveguides. Even though the effective non-linearity is reduced and depends on the modulation depth of the d-coefficient, an important advantage of QPM is that phase-matching can always be achieved between the fundamental modes of the two wavelengths by choosing the appropriate periodicity.

Different electrode geometries were investigated in a series of experiments. Initial attempts at SHG failed due to severe waveguide losses caused by the deformation of the polymer under the finger electrodes during poling. That is, the polymer under the electrodes was squeezed when a strong field was applied, leading to a periodic

perturbation which scattered the light out of the waveguide. The surface profile of the polymer waveguide was measured after poling using a phase shift interferometer (PSI) set-up, as already reported in detail elsewhere[6]. Fig. 1 shows a gray scale coded two-dimensional map of the thickness variations. The white regions show the imbedded areas corresponding to the digital electrode grating, while the line scan below shows the deformation amplitude of 300 nm in the poled waveguide device.

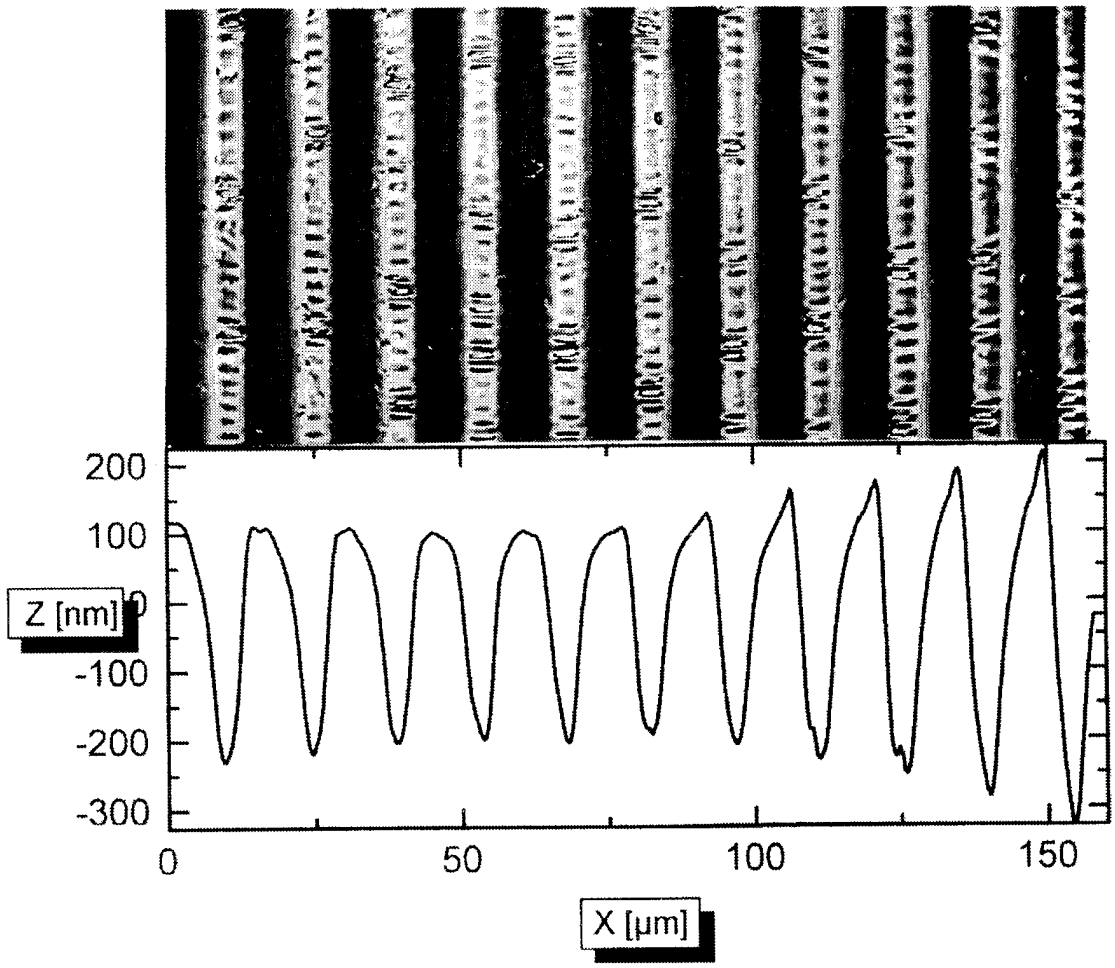

Fig. 1 Gray scale coded two-dimensional map of the polymer surface. The white regions show the depressed areas corresponding to the digital electrode pattern, as also illustrated in the line scan below.

Systematic investigations with different grating periods exhibited a strong increase in the deformation amplitude for finer electrode gratings. For large periods almost no deformation is observed except at the edges of the electrodes. These results can be explained by the electrostatic forces during the poling and the resulting viscous flow of the polymer in the rubbery state. For large grating periods, a similar flow of the polymer is, as observed, only possible near the edges of the electrodes. Thus, the preparation of the digital electrode on the substrate should minimize the deformation of the polymer waveguide.

In the next iteration, new samples were prepared on a fused silica substrate, choosing the lower electrode as the digital electrode (Fig. 2). After depositing and photolithographic patterning of the lower aluminum electrode with a period of 14 μm, a stack of three polymer layers was spin coated. Subsequently, a plain aluminum electrode was deposited on top. The samples were poled by applying an electric field of 100V/μm between the two electrodes. The maximum d-coefficient for this poling field has been measured previously[3] to be d_{33}=25pm/V at 1.55μm. After removal of the upper electrode, channel waveguides were created by photobleaching through a mask. Finally, the samples were diced into pieces of different lengths for endfire coupling.

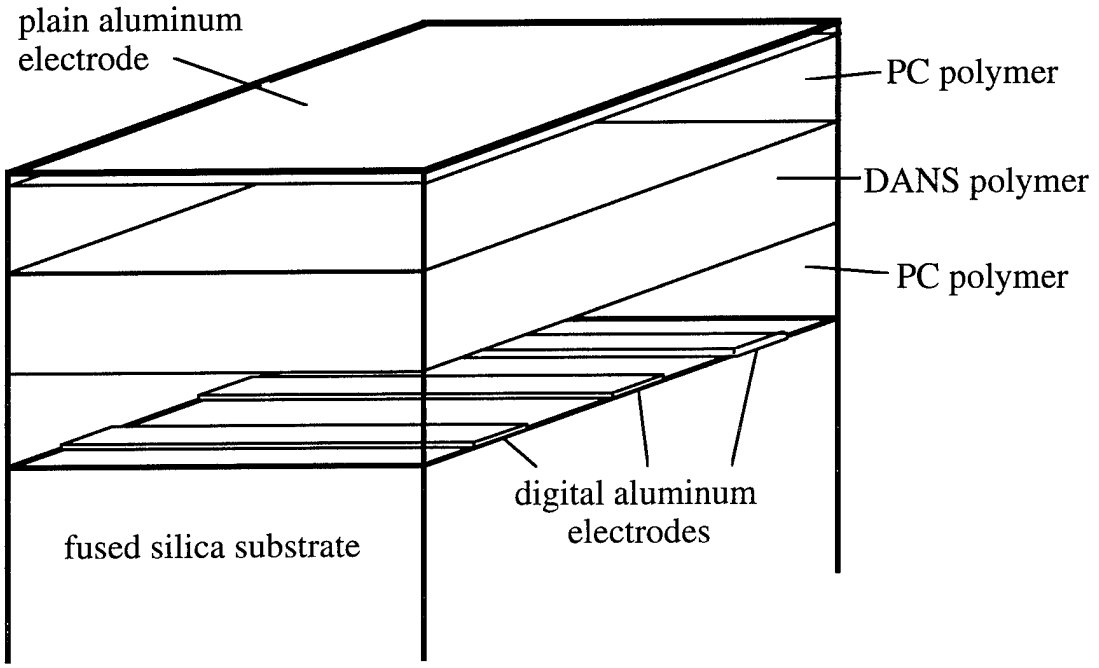

Fig. 2 Sample construction (electrode grating period 14 μm)

A surface scan with a profilometer indicated only a slight periodic deformation of about ±0.02 μm. The waveguide losses were therefore greatly reduced (<5 dB/cm) with respect to the earlier experiments[3], and a 15% throughput could be achieved in a 0.8 cm long monomode channel waveguide.

The second harmonic generation (SHG) experiments were performed with a tuneable NaCl:OH^- color center laser, pumped by a mode-locked Nd:YAG laser. The system produces 6..9 ps-pulses in the wavelength range of 1.5...1.7 μm. The phase-matching curve (Fig. 3) shows a classical $\mathrm{sinc}^2(\Delta\beta L)$ response with detuning $\Delta\beta L$. Based on the width of the peak, the phase matching length was determined l_{PM}=0.2 cm, which is very close to the sample length of L=0.25 cm.

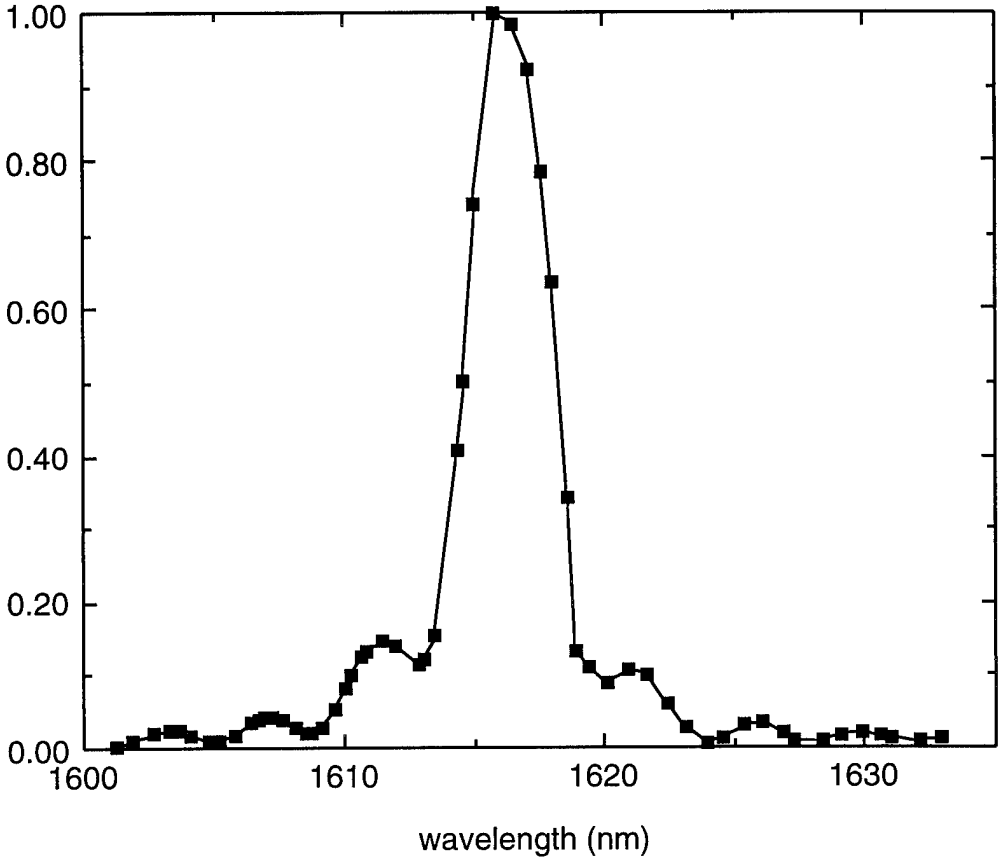

Fig. 3 Normalized phase-matching tuning curve

The figure of merit, however, is still rather small $\eta=P_{2\omega}/P_{\omega}^2L^2$ = 0.05%/W/cm^2. This low conversion efficiency is most likely due to the poor modulation depth of the non-linear coefficient. The polymer stack has a total thickness of 6.3 μm, whereas the distance between two fingers of the digital electrode is 7 μm. This allows a large leakage of the poling field into the regions that should remain unpoled for maximum conversion.

In summary, quasi-phase-matching has been demonstrated in a low loss polymeric channel waveguide. Phase-matching was maintained over 0.2cm, but this length can be increased by opimizing the waveguide design. The conversion efficiency is still low, and it is essential to increase the modulation depth of the d-coefficient in order to make use of the large non-linearity of the material.

References:

1. J.A. Armstrong, N. Bloembergen, et al., Phys. Rev., vol. 127, pp.1918-1939, 1962
2. G. Khanarian, R.A. Norwood, et al., Appl. Phys. Lett. **57** (1990) 977
3. M. Jäger, G.J.M. Krijnen, et al., CLEO 1995
4. G.L.J.A. Rikken, C.J.E. Seppen, S. Nijhuis, E. Meijer, Appl. Phys. Lett.**58** (1991) 435
5. G. Marowsky, F. Sieverdes, Proc. SPIE, **1775** (1992) 178
6. W. Brinker, S. Yilmaz, S. Bauer, et al., Optics Letters, Vol. 20, No. 8 (1995) 816

Enhanced Cerenkov-Radiative SHG with UV Induced Nonlinear Optical Susceptibility-Corrugation

Heihachi Sato, Hiroaki Matsuno and Iwao Seo*

Department of Electrical Engineering, National Defense Academy, Yokosuka 239, Japan.
[Phone (0468)41-3810, FAX (0468)44-5903]
*Tsukuba Research Center, Mitsubishi Chemistry Co. Ltd., Inashiki, Ibaraki 300-03, Japan.
[Phone (0298)87-1022, FAX (0298)87-7228]

It has been well recognized that introducing corrugative configuration into nonlinear optical (NLO) susceptibility $\chi^{(2)}$ results in an extreme enhancement of SHG power with quasi-phase-matching (QPM) scheme. The authors et al have also demonstrated significant SHG enhancement with the NLO corrugation even in the Cerenkov-radiative schemes[1-3]. In these recent works the NLO corrugations have been electrically introduced with either contact-electrode or corona discharges. However, organic polymers have, in general, tendency to change their optical properties, i.e. refractive index and NLO susceptibility, with ultra-violet (UV) sbsorption. Fortunately, it has been found from spectroscopy that vinylidene cyanide/vinyl acetate (VDCN/VAc) copolymer has a strong absorption band around 200 nm wavelength. In addition, it has also been preliminarily expected that the UV irradiation tends to reduce or dissipate its NLO susceptibility and the refractive index due to dissociation of the side chain in VDCN/VAc copolymer. In the present paper we shall thus attempt to enhance the Cerenkovian SHG power with a periodic or chirped NLO $\chi^{(2)}$ corrugation by irradiating ArF 193 nm laser source, together with discussion of the optimum UV irradiation.

Since dependence of the index on the UV irradiation intensity should reflect back to that of NLO $\chi^{(2)}$ susceptibility, the refractive index was measured as a function of UV exposure time of ArF 193 nm laser (Lambda Phys.:EMG-202MSC) source as in Fig.1. About 10^{-3} of index de

crease can be obtained with the exposure time of ~5 minutes, whereas the NLO film was damaged with the exposure time longer than 5 minutes. This index reduction was also confirmed by looking at the beam confinement within the channel guide made of the UV irradiation. Thus, the condition of the UV irradiation above was used for making the NLO $\chi^{(2)}$ corrugation. Before inducing the NLO $\chi^{(2)}$ corrugation into VDCN/VAc film by UV irradiation, the film has been preliminarily poled uniformly with applying the electric field (~1MV/cm) for 15 minutes at 182℃ as in our previous work [2]. The experimental setup is shown in Fig.2:(a) processing of UV irradiation with chirped periodic mask and (b) schematic diagram for the Cerenkov-radiative SHG scheme, just the same as used in ref.2 except for the UV induced NLO corrugation. A pulsed Nd:YAG 1.06 μm laser (NEC:SL-129) was used as the fundamental wave source. After passing through IR filter F_1, the beam was coupled into the NLO film (VDCN/VAc) with a ZnSe prism. The Cerenkovian SHG power filtered out by an interference filter (0.53 μm) F_2 was detected by a photomultiplier, and its waveform was observed at CRT, together with the fundamental waveform bypassed by a beam splitter BS. For satisfying the Cerenkov-radiative scheme the NLO film on the substrate (BK-7) with Au film was sandwiched by a fused silica plate. For comparison both uniformly periodic NLO $\chi^{(2)}$ structure with 20 μm period, and chirped periodic NLO $\chi^{(2)}$ structure with the average period 20 μm and chirping period 200 μm were prepared with the UV irradiation.

Typical SHG waveforms observed with various NLO $\chi^{(2)}$ schemes are depicted in Fig.3, showing that the UV induced NLO $\chi^{(2)}$ corrugations effectively enhance its SHG power comparable to or greater than with the electrically poled films. The relationships between the SHG power $P_{2\omega}$ and the square of fundamental power P_{ω}^2 are illustrated in Fig.4 for various NLO $\chi^{(2)}$ configurations. From this it is well found that the enhancement factor of 7.3 was obtained to that of uniformly poled scheme, while about six times of SHG enhancement was recognized with the same NLO $\chi^{(2)}$ corrugation induced with the contact-electrode discharge. Depending on the UV irradiation time the film tends to be opaque, so that the over-exposed region in the film may comes up to be lossy to origin of SHG power dissipation. More about this point and physical mechanism of NLO $\chi^{(2)}$ disappearance will also be described with IR spectroscopy.

References

1. Y. Azumai and H. Sato, Jpn. J. Appl. Phys. **32**, 800(1993).

2. H. Sato, Y. Azumai and H. Nozawa, Opt. Lett. **19**, 93(1994).

3. H. Sato and Y. Azumai, Proc. SPIE(Nonlinear Optical Properties of Organic Materials Ⅶ) **2285**, 272(1994).

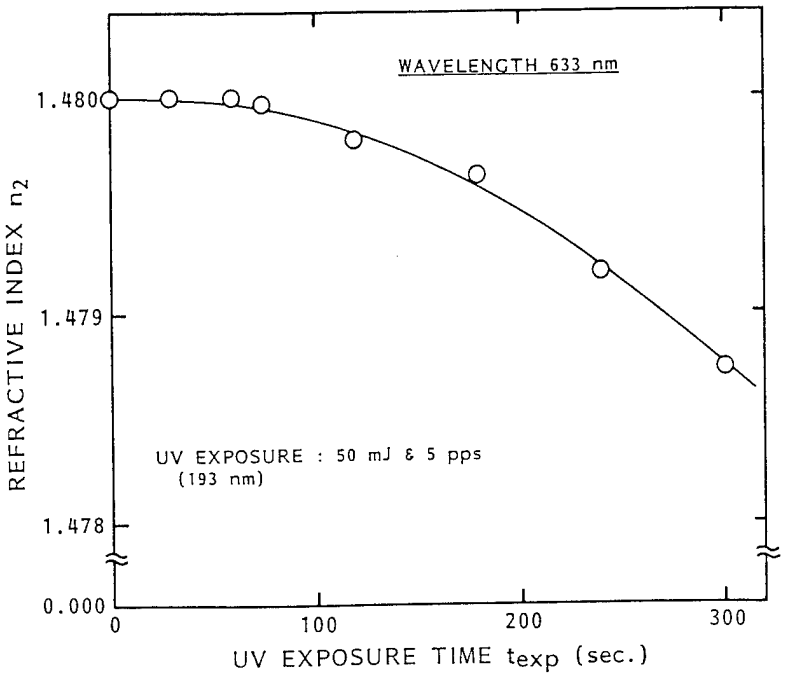

Fig.1 Dependence of refractive index on UV exposure time t_{exp}.

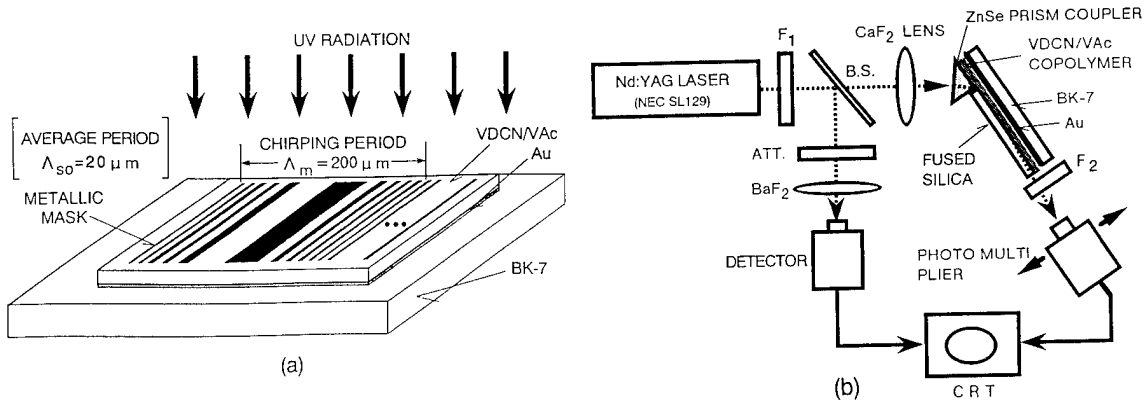

Fig.2 Experimental setup : (a) processing of UV induced NLO $\chi^{(2)}$ (chirped periodic) corrugation and (b) schematic diagram for the Cerenkov-radiative SHG scheme.

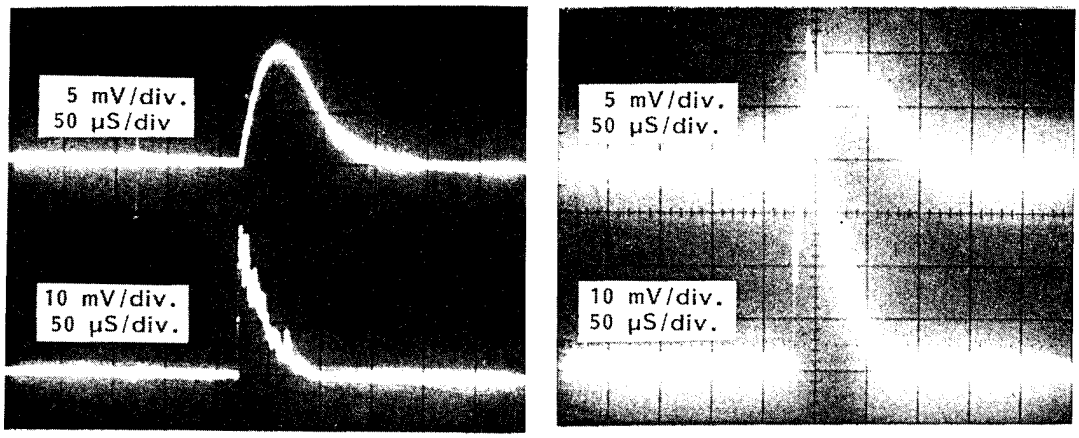

(a) Uniform NLO $\chi^{(2)}$ (b) Periodic NLO $\chi^{(2)}$

Fig.3 Observed SHG and fundamental waveforms (upper : fundamental , lower : SHG) for various NLO $\chi^{(2)}$ schemes .

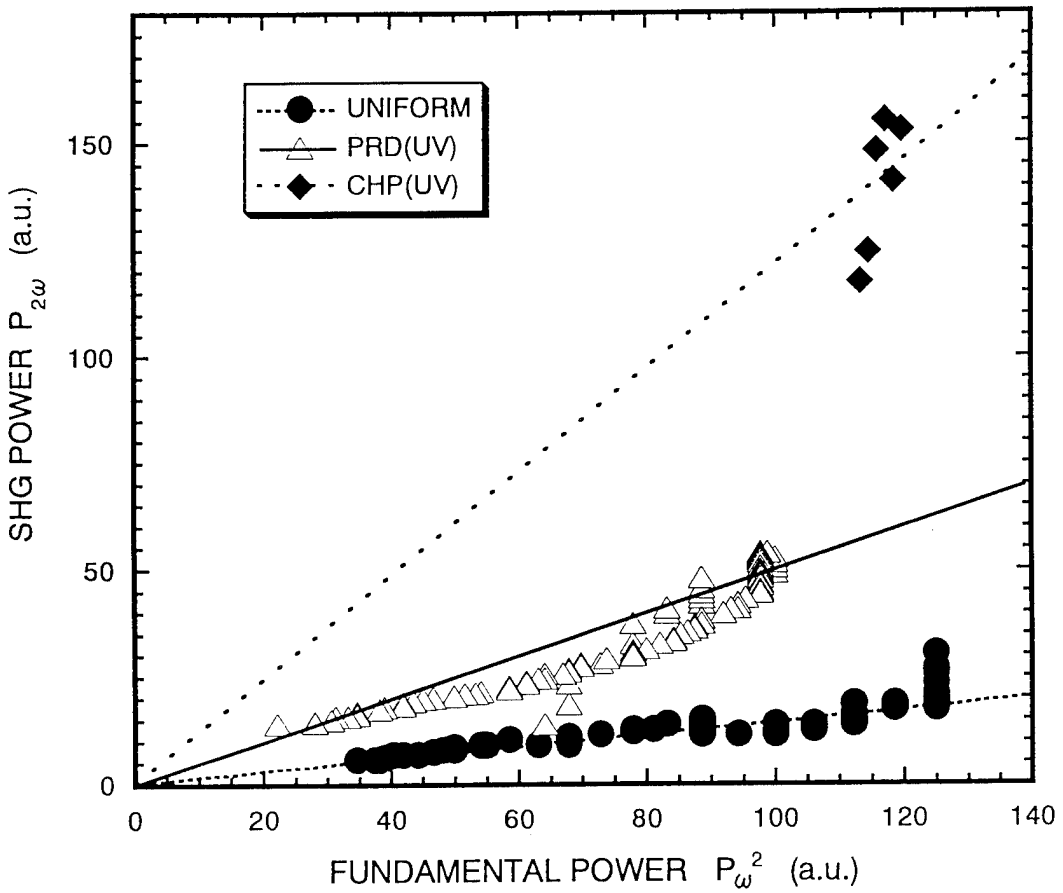

Fig.4 Relationships between SHG power $P_{2\omega}$ and square of fundamental power P_{ω}^{2} for various NLO $\chi^{(2)}$ schemes, where UNIFORM , PRD(UV) and CHP(UV) denote uniformly poled $\chi^{(2)}$, periodic NLO $\chi^{(2)}$ with 20 μm period and chirped NLO $\chi^{(2)}$ with chirping period 200 μm and average period 20 μm .

Frequency Doubling in a Poled Polymer Waveguide Using Anomalous Dispersion Phase-Matching

T.C. Kowalczyk, K.D. Singer
Case Western Reserve University
Cleveland, OH 44106
Phone: (216) 368-4023
FAX: (216) 368-4671

P.A. Cahill
Sandia National Laboratories
Division 1811
Albuquerque, NM 87185-1407
Phone: (505) 844-5754
FAX: (505) 844-9624

Many technological advances can be realized from the development of coherent short wavelength sources, particularly in the fields of information display and storage. One approach to producing short wavelengths is to frequency double (existing and inexpensive) near-IR semiconductor lasers using a nonlinear optical process, second harmonic generation (SHG). Large intensities are necessary to drive such nonlinear interactions and these intensities can be achieved even with continuous wave lasers by spatially confining light to a waveguide. Waveguide geometry can be compact and may allow diffraction free propagation. Poled polymers are interesting materials for second harmonic generation because they have large nonresonant nonlinearities, low losses, and are easily processed.

Large SHG conversion efficiencies require materials with large nonlinearities, transparency at the fundamental and harmonic wavelengths, spatial overlap of the fundamental and harmonic fields, and phase-matching over long interaction lengths. Of these requirements, phase-matching is probably the most important and challenging hurdle in obtaining efficient second harmonic generation. A variety of phase-matching schemes including modal dispersion phase-matching (MDPM), birefringent phase-matching (BFM), Cerenkov phase-matching (CFM), and quasi-phase-matching (QPM)

have been employed for frequency doubling.[1] In this paper we describe second harmonic generation in a poled polymer waveguide using anomalous dispersion phase-matching (ADPM). In anomalous dispersion phase-matching, a nonlinear chromophore with an absorption peak between the fundamental and harmonic wavelength is doped into a host material with normal dispersion. Fig. 1 shows the structure and absorption spectrum of the anomalous dispersion dye, a thiobarbituric acid (TBA) derivative along with the refractive index dispersion of the guest-host system, TBA doped polymethylmethacrylate (PMMA).. The synthesis and characterization of this chromophore have been reported previously.[2] At a precise concentration, the normal dispersion of the host material at the harmonic wavelength is canceled by the anomalous dispersion of the guest chromophore. ADPM requires chromophores to have a transparency window beyond the main electronic absorption maximum. This requirement places serious demands on dopant chromophores because the phase-matchable interaction length for lossy materials will be limited to the 1/e absorption length of the composite system. Nevertheless, ADPM offers many advantages over conventional phase matching techniques. First, the optical nonlinearity-transparency trade-off can be overcome by using chromophores that have strong absorption in the visible part of the spectrum and results in chromophores with exceptionally large molecular susceptibilities.[3] Second, ADPM allows phase-matching between lowest order fundamental and harmonic modes.

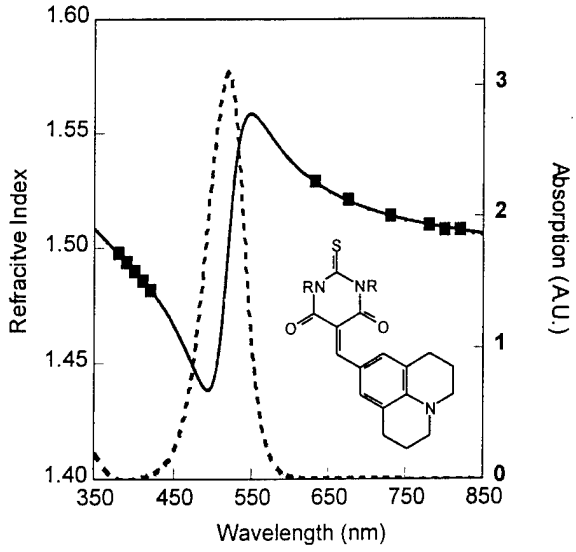

Figure 1. Absorption spectrum of 6% TBA-PMMA and resulting dispersion of the guest-host system. Data points represent refractive index measurements and the solid line a fit to a two term Sellmeir equation.

Refractive indices were measured with TM polarized light using the prism coupling technique. Refractive indices at the fundamental wavelength were observed to increase with concentratrion (normal dispersion) while those at the harmonic decrease with

increasing concentration (anomalous dispersion). Data for 6% TBA-PMMA is shown in Fig. 1. The samples were then poled and the refractive indices remeasured. Because of the quantized mode structure of a waveguide, fundamental and harmonic effective indices must be matched. Fig. 2 shows the TM effective index for 6% TBA-PMMA films calculated as a function of waveguide thickness from bulk refractive index measurements. The intersection point in Fig. 2 predicts phase-matching for a 2.0 μm thick film. Experimental adjustment of the phase-matching condition is achieved by changing the thickness of the waveguide, and hence the effective mode indices. Slab waveguides of various thickness were prepared by casting of thin films.

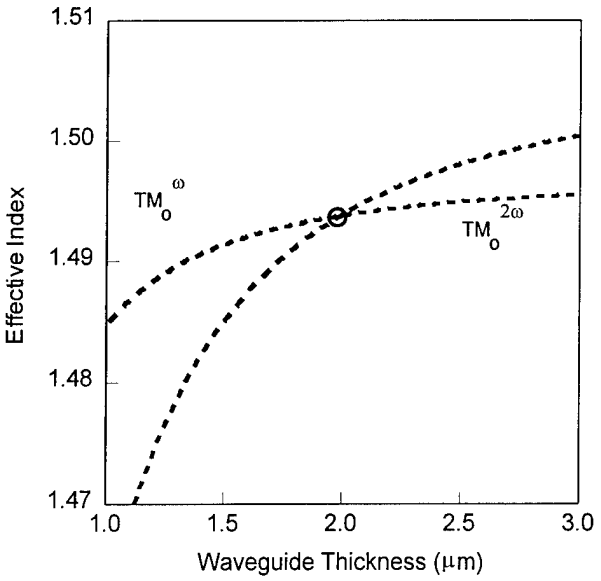

Figure 2. Effective indices plotted as a function of waveguide thickness for 6% TBA-PMMA. The phase-matching condition is satisfied at the intersection of the two curves.

Light from a frequency tripled Nd:YAG pumped optical parametric oscillator (815 nm) was in-coupled and out-coupled from the waveguide through a high index prism. Part of the fundamental beam was passed through a quartz wedge which served to eliminate shot-to-shot fluctuations. Harmonic light was collected using photo-multiplier tubes after appropriate filtering and attenuation. The measurement was repeated for samples of different thickness. Film thicknesses were measured independently using a profilometer. In Fig. 3, the relative amount of second harmonic power is plotted as a function of phase-mismatch using the effective index curves (Fig. 2). The peak in Fig. 3 corresponds to the film of thickness 2.0 μm, in excellent agreement with the calculated phase-matching thickness in Fig. 2. Overall, Fig. 3 shows a five-fold increase in second harmonic power at the calculated phase-matching thickness, and verifies phase-matching due to anomalous dispersion.

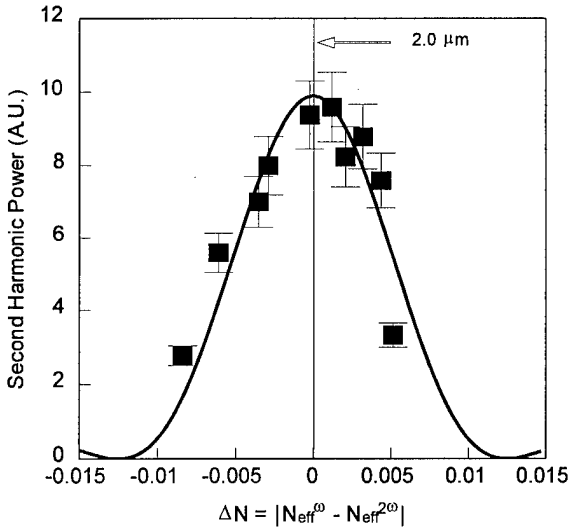

Figure 3. Second harmonic power measured as a function of waveguide thickness. Solid line is a fit to the $sinc^2(x)$ function using the amplitude and propagation length as adjustable parameters.

In summary we have demonstrated anomalous dispersion phase-matched second harmonic generation in a poled polymer waveguide at a fundamental wavelength of 815nm. The experimetally measured conversion efficiency was $7x10^{-4}$% for 200W of fundamental power and a very short, 35 μm, propagation length due to single prism coupling. Experiments are currently under way to increase the interaction length and nonlinearity.

This work was supported by the U.S. Department of Energy under contract DE-AC04-94AL85000, AFOSR under grant #49620-93-1-0202, and Amoco Chemical Company.

1. G.I. Stegeman and W. Torruellas, MRS Proc., A.F. Garito, A. Jen,C. Lee and L.R. Dalton, ed., Materials Research Society, Pittsburgh, **328**, 397 (1994).

2. P.A. Cahill, D.R. Tallant, T.C. Kowalczyk, and K.D. Singer, "Molecular to Material Design for Anomalous-Dispersion Phase-Matched Second Harmonic Generation", Proc. SPIE, Vol. 1560, pp. 130-138, 1991.

3. L.T. Cheng, W. Tam, and A. Feiring, "Quadratic Hyperpolarizabilities of Fluorinated Sulfonyl and Carbonyl Aromatics: Optimization of Nonlinearity and Transparency Trade-off", Proc. SPIE, Vol. 1337, pp. 203-214, 1990.

Quasi-phasematched sum frequency generation in active-passive hybrid waveguides

S. Lehmann, G. Marowsky

Laser-Laboratorium Göttingen e.V.

Hans-Adolf-Krebs-Weg 1,

D-37077 Göttingen, Germany

Tel.: + 49-551-50 35 30, Fax: + 49-551-50 35 99

Nonlinear optical interactions in waveguides have attracted considerable interest in the past few years. Various classes of materials have been investigated for this purpose. Of these, optically nonlinear polymers have been the focus of intensive research [1]. Their merits render them attractive for use in the development of optoelectronic devices. Quasi-phasematching is a versatile technique for second-order nonlinear processes. The phase-velocity mismatch between interacting waveguide modes at frequencies ω_i ($i = 1,2,3$) is compensated for by a spatial modulation of the material nonlinearity with a

period corresponding to the coherence length [2,3]. Active-passive hybrid waveguides combine the high optical quality of glass waveguides with the strong nonlinearity of poled polymers. Here, the guided modes interact via the evanescent field. For sum frequency (SF) generation in isotropic materials the phase mismatch is large, i.e. the coherence length is only a few microns, which increases by at least two orders of magnitude upon utilizing the mode dispersion of the waveguide [4].

The diffused channel waveguide (type BGG36) was purchased from IOT (Waghäusel, Germany) with a diameter of 10 μm. A 2 μm thick film of 2 wt.% DANS (4-Dimethylamino-4'-nitrostilbene) in PMMA (poly (methyl methacrylate)) was spin-coated from solution on top of the waveguide. After corona-poling at 5 kV normal to the surface the second-order susceptibility of the film was 1 pm/V. Two prisms were used for coupling the emission of a Nd:YAG laser and a dye laser (580 nm) into the waveguide and extracting the SF-signal at 375 nm. The mode spectrum vs. the coupling angle is shown in Fig. 1 (dashed curve). Only the higher order modes emerge due to the larger coherence length. The angular position of the lower order modes obtained by separately performed m-line-measurements are marked. The fundamental mode is TM_{00}, the higher order modes TM_{Ai} (i = 1, 2, 3) have asymmetric profiles. The total power of the pump beams inside the guide was 1 kW at 1064 nm and 80 W at 580 nm. The coherence length was (50 ± 5) μm for the conversion of the two pump beams propagating in the fundamental modes into higher order modes at 375 nm. The film was periodically bleached corresponding to the coherence length with 532 nm radiation

focused with a microscope objective to achieve quasi-phasematching. The SF-signal increased by a factor of 5 which is shown in Fig. 1 (solid curve). The arrow marks a mode which was not present before bleaching and may be attributed to light scattered into this mode from the higher order modes. The conversion efficiency was 10^{-8} for the non-optimized system. Calculations show that an increase of several orders of magnitude is possible by matching the refractive indices of the waveguide and the film, and by controlling the waveguide mode dispersion. In conclusion, we have shown, for the first time, that photobleaching is an attractive method for quasi-phasematched sum frequency generation in hybrid waveguides. Work is in progress to increase the efficiency and apply the method to difference frequency generation.

References

[1] D.M. Burland, R.D. Miller, C.A. Walsh, Chem. Rev. **94**, 31 (1994)

[2] S. Somekh, A. Yariv, Opt. Comm. **6**, 301 (1972)

[3] G. Marowsky, E.J. Canto-Said, S. Lehmann, F. Sieverdes, Phys. Rev. B **48**, 18114 (1993)

[4] G. Marowsky, S. Lehmann, D. Neuschäfer, E. Bär, H. Hsiung, L.-T. Cheng, J.M. Rodriguez-Parada, Appl. Phys. B **58**, 501 (1994)

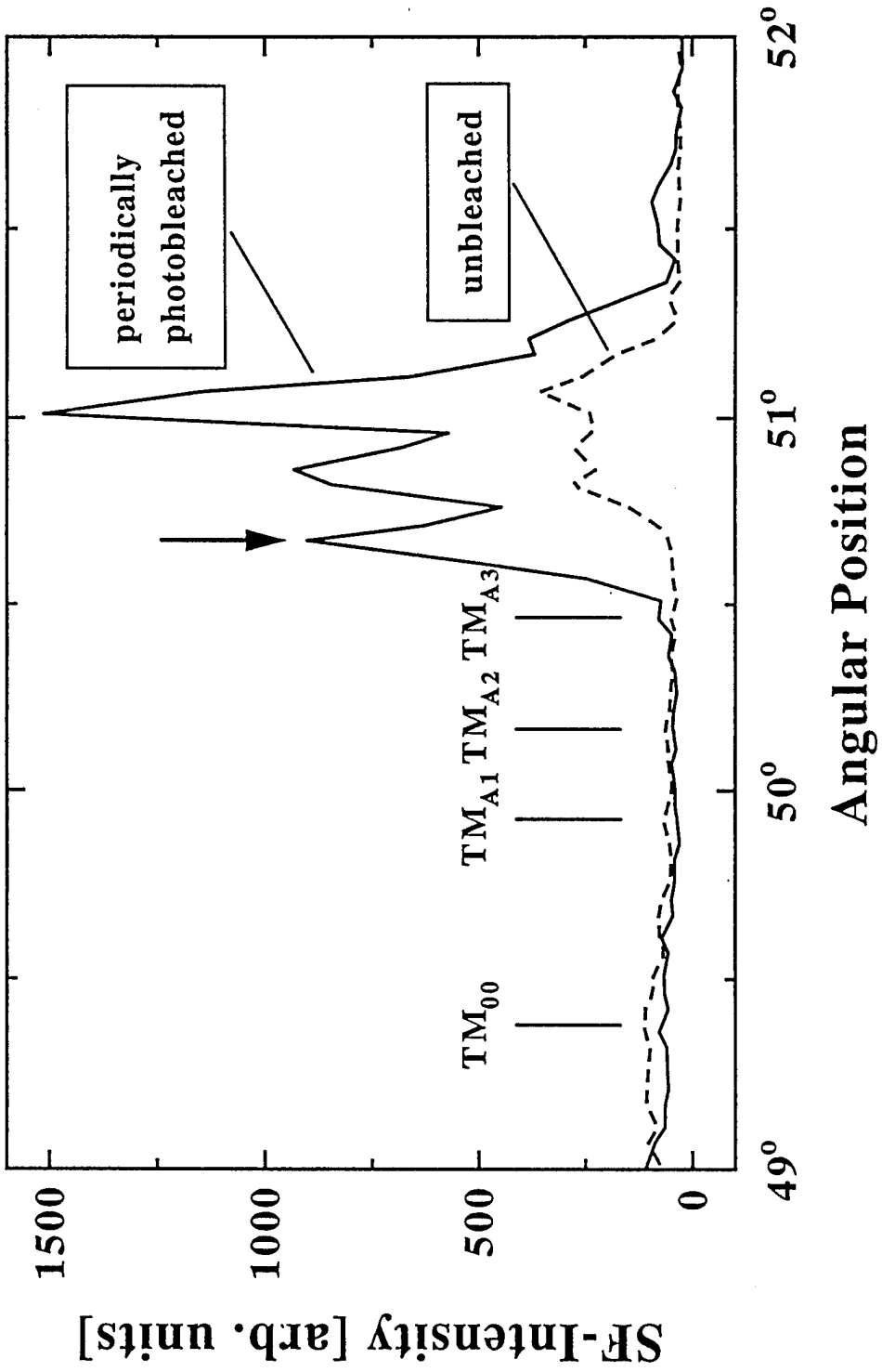

Fig. 1: Angular position of waveguide modes at 375 nm before (dashed) and after (solid) photobleaching.

Quasi-phase-matched Second Harmonic Generation in an Electro-optic Polymer Waveguide

Satoru Tomaru, Toshio Watanabe, Makoto Hikita,
Michiyuki Amano, Yoshito Shuto and Hiroki Itoh
NTT Opto-electronics Laboratories
Tokai,Naka-gun, Ibaraki, 319-11 Japan
TEL 81-292-87-7749 FAX 81-292-87-7870

Itaru Yokohama and Masaki Asobe
NTT Opto-electronics Laboratories
Atsugi-shi, Kanagawa, 243-01 Japan
TEL 81-462-40-3245 FAX 81-462-40-4303

Quasi-phase-matched(QPM) technique is very attractive for realizing frequency conversion devices, because it is easy to realize frequency conversion with high efficiency and to obtain a collimating beam. Therefore, many QPM studies have been undertaken mainly using $LiNbO_3$ waveguides.[1-3] On the other hand, nonlinear organic materials have received considerable attention due to their large nonlinear coefficient. However, there have been few reports on quasi-phase-matched frequency conversion using these materials[4,5] because they are difficult to fabricate into waveguides with a precise periodic poling structure.

In the paper, we report quasi-phase-matched second harmonic generation (QPM-SHG) in a waveguide composed of a nonlinear optical polymer. Recently, we have succeeded in developing a new waveguide fabrication technique which we call the 'serially grafted technique', using two different polymers, a UV cured resin and an electro-optic(EO) polymer.[6] The advantage of this is its ability to connect different waveguides with low loss. So, we applied the technique in order to realize QPM-SHG devices with a precisely controlled periodic poling waveguide structure.

The core materials in the waveguide with a QPM structure which we fabricated were EO polymer and UV cured resin. The cladding material was also the UV cured resin. The EO polymer was a nonlinear organic dye branched polymer which was composed of PMMA and nonlinear optical diazo dye.[7] The polymer is a good nonlinear waveguide material which exhibited a d_{33} value of 80 pm/V and a loss of 0.65 dB/cm in the form of a single-mode waveguide operating at 1.3 μm. The refractive index of the UV cured resin forming

the core and cladding layer can be easily controlled.[8] This controllability makes it easy to form a periodic laminar structure composed of EO polymer and UV cured resin with almost the same refractive index and also to realize a single-mode waveguide.

Figure1 shows the method used to fabricate of the periodic waveguide. First, the undercladding layer and core EO polymer are spin-coated on a Si substrate. After forming periodic patterns on the EO polymer layer by conventional photolithgraphy, the EO polymer is etched by O_2 reactive ion etching (O_2RIE) until the surface of the undercladding layer is exposed. Next, the periodic patterned EO polymer is covered with UV cured resin whose refractive index is the same as that of the EO polymer. Then, the UV resin layer is etched using the O_2RIE process until the top surface of the patterned EO polymer is exposed. This process forms a core layer composed of EO polymer and UV cured resin whose refractive index difference is controlled to within 0.001. Next, the channel waveguide patterns are formed on the core layer by a conventional photolithographic process. Then by using the O_2RIE process again, the core ridge composed of EO polymer and UV cured resin is formed. By covering the core ridge with UV cured resin, a channel waveguide with a periodic structure can be obtained. Finally, the waveguide is poled by applying a high electric voltage through upper and lower electrodes. This poling process provides the waveguide with a periodic poled structure. The periodic length (Λ) in the waveguide can be controlled easily by changing the mask pattern. In this experiment, a waveguide with a periodic length in the10μm to 90μm range with the intervals of 1μm was formed on the same substrate. Table 1 shows the refractive indices of the core materials (EO polymer and UV cured resin), cladding material (UV cured resin) and other waveguide parameters. Figure 2 shows one example of the fabricated periodic waveguide and its near field pattern at 1.55μm. The waveguide loss was lower than 3 dB/cm at 1.55μm. By using parameters in table 1, we can estimate the periodic length for phase-matched SHG wavelength with the Marcatili method.[9] The poling voltage was typically about 40V/μm. Under the same poling condition, the coefficient (d_{33} value) of the EO polymer thin film was found to be about 20 pm/V. Therefore, the effective d (d_{eff}) value in launching a TM mode incident light into the waveguide was estimated to be about 6 pm/V ($d_{eff}=d_{33}/\pi$.).[4]

SHG experiments were performed with 5mm long QPM waveguides using a color center laser (repetition frequency: 100MHz, pulse width:10ps) with a 1.48-1.65μm fundamental wavelength. TM_{00} mode incident light was launched into the waveguide by end-fire coupling. The observed SHG intensity shows a strong dependent on the

periodic length (Λ). Figure 3 shows the relationship between the periodic length and the phase-matched SHG wavelength. When the fundamental wavelength was 1.587μm, the SHG intensity was strongest in the waveguide with a periodic length of 32μm. The SHG efficiency was found to be about 10^{-3} /W.

In conclusion, we have succeeded in realizing QPM-SHG in a periodic waveguide composed of EO polymer and UV cured resin by using a new developed waveguide fabrication technique (serially grafted technique). The typical SHG efficiency of a 5mm long QPM waveguide was about 10^{-3}/W. The efficiency will be improved by more than one order by optimising the waveguide parameters and poling conditions. Therefore, the QPM waveguide will be a key component in nonlinear optical devices, such as frequency conversion devices and cascade devices.

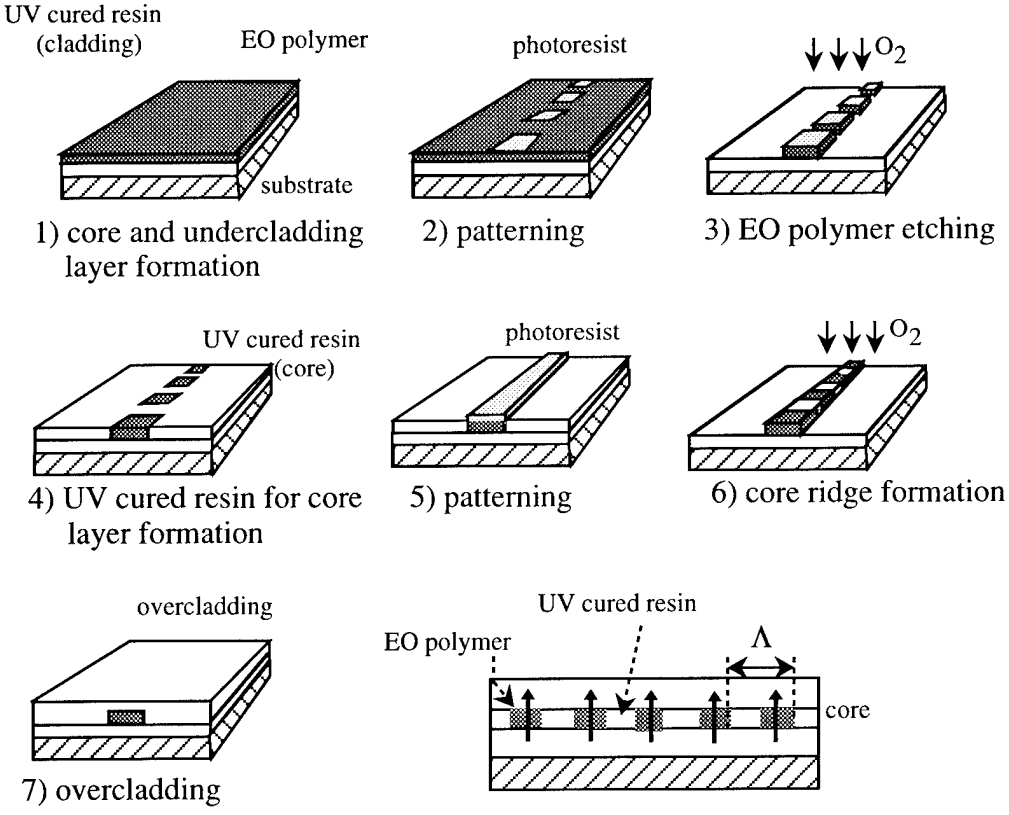

Fig.1 Periodic waveguide fabrication method based on 'serially grafted technique'.

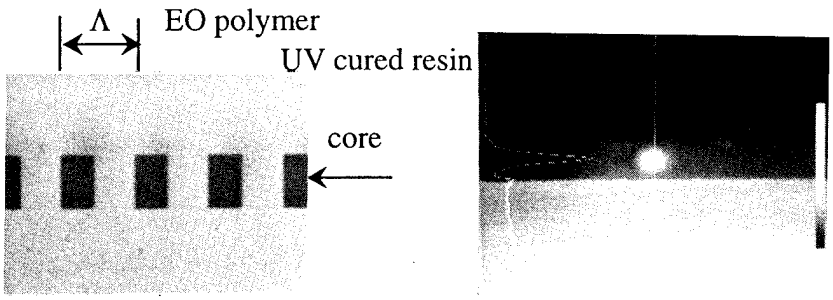

Fig.2 Photograph of the periodic waveguide and its near-field pattern at 1.55μm.

Table 1 Waveguide parameters of QPM waveguide.

	core		cladding
	EO polymer	UV resin	UV resin
n at 1.55μm	1.544	1.544	1.529
width	6μm		—
height	2μm		4μm
periodic length(Λ)	10-90μm (intervals of 1μm)		

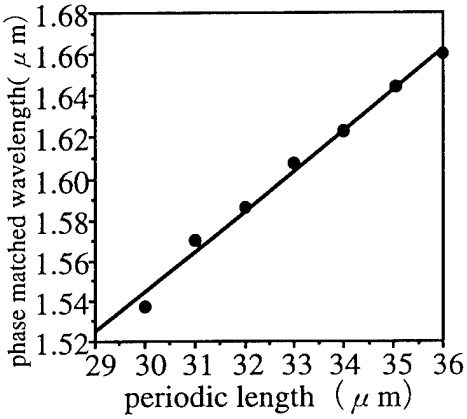

Fig.3 Relationship between the periodic length and phase-matched SHG wavelength.

References

1.Yamada, M.,Nada, N., Saito, M., and Watanabe,K., Appl.Phys. Lett.,1992,62, pp.435-436

2.Lim, E., Fejer, M. M., Byer, R. L., Electron.Lett.,1989, 25, pp.174-175

3.Mizuuchi, K., Yamamoto, K., and Taniuchi, T., Appl.Phys.Lett., 1991,59, pp.1538-1540

4.Suhara, T., Morimoto, T. and H.Nishihara, 1993, MOC/GRIN'93, pp76-79

5.Khanarian, G. and Norwood, R.,1990, SPIE 1337,pp.44-52

6.Watanabe, T., Amano, M., Hikita, M., Shuto, Y, and Tomaru, S., Appl.Phys.Lett, 1994 65, pp1205-1207

7.Amano, M., Watanabe, T, Hikita, M., Shuto, Y.,Tomaru, S., Yaita. M.,and Nagatsuma, T.,1994, Proc.SPIE2143, pp68-79

8.Murata, N. and Nakamura, K., J.Adhesion,1991,35,pp.251-267

9.Marcatili,E.A.J.,Bell.Syst.Tech.J.,1969,48,pp2071-2102

Bulk-type phase-matched SHG devices of poled polymer

X. T. Tao, T. Watanabe, H. Ukuda, and S.Miyata

Faculty of Technology, Tokyo University of
Agriculture and Technology, 2-24-16 Nakamachi, Koganei-shi,
Tokyo 184, JAPAN FAX: 0423-86-1084

Bulk phase-matched second-harmonic generation has been realized from a drawn and poled polymer by prism and end-fire coupling at 1.064 μm.

Introduction:

Polymeric second-order nonlinear optical (NLO) materials have been studied extensively in recent years for applications in communication and optical signal processing[1-2]. Most of the earlier works were concerned with the synthesis and the general properties such as nonlinear optical coefficients and temporal stability. Only a few studies have been reported on phase matched second harmonic generation (SHG)[3]. In fact, phase matching is the first important condition to achieve high conversion efficiency of SHG. It has been proposed that the mode dispersion of fundamental and second-harmonic waves was used to achieve phase matching, in which very precise control of film thickness was required. This is not easy for poled polymer films generally obtained by spin-coating. To avoid this difficulty, the use of Cerenkov radiation and non-collinear light path have been proposed. But in all these methods the obtainable SHG conversion efficiency was limited by the small over-lap integrals for different modes. In order to maximize the overlap integral, the quasi-phase matching (QPM)[4] mthods by altering $\chi^{(2)}$ singal or periodic poling have been proposed. But again the precise control of periodicity should be needed, which is also very difficult. We found main-chain polymers with Λ-type charge transfer chromophores have positive birefringence, by drawing and poling, the birefringence can be increased and controlled to realize bulk phase-matching.[5] Here we describe the recent progress of bulk phase-matching of poled polymers.

Experiment and results:

1.Sample preparation

The free-standing films were drawn and poled simultaneously by zone drawing and poling apparatus developed by ourself, Fig. 1. is the schematic set-up used in the experiment.

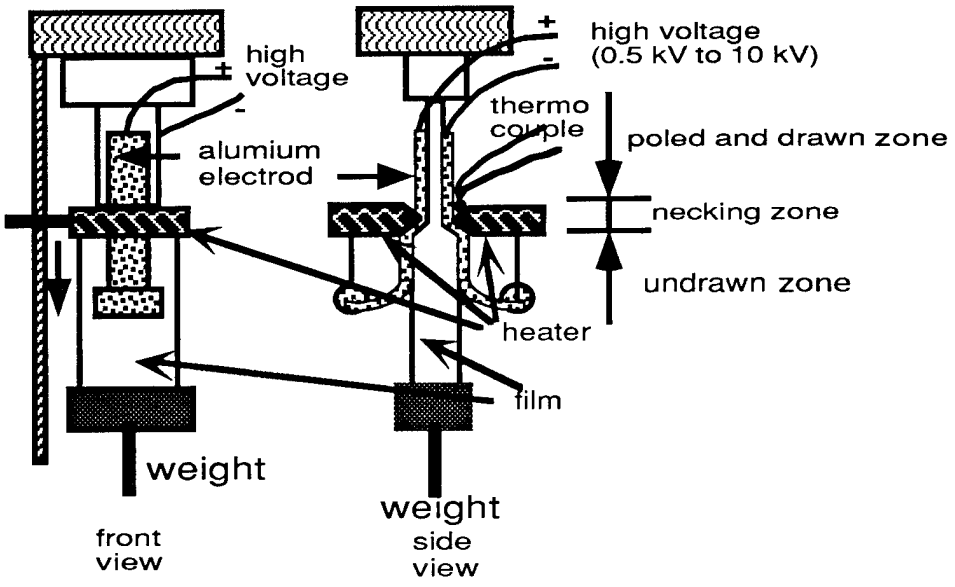

Figure 1. Schematic set-up of zone drawing and poling.

2.Phase matching experiment

The geometry of the drawn polymer was shown in Fig.2. The refractive indices are defined as n_x, n_y, and n_z for the polarization vector in the film normal direction, the transverse

direction in the plane of the film and parallel to the draw direction, respectively. The θ and ϕ are polar coordinates (referred to z and x, respectively).

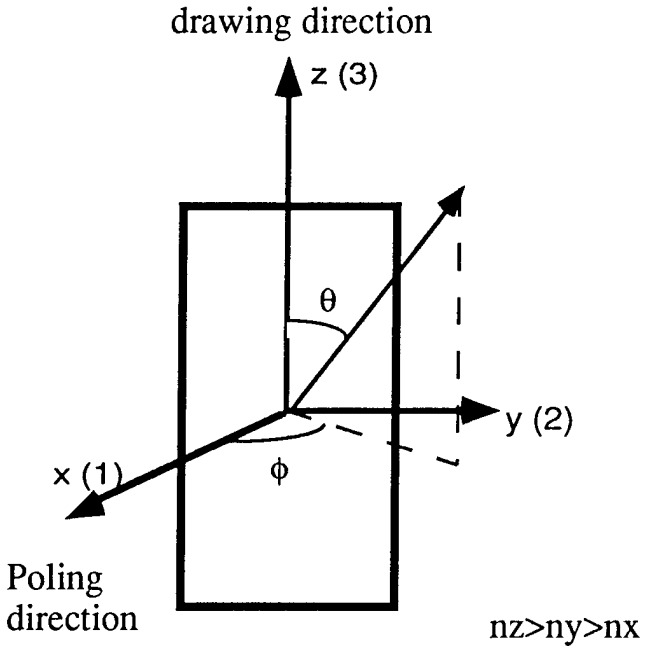

Fig. 2. Geometry of polymer film samples

Using the refractive indices of polymer with draw ratio of 1.18, the type I phase matching characteristics has been calculated. Cutting films with the calculated phase-matching directions, the phase-matched SHG has been observed in experiment by using a Nd:YAG laser with 1064 nm fundamental wavelength by prism and end-fire coupling. Fig.3 is the schematic set-up for the phase-matched SHG through end-fire coupling and Fig. 4 is the relationship of SH intensity and rotation angle.

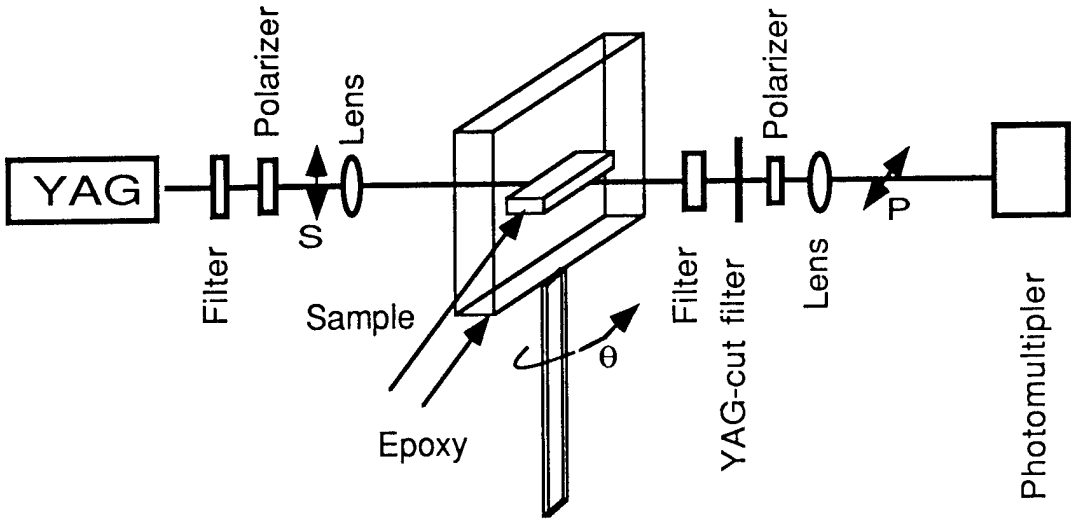

Fig. 3. Schematic setup for phase-matched second-harmonic generation experiment. The incident light is S-polarized and the output light is P-polarized.

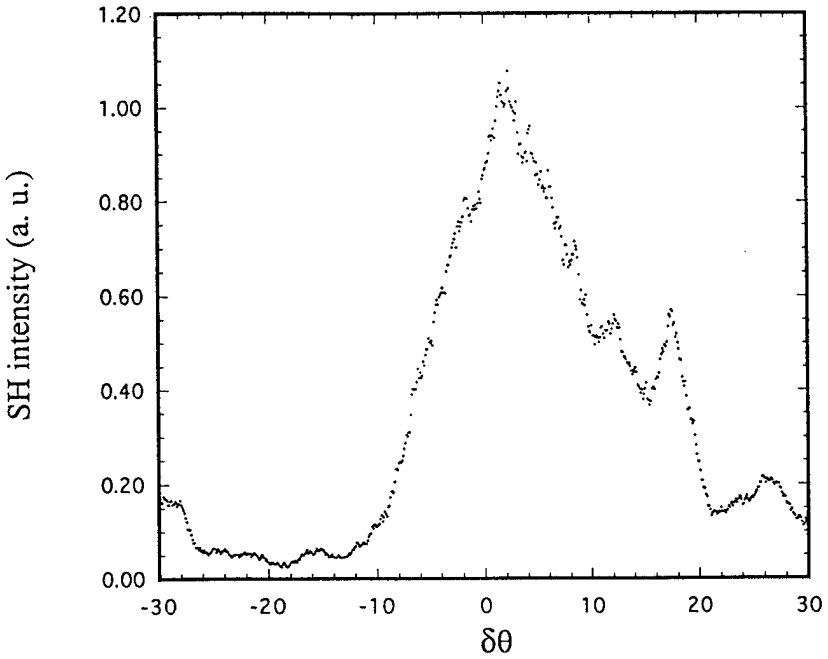

Fig. 4. The dependence of phase-matched SHG intensity of polyurea with draw ratio of 1.18 on angle of δθ.

Refrences:
(1) D. S. Chemla, J. Zyss, Eds."Nonlinear optical properties of organic molecules and crystals" (Academic press New york, 1987)
(2) S. Miyata, ed."Nonlinear optics, fundamentals, materials and devices" (North Holland,1992)
(3) O. Sugihara, T.Kinoshita, M.Okabe, S.Kunioka, Y.Nonaka, and K.Sasaki, Appl. Optics, 30, 2957 (1991).
(4) M.M.Fejer, G.A.Magel, D.H.Jundt, and R.L.Byer, IEEE J. Quan.Elec. 28, 2631, (1992)
(5) X. T. Tao, T. Watanabe, D. C. Zou, H. Ukuda and S. Miyata, J. Opt. Soc. Am. B, in press.

Thin Films of Organic Salts with Large Optical Non-Linearities by Organic Vapor Phase Deposition.

P.E. Burrows, S.R. Forrest and T. Buma,
Advanced Technology Center for Photonics and Optoelectronic Materials (ATC/POEM)
Department of Electrical Engineering
C436 Equad, Olden Street,
Princeton University
Princeton NJ 08544
Phone: 609-258-4204 Fax 609-258-1954

L.S. Sapochak and J. Schwartz,
Advanced Technology Center for Photonics and Optoelectronic Materials (ATC/POEM)
Department of Chemistry
Princeton University
Princeton NJ 08544

V.S. Ban and J.L. Forrest,
PD-LD Inc.
209 Wall St., Princeton NJ 08540

Recently, single crystals of organic and organometallic salts[1-3] have been shown to possess extremely large second order ($\chi^{(2)}$) NLO effects leading to a high second harmonic generation (SHG) efficiency. The naturally non-centrosymmetric crystal structures of these compounds eliminates the need for external poling as required for guest-host polymeric systems. Furthermore, these salts have a high optical damage threshold and sufficient stability with respect to temperature to withstand many conventional semiconductor fabrication processes. In particular, highly pure single crystals of the salt, 4'-dimethylamino-N-methyl-4-stilbazolium tosylate (DAST)[1], have been shown to have a value of $\chi^{(2)}$ at least 10^3 times greater than that of urea.

For many applications such as waveguide devices, it is desirable to grow NLO materials into optical quality thin films. Although thermal evaporation in a high vacuum environment has been used to grow thin films of many organic and inorganic materials, the technique is not always applicable to organic salts. For example, when heated in vacuum, DAST decomposes before vaporization. Attempts at growth of DAST by double-source co-evaporation of two neutral precursors have also been unsuccessful, due in part to the radically different vapor pressures of the precursors,[4] resulting in highly nonstoichiometric growth.

In this paper we apply the techniques of vapor phase epitaxy[5] (VPE) to grow films of DAST by the reaction of two volatile organic materials in a hot-wall reactor. The proposed reaction scheme is shown in Fig. 1. In step 1, thermal demethylation of 4'-dimethylamino-N-

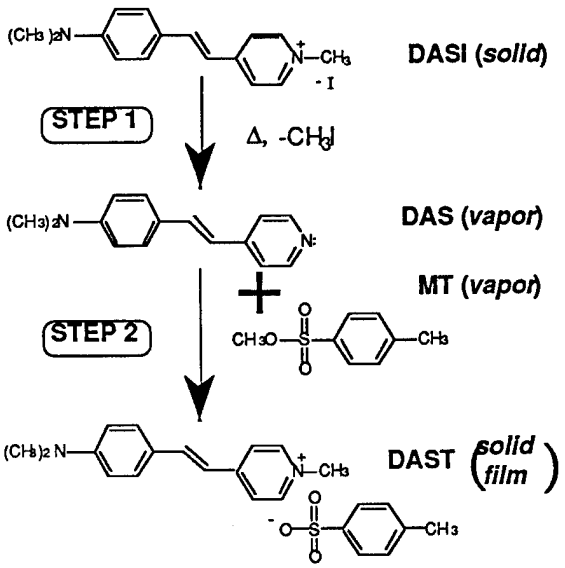

Figure 1: Proposed reaction scheme for the production of DAST by the reaction of DASI with MT.

methyl-4-stilbazolium iodide (DASI) gives neutral DAS with the elimination of volatile CH_3I. In step 2, the DAS reacts with MT, resulting in methylation of the pyridine ring at the nitrogen atom. The resulting stilbazolium and tosylate ions form DAST crystals.

The OVPD reactor designed to grow DAST by the above scheme is shown schematically in Fig. 2. The reaction tube is a glass cylinder of diameter 2.5 cm and length 45 cm. A 2.5 cm^3 alumina crucible is filled with approximately 1g of DASI and placed approximately 15 cm into the reaction tube. The crucible is heated by means of one

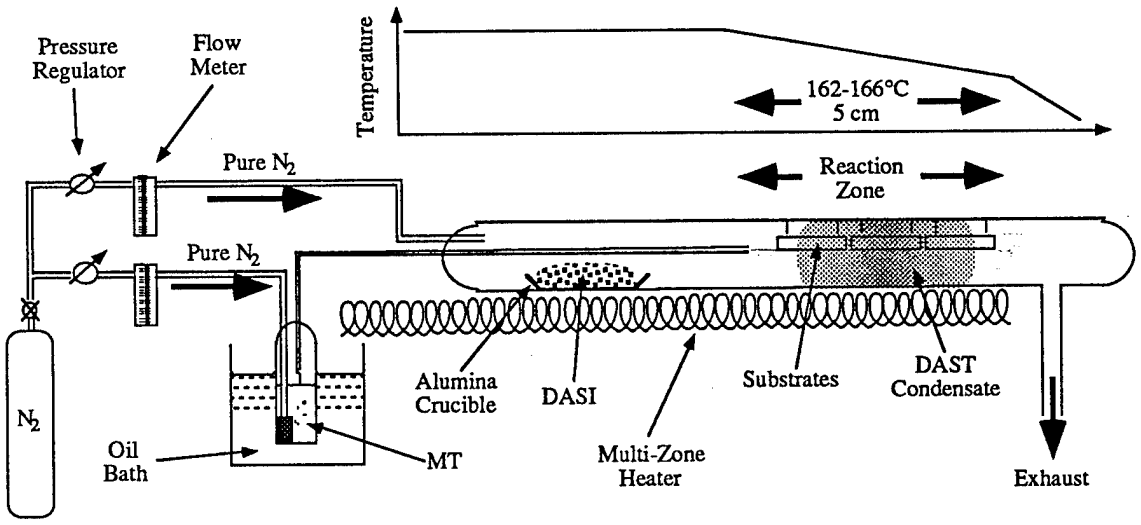

Figure 2: Schematic of the OVPD chamber, showing the layout and temperature gradient of the reactor zone.

zone of a multi-zone heater wrapped around the reaction tube. A regulated stream of pure N_2 gas is introduced into the hot end of the tube to provide a slight pressure gradient, causing the DAS vapor to flow along the reactor tube. The temperature of the reactor is monitored by a chromel-alumel thermocouple inserted into a thin-walled glass tube which runs the length of the reactor. MT is loaded into a 30 cm^3 bubbler, the temperature of which is maintained by a silicone oil bath. Pure nitrogen gas, regulated to 5 psi, passes through a flow meter and bubbles through the MT, thereby carrying MT vapor through a glass transfer tube (heated to >100°C) into the reaction tube, approximately 5 cm beyond the DASI crucible (to prevent reactions in the crucible). The DAS vapor mixes with the MT vapor in the reaction zone, along which a temperature gradient is

maintained, and reacts to form DAST on substrates supported along the length of the tube. Excess unreacted MT vapor, and any volatile side-reaction products, are exhausted from the cold end of the reactor.

We observe the growth of reddish-brown reaction product under various conditions. The purest DAST is obtained at temperatures between 162 and 166°C in the reaction zone, with the DASI crucible at 253±2°C, the MT bubbler at 55±2°C and the bubbler and purge gas flows at 15 cm^3/min and 400 cm^3/min, respectively. Optical micrographs of DAST films grown by OVPD under these conditions on various substrates are shown in Fig. 3. On gold-coated glass slides, we observe regions of crystalline film growth with a clear alignment direction, as illustrated by the light and dark areas observed in a polarized-light micrograph (Fig. 3a). The mean film thickness is estimated by interference microscopy to be 500 nm after 100 minutes of growth, giving an average growth rate of 0.8 Å/s, although the film is highly non-uniform in both thickness and coverage, suggesting a columnar growth mode. Growth on glass (Fig. 3b), however, yields separated islands of material, implying that the DAST film does not wet the surface. It is apparent from Fig. 3 that surface interactions greatly influence film nucleation, as is typical in comparable inorganic crystalline growth techniques. Optical quality thin films may therefore be achievable by using substrates which provide more favorable physical interactions with the DAST film to induce a "quasi-epitaxial" growth mode.[6,7]

Figure 3(a): Polarized light micrograph of film grown on gold coated glass slides, showing region of continuous, aligned, polycrystalline growth Scale bar is 10μm.

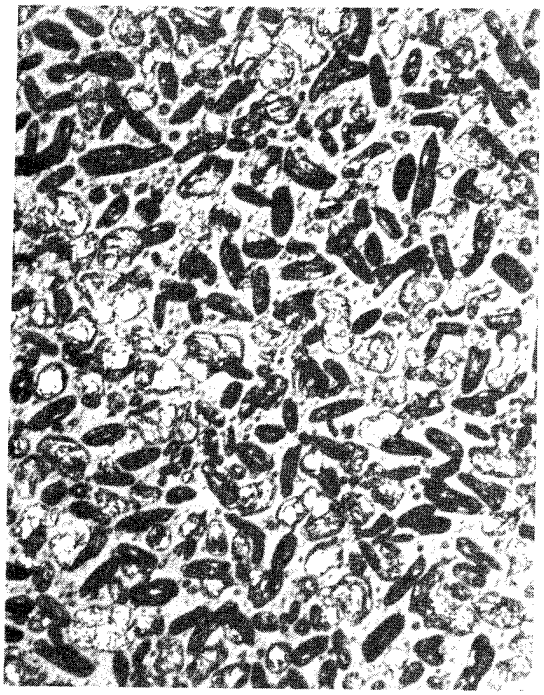

Figure 3(b): Optical micrograph of DAST film grown on glass under similar conditions.

Confirmation of the stoichiometric composition of the reaction products was accomplished by one dimensional (1D) and two dimensional (2D) ^{1}H NMR spectroscopic analysis of OVPD films dissolved in dimethyl sulfoxide-d_6 (DMSO-d_6). The ^{1}H NMR spectrum of a film sample grown under the optimum conditions described above shows all of the peaks assigned to DAST, with no detectable impurities in the aromatic region. Based on the limits of sensitivity and integration accuracy of NMR measurement, the DAST film is >95% pure. Having demonstrated the *chemical* purity of the OVPD DAST films using ^{1}H NMR, we employ SHG intensity measurements to semi-quantitatively determine the degree to which the non-centrosymmetric *crystal structure* of DAST is achieved. To measure the SHG efficiency of the films, a 1.06μm wavelength Nd:YAG laser beam was passed though a H_2 Raman-shifter to obtain an excitation wavelength of 1.9μm. The frequency doubled light is then at 0.95μm, and both the fundamental and the SHG signal are beyond the absorption band of DAST. The SHG intensity at 0.95μm of the film was found to be approximately 10% of the intensity obtained from a "bulk" DAST powder sample. Given the fact that the film was very thin and discontinuous (resulting in poor coupling and no phase match to the excitation source), this result qualitatively indicates a surprisingly high SHG efficiency, indicating the presence of significant amounts of the SHG-active phase of DAST. The presence of other, non-SHG active phases, however, can not be ruled out.

In summary, we have presented a new technique for the growth of extremely pure, strongly NLO-active films of DAST via the chemical reaction of two organic vapors in a hot-wall reactor. By using different reactants, and with the appropriate combinations of bubblers and solid-sources, this technique can be applied to yield thin films of many different highly polar, NLO-active organic and organometallic salts, which is not possible by established methods of thin film growth. We expect this technique to open up an entirely new range of materials and numerous novel photonic device applications.

The authors thank Dr. S.R. Marder for advice and for providing pure DAST samples, Prof. M.E. Thompson for helpful discussions, and Dr. D. Strickland for assistance with the NLO measurements. This work was funded by the AFOSR (C. Lee and G. Pomrenke), the NSF MRSEC Program and a 1994 Phase I BMDO SBIR contract (J. Pazik).

References.

1. J.W. Perry, S.R. Marder, K.J. Perry and E.T. Sleva, Proc. SPIE **1560,** 302 (1991).

2. S.R. Marder, J.W. Perry, W.P. Schaefer, B.G. Tiemann, P.C. Groves and K.J. Perry, Proc. SPIE **1147,** 108 (1989).

3. S.R. Marder, J.W. Perry and W.P. Schaefer, Science 245, 626 (1989).

4. S.R. Forrest, P.E. Burrows, E.I. Haskal and Y. Zhang, Proc. Mat. Res. Soc. Symp. Proc. **328**, 37 (1994).

5. T.P. Pearsall (ed.) "GaInAsP Alloy Semiconductors," *Wiley*, NY, 1982.

6. S.R. Forrest and Y. Zhang, Phys Rev B, **49**, 11297 (1994).

7. S.R. Forrest, P.E. Burrows, F.F. So and E.I. Haskal, Phys Rev B, **49**, 11315 (1994).

Thursday, September 14, 1995

Electroluminescent Polymers

ThC 1:30 pm-2:15 pm
Holladay Room

Kenneth D. Singer, *Presider*
Case Western Reserve University

High Efficiency White and Colored Organic Electroluminescence

R. H. Jordan
A. Dodabalapur
M. Strukelj
L. J. Rothberg
R. E. Slusher
T. M. Miller

AT&T Bell Laboratories
Murray Hill, NJ 07974

The need for light weight, low power multicolor displays and backlights has spurred interest in thin–film, organic electroluminescent (EL) devices. A typical organic EL device consists of an indium–tin oxide anode (ITO) layer on a glass substrate, and sequential layers of bis(triphenyl)diamine (TAD, hole transporter), tris(8-hydroxyquinoline)aluminum (AlQ, electron transporter and green light–emitter), and a low work function metal cathode (e.g., Al or Mg:Ag).[1] Device efficiency, stability, and spectral output can be tailored by incorporating intermediate layers of organic hole–blockers[2] or blue–emitters,[3] or doping AlQ with narrow spectral linewidth organic dyes.[4] Cavity resonance effects have been employed in lithographically patterned optical microcavities to select single[5] or multiple[6] colors out of broad spectrum organic emitters like AlQ. Device efficiency is a critical parameter, especially for liquid crystal display backlight applications. We will describe an approach for white light EL and an approach for enhancing device efficiency.

White light electroluminescence, of interest for backlights, is achieved by sandwiching a thin layer of a blue-emitting species, 2-naphthyl-4,5-bis(4-methoxyphenyl)-1,3-oxazole, (denoted NAPOXA), between TAD and AlQ (Figure 1(a)). NAPOXA, the intermediate emitting layer, is a new chemical compound based on a class of substituted oxazoles, and has a broad luminescence spectrum which spans the range 400—650 nm with a significant fraction of emission occurring at blue wavelengths. Figure 2 shows EL spectra for (a) 600 Å TAD/600 Å AlQ device, (b) 600 Å TAD/150 Å NAPOXA/600 Å and (c) 600 Å TAD/150 Å NAPOXA/300 Å AlQ/200 Å AlQ + 0.5% DCM 1/200 Å AlQ. (The organic dye DCM 1 was added to broaden the spectrum.) Photometric coordinates standardized by the Commission Internationale de l'Eclairage[7] (CIE) describe perceived device color; white is defined as (CIE; 0.33, 0.33). The CIE coordinates of the emitted light of the described structures are (a) (CIE; 0.39, 0.56), (b) (CIE; 0.28, 0.46), and (c) (CIE; 0.31, 0.41). Bright EL of 4000 cd/m^2 was achieved with device configuration (c).

Enhanced efficiency from EL devices was obtained by matching the narrow electroluminescence spectral width of pyrromethene dye–doped AlQ with the optical mode width of the microcavity. The microcavity is comprised of a broad bandwidth (> 200 nm) titanium dioxide and silicon dioxide quarter–wave dielectric–stack reflector (peak reflectivity 80% at 550 nm), a silicon nitride spacer layer (used to modify cavity length), an ITO electrode, the organic layers, and a highly reflecting Al or Al:Li electrode (Figure 1(b)). A portion (~ 100 Å) of the AlQ layer is doped with the organic dye pyrromethene (PM 580).[8] Doping a non–cavity device narrows the EL spectral width from 85 nm (undoped AlQ) to 45 nm, FWHM, for dye doping levels from 0.3% to 3.0% (by weight). Both the doped and undoped EL spectra peak at 545 nm. Preliminary experimental results show an increase in external quantum efficiency by a factor of 1.2 when the microcavity supports a single optical mode that is matched with the narrow dye–doped AlQ emission. Optimized mode matching is predicted to give a factor of $2n^2$ enhancement of surface–emitted, integrated luminescence over that of a non–cavity device, where n if the refractive index of the device. Using a typical refractive index value $n \cong 1.5$ predicts an enhancement factor of 4.5. The cavity narrows the spatial distribution of radiation from the emitting layer and redirects light that would be lost to total internal reflection in the absence of a cavity. These large enhancement factors necessitate a match between the cavity and emitter spectral widths, which requires a narrow spectral width emitter (dye–doped AlQ) rather than a wide spectral width emitter (AlQ). The enhancement techniques described here, combined with recently reported increased efficiencies of typical organic EL devices, may yield the very high device efficiencies required for backlight applications where white light is not required and ultralow power is essential.

[1]C. W. Tang and S. A. VanSlyke, Appl. Phys. Lett. **51**, 913 (1987)
[2]J. Kido, M. Kimura and K. Nagai, Science **267**, 1332 (1995)
[3]M. Strukelj, R. H. Jordan and A. Dodabalapur, J. Am. Chem. Soc. (1995) (to be published)
[4]C. W. Tang, S. A. VanSlyke and C. H. Chen, J. Appl. Phys. **65**, 3610 (1989)
[5]A. Dodabalapur, L. J. Rothberg, T. M. Miller and E. W. Kwock, Appl. Phys. Lett. **64**, 2486 (1994)
[6]A. Dodabalapur, L. J. Rothberg and T. M. Miller, Appl. Phys. Lett. **65**, 2308 (1994)
[7]*Colorimetry* (Central Bureau of the CIE, Vienna, 1986).
[8]R. E. Hermes, T. H. Allik, S. Chandra and J. A. Hutchinson, Appl. Phys. Lett. **63**, 877 (1993)

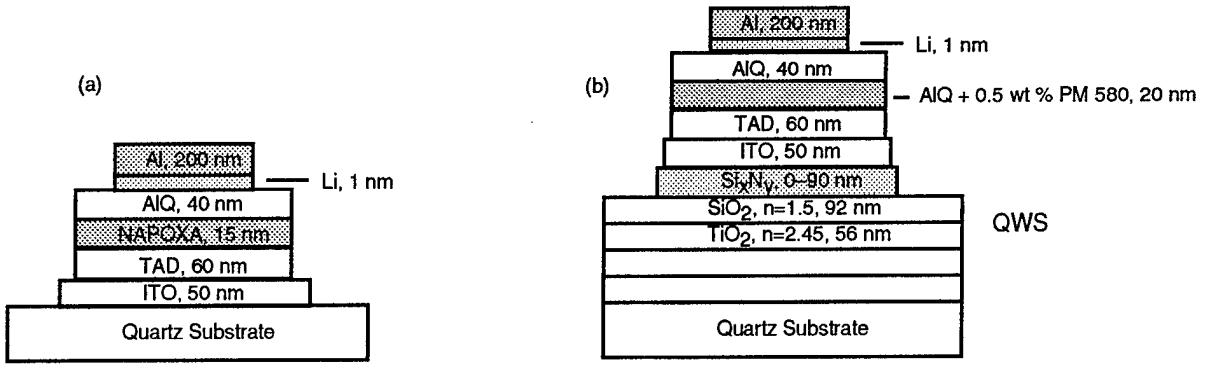

Figure 1. (a) Schematic of broad emission spectrum electroluminescent device with new species 2-naphthyl-4,5-bis(4-methoxyphenyl)-1,3-oxazole (NAPOXA). (b) Schematic of narrow emission spectrum emitting microcavity electroluminescent device.

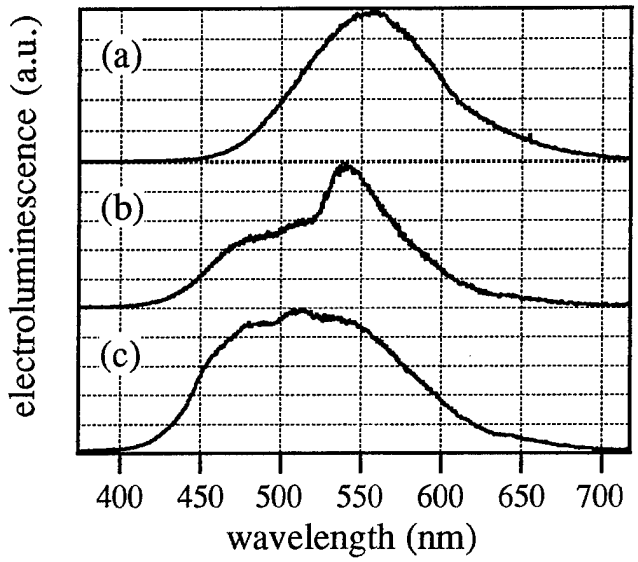

Figure 2. Normalized electroluminescent spectra for (a) 600 Å TAD/600 Å AlQ device, (b) 600 Å TAD/150 Å NAPOXA/600 Å and (c) 600 Å TAD/150 Å NAPOXA/300 Å AlQ/200 Å AlQ + 0.5% DCM 1/200 Å AlQ.

Polymer Light-Emitting Electrochemical Cells

Qibing Pei, Gang Yu, Chi Zhang, Yang Yang and Alan J. Heeger
UNIAX Corporation
6780 Cortona Drive
Santa Barbara, CA 93117

Electrochemistry provides a convenient means of reversibly doping conjugated polymers *n*-type (electron carriers) or *p*-type (hole carriers). When such charge carriers are introduced by electrochemical doping, they are compensated by counter-ions from the electrolyte. At high doping levels, the material becomes metallic, leading to low resistance contacts and easy charge injection (both *n*-type and *p*-type, respectively). [1-5]

The active medium of a polymer light-emitting electrochemical cell (LEC) is a semiconducting and luminescent polymer with sufficient ionic species as additive to provide the counterions necessary for *p*-type and *n*-type doping. In addition, since the ions must be mobile during the *in-situ* electrochemical doping, an ionically conductive material is required. That ionically conducting material can be the semiconducting and luminescent polymer, possibly enhanced by blending with a known ion transport polymer, for example, poly(ethylene oxide), PEO. This blend is sandwiched between two metal electrodes as shown in Fig. 1. The doping profile is changed in a controlled fashion through reversible electrochemical oxidation and reduction to form a *p*-type layer on one side, an *n*-type layer on the opposite side, and a *p-n* junction at the interface between the two. *Light emission is from the compensated region within the p-n junction.*

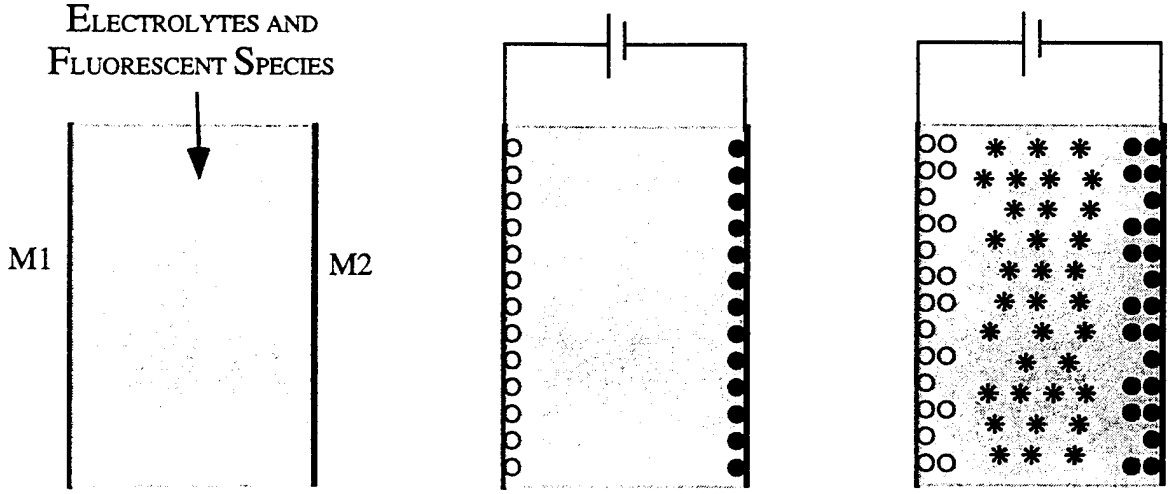

*Figure 1: Schematic diagram of the electrochemical processes in a light-emitting electrochemical cell (LEC). ∘ An oxidized species (p-type doped); • A reduced species (n-type doped); * A neutral electron-hole pair.*

Due to the presence of the electrolyte in the active layer of the polymer LEC, thin double layers form at both the M_1/active layer and M_2/active layer interfaces. When a sufficiently high

voltage (V) is applied between M_1 and M_2, electrochemical doping is initiated, and charge is injected from the electrodes into the active layer. If M_1 is wired as the anode and M_2 as the cathode, the luminescent polymer adjacent to the surface of M_1 is oxidized and *p*-type carriers are introduced, while the polymer adjacent to the surface of M_2 is reduced and *n*-type carriers are introduced. On both the *n*-type side and the *p*-type side, the electrochemical potential locally readjusts with an associated redistribution of the compensating ionic species. This process is depicted schematically in the middle panel of Figure 1.

Under the influence of the field due to the applied voltage, the *p*-type carriers (holes) move from the anode toward the cathode, and the *n*-type carriers (electrons) move from the cathode toward the anode. Between the regions of *n*- and *p*-type doping, the holes propagating toward the cathode and the electrons propagating toward the anode meet in a region which defines an electrochemically induced *p-n* junction. Within the electrochemically induced *p-n* junction, the electrons and holes combine to form neutral pairs which radiatively decay to the ground state. This process is depicted schematically in the final panel of Figure 1.

Conjugated polymers such as poly(1,4-phenylene vinylene) (PPV) and its soluble derivatives are attractive for use in the active layers of the LEC's. PPV is luminescent in its neutral (undoped) state, is readily oxidized and reduced electrochemically, and is electrically conductive following electrochemical oxidation or reduction. The color of the light emitted by an LEC is determined by the energy gap of the semiconducting polymer in which the p-n junction is formed and can be changed in a straightforward way by substituting a different conjugated polymer in the active layer. LEC's which emit orange light were fabricated by using the soluble derivative of PPV, poly(5-(2'-ethylhexyloxy)-2-methoxy-1,4-phenylene vinylene), or MEH-PPV, as the fluorescent redox species. To prepare these prototype devices, a thin polymer layer containing a 1:1 ratio (by weight) of MEH-PPV and PEO was spin-cast from solution in pyridine onto ITO-coated glass substrates; The PEO was added to improve the ionic mobility. The polymer layer also contained lithium trifluoromethanesulfonate such that the molar ratio of the (CH_2CH_2O) moeties in the PEO to salt was 20:1. Finally, a thin layer of aluminum (400 Å) was evaporated onto the polymer film.

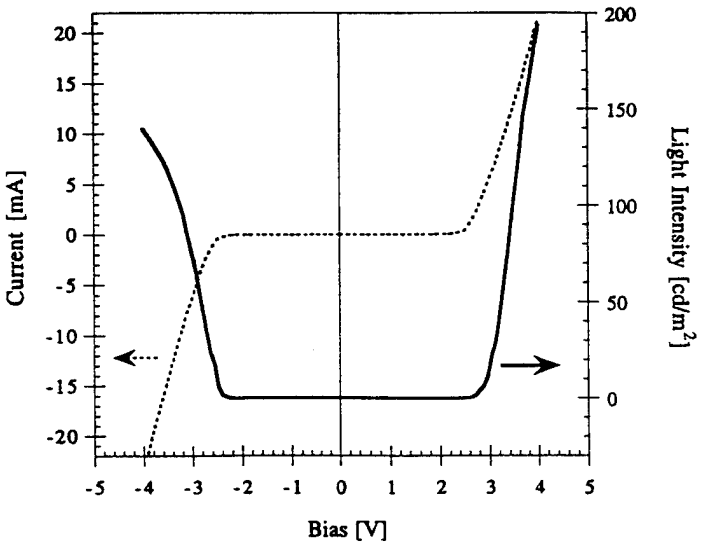

Figure 2: Light output vs. voltage and current vs. voltage for ITO/MEH-PPV + PEO/Al light-emiting electrochemical cells with the ITO contact wired as the anode.

Typical current vs voltage (I-V) and light vs. voltage data for these yellow-orange emitting devices are presented in Figure 2. The apparent threshold voltages for appreciable current injection and for detection of visible light emission are below 25V for both forward bias scans (sweeping from 0 to 4 V) and reverse bias scans (sweeping from 0 to -4 V). In a darkened room, light emission can be observed for V>2.1 V. The forward and reverse bias I-V and light vs. voltage curves obtained from LECs are nearly symmetric about zero bias, in contrast to the diode-like behavior exhibited by "conventional" polymer LEDs. [8]

Figure 3 shows the spectrally resolved light outputs from one of the MEH-PPV devices upon application of a voltage of either polarity, demonstrating that the LEC is bipolar. The spectrum of emitted light is seen to be the same in either case, indicating that the emission is independent of which electrode serves as the anode and which serves as the cathode. The photoluminescence spectrum, included for comparison, is seen to be slightly red-shifted.

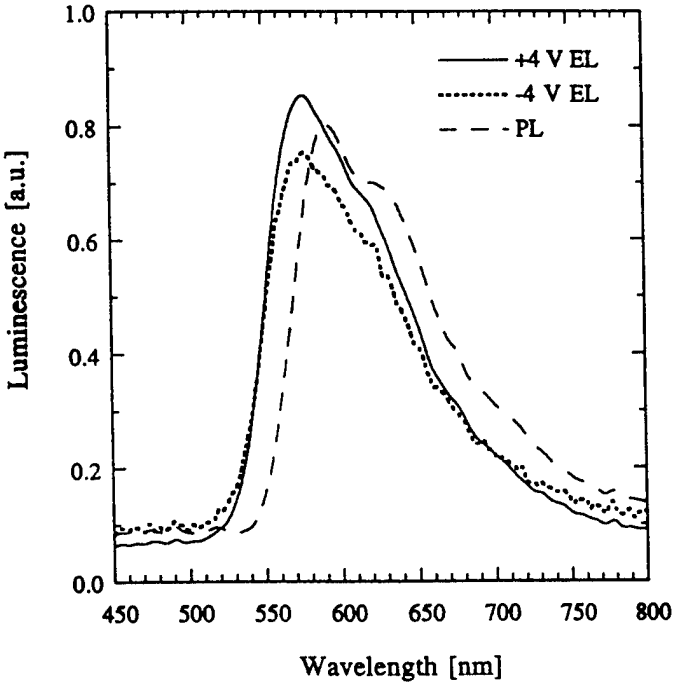

Figure 3: Electroluminescence and photoluminescence spectra of a thin layer of an admixture of MEH-PPV and poly(ethylene oxide) with a lithium salt. The electroluminescence spectrum was generated by incorporation of the layer in an ITO/MEH-PPV + PEO/Al polymer light-emitting electrochemical cell (see text for detailed description).

In addition to the prototype LECs fabricated with MEH-PPV, similar devices, which emitted green and blue light, were fabricated. In all cases, turn-on occurred at a bias voltage approximately equal to the measured optical gap, as expected for a *p-n* light-emitting junction.[9] For these initial devices, the external quantum efficiencies ranged from approximately 0.1% photons *per* electron to approximately 2% photons *per* electron with different materials in the active layer.

LECs have a number of specific and important advantages over the "conventional" polymer light emitting diode:

(i) As *p-n* junctions, they "turn on" at an applied voltage approximately equal to the energy gap, $eV_{on}=E_g$. For visible light emission, V_{on} is always less than 3V.

(ii) Since carrier injection occurs via ohmic contacts into the doped *n*-type and *p*-type regions, respectively, stable metals such as Al, Au, etc. can be used to form these contacts. This is in contrast with the tunnel diode polymer LED,[8] where low work function, reactive metals are needed to achieve efficient electron injection.
(iii) Even more important, there is no need to match the work functions of the anode and cathode to the π and π^* energies of the luminescent polymer, as must be done for the tunnel diode device.[8] Consequently, the same electrode materials can be used for either small gap or wide gap materials, thus promising significant manufacturing advantages for multicolor displays.

The polymer light-emitting electrochemical cell constitutes a radically new approach to the construction of organic light emitting devices; a light-emitting *p-n* junction diode is created *in-situ* through simultaneous *p*-type and *n*-type electrochemical doping of a thin film of conjugated polymer which contains added electrolyte to provide the necessary doping counterions. This novel light-emitting device offers both opportunities and challenges. for example, since the *p-n* junction is created *in-situ*, the thickness (t) of the luminescent polymer layer is less critical than in the conventional polymer LED where the tunneling injection current is exponentially sensitive to the electric field (E); $I \propto \exp[-\kappa/E]=\exp[-\kappa t/V]$ and κ is a constant.[8] Moreover, the use of pre-patterned interdigitated electrodes enables the polymer LEC to be fabricated simply, in a single step, with little sensitivity to film thickness. On the other hand, performance optimization will require the synthesis of novel multi functional polymers; polymers which are semiconductors, which are luminescent, and which simultaneously exhibit high ionic mobility.

Acknowledgment: We thank Dr. F. Klavetter for preparing solutions of MEH-PPV and tetrabutylammonium-doceylbenzenesulfonate, and for discussions of the mechanism of operation of the light-emitting electrochemical cells, and Dr. N. Colaneri for numerous discussions.

References:

1. a) D. MacInnes, M.A. Druy, P.J. Nigrey, D.P. Nairns, A.G. MacDiarmid and A.J. Heeger, Chem. Commun., 318 (1981).
b) P.J. Nigrey, A.G. MacDiarmid, and A.J. Heger, Mol. Cryst. Liq. Cryst. 83, 1341 (1982).
2. J. Chen and A.J. Heeger, Phys. Rev. B, 33, 1 (1986).
3. F. Moraes, J. Chen, T.-C. Chung and A.J. Heeger, Synth. Met. 11, 271 (1985).
4. M. Ozaki, D.L. Peebles, B.R. Weinberger, C.K. Chiang, S.C. Gau, A.J. Heeger and A.G. MacDiarmid, Appl. Phys. Lett. 35, 83 (1979).
5. *Handbook of Conducting Polymers*, ed. by T. Skotheim, (Marcel Dekker, New York, 1986).
6. Q. Pei and F. Klavetter, U.S. Patent Application #08/268763 (June 28, 1994).
7. An alternative model has been proposed by F. Klavetter (to be published).
8. I.D. Parker, J. Appl. Phys. 75, 1656 (1994).
9. S.M. Sze, *Physics of Semiconductor Devices* (Wiley, New York, 1981).

Thursday, September 14, 1995

Organics Towards Devices

ThD 2:15 pm-3:45 pm
Holladay Room

Kenneth D. Singer, *Presider*
Case Western Reserve University

EFFECTS OF DRAWING ON SECOND-ORDER NONLINEAR OPTICAL COEFFICIENTS OF POLED POLYMERS

T. Watanabe, X. T. Tao, M. Nakayama, J. Kim, T. Deguchi and S. Miyata.

Tokyo University of Agriculture and Technology
Koganei-shi Tokyo 184, Japan

TEL 81-423-88-7054

FAX 81-423-86-1084

Introduction

Recently organic nonlinear optical (NLO) materials have been extensively investigated because of their large second-order nonlinear optical coefficients and ultra fast response in the field of optoelectronics[1]. In order to obtain a highly efficient second harmonic generation (SHG), the materials match the phase velocity over the long propagation distance for light at fundamental and harmonic waves. To realize phase-matching, a general technique is using natural birefringence in certain anisotropic crystal to compensate the refractive index dispersions between the fundamental and second harmonic wavelength and fulfill $n\omega = n2\omega$. The advantages of birefringence phase-matching is that one can satisfy this condition relatively easy by rotating the crystal. Recently the bulk-type phase-matched SHG was observed for the first time from poled polymers with large positive birefringence[2]. The conversion efficiency of this SHG device is not enough because of small nonlinear optical coefficients. Large off-diagonal tensor components are required to improve the conversion efficiency of bulk type SHG devices. However the molecular design concept and their assembly to optimize off-diagonal tensor component are not clear. In this presentation, the effects of drawing on second order nonlinear optical coefficients of poled polymers will be discussed using Λ type main chain polymers and a side

chain polymer.

Experimental

The chemical structures of samples used in this experiment are shown in Figure 1. The details of synthetic scheme was described in elsewhere[3]. The origin of nonlinearity for Λ type polymer is based on two dimensional charge transfer[4], whereas the origin of side chain polymer is based on one dimensional charge transfer.

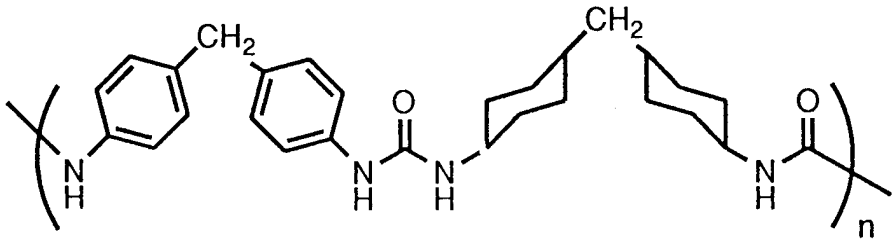

Λ type polymer

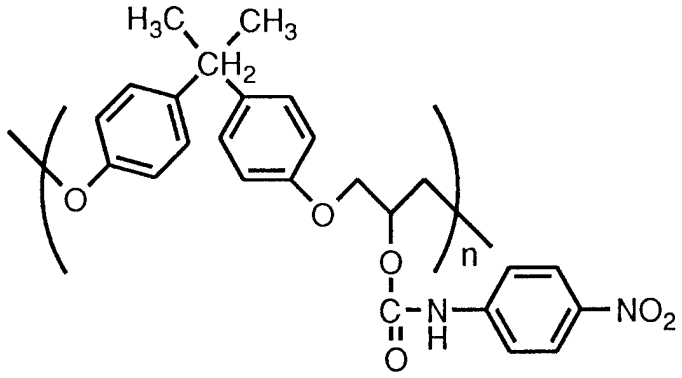

Side chain polymer

Figure 1. Chemical structure of polyurea (Λ shaped polymer) and side chain polymer.

All free standing films were prepared from solvent casting. The film was stretched above their glass transition temperature (Tg) and poled below Tg. Nonlinear optical coefficients of thin films were measured according to the Maker-fringe technique. The refractive index of polymers were determined using prism coupling method. The molecular

hyperpolarizabilities were calculated using MOPAC-PM3 method.

Results and Discussion

Coordinate axes of stretched polymer were defined as follows. The x axis represents the drawing direction and y axis corresponds to perpendicular to the chain. Z is parallel to the poling direction . The point group of stretched and poled films belongs to $2mm$. There are five independent non-zero tensor components. Figure 2. shows the nonlinear optical coefficients of main chain polymer as a function of draw ratio. The ratio of d_{31}/d_{32} for Λ type polymer increases with the draw ratio. In contrast, there is no difference between d_{31} and d_{32} of side chain polymer due to randomly oriented nonlinear optical chromophores except poling direction.

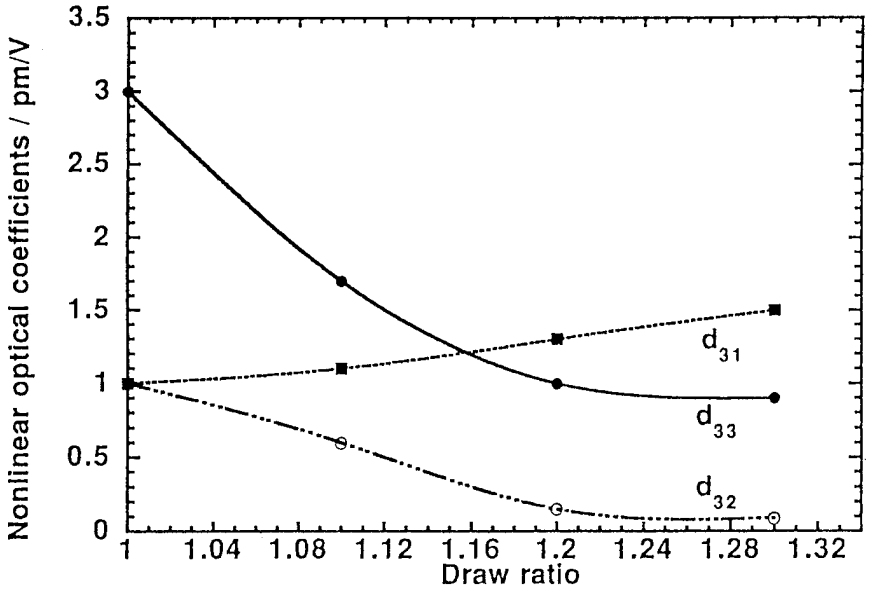

Figure 2. Nonlinear optical coefficients as a function of draw ratio.

Table 1. Molecular hyper polarizability of model compounds of polymer. ($x10^{-30}$ esu); Urea and PCNB are model compounds of main chain and side chain polymer respectively.

Sample	βxxx	βxyy	βxzz
Urea	0.34	-0.62	0.14
PCNB	6.15	-0.65	1.24

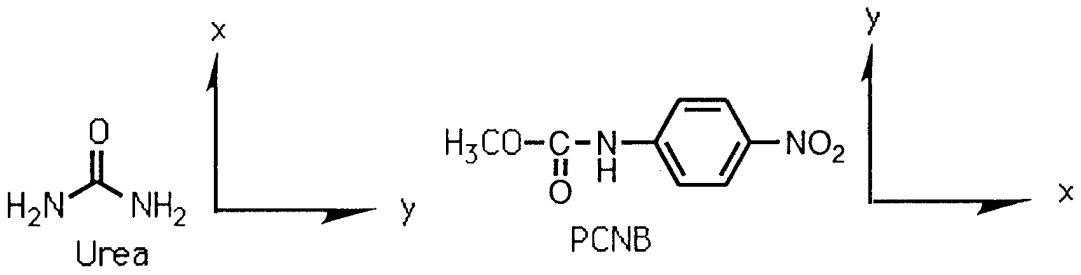

Figure 3. Chemical structure of model compounds.
x and y axes are used as a molecular frame.

Further, tensor ratio of d_{33}/d_{31} for side chain polymer did not vary with drawing whereas d_{31} of main chain polymers became larger than d_{33}. These results suggest that bulk nonlinearity of main chain polymer seems to reflect the orientation of polymer chain. In order to know the origin of bulk nonlinearity molecular hyperpolarizability was calculated using model compounds. The large ratio of d_{31}/d_{32} for Λ type polymer is ascribed to the highly aligned βxyy components which is largest tensor component incorporated to polymer chains.

The tensor ratio, d_{33}/d_{31} of Λ type polymer is found to be in a range not normally achieved in other ordered systems, such as liquid crystals and Langmuir-Blodgett films and suitable for the bulk type phase-matching.

References

1 D. S. Chemla and J. Zyss, *Nonlinear Optical Properties of Organic Molecules and Crystals*, (Academic Press, Inc., Orland, 1987)

2 X. T. Tao, T. Watanabe, D. C. Zou, H. Ukuda and S. Miyata, J. Opt. Soc. Am. B, in press)

3 X. T. Tao, T. Watanabe, D. C. Zou, S. Shimoda, H. Sato and S. Miyata, Macromolecules, **28**, 2637(1995)

4 H. S. Nalwa, T. Watanabe and S. Miyata, Opt. Mater., **2**, 73(1993)

A Study of Neodymium-Chelate-Doped Polymer Waveguides

Sihan Lin, Robert J. Feuerstein, and Alan R. Mickelson

Department of Electrical and Computer Engineering
University of Colorado, Boulder, Colorado 80309-0425
Telephone: (303) 492-1670, Fax: (303) 492-5323

INTRODUCTION

The promise of switched high speed optical interconnects has stimulated research on electro-optic (EO) polymeric devices due to their potentially low cost and the flexibility of fabrication, as well as the possibility of forming multilayer structures [1-3]. As in other integrated optical (IO) devices, loss in polymer devices is a serious issue and a major limitation to the application of IO devices.

By incorporating rare earth (RE) ions into fused silica fibers, glass, and $LiNbO_3$ substrates, low threshold lasers and optical amplifiers have been successfully fabricated [4-6]. Recently, a $NdCl_3$-doped photo-lime-gelatin thin-film optical amplifier has been demonstrated [7]. Such doping provides a solution to the IO loss problem. By pumping devices throughout their active region, one can achieve transparent operation.

Polymer thin film coating allows for the optical channels and devices to be built on top of electrical connections [8]. Electronic packaging polymers such as polyimides have been used for optical devices [3]. The fluorinated polyimides are more suitable for optical applications than the unfluorinated polyimides due to lower optical loss. In addition to the merits of the polyimides, such as high thermal stability and excellent mechanical properties, the fluorinated polyimides are the least moisture sensitive and most optically transparent due to the flouro group moving the electronic absorption bands towards the shorter wavelengths [9]. However, incorporating RE salt ions into such polymers is difficult, if one wants to spin-coat the polymer. This is not necessarily true for chelated versions of the rare-earth ions, since the organic ligand of the chelate allows for some degree of solubility in polymer solvents.

In this paper, we report a study of neodymium (Nd) chelate doping into polymers, and the fabrication of the neodymium chelate doped polyimide waveguides and their photoluminescence.

SOLUBILITY STUDY AND PROCESSING

The doping was implemented by dissolving a chelate into a solvent, and then mixing it with the polymer solution. We used the same solvent for the dopant and the polymer to avoid the complexity of finding solvent combinations to get good spin properties of the solution. The aggregation, or crystallization of the dopant, was examined on a thick film of the doped polymer.

We have studied several optical polymers with different neodymium chelates in variety of solvents. We have used polymethylmethacrylate (PMMA), PMMA/DR1(side-chained), polystyrene, Ultem®(polyimide), and Ultradel® 9000 series (fluorinated polyimides) as host polymers. We have used tris(2,2,6,6,-tetramethy1-3,5-heptanedionato) neodymium (Nd $(TMHD)_3$), Nd hexafluoroacetylacetonate, Nd trifluoroacetylacetonate, and Nd i-propoxide for the active RE dopant. To get good quality spin-coated film, high boiling point solvents were used. We have used anisole, γ-butyrolactone, chlorobenzene, cyclodentanone, dyglyme and toluene. Table I lists some of the results on solubility studies.

The above experiments determined that the best materials for the chelate doped polymer are those of the Ultradel® 9000 series fluorinated polyimides doped with neodymium hexafluoroacetylacetonate chelate in γ-butyrolactone.

The polyimides used in this study were Ultradel® 9020D and ADP 94003 which were commercially available from the Amoco Chemical company. They are fluorinated photosensitive polyimides. The Nd chelate used in the study is shown in Fig. 1, and is commercially available from Strem Chemicals.

Table I. Selective results of chelate doping in polymers

	Nd (TMHD)3	Nd hexafluoroacetylacetonate	Nd trifluoroacetylacetonate
PMMA	aggregation & poor adhesion	aggregation & poor adhesion	aggregation & poor adhesion
Polystyrene	aggregation & poor adhesion	aggregation & poor adhesion	aggregation & poor adhesion
Ultem®	no solvent dissolves both	no solvent dissolves both	no solvent dissolves both
Ultradel® 9000 series	no solvent dissolves both	good solubility & optical quality	no solvent dissolves both

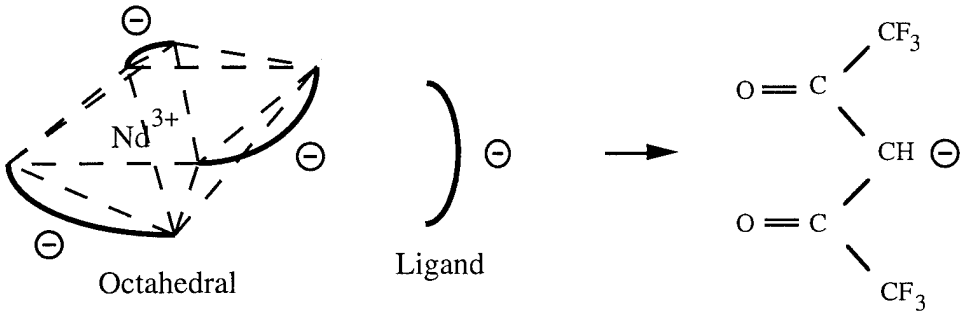

Fig. 1 Neodymium hexafluoroacetylacetonate (Nd $(CF_3COCHCOCF_3)_3$)

The chelate was first dissolved in γ-butyrolactone and then mixed with the polymer solution. The mixed solution was stirred overnight. Filtration was found necessary to reduce the optical loss.

The doped fluorinated polyimide was processed as follows. After spin coating, the film was baked on a hot plate at 100°C for 3 minutes to remove the residue solvent. Then it was exposed under a UV lamp to crosslink the polymer. The dose was about 1 J/cm^2. After exposure it was baked in a nitrogen purged oven at 175 °C for 30 minutes. If a structure was patterned under a UV source, the sample needed to be developed on a spinner head. The developer was sprayed onto the sample while it was spinning at 1000 rpm. However, high temperature processing influences the chelate. Since the chelate has a melting point around 155 °C, sublimation was observed and became noticeable if the processing temperature exceeded 200 °C. The processing temperature has been kept below 200 °C, and the baking time as short as possible to avoid the loss of chelates.

Two configurations of channel waveguides were used in the study. In the first structure, a low index polyimide was spun on a fused quartz substrate. After soft bake the films were exposed to a UV source through a waveguide trench mask. After developing the waveguide trenches were obtained. The doped polyimide with a higher index of refraction filled the trenches by spin coating. An acrylate cladding layer was spun on for the cladding. In the second structure, the doped polyimide film was patterned to the rib waveguides on fused quartz substrate and then it was covered by a UV curable acrylate layer.

The endfaces were prepared by a wafer dicing saw. An adhesion promoter was found essential to achieve good optical quality endfaces since it significantly improved the adhesion between the fused quartz substrate and the polyimide film. The peeling of the film at endfaces during cutting was eliminated. The loss due to the roughness of saw cutting marks was negligible when the spindle speed and the forward cutting speed were properly set.

ABSORPTION AND LUMINESCENCE MEASUREMENTS

The absorption spectrum of the doped polymer thin film has been used to determine the existence of Nd^{3+} ions and therefore has been used as a general technique to evaluate the processing. From the absorption spectra of pre- and post-processed films, one can determine the change of the concentration of Nd^{3+}.

To get enough absorption, the film was prepared with thickness of around 100 μm. The absorption spectrum was measured on a VARIAN CARY-2400 spectrophotometer. Fig. 2 shows the spectrum of doped film after the bake. The corresponding excited state level of each absorption peak is marked next to the peak. There is almost no change in absorption seen between 110 °C soft bake and this data. However, a 50% absorption drop has been observed after 300 °C hard bake.

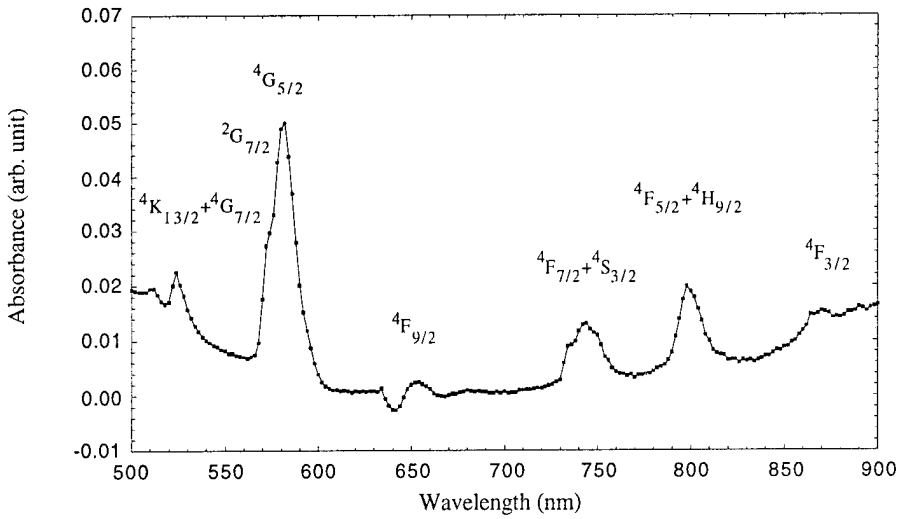

Fig. 2 Absorption spectrum of the Nd chelate doped polyimide after 175 °C bake.

We estimated the ground state absorption crosssection from the insertion loss of the waveguide measured at 799 nm (peak absorption) and 834 nm (background absorption). On samples of $1.0 \times 10^{20}/cm^3$ Nd^{3+} concentration the absorption cross section is measured to be 1.0×10^{-20} cm^2 at 799 nm for the rib waveguides (covered by acrylate cladding) and 4.5×10^{-20} cm^2 for trench waveguides. The low neodymium absorption of the rib waveguides can be explained by the fact that during the processing of the rib waveguides the developer removed most of the chelates since the developer contained the solvent dissolving the chelate.

The photoluminescence (PL) indicates the radiative relaxation transitions of the excited states. We have observed PL on the two channel waveguide structures and on slab waveguides as well. Fig. 3 shows the PL spectrum of a Nd^{3+} doped channel waveguide at 1.058 μm. The PL at 0.9 μm and 1.3 μm was barely detectable.

The lifetime of the metastable state can reveal information such as the quenching due to the interaction of the ions and surroundings. We used a phase-shift method to measure the life time[10] of $^4F_{3/2}$. The measured lifetime was extremely short (< 10 μs) compared to the typical lifetime (> 259 μs) in an inorganic host. The origin of the short lifetime is being studied.

The determination of the precise concentration of the Nd^{3+} and the absorption crosssection are in progress.

A low loss all-polyimide structure can be implemented if we can use more thermally stable chelates. One can choose heavier ligands for the chelate to increase the thermal stability. Therefore, the boiling point can be increased and the sublimation can be suppressed. In this case the polyimides can be processed under higher temperature, and the optical loss due to incomplete removal of the solvent and water in the polymer film can be reduced. Meanwhile the polyimide can be used for the cladding layer without the worry of losing more chelates due to sublimation, boiling, and decomposition.

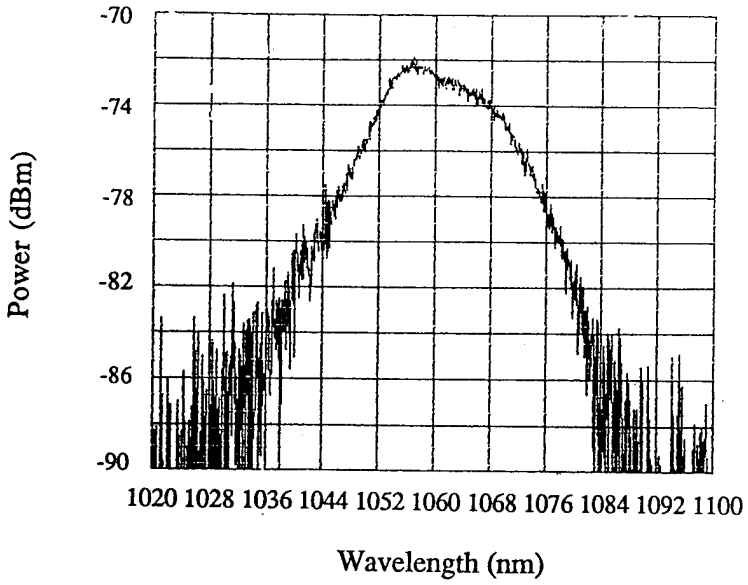

Fig. 3 The $^4F_{3/2}$ PL spectrum of a Nd chelate doped channel waveguide at 1.058 μm. The waveguide was pumped by a 28 mW diode laser at 804 nm.

CONCLUSIONS

We have studied several optical polymers doped with various chelates using different solvents. Only the fluorinated-chelate doped fluorinated-polyimides exhibited good optical quality and PL at 1.06 μm wavelength. The PL signal was weak and the lifetime was short compared with PL of Nd doped inorganic host materials. The doped polymers need to be studied further . This demonstration shows the possibility of lossless polymer optical devices by incorporating an organic version of RE ions into a polymer and pumping it with a low cost laser diode.

REFERENCES

[1] E. van. Tomme, P. P. van.Daele, R. G. Baets and P. E. Lagasse, "Integrated optic devices based on nonlinear optical polymers," *IEEE J. Quantum Electron.*, Vol. 27, pp. 778-787 (1991).

[2] T.A. Tumolillo, Jr. and P. R. Ashley, "Fabrication and design considerations for multilevel active polymer devices," *SPIE* Vol. 2025, pp. 507-515 (1993).

[3] S. Ermer, J. F. Valley, R. Lytel, G. F. Liscomb, T. E. Van Eck, and D. G. Girton, "DCM-polyimide system for triple-stock poled polymer electro-optic devices," *Appl. Phys. Lett.*, Vol. 61, no 19, pp. 2272-2274 (1992).

[4] J. Stone and C. A. Burns, " Neodymium-doped silica lasers in end-pumped fiber geometry," *Appl. Phys. Lett.* Vol. 23, pp. 388-389 (1973).

[5] H. Yajima, S. Kawase, and Y. Sekimoto, "Amplification at 1.06 μm using a Nd: glass thin-film waveguide," *Appl. Phys. Lett.*, Vol. 21, pp. 407-409 (1972).

[6] E. Lallier, J. P. Pocholle, M. Papuchon, M. de Micheli, M. J. Li, Q. He, and D. B. Ostrowsky, C. Grezes-Besset and E. Pelletier, "Nd:MgO:$LiNbO_3$ waveguide laser and amplifier," *Opt. Lett.*, Vol. 15, no. 12, pp. 682-684 (1990).

[7] R. T. Chen, M. Lee, S. Natarajan, C. Lin, Z. Z. Ho, and D. Robinson, "Single-mode Nd^{3+}-doped graded-index polymer waveguide amplifier," *IEEE Photonics Technol. Lett.*, Vol. 5, pp. 1328-1331 (1993).

[8] D. H. Hartman, G. R. Lalk, J. W. Harse, and R. R. Krchnarek , "Radiant curved polymer optical waveguides on printed circuit boards for photonic interconnection use," *Appl. Opt.*, Vol. 28, no. 1, pp. 40-47 (1989).

[9]T. C. Kowalczyk, T. Kosc, K. D. Singer, P. A. Cahill, C. H. Seager, M. B. Meinhardt, A. J. Beuhler, and D.A. Wargowski, "Loss Mechanism in polyimide waveguides," *J. Appl. Phys.*, Vol. 76, no. 4 pp. 2505-2508 (1994).

[10] E.A. Bailey, Jr., and G. K. Follefson, "The determination of the fluorescence lifetimes of dissolved substances by a phase shift method," *J. Chem. Phys.*, Vol. 21, no. 8, pp. 1315-1322 (1953).

Optical Second Harmonic Generations of the Thermotropic Liquid Crystalline Main-Chain Polymer (Aromatic Polyesters)

Tadahiro Asada

Department of Polymer Chemistry, Graduate School of Engineering, Kyoto University, KYOTO, 606 JAPAN
Tel: +81-75-753-5629 Fax: +81-75-751-2769

INTRODUCTION

To improve the stabilities and processabilities, blend or graft polymerization of nonlinear optical organic materials with polymers has been intensively studied by many researchers (1-3). However, it was pointed out that there remain problems in the durability (4). To the contrary, the main-chain type nonlinear optical polymers are expected to be durable and good nonlinear optical materials for various applications, because these materials have been developed to be high performance materials.

Some liquid crystalline polymers were reported to exhibit very large optical nonlinearities (5). The merits of the liquid crystalline polymers for the second harmonic generation are that the molecular structure of a polymer chain is noncentrosymmetric and also they are easily oriented to construct the noncentrosymmetric crystal structure, when they are processed in the liquid crystal state.

The second harmonic generations of the liquid crystalline main-chain type copolymers of 2-hydroxy-6-naphthoic acid (HNA) with 4-hydroxy-benzoic acid (HBA), with various composition ratios were investigated. It

was found that the second harmonic generation of the films was greatly affected not only by polymerization conditions but also the processing conditions of the films. The relationship between structure (molecular and bulk) and second harmonic generation has been studied experimentally (NMR, IR and X-ray diffraction studies) and also molecular simulation method.

EXPERIMENTAL SECTION

The chemical structure of the copolymer synthesized is as follows:

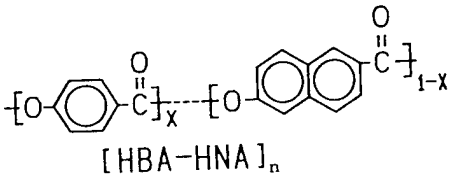

Varieties of copolyesters which have various composition ratios were prepared: the molar ratio of HBA : HNA = (90:10, 80:20, 70:30, 60:40, 50:50, 40:60, 30:70, 20:80, 10:90) etc.

The preparation of these wholly aromatic copolyesters requires a melt condensation of 6-acetoxy-2-naphthoic acid with 4-acetoxy benzoic acid at high temperatures (Ca.360°C) in N_2 atmosphere. The acetic acid was collected during polymerization.

The films of the samples were processed in various conditions, such as in a heating roller extension (Nito HR-3) and instant two-opposite way-extension method (a new technique developed by us).

The second harmonic generation of the samples was evaluated by both the powder (for as polymerized samples) and also Maker Fringe Method (6). Nd: YAG lazer (Spectron, SL401) was used as the light source (wavelength=1064nm). The experimental apparatus for the second harmonic generation measurement has been described previously (7). The second harmonic nonlinear optical coefficient d_{33} of the films were

evaluated by Marker Fringe Method, compared with standard Y-cut quartz d_{11}.

RESULTS AND DISCUSSIONS

Table1 shows the relation between the second harmonic generation intensities measured by the powder method and compositions for the copolyesters.

Table 1 Comparison of the Second Harmonic Generation and Compositions of the Copolyesters

Composition(X)	0.9	0.8	0.7	0.6	0.5	0.4	0.3	0.2
SHG intensities(a.u.)	-	2.0	2.5	2.5	2.0	1.5	-	-

The results shown in Table 1 are rather qualitative, we can know only that which composition is rather active in second harmonic generation.

We obtained nonlinear optical coefficients for film samples. For highly oriented film sample of composition X=0.6, d_{33} Ca. 5pm/V was obtained.

We found, however, the second harmonic generation of samples were completely different from each other, if the polymerization conditions of the polymers were changed, for examples, the evacuation of the gas of acetic acid, the polymerization time etc., even though the components compositions of the sample were the same. Two quite different samples were obtained with the same composition ratio. The IR spectra show no apparent difference between them. The difference, however, is seen on the X-ray diagrams as shown in Fig.1. From Table 1 and Fig. 1, it is apparent that the activity of the second harmonic generations of the copolyesters depends on the compositions of the sample and also the crystal structure of the sample, which is considered to be affected by the distribution manner of the components.

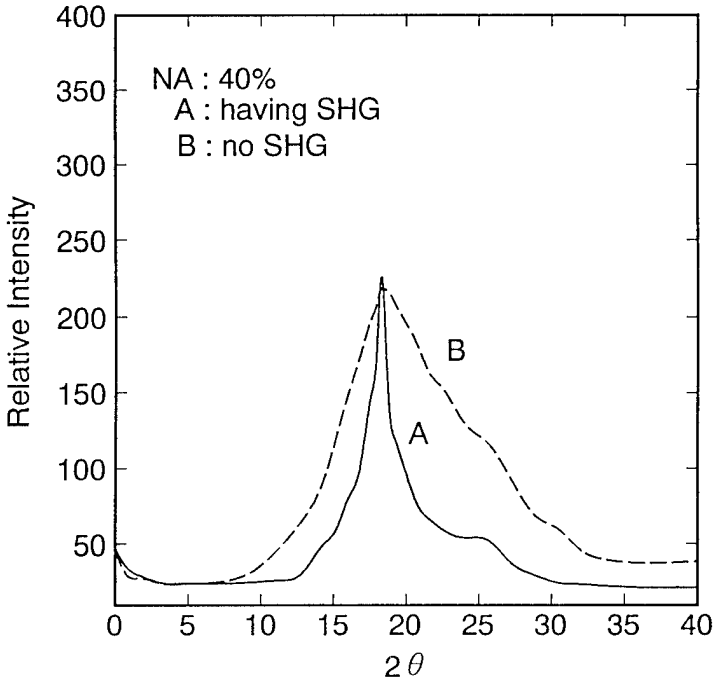

Fig. 1. X-ray diffraction diagrams for the samples (X=0.4) and SHG

We calculated hyperpolarizability (β) for molecular simulation models by Molecular Orbital Method. The results tells that the composition distribution and conformation also change greatly the amount of β values.

REFERENCES

1) K. D. Singer,M. G. Kuzyk,and J. E. Sohn, J. Opt. Soc. Am., B4, 968(1987).

2) H. Nakanishi, Solid Physics, 24, 873(1989).

3) J. D. Makanzie, C. Y. Li, and Y. Xu, Chem. Express, 6, 903(1991).

4) S. Umegaki, Sen-i Gakkai Preprints, G-123(1994).

5) G. R. Meredith, J. G. Vanadusen, and D. J. Williams, "Nonlinear Optical Properties of Organic and Polymeric Materials", ACS Symposium Series, 109(1983).

6) J. Jerphagonon and S. K. Kurts, J. Appl. Phys., 41, 1667(1987).

7) T. Asada, Mol. Cryst. Liq. Cryst., 254, 125(1994).

Diagnostics of femtosecond laser pulses using films of poly(p-phenylenevinylene) (PPV) .

B. Luther-Davies, M. Samoc, A. Samoc, M. Woodruff,
Laser Physics Centre, Australian National University, Canberra, ACT 0200, tel (06)2490031, FAX: (06)2490029
J.Swiatkiewicz, Photonics Research Laboratory, State University of New York at Buffalo, NY 14260
R. Trebino , K.W. Delong, Sandia National Laboratories, Livermore, California 94551

Poly(p-phenylenevinylene), abbreviated PPV, is a conjugated polymer having a very high third-order optical nonlinearity which we are investigating for possible use in ultrafast photonic switching at 800 nm [1]. A result from these investigations is that PPV can be very useful as an active material in devices used to diagnose very short laser pulses.

One example of such a use of PPV is a simple single-shot autocorrelator which uses two-photon induced fluorescence. Since the two-photon absorption coefficient of PPV at 800 nm is very high (reaching 80 cm/GW) [1] and the fluorescence is efficient, autocorrelation can readily be observed both with a mode-locked train from a femtosecond Ti-sapphire laser and with low repetition rate amplified pulses from a regenerative Ti-sapphire amplifier using the geometry shown in figure 1.

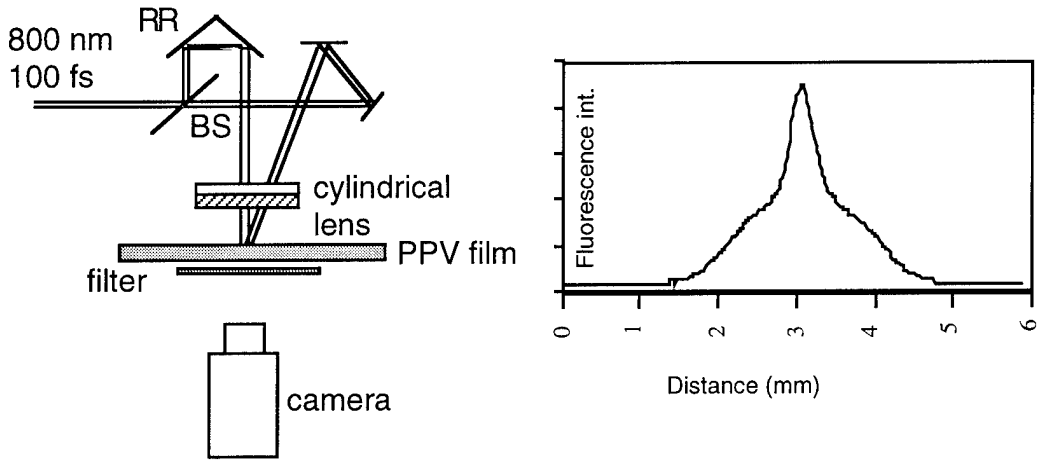

Fig.1 A scheme of a single-shot autocorrelator and a trace showing an autocorrelation signal superimposed on a two-photon fluorescence profile observed with a CCD camera using a thin PPV film. The autocorrelation pulse width is about 150 fs.

More quantitative intensity autocorrelation data can be obtained by monitoring the intensity of the self diffracted signal as a function of delay between two pulses crossing in a PPV film about 1 μm thick in the geometry shown in figure 2. The very high nonlinearity of PPV ($n_2 \approx 1 \times 10^{-11}$ cm^2/W) [1] also permits a more sophisticated diagnostic technique: frequency resolved optical gating (FROG) [2]. Here frequency resolution is included and the full information on the laser pulse properties can be extracted from measurement of the frequency spectrum as a function of time using the same self-diffraction geometry (figure 2).

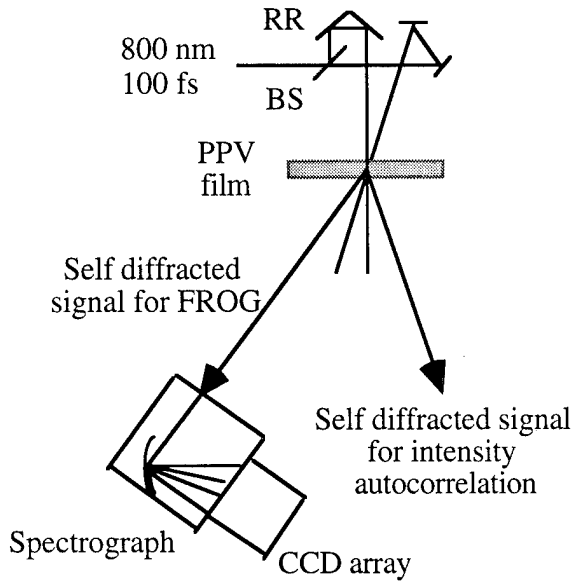

Fig. 2 Multiple-shot intensity autocorrelation or FROG signals can be recorded using self-diffracted beams from a PPV film . For FROG the emission is dispersed by a spectrograph. and the spectra recorded as a function of the delay of one of the beams (varied by scanning the retro reflector, RR ,position)

FROG data can be converted into information on the phase and amplitude of the laser pulse using techniques described in [2]. Single shot measurements can also be performed and these are especially useful for "live" monitoring of the pulse properties. For single shot recording the beams are focussed with a cylindrical lens into the sample as in Fig.1, and the self-diffracted signal is imaged through the spectrograph onto a CCD camera so that frequency and time axes are orthogonal. FROG traces could be obtained in this single-pulse geometry at pulse energies as low as a few tenths of a microjoule with the pulse width of 100 femtoseconds using a sub-micron thick PPV film.

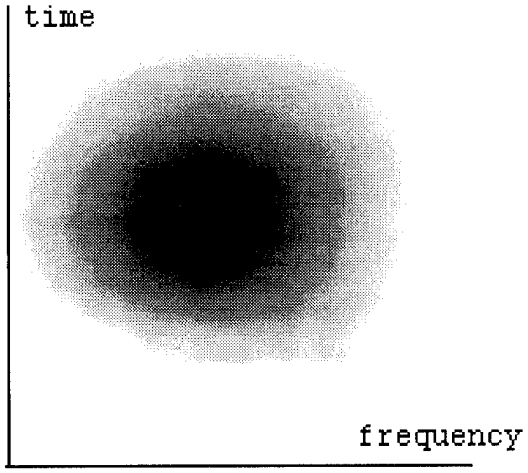

Fig.3 An example of a 2D FROG profile obtained in a multiple shot experiment. Relatively symmetric shape of the intensity map is an indication of good quality of the pulse. The pulse parameters obtained from this scan are: autocorrelation half width=241 fs, spectral halfwidth=3.98 nm

References

1. A. Samoc, M. Samoc, B. Luther-Davies and M. Woodruff, Optics Letters, in press
2. D.J. Kane and R. Trebino, Optics Letters, 18, 823 (1993); R. Trebino and D.J. Kane, J.Opt.Soc.Am. A10, 1101 (1993)

This research has been carried out on behalf of the Harry Triguboff AM Research Syndicate

Polarized Electroluminescence in Liquid Crystalline Main Chain Polymers Containing Arylene Vinylene Units

R. Festag, A. Greiner, G. Lüssem, C. Schmidt, V. Stümpflen, J.H. Wendorff

Institute for Physical Chemistry and Center for Materials Science
Philipps University Marburg
35032 Marburg
Germany

FAX: +49 6421 288916 Tel.: +49 6421 285964

Polymers carrying arylene vinylene units have recently met with great interest because of their potential use in light emitting diodes (LED). This contribution is concerned with the combination of the electroluminescence properties characteristic of arylene vinylene polymers with the peculiar order characteristic of the liquid crystalline state within one material. New possibilities for manufacturing and applications of such materials are envisioned to result. The concept is to exploit the self-organization taking place in liquid crystalline material and the strong coupling of the orientational order to substrate effects and external fields in order to control the state of orientation of the chromophores and thus the polarization of the emitted light as well as its spatial distribution. The arylene vinylene units are incorporated for this end into a chain backbone and they are separated along the backbone by flexible spacers. Such polymers can be expected to display a glassy state, good processing characteristics and a long term stability of films manufactured from it. Such films are not necessarily liquid crystalline and soluble.

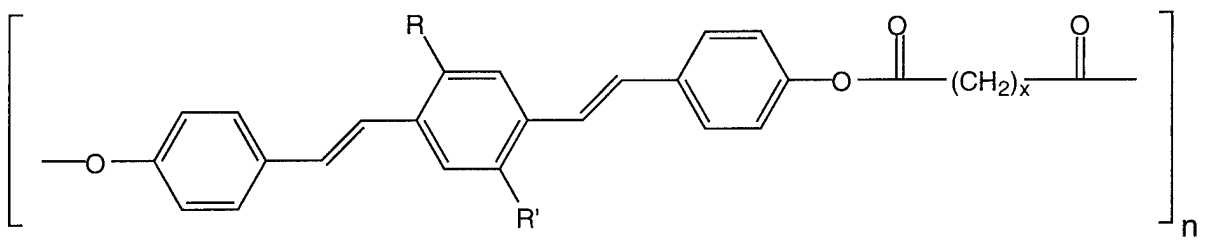

Fig. 1: Chemical structure of the main chain polymers

We were able to obtain soluble and liquid crystalline main chain polymers by attaching lateral subsitutents. The number, the size and the polarity of the substitutents were varied. The arylene vinylene units are separated via spacers of different length in order to control the mesophase range and the glass transition temperature (see Fig. 1).

The bilaterally substituted compounds were found to display no mesophase, but the compounds substituted only in the 2-position exhibit a mesophase in a broad range independent of the polarity of the substituent (see Tab. 1, for the case of the compounds with spacer length x=8). A remarkable stabilization of the mesophase takes place if dipolar groups are used as lateral substitutents. The compound with the CF_3 substitutent shows no crosslinking of the arylene vinylene units in the anisotropic phase at 260°C even after several hours. The very high clearing temperatures and the absence of crosslinking makes this compounds a promising material for high performance applications.

Substitutents	T_G	T_{Cl}
R = Phenyl, R' = H	84	166
R = NO_2, R' = H	60	305 (decomp.)
R = CF_3, R' = H	57	295
R = R' = CH_3	63	--

Tab. 1: Transitions temperatures [°C] for the compounds with spacer length x=8 and different subsitutents

The mesophase structure was characterized by X-ray scattering. The investigations were performed both on drawn fibers and on the isotropic material in the glassy state. We will discuss, in the following, the results obtained for the compound with x=10 and the phenyl substitutent as an example (T_G=77°C, T_{Cl}=179°C).

The fiber diagram (see Fig. 2a) shows the amorphous halo located on the equator and the layer reflections perpendicular to it along the meridian i.e. along the drawing direction. The narrow azimutal width of the reflections have to be taken as an indication of a high orientational order in the fibers. The diagram displays, however, not all reflections for experimental reasons. Additional information is available from

small angle scattering experiments on an oriented fiber. The scattering diagram (Fig. 2b) shows the presence of three distinct reflections. They can be attributed to a layer structure and be indexed as (100), (200), (300). The wide angle X-ray diagram reveals an amorphous halo. The structure displayed by the arylene vinylene polymers corresponds thus to a smectic A phase. Similar results were obtained for all compounds independent of the lateral substituent.

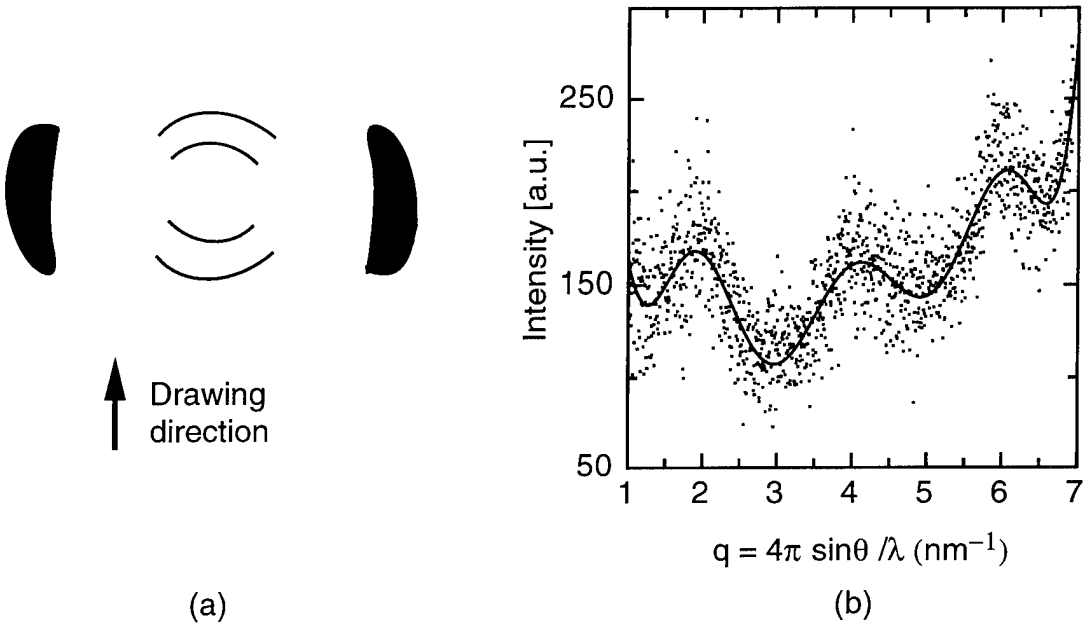

Fig. 2: a) Schematic representation of the flat camera X-ray diagram for a drawn fiber (diagram displays the (300) and (400) layer reflections)
b) SAXS-diagram of a drawn fiber

In order to make use of the distinct properties of these materials and to investigate their principle aptitude for electroluminescent applications we oriented a thin film of the polymer macroscopically by mechanical deformation within the mesophase. The film was subsequently cooled down into the glassy state. An estimate of the achieved degree of orientation was obtained by measuring the UV-dichroism of the sample (Fig. 3). The absorption of the system turned out to large along the direction of the mechanical deformation and small perpendicular to it. The transition dipole moment of the chromophores is thus oriented predominantly along the deformation direction.

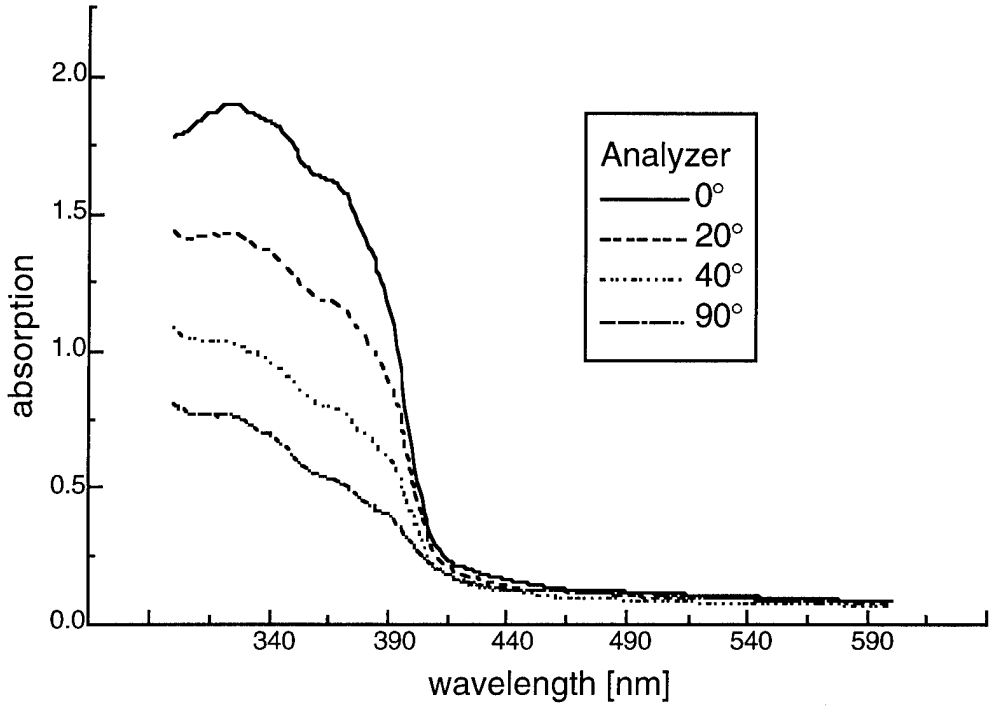

Fig. 3: Absorption of incoming light by an orientated sample vs. wavelength for different positions of the analyzer in relation to the direction of deformation

Depending on spacer length, a macroscopic order parameter in the range between 0.2-0.4 was extracted. Preliminary results of investigations on the polarized fluorescence emission of these systems seem to confirm the results of the UV-dichroitic studies.

In conclusion, we have shown that the new liquid crystalline arylene vinylene polymers are thermally stable, soluble, possess a broad liquid crystalline phase and can be oriented macroscopically quite easily. These systems exhibit a polarized emission in LED-applications.

Thursday, September 14, 1995

Processing

ThE 4:15 pm-5:45 pm
Holladay Room

Hilary Lackritz, *Presider*
Purdue University

Optically initiated orientation of nonlinear photoisomers

R. A. Hill and A. Knoesen
Department of Electrical and Computer Engineering
University of California, Davis, CA 95616
(916) 752-8023 phone
(916 752-8428 fax

D. R. Yankelevich
Centro de Investigación Científica y de Educación Superior de Ensenada
Departamento de Física Aplicada, Ensenada, Mexico 22860

R. Twieg
IBM Almaden Research Center
San Jose, CA 95120

Second order nonlinearities can be imposed in a disordered polymer film by poling. Electric field poling is the most common technique but poling can also be achieved optically. In optical poling, a sample is irradiated with linearly polarized light and the nonlinear molecules undergo successive isomerizations, contractions and relaxations and eventually become aligned perpendicular to the incident polarization.[1] This photoisomerization can also increase the mobility of the nonlinear molecules within the polymer and permit improved alignment to an electric field.[2] The previous reports of optically induced reorientation have used continuous-wave illumination and required long exposure times.[3-11] However, the trans-cis photoisomerization has been shown to be extremely fast.[12] We are investigating the dynamics of the trans-cis isomerization and orientation of nonlinear stilbene molecules in the presence of an electric field by monitoring the changes in the second order nonlinearity. In our research we have used short optical pulses to initiate molecular reorientation by photoisomerization. The unstable cis-isomer of azobenzene is used to enable a transition between two states which both involve the stable trans-isomer. Because of the extreme speed with which the photoisomerization can be initiated, it could find an application in digital optical storage.

An explanation of an alignment cycle is illustrated in Figure 1. In the initial steady state, the molecules are locked into a given orientation by the local polymer environment. Upon isomerization to the cis-isomer, the molecules are able to move within that environment due to the contracted size of the cis-isomer. The molecules will then slowly relax back to the trans-isomer. The oriented state is generated by applying an electric field to the material while the mobility of the molecules in the polymer environment is increased. The applied field will orient the molecules and, upon relaxation to the trans-isomer, they will once again become locked into the local polymer environment. Once locked into the local environment, the applied field can be removed and the molecules will remain aligned for months. This oriented state can be read by using a second harmonic generation (SHG) probe. A randomization cycle follows a similar sequence but without the applied electric field. In this case, once the mobility of the molecules has been increased by photoisomerization, the molecules are allowed to randomly reorient within the polymer. Once the molecules relax back to the trans-isomer, they will become locked into this random orientation. Due to the random orientation, no signal will be detected by the SHG probe used to read the state of alignment.

Initial experiments have been performed using a sidechain polymer which is a poly(methyl methacrylate) backbone onto which a pseudo-stilbene Disperse Red 1 is attached.[13] In these experiments, the photoisomerization was performed with ~10 nanosecond pulses centered at 532 nm, generated by a doubled Q-switched Nd:YAG laser. The recorded state was read by second harmonic generation using an *in situ* probe. These initial experiments indicated that in addition to the photoisomerization effect, some thermal energy is necessary to complete a change of state. This was most noticeable during a randomization cycle. It was found that approximately five times as much energy was required for randomization than for alignment. Work is continuing to further quantify this effect and to investigate the dynamics in other nonlinear materials.

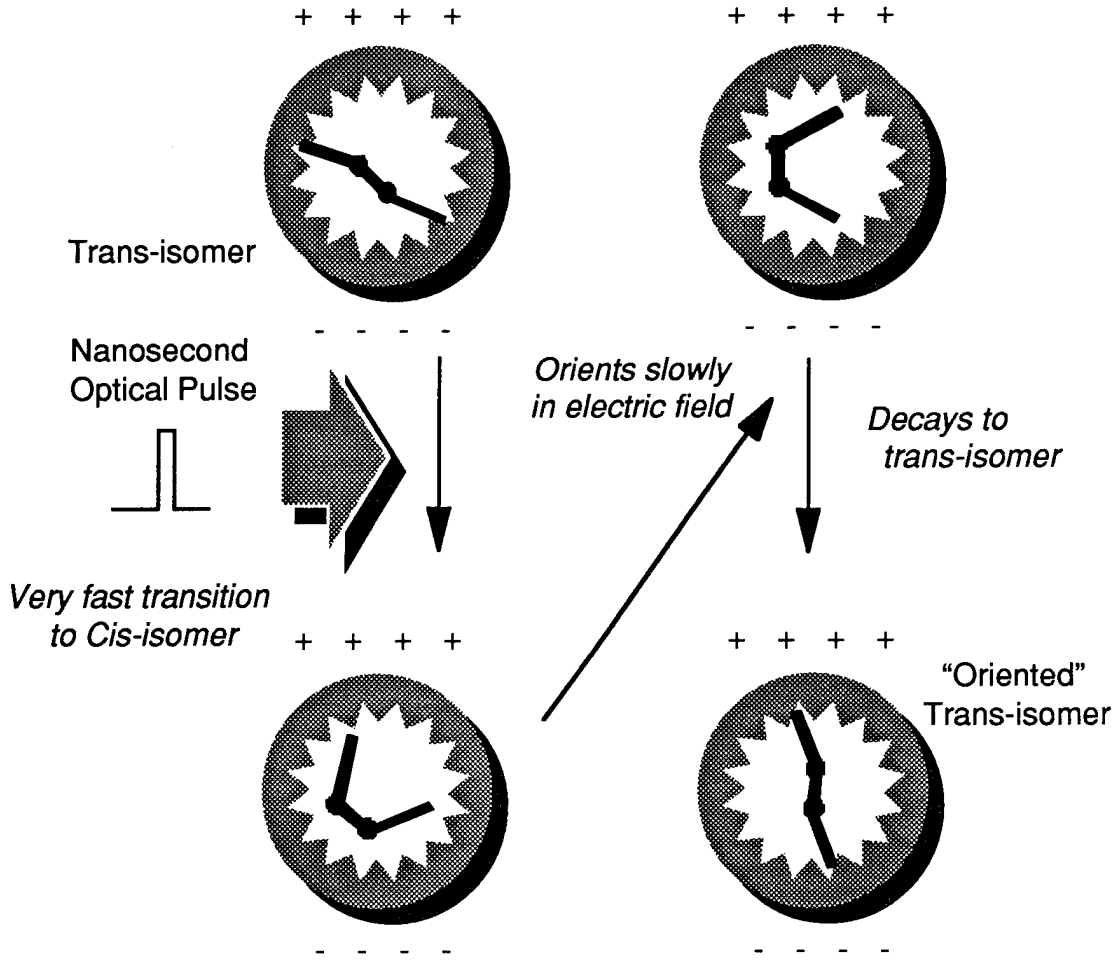

Figure 1. Optically initiated molecular alignment. In the presence of an electric field, a short optical pulse photoisomerizes the molecules. These cis-isomers have increased mobility in the polymer and are able to align with the applied electric field during relaxation back to the stable trans-isomer. After relaxation, the molecules are once again locked into the local polymer environment and the field can be removed.

REFERENCES

1. A. Natansohn, S. Xie, and P. Rochon, Macromol., **25**, 5531 (1992).
2. A. Petri, S. Kummer, H. Anneser, F. Feiner, and Ch. Bräuchle, Ber. Bunsenges. Phys. Chem., **97**, 1281 (1993).
3. T. Todorov, L. Nikolova, and N. Tomova, Appl. Opt., **23**, 4309 (1984).
4. M. Eich and J. Wendorff, J. Opt. Soc. Am. B, **7**, 1428 (1990) and references therein.
5. Z. Sekkat and M. Dumont, Appl. Phys. B, **53**, 121 (1991).
6. P. Rochon, J. Gosselin, A. Natansohn, and S. Xie, Appl. Phys. Lett., **60**, 4 (1992).
7. Z. Sekkat and M. Dumont, Appl. Phys. B, **54**, 486 (1992).
8. Z. Sekkat, D. Morichère, M. Dumont, R. Loucif-Saïbi, and J. A. Delaire, J. Appl. Phys., **71**, 1543 (1992).

9. Z. Sekkat and M. Dumont, Mol. Cryst. Liq. Cryt. Sci. Technol. - Sec. B: Nonlinear Optics, **2**, 359 (1992).
10. R. Loucif-Saïbi, K. Nakatani, J. A. Delaire, M. Dumont, and Z. Sekkat, Chem. Mater., **5**, 229 (1993).
11. F. Chaput, D. Riehl, Y. Lévy, and J.-P. Boilot, Chem. Mater., **5**, 589 (1993).
12 R. J. Sension, S. T. Repinec, A. Z. Szarka, and R. M. Hochstrasser, J. Chem. Phys., **98**, 6291 (1993) and references therein.
13. R. A. Hill, S. Dreher, A. Knoesen, and D. R. Yankelevich, Appl. Phys. Lett. **66**, (1995).

Electro-optic And Second Harmonic Generation Studies Of Dye-Doped Polymers

Fassil Ghebremichael and Hilary S. Lackritz
Purdue University
School of Chemical Engineering
West Lafayette, IN 47907-1283
Phone: (317) 494-4065
FAX: (317) 494-0805

I. INTRODUCTION

The linear electro-optic (EO) effect, in conjunction with second harmonic generation (SHG) has been used to study temperature and electric field effects on dye-doped guest-host systems. An interferometric technique with *in-situ* poling was used to probe the poling field-induced molecular alignment of the chromophores as a function of temperature. The doped polymer systems were thin films of 4-dimethylamino-4'-nitrostilbene or disperse red 1 chromophores doped into poly(methyl methacrylate). For small poling fields, this technique revealed the linear dependency of the electro-optic-coefficient, r, and thus the second order susceptibility $\chi^{(2)}$ of the material, on low poling fields. It was also possible to detect the β-relaxation, the secondary transition occurring below the glass transition temperature, which until now has not easily been seen in studies using optical techniques.

II. EXPERIMENT

The dye-doped system was PMMA and 1% wt., 2% wt. and 4 % wt. 4-dimethylamino-4'-nitrostilbene (DANS) or 10% wt. disperse red 1 (DR1) in chloroform at a solids:solvent ratio of 15:85. Films were then prepared by spin coating the solutions on 1" x 2" indium tin oxide (ITO) coated glass substrate pieces. Two such films were then joined resulting in an ITO-film-ITO sandwich configuration of about 5 μm thickness.

The EO experimental set-up was a Mach-Zehnder interferometer with one of its arms consisting of the film mounted on a heating block as shown in Fig. 1. It was necessary to incorporate an electronic feed-back system to compensate for the large thermal drifts caused by the heating of the sample-mount block. The electronics of the feedback system did not adjust for the high frequency modulated electro-optic effect.

The output of the interferometer shown in Fig. 1 may be written as

$$I_\Omega(t,\theta) = I_1 + I_2 + 2\sqrt{I_1 I_2}\cos\left[\phi(\theta) + \phi_\Omega(t)\right], \text{ with } \phi(\theta) = \phi_2 - \phi_1(\theta). \qquad (1)$$

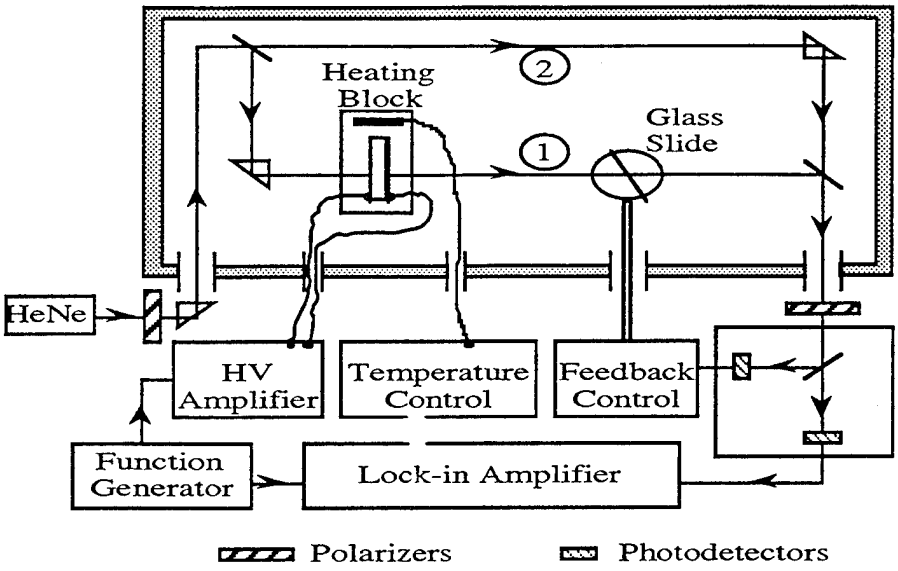

Figure 1. Electrooptic set-up

For an s-s polarization, the modulation phase, $\phi_\Omega(t)$, is given by[1]

$$\phi_\Omega(t) = \frac{\pi n^3 r_{113}}{\lambda} V_\Omega(t), \qquad (2)$$

where r_{113} is the EO coefficient which is proportional to the second order susceptibility, $\chi^{(2)}_{113}$, V is the modulation voltage at frequency Ω (=1KHz), and n is the index of refraction at V= 0.

When $V_\Omega(t)$ in Eq. (2) is a saw-tooth function, the fundamental Fourier component of Eq. (1), which the lock-in amplifier was set to measure is

$$I_\xi(\theta) = 2I_0 \frac{|\sin\xi|}{|\pi^2 - \xi^2|} \sqrt{\xi^2 \cos^2[\phi(\theta)] + \pi^2 \sin^2[\phi(\theta)]}\,, \text{ with } \xi = \frac{\pi n^3 r_{113} V_0}{2\lambda}. \qquad (3)$$

III. RESULTS AND DISCUSSIONS

The dependence of the intensity of Eq. (3) on $\phi(\theta)$ is shown in Fig 2. The reference output signal was used to control the feed-back system for maximum interferometer sensitivity.

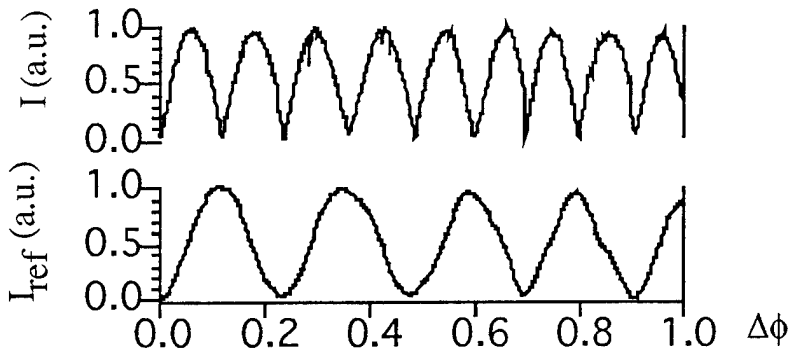

Figure 2. Determination of the interferometer sensitivity.

The cusp associated to the absolute value sign in Eq. (3) is evident from the lock-in amplifier output intensity, Fig. 2. By detecting the EO effect at several amplitudes of the ac fields and fitting the result to Eq. (3) significantly minimized the measurement errors due to RF pick-up and thermal fluctuations. Figure 3 shows the linear dependence of the second order susceptibility on small applied fields, vdc.

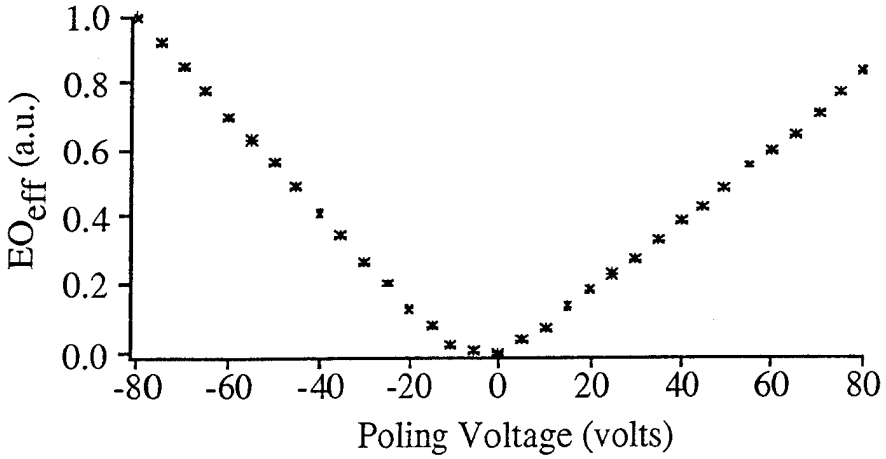

Figure 3. Poling field dependence of the effective electro-optic coefficient.

Figure 4 shows typical data with a large increase at T_g (≈98 °C) followed by a pronounced peak, and it also shows a smaller secondary peak at about 70 °C. The secondary peak in the EO signal is attributed to the β-transition of the polymer. The physical significance of the data can be derived from the models for doped polymer systems by Liu *et al.*, where the chromophore relaxation is described by rotational Brownian motion[2] or Kuzyk *et al.* in which the mobility parameter is a function of the elasticity of the polymer matrix.[3] As the polymer becomes soft near or above T_g, the order parameter increases resulting in a better molecular alignment, thus a higher second order parameter and consequently a higher EO coefficient.

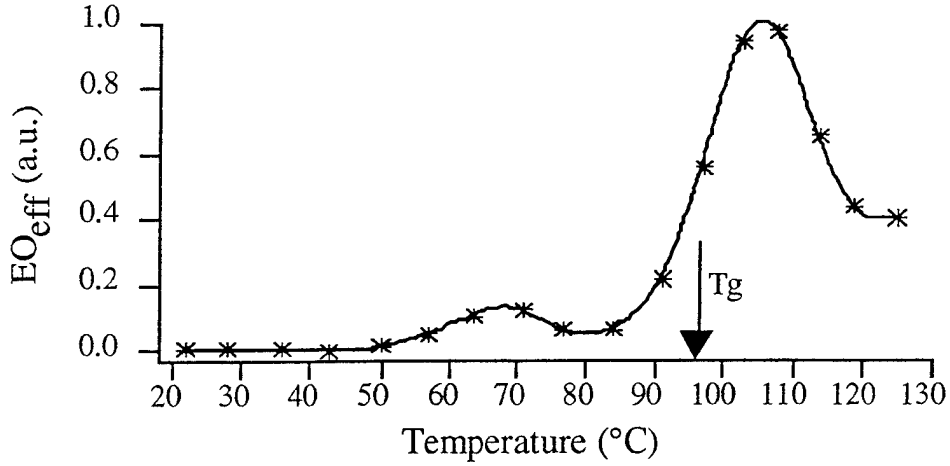

Figure 4. Temperature dependence of the effective electro-optic coefficient.

The first sub-T_g phase transition, the β-transition has been seen in studies of thermal stimulated discharge, dielectric relaxation, and dynamic mechanical analysis experiments.[4] The presence of the secondary relaxation has also been speculated based upon second harmonic generation data.[5] The α- and β-transitions do not have the same relaxation times, thus have different resonant frequencies. As long as the modulation frequency is far from the respective resonant frequencies, the amplitudes of the peaks can be used to deduce the relative contributions of the two transitions to the chromophores mobility.

IV. CONCLUSION

With this novel technique incorporating *in-situ* poling, it was possible to study the electro-optic effect as a function of temperature and poling field. It was shown that for poling fields to about ± 20 MV/m, the EO coefficient depended linearly on the applied field. The feed-back system incorporated in the set-up helped with the drifts due to large induced thermal variations and also with the subtle temporal drifts that plague almost all interferometers. The regulation of the interferometer intensity fluctuations to less than 0.5% for relatively long times contributed significantly to the successful reproducibility of experiments. This technique has displayed its versatility in measuring the EO effect as a function of several parameters in one experimental set-up. It was shown how this technique encompasses several experiments, by comparing the results to several independent and dispersed works. It has also been demonstrated for the first time that optics may be used to study the thermal and temporal characteristics of the secondary mechanical relaxation of the polymer system. It is important to understand all the mechanical, thermal and temporal behaviors of these device oriented polymer systems before they can actually be commercially presented.

V. REFERENCE

1. B. E. A. Saleh, and M. C. Teich, Fundamentals of Photonics, John Wiley and Sons, Inc. New York (1991).
2. Lee-Yin Liu, D. Ramkrishna, and H. Lackritz, *Macromolecules,* **27** (21), 5987 (1994).
3. M. G. Kuzyk, R. C. Moore, and L. A. King, J. Opt. Soc. Am. **B7**, 64 (1990).
4. N. G. McCrum, B. B. Read, and G. Williams, Anelastic and Dielectric Effects in Polymeric Solids, Wiley, London (1967).
5. F. Ghebremichael, M. G. Kuzyk, and C. W. Dirk, Nonlinear Optics **6**, 123 (1994);

Relaxation Processes in Nonlinear Optical Side-Chain Polyimide Polymers

P.G. Kaatz, Ph. Prêtre, U. Meier, U Stalder and P. Günter
Nonlinear Optics Laboratory, Institute of Quantum Electronics
ETH Hönggerberg, CH-8093 Zürich, Switzerland, Phone +41-1-633 31 66, Fax +41-1-633 10 56

B. Zysset, M. Stähelin, M. Ahlheim, and F. Lehr
SANDOZ Optoelectronics Research, SANDOZ Huningue SA
Avenue de Bâle, F-68330 Huningue, France Phone + 33-89-69 61 74

1. Introduction

Optical, nonlinear optical and electro-optic properties of modified side-chain polyimide polymers as shown in Fig. 1 have been determined. Relaxation processes in these nonlinear optical (NLO) polymers are of considerable interest for obtaining a better understanding of the long-term stability of potential devices fabricated from these materials. The relaxation mechanisms of the side-chain chromophores have been investigated above and below the glass transition by second-harmonic decay, dielectric relaxation and differential scanning calorimetry measurements. We find that the time-temperature relaxation behavior of the NLO chromophores in a variety of polymer systems can be understood in terms of current phenomenological descriptions of the glass transition with the aid of a scaling relation.

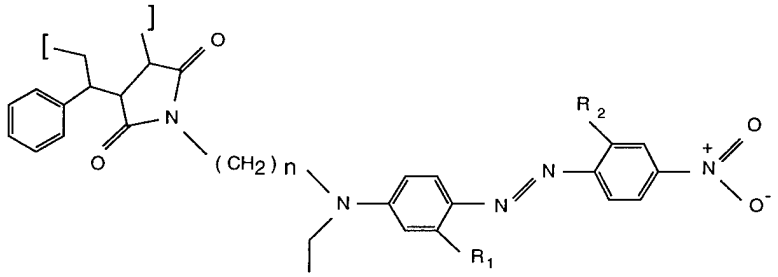

Polymer	n	R_1	R_2	Tg [°C]
A-095.11	3	CH_3	H	137
A-097.07	3	CH_3	Cl	149
A-148.02	2	H	H	172

Fig.1: Modified NLO side-chain polyimide polymers. The alkyl amino functionalized NLO azo chromophores with the various substitution patterns were attached via a two or three carbon spacer linkage to an alternating styrene-maleic-anhydride copolymer.[1]

2. Optical and Nonlinear Optical Properties of the NLO Polymers

The optical and nonlinear optical properties of the NLO polymers investigated in this study are given in the following table. Detailed results can be found elsewhere.[2]

Polymer	A-095.11	A-097.07	A-148.02	Poling field
λ_0 [nm]	491	510	470	
n @ 633 nm	1.84 ± 0.01	1.89 ± 0.01	1.80 ± 0.01	
n @ 1313 nm	1.65 ± 0.01	1.67 ± 0.01	1.66 ± 0.01	
d_{31} @ 1338 nm [pm/V]	23 ± 3	23 ± 7	19 ± 5	corona
r_{13} @ 1313 nm [pm/V]	6.7± 0.4	2.3 ± 0.2	6.5 ± 0.3	150 V/µm

The optical properties were determined by transmission spectroscopy[3], NLO data were obtained with a standard Maker Fringe technique[4] and electro-optic coefficient were measured either in an interferometric[5] or an ellipsometric configuration[6].

3. Modeling Structural Relaxation in Polymeric Glasses

A useful functional representation for describing the non-exponentiality of structural relaxations in polymeric glasses in the time domain is the stretched exponential or Kohlrausch-Williams-Watts[7] (KWW) function

$$\phi(t) = exp\,-(t/\tau)^b\ , \tag{1}$$

with $0 < b \leq 1$. The issue of nonlinearity of structural relaxations was addressed by Tool by introducing the concept of fictive temperature, T_f which describes the influence of the actual structure of a glass on the relaxation time τ. A calculation procedure for T_f was introduced by Narayanaswamy[8] and further developed by Moynihan.[9]

The structural relaxation time of polymeric liquids, as interpreted by DiMarzio and Gibbs[10] involves the cooperative rearrangement of a number of molecular segments of the polymer molecule. Adams and Gibbs[11] subsequently obtained an expression for the structural relaxation time in terms of the configurational entropy S_c. Hodge has shown that the following expression can be derived for the relaxation time associated with the cooperative chain rearrangements:[12]

$$\tau = A\,exp\left(\frac{B}{T(1-T_2/T_f)}\right) \tag{2}$$

where $B{\cdot}R$ is an activation energy with R the gas constant, T is the temperature, and A is a time parameter. We assume that the temperature T_2 in this formulation is equivalent to the "Kauzmann temperature",[13] T_K, which is described by $S_c = 0$.

Extended DSC (Differential Scanning Calorimetry) measurements of the polyimide NLO polymers indicate the following correlation between the parameters A, B, and T_2 :[14]

$$A = \tau_g\ exp\left(\frac{-B}{T_g - T_2}\right) \tag{3}$$

with τ_g the relaxation time at T_g, typically in the range of 10 - 100 s.

Above the glass transition the polymer system is in thermal equilibrium and therefore, T_f equals T. Together with the replacement of A in Eq. (2) this yields the functional form of the Vogel-Fulcher (VF) equation for the normalized relaxation time $\tau_n = \tau / \tau_g$:

$$ln\ \tau_n = -\frac{B}{T_g - T_2} + \frac{B}{T - T_2}. \tag{4}$$

Below the glass transition T_f reaches a final limiting value in simple cooling processes, i.e. without sub-T_g annealing. Assuming the final fictive temperature to be T_g, we obtain the following temperature dependence of the normalized relaxation time;

$$ln\ \tau_n \approx \frac{B}{T_g - T_2}\frac{T_g - T}{T} = 2.303 C_1^g \frac{T_g - T}{T}\ . \tag{5}$$

This result indicates that the primary or α-relaxation processes should have an Arrhenius temperature dependence below the glass transition. In addition, from the "universality" of the Williams-Landel-Ferry[15] (WLF) parameter C_1^g, one might expect normalized relaxation times to scale with the scaling parameter $(T_g - T)/T$, at least in the same class of glass forming liquids.

4. Dielectric Relaxation Measurements above the Glass Transition

A Hewlett-Packard HP 4129A LF Impedance Analyzer with a frequency range of 5 Hz to 13 MHz was used for dielectric measurements to investigate the relaxation of the side-chain chromophores above the glass transition temperature. The impedance measurements were done according to the "lumped circuit" method in either a parallel or series configuration. The dielectric loss was fitted to the Fourier transform[7] of the KWW stretched exponential function. Vogel-Fulcher and WLF parameters for the side-chain polymers are listed in the following table.

Polymer	B [10^3 K]	T_g [K]	T_2 [K]	C_1^g	$\log(\tau_g$ [s]/1s)
A-095.11	1.5±0.3	410	356±9	12±3	1.3±0.6
A-097.07	1.2±0.2	422	377±7	12±2	2.1±0.3
A-148.02	1.5±0.4	445	389±15	11±4	1.0±0.3

5. Second Harmonic (SHG) Decay Measurements below the Glass Transition

Relaxation of the side-chain chromophores below the glass transition was investigated by the decay of the SHG signal from corona and electrode poled films at fixed temperature over several decades in time. The time dependence of the decay of the normalized SHG ***d*** coefficient was usually well represented by the stretched exponential function. An example of normalized decay traces for A-095.11 is shown in Fig. 2.

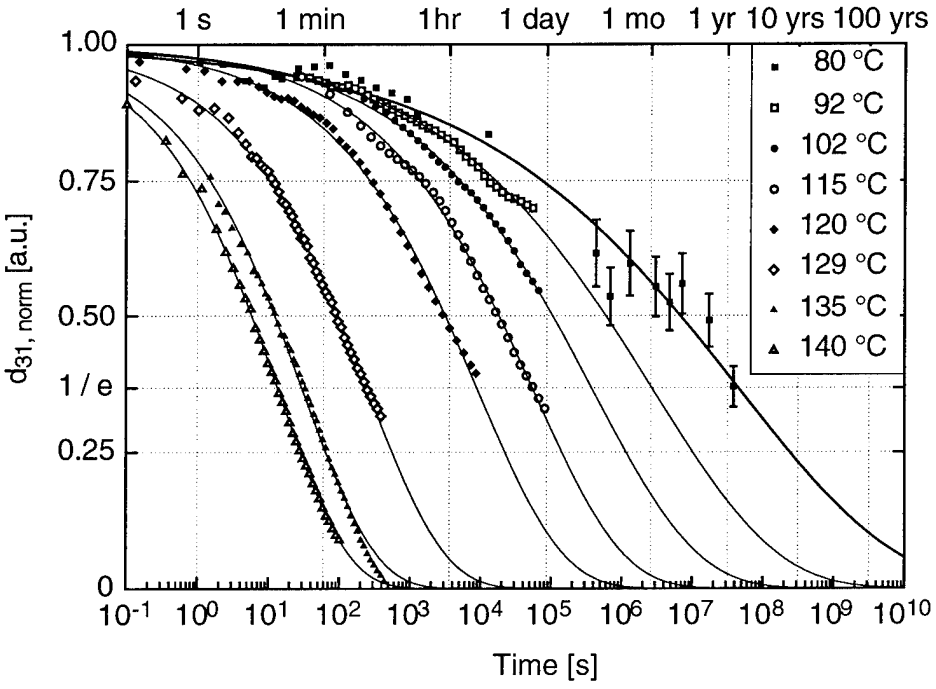

Fig. 2:

SHG relaxation traces for A-095.11 for different decay temperatures.

6. Scaling of Relaxation Times for Nonlinear Optical Polymers

Relaxation times from dielectric and SHG decay measurements are shown in the scaling graph.

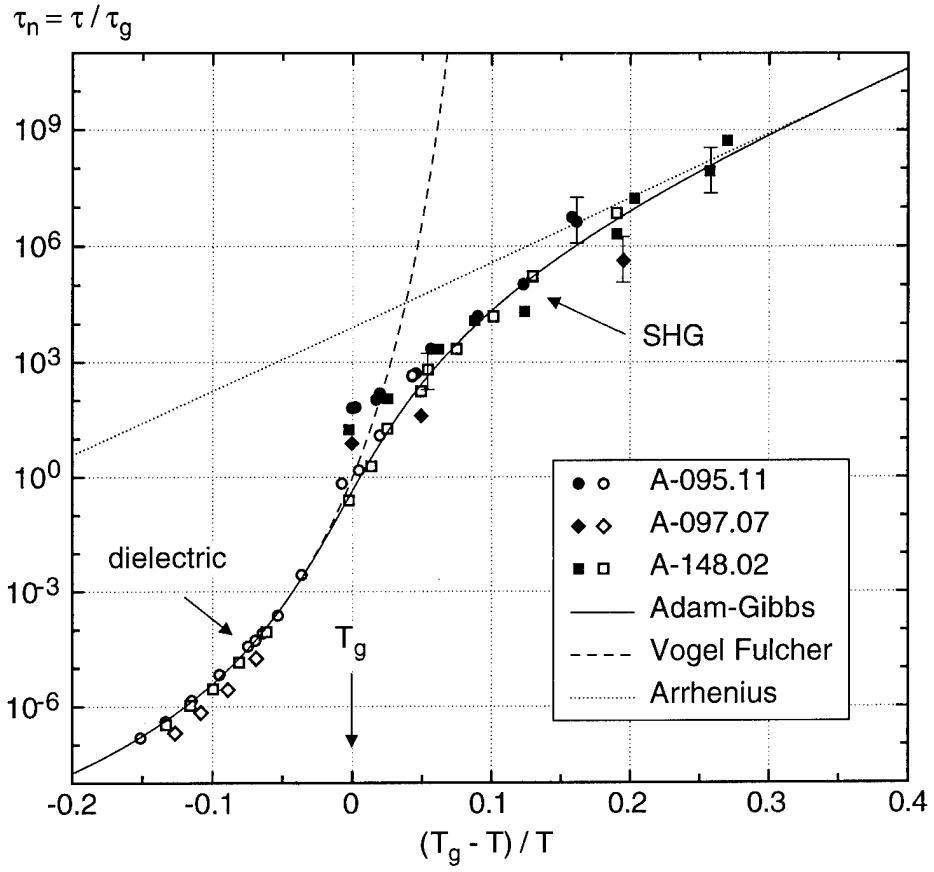

Fig. 3:
Scaling of normalized relaxation times for NLO side-chain polymers. Filled points belong to corona poled, open points to electrode poled films.
The solid line is calculated according to the Tool - Narayanaswamy procedure based on the Adam-Gibbs model for the relaxation time τ. Input parameters are taken from dielectric measurements.
The Vogel-Fulcher law fitted to dielectric data is given by the dashed line. Far below the glass transition, the relaxation is of Arrhenius type with an activation energy of $1.3 \cdot 10^5$ J/mol.

It is seen that the relaxation behavior of the NLO chromophores both above and below the glass transition can be modeled using the Tool / Narayanaswamy procedure with the appropriate WLF parameters for the NLO polymer. This procedure including our minor modification provides an excellent framework for the nonlinear extension of the liquid state relaxation behavior through the glass transition as suggested by the consistency between observed and calculated relaxation times below the glass transition.

7. References

(1) Ahlheim, M.; Lehr, F., *Makromol. Chem.* **1994**, *195*, 361-373.
(2) Prêtre, P.; Kaatz, P.; Bohren, A.; Günter, P.; Zysset, B.; Ahlheim, M.; Stähelin, M.; Lehr, F., *Macromolecules* **1994**, *27*, 5476 - 5486.
(3) Manificier, J. C.; Gasiot, J.; Fillard, J. P., *J. Phys. E: Sci. Instrum.* **1976**, *9*, 1002-1004.
(4) Jerphagnon, J.; Kurtz, S. K., *J. Appl. Phys.* **1970**, *41*, 1667.
(5) Bosshard, C.; Sutter, K.; Schlesser, R.; Günter, P., *J. Opt. Soc. Am.* **1993**, *B10*, 867.
(6) Teng, C. C.; Man, T. H., *Appl. Phys. Lett.* **1990**, *56*, 1734-1736.
(7) Williams, G.; Watts, D. C.; S.B., D.; North, A. M., *Trans. Far. Soc.* **1971**, *67*, 1323.
(8) Narayanaswamy, O. S., *J. Am. Cer. Soc.* **1971**, *54*, 471.
(9) Moynihan, C. T.; Crichton, S. N.; Opalka, S. M., *J. Non-Cryst. Solids* **1991**, *131-133*, 420.
(10) DiMarzio, E. A.; Gibbs, J. H., *J. Chem. Phys.* **1958**, *28*, 373.
(11) Adam, G.; Gibbs, J. H., *J. Chem. Phys.* **1965**, *43*, 139 - 145.
(12) Hodge, I. M., *Macromolecules* **1986**, *19*, 936.
(13) Kauzmann, W., *Chem. Revs.* **1948**, *43*, 219.
(14) Kaatz, P.; Prêtre, P.; Meier, U.; Stalder, U.; Günter, P.; Zysset, B.; Ahlheim, M.; Stähelin, M.; Lehr, F., in preparation
(15) Williams, M. L.; Landel, R. F.; Ferry, J. D., *J. Am. Chem. Soc.* **1955**, 3701.

Towards a physical interpretation of the activation volume for chromophore reorientation in corona poled polymers

Shane C. Brower and L. Michael Hayden, University of Maryland Baltimore County
Dept. of Physics, 5401 Wilkens Ave., Baltimore, MD 21228 Phone: 410-455-3290
Fax: 410-455-1072 Internet: brower@umbc9.umbc.edu, hayden@umbc7.umbc.edu

Recently we reported[1, 2] on a technique for measuring the decay of the second order optical susceptibility $\chi^{(2)}$ as a function of temperature and pressure in poled nonlinear optical (NLO) polymeric materials. This approach utilizes second harmonic generation (SHG) to monitor the rotational reorientation of the NLO chromophores in such systems and yields structural information directly related to the reorientation process in poled polymers.

Initially we applied our technique to a system consisting of the dye Disperse Red 1 (DR1) dissolved in poly(methyl methacrylate) (PMMA).[1,2] Figure 1 shows the results of monitoring the decay of $d_{31} = \frac{1}{2}\chi_{zxx}$ in DR1/PMMA versus time at 99°C and various pressures.

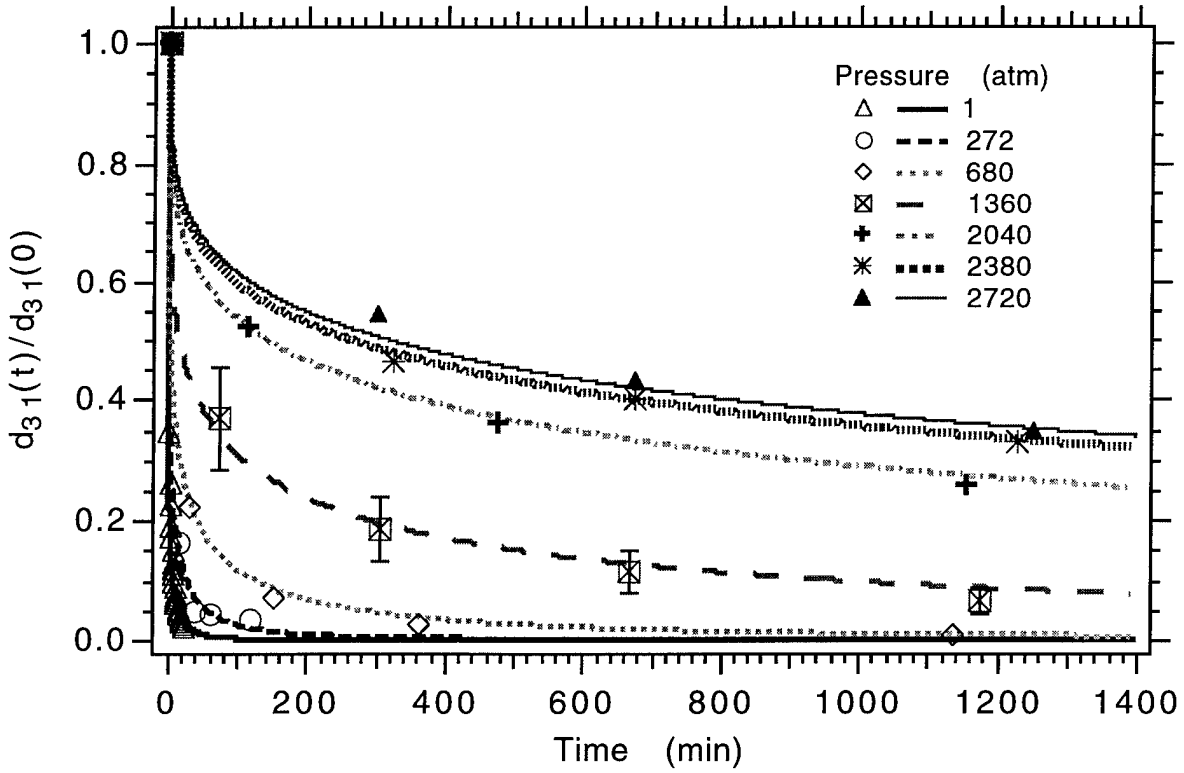

Figure 1. Decay of d_{31} in corona poled films of DR1/PMMA at 99°C and various pressures. The solid curves are generated from the average values of τ and β obtained from fits of the data for several samples to the Kohlrausch-Willimas-Watts stretched exponential. A representative data set is included with each curve. The error bars on the data for 1360 atm. are typical of each of the data sets.

At each pressure, the relaxation of $\chi^{(2)}$ could be fit quite well by a Kohlrausch-Williams-Watts (KWW) stretched exponential[3],

$$d_{31}(t) = d_{31}(0)\exp\left[-\left(t/\tau(P)\right)^{\beta}\right] \tag{1}$$

where P is pressure, $\tau(P)$ is the time required for d_{31} to decay to $1/e$ of its original value and β is a measure of the width of the distribution of relaxation times associated with the decay process. The decay of $\chi^{(2)}$ was monitored for several individual samples at each pressure, yielding a mean decay time and decay distribution width for that pressure. Defining the pressure shift factor a_P by $a_P = \tau(P)/\tau(P_o)$, where P_o is atmospheric pressure, we observed that $ln\ a_P$ varied linearly with pressure up to approximately 1500 atmospheres as shown in Figure 2.

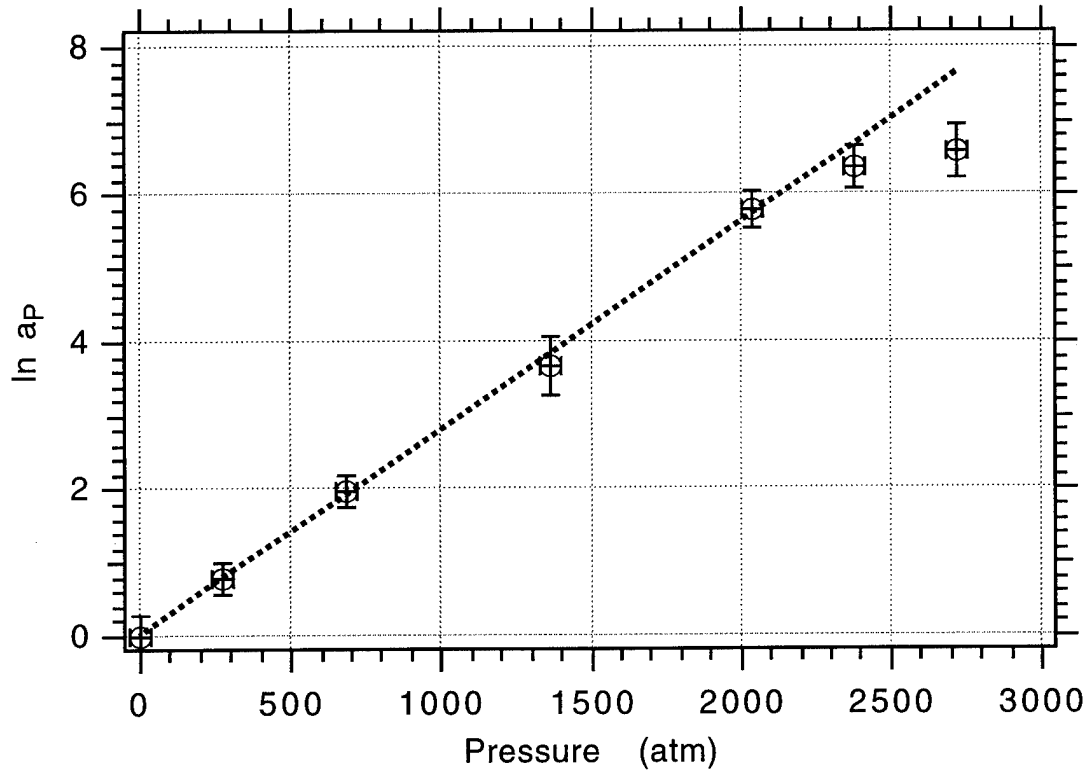

Figure 2. Natural log of the shift factor a_P vs pressure for the DR1/PMMA system described in Figure 1.

Above 1500 atmospheres the rate of increase of $ln\ a_P$ with pressure decreased dramatically. The initial linear dependence of $ln\ a_P$ on pressure suggested that below 1500 atm the reorientation of the DR1 chromophores was an activated process and allowed us to calculate an activation volume for the process by fitting the linear region of the data in Figure 2 to the equation

$$\ln a_P = \frac{\Delta V^*}{RT}\left(P - P_o\right) \tag{2}$$

where R is the gas constant, T is temperature and ΔV^* is the activation volume.

Measuring the activation volume for chromophore reorientation in poled polymers yields size related information that is potentially useful in determining the mechanism governing chromophore reorientation in poled polymers. However, we must first determine the physical nature of the activation volumes, i.e. what do the activation volumes correspond to physically?

To that end, we have measured the activation volumes for a series of guest-host materials formed by individually dissolving the dyes Disperse Red 1 (DR1), Disperse Orange 3 (DO3) and *N,N* dimethyl-*p*-nitroaniline (DpNA) in poly(methyl methacrylate) (PMMA), polycarbonate (PC), and polystyrene (PS).[4] For each of these materials, $ln\, a_P$ exhibited qualitatively the same behavior versus pressure as that observed for DR1/PMMA in Figure 2 -- an initial linear pressure dependence followed by a rapid decrease in the slope. This allowed us to extract an activation volume for chromophore reorientation in each of the systems. These results are contained in Table 1.

Table 1.

Activation volumes in Å^3 for various guest-host polymer systems. (Below each chromophore is shown its van der Waals volume)

	PMMA	PS	PC
DR1 (270 Å^3)	160 ± 20	352 ± 8	320 ± 20
DO3 (202 Å^3)	180 ± 20	380 ± 10	210 ± 30
DpNA (142 Å^3)	50 ± 5	270 ± 20	170 ± 5

For an activated process, the activation volume is normally identified as the volume of the transition state between the original and final configurations of the system. For the case of chromophore realignment in a poled polymer, the transition state is related to the intermediate configurations of the polymer and/or dye molecules during the passage from the original poled state to the final randomized state. Thus the activation volume is somehow related to the motions of these various molecules during the reorientation process.

One possibility for the physical correspondence of the activation volume for rotational reorientation in poled polymers is that the activation volume is equivalent to the average volume swept out by the chromophores during reorientation. However, we demonstrated that such an equality between activation volume and chromophore swept volume is incompatible with the observed variations in activation volume between polymer systems as seen in Table 1.[4] For example, if the activation volume for chromophore reorientation is equivalent to the average volume swept out by the chromophores during rotation, one would predict that for a given dopant the activation volume for rotational reorientation should be independent of the host polymer, i.e. when rotating through the same angular displacement about the same point of rotation, a given molecule will sweep out the same amount of volume irrespective of the surrounding environment. However, the results in Table 1 show that for a given dopant, the activation volume does in fact vary form host to host. Similarly, again assuming activation volumes to represent chromophore swept volumes, one would expect there to be a direct relationship between chromophore size and activation volume for a given polymer host. Again we see from Table 1 that in general there is not a direct relationship between dopant size and activation volume within the same host polymer. Therefore, the data in Table 1 imply that the activation volume for chromophore reorientation is not equivalent to the average chromophore swept volume.

It has been demonstrated in a variety of guest-host and side-chain polymer systems that the rotational reorientation of the guest molecules is directly coupled to the motion of the polymer host.[5,6] In addition, these studies found that in a given polymer host, the reorientation of similar sized dopants is coupled to the same polymer constituent motion,[6(a),(b)] while the reorientations

of substantially different sized dopants are coupled to different types of polymer motion.[5,6(a),(b),(d)] This coupling between chromophore reorientation and polymer segmental motion suggests that perhaps the activation volumes we measured for a given system are related to the size or motion of the polymer constituents to which the chromophore reorientation was coupled. If this is true, then all chromophores whose reorientations are coupled to the same polymer component motion should have the same activation volumes. Furthermore, these activation volumes should be different from those for dopants whose rotations are coupled to the motion of different parts of the polymer or different motions of the same polymer component. As a result, for a given polymer host, as the dopant molecule is changed such that chromophore reorientation becomes coupled to different polymer constituent motions, the measured activation volume should exhibit a corresponding incremental change. This is precisely the type of behavior exhibited by the activation volumes in Table 1. Specifically, for PMMA both DR1 and DO3 have the same activation volume within experimental error, and this activation volume is much larger than that for DpNA. Similarly, in PS the activation volumes for DR1 and DO3 are approximately the same and significantly larger than the activation volume for DpNA. Finally, in PC the activation volumes for DO3 and DpNA are almost equal and substantially lower than the activation volume for DR1. Moreover, the activation volumes for DR1 and DpNA in PS are seen to correlate with the proposed chromophore reorientation/polymer constituent motion couplings of these systems. That is, Dhinojwala et. al.[6(b)] have observed that the reorientation of DR1 in PS is coupled to the large scale segmental motion of the PS backbone associated with its α-transition. On the other hand, these same researchers found[6(d)] that the reorientation of DpNA in PS was only partially coupled to the PS α-transition dynamics, with the remainder of the reorientation occurring independently of the motion of the polymer matrix. Therefore, if activation volume is a function of the size or motion of the host polymer components to which the chromophore reorientation is coupled, we would expect DR1/PS and DpNA/PS to have different activation volumes, which in fact they do. The agreement between the measured activation volumes and the observed couplings of chromophore reorientation and polymer motion in DR1/PS and DpNA/PS, along with the "grouping" of activation volumes for each polymer host in Table 1 imply that the activation volume for chromophore rotational motion is a function of the motion of the polymer components to which the reorientation is coupled.

Further study is necessary to determine if the suggested relationship between polymer constituent motion and the activation volume for chromophore rotation exists, and if so, to quantify this relationship. To do so, we are currently investigating a series of guest- host systems in which n-alkyl-aminonitrotolanes are individually doped into PMMA, PEMA, and PIBMA. In this study the size of the dopants is being incrementally varied over a wide range in order to fully probe the various coupling possibilities between chromophore reorientation and the motion of the various polymer components. In addition to measuring the activation volumes for chromophore reorientation in these systems, we are comparing these activation volumes to the activation volumes for molecular motion of the neat polymers obtained from dielectric relaxation measurements in the literature. The results of this current study will be presented.

References:

[1]S. C. Brower and L. M. Hayden, *Appl. Phys. Lett.*, **63**, 2059 (1993).

[2]S. C. Brower and L. M. Hayden, *Organic Thin Films for Photonic Applications Technical Digest 1993*, (Optical Society of America, Washington, D.C., 1993), **17** 292.

[3]F. Kohlrausch, *Pogg. Ann. Physk.*, **119**, 352 (1863); G. Williams and D. C. Watts, *Trans. Faraday Soc.*, **66**, 80 (1970).

[4]S. C. Brower and L. M. Hayden, *J. Poly. Phys. B*, submitted

[5]Q. Tran-Cong, S. Chikaki, and H. Kanato, *Polymer*, **35**, 4465 (1994).

[6](a)A. Dhinojwala, G. K. Wong, and J. M. Torkelson, *Macromolecules*, **26**, 5943 (1993); (b) A. Dhinojwala, G. K. Wong, and J. M. Torkelson, *J. Chem. Phys.* , **100**, 6046 (1994); (c) A. Dhinojwala, J. C. Hooker, and J. M. Torkelson, *J. Non-Cryst. Solids*, **172-174**, 286 (1994); (d) J. M. Torkelson and A. Dhinojwala, *Bull. Am. Phys. Soc.*, **40**, 233, (1995)

Current flow in doped and undoped electro-optic polymer films during poling

D. G. Girton, W. W. Anderson, J. A. Marley, T. E. Van Eck, and S. Ermer

Lockheed Research and Development Division
Department 97-80, Building 202
3251 Hanover St., Palo Alto, CA 94304
415 354-5133 Voice, 415 354-5400 Fax
Girton_Dexter@mm.rdd.lmsc.lockheed.com

Electric-field poling is used to achieve a macroscopic alignment of the chromophores responsible for the electro-optic (EO) effect in polymer films.[1] In EO polymer devices this chromophore doped layer, referred to as the "core" layer, is usually stacked between two polymer "cladding" layers of lower index which confine transmitted light to the core layer. These polymer films are formed by spin coating using standard semiconductor equipment and manufacturing processes. The polymer films are amorphous as spun and cured, so the polarizable chromophores are randomly arranged, and therefore no second-order electro-optic effects occur. Electric-field poling has been used to make a variety of EO polymer devices[2,3,4,5], but the process is not well understood. In electric field poling the EO polymer is heated above its glass transition temperature T_g, a voltage is applied by electrodes to align the nonlinear chromophore molecules in the direction of the field, and the material is cooled back to room temperature under the influence of the electric field. While the voltage is applied to the cladding/core/cladding stack of films, the electric field divides in some manner so that a portion of the applied voltage appears across each of the film layers, as illustrated in Figure 1.

To achieve the maximum chromophore alignment during poling it is necessary to have a large fraction of the applied field appear across the core layer. Assuming the simple electrical resistance model shown in Figure 1, the voltage fraction appearing across the core layer depends on the ratio of the cladding to core resistivity (or core to cladding conductivity), and this fraction is high only when the resistivity of the cladding is low compared to the core. Thus, based on the model, the resistivity of each layer significantly influences the effectiveness of chromophore alignment during poling. We present a simple technique for measuring current flow in polymer films during poling, along with measured values for particular polymers, and we present data on fabricated Mach-Zehnder modulators which support the resistance model shown in Figure 1. For simplicity, the resistivity of the top and bottom claddings were assumed to be equal, and layer-to-layer interface charges were not accounted for.

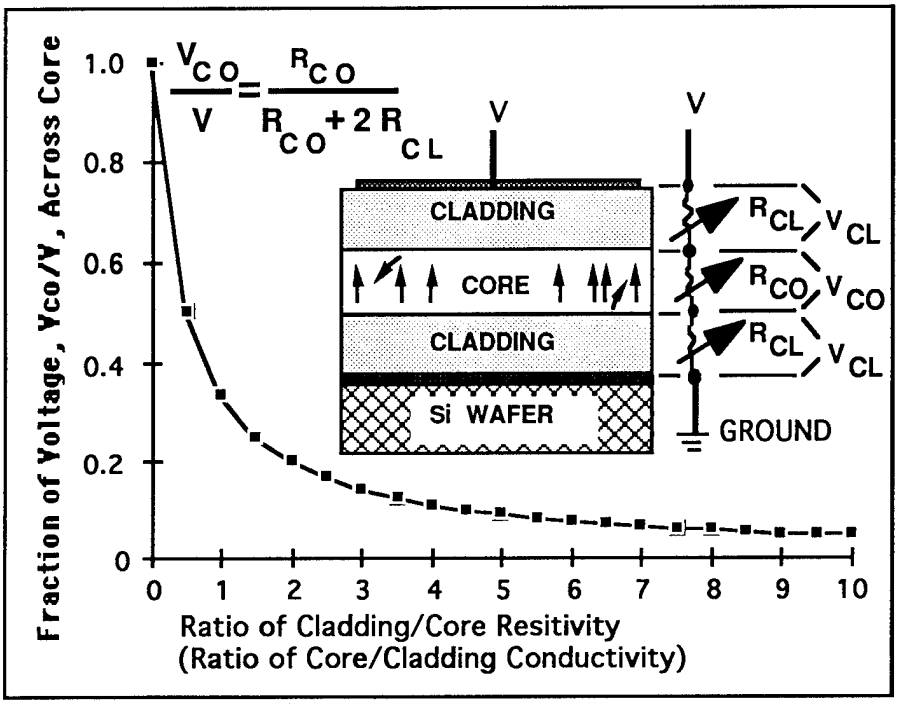

Figure 1. Fraction of voltage appearing across EO polymer core layer vs. cladding/core resistivity ratio. Arrows across resistors indicate resistivity may vary with applied voltage and with time.

The cladding materials in this work were based on Amoco Ultradel® 4212 polyimide, and an in-house UV curable acrylate . The core material was a guest-host mixture of Amoco 4212 and the laser dye DCM[6], with a T_g near 200 °C. The measurement techniques described here can be extended to a wide range of single or multilayer polymer materials.

Although current flow in selected polyimides has been studied by some workers[7,8], the mechanisms of charge transport are not well understood, and little has been done to understand transport in chromophore doped polymer films. The need to build EO devices with low switching voltages, as required for system application, provides motivation to achieve good poling and thus utilize the potential that a particular chromophore has to offer. To achieve effective poling it will be necessary to study and understand the conduction mechanisms in doped and undoped polymer films. Manufacturers can then synthesize materials with controlled conductivities which can be used to build practical EO polymer devices.

Samples for conductivity measurements were prepared by starting with Si wafers on which 2 μm of thermal oxide had been grown, and then a 0.5 μm thick film of Al (with 1% Si, 2% Cu) was deposited by sputtering. Single layer polymer films were spin coated and cured. Using the same procedure, a series of Mach-Zehner modulators was built at the same time. The single layer thicknesses of the samples shown in Figure 4 were: 1.9 μm for 4212:DCM core, 2.8 μm for 4212 cladding, and 2.7 μm for acrylate cladding. After each layer was cured, a solid, round gold electrode was evaporated through a shadow mask, giving an area of 1 cm^2. The mask was separated about 5 mils from the polymer surface to avoid contamination and scratches which might affect the results. This mask contained 12 such round holes which were spread over a 100 mm Si wafer so that each sample could be separated by cleaving after evaporation. Contact with the Al ground plane was achieved by scratching through the polymer using a sharp tool. Each sample was cleaned of Si and polymer chips by a high pressure blast of semiconductor grade N_2, and then stored permanently in an N_2 dessicator. Water or other chemical contact with the films was avoided in order to prevent contributions from these sources in the measured currents. Care was taken to minimize sample-to-sample variations by using all 12 samples from one wafer for a trend study where possible, and other wafers that were needed were built at the same time using the same conditions.

Each sample was tested on a water-cooled hot plate (Lucas/Signatone Corp.), housed in an N_2 purged enclosure as shown in Figure 2. The hot plate surface temperature was controlled via thermocouple feedback to a programmable temperature controller (Omega Corp.) with ramp and soak capability. The 2 μm thick SiO_2 film on the Si wafer was thin enough to permit good heat transfer to the polymer film, while providing additional electrical isolation from low level noise sources originating in the hot plate. A fine gold wire, which contacted the gold top electrode, was electrically connected to a dc power supply, and a picoammeter measured the current, as shown in Figure 2. A personal computer timed the measurements and stored the resulting current values. The entire process of sample preparation, testing, and storage was carried out in a Class 10 clean room to minimize particulate contamination.

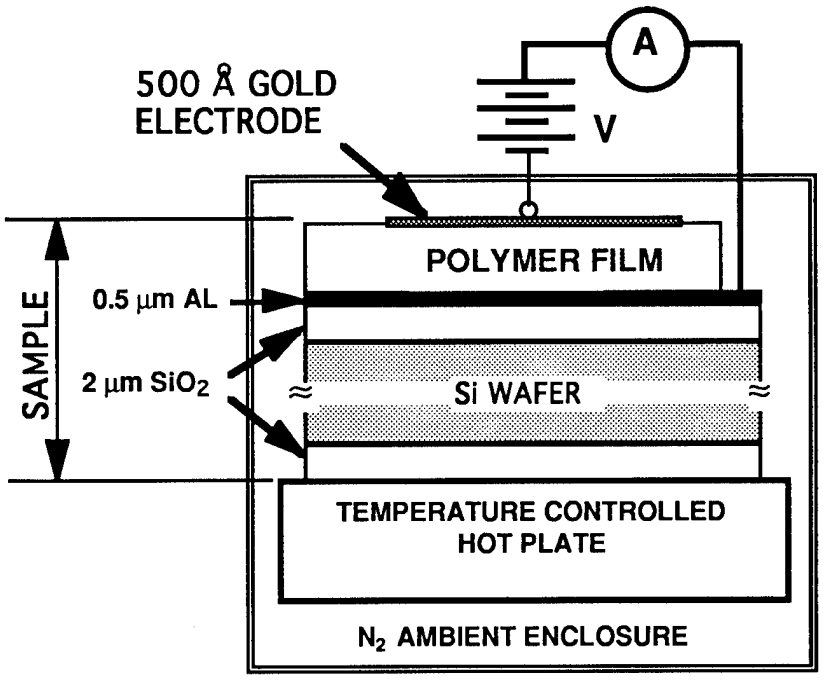

Figure 2. Polymer conductivity sample in test on a hot plate, and electrical schematic with power supply V and picoammeter A.

Each sample was heated in an N_2 environment using the temperature profile shown in Figure 3. The purpose of the 120 ^oC segment is to drive off absorbed moisture. The sample electrodes were shorted together until the beginning of the 190 ^oC segment, and then a dc voltage was applied throughout the test time. Due to history effects in polymer films[7], each sample was tested only once. This procedure duplicated the poling procedure for the concurrent Mach-Zehnder modulator devices, except the poling time was longer for the conductivity samples in order to indicate current trends.

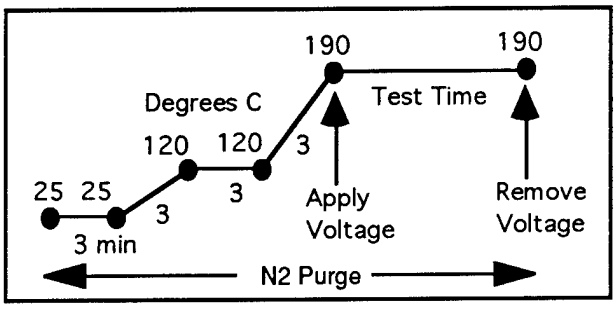

Figure 3. Temperature profile of conductivity sample under test.

Typical current values for the films tested at 190 ^oC, for several fields, are shown in Figure 4. The data show that the 4212:DCM core film is one to two order of magnitude more conducting than the 4212 cladding film, while the acrylate cladding is somewhat more conducting than the core. The core layer starts out with the same characteristics before doping, but the addition of the chromophore dopant raises the conductivity in two ways: First, the DCM is not prepared to microelectronic specifications and therefore may be contaminated with ionic impurities which would increase the current. The magnitude of this ionic contribution is unknown. It would become very small as the ions are swept toward one electrode. Second, most small molecules have a plasticizing effect on polymers, lowering the T_g, and this should increase the current. The cause of the higher conductivity in the acrylate cladding is unknown.

Current in some of the films decreased with time, while others increased and then decreased during the measurement period. The causes of these trends are not understood and are the subject of further investigation. Chemical rearrangements may occur during the poling period, and effects such as chromophore diffusion, residual solvent diffusion, and movement of ionic charges may contribute to the measured current. The current in the 4212:DCM core layer appears to be more voltage dependent than in the 4212 cladding layer. Thus it can be seen that the conductivity of these films vary with voltage and time. Based on these single film measurements, the resistance model of Figure 1 implies that the field across the core layer in a three layer stack could vary significantly with voltage and time during the poling process, according to the ratio of the core/cladding conductivities.

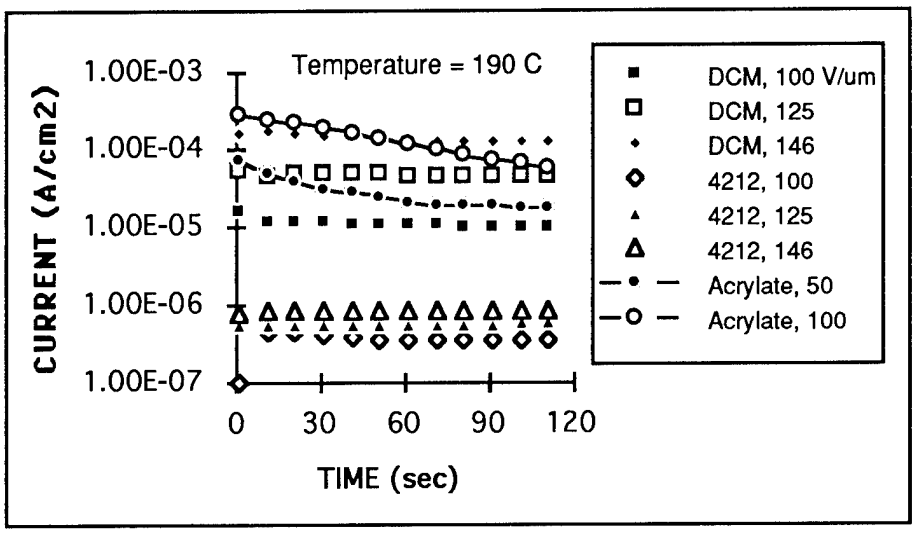

Figure 4. Plot of current vs. time for 4212:DCM core, 4212 cladding, and acrylate cladding, for several fields.

The Mach-Zehnder modulators that were fabricated concurrently with the conductivity samples resulted in device EO coefficient values , r33, as shown in Figure 5. The acrylate cladding yielded significantly higher values of r33. This supports the resistance model since acrylate cladding is much more conductive that the 4212 cladding. The cause of the saturation in r33 is unknown and is the subject of further investigation.

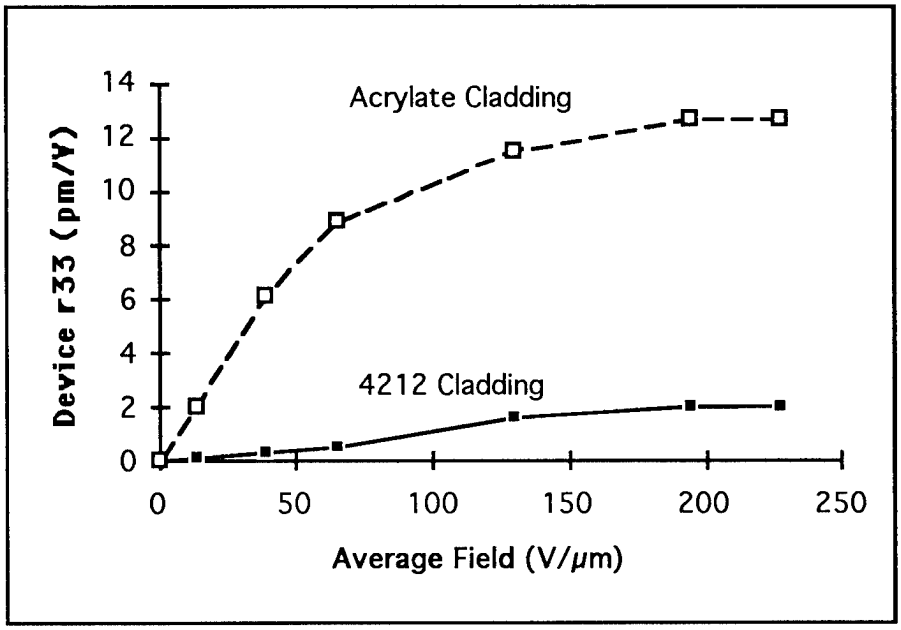

Figure 5. Device r33 vs. average poling field for Mach-Zehnder modulators with different claddings.

In summary, a technique for measuring current flow in electro-optic polymer films during poling has been presented, along with measurements on single layer films as a function of time and applied field. Mach-Zehnder modulators were built up from these single films, and the modulator r33 values tended to support a simple resistor analog for a multilayer films. The role of ionics was discussed but their effect on conductivity was not determined. Further work is needed to understand more completely how electric fields divide in multilayer stacks, and how this affects poling efficiency.

1) K. D. Singer, J. E. Sohn, and M. G. Kuzyk, "Orientationally Ordered Electro-optic Materials", in Nonlinear Optical and Electro-active Polymers, P.N. Prasad and D.R. Ulrich, ed., Plenum Press, New York (1988), p. 189.
2) D. G. Girton, S. L. Kwiatkowski, G. F. Lipscomb, and R. S. Lytel, Appl. Phys. Lett. **58**, 1730 (1991).
3) C. C. Teng, Appl. Phys. Lett. **60**, 1538 (1992).
4) G. R. Möhlmann W. H. G. Horsthuis, A. McDonach, M. J. Copeland, C. Duchet, P. Fabre, M. B. J. Diemeer, E. S. Tramel, F. M. M. Suyten, E. Van Tamme, P. Baqero, and P. Van Daele, Proc. SPIE 1337, 215 (1990).
5) T. E. Van Eck, A. J. Ticknor, R. S. Lytel, and G. F. Lipscomb, Appl. Phys. Lett. **58**, 1588 (1991).
6. S. Ermer, J.F. Valley, R. Lytel, G.F. Lipscomb, T.E. Van Eck and D.G. Girton, Appl. Phys. Lett. **61**, 2272 (1992).
7) H. J. Neuhaus, D. R. Day, and S. D. Senturia, J. Electron. Mat. **14**, 379, (1985).
8) F. W. Smith, H. J. Neuhaus, and S. D. Senturia, J. Electron. Mat. **18**, 93, (1987).

Electric Field Effects in Poled Polymer Thin Films

Mark H. Ostrowski and Hilary S. Lackritz
Purdue University, School of Chemical Engineering
West Lafayette, IN 47907-1283
Phone (317) 494-4065
FAX (317) 494-0805

INTRODUCTION

Polymer thin film systems have been explored as potential materials for nonlinear optical (NLO) device applications using second order nonlinear optical effects such as second harmonic generation and linear electrooptic effect for photonic devices including waveguides and frequency doublers. For second order nonlinear effects to be observed, a noncentrosymmetric orientation of the NLO chromophores, which is obtain by poling with a large magnitude electric field, is necessary. The effects of the electric field during and following poling are poorly understood. During poling, charge is injected into the polymer film affecting the local electric field that the NLO chromophores senses. After poling, these charges that have become trapped in the polymer film system affect the decay of the NLO properties of the film. Therefore, to make efficient nonlinear optical devices, it is necessary to understand the electric field effects on the thermal and temporal stability of chromophore orientation within the polymer thin film system as a function of processing. Electroreflection and dielectric relaxation measurements were performed on poly(methyl methacrylate) doped with 4-dimethylamino-4'-nitrostilbene (DANS).

EXPERIMENTAL PROCEDURE

Electroreflection measurements were made within the absorption spectrum of the chromophores which was measured using a Spectronic ultraviolet-visible (UV-Vis) spectrophotometer. A 0.1 - 1 kHz AC voltage was applied across the film to create electric fields

approaching 10^6 V/cm. A collimated beam from a Hg-Xe 1 kW lamp was passed through a monochromator and reflected from the sample. A photodiode connected to a lock-in amplifier which was phased locked to the frequency of the applied field was used to observe the reflected beam.. Another photodiode was used to measure the change in intensity, if any, of the light from the lamp which was used as a reference source. The output of both photodiodes was recorded as a function of optical wavelength. A spectrum of the sample without the applied electric field was also obtained. The electroreflection setup is shown in Figure 1. In addition, dielectric relaxation measurements were performed using a GenRad 1689 dielectric bridge. The frequency range is from 12 Hz to 100 kHz. An oven with 0.1°C accuracy was used to control the temperature during the experiment.

RESULTS AND DISCUSSION

Electroreflection experiments were performed to characterize the electric field at the electrodes. This is obtain by comparing the derivatives of the absorption spectrum to the change of the absoprtion spectrum due to an applied electric field. The first derivative of the zero-field spectrum for a 5 wt% DANS doped in PMMA film was obtained In Figure 2, the fundamental and second harmonic spectra for a 5 wt% DANS doped in PMMA film are shown. The spectral dependence shows no obvious relation to the derivative of the zero-field spectrum. Samples tested for electroreflection signal well to the red of their absorption bands showed minimal signal, arguing against a contribution to the signal from interference in the film modulated by electrostriction. The fundamental and second harmonic spectra displayed in Figure 2 match one other to within the accuracy of the experiment. This similarity would necessarily occur if reflection occurred from the front surface only. However, this is not the case. A measurable signal penetrates through the polymer film and through the semi-transparent gold electrode on the rear surface. The spectral match indicates that the DC field has the same spatial dependence as the applied field which is uniform across the film. This implies that the field responsible for the signal at the fundamental is largely due to charge localized at or near the electrodes. This

field may simply be due to the difference between the work functions of the two electrodes, and would be present even if the polymer did not conduct at all, since the Fermi levels of the two electrodes would equilibrate through the external circuit.

Dielectric relaxation measurements were performed on films consisting of PMMA doped with 4 wt% DANS. The normalized dielectric loss curve as a function of normalized frequency is shown in Figure 3. These curves at different temperatures were fitted using the Havriliak-Negami equation. The results are shown in Table 1. Both α and β decrease slightly and τ decreases significantly with increasing temperature. This decrease in a suggests an increase in intermolecular coupling. The relaxation times obtain from dielectric relaxation measurements will be used with the relaxation times from second harmonic generation experiments to determine the relaxation time as a function of temperature.

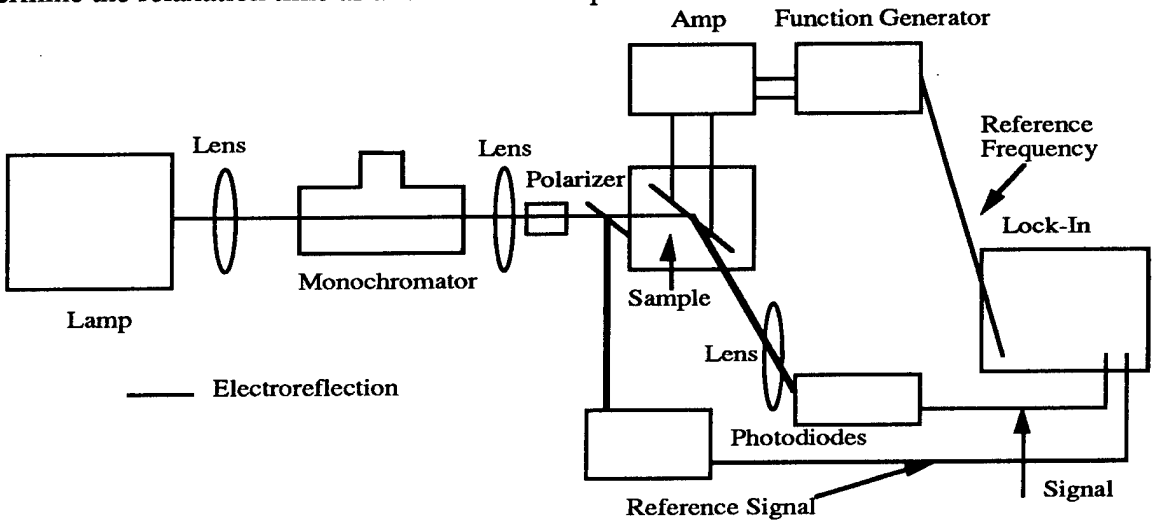

Figure 1. Electroreflection setup.

Table I. Havriliak-Negami Parameters

Temp	α	β	τ	Freqmax
100°C	0.44	0.99	290 μs	3470 Hz
110°C	0.38	0.99	115 μs	7200 Hz
120°C	0.35	0.81	70 μs	21300 Hz
130°C	0.33	0.74	11 μs	52700 Hz

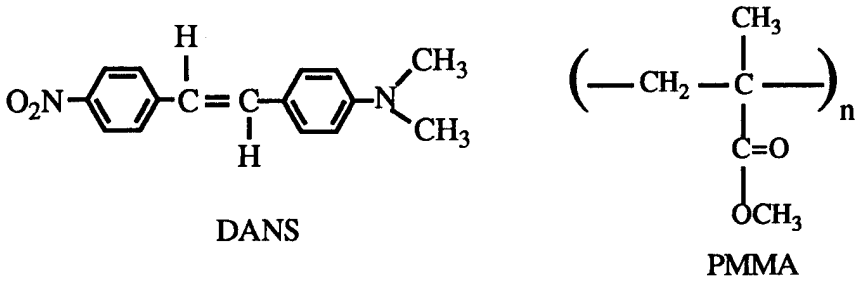

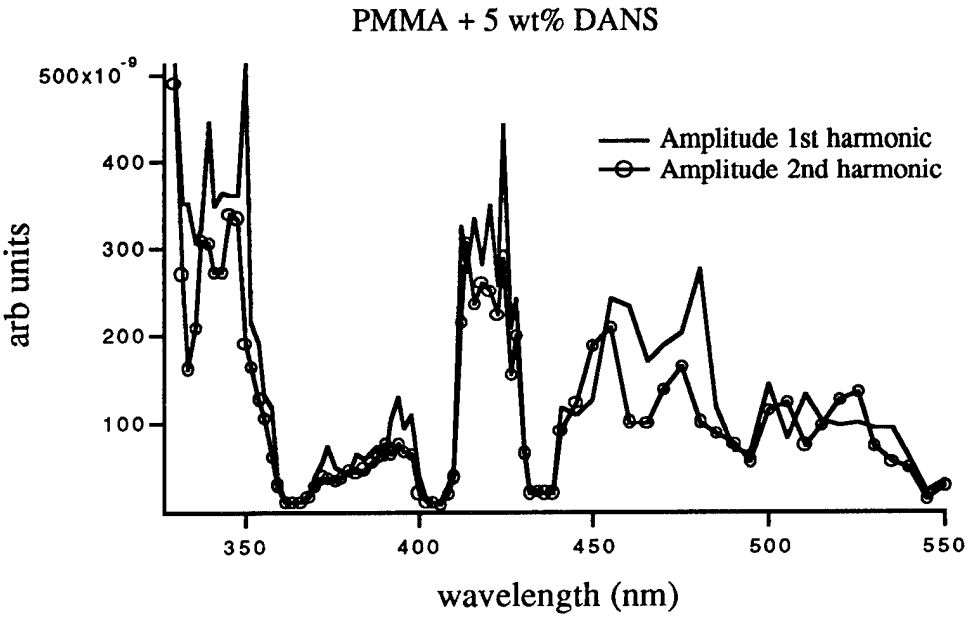

Figure 2. First and second harmonic spectra of 5wt% DANS + PMMA and structures.

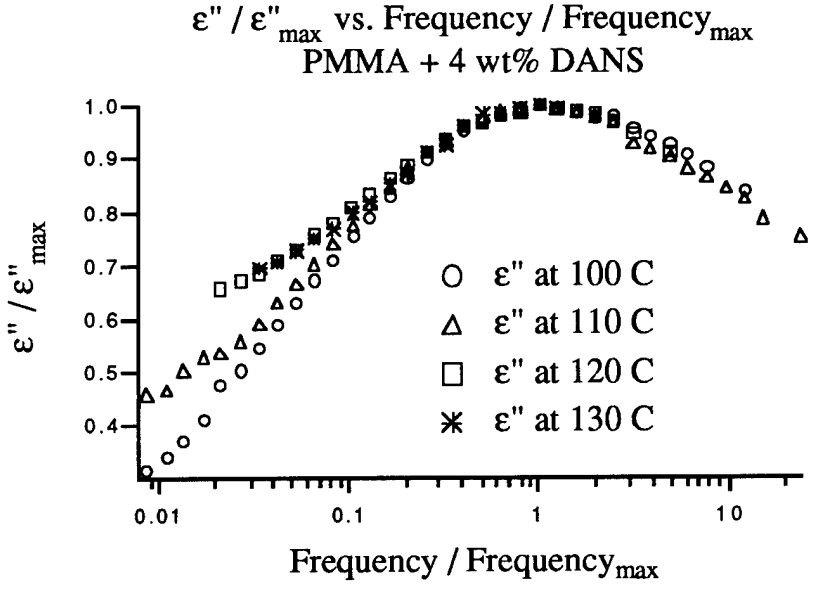

Figure 3. $\varepsilon''/\varepsilon''_{max}$ vs. normalized frequency for 4 wt% DANS doped in PMMA.

ORGANIC THIN FILMS FOR PHOTONICS APPLICATIONS

TECHNICAL PROGRAM COMMITTEE

Kenneth Singer, *Case Western Reserve University, Chair*
Charles Y.-C. Lee, *Air Force Office of Scientific Research, Chair*
Hilary S. Lackritz, *Purdue University, Program Chair*
George I. Stegeman, *University of Central Florida/CREOL, Program Chair*
***Gary C. Bjorklund,** *Optivision Inc.*
Julian Bristow, *Honeywell Technology Center*
Susan Ermer, *Lockheed Research and Development Division*
Anthony F. Garito, *University of Pennsylvania*
Alan Heeger, *University of California, Santa Barbara*
Yasuhiro Koike, *Keio University, Japan*
Mark G. Kuzyk, *Washington State University*
Geoffrey A. Lindsay, *U.S. Navy*
Rick Lytel, *Akzo Nobel Electronic Products, Inc.*
Seth Marder, *California Institute of Technology*
Tobin Marks, *Northwestern University*
W. E. Moerner, *IBM Almaden Research Center*
Peter Palffy-Muhoray, *Kent State University*
Paras N. Prasad, *State University of New York at Buffalo*
William H. Steier, *University of Southern California*
James T. Yardley, *AlliedSignal Inc.*

INTERNATIONAL ADVISORY COMMITTEE

Donal D. C. Bradley, *University of Sheffield, UK*
Peter Gunter, *Swiss Federation Institute of Technology, Switzerland*
Winfried Horsthuis, *Akzo Nobel Electronic Products, The Netherlands*
François Kajzar, *CEA Saclay, France*
Toshikuni Kaino, *NTT Opto Electronics Laboratory, Japan*
Wolfgang Knoll, *Max-Planck-Institut fur Polymerforschung, Germany*
Seizo Miyata, *Tokyo University of Agriculture and Technology, Japan*
Hachi Nakanishi, *Tohoku University, Japan*
Almira Natansohn, *Queen's University, Canada*
Andre P. Persoons, *University of Leuven, Belgium*
Hiroyuki Sasabe, *Institute of Physical and Chemical Research (RIKEN), Japan*
Guiseppe Zerbi, *Politecnico di Milano, Italy*
Joseph Zyss, *Centre National d'Etudes des Telecommunications, France*

*OSA Technical Council Representative